

THEORY AND RESEARCH IN ENGINEERING II

VOLUME I

EDITOR: DOÇ. DR. MIHRİBAN KALKANCI

İmtiyaz Sahibi / Publisher • Yaşar Hız
Genel Yayın Yönetmeni / Editor in Chief • Eda Altunel
Kapak & İç Tasarım / Cover & Interior Design • Gece Kitaplığı
Editör / Editor • Doç. Dr. Mihriban Kalkancı
Birinci Basım / First Edition • © Aralık 2020
ISBN • 978-625-7319-06-5

© copyright

Bu kitabın yayın hakkı Gece Kitaplığı'na aittir.

Kaynak gösterilmeden alıntı yapılamaz, izin
almadan hiçbir yolla çoğaltılamaz.

The right to publish this book belongs to Gece Kitaplığı.
Citation can not be shown without the source, reproduced in any way
without permission.

Gece Kitaplığı / Gece Publishing
Türkiye Adres / Turkey Address: Kızılay Mah. Fevzi Çakmak 1. Sokak
Ümit Apt. No: 22/A Çankaya / Ankara / TR
Telefon / Phone: +90 312 384 80 40
web: www.gecekitapligi.com
e-mail: gecekitapligi@gmail.com



Baskı & Cilt / Printing & Volume
Sertifika / Certificate No: 47083

Theory and Research in Engineering II

EDITOR

DOÇ. DR. MIHRIBAN KALKANCI

CONTENTS

CHAPTER 1 HOUSING DAMAGE ESTIMATOR FOR EARTHQUAKES: AN AUTOMATED MACHINE LEARNING APPLICATION FOR 2015, NEPAL EARTHQUAKE Emre S. OZMEN.....	1
CHAPTER 2 INNOVATIVE TECHNIQUES IN CLOTHES PRODUCTION: COSTUME (TEKMET) PRODUCED USING TEXTILE AND METAL MATERIALS Gülhan PINARLIK & Gökhan YILDIRIM.....	21
CHAPTER 3 DETERMINATION OF THE IDEAL FLOW RATE IN DRYING OF TABLE SALT Sultan KEPÇEOĞLU & Aytaç MORALAR& Soner ÇELEN.....	35
CHAPTER 4 SURFACE CHARACTERIZATION FOR NANOTECHNOLOGICAL APPLICATIONS Ceyda BİLGİÇ & Şafak BİLGİÇ	47
CHAPTER 5 TRANSMISSION LINE LOADING REGULATION AND POWER LOSS MINIMIZATION IN ELECTRICAL POWER SYSTEMS BY USING FACTS DEVICES Serhat Berat EFE	67
CHAPTER 6 GRAVITATIONAL WATER VORTEX POWER PLANTS Ahmet TEBER	93
CHAPTER 7 VERMICULITE FILLED POLYMER COMPOSITES Ozan TOPRAKCI & Mukaddes Sevval CETIN & Hatice Aylın KARAHAN TOPRAKCI.....	125
CHAPTER 8 DESIGN AND IMPLEMENTATION OF A MOBILE CULTURAL HERITAGE KNOWLEDGE MANAGEMENT SYSTEM FOR THE INTERNET OF ARCHEOLOGICAL THINGS Mehmet Erkan YÜKSEL & Hüseyin FIDAN.....	145

CHAPTER 9 INNOVATIVE SUPERHYDROPHOBIC MATERIALS DESIGNED WITH INSPIRATION FROM NATURE Ceyda BİLGİÇ & Şafak BİLGİÇ	163
CHAPTER 10 THE NOVEL MANUFACTURING TECHNIQUES OF THE AIRBORNE PARTS Tamer SARAÇYAKUPOĞLU.....	179
CHAPTER 11 TOPOLOGIES OF ISOLATED AND NON-ISOLATED DC-DC PWM CONVERTERS IN SOLAR PV APPLICATIONS Naim Suleyman TING & Yakup SAHIN	195
CHAPTER 12 FLEXIBLE PIEZORESISTIVE STRAIN SENSORS BASED ON CARBONACEOUS FILLER/THERMOPLASTIC ELASTOMER COMPOSITES Mukaddes Sevval CETIN & Ozan TOPRAKCI & Hatice Aylin KARAHAN TOPRAKCI.....	215
CHAPTER 13 MINI-REVIEW: SOME ARTICLES IN THE FIELD OF BIOTECHNOLOGY Sevcan Aytaç KORKMAZ & Sümeyye GÜVENDİ GÜNDOĞDU	237
CHAPTER 14 BIOTECHNOLOGY STUDIES FOR MINI-REVIEW Sevcan AYTAÇ KORKMAZ & Veysel ÇAKIR	251
CHAPTER 15 A HOUSE OF QUALITY APPLICATION BASED ON A DECISION SUPPORT SYSTEM FOR THE CREDIT CARD MONITORING UNIT OF A BANK Yeliz BURUK SAHIN & Ezgi AKTAR DEMİRTAS	263
CHAPTER 16 SOFTWARE DEVELOPMENT FOR MANIFOLD LINE HYDRAULIC DESIGN-I: METHODOLOGY AND DESIGN PRINCIPLES Gürol YILDIRIM.....	281

CHAPTER 17 SOFTWARE DEVELOPMENT FOR MANIFOLD LINE HYDRAULIC DESIGN-II: STEPS OF ALGORITHM, IMPLEMENTATION AND COMPUTER VISUALIZATION Gürol YILDIRIM	299
CHAPTER 18 SOFT SWITCHING CONCEPT IN PULSE WIDTH MODULATION POWER ELECTRONICS CONVERTERS Yakup SAHIN & Naim Suleyman TING	315
CHAPTER 19 CHANGE IN KEY MECHANICAL DESIGN QUANTITIES OF BI-2212 SUPERCONDUCTING SYSTEM WITH VARIOUS ANNEALING AMBIENT Asaf Tolga ULGEN & Gürcan YILDIRIM	331
CHAPTER 20 GEOGRAPHIC INFORMATION SYSTEM (GIS) AND MULTI CRITERIA DECISION ANALYSIS (MCDA) BASED APPLICATION FOR IDENTIFYING SUITABLE WIND TURBINE LOCATIONS IN KAHRAMANMARAS, TURKEY Ozan ARTUN	349
CHAPTER 21 DETERMINATION OF WELDING PARAMETERS OF POLYPROPYLENE SHEETS OF JOINED BY FRICTION STIR WELDING İhsan KÜÇÜKRENDECI.....	371
CHAPTER 22 FERROCHROMIUM SLAG UTILIZATION IN HOT MIX ASPHALT Altan YILMAZ	387
CHAPTER 23 A NOVEL RESEARCH ON DIFFERENT TYPES OF CELLULOSE USED IN COATING INDUSTRY Bilge ÇELİK & Nil ACARALI	403
CHAPTER 24 UP-TO-DATE APPROACHES TO WORKPLACE NUTRITION RELIGIONS Abdulkadir BİNGÖLBALİ & Dilek ÖZTAŞ & Ergün ERASLAN	419

CHAPTER 25 THE MODEL OF PREVENTING PSYCHOSOCIAL RISKS IN WORKPLACES WITH THE RISK ASSESSMENT METHOD A STUDY EXAMPLE FOR TURKEY MOBBING ISSUE Adnan KARABULUT & Dilek ÖZTAŞ & Ergün ERASLAN	439
CHAPTER 26 MEASUREMENT OF LOW FREQUENCY ELECTROMAGNETIC RADIATION LEVELS AT MUŞ CENTER POINTS AND PREDICTION BY USING TIME SERIES MODELS Zeydin PALA & İbrahim Halil ÜNLÜK & Çağrı ŞAHİN	455
CHAPTER 27 THE STATE AND IMPORTANCE OF FPGAs IN COMPUTATIONAL ELECTROMAGNETICS Ali Recai CELİK	477
CHAPTER 28 ON PERFORMANCE OF FLOWER POLLINATION ALGORITHM IN TRAINING ADAPTIVE-NETWORK-BASED FUZZY INFERENCE SYSTEM (ANFIS) Ceren BAŞTEMUR KAYA.....	489

Chapter 1

HOUSING DAMAGE ESTIMATOR FOR EARTHQUAKES: AN AUTOMATED MACHINE LEARNING APPLICATION FOR 2015, NEPAL EARTHQUAKE



Emre S. OZMEN¹

¹ Graduate School, Nisantasi Universitesi, Maslak, Istanbul 34398 Turkey, Tel: +90 212 210 1010, emre.ozmen@nisantasi.edu.tr

1. Gorkha (2015, Nepal) Earthquake

Gorkha earthquake (also known as the Nepal earthquake) with a magnitude of 7.8, nearly 10,000 people died and 20,000 injured on the 25th of April, 2015. It is reported as the worst natural disaster after the 1934 earthquake. Due to its center and occurrence (11:56am) time, as a blessing, it is recorded that both the capital of Nepal and outdoor rural workers were relatively less effected than it normally can. [1] However, it did not prevent hundreds of thousands of Nepalese from being homeless for months and outbreaks. It also triggered activities on Mouth Everest and avalanches were followed by. [2] The effects on rebuilding economy were calculated around \$5billion dollars.

2. Post-disaster Data Collection and Challenge

To scrutinize the facts about its damage on particular of housing, National Planning Commission Secretariat of Nepal worked with Kathmandu Living Labs and the Central Bureau of Statistics and conducted a survey. It ended with one of the largest post-disaster data collection ever attempted, consisting of valuable information on earthquake statistics, household conditions, and socio-economic-demographic impact. Commission declared that the data collected using mobile technology first targeted to identify beneficiaries eligible for government help, but it also served researcher, other governments.

On year 2020, DrivenData Inc. that is known with hosting data science challenges for intermediate-level practices, started a competition about 2015 Nepal earthquake's household damage modelling. [3] The dataset consists of around 300K rows (houses) with 39 labels and mostly refers to building characteristics. Data type is dominated by binary, where 30% refers to int and categorical. The target of data set as damage_grade and it is represented out of 3 per ordinal order, where 3 tied with serious

The remaining 38 labels are described as below:

- categorical: There are 7 columns in this data type
 - 3 of them are linked with foundational attributes, gradually differs from 3-to-6 categories
 - 3 of them are linked with floor/roof types that were used, gradually differs from 3-to-4 categories
 - 1 refers to ownership status with 4 categories
- int: There are 8 columns in this data type
 - 3 of them are linked with geospatial location, gradually from 1-to-3 refers to density
 - 4 of them are attributes with dimensions of the house, in respect to height, area as well as # of floors
 - 1 refers to household numbers

- binary: There are 25 columns in this data type
 - 7 of them are linked with engineering level
 - 7 of them are linked with material types; stone, mud and its derivatives, mortar and its derivatives, timber and its derivatives
 - 7 of them are linked with functional types; government, hospital, education, resorts etc

3. Performance Metrics

The fact that the target is based on an ordinal number, both categorization and regressions techniques can be applied. Although performance metrics may depend on model chosen, low error, high precision/recall approach will be applied as a holistic approach. F1 as a demonstration of both precision/recall can be interpreted as one the scores. F1 is defined as:

$$F1 = \frac{2 \times Pre \times Rec}{Pre + Rec}, \text{ where } Pre = Precision, Rec = Recall$$

$$Pre = \frac{TP}{TP + FP}, Rec = \frac{TP}{TP + FN}$$

TP = True Positive, FP = False Positive, FN = False Negative

4. Automated Machine Learning Methodology Exploration

Machine learning is a taxonomy created to replace the existing taxonomy with predictions. [4] However, there is one major distinction between them. The former is more event based, where the latter is more rule based. In other words, to make some predictions you either set rules or train your model with what happened without rules. [5, 6] Knowing that the polarization between regression and classification is not always needed as mentioned earlier, the possibility of discovering a huge data (like we have here, 300K houses with 40 columns) with no bindings excites practitioners. However, practicality perspective setting boundaries so wide might jeopardize study in the sake of necessity of dealing with more than 10 different models from regression and classification domains. [7] From this regard, automated machine learning (AML) concept can be utilized to both have the advantages of omni-model environment and test AML's performance.

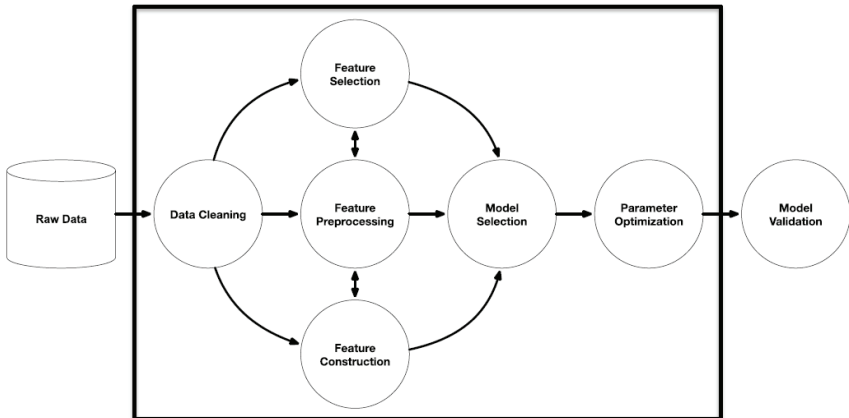


Figure 1: Tree-based pipeline (Olson, 2016)

A typical machine learning scientist's list of tasks vary from data gathering to visualization, usually requires significant time for data cleansing, feature processing per construction and selection, model selection with more than 10 options maybe 20 with its derivatives, parameter optimizations, model validation and maybe even production. [8] Most major companies created different roles for this group of iterative tasks such as including data curator, data steward, data engineer, data architect and data scientist. If this is not the case, AML can help one individual with many hats. In the end, AML's commitment is to manage all except raw data and model validation. To be specific:

- Works with many models including Boost, Naïve ayes, Decision Tree, Random Forest, Linear Models, Gradient Descent, Logistic Regression, Multinomials, Support Vector
- Adjusts default parameters in a way to find the best fit
- Finds best algorithms
- Optimize the entire workflow, multi-arm bandit

There are many attempts in respect to AML, in both open source and commercial arena, to mention few for the former:

- auto-Weka is a Java library, built on Weka
- auto-sklearn is a Python library, optimizes per Bayesian
- TPOT works with Python
- auto-keras is a Python library, has very powerful classification/regression models for not only structured data, but also images and texts
- H20 AutoML is developed with Java, works with Python, R and Scala

5. Application with H2O AutoML

Amongst all, H2O AutoML has distinctive features per three aspects, it is explicit in terms of model names (and flexible in terms of inclusions or exclusions), gives confusion matrix if it applies and proposes important factors. [9] To be more specific, H2O AutoML requires only two data and two stopping parameters. On the other hand, it handles a total of 27 parameters to burst the control on user hands. [10]

First H2O is initiated.

```
import h2o
from h2o.automl import H2OAutoML
h2o.init()

Checking whether there is an H2O instance running
at http://localhost:54321 ..... not found.
Attempting to start a local H2O server...
; Java HotSpot(TM) 64-Bit Server VM (build
25.261-b12, mixed mode)
Starting server from
C:\Users\emreo\miniconda3\lib\site-
packages\h2o\backend\bin\h2o.jar
Ice root:
C:\Users\emreo\AppData\Local\Temp\tmpnjlg22vp
JVM stdout:
C:\Users\emreo\AppData\Local\Temp\tmpnjlg22vp\h2o
_emreo_started_from_python.out
JVM stderr:
C:\Users\emreo\AppData\Local\Temp\tmpnjlg22vp\h2o
_emreo_started_from_python.err
Server is running at http://127.0.0.1:54321
Connecting to H2O server at
http://127.0.0.1:54321 ... successful.
```

```
H2O_cluster_uptime: 06 secs
```

```
H2O_cluster_timezone: America/New_York
```

```
H2O_data_parsing_timezone: UTC
```

H2O_cluster_version:	3.30.0.6
H2O_cluster_version_age:	3 months and 3 days
H2O_cluster_name:	H2O_from_python_emreo_oxt8zm
H2O_cluster_total_nodes:	1
H2O_cluster_free_memory:	3.521 Gb
H2O_cluster_total_cores:	8
H2O_cluster_allowed_cores:	8
H2O_cluster_status:	accepting new members, healthy
H2O_connection_url:	http://127.0.0.1:54321
H2O_connection_proxy:	{"http": null, "https": null}
H2O_internal_security:	False
H2O_API_Extensions:	Amazon S3, Algos, AutoML, Core V3, TargetEncoder, Core V4
Python_version:	3.7.7 final

Data can be automatically split into training and test dataset, however here, data already came in a split way.

In [1]:

```

train =
h2o.import_file(r"C:\Users\YourUsername\Desktop\t
rain_quake.csv")
test =
h2o.import_file(r"C:\Users\YourUsername\Desktop\t
est_quake.csv")

Parse progress: | ████████████████████████████████████████████████████████████ |
100%
Parse progress: | ████████████████████████████████████████████████████████████ |
100%
```

Features and target were identified.

model_id	mean_per_class_error	logloss	rmse	mse
DRF_1_AutoML_20201003_232545	0.414617	1.14618	0.480915	0.231279

Out[5]:

In [6]:

aml.leader

Model Details

=====

H2ORandomForestEstimator : Distributed Random Forest

Model Key: DRF_1_AutoML_20201003_232545

Model Summary:

	number_of_trees	number_of_internal_nodes	model_size_in_bytes	min_depth	max_depth	mean_depth	min_leaf_size	max_leaf_size	mean_leaf_size
0	2.0	6.0	849631.0	20.0	20.0	20.0	855.0	142.0	112.0

ModelMetricsMultinomial: drf

** Reported on train data. **

MSE: 0.2616145729335327

RMSE: 0.511482720073252

LogLoss: 3.1327581170891725

Mean Per-Class Error: 0.43795864384785194

Confusion Matrix: Row labels: Actual class;
Column labels: Predicted class

	1	2	3	Error	Rate
0	5831.0	8015.0	1248.0	0.613688	9,263 / 15,094
1	4340.0	70191.0	15184.0	0.217622	19,524 / 89,715
2	668.0	24631.0	27127.0	0.482566	25,299 / 52,426
3	10839.0	102837.0	43559.0	0.343982	54,086 / 157,235

Top-3 Hit Ratios:

	k	hit_ratio
0	1	0.656018
1	2	0.933539
2	3	1.000000

Up above is the first branch, where below shows the second branch. Accuracy, aka F1 is almost (from 0.66 to) 0.7 after 5 tours of cross-validations, which is closer to winning score.

MSE: 0.23127907948492804

RMSE: 0.480914836000022

LogLoss: 1.146178551822972

Confusion Matrix: Row labels: Actual class;
Column labels: Predicted class

	1	2	3	Error	Rate
0	10226.0	14145.0	753.0	0.592979	14,898 / 25,124
1	5747.0	124045.0	18467.0	0.163322	24,214 / 148,259
2	708.0	41815.0	44695.0	0.487548	42,523 / 87,218
3	16681.0	180005.0	63915.0	0.313257	81,635 / 260,601

Top-3 Hit Ratios:

k	hit_ratio
0	1 0.686743
1	2 0.957026
2	3 1.000000

Cross-Validation Metrics Summary:

		mean	Sd	cv_1	cv_2	cv_3	cv_4	cv_5
		n		_vali	_vali	_vali	_vali	_vali
0	accuracy	0.68 674 3	0.004 98712	0.67 7864	0.68 9428	0.68 8142	0.89 121	0.68 915
1	err	0.31 325 6	0.004 98712	0.32 2135	0.31 0571	0.31 1857	0.37 875	0.31 084

		mean	Sd	cv_1 _vali	cv_2 _vali	cv_3 _vali	cv_4 _vali	cv_5 _vali
2	err_count	163 27.0	260.0 721	1679 0.0	1618 7.0	1625 4.0	1620 3.0	1620 1.0
3	logloss	1.14 617 7	0.207 669	1.51 5895	1.02 6942	1.04 5588	1.02 286	1.06 017
4	max_per_class_error	0.59 301 8	0.008 7694	0.60 8197	0.58 9768	0.58 5993	0.88 855	0.59 234
5	mean_per_class_accuracy	0.58 536 7	0.005 9955	0.57 4786	0.58 7278	0.58 7304	0.58 965	0.58 781
6	mean_per_class_error	0.41 463 3	0.005 9946	0.42 5213 9	0.41 2215	0.41 2963	0.41 045	0.41 218
7	mse	0.23 127 6	0.003 8536	0.23 8031 1	0.22 8675	0.22 9034	0.23 067	0.22 997
8	r2	0.38 201 7	0.012 3747	0.36 0085	0.38 8858	0.38 7967	0.38 8377	0.38 515
9	rmse	0.48 001 6	0.003 9866	0.48 7843	0.47 8223	0.47 8603	0.48 0168	0.47 956

Scoring History:

	times tamp	dur atio n	number_ of_trees	trainin g_rmse	training _logloss	training_classi fication_error
0	2020- 10-03 23:26 :23	37.8 93 sec	0.0	NaN	NaN	NaN
1	2020- 10-03 23:26 :28	42.2 62 sec	2.0	0.5114 83	3.13275 8	0.343982

Variable importance would not significantly change from one model to another. Per top factors, geospatial location looks like dominating other. Floor type derivatives, age of the building, foundation type and area percentage are also significant attributes.

Variable Importances:

	variable	relative_importa nce	scaled_import ance	percentage
0	geo_level_1_id	17334.062500	1.000000	0.220961
1	geo_level_2_id	7466.929688	0.430766	0.095183
2	geo_level_3_id	5873.937500	0.338867	0.074876
3	building_id	4998.819336	0.288381	0.063721
4	other_floor_type	4635.594238	0.267427	0.059091

	variable	relative_importance	scaled_importance	percentage
5	age	4103.796387	0.236748	0.052312
6	foundation_type	4081.254883	0.235447	0.052025
7	area_percentage	3984.306885	0.229854	0.050789
8	ground_floor_type	3447.547852	0.198889	0.043947
9	height_percentage	3026.006592	0.174570	0.038573
10	count_floors_pre_eq	1828.075317	0.105461	0.023303
11	has_superstructure_cement_mortar_brick	1784.335083	0.102938	0.022745
12	position	1531.578491	0.088357	0.019523
13	roof_type	1530.040283	0.088268	0.019504
14	has_superstructure_mud_mortar_stone	1443.995361	0.083304	0.018407
15	count_families	1268.828247	0.073199	0.016174
16	has_superstructure_timber	1258.311279	0.072592	0.016040
17	land_surface_condition	1230.474854	0.070986	0.015685
18	plan_configuration	966.522949	0.055759	0.012320

	variable	relative_importance	scaled_importance	percentage
19	has_superstructure_ba mboo	790.166809	0.045585	0.010072

```
See the whole table with table.as_data_frame()
```

```
Out[6]:
```

Due to decision tree nature, we are producing our prediction based on probabilities, where the highest determines the damage types. Here is shown a demonstration with head of the data.

```
In [7]:
```

```
preds = aml.leader.predict(test)  
preds
```

```
drf prediction progress: |██████████████████████████████████████████|  
100%
```

predict	p1	p2	p3
3	0	0.250845	0.749155
2	0.0039452	0.727689	0.268366
2	0.0245312	0.847322	0.128147
1	0.666667	0.333333	0
3	0.00146907	0.17418	0.824351
2	0.141407	0.581733	0.27686
1	0.576923	0.423077	0
3	0.0212464	0.315511	0.663242
2	0.0180474	0.565369	0.416583
2	0	0.921306	0.0786937

5.2 All Models (Classification and Regression)

Replication for larger set of models.

In [8]:

```
train          =
h2o.import_file(r"C:\Users\YourUsername\Desktop\t
rain_quake.csv")
test          =
h2o.import_file(r"C:\Users\YourUsername\Desktop\t
est_quake.csv")
```

```
Parse   progress: |██████████████████████████████████████████|
100%
```

```
Parse   progress: |██████████████████████████████████████████|
100%
```

In [9]:

left intentionally blank

```
x = train.columns
y = "damage_grade"
x.remove(y)
```

This time `max_models` is selected with 20 models, if applies.

In [10]:

```
aml = H2OAutoML(max_models=20, seed=1)
aml.train(x=x, y=y, training_frame=train)
```

```
AutoML progress: |███
22:19:05.835: AutoML: XGBoost is not available;
skipping it.
```

```
██████████████████████████████████████████████ Failed polling AutoML progress
log: [WinError 32] The process cannot access the
file because it is being used by another process:
'C:\Users\emreo\AppData\Local\Temp\tmpwve5u
jam.csv'
```

```
██████████████████████████████████████████████ Failed polling AutoML progress
log: [WinError 32] The process cannot access the
file because it is being used by another process:
```



```
'C:\\Users\\emreo\\AppData\\Local\\Temp\\tmp9gfk0
t7e.csv'
```

```
Failed polling AutoML progress log: [WinError
32] The process cannot access the file because it
is being used by another process:
'C:\\Users\\emreo\\AppData\\Local\\Temp\\tmpkukga
xmc.csv'
```

```
Failed polling AutoML progress log: [WinError
32] The process cannot access the file because it
is being used by another process:
'C:\\Users\\emreo\\AppData\\Local\\Temp\\tmppmq_s
o3d.csv'
```

```
| 100%
```

5.3 Winning Model

Leaderboard.head brings us the top ten, Stacked Ensemble with regression leads the run, our DRF makes only a number 6 here.

```
In [11]:
```

```
aml.leaderboard.head()
```

model_id	mean_residual_deviance	rmse	mse	mae	rmsle
StackedEnsemble_AllModels_AutoML_20200729_22	0.200279	0.44752	0.20027	0.3507	0.14587
StackedEnsemble_BestOfFamily_AutoML_20200729	0.200869	0.44818	0.20086	0.3517	0.14610
GBM_grid_1_AutoML_20200729_221905_model_4	0.201596	0.44899	0.20159	0.3550	0.14655
GBM_5_AutoML_20200729_221905	0.206886	0.45484	0.20688	0.3612	0.14858
GBM_grid_1_AutoML_20200729_221905_model_2	0.208152	0.45623	0.20815	0.3593	0.14891
DRF_1_AutoML_20200729_221905	0.209826	0.45806	0.20982	0.3649	0.14954
GBM_4_AutoML_20200729_221905	0.210362	0.45865	0.21036	0.3672	0.14962
GBM_3_AutoML_20200729_221905	0.214197	0.46281	0.21419	0.3724	0.15103

model_id	mean_residual_deviance	rmse	mse	mae	rmsle
XRT_1_AutoML_20200729_221905	0.214246	0.46286	0.21424	0.3760	0.15080
GBM_2_AutoML_20200729_221905	0.217049	0.465885	0.217049	0.37613	0.152045

Out[11]:

Unlike probabilities of DRF, prediction makes float numbers here. To be able to submit, they were rounded to up.

In [12]:

```
pred = aml.predict(test)
pred
```

```
stackensemble prediction progress: | ██████████
100%
```

predict

2.80101

2.23104

2.16015

1.26562

2.80709

2.07994

1.33965

2.91986

2.16437

2.10983

Out[12]:

7. References

- [1] Mahr, K., Adkin, R. (2015). Fresh earthquake kills scores in Nepal and India. Retrieved from <https://www.reuters.com/article/us-quake-nepal/fresh-earthquake-kills-scores-in-nepal-and-india-idUSKBN0NX0JO20150512>
- [2] Sharma, G. (2020). Five years after Nepal's quake, lockdown stops reconstruction. Retrieved from <https://www.reuters.com/article/us-nepal-quake-anniversary-idUSKCN2270LM>
- [3] Bull, P. (2014). Introducing Drivendata. <https://www.drivendata.co/blog/introducing-drivendata/>
- [4] Gijssbers, P., LeDell, E., Thomas, J., Poirier, S., Bischl, B., & Vanschoren, J. (2019). An open source AutoML benchmark. arXiv preprint arXiv:1907.00909.
- [5] Guyon, I., Sun-Hosoya, L., Boullé, M., Escalante, H. J., Escalera, S., Liu, Z., ... & Statnikov, A. (2019). Analysis of the AutoML Challenge Series. *Automated Machine Learning*, 177.
- [6] Saikia, T., Marrakchi, Y., Zela, A., Hutter, F., & Brox, T. (2019). Autodispnet: Improving disparity estimation with automl. In *Proceedings of the IEEE International Conference on Computer Vision* (pp. 1812-1823).
- [7] Hutter, F., Kotthoff, L., & Vanschoren, J. (2019). *Automated machine learning: methods, systems, challenges* (p. 219). Springer Nature.
- [8] Olson, R. S., Bartley, N., Urbanowicz, R. J., & Moore, J. H. (2016, July). Evaluation of a tree-based pipeline optimization tool for automating data science. In *Proceedings of the Genetic and Evolutionary Computation Conference 2016* (pp. 485-492).
- [9] H2O.ai, H2O AutoML. (2017). Retrieved from <http://docs.h2o.ai/h2o/latest-stable/h2o-docs/automl.html>. H2O version 3.30.0.1.
- [10] LeDell, E. (2018). The different flavors of AutoML. Retrieved from <https://www.h2o.ai/blog/the-different-flavors-of-automl/>

Chapter 2

INNOVATIVE TECHNIQUES IN CLOTHES PRODUCTION: COSTUME (TEKMET) PRODUCED USING TEXTILE AND METAL MATERIALS



Gülhan PINARLIK¹

Gökhan YILDIRIM²

1 Usak University, Vocational School of Technical Sciences, Textile, Clothing, Footwear and Leather, Usak-Turkey, gulhan.pinarlik@usak.edu.tr

2 Usak University, Vocational School of Technical Sciences, Department of Mechanical and Metal Technologies, Usak-Turkey, gokhan.yildirim@usak.edu.tr

1. INTRODUCTION

It will not be possible for the textile industry to keep up with the rapidly changing and developing fashion trends, unless it gets a bigger share from the market with innovative products, integrates with different disciplines in design and makes production in the light of creative ideas using different materials. Other than textile materials, paper, ceramic, metal, natural objects such as leaves, branches, waste etc. can be used as materials in design [1].

Before the 20th century, any change in model techniques and/or style, was considered as an innovation. As of the 20th century, the search for an artistic expression, regarding new materials and new cloth production methods, has begun [2].

As a completely new technique, 3D printing makes its appearance in textile sector. Even though 3D printers are first used in 1984 by Chulk Hull of 3D Systems, it becomes popular in the textile applications after 2010 [3]. It is still not widely used in the industry but it is especially important for independent designers to easily turn their ideas into products [4][5]. It eliminates complicated production processes and enables the design to be produced in only one move. With the use of 3D printers in textile design, clothes can be produced as a whole, as shown in Figure 1.



Figure 1 All garment produced using a 3D printer [3].

In addition, surfaces can be obtained with 3D printers, as seen in Figure 2. These will be presented as an alternative to woven or knitted surfaces that form the basis of the textile surface in the future [4].

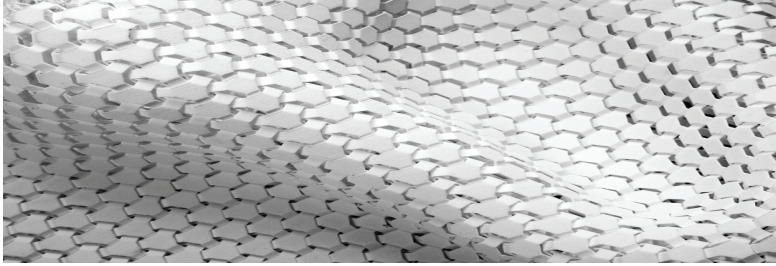


Figure 2 Fabric produced with a 3D printer [5].

Innovation turns creative ideas into industrial products. Innovation can also be defined as turning designs into marketable high value-added products. The design made during the process, transforms into a new work idea and holds great importance for maintaining continuity of businesses.

Using unusual materials and innovative methods rather than conventional ones creates a new insight in textile design. Only innovative and creative designs which combines various disciplines like art, engineering, science can find their ways into today's industry.

2. MATERIAL AND METHOD

2.1. Materials

In this study, felt was chosen as the main material of the garment, as the costume was inspired by Mevlana and his clothes. The main material is preferred since it keeps an upright position and gives an “aba” appearance when worn. In the designed costume, lining was sewn in order to prevent the fluff falling from felt sticking to the clothes underneath and also to prevent the embroidery lines from being seen. Lozenge patterned tulle was also used in the costume decorations. It is aimed to give movement to the costume and appeal to the eyes. Silver color was chosen for tulle to match the chain accessories and embroidery yarn used. Additionally, the edge details were cut into triangles as a transition to the metal accessories. Properties of the main material, lining material and tulle used in the designed costume are given in Table 1 below.

Table 1 Properties of main material, lining material and tulle

Material Type	Size (m)	Weight (gr / m ²)	Color
Synthetic Felt	2 x 1	640	Black

Lining (Shirting)	2 x 1	125	Black
Decorative Diamond Patterned Tulle	1x 0,5	65	Silver

Instead of conventional sewing method, bolts and nuts, which are used to fasten machine parts, are used as a joining method in the designed costume. The purpose of using a different joining technique in the designed costume is the increasing interest to new viewpoints in the textile sector and increasing share of innovative design companies. Dressing is one of our primary needs, however, not all textile products are necessities so that people look for a particular reason to buy a textile product. New techniques, new styles, new materials may be appealing to the customers. As the demand for conventionally produced textile materials decreases, designers offer more innovative designs to increase their sales. Unconventional use of bolts and nuts in this design serves for boosting demand in the market. Properties of bolts and nuts used in the costume are given in Table 2 below.

Table 2 Properties of bolts and nuts used in joining

Material Type	Feature	Quantity	Color
M6 Bolt	Countersunk Head	22	Silver
M6 Nut	Cap (Acone)	22	Silver

Metal accessories are mainly used in the costume to attract attention. Metal appearance is preferred in all accessories. The accessories and their properties are given in Table 3 below.

Table 3 Accessories used and their features.

Accessory					
Name	Material	Weight	Size	Piece	Color
Rosary Grain	Metal Wire	0,327 gr	Ø 6 mm	23 Pieces	Silver
Bead	Plastic	0,016 gr	Ø 3 mm	139 Pieces	Silver
Bead Nail	Metal Wire	0,149 gr	30 mm'lik	23 Pieces	Silver
Embroidery Yarn	Metallic Yarn	Nm 3,5/10	---	---	Silver
Needlepoint Yarn	Polyester	Nm 10/3	---	---	Gray

Sewing Yarn	Polyester	Ne 42/2	---	---	Black
Chain	Metal	0,179 gr/1 pod	Wire thickness:1.2 mm	271 bakla	Silver
5 cm Triangle	Steel	~20 gr	Δ Equilateral 50 mm	5 Adet	Black
5 cm Triangle	Aluminum	~7 gr	Δ Equilateral 50 mm	7 Adet	Silver
7 cm Triangle	Steel	~40 gr	Δ Equilateral 70 mm	8 Adet	Black
7 cm Triangle	Aluminum	~13 gr	Δ Equilateral 70 mm	5 Adet	Silver

2.2. Method

In the design process, a sketch is drawn on a silhouette at first. Then, the technical drawings of the costume are prepared in three parts according to the male mannequin's measurements and transferred to a model. The accessories are marked on the model regarding the drawings. After determining the accessories, the embroideries are placed on the model to make it flamboyant. The picture of the designed costume drawn by hand on the silhouette is given in Figure 3 below and the dimensions of the costume are given in Figure 4.



Figure 3 Dress-up picture of the costume drawn by hand on the silhouette.

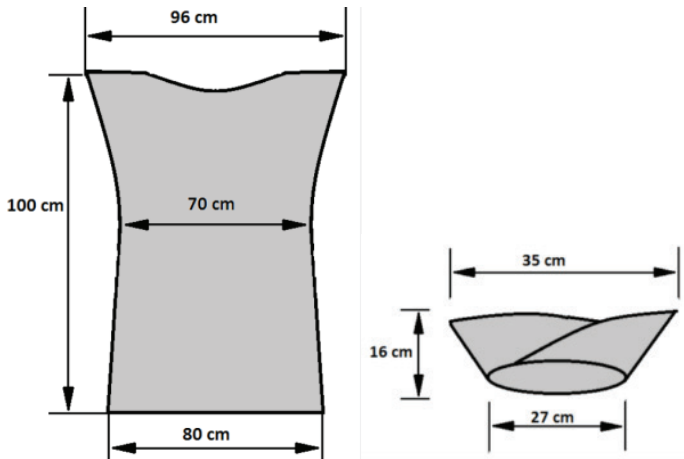


Figure 4 Dimensions of the designed costume.

The felt was cut according to the designed model. Then, the decorative diamond-patterned tulle fabric was applied to the felt. While being applied, the edges of the decorative diamond patterned tulle fabric are cut in triangles to form a transition between fabric and metal accessories. Triangular pattern is used on the left shoulder and also on the back of the shoulder as shown in Figure 5.



Figure 5 Applique details of decorative diamond-patterned tulle fabric

As shown in Figure 6, six chains are mounted on the shoulders of the right front part and a bead nail is attached to each of the chain ends. A zigzag pattern is applied to the mounted section by using silver embroidery yarn and chain embroidery technique. The lower corner of the triangle, where the zigzag pattern meets the chain, and also some part of the chains are garnished with silver-colored plastic beads. An asymmetrical appearance is provided by choosing different lengths of the chains.

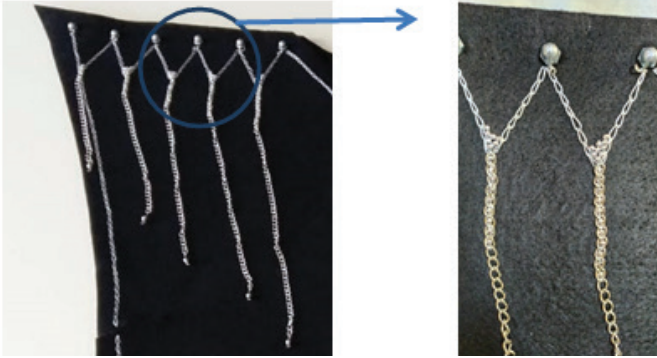


Figure 6 Shoulder details of the right front part

Since the front part of the costume will not be buttoned up, it is decorated with chains instead of using buttons and buttonholes as shown in Figure 7. Three rosary beads were mounted on each end of the chains with the help of bead nails. This detail is used on the right and left front of the costume.



Figure 7 Details of the front part

The main decoration in the design is chosen as “S” twist as it is the main pattern in metal ornamental blacksmithing. Figure 8 shows the “S” twist used in metal ornamental blacksmithing.

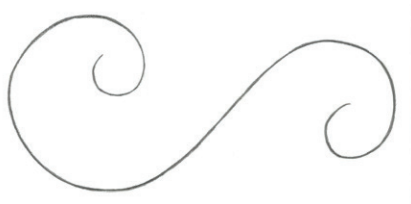


Figure 8 “S” twist used in metal ornamental blacksmithing

Existing embroidery patterns are tried; however, the embroideries are observed to be unpretentious and weak due to thick fabric (felt) use. For this purpose, “Chain” embroidery was developed and a new embroidery pattern was created. This embroidery is thicker and bulkier than chain embroidery. The new embroidery is named as “Circular Chain”. The stages of the newly designed “Circular Chain” embroidery are shown in Figure 9 below. The stages have shown in Figure 9 (a), (b), (c) and (d) are the known chain embroidery stages. With the yarn shown in blue in Figure 9 (e), S turns are made around the chain embroidery. In Figure 9 (f), S turns are given around the chain embroidery with the yarn seen in yellow in the other direction and the embroidery has taken its final form. Figure 9 (g) shows the final version of the embroidery, which is embroidered with silver embroidery yarn on the felt.

S twist pattern is embroidered with this new technique on the right and left front parts. In the back of the cloth, a new pattern is formed by rotating S twist pattern around the edge of S. The new pattern is two horizontal S twists and it is embroidered with circular chain technique. The rotation of these S twists is inspired by Mevlana’s rotation during the Semâ Ceremony.

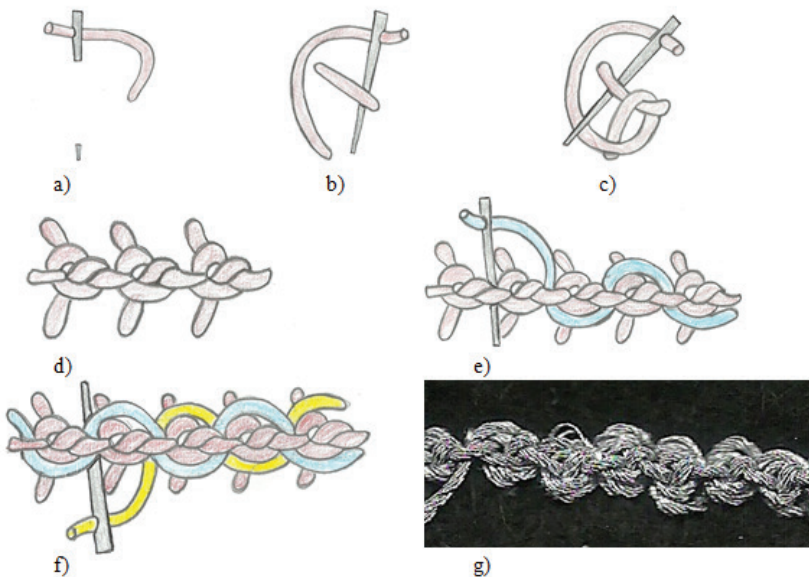


Figure 9 Stages of the newly designed “Circular Chain” embroidery

Also, the edges of the costume are embroidered with a plain chain stitch. The edges of the triangular metal accessories used in the skirts of the costume are contoured by using silver embroidery yarn using the handle embroidery technique.

Today, CNC machinery is used to cut and shapes materials such as sheet metal, iron, steel, aluminum, wood, plexiglass and so on. As accessories, aluminum and steel parts are shaped in the form of equilateral triangles with 7 and 5 cm sides by using CNC, a computer controlled production tool. After shaped, the triangular accessories are drilled on the corners in the dimensions given in Figure 10. Then, they are placed on the costume by using plastic beads and gray yarn.

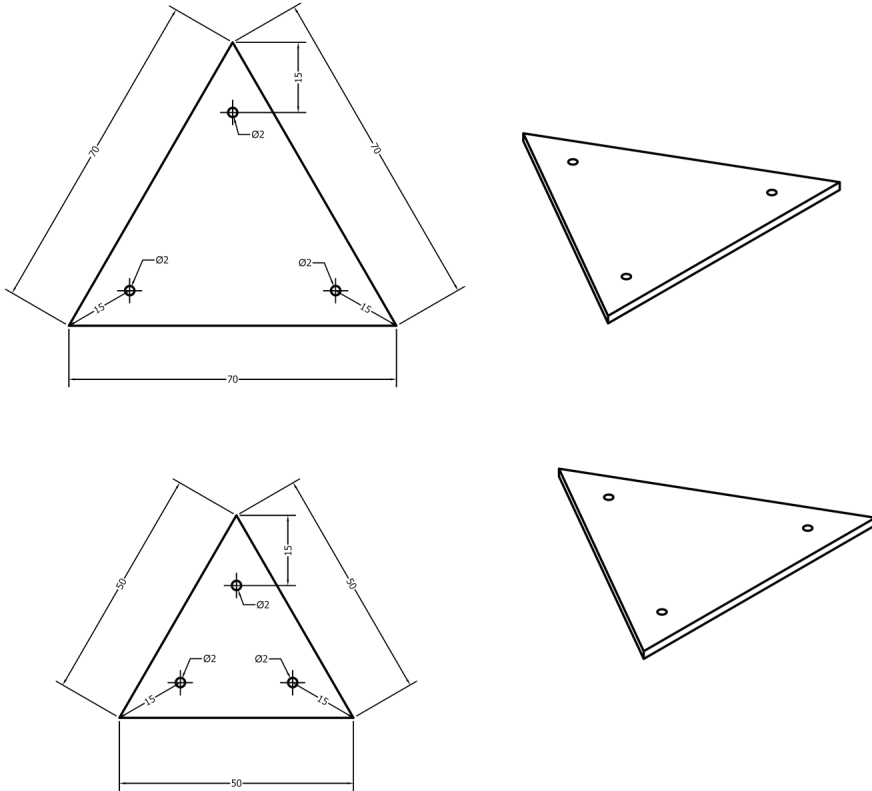


Figure 10 Autodesk Inverter drawings and dimensions of triangles used as accessories.

Plastic beads are used to prevent metals from cutting the yarn and also to give a rivet-like appearance.

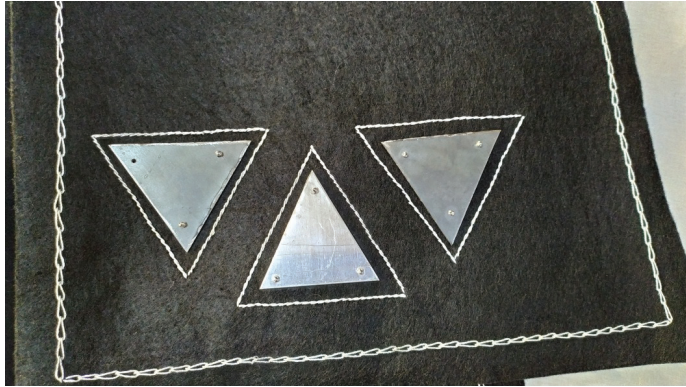


Figure 11 The image of the triangles used as accessories on the garment.

After the processing and lining process of the designed costume was completed, a total of 22 pieces of silver-colored M6 countersunk bolts are fastened with silver-colored M6 cap (acorn) nuts. Six are used on each of the shoulders and five are used on the sides. No stitches are used to join the front and back parts of the garment. Instead, bolts and nuts used in assembling machine parts were chosen (Figure 12). A countersunk bolt with countersunk was chosen in order to level the bolt surface and fabric to ensure that this connection does not disturb the body of the wearer. In order to complete the connection and also to draw attention on the costume, a cap nut is preferred. Figure 13 shows silver-colored M6 countersunk bolts and silver-colored M6 cap (acorn) nuts.

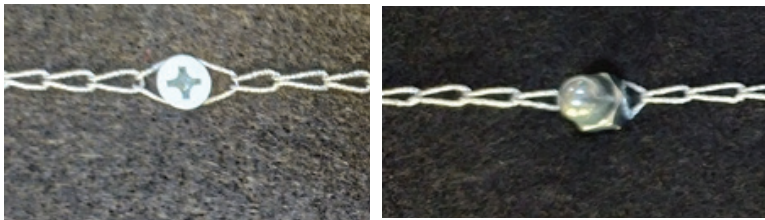


Figure 12: Assembling the Costume with Bolts and Nuts



Figure 13: Silver-Colored M6 Countersunk Bolts and Silver-Colored M6 Cap (Acorn) Nuts

The headdress, shown in Figure 13, is designed to be compatible with the costume as an accessory. The headdress consists of two parts. It is made by using the remaining materials from the costume. The headboard is decorated with chains and embroidery. A lining is sewn inside so that it is easy to wear and does not disturb the head.



Figure 13 Headgear

RESULTS

The results of the study are as follows;

3. The picture of the designed and produced costume with the headdress is shown in Figure 14.



Figure 14 Designed, produced costume and headdress

- A costume is designed by using textile and metal materials together.
- The bolt and nut connection, which is used in the assembly of machine parts, is used as a new technique in the assembly of textile products successfully. It has been proven that a method other than sewing, which is essential in textile products, can be used.
- The “S” twist motif used in metals is successfully used as a pattern in costume design.
 - The pattern obtained by rotating the “S” twist on the back details is inspired by the rotation of the whirling dervishes and the triangular metal details added to the pattern also represent them.
 - The “Chain” embroidery design is improved and a new embroidery pattern is created since the former is unpretentious and weak due to thick fabric (felt). The new embroidery is thicker and bulkier than chain embroidery. It is named as “Circular Chain”.
- The weight of the costume is increased due to the use of felt and metal accessories. It is necessary to reduce the weight with lighter fabrics and light metal accessories.
- The “S” twists embroidered on the front piece are inspired from the whirling dervishes’ stance. However, the posture of his hands is not represented in embroidery. It can be modified so that it poses more similarity and becomes more interesting.
- An alternative is created to the design, embroidery, joining method and material because the interest to textile products may decrease over time and new models should be introduced periodically.

REFERENCES

- MARTINEZ, E. H. V., Moda Tasarımında Sanatsal İfade Önerisi Olarak Alternatif Malzemeler: Seramik Elbiseler, Sanat ve Tasarım Dergisi, Anadolu Üniversitesi, Sf:162-181
- GÖNÜL İ. S., BAĞRIŞEN, Y., (2016), 20.yy.dan Günümüze Giyim Tasarımında Deneysel Yaklaşımlar, İdil Sanat ve Dil Dergisi, Cilt 6/2016, Sayı 28,Sf:91-105 ISSN:2146-9903
- YILDIRAN, M., ZAIMOĞLU, Ö., (2017), Moda Tasarımında İnovatif Bir Yöntem: Üç Boyutlu Yazıcılar İle Giysi Tasarımı Uygulamaları, İdil Sanat ve Dil Dergisi, cilt:6/2017, Sayı: 38, Sf:2949-2976, ISSN:2146-9903
- DÜZGÜN, D.E., ÇETİNKAYA, K., (2019), Moda Alanında 3 Boyutlu Baskı Teknolojileri Kullanımı, International Journal of 3D Printing Technologies and Digital Industry, Cilt:3 Sayı:1 Volume:3 Number:1 Pages 19 - 31 ISSN:2602-3350
- Yıldırım, M., (2016), Moda Giyim Sektöründe Üç Boyutlu Yazıcılarla Tasarım ve Üretim, Süleyman Demirel Üniversitesi Güzel Sanatlar Fakültesi Hakemli Dergisi ART-E Mayıs-Haziran'16 Sayı:17 ISSN 1308-2698, Sf: 155-172
<http://fashiontribes.typepad.com/fashion/2015/04/future-of-fashion-3d-printed-dress-kinematics-cloth.html>, Erişim Tarihi: 20.06.2018
- RIFKIN, J., (2012). The Third Industrial Revolution: How the İnternet, Green Electricity, and 3-D Printing are Ushering in a Sustainable Era Of Distributed Capitalism, World Financial Review, 1.
<https://www.sculpteo.com/blog/2016/01/27/making-wearable-3d-printed-clothes/>, Erişim Tarihi: 20.06.2018
- Erbıyıklı, N ., (2011), Tekstil ve Moda Tasarımı Açısından Sanat ve Bilim, Akdeniz Sanat , 4 (7) , 0-0 , Retrieved from <https://dergipark.org.tr/en/pub/akdenizsanat/issue/27654/291449>

Chapter 3

DETERMINATION OF THE IDEAL

FLOW RATE IN DRYING OF TABLE SALT



Sultan KEPÇEOĞLU¹

Aytaç MORALAR²

Soner ÇELEN³

1 Sultan KEPÇEOĞLU, ASOS Proses Makina San. ve Tic. A.Ş

2 Aytaç MORALAR, Tekirdağ Namık Kemal University

3 Soner ÇELEN, Tekirdağ Namık Kemal University

1. INTRODUCTION

Salt, which has been used as a nutrient since ancient times, is one of the most important inputs of the chemical industry in our age. Salt is expressed with the symbol NaCl [1]. The salt mine exists in two forms in the natural environment: dissolved salts and solid salts. Dissolved salts are found in the form of sea, lake, and groundwater. Solid salts can be found in underground salt mines as rock salt [2].

The method of keeping the foods by drying is the oldest keeping method the mankind have learned from nature and have been using since the ancient history. Since the amount of water in the food is reduced by the drying process, the possibility of enzymatic and microbiological deterioration is considerably reduced [3]. Today, salt is used extensively, especially in food, agriculture, animal husbandry, medicine, traffic, and industry, directly or indirectly [2, 4]. Salt is one of the most popular spices in the food industry. It is usually produced by extracting from seawater, purifying and drying. In one of the production technologies, crystal sea salt is dried, pulverized, packaged, and distributed to the market.

While the salt is pure, it consists of approximately 40% Sodium and 60% Chlorine. Its hardness is 25 and its specific weight varies between 2.1-235 g / cm³. Its melting point is 800.8 ° C and its boiling point is 1412 ° C. As it is produced from nature, its color is gray, yellow, red, even blue and green. However, while in pure form, salt is colorless [1].

In Turkey, crude salt production from seawater, from the lake, Rock (Underground Mining), and Resources (Underground) in four different ways, including the saltwater is produced. 63% of the lake's salt production in Turkey, 30% of the sea, rock, 6%, and 1% are realized as a source of salt. Salt consumption is 67% in the chemical industry, 5% in the food industry and animal husbandry, 15% in the snow and ice struggle for highways, 3% in table salt, and 10% in other industrial uses. The production and consumption of salt, which is intertwined with the human life process, gains importance in this respect [5].

Drying is a fundamental process of immense commercial importance in all industrial applications ranging from food, agriculture, mining, and even manufacturing sectors [6].

Fluidized bed drying has a special position. It is among the modern drying methods due to its unique advantages. These advantages include ease of use and maintenance, good mixing between solids, intense heat, and mass transfer gas phases [7]. The gas velocity in the fluidized bed must be adjusted very carefully. The contact between the powdered or granular dried material and the fluidizing gas is very good. Therefore, heat transfer between drying air and particles is also effective. With this drying system,

it is possible to dry the materials without any drawback in large temperature differences. The most important advantage of this system, where automatic loading and unloading is possible, is the completion of the drying process in a short time. [8].

In this study, it is aimed to determine the appropriate air velocity in the drying of salt in a fluid bed dryer.

2. MATERIAL AND METHOD

The salt (NaCl) used in this study is the lake salt taken from İzmir Salt Lake and it was obtained from a local company. The salt that is subjected to drying in the experiments is not the raw salt, it is the salt brought to the drying conditions through certain processes (pretreatments, evaporation, grinding, washing, centrifugation etc.) in the specified enterprise. Salt is generally of different grain sizes and is also available in the form of particles. The salt was filled with 100 g glass containers from the facility and closed so as not to absorb the humidity of the ambient air, it was moved to the location of the experiment set and kept in these containers until the experiments were carried out (Figure 1).

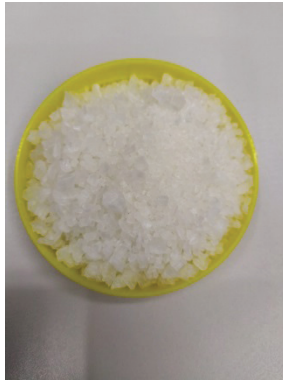


Figure 1. *Salt used in the experiments*

The product is placed in the desired bed height of the fluid bed dryer used in drying trials and shown in Figure 2. A cork type sieve is placed between the sample container and the hot air supply line. The desired airspeed (Fan) and drying air temperature (Heater) value are entered from the control panel according to the process values. The sample cup top is made of glass to see the boiling motion. In order to avoid product loss, a cloth filter can be attached to the dryer outlet, not to see the product loss during the trials (which is seen as another way to understand which airspeeds are ideal). To measure under-screen pressure, a manometer is attached to the hot air supply line.

In the prepared test setup, a 3% moist salt product is formed at 200 mm cake height, at an air temperature of 208.3 °C, at air velocities of 0.7 m / s, 0.8 m / s, 1.3 m / s, 1.5 m / s, 2.5 m / s and 2.9 m / s, respectively. The trials were repeated during the six different test periods calculated. At the end of the calculated period of each trial, drying was stopped and the moisture values were measured in the product's moisture analyzer. At the end of the drying process, the total product remaining in the chamber is weighed and the product loss is calculated.

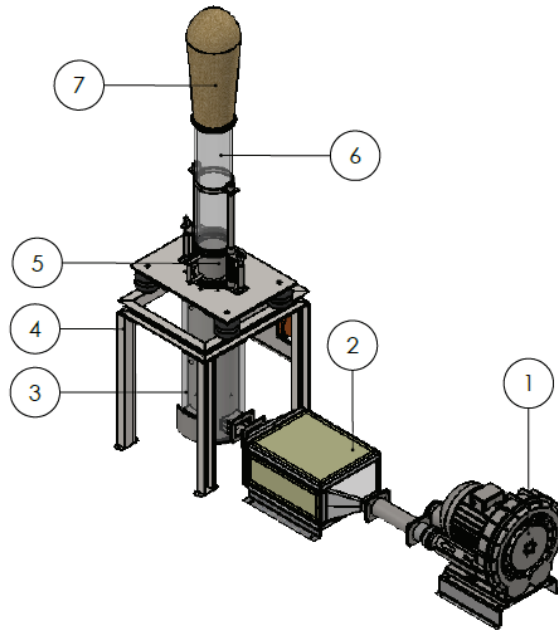


Figure 2. Fluid bed dryer1: Fan (TMM - Type: EJ9KB - Power: 4kW - Flow: 470 m³ / h - Maximum Pressure: 225 mbar), 2: Resistance Heater (Max.180-250 °C), 3: Hot Air Supply Line, 4: Chassis, 5: Sample Cup, 6: Sight Glass Column, 7: Cloth Filter

Figure 3 illustrates a sieve analyzer (Loyk ESM-200, Turkey) that was measured on the product particle size distribution. Mesh sieve with large hole diameters is at the top and meshes with gradually shrinking hole diameters are placed in order and shaking motion is given. The product accumulates on the mesh with hole diameters that are too small to pass through the shaking motion. When the process is finished, the samples on the sieve are weighed and the grain size distribution results.

In the MFIX analysis program, a two-dimensional analysis was performed to see the boiling movement of the product according to the input speeds.



Figure 3. Sieve analyzer

3. RESULTS AND DISCUSSION

The layer thickness (cake height) of the salt with a density of 1.084 g / ml, a specific heat of 0.88 kJ / kg K, and initial humidity of 3% was taken as 200 mm. Sieve analysis results of six different tests are given in Table 1.

Table 1. Sieve analysis results

SIEVE ANALYSIS RESULTS						
Sample Amount (g) :		10				
Revolutions per minute (rev/min) :		100				
Test time (min) :		10				
Sieve no	Particle Size (μ)	Hole Size (mesh)	Empty sieve weight (g)	Full screen weight (g)	Sample weight (g)	Weight value %
1	5000	4	374.2	374.8	0.6	6
2	3500	6	383.4	383.8	0.4	4
3	1020	20	340.4	345	4.6	46
4	850	20	347.4	349.6	2.2	22
5	<596	30	328	329.8	1.8	18
under sieve-			340	340.4	0.4	4
					Total = % 100	
Test Result:						

interspace	>5000 (μ)	5000- 3500 (μ)	3500-1020 (μ)	1020-850 (μ)	850-596 (μ)	<596 (μ)
Sample amount %	6	4	46	22	18	4

sieve diameter=7 cm

Calculations for the ideal boiling of 3 kg, 3% moist salt product at 208.3 ° C air temperature, 0.7 m / s, 0.8 m / s, 1.3 m / s, 1.5 m / s, 2.5 m / s and 2.9 m / s it is made. At equation 1 was found between 1 and 30.14 kJ for the energy consumed until the water in the product reached the boiling point. With the help of the same formula, the energy spent to heat the product was 102.46 kJ and the energy required for the evaporation of the water coming to the boiling point was 203.13 kJ. By collecting the calculated energies, the total energy required for drying was found at 335.70 kJ (and the mass airflow required at 208.3 ° C was 1.74 kg/s.

$$Q = m.c.\Delta T \quad (1)$$

The results of the tests carried out at the speeds of 0.7 m / s, 0.8 m / s, 1.3 m / s, 1.5 m / s, 2.5 m / s and 2.9 m / s are given in Table 2. Total test times were 4.584 min, 4.011 min, 2.262 min, 2.139, 1.284 min, and 1.107, respectively.

Table 2. Flow rate results of trials at different air velocities

	UNIT	TEST 1	TEST 2	TEST 3	TEST 4	TEST 5	TEST 6
Pipe Diameter	m	0.125	0.125	0.125	0.125	0.125	0.125
Air Speed	m/s	0.7	0.8	1.3	1.5	2.5	2.9
Air flow	m ³ /s	0.009	0.01	0.016	0.018	0.031	0.036
Volumetric Air Flow	m ³ /min	0.515	0.589	0.957	1.104	1.841	2.135
Mass Air Flow	kg/min	0.379	0.433	0.768	0.812	1.354	1.57
Total Test Time	min	4.584	4.011	2.262	2.139	1.284	1.107

In the prepared test setup, a 3% moist salt product is formed at 200 mm cake height, at an air temperature of 208.3 ° C, at air velocities of 0.7 m / s, 0.8 m / s, 1.3 m / s, 1.5 m / s, 2.5 m / s and 2.9 m / s, respectively. The trials were repeated during the calculated test times. At the end of the calculated period of each trial, drying was stopped and the moisture values

were measured in the product's moisture analyzer. At the end of the drying process, the total product remaining in the chamber is weighed and the product loss is calculated and the results are shown in Table 3.

Table 3. *Data used in tests*

	UNIT	TEST 1	TEST 2	TEST 3	TEST 4	TEST 5	TEST 6
Product initial density	g/ml	1.084	1.084	1.084	1.084	1.084	1.084
Initial moisture	%	3	3	3	3	3	3
Final moisture	%	0.0801	0.0797	0.0680	0.0712	0.0632	0.0600
Test Time	min	4.58	4.01	2.26	2.14	1.28	1.11
Initial product amount	g	3000	3000	3000	3000	3000	3000
Final product amount	g	2930	2920	2730	2598	2213	2012
Product loss	%	2.33	2.67	9.00	13.40	26.23	32.93
Static cake height	mm	200	200	200	200	200	200
Drying air temperature	°C	208.3	208.3	208.3	208.3	208.3	208.3
Air speed (fluidized)	m/s	0.7	0.8	1.3	1.5	2.5	2.9
Pressure drop caused by the sieve	mbar	0.493	0.647	1.778	1.717	6.447	6.482
Pressure drop caused by the under-sieve product	mbar	12.065	12.688	16.525	20.585	27.04	28.086
Sieve code	-	Sieve	Sieve	Sieve	Sieve	Sieve	Sieve

As a result of the calculated periods, it was concluded that the product was dry and the ideal boiling speeds observed in the analyzes match the reality.

In the MFIX analysis program, a two-dimensional analysis was performed to see the boiling movement of the product according to the input speeds. Boiling images in the fifth second are shown in Figure 4.

In Figure 4, boiling was not observed because the gravity effect (pressure drop created by the bed) caused by the test1 and test2 product beds was insufficient. The increasing air velocity in Test3 and Test4 overcomes the pressure drop and boils. In Test5 and Test6, it is clearly understood from the boiling movement that the air velocity is too high for the bed height. In summary, since the product does not boil at low speeds, drying does not occur, while high-speed product loss occurs and it

can be accepted as the most important criterion in the ideal speed drying process. It is observed that boiling at speeds of 1.3 m / s and 1.5 m / s is ideal. Time-dependent temperature graphs in the MFIX analysis program are shown in Figure 5.

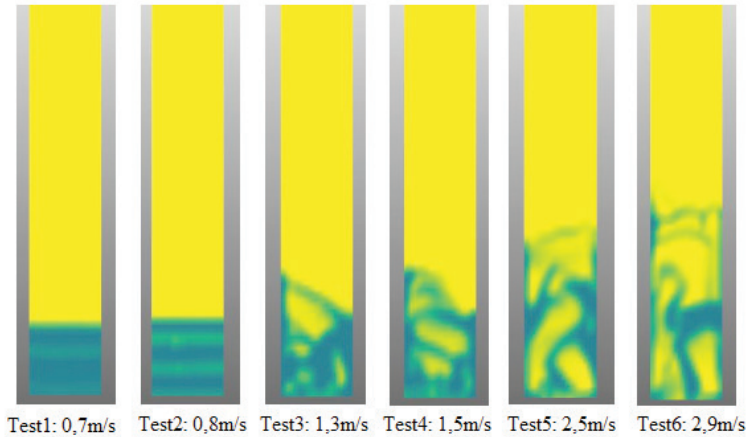
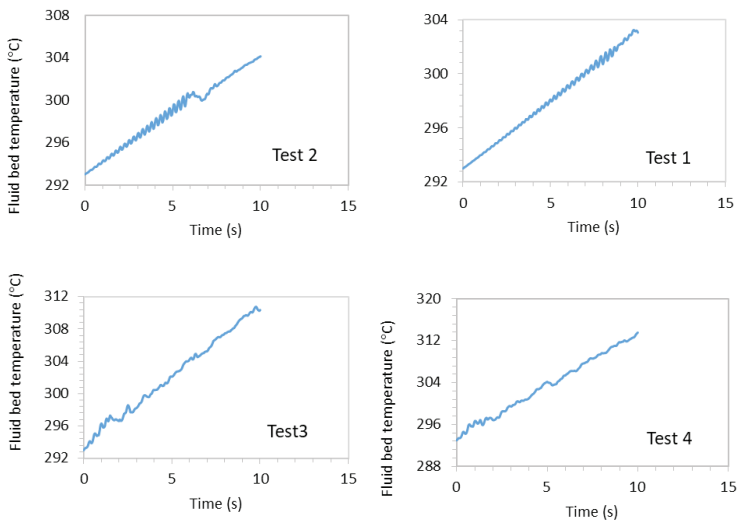


Figure 4 MFIX analysis results



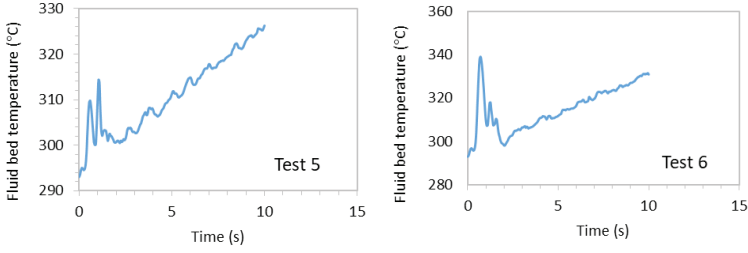


Figure 5 Time-dependent temperature change

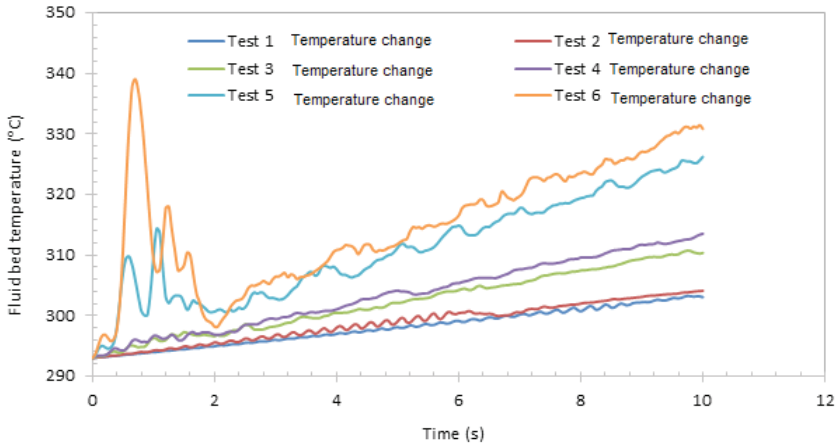


Figure 6 Temperature change of tests

In Figure 6, the bed temperature increases linearly and slowly in the air velocities before boiling. At the speeds that boil, the bed temperature increases rapidly and linearly. At high speeds, the bed temperature changes instantaneously (irregularly) due to air explosions and non-ideal boiling movements in the product. Drying time and ideal drying temperature depend on airspeed.

In the Solidworks simulation program, pressure losses caused by the sieve plate were examined. Since the results are very small and the scale range of the manometer in the test device is large, the results of the analysis here are included in the Figure 7. The minimum / maximum pressure values of the tests were found as 1013.13 / 1013.68, 1013.17 / 1013.81, 1012.97 / 1014.71, 1013.03 / 1014.72, 1012.33 / 1018.05 and 1012.29 / 1018.65, respectively.

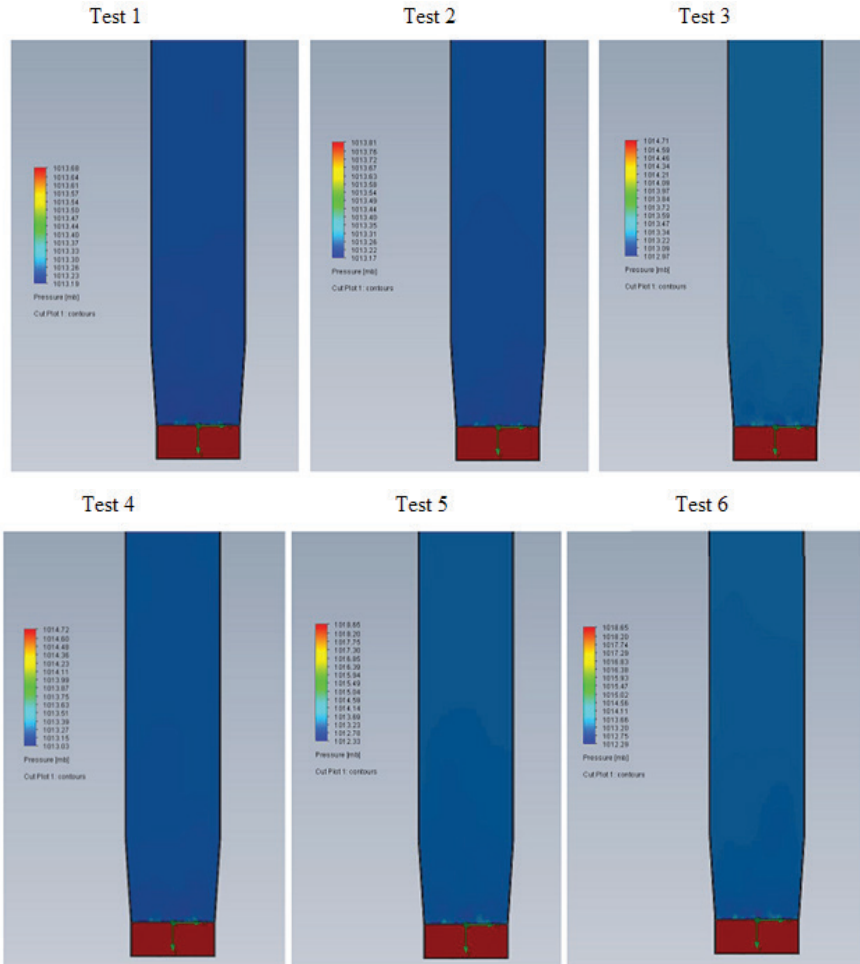


Figure 7 Pressure losses created by the sieve plate in the Solidwork program

4. CONCLUSIONS

Calculations for the ideal boiling of 3 kg, 3% moist salt product at 208.3 ° C air temperature, 0.7 m / s, 0.8 m / s, 1.3 m / s, 1.5 m / s, 2.5 m / s and 2.9 m / s it is made. The total energy required for drying was 335.70 kJ and the required mass airflow at 208.3 ° C was 1.74 kg/s. In addition, a two-dimensional analysis was performed to see the boiling movement of the product according to the input speeds in the analysis program. Boiling at speeds of 1.3 m / s and 1.5 m / s was ideal.

Acknowledgements

We thank ASOS Proses Makine San. ve Tic. A.Ş. for allowing the use of its laboratories as authors.

REFERENCES

- [1] Ergin, Z., Tuzun üretim teknolojisi ve insan sađlıđındaki yeri, *Bilimsel Madencilik Dergisi*. 1988, 27(1), 9-30.
- [2] Güngörmez, H., In terms of economic activity: Tuzluca kaya, *Cođrafya Dergisi*. 2015, 30, 26-37.
- [3] Moralar, A. and Çelen, S., Determination of some parameters of dried carrot by microwave method, *El-Cezeri Journal of Science and Engineering*. 2020, 7(1), 31-42.
- [4] Çelen S, Arda S. O. ve Karataşer M. A., Güneş Enerji Destekli Mikrodalga Konveyör Kurutucu Kullanılarak Kuruma Davranışının Modellenmesi, *El-Cezeri Fen ve Mühendislik Dergisi*. 2018, 5(1), 267-271.
- [5] Ersöz, M.A., Dođan, H., Investigated By Experimentally for Drying Lake Salt in a Fluid Bed Continuous Dryer, *Pamukkale University Journal of Engineering Sciences*. 2010, 16(2), 155-163.
- [6] Jafari, H., Farahbod, F., The experimental survey on the rotary dryer performance: drying of wetted salt from effluent bio wastewater, *Journal of Applied Biotechnology & Bioengineering*. 2017, 4(3), 567-570.
- [7] Sizgek, E., Sizgek, G. D., Drying characteristic of porous ceramic microspheres in a microwave heated fluidised bed, *Chem. Eng. Technol*. 2002, 25(3), 287-292.
- [8] Güngör, A., Özbalta, N., Endüstriyel kurutma sistemleri, III. Ulusal Tesisat Mühendisliđi Kongresi ve Sergisi Bildiriler Kitabı, İzmir.1987, (2), 737-747.

Chapter 4

SURFACE CHARACTERIZATION FOR NANOTECHNOLOGICAL APPLICATIONS



Ceyda BİLGİÇ¹
Şafak BİLGİÇ²

1 Assoc. Prof. Dr., Department of Chemical Engineering, Eskisehir Osmangazi University, Eskisehir, Turkey, Orcid No: 0000-0002-9572-3863

2 Assist.Prof.Dr. Department of Civil Engineering, Eskisehir Osmangazi University, Eskisehir, Turkey, Orcid No: 0000-0002-9336-7762

1. Introduction

Nanotechnology comes into our lives with many applications such as; self-cleaning paints, non-contaminating fabrics, coatings as hard as concrete to diamond, killing cancer cells without damaging the body, creams that do not lose their effect for days, socks that do not smell because they kill bacteria, and microbe-free refrigerators. As an application of nanotechnology, it is possible to prepare smart surfaces that water-repelling (hydrophobic) and water-loving (hydrophilic). Many surfaces such as automobile glasses that do not require superhydrophobic wipers, non-fogging bathroom mirrors and vehicle interior windows, self-cleaning building exteriors (figure 1), non-clogging stent walls, ship exterior paints that algae and marine animals cannot adhere, and friction-free surfaces can be prepared.

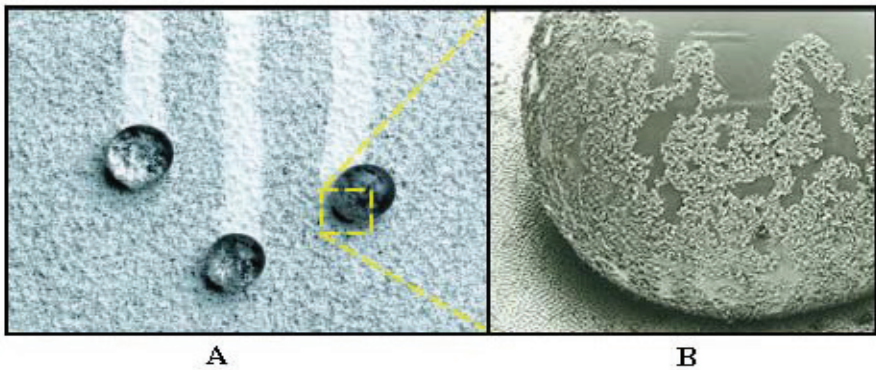


Figure 1. Self-cleaning building exterior. A- self-cleaning nano-paint B- close up view of the droplet (Özgür et al., 2007:52)

Hydrophobic surfaces are a form of nanotechnology that is used in many areas of industry and new ones are being added to these areas every day. The interest in hydrophobic surfaces has been emerging for the first time by investigating the reasons why the lotus leaves are always clean. The leaf surface is covered with a material with low surface free energy as well as having nano-scale hairs present on the rough structure. With a combination of both of these two properties, it has been determined that the lotus leaf surface has a hydrophobic property. Thus, due to the air trapped in the nanoscale spaces, the liquid drop on its surface contacts the surface with a very small area.

In this way, the liquid drop can remain on the surface with a high contact angle thanks to the surface tension, close to a spherical shape. It can also roll off the surface with a small slope. During rolling, the liquid drop cleans the surface of the material by taking away the dirt and dust particles on the

surface (Neinhuis and Barthlott, 1997:667). Because of these properties, hydrophobic/superhydrophobic surfaces have found many applications in industry such as; improving corrosion resistance, self-cleaning surfaces, prevention of icing and fogging, oil and water separation, battery manufacture technology, optical devices, water purification, membrane separation, and anti-bacterial surfaces, and medical applications.

The wetting behavior of the solid surface is very important for both practical applications and basic research. The hydrophilic or hydrophobic property (wettability) of the surface can be characterized by measuring the surface tension between the surface and the water droplet. If the contact angle is less than 90° , the surface is called hydrophilic, it is greater than 90° , it is called hydrophobic, it is between 150° and 180° , is named superhydrophobic. Contact angle (CA); depends on many factors including surface energy, roughness, method of surface preparation, and surface cleanliness (Bhushan and Jung, 2007:1033). Changes the wettability of the solid surface depends on the chemical properties and microstructure of the surface.

Hydrophobic surfaces can be prepared both by using low surface energy materials (such as fluoride or alkyl compounds) (chemical method) and by controlling the surface roughness (geometric method). Chemical modification of the flat surface can maximum increased the contact angle up to 120° , while the contact angle can be increased above 150° by increasing the surface roughness by adding nanoscale particles to the structure. With the creation of surface roughness or air pockets, the surface area increases, and the hydrophobicity of the surface is increased (Hsiang et al., 2007:420).

Non-wetting, in other words, water repellency (hydrophobicity) or vice versa, wettability (hydrophilicity), and surface energy terms encountered in the many disciplines, including construction, chemistry, food, textile, paint, glass, pharmacy, mining, electrical electronics, metallurgy, and materials, etc. It occurs during the production of materials or products in many different industrial areas. Some of them can be listed as follows: water-repellency, ie non-wetting fabric in textile (Liu et al., 2012:17426; Fang et al., 2017:2039), to obtain non-stick surface's in the metal industry, the metal surface was coated with teflon etc. materials (Arukalam et al., 2016:220; Gnedenkov et al., 2016:1241; Zdziennicka, et al., 2009:243), , in the paper industry, the paintability and print quality of the paper surface (Gao et al., 2015:24; Asano and Shiraishi, 2015:55; Azemar et al., 2015:10), in mining, ore enrichment by flotation and solid-liquid separation by precipitation method (Raza et al., 2014:10137), in the food, cosmetics and paint industry ensuring the stability of emulsified products (Kapilashrami et al., 2004), in pharmaceutical to form drug (pill) formulations (Hölck, et

al., 2012:1285), in the electrical and electronics industry; the production of electronic circuits and the determination of the product quality in the production of insulation material (Syakur, et al., 2012:284), especially in the construction industry; coating with hydrophobic materials to protect the basic structures of buildings against groundwater (Le and Nunes, 2016:1), in the material field, to obtaining a super hydrophobic product or surface (Chakradhar, et al., 2011:8569) and in biomaterial production (Huebsch and Mooney, 2009:426; Mockenhaupt et al., 2008). Determining the wettability or non-wettability of a solid measured by the surface energy of that solid (figure 2).

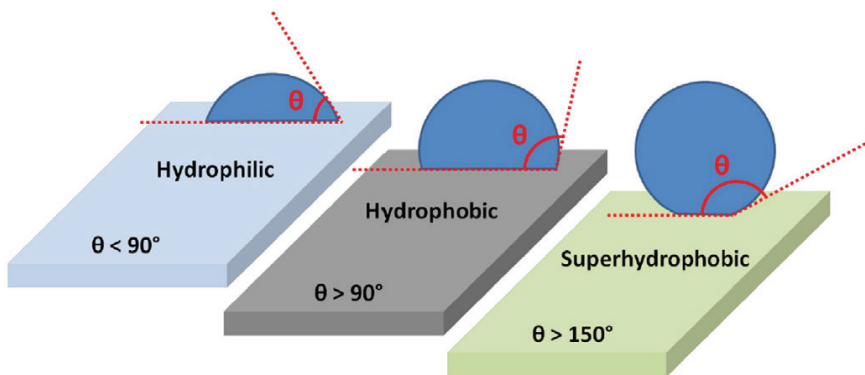


Figure 2. The states of surfaces with different contact angles (Oberli et al., 2014:47)

There have not been many studies on the investigation of wettability and determination of surface energies. Syakur et al. 2012, added silicone rubber and silica sand to the epoxy and examined its hydrophobic character and electrical insulating ability and electrical insulating ability. As a result, both properties of silicone rubber increase positively while they determined that adding 10-20% silica by weight to epoxy does not affect these properties (Syakur et al. 2012:284). Atta et al. 2016, measured the water contact angle of epoxy coatings containing CaCO_3 nanoparticles whose surface was modified with fatty acids. They found that the contact angle increased significantly with the addition of modified calcite (Atta et al., 2016:577).

In today's world, eliminating environmental pollution with traditional methods using water and chemicals will soon become impossible, given the increasing population and decreasing energy resources. Therefore, in recent years, individual and industrial level cleaning and environmental treatment issues have been among the topics of great interest to researchers. For this purpose, self-cleaning dyestuffs have started to be produced, and studies on bringing the self-cleaning feature to textile surfaces have come to the

fore. With the use of self-cleaning textile surfaces in daily life, reduction in cleaning costs is achieved by minimizing the use of water and electricity and conserving energy resources. Thus, it is aimed to develop sustainable innovative cleaning methods.

Inspirations from nature give researchers a remarkable perspective in experiencing nanotechnological developments. For example, the gecko, a type of lizard, can hold onto the surface on which it is located, thanks to the nano-structured hairs on its feet. Figure 3 shows the gecko lizard and the nano-structured hairs on its feet.



Figure 3. Micro and nano-structured hairs on the Gecko feet (Bozkaya, 2006)

Lotus leaves have also nano-sized roughness. As a result of these leaves being nano-rough, a drop of water on the leaf surface rests on the nanoparticle contact with air much more than on a normal surface. Therefore, the surface tension of the water droplet prevents the drop from slipping and allows it to roll from the surface. Dirt particles on the surface are also effectively transported by the rolling liquid droplet. Thus, the surface gains self-cleaning quality. The lotus leaf and the water drop on it are shown in figure 4.



Figure 4. Leaves of Lotus Plant (Özdoğan et al., 2006:287)

Studies on self-cleaning surfaces have been an area that researchers have focused on in recent years. Metal oxides such as TiO_2 , SiO_2 , ZnO , and MgO are used to obtain self-cleaning surfaces. Today, nanoparticles of said metal oxides are combined with textile materials to form nano-composites or these composites are transferred to the textile surface as a nano thin layer by different methods. Self-cleaning textile and glass surfaces thanks to the TiO_2 coating, and self-cleaning dyestuffs obtained by adding titanium dioxide nanoparticles attract great attention today.

2. Basics of self-cleaning

2.1. Surface free energy / Surface tension

The atoms on the surface of the dense phase material interact with a very different environment than the atoms on its inner surface. This difference is due to the asymmetrical environment, for example; each atom of the bulk material is again surrounded by the same single type of atom. But on the surface, the situation is different, they are exposed to different influences as they interact with their close or distant neighbors around them. Therefore, these atoms have a different distribution of energy according to the atoms inside. Especially for liquids, this situation undesirably increases the energy of the liquid molecules. To reduce this energy, a force is created by the surface. To this in solids; the surface free energy in liquids is called surface tension and is represented by (γ).

Many aquatic insects live according to the laws of physics. For example; a water spider; walks on the membrane formed due to surface tension on the water. There is a dense velvety weave of hydrophobic (water-repellent) hairs covered with wax to prevent them from sticking to water (figure 5). Moreover, the legs of the water repellent (*Gerris remigis*) have a water contact angle of about 167° . It is therefore characterized by durable and robust super hydrophobicity (Liu et al., 2013:503).



Figure 5. Water spider (Yenice E.,2015)

2.2. Surface roughness

The most important factors affecting the contact angle are the surface energy and roughness of the solid. Surface energy arises as a result of surface tension. In a crystal structure, an atom in the crystal can stably hold its place as it is subjected to pulling force from all directions. However, it is not concerned with the same situation for surface atoms. The surface atom feels half the tensile force applied to an atom inside and therefore tends to rupture from the surface, which creates surface tension. The lower the surface tension, the smaller the contact angle. The increase in surface roughness causes both hydrophilic and hydrophobic properties to increase. The maximum contact angle that can be reached without roughness does not exceed 120° for a hydrophobic surface. As the roughness causes air compression between the surface and the water drop, the interaction between it decreases, so the contact angle increases on hydrophobic surfaces (Sas et al., 2012:824).

In many studies in the literature, it is stated that surface roughness is one of the most important factors in the production of superhydrophobic and superoleophobic surfaces. The contact area between the surface and the liquid is minimized by increasing the surface roughness with the

chemicals used and thus superhydrophobic and superoleophobic surfaces can be produced (Lafuma and Quere, 2003:457).

Hong et al. created a water-repellent surface for automobile safety glasses by the sol-gel process. Surfaces are coated with a spray coating method consisting of a silica substrate and a fluorocarbon layer that provides surface roughness and also increases chemical and mechanical resistance. The mentioned method consists of two independent steps. The first step is to produce silica sols and water repellent coating solutions. The second step is the heat treatment for sputter deposition and curing. Silica sol was obtained by a two-step aging process: in the first aging, a basic catalyst such as NH_4OH was added to a mixture of tetraethylortosilicate (TEOS) and ethanol, and in the second aging was performed by adding an acidic catalyst. Water-repellent coating solution for was made by the hydrolysis reaction by the addition of fluoroalkylsilane, HCl and H_2O . After the glasses were cleaned, drying and heat treatment was carried out at 100-500 °C on spray-coated silica glass. Then the water repellent solution was spray coated on the silica layer and the system was heated at 100-150 °C and cleaned with alcohol. Thanks to the coating developed within the scope of the study, the contact angle of the surface was increased up to 112°, but as a result of the safety tests, it was observed that the abrasion resistance decreased as the surface roughness increased (Hong et al., 1999:274).

Erbil et al. investigated that the effect of polymer concentration, film formation temperature and lack of solvent on the homogeneity, surface roughness and water contact angle of isotactic polypropylene coating. The profile of a water droplet on a smooth polymer surface has a contact angle of 104°. Increasing the initial concentration of the polymer increased the final coating thickness and surface roughness, hence contact angles up to 149°. This surface provides a homogeneous initial precipitate layer grown on the network and creates a more homogeneous final coating. Changing the drying temperature and drying conditions affected homogeneity. Furthermore they were able to create a superhydrophobic polymer coatings on a variety of substrates, including aluminum foil, stainless steel, teflon, high density polyethylene and polypropylene other than glass slides. The only condition for applying this method to various surfaces is that the solvent mixture does not dissolve the underlying material. The disadvantage of this method is that after a long time deterioration of strength (Erbil et al., 2003:1377).

Zhang et al., a new, simple and low cost method has been developed to improve the surface properties of the TiO_2 film. Degussa P25- TiO_2 nanoparticles-glazed ceramic tiles on tetraethyl orthosilicate (TEOS) was modified with. The effects of tetraethyl orthosilicate modification were investigated on the microstructure, crystal structure, hydrophilicity,

photocatalytic activity and stability of the films. In their study, the modified P25-TiO₂ / TEOS particles compared to pure P25-TiO₂ particles, have found that the better dispersion, the higher surface area, the greater surface roughness, and and have found that a smaller particle size exhibited. After 10 days in a dark place the coatings have better hydrophilicity and higher photocatalytic activity under visible light irradiation were observed. Therefore, they concluded that the P25-TiO₂/TEOS films have good wash resistance and would be a suitable candidate for practical applications (Zhang et al., 2013:141).

3. Theoretical basis about wettability

3.1. Wettability

Wetted the spread of a liquid on the solid surface and covering the surface at a certain rate and wetting of the solid surface to be covered by any liquid to a certain extent, the degree to which this phenomenon occurs is called wettability. The contact angle gives information about the wettability property of a material and the surface energy of a solid surface. According to the wetting theory, when a droplet is deposited on a solid surface, the fluid dynamics of both the solid and liquid phases are affected by different physical and chemical factors. These factors are fluid dynamics of both solid and liquid phases, surface tension, density and solid-liquid temperatures, the viscosity of the liquid, surface roughness, and shape of the solid. Contact angles vary depending on the tensions between the three surfaces (Zhang et al., 2013:141)

If the contact angle is greater than 90°, the surface is hydrophobic and the liquid material cannot penetrate through the pores in the solid material and cannot fully wet the solid material. Fully wetting is observed when the contact pain is 0°. Surface energy, adhesion, and wettability increase as the contact angle decreases, and the larger the contact angle, the lower the surface energy, wettability, and adhesion (Zhang et al., 2013:141). The wetting event can be divided into two general classes: Equilibrium wetting occurring where a liquid and solid in contact are not intervened from outside and dynamic wetting in which the liquid or solid (or both) is in the transition to other phases during the wetting period. The wetting event can be divided into two general classes: equilibrium wetting where a liquid and solid in contact is not intervened, and the liquid or solid (or any It is the dynamic wetting in which the two) are in transition to other phases during the soaking period. A static contact angle is obtained if the system is in equilibrium and a dynamic contact angle if it is variable (Aydar, 2012).

When the surface of the wetting properties is analyzed; wetting properties is characterized by the main parameter is the is the static or dynamic contact angle with the solid of the liquid. The contact angle

depends on many factors; surface energy, surface roughness and whether the surface is clean or not, etc. If the liquid wets the surface (hydrophilic surface), the static contact angle value of $0^\circ \leq \theta \leq 90^\circ$, the liquid does not wet the surface (hydrophobic surface), the contact angle value is $90^\circ \leq \theta \leq 180^\circ$. Surfaces show hydrophilic properties; composed of polar molecules having high surface energy, and show hydrophobic properties; composed of non-polar molecules having low energy surfaces. Contact angle 10° less than the super hydrophilic surfaces, while surfaces with a contact angle between 150° and 180° is known as superhydrophobic (Bhushan and Jung, 2011:1).

The relationship between the construction methods of superhydrophobic surfaces, surface morphology, and wettability was explained in theory by Ma and Hill. Extensive information has been given on the techniques of making non-wetting solid surfaces created by using polymer and sol gel chemistry. With the combination of micrometer and nanometer roughness scale, it has been emphasized that when used in low surface energy materials, the contact angle is greater than 150° and these types of surfaces are called superhydrophobic surfaces. The current situation and recent developments regarding superhydrophobic surfaces are explained in their studies (Ma and Hill, 2006:193).

Yüce et al. were investigated that the surface hydrophobicity of polystyrene nanoparticle nanocomposites as a function of nanoparticle. The contact angle change depending on the surface composition or surface roughness on the polystyrene surface was examined. Silica nanoparticles with polystyrene, chloroform and dimethylsilyl hydrophobic surface groups were used in the study. The coating was made on slides with the spin coating method. Characterization was made using contact angle measurement, scanning electron microscopy and atomic force microscope techniques. It has been found that in the case of good dispersion of nanoparticles, the cosine of the water contact angle ($\cos \theta$) decreases linearly with increasing mass percentages of the nanoparticles. This situation has shown that the composite surface includes the smooth polystyrene regions and the rough nanoparticle regions. Two-component (polymer and nanoparticle) composite surfaces where only the surface composition changes but the surface roughness is kept constant for each component are modeled the Cassie-Baxter model. The cosine of the water contact angle sharply decreased at the start of a transition as the nanoparticles formed clusters of broad size distribution. This behavior is modeled as a transition from the Wenzel regime to the Cassie-Baxter regime on a critical roughness length scale. This is because the Laplace pressure prevents the water droplet from penetrating the surface fluctuations (Yüce and Demirel, 2008).

3.2. Wetting models

Contact angle measurements, first described by Thomas Young in 1805, are still used to characterize the surface properties of solids such as non-wetting and surface energy and to determine liquid-solid interface and solid surface energy at minimum equilibrium distance, is one of the simplest and most accurate methods (Young, 1804:65; Bormashenko, 2014:92). The expression of contact angle (θ) depending on the surface and interface energies is also known as the famous Young's equation and is schematized in figure 6a.

Young's equality is based on the ideality of surfaces. Ideal substrate; they are chemically homogeneous, perfectly smooth surfaces. Accordingly, hysteresis is not concerned since there is no difference in advancement and regression contact angles for ideal systems. On the other hand, on the real (heterogeneous and rough) surfaces, since different angles may occur along the lines that the drop touches, an angle that exactly fits the Young equation cannot be observed (Aydar 2012).

The droplets form a three-phase contact line suitable for solid-liquid, solid-air, and liquid-air interfaces as shown in Figure 2. The forces created by the surface tension at each interface attract the drops on the solid surface and determine their shape (Sas et al., 2012:824; Blossey, 2003:301). According to Young's equation (1), the cosine of the equilibrium water contact angle (θ) is directly proportional to the difference of interface forces per unit length of solid-air and solid-liquid, while inversely proportional to the liquid-air interface force (Shirtcliffe, 2010:124).

$$\cos \theta = \frac{\gamma_{sv} - \gamma_{sl}}{\gamma_{lv}} \quad (1)$$

In liquids, there is a dynamic balance between the liquid surface and the inside of the liquid. Therefore, the free surface energy is the same at all points, but for solid surfaces, the free surface energy is not equal at all points. The equilibrium contact angle depends on surface conditions. The wetting behavior of smooth (ideal) and rough solids was developed by Young and Wenzel, Cassie-Baxter equations, respectively.

3.2.1. Wenzel's Equation

During the studies to give water repellency to textile surfaces, Wenzel (1936) revealed that surface roughness can significantly alter the water contact angle (Wenzel, 1936:988). According to Wenzel's equation (2), water progresses following all topological variations on the surface (Figure

6b). Wenzel's equation is called homogeneous wetting, in which Young contact angle (θ) and surface roughness (r) are used to find the water contact angle on the rough surface.

$$r(\gamma_{sv} - \gamma_{sl}) = \gamma_{lv} \cos \theta_W^* \quad (2)$$

where θ_W^* is Wenzel's contact angle affected by surface roughness; modified Wenzel's equation is:

$$\cos \theta_W^* = r \cos \theta \quad (3)$$

The roughness parameter (r) is found as the ratio of the liquid-solid contact area to the geometric projection of the liquid-solid interface. If the roughness parameter is equal to 1, the surface becomes a smooth ground, and Wenzel's equation converted Young's equation. However, it is accepted that this parameter is always greater than 1 for rough surfaces and that it causes an increase in the contact angle of hydrophobic surfaces (Sas et al., 2012:824; Sanjay et al., 2012:76).

Solid surfaces are seldom homogeneous. The microscopic surface roughness comprising tangential direction at the three phase contact line is not parallel to the macroscopic solid surface. Wenzel was the first to try to uncover the relationship between surface roughness and actual contact angle. He stated that in parallel with the increase in surface roughness, the hydrophobic behavior of the material also increase. This behavior is associated with the increase in surface roughness provided by the surface area (Lee and Owens 2010:3247).

3.2.2. Cassie-Baxter's Equation

Wettability of rough, chemically heterogeneous, two-component surfaces; often defined by the Cassie-Baxter model (Figure 6c). Cassie-Baxter (1944) proposed another model to explain the roughness effect on the behavior of the drop on the surface. In contrast to Wenzel, wetting is assumed to be heterogeneous in this model; the air is trapped in the surface voids by the liquid. In this case, the contact area between liquid and solid is minimized, while the area between liquid and air is maximized. Thus, the liquid is forced to form spherical drops (Cassie and Baxter, 1944:546; Sas et al., 2012:824; Sanjay et al., 2012:76).

Their model consists of two parts. The first part includes a surface fraction, f_1 , and contact angle of θ_1 and the other part includes f_2 and θ_2 (Cassie and Baxter, 1944:546). Hence, in Cassie and Baxter's equation, the contact angle is defined as Eq. (4):

$$\cos \theta = f_1 \cos \theta_1 + f_2 \cos \theta_2 \quad (4)$$

where θ is the contact angle in the model of Cassie and Baxter and f_1 is the fraction of surface area with contact angle θ_1 ($f_1 + f_2 = 1$). If only air is present between solid and liquid, θ_2 will be 180° . Therefore, Eq. (4) can be written as Eq. (5):

$$\cos \theta_{CB} = f_s (\cos \theta_s + 1) - 1 \quad (5)$$

where f_s is the fractional solid surface with a contact angle of θ_s . In addition to the models listed, more improved models have been provided in references to predict the specific modes of wetting (Lopes et al., 2013:24530; Sas et al., 2012:824).

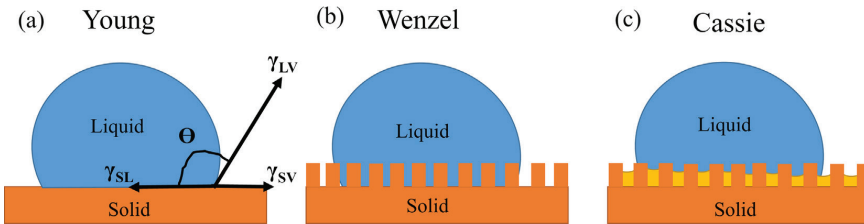


Figure 6. Different wetting models (Barati Darband et al.,2020:1763)

4. Conclusions

Nanotechnology is a technology that deals with structures and processes on the order of one billionth of a meter. New properties of materials that are reduced to a nanoscale size that cannot be observed on a macro-scale are emerging. Two basic strategies known as top-down and bottom-up are used to reduce materials to nanosize. While physical methods are used in the top-down strategy, chemical methods are used in the bottom-up strategy.

Due to the important properties given to materials, nanotechnology has been used widely in composite applications and the production of nanocomposites has gained speed. Nanocomposites consist of two components as filling and matrix materials. While filling materials are nano-sized particles, tubes, and fibers, matrix materials are polymer, metal, ceramic, and their derivatives. The most commonly used matrix material is thermoplastic polymer matrices. The main reasons for this are the ease of processing, mechanical properties, flexible structure, and low density of polymers. In the production of polymer nanocomposites, melt blending, solvent method, and in-situ polymerization methods are widely used.

In this article, developments about surface characterization and its applications in nanotechnology and studies on this subject are compiled. Hydrophobicity or severe water repellency of the surface finds important solutions in many application areas such as self-cleaning, coating, corrosion resistance, biotechnology, and low friction coatings. It is possible to adjust the surface topography by selecting the design parameters of the surface appropriately, and thus to obtain the hydrophobicity afterward.

Acknowledgments

This study is a part of a project (2020-3139) supported by the Research Fund of Eskişehir Osmangazi University.

References

- Arukalam, I. O., Oguzie, E. E., Li, Y. (2016). Fabrication of FDTS-modified PDMS-ZnO nanocomposite hydrophobic coating with anti-fouling capability for corrosion protection of Q235 steel. *Journal of Colloid Interface Science*, 484, 220-228.
- Asano, H., Shiraishi, Y. (2015). Development of paper-based microfluidic analytical device for iron assay using photomask printed with 3D printer for fabrication of hydrophilic and hydrophobic zones on paper by photolithography. *Analytica Chimica Acta*, 883, 55-60.
- Atta, A. M., Al-Lohedan, H. A., Ezzat, A. O., Al-Hussain, S. A. (2016). Characterization of superhydrophobic epoxy coatings embedded by modified calcium carbonate nanoparticles. *Progress in Organic Coatings*, 101, 577-586.
- Aydar, A. Y. (2012). Determination of Contact Angle of Olive oil and Canola Oil on a PTFE surface at Elevated Temperatures. *Master of Science Thesis*, NCSU.
- Azemar, F., Fay, F., Réhel, K., Linossier, I. (2015). Development of hybrid antifouling paints. *Progress in Organic Coatings*, 87, 10-19.
- Darband, G. B., Aliofkhaezrai, M., Khorsand, S., Sokhanvar, S., Kaboli, A. (2020). Science and engineering of superhydrophobic surfaces: review of corrosion resistance, chemical and mechanical stability. *Arabian Journal of Chemistry*, 13(1), 1763-1802.
- Bhushan, B., Jung, Y. C. (2011). Natural and biomimetic artificial surfaces for superhydrophobicity, self-cleaning, low adhesion, and drag reduction. *Progress in Materials Science*, 56, 1-108.
- Bhushan, B., Jung, Y. C. (2007). Wetting study of patterned surfaces for superhydrophobic. *Ultramicroscopy*, 107, 1033-1041.
- Blossey, R. (2003). Self-cleaning Surfaces-Virtual Realities. *Nature Materials*, 2, 5, 301-306.
- Bormashenko, E. (2014). Progress in understanding wetting transitions on rough surfaces. *Advances in Colloid and Interface Science*, 222, 92-103.
- Bozkaya, Y. (2006). *Anadolu Üniversitesi İleri Teknolojiler Araştırma Birimi*, 2006.
- Chakradhar, R. P. S., Kumar, V. D., Rao, J. L., Basu, B. J. (2011). Fabrication of superhydrophobic surfaces based on ZnO-PDMS nanocomposite coatings and study of its wetting behaviour. *Applied Surface Science*, 257, 8569-8575.
- Cassie, A, Baxter, S. (1944). Wettability of Porous Surfaces. *Transactions of the Faraday Society*, 40, 546-551.

- Erbil, H. Y., Demirel A. L., Avcı Y., Mert O. (2003). Transformation of a simple plastic into a superhydrophobic surface. *Science*, 299, 1377-1380.
- Fang, L. J., Li, Y. H., Liu, P. F., Wang, D. P., Zeng, H. D., Wang, X. L., Yang, H. G. (2017). Facile fabrication of large-aspect-ratio g-C₃N₄ nanosheets for enhanced photocatalytic hydrogen evolution. *ACS Sustainable Chemistry & Engineering*, 5 (3), 2039-2043.
- Gao, Z., Zhai, X., Liu, F., Zhang, M., Zang, D., Wang, C. (2015). Fabrication of TiO₂/EP super-hydrophobic thin film on filter papersurface. *Carbohydrate Polymers*, 128, 24-31.
- Gnedenkov, S. V., Sinebryukhov, S. L., Egorkin, V. S., Vyaliy, I. E. (2016). Wettability and electrochemical properties of the highly hydrophobic coatings on PEO-pretreated aluminum alloy. *Surface and Coatings Technology*, 307(C), 1241-1248.
- Hsiang, H., Liang, M. T., Huang, H. C., Yen, F. S. (2007). Preparation of superhydrophobic boehmite and anatase nanocomposite coating films. *Materials Research Bulletin*, 42, 420-427.
- Hong, B. S., Han, J. H., Kim, S. T., Cho, Y. J., Park, M. S., Dolukhanyan, T., Sung, C. (1999). Endurable Water-Repellent Glass for Automobiles. *Thin Solid Films*, 351(1-2), 274-278.
- Hölck, O., Bauer, J., Wittler, O., Michel, B., Wunderle, B. (2012). Comparative characterization of chip to epoxy interfaces by molecular modeling and contact angle determination. *Microelectronics Reliability*, 52(7), 1285-1290.
- Huebsch, N., Mooney, D. J. (2009). Inspiration and application in the evolution of biomaterials. *Nature*, 462, 426-432.
- Kapilashrami, A., Eskilsson, K., Bergström, L., Malmsten, M. (2004). Drying of oil-in-water emulsions on hydrophobic and hydrophilic substrates. *Colloids Surfaces A: Physicochemical Engineering Aspects*, 233(1-3), 155-161.
- Lafuma, A., Quere, D. (2003). Superhydrophobic States. *Nature Materials*, 2, 457-460.
- Le, N. L., Nunes, S. P. (2016). Materials and membrane technologies for water and energy sustainability. *Sustainable Materials and Technologies*, 7, 1-28.
- Lee, H. J., Owens, J. R. (2010). Design of Superhydrophobic Ultraoleophobic Nycos. *Journal of Materials Science*, 45, 3247-3253.
- Liu, K., Tian, Y., Jiang, L. (2013). Bio-inspired superoleophobic and smart materials: design, fabrication, and application. *Progresses Material Science*, 58(4), 503-564.
- Liu, Y., Xin, J.H., Choi, C. H. (2012). Cotton fabrics with single-faced superhydrophobicity. *Langmuir*, 28, 17426-17434.

- Lopes, D. M., Ramos, S. M. M., Oliveira, L. R., Mombach, J. C. M. (2013). Cassie-Baxter to Wenzel state wetting transition: a 2D numerical simulation. *RSC Advances*, 3, 24530-24534.
- Ma, M., Hill, R. M. (2006). Superhydrophobic surfaces. *Current Opinion in Colloid & Interface Science*, 11, 193-202.
- Mockenhaupt, B., Ensikat, H., Spaeth, M., Barthlott, W. (2008). Superhydrophobicity of biological and technical surfaces under moisture condensation: Stability in relation to surface structure. *Langmuir*, 24, 13591–13597.
- Neinhuis, C., Barthlott, W. (1997). Characterization and distribution of water-repellent, self-cleaning plant surfaces. *Annals of Botany*, 79(6), 667-677.
- Oberli, L., Caruso, D., Hall, C., Fabretto, M., Murphy, P. J., Evans, D. (2014). Condensation and freezing of droplets on superhydrophobic surfaces, *Advances of Colloid and Interface Science*, 210, 47-57.
- Özdoğan, E., Demir, A., Seventekin, N. (2006). Lotus Etkili Yüzeyler. *Tekstil ve Konfeksiyon*, 16(1), 287-290.
- Özgür, H., Gemici, Z., Bayındır M. (2007). Akıllı Nanoyüzeyler. *Bilim ve Teknik Dergisi*, 473, 52-56.
- Raza, A., Ding, B., Zainab, G., El-Newehy, M., Al-Deyab, S. S., Yu, J. (2014). In situ cross-linked superwetting nanofibrous membranes for ultrafast oil/water separation. *Journal of Materials Chemistry A*, 2, 10137-10145.
- Sanjay, S. L., Annaso, B. G., Chavan, S. M., Rajiv, S. V. (2012). Recent Progress in Preparation of Superhydrophobic Surfaces: A Review. *Journal of Surface Engineered Materials and Advanced Technology*, 2(2), 76-94.
- Sas, I., Gorga, R. E., Joines, J. A., Thoney, K.A., (2012). Literature Review on Superhydrophobic Self-Cleaning Surfaces Produced by Electrospinning. *Journal of Polymer Science Part B-Polymer Physics*, 50(12), 824-845.
- Syakur, A., Berahim, H., Rochmadi, T. (2012). Hydrophobic Contact Angle and Surface Degradation of Epoxy Resin Compound with Silicon Rubber and Silica. *Electrical and Electronic Engineering*, 2(5), 284-291.
- Shirtcliffe, N. J., McHale, G., Atherton, S., Newton, M. I. (2010). An Introduction to Superhydrophobicity. *Advances in Colloid and Interface Science*, 161(1), 124-138.
- Wenzel, R. N. (1936). Resistance of Solid Surfaces to Wetting by Water. *Industrial & Engineering Chemistry*, 28(8), 988-994.
- Yenice, E. (2015). Plazma Destekli Kimyasal Buhar Biriktirme Yöntemi ile Su İtici Nano Kaplama Sentezi ve Karakterizasyonu. *Selçuk Üniversitesi Fen Bilimleri Enstitüsü Kimya Mühendisliği*, 70 p.
- Young, T. (1804). An Essay on the cohesion of fluids. *Philosophical Transactions of the Royal of London*, 95, 65-87.

- Yüce, M. Y., Demirel, A. L. (2008). The effect of nanoparticles on the surface hydrophobicity of polystyrene. *European Physical Journal B.*, 64, 493-497.
- Zdziennicka, A., Szymczyk, K., Janczuk, B. (2009). Correlation between surface free energy of quartz and its wettability by aqueous solutions of nonionic, anionic and cationic surfactants. *Journal of Colloid Interface Science*, 340, 243-248.
- Zhang, P., Tian, J., Xu, R., Ma, G. (2013). Hydrophilicity, photocatalytic activity and stability of tetraethyl orthosilicate modified TiO_2 film on glazed ceramic surface. *Applied Surface Science*, 266, 141-147.

Chapter 5

TRANSMISSION LINE LOADING REGULATION AND POWER LOSS MINIMIZATION IN ELECTRICAL POWER SYSTEMS BY USING FACTS DEVICES



Serhat Berat EFE¹

¹ Serhat Berat EFE, Bandırma Onyedi Eylül University, Dept. of Electrical Engineering, 10200, Bandırma.

INTRODUCTION

Electrical energy demand is increasing rapidly in proportion to technological developments. As the electrical energy generation capacity is limited, it is vital to use the generated energy in the most efficient way (Cengiz et al., 2017). However, limited energy resources have led system planners to look for new techniques to improve the power system performance (Albatsh et al., 2017 & Kocaman et al., 2015). Electric power systems are designed to be stable in both steady state and various operating conditions. As the population and economy are growing, flexibility, reliability and capacity of the existing systems should be increased (Bakır et al., 2018; Kocaman et al., 2020 & Ikbal et al., 2019). Controlling and optimization of power systems are the easiest and most appropriate approaches to achieve this aim (Yıldırım et al., 2017 & Cengiz et al., 2017). However, nonlinear conditions that may occur during operation of actual power systems adversely affect such flows. While the conventional methods have limited capabilities to optimize power systems in case of nonlinearity, one of the proposed solutions is upgrading existing power systems using flexible alternating current transmission system (FACTS) controllers (Haddadi et al., 2011; Li et al., 2000 & Gotham et al., 1998). In this regard, various FACTS devices have been developed and used for whole system optimization. However, it is necessary to perform certain analyses concerning both planning and operating sections of power systems. One of the most important analyses is power flow analysis, which provides data for optimal power flow studies (Allaoua et al., 2009). Power flow analysis allows system engineers to plan the operation of power systems under existing conditions and to optimize power systems according to the requirements of future applications.

Power system engineers and planners should perform an adequate and effective power flow analysis for continuous operating and advanced controlling the system components. As there are numerous and efficient power flow analysis techniques available in the literature to analyze the power system (Farag et al., 2011; Haque 2000; Li et al., 2014 & Li et al., 2016), a power flow analysis algorithm should have following capabilities:

(i) Quick convergence performance for immediate detection of system transients.

(ii) General design for ability of quick and easy adaptation.

The power flow analysis techniques that available in literature have disabilities to handle modern power systems (Ghatak et al., 2017). These limitations are major disadvantages of such algorithms.

Researchers were studied various components and devices are developed to adapt conventional power flow analysis methods with modern power systems (Bhullar et al., 2017; Pourbagher et al., 2018). As the FACTS devices are components developed for this purpose, among them, unified power flow controller (UPFC) is the most effective to regulate active and reactive power flows in power systems due to its regulation and optimization capability.

UPFC is designed as two controlled converters linked back-to-back with a DC link. Usually, the shunt voltage source converter (VSC) is considered as a static synchronous compensator (STATCOM) (Alamelu et al., 2015) and series one as a static synchronous series compensator (SSSC) (Shojaeian et al., 2013). The shunt component injects a current into the system while the series component injects a series voltage (Shahgholian et al., 2017).

The literature review shows that researchers have generally attempted to control converter units using various methods and algorithms, including intelligent systems, such as artificial neural networks, fuzzy logic, and genetic algorithm (Albatsh et al., 2017; Nahak et al., 2017; Sarker et al., 2014; Hashemi et al., 2014 & Morsli et al., 2012). FACTS devices are designed and discussed in general terms at (Ghatak et al., 2017 & Lei et al., 2017) and UPFC at (Mehrjerdi et al., 2017 & Tumay et al., 2004) in detail.

In this context, this study focused on developing an efficient control strategy for unified power flow controller based on the Newton – Raphson power flow analysis method for transmission line loss minimization and loading regulation to show the advantages of FACTS devices on power system optimization. A comprehensive model that consist of incorporating power flow analysis algorithm and unified power flow controller was designed, which uses overall system data. The results obtained show that proposed method has quick response capability to regulate line loadings and decreasing line power losses.

The proposed advanced control model incorporating the Newton – Raphson (NR) power flow analysis method with UPFC was designed under the MATLAB / Simulink platform, where the code section of algorithm was compiled with the MATLAB editor. The performance of the developed method was validated in terms of both transmission line loading regulation and transmission power loss minimization on the IEEE-30 bus system by comparing the results with the pre-known values given in the literature using two scenarios which were line fault and generator outage. After validating the proposed model, its advantages and performance were further discussed based on the results of two case studies; line fault and generator outage.

In the literature, researchers were focused on controlling such devices by intelligent methods. Beside the advantages of these methods, computation time arises proportionally with the systems getting complex. In addition, system design and operation are relatively difficult. Proposed technique is based on conventional power flow algorithm and UPFC structures, which have less computation time and simple design.

The main contribution and highlights of this method can be given as follows:

- This approach differs by using all over system data and contains an algorithm that repeating in a sequence for continuous optimization from references (Tumay et al., 2004) and (Ambriz-Perez et al., 1998) that focused on an integrated model consist of UPFC and NR algorithm.
- The structure of the proposed model is similar as closed-loop feedback control algorithm that widely studied in literature like in references (Kumar et al., 2017 & Sereeter et al., 2017). However, this study uses all system data and performs power flow analysis periodically by timer subprogram to determine system changes and regulate them.

NEWTON-RAPHSON POWER FLOW ANALYSIS METHOD

It is necessary to define NR power flow algorithm for better understanding of proposed technique. Power systems can be described as a network of buses and branches. Network buses can be classified as slack bus, generator bus (PV bus) and load bus (PQ bus). Each bus in the power network is fully characterized by the following four electrical quantities:

- $|V_i|$: voltage magnitude
- δ_i : voltage phase angle
- P_i : active power (W)
- Q_i : reactive power (VAr)

The power flow problem concerns the computation of the voltage magnitude $|V_i|$ and angle δ_i in each bus of a power system, where power generation and consumption are given (Sereeter et al., 2017).

In the literature, power flow analysis is widely undertaken using the NR method, in which an NR iteration is used to solve a nonlinear system of equations $F(\vec{x}) = 0$. As this method is relatively more robust for most starting values, it is vital to select these values carefully for best convergence or speed of iteration. The NR iterative method can be described generally as:

$$y = f[x(0)] + J(0)[x - x(0)] \quad (1)$$

and in terms of x

$$x = x(0) + J(0)^{-1}[y - f(x(0))] \quad (2)$$

In (1) and (2), J is partial derivatives matrix called the Jacobian. For the iteration count i , (2) can be rewritten as:

$$x_{i+1} = x_i + J_i^{-1}[y - f(x_i)] \quad (3)$$

Equation (3) is the general representation of the NR iterative method. The application of the algorithm for power flow analysis can be given as follows:

$$V_{i+1} = V_i + J_i^{-1}[S - f(V_i)] \quad (4)$$

In (4), S is the specified complex power at any (P, Q) busbar and $f(V)$ is the calculated power value at that busbar based on the current values of computed voltage. Thus, (4) can be rewritten as:

$$\Delta S_i = J_i \Delta V_{i+1} \quad (5)$$

Equation (5) is the fundamental representation of the NR algorithm for power flow analysis. Convergence can be obtained by comparing ΔS power mismatches against a pre-specified value, rather than voltage comparison. As the equations are in complex form, solutions can be provided using cartesian or polar representations (Powell 2004). In this study, polar forms of equations were used to create the algorithm. The shortened form of polar representation of the NR algorithm for power flow solutions obtained from (Powell 2004) can be given as:

$$\begin{bmatrix} \Delta P \\ \Delta Q \end{bmatrix} = \begin{bmatrix} J_1 & J_2 \\ J_3 & J_4 \end{bmatrix} \begin{bmatrix} \Delta \delta \\ \Delta V \end{bmatrix} \quad (6)$$

Moreover, the expanded version of (6) can be written as:

$$\begin{bmatrix} \Delta P \\ \Delta Q \end{bmatrix} = \begin{bmatrix} \frac{\partial P}{\partial \delta} & \frac{\partial P}{\partial V} \\ \frac{\partial Q}{\partial \delta} & \frac{\partial Q}{\partial V} \end{bmatrix} \begin{bmatrix} \Delta \delta \\ \Delta V \end{bmatrix} \quad (7)$$

For the general formation of (7), a busbar named “k” (Figure 1) can be used.



Figure 1 Busbar structure for formulation

If

$$S_k^* = V_k^* \sum_{j=1}^n Y_{kj} V_j \quad (8)$$

and polar representation of the node according to the aim of proposed study is

$$\begin{aligned} V_k &= |V_k| e^{j\delta_k} \\ V_j &= |V_j| e^{j\delta_j} \\ Y_{kj} &= |Y_{kj}| e^{j\theta_{kj}} \end{aligned} \quad (9)$$

then, (7) can be rewritten as:

$$S_k^* = |V_k| \left| \sum_{j=1}^n |Y_{kj}| |V_j| e^{j(\theta_{kj} + \delta_j - \delta_k)} \right. \quad (10)$$

As (7) is formed using the active and reactive powers, it is necessary to provide equations for obtaining these values. In the following equations, the Jacobian elements are also taken into account.

$$P_k = |V_k| \sum_{\substack{j=1 \\ j \neq k}}^n |Y_{kj}| |V_j| \cos(\delta_k - \delta_j - \theta_{kj}) + \quad (11)$$

$$+ |V_k|^2 |Y_{kk}| \cos(-\theta_{kk})$$

$$Q_k = |V_k| \sum_{\substack{j=1 \\ j \neq k}}^n |Y_{kj}| |V_j| \sin(\delta_k - \delta_j - \theta_{kj}) + \quad (12)$$

$$+ |V_k|^2 |Y_{kk}| \sin(-\theta_{kk})$$

Another major calculation for power flow analysis using the NR method is, as mentioned in (7), determining the Jacobian matrix elements. The contents of the Jacobian submatrices in polar coordinates are given in (Powell 2004) and these equations are used to construct the algorithm.

UPFC STRUCTURE

UPFC, one of the most important FACTS devices, has the advantages of both SSSC and STATCOM. Voltage magnitude, phase angle and impedance can be controlled by UPFC without violating operating and security limits. It is capable of controlling each of the three variables of voltage magnitude, active and reactive power flow simultaneously, as well as any combination of them, and also can be used for voltage regulation, series compensation, and phase angle regulation in power systems (Acharjee 2016). General representation of a UPFC connected between two busbars is given in Figure 2.

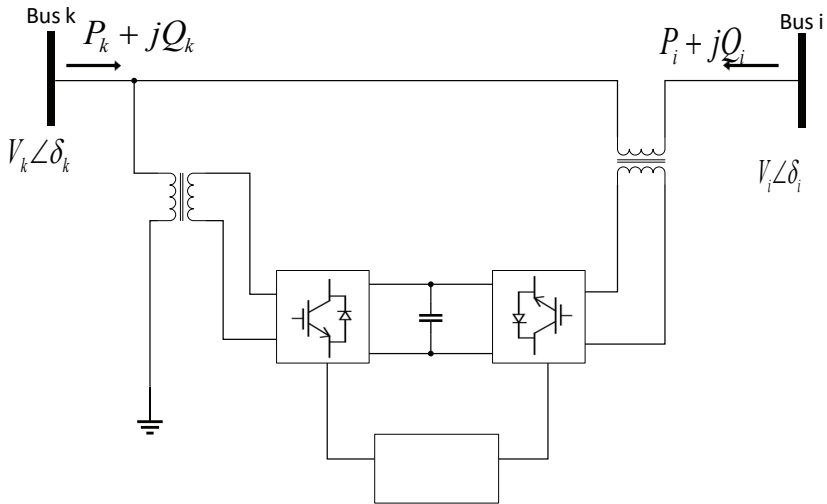


Figure 2 UPFC structure and application

According to the aim of the proposed method, UPFC (Figure 2) was modified by adding a controlling unit. VSC1 and VSC2 converters were controlled by the determination of triggering angles via this unit. UPFC elements need to be explained in detail to provide a clear understanding of the overall structure. DC voltage is inverted to a pure AC signal. The magnitude and frequency of this signal is pre-defined with tolerance for system stability.

The shunt converter transmits the injected real power obtained from the network to the series branch over the DC line. In addition, the shunt branch has the ability to control reactive power. The DC line is used for power exchange between the two converters. On the other hand, the series converter controls the power flows of power lines. UPFC has become an ideal AC-to-AC converter with these advanced capabilities (Efe 2018).

As UPFC consists of two units, series and shunt, the mathematical model of this device can be obtained using these parts separately. This allows an advanced control of UPFC by simplifying the complex structure.

a. Series Unit

The equivalent circuit of the series unit is given in Figure 3.

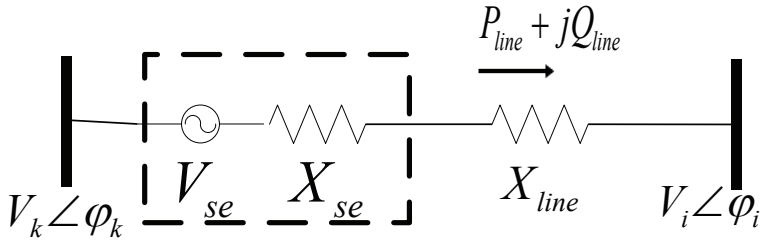


Figure 3 Series unit

This unit can be represented as an ideal controllable voltage source V_{se} with a series reactance X_{se} . If k is the sending bus and i is the receiving bus, where V_k is the voltage of bus k and V_i is the voltage of bus i , then the active and reactive power flows of the series unit are carried by the I_{line} line current as expressed in (13) and (14), respectively.

$$P_{line} = \frac{V_{se}V_i(\cos(\varphi_{se} - \varphi_i))}{jX_{line}} - \frac{V_kV_i \cos \varphi_i}{jX_{line}} \quad (13)$$

$$Q_{line} = \frac{V_k^2 - V_kV_i \sin \varphi_i}{jX_{line}} \quad (14)$$

$$b. \text{ Shunt Unit} \quad \frac{V_{se}^2 - V_{se}V_i \sin(\varphi_{se} - \varphi_i)}{jX_{line}} + \frac{2V_kV_{se} \sin \varphi_{se}}{jX_{line}}$$

The shunt unit is shown in Fig. 4.

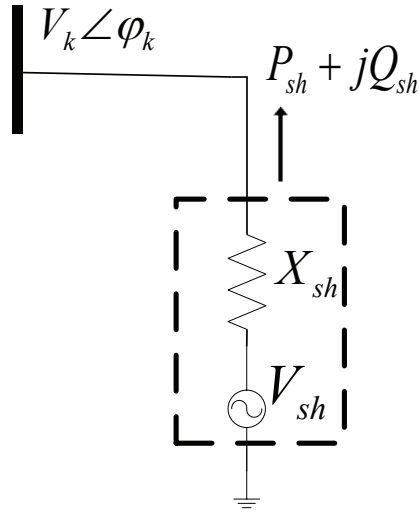


Figure 4 Shunt unit

The total power flow through the shunt unit is summarized in (15)

$$\begin{aligned}
 P_{sh} + jQ_{sh} &= V_k I_{sh}^* \\
 &= \frac{V_k V_{sh} \cos \varphi_{sh}}{jX_{sh}} - j \frac{V_k^2 - V_k V_{sh} \sin \varphi_{sh}}{jX_{sh}}
 \end{aligned} \tag{15}$$

Similar to the series unit, this section can also be defined with an ideal controllable voltage source V_{sh} and a reactance X_{sh} .

For both units, the firing angles are updated using (16):

$$a^{t+1} = a^t \pm \Delta a \tag{16}$$

where Δa is the change in firing angle both decrement and increment, a is the firing angle, and t is the iteration number.

PROPOSED METHOD

The designed UPFC structure comprised two units: System data were collected by the hardware section designed using the MATLAB / Simulink platform and the code-based section was based on the NR power flow algorithm to optimize and regulate the system created by MATLAB editor. The code-based section also consisted of two sub-sections for data

preparation and NR algorithm. Both sections were obtained using the equations given in sections II and III.

Power flow algorithm includes a subprogram used for forming the bus admittance matrix (Y-matrix) in four steps:

-
- Step 1.* Collect bus data and line data
 - Step 2.* Initialize Y-bus
 - Step 3.* Form the diagonal elements
 - Step 4.* Form the off - diagonal elements
-

The proposed method was designed for online use. Therefore, a timer sub-program was added to allow repeating power flow analysis at pre-set intervals to observe the whole system periodically. Figure 5 presents the general flowchart of the NR power flow analysis including the data preparation section and timer sub-program.

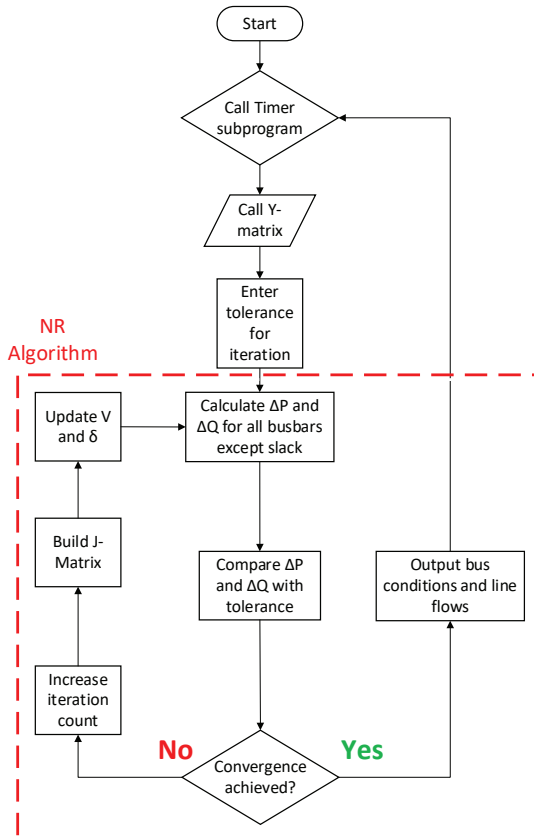


Figure 5 NR Flowchart

An integrated system incorporating the NR algorithm and data collecting units was created using MATLAB/Simulink. The structure of the designed system is shown in Figure 6, and the internal structure of the main controller block is given in Figure 7.

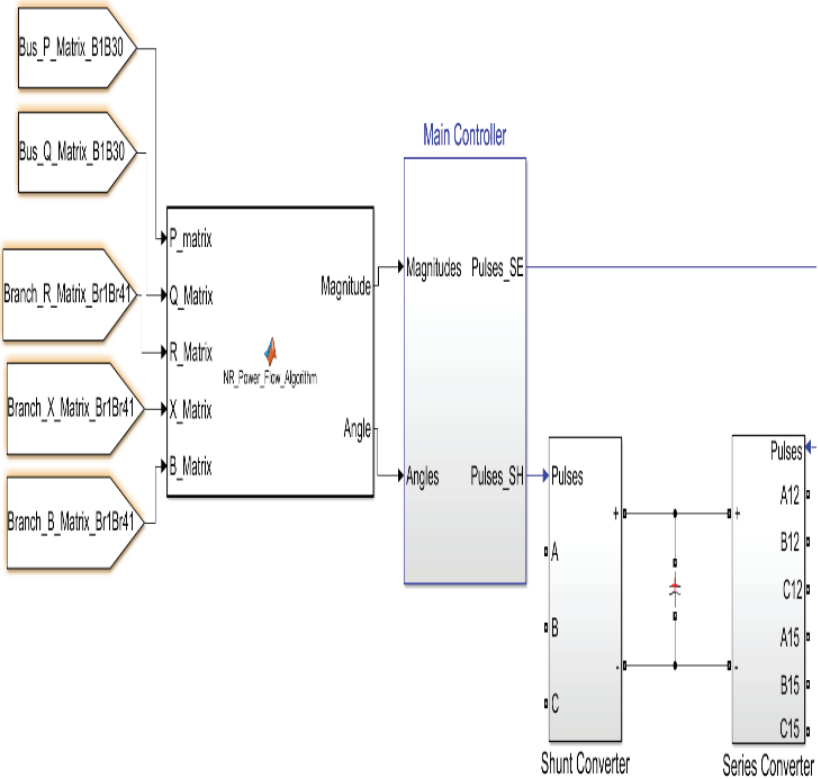


Figure 6 Proposed system

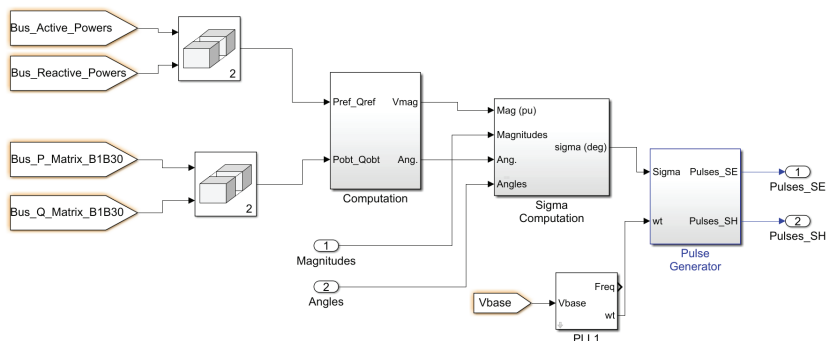


Figure 7 Main controller

The branch data and system power values were fed into the system to be used in the power flow algorithm block presented in Figure 6. The busbar and line parameters of P, Q, R, X and B values collected from the system were converted to the matrix form and used by the power flow algorithm block to generate the actual magnitude and angle values. These values were compared to the reference values in the main controller generated by the computation block given in Figure 7. The sigma value was calculated using this comparison and the pulse generator adjusted the series and shunt pulses. The series and shunt converters were connected via a capacitor with a value of 5 millifarads. The active trigger time of pulses was determined by the comparison of the obtained and reference values. Since the proposed method used the overall system data, the pulses were adjusted more accurately (Efe 2018 & Efe 2018).

The system capabilities were tested on different operating conditions of power system. These processes were detailed in the following sections.

LINE FLOW REGULATION

Major losses occur at the transmission section of power systems. One of the vital studies concerning power utilities is the improvement of transmission conditions. FACTS devices are most effective in improving the transmission line losses (Hingorani et al., 1999). On the other hand, researchers have made progress in estimating such losses for better results and precautions. Classical calculations are inadequate due to the instantaneous changes during operation. This requires interfering with analyses momentarily for better regulation. Therefore, the proposed study focused on online regulation of line active and reactive power flows.

A computer with an Intel Core i7 processor and 16 GB RAM was used to simulate the proposed model under MATLAB/Simulink platform. Three cases were used to test the proposed system. In the first case, the standard IEEE-30 bus system was used, and it was aimed to validate the proposed system based on a pre-known value. The results of proposed method were compared with the results of (PowerWorld Simulator 2020; Al-Roomi 2015) for simulation and (Zimmerman et al., 2011) for code based sections, and convergence was achieved. Simulations for steady state operating can be repeated by using (PowerWorld Simulator 2020 & Al-Roomi 2015).

As the system was designed to be used in dynamic systems, after this validation process, the behavior of this system under line fault conditions was determined in the second case, and the generator outage conditions were tested in the third case. Details were given in following subsections.

A- Validation on the Standard IEEE-30 Bus System

In this case, the standard IEEE-30 bus system proposed in (Christie 1993) was used for the comparison of the UPFC-connected system results. The designed UPFC was placed between buses 12 and 15 at branch 18. This structure is illustrated in Figure 8.

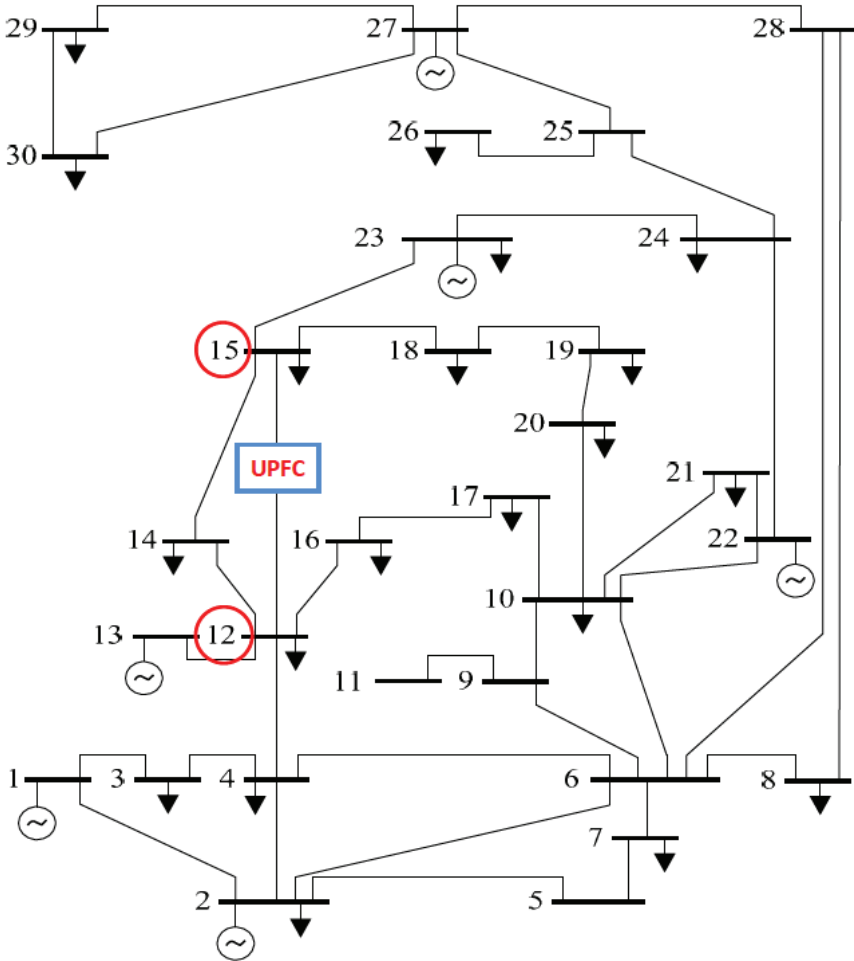


Figure 8 IEEE-30 bus system with UPFC placement

The proposed method was validated by two ways: First, the bus voltage magnitudes per unit were compared to the values given in the literature (Figure 9). The base apparent power of the system was 100 MVA. In the second step, the line active and reactive losses of the selected lines were compared (Table 1).

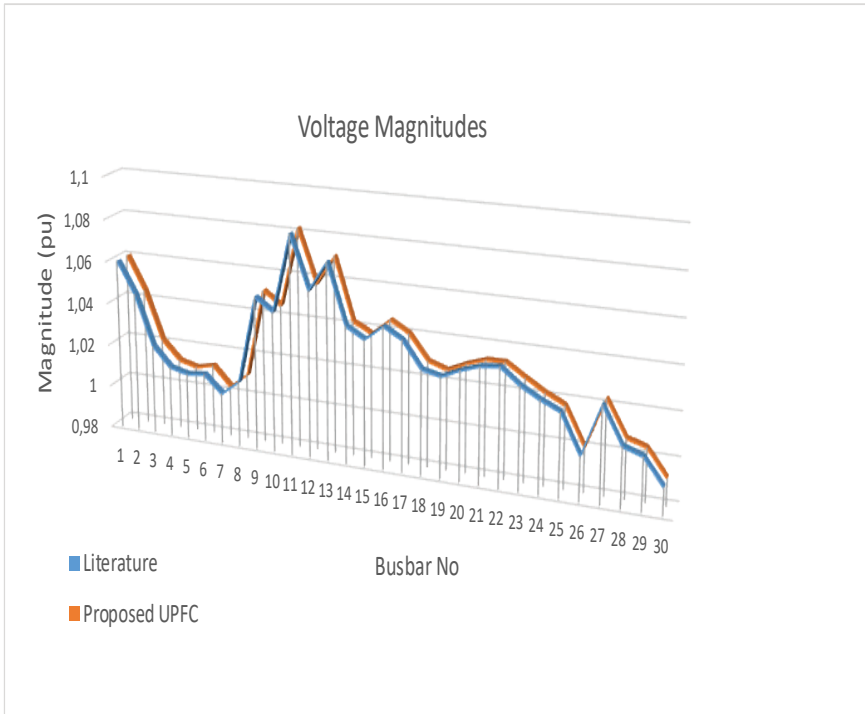


Figure 9 Voltage magnitude comparison

Table 1 Loss Comparison of Selected Lines

Between Buses	Iterative Method		Proposed Method	
	Active Power Loss (MW)	Reactive Power Loss (MVar)	Active Power Loss (MW)	Reactive Power Loss (MVar)
1-2	5.213	15.61	5.202	14.88
1-3	3.108	11.36	3.089	10.87
2-4	1.018	3.1	1.011	3.06
2-5	2.943	12.36	2.931	11.87
2-6	1.946	5.9	1.929	5.846
4-6	0.632	2.2	0.627	2.18
4-12	0	4.69	0	4.53
6-7	0.381	1.17	0.376	1.144
6-9	0	1.62	0	1.57
12-15	0.217	0.43	0.216	0.424
12-16	0.054	0.11	0.054	0.109
16-17	0.008	0.03	0.008	0.029

According to the comparisons shown in Fig. 10 and Table 1, the proposed model could be accepted as validated since the results were consistent with those of the NR based system described in the literature. In

addition, the proposed method was successful at decreasing power losses, especially reactive power losses. This proves that the proposed system is appropriate for use in power flow studies.

B- Line Fault Conditions

Determination of transmission line faults is important because of correcting permanent faults in a short time. In addition to their adverse effects on operation, these faults can also affect the parameters concerning planning section in power flow analysis. Different events, such as insulation breakdown and lightning are common causes of power system faults. Line faults occur in a very short period; therefore, their distortions cannot always be observed in detail.

Failure in a line due to a fault condition in a power system causes the transferring active and reactive power flows of that line to unfaultry lines. Unfortunately, this transfer cannot be linear. In this case, the major advantage of the proposed method is that line loadings can be optimized. Thus, both line losses can be minimized and busbar loading values can be adjusted.

One of the most important advantage of the proposed method is that it allows observing and regulating possible effects of line faults on a power system. According to the validation of the method for such conditions, a line fault was assumed to occur on the line between buses 4 and 6.

The system was simulated for 5 seconds with the fault starting at the 1.7th second and ending at the 3.7th second. For a fast response, the timer subprogram was adjusted to 0.5 seconds.

The system performance was expected to be observed via line loading values from buses 2 to 6. When the system was simulated, the loading value was increased from 89% to 145.9%. Addition of the developed UPFC structure to the system, regulated the line loadings and decreased this value to 125% for fault conditions. According to this decrement, the line active power losses were decreased from 3.2278 MW to 2.7718 MW and the reactive power losses were reduced from 9.7862 MVAR to 8.4036 MVAR. The optimized power losses for the other lines are given in Table 2 in relation to the data in Table 1.

These values are the most significant ones that obtained for such condition. For safety and to avoid any possible blackout situation, maximum loading was limited to 125% at all lines.

Table 2 Line Loss Comparison for Line Fault Conditions

Between Buses	Line Loading value for normal operation conditions (%)	Line Loading value during fault (%)	Line Loading value during fault with UPFC (%)	Losses During Fault Without Proposed UPFC		Losses During Fault With Proposed UPFC	
				Active Power Loss (MW)	Reactive Power Loss (MVA _r)	Active Power Loss (MW)	Reactive Power Loss (MVA _r)
1-2	126.7	144.4	124.8	6.0114	18.0006	5.2074	15.5931
1-3	63.7	48.4	54.6	2.3894	8.7333	2.7016	9.8747
2-4	64.6	23.4	41.1	0.3731	1.1362	0.6568	2.0002
2-5	60.8	73.8	59.7	3.6144	15.1798	2.9306	12.3078
4-6	81	0	0	0	0	0	0
4-12	71.5	103.9	75.2	0.0000	6.8957	0.0000	5.00238
6-7	29.1	16.8	25.5	0.2226	0.6834	0.3386	1.03974
6-9	44.5	29.3	33	0.0000	1.0792	0.0000	1.21832
12-15	56.6	81	59.4	0.3142	0.6226	0.2310	0.45765
12-16	47.2	103.3	75.9	0.1196	0.2436	0.0881	0.17938
16-17	23.7	81.8	66.3	0.0279	0.1048	0.0227	0.08511

The regulation process was performed by regulating the busbar voltage amplitudes. This procedure is also the purpose of all power flow analysis algorithms.

Busbar voltage comparisons are given in Table 3 to offer a clear understanding of the effects of the proposed method on the operational system values.

Table 3 Busbar Average Voltage Amplitudes comparison for fault conditions

Bus No	Normal Operating	Without UPFC	With UPFC
1	1.0600	1.0600	1.0600
2	1.0431	1.0384	1.0429
3	1.0207	1.0207	1.0206
4	1.0118	1.0111	1.0115
5	1.0100	1.0071	1.0097
6	1.0103	1.0044	1.0100
7	1.0024	0.9974	1.0022
8	1.0100	1.0051	1.0098
9	1.0509	1.0454	1.0506
10	1.0451	1.0363	1.0433
11	1.0820	1.0820	1.0820
12	1.0571	1.0577	1.0565
13	1.0710	1.0710	1.0710
14	1.0423	1.0423	1.0423
15	1.0377	1.0348	1.0369
16	1.0444	1.0386	1.0441
17	1.0399	1.0325	1.0393

18	1.0282	1.0228	1.0267
19	1.0257	1.0190	1.0246
20	1.0297	1.0224	1.0288
21	1.0327	1.0240	1.0313
22	1.0333	1.0246	1.0324
23	1.0272	1.0221	1.0260
24	1.0216	1.0141	1.0202
25	1.0173	1.0077	1.0157
26	0.9997	0.9899	0.9960
27	1.0232	1.0127	1.0202
28	1.0068	1.0011	1.0064
29	1.0034	0.9926	1.0016
30	0.9919	0.9810	0.9889

C- Generator Outage Conditions

In modern power systems, loads are supplied by multi nodes. These supplements can be conventional, such as hydro and thermal or distributed generators; e.g., renewable energy sources. For both systems, any outage that is possible to occur at a generating unit directly affects the system in proportion to the capacity of generating unit. For the validation of the proposed method in the third case, generator 2 was disconnected from the power network.

It took 131 milliseconds for five iterations to reach convergence in the case of generator outage. The convergence graphs for the line fault, generator outage and normal operating conditions are given in Fig. 10.

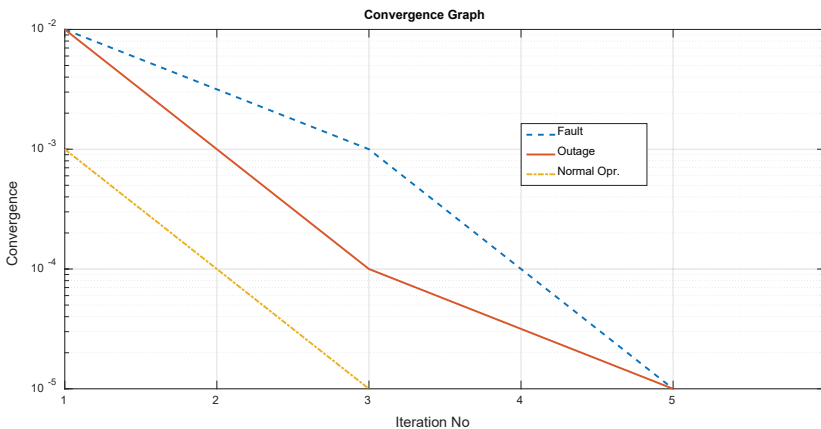


Figure 10 Convergence graph

According to the purpose of study, an outage was supposed to occur at generator 2 to observe the optimization ability of the proposed method under these conditions. Similar to the line fault conditions, the system was simulated for 5 seconds and the fault started at the 1.7th second and ended at the 3.7th second. For a fast response, the timer subprogram was adjusted to 0.5 seconds.

The comparison of line losses is given in Table 4. The table also includes the line loading values for a clear comparison. The simulation results demonstrate the system performance during outage.

Table 4 Line Loss Comparison for Generator Outage Conditions

Between Buses	Line Loading value during outage (%)	Line Loading value during outage with UPFC (%)	Losses During Outage Without Proposed UPFC		Losses During Outage With Proposed UPFC	
			Active Power Loss (MW)	Reactive Power Loss (MVar)	Active Power Loss (MW)	Reactive Power Loss (MVar)
1-2	151.7	125	6.3159	18.9125	5.2157	15.6181
1-3	70.1	66.1	3.4610	12.6501	3.2707	11.9545
2-4	61	62	0.9727	2.9621	0.9908	3.0173
2-5	61.4	60.9	3.0074	12.6305	2.9895	12.5552
2-6	87.7	88.3	1.9404	5.8830	1.9580	5.9363
4-6	86.1	84	0.6798	2.3663	0.6647	2.3137
4-12	70.8	71	0.0000	4.6993	0.0000	4.7230
6-7	30.5	29.8	0.4041	1.2409	0.3957	1.2151
6-9	45.9	44	0.0000	1.6909	0.0000	1.6244
12-15	58.4	57.1	0.2266	0.4490	0.2220	0.4399
12-16	50.1	48	0.0580	0.1181	0.0557	0.1134
16-17	26.4	24.3	0.0090	0.0338	0.0083	0.0312

CONCLUSION

This study proposed a simple and effective line loading regulation and loss minimization technique for dynamic power systems by using FACTS devices. Regulator was designed with UPFC that incorporates with NR algorithm. The method was based on the NR power flow analysis algorithm because of its rapid convergence characteristic.

Proposed method can be summarized as follows; data were collected from all busbars that necessary for NR algorithm. Collected data were formed as matrix form for processing and NR power flow algorithm performed. Amplitude and angle values, which are output of algorithm, were sent to main controller. These parameters were compared with reference values in main controller. Series and shunt pulses were generated for UPFC by this comparison. Reference data are nominal system operating values.

Proposed method differs from previous studies by using all over system data to avoid any calculation errors and contains an algorithm that repeating in a sequence for continuous optimization.

In addition, this study has significant advantages of using all system data and performing power flow analysis periodically by timer subprogram

to determine system changes and regulate them. This approach also allows regulating system in case of any fault type and location.

As the purpose of study, proposed method was tested on two cases of line fault and generator outage after validation, and the system showed satisfactory performance on the decrement of transmission line losses. Another advantage of the developed system is that it can be adapted to any number of buses, which means it has a general design.

REFERENCES

- Cengiz, Ç., Kaynaklı, M., Gencer, G., Eren, M., Yapıcı, İ., Yıldırım, S. & Cengiz, MS. 2017. Selection Criteria and Economic Analysis, International Conference on Multidisciplinary, Science, Engineering and Technology Bitlis Book of Abstracts pp. 27-29.
- Albatsh, F.M., Mekhilef, S., Ahmad, S. & Mokhlis, H. 2017. Fuzzy Logic Based UPFC and Laboratory Prototype Validation for Dynamic Power Flow Control in Transmission Lines. *IEEE Transactions on Industrial Electronics* 64 (12): 9538-9548.
- Kocaman, B. & Abut, N. 2015. The Role of Energy Management in Microgrids with Hybrid Power Generation System. *Bitlis Eren University Journal of Science and Technology*, 5 (1): 31-36.
- Bakır, H., Öztürk, A. & Tosun, S. 2018. Investigation of Power Flow Effect of Serial and Parallel FACTS Devices. *Balkan Journal of Electrical and Computer Engineering* 6: 6-11.
- Kocaman, B. & Abut, N. 2020. The Role of Static VAR Compensator at Reactive Power Compensation. *European Journal of Technique* 10 (1): 143-152.
- Ikbal, A., Aftab, M.A., Hussain, S.M.S. & Gupta, S. 2019. Software defined networks for smart substations in an active distribution system. *Journal of Engineering Research* 7 (1): 1-11.
- Yıldırım, S., Yapıcı, İ., Atiç, S., Eren, M., Palta, O., Cengiz, Ç., Cengiz, MS. & Yurci, Y. 2017 Numerical Analysis of Productivity and Redemption Periods in Illumination, *Imeset Book of Abstracts, Int. Mult. Sci. Eng. Tech* pp. 12-14.
- Cengiz, MS., Eren, M., Cengiz, Ç., Yıldırım, S., Yapıcı, İ., Yurci, Y., Atiç, S. & Palta, O. 2017. Numerical analysis of warming and warming problem in LED lamps. *Imeset International Conference Baku Book of Abstracts*, 12-14 July 2017. Baku
- Haddadi A.M. & Kazemi, A. 2011. Optimal Power Flow Control by Rotary Power Flow Controller. *Advances in Electrical and Computer Engineering* 11 (2): 79-86.
- Li, N., Xu, Y. & Chen H. 2000. FACTS-Based Power Flow Control in Interconnected Power Systems. *IEEE Transactions on Power Systems* 15 (1): 257-262.
- Gotham, D.J. & Heydt, G. T. 1998. Power Flow Control and Power Flow Studies for Systems with FACTS devices. *IEEE Transactions on Power Systems* 13 (1): 60-65.

- Allaoua, B. & Laoufi, A. 2009. Optimal Power Flow Solution Using Ant Manners for Electrical Network. *Advances in Electrical and Computer Engineering* 9 (1): 34-40.
- Farag, H.E., El-Saadany, E. F., El Shatshat, R. & Zidan, A. 2011. A generalized power flow analysis for distribution systems with high penetration of distributed generation. *Electric Power Systems Research* 81 (7): 1499-1506.
- Haque, M.H. 2000. A general load flow method for distribution systems. *Electric Power Systems Research* 54 (1): 47-54.
- Li, H., Zhang, A., Shen, X. & Xu J. 2014. A load flow method for weakly meshed distribution networks using powers as flow variables. *International Journal of Electrical Power and Energy Systems* 58: 291-299.
- Li, H., Jin, Y., Zhang, A., Shen, X., Li, C. & Kong, B. 2016. An improved hybrid load flow calculation algorithm for weakly-meshed power distribution system. *International Journal of Electrical Power and Energy Systems*, 74: 437-445.
- Ghatak, U. & Mukherjee, V. 2017. An improved load flow technique based on load current injection for modern distribution system. *International Journal of Electrical Power and Energy Systems* 84: 168-181.
- Bhullar, S. & Ghosh, S. 2017. A novel search technique to solve load flow of distribution networks. *Journal of Engineering Research* 5 (4): 59-75.
- Pourbagher, R., & Derakhshandeh, S. Y. 2018. A powerful method for solving the power flow problem in the ill-conditioned systems. *International Journal of Electrical Power and Energy Systems* 94: 88–96.
- Alamelu, S., Baskar, S., Babulal, C.K. & Jeyadevi, S. 2015. Optimal siting and sizing of UPFC using evolutionary algorithms. *International Journal of Electrical Power and Energy Systems* 69: 222-231.
- Shojaeian, S. & Soltani, J. 2013. Low frequency oscillations damping of power system including unified power flow controller based on adaptive backstepping control. *Revue Roumaine Des Sciences Techniques* 58 (2): 193-204.
- Shahgholian, G., Mahdavian, M., Janghorbani, M., Eshaghpour, I. & Ganji, E. 2017. Analysis and Simulation of UPFC in Electrical Power System for Power Flow Control. *Proceedings of the 14th International Conference on Electrical Engineering/Electronics, Computer, Telecommunications and Information Technology (ECTI-CON)*. Phuket, Thailand.
- Nahak, N. & Mallick, R.K. 2017. Damping of power system oscillations by a novel DE-GWO optimized dual UPFC controller. *International Journal Engineering Science and Technology* 20 (4): 1275-1284.

- Sarker, J. & Goswami, S. K. 2014. Solution of multiple UPFC placement problems using Gravitational Search Algorithm. *International Journal of Electrical Power and Energy Systems* 55: 531-541.
- Hashemi, Y., Kazemzadeh, R., Azizian, M. R. & Yazdankhah, A. S. 2014. Concurrently attuned design of a WADC-based UPFC PSDC and multiinput PSS for improving power system dynamic performance. *Turkish Journal of Electrical Engineering and Computer Sciences* 22 (2): 243-261.
- Morsli, S., Tayeb, A. & Mouloud, D. 2012. A robust adaptive fuzzy control of a unified power flow. *Turkish Journal of Electrical Engineering and Computer Sciences* 20 (1): 87-98.
- Ghatak, U., & Mukherjee, V. 2017. A fast and efficient load flow technique for unbalanced distribution system. *International Journal of Electrical Power and Energy Systems* 84: 99-110.
- Lei, J., An, T., Du, Z. & Yuan, Z. 2017. A General Unified AC / DC Power Flow Algorithm with MTDC. *IEEE Transactions on Power Systems* 32 (4): 2837-2846.
- Mehrjerdi, H. & Ghorbani, A. 2017. Adaptive algorithm for transmission line protection in the presence of UPFC. *International Journal of Electrical Power and Energy Systems* 91: 10-19.
- Tumay, M. & Vural, A. M. 2004. Analysis and Modeling of Unified Power Flow Controller: Modification of Newton – Raphson Algorithm and User-Defined Modeling Approach for Power Flow Studies. *Arabian Journal for Science and Engineering* 29 (2): 135–153.
- Ambriz-Pérez, H., Acha, E., Fuerte-Esquivel, C.R. & De la Torre, A. 1998. Incorporation of a UPFC model in an optimal power flow using Newton's method. *IEE Proc. - Gener. Transm. Distrib.* 145 (3): 336-344.
- Kumar, B.V. & Srikanth, N.V. 2017. A hybrid approach for optimal location and capacity of UPFC to improve the dynamic stability of the power system. *Applied Soft Computing* 52: 974-986.
- Sereeter, B., Vuik K., & Witteveen, C. 2017. Newton power flow methods for unbalanced three-phase distribution networks. *Energies* 10 (10): 1-20.
- Powell, L. 2004. *Power System Load Flow Analysis*. McGraw-Hill.
- Acharjee, P. 2016. Optimal power flow with UPFC using security constrained self-adaptive differential evolutionary algorithm for restructured power system. *International Journal of Electrical Power and Energy Systems* 76: 69-81.
- Efe, S.B. 2018. UPFC Based Real-Time Optimization of Power Systems for Dynamic Voltage Regulation. *Computer Modeling in Engineering & Sciences* 116 (3): 391-406.

- Efe, S.B. 2018. Jacobi Method based unified power flow controller design for dynamic power systems. Dicle University Journal of Engineering 9 (2): 601-607.
- Hingorani, N.G. & Gyugyi, L. 1999. Understanding FACTS: concepts and technology of flexible AC transmission systems. IEEE Press, NY.
- PowerWorld Simulator Version 21 Glover, Overbye & Sarma Edition, August 31, 2020.
- Al-Roomi, A.R. (2015). Power Flow Test Systems Repository <https://al-roomi.org/power-flow>.
- Zimmerman, R.D., Murillo-Sanchez, C.E. & Thomas R.J. 2011. Matpower: Steady-State Operations, Planning and Analysis Tools for Power Systems Research and Education. IEEE Transactions on Power Systems 26 (1): 12-19.
- Christie, R. 1993. Power Systems Test Case Archive.

Chapter 6

GRAVITATIONAL WATER VORTEX POWER PLANTS



Ahmet TEBER¹

¹ Assist. Prof. Dr. , Bayburt University, Technical Scientific Vocational School, Department of Electricity and Energy, Bayburt, Turkey, ahmetteber@bayburt.edu.tr, ORCID: 0000-0002-7361-2302. This chapter has been supported by Bayburt University Scientific Research Projects Coordination Department. Project No. 2019/01-69001-01

INTRODUCTION

Besides increasing carbon emissions, growing energy demand, and the cost for establishing energy systems against to reduction of fossil fuels have lead policymakers and engineers to consider renewable and sustainable resources for energy generation. Based on OECD energy reports between 2000-2019 in the OECD countries, renewable energy production has been increasing from 6,04% to 10,81% of primary energy supply (OECD 2020) [1]. Hydropower corresponds to 15,8% out of 26,2% of predictable renewable energy portion of worldwide electricity generation as of the beginning 2019 (REN21 2020) [2]. Significant developments in the hydropower sector by 2060 suggest that more than fifty percentage of energy consumption of the world will be reinforced by renewable resources (Ak, Kentel, and Kucukali 2017) [3]. Developments in the history of water wheels brought researchers to find out newer hydropower technologies. Since most of the larger traditional hydropower resources have already been reached approximately the best technology, with that perspective, the development of small and low head hydropower resources is under focus by researchers. Therefore, the classification of hydropower plants is required to understand what point it has ended so far. Although no agreement on the small hydropower definition in European Union (EU) members has been observed, it is accepted that the installed power is 10 MW or less than 10 MW according to the classification established by the European Small Hydropower Association (ESHA) (Kosnik 2010).

According to the classification of hydropower systems (HPS), HPS are classified into two categories as potential and type of hydropower. Under the type of HPS, impoundment type and run-off river type come into prominence. The run-off river type does not require significant water storage in a reservoir with the help of natural conditions of sufficient water flow and volume exists. Depending on advantages and disadvantages of HPS as a trade-off matter, run-of-river systems are a very conservationist alternative to generate electricity for either on-grid or off-grid systems, which are likely under the attention of researchers and people who lives in rural areas nowadays.

A famous example of run-off-river systems is the gravitational water vortex power plant (GWVPP). There exist applications and research studies regarding GWVPP using different strategies on particular aspects. They are not only theoretical one that consists of numerical studies but also experimental one that covers laboratory and commercial installations relying on numerical results by Computational Fluid Dynamics' (CFD) approaches.

This chapter provides a basic tutorial and an installation process on the fundamental aspects of GWVPP systems including fundamentals of the technology, which is required supporting proposals. Besides that, general

approach for CFD modeling with an example of GWVPP velocity and pressure simulation has been done.

DEFINITION OF GRAVITATIONAL WATER VORTEX POWER PLANT

GWVPP is sustainable & renewable energy resources as an emerging technology, which generates energy. It is classified under micro-scale hydropower including vortex turbine system. The technology especially built right next to a stream based on a circular basin with a central orifice by using an upstream and an outlet canals. General view including turbine-generator system is represented in Figure 1.

Generating a stable water vortex above an orifice drives a water turbine, which is positioned at a suitable height. Therefore, this system is able to convert energy in a moving flow into rotational energy using a low head up to 5m, although most convenient researches are built between 0.5m and 3m (Dhakal, R., Shrestha, S., Neupane, H., Adhikari, S. and Bajracharya 2020).

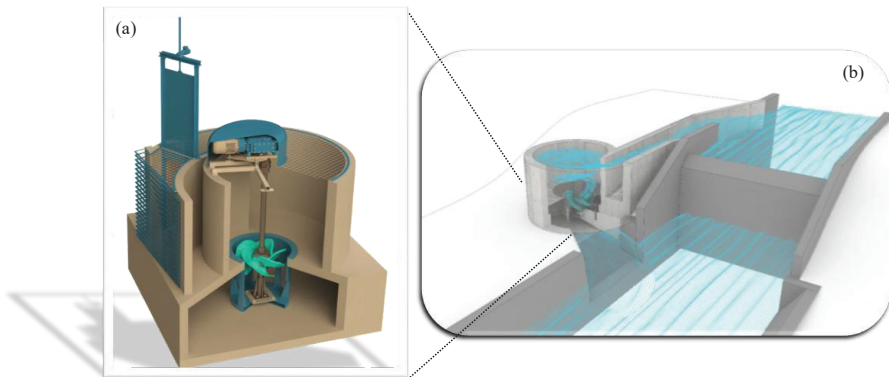


Figure 1. *Gravitational Water Vortex Power Plant (a) General Illustration (Cooke 2018), (b) Turbine-Generator System (Kumar 2020)*

System Description

A GWVPP system as installed either on-grid or off-grid can build using facilities that requires comprehensive scheduling, detailed construction, and well-organized operation. A typical schematic of GWVPP is presented in Figure 2.

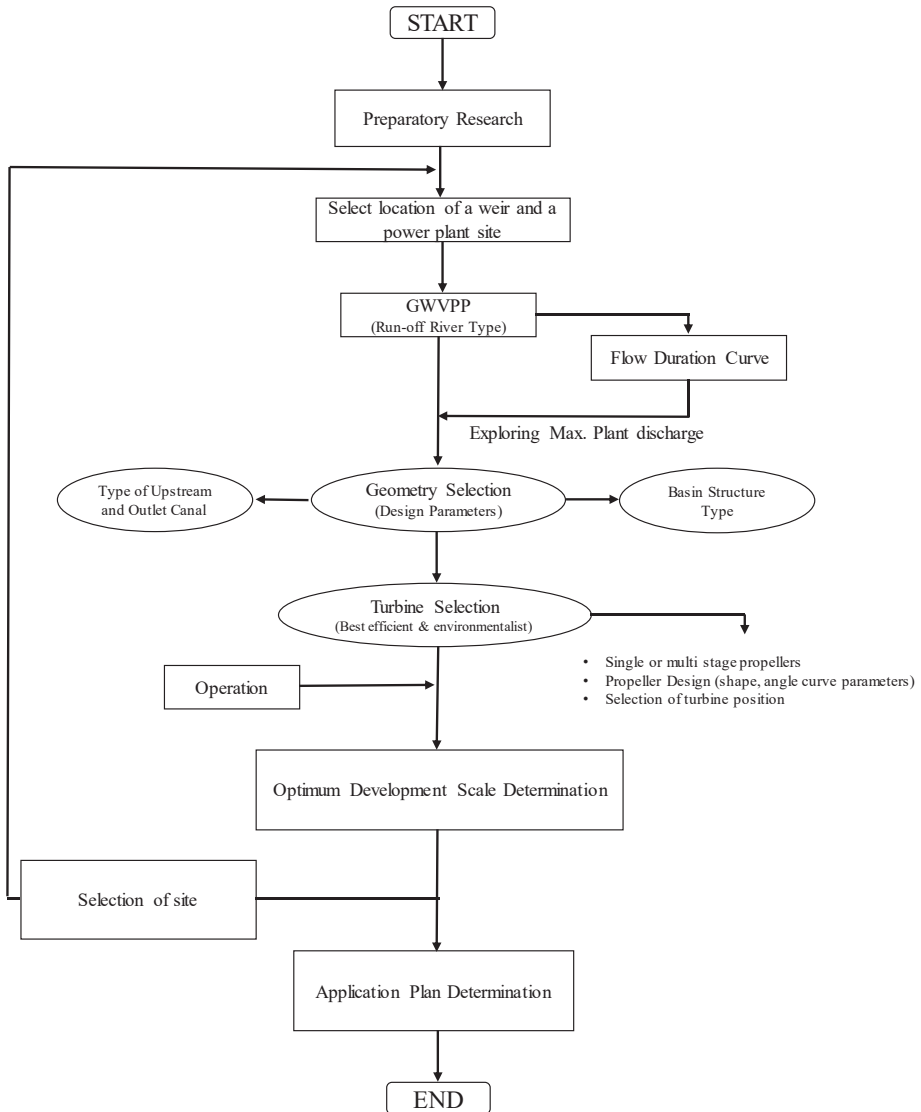


Figure 2. Flow Diagram of a Gravitational Water Vortex Power Plant

FUNDAMENTALS

Free-surface vortex flows are related to emerging technologies such as a GWVPP. The water flow produces a free-surface non-rotational vortex of a hydroelectric turbine located at the center of a basin structure. In order to generate power, a momentum difference is then created by placing a load between turbine blade and vortex flow. Vortexes must be carefully studied during the operation of hydroelectric power plants so as not to cause very harmful consequences. GWVPPs are modeled by CFD modeling tools to

generate power. Yet, simple analytic methods are still vital to provide analytical and numerical approaches for design choices and predictions. Therefore, at that point, the water vortex theory can be started with the classification of vortices. The other subtitles will be covering the other important parameters of vortices.

Vortices Systematization

A circulation determines the vortex strength known as the vortex behavior.

$$\Gamma = 2nrV_{\theta} \quad (1)$$

where Γ is influenced by three parameters as basin structure geometry, Fr (Froude number), S/D (the relative submergence) (Hamed Sarkardeh, Amir Reza Zarrati, Ebrahim Jabbari 2011). An important parameter for generation free surface vortex is an air-core that is possible formation down the centerline of the vortex. Therefore, G.E. Hecker is classified free surface vortex with an increment of water density in six categories as (i) surface dimple, (ii) surface swirl, (iii) coherent swirl, dye core up to intake, (iv) vortex that attracts floating debris, but not air, (v) vortex that pulls air bubbles into inlet, and (vi) full air-core for intake (Hecker 1987). It was found that the possible impact increases from vortex type (i) through vortex type (vi) associated with full air-core.

Due to reliability and safety, which comes first to consider/generate safe electricity, Sarkardeh et al. later distinguished free surface vortices into three essential categories according to the effect on the intake. The following classification was represented as following contents: Strongest type (Vortex A): Air bubbles extend from the water surface towards the intake. Due to the formation of a steady air-core at vortex midpoint, such vortex, which increases the air steady transmission to intake should be avoided. Stronger type (Vortex B): The vortex rotation extends downward so that it can pull debris together. Safest type accepted by researchers (Vortex C): It is related a slight dimple and the weak rotation.

Theoretical Vortices' Models

A vortex is defined as the movement of a large number of material particles around a concentric point (Lugt 1983; Mulligan 2015). Also, Vortex flow is described in cylindrical coordinates at radial spot (r) from the rotation center. Here, V_{θ} , V_r , and V_z are defined the tangential, radial, and axial velocities, respectively. In a basin structure of GWVPP without an impeller, a free-surface vortex creates fluid spin around a common center that coincides with an orifice at the basin structure base.

Researchers have been working on physical models including mathematical equations to investigate the mechanisms under free-surface vortices. In vortex theory, a vortex consists of concentric circular flow lines around a point. At that point, the velocity is constant along any streamline whereas the velocity varies between streamlines. If there is no applied outer force to the system except gravity, the flow turns becoming irrotational formation (H. A. Einstein 1951). Therefore, the tangent velocity V_θ increases inversely proportional with the radius because of the angular momentum. This is accepted as the normalized form of the potential vortex model. M. K Domfeh et al. (Domfeh et al. 2020) summarized vortex models characteristics using the equations by various authors.

Table 1 represents the vortex models according to the creation year below:

Table 1. *Analytic Vortex Models*

Sources	Model Equations
Einstein and Li (H. A. Einstein 1951)	$V_{\theta} = \frac{\Gamma}{2\pi r}$
Rankine (WJM Rankine 1872)	$V_{\theta} = \begin{cases} \frac{\Gamma}{2n} \frac{r}{r_m^2}, & r \leq r_m \\ \frac{\Gamma}{2n}, & r > r_m \end{cases}$
Hite and Mih (Hite and Mih 1994)	$V_{\theta} = \frac{\Gamma}{2nr_m} \frac{2R}{1+2R^2},$ $V_r = \frac{-v_e}{r_m} \frac{8R}{1+2R^2},$ $V_z = v_e \frac{z}{r_m^2} \frac{16}{(1+2R^2)^2},$ $\frac{H_r - H_0}{H} = \frac{2R^2}{1+2R^2}$
Burgers and Rott (Rott 1959)	$V_{\theta} = \frac{\Gamma}{2nr} \left[1 - e^{-\left(\frac{r}{r_0}\right)^2} \right],$ $r_0 = 2 \left(\frac{\nu}{a} \right)^{1/2} \text{ and } a = \frac{\partial V_z}{\partial z}$
Odgaard (Odgaard 1986)	$V_{\theta} = \frac{\Gamma}{2nr} \left[1 - e^{-1.25 \left(\frac{r}{r_m}\right)^2} \right],$ $V_r = -k_1 r, \quad V_z = 2k_1 z$
Rosenhead (Rosenhead 2011)	$V_{\theta} = \frac{\Gamma}{2n} \left(\frac{r}{r_c^2 + r^2} \right)$
Vatistas (Vatistas, Kozel, and Mih 1991)	$V_{\theta} = \frac{\Gamma}{2nr_m} \frac{R}{\sqrt{1+R^4}},$ $\frac{H_r - H_0}{H} = \frac{2}{n} \arctan(R^2)$
Anwar (H. O. Anwar 1965)	$V_{\theta} = v_{\theta_0} \sqrt{1 - 2 \frac{1 - \sqrt{1 - (2n)^2}}{1 + \sqrt{1 + (2n)^2}} \log_e \frac{\tan \varphi}{\tan \varphi_0}}$ $, \quad \varphi = \tan^{-1} \left(\frac{r}{z} \right), n = 0.498$

Chen (Chen et al. 2007)

$$V_{\theta} = \frac{\Gamma}{2nr_m} \frac{2R}{1+2R^2} (1+ah_1z'),$$

$$V_r = \frac{v}{r_m} \frac{8R}{1+2R^2} [1+ah_1z'],$$

$$V_z = \frac{16v_e}{r_m^2 (1+2R^2)^2} \left[\frac{(1+ah_1z')}{a} + (1+ah_1z') \right]$$

$$, \frac{H_r - H_0}{h_1} = \frac{2r^2}{r_m^2 + 2r^2} (1+az)^2$$

Wang (Wang, Jiang, and Liang 2011)

$$V_{\theta} = \frac{\Gamma}{2nr_m} \frac{m_1 R}{1+m_2 R+R^2},$$

$$V_r = \frac{-Q}{4ndr_m} \frac{4 \times 0.928 R}{1-0.7R+R^2},$$

$$V_z = \frac{-Q}{4nd} \frac{3 \times 0.928}{(1-0.7R+R^2)^2},$$

$$\frac{H_r}{H_{\infty} - H_0} = \frac{R^2 + 0.35R}{R^2 + 0.35R + 1},$$

$$m_1 = 0.928 \text{ and } m_2 = -0.7$$

When considering some of parameters used for analytic vortex models are Q is the discharge and d is the orifice diameter, a is the approach flow factor when Γ_v is the strength of vortex. ω is vortex angular speed at center, r and r_m are the radius and the radius when tangential velocity reaches maximum, respectively. v and v_e are the kinematic and effective viscosity, respectively. Γ denotes the outer zone circulation, a is an axial gradient, k_1 is the proportionality factor. H , H_r , and H_0 is the water head, the water surface head at r , the water surface elevation at the center, in that order. H_{∞} is the depth unaffected by the air-core, $R=r/r_m$ is the dimensionless or normalized radius, h , h_0 , h_1 refer to the air core depth (while R approaches infinity), the submergence depth, the total depth of air-core, $z'=z/h_1$.

Dimensionless Analysis

In GWVPP theory, the flow and rotational strength are under authority with the circulation parameter (Γ), which is also related with the approach flow geometry (Mulligan et al. 2019). Therefore, the circulation parameter must be correlated with the inlet width (b), the water depth (h_{in}) and tangential velocity (V_{θ}) at the plant's inlet via $V_{\theta} = (Q/b)h_{in}$. In that way, vortex strength is found as the following expression below:

$$\Gamma_v = \frac{2\pi r_{in} Q}{bh_{in}} \quad (2)$$

After some empirical studies, Mulligan et al. found that a simple relationship for the discharge between the dimensionless parameters under executive by:

$$Q = \frac{k_\alpha}{\left(\frac{5\alpha d}{h_{in}}\right)^{n_\alpha}} \sqrt{gd} \quad (3)$$

Here, k_α and n_α are the supplementary experimental constraints. They are defined as $k_\alpha = -0.12\alpha^3 + 0.79\alpha^2 - 0.62\alpha + 0.36$ and $n_\alpha = 0.05\alpha^2 - 0.39\alpha - 0.55$ for $1.3 \leq \alpha \leq 6.22$. For the dimensional analysis, intake submergence is to play a role affecting the free-surface vortex formation. Studying the relationship between vortex formation and submergence at intake leads engineers to investigate boundaries for designs, where vortices would be harmful on the operation of the hydraulic structure or basin. Therefore, the term of critical submergence is defined as the depth (Domfeh et al. 2020), in which the vortex air-core is developed as a function of various variables such as the intake velocity (V), the intake diameter (D), the intake geometry's measure (L), Γ , the acceleration due to gravity (g), the surface tension (σ), the dynamic water viscosity (μ), and the water density (ρ). There exists a number of empirical and analytical formulas to evaluate critical submergence such as Gordon (Grant 1997), Hecker (Hecker 1987), and Knauss (Knauss J. 1987). The air-vortex, which is related variables above results in relative critical submergence (S_{rc}) as a function of Γ / VD , L / D , the Froude number ($F_r = V / \sqrt{gD}$), the Reynolds number ($R_e = VD / \nu$), and Weber number ($W_e = V(\rho D / \sigma)^{1/2}$). Even though F_r is a prominent parameter for vortex intensity, researchers in fluid dynamics have been working on various equations for the relative critical submergence and other dimensionless parameters including F_r and R_e .

Water Vortex-Turbine Interaction

Revised model of tangential velocity was proposed to clarify stronger axial gradients near the core (Timilsina, Mulligan, and Bajracharya 2018):

$$v_\theta(r) = \frac{\Gamma_v}{2\pi r} \left(1 - \left(\frac{h}{5\alpha d} \right)^{\frac{2r}{d}} \right) \quad (4)$$

where tangential velocity is $v_\theta(r) = \Gamma_v / 2\pi r$ in ideal condition. By substituting this equation from the radial momentum equation (in the Navier-Stokes equations), pressure profile can be achieved by:

$$h_r = h_{in} - \frac{\rho \Gamma^2}{8\pi^2} \left(\frac{1}{r^2} - \frac{1}{r_{in}^2} \right) \quad (5)$$

The equations above can be primarily used for the estimation the velocity ranges near to the core when defining the maximum value of angular velocity to propose turbine component. When turbine impeller is mounted, the GWVPP system can behave quite strangely. A torque is produced via turbine shaft because of a load on a turbine generator. Then, momentum differences are occurred in the velocity field around the propeller. At zero conditions, the torque causes a reduction in the initial water level, which affects overall flow field. For example, reaction turbines are partially based on that feature resulting in head difference with a better performance and power output estimation. That effect can be measured using the equations on vortex models above. While the tangential velocity controls the flow field, the axial velocity signifies a large flow portion around the turbine. The flow can be predicted with continuity feature over the vortex core (or the orifice or turbine intake), which should not be ignored to get maximum efficiency taking into account the turbine shape.

Viscosity Effects, Scale Effects and Surface Tension

Viscous effects can be ignored at high Reynolds number according to the experiences of the most researchers (Gulliver 1983). However, the threshold level (or the highest RE value) can be contradict among different researchers. Anwar et al. completed two studies to observe Reynold number on weak vortex formation and a horizontal flume. The cut-point for the highest value of Reynold number by different researchers are listed in Table 2.

Table 2. *Cut-point for the Highest Reynolds Number*

	Zielinski and Villemonte (P.B. Zielinski , J.R. Villemonte 1968)	Daggett and Keulegan (GH Keulegan 1974)	Anwar(Anwar 2013; Anwar, Weller, and Amphlett 1978)
Re	1x10 ³	3.2x10 ⁴	1x10 ³ 3x10 ³

Since the forces affect vortex characteristics scale differently, the forces of gravitational, viscous, and surface tension between the model and the prototype are need to be checked along similarity related to equality of inertial forces' ratios. Due to the Reynolds number, it is difficult to accommodate Froude and Weber number scaling, simultaneously. Scaling is used with one of these parameters, assuming the inequality of the other force ratios are ignored.

At intake, surface tension influences developing the free surface vortices. It is assumed by the researchers that surface tension is negligible

beyond certain limits. At the conditions of $3 \times 10^3 < Re < 7 \times 10^5$, $120 < \rho(V^2 D / \sigma) < 34000$ for a cylindrical tank, and $W_e > 1.5 \times 10^4$ for horizontal and vertical intakes, σ can be negligible. Also, when the water surface is depressed considering significant value only at $W_e < 1.5 \times 10^4$.

Theoretical Power Output

In the GWVPP technology, water passes through the canal, goes into the basin structure tangentially, creating a strong vortex circulation. Then, velocity near the core rotates coaxially placed runner. The maximum power that can be obtained for any hydropower turbine is defined by:

$$P = \rho g Q H$$

where Q is the flow rate and H is the gross head at the site. Based on reaction turbine principals, the maximum power output obtained on shaft is considered by itself (Williamson, Stark, and Booker 2014) as:

$$P = \rho g Q \varphi_v (H - h_1 - h_2 - h_3)$$

where φ_v is the vortex turbine's efficiency, h_1 , h_2 and h_3 are the head loss across the radius, the head loss at the outlet, and the output kinetic energy, respectively. Therefore, it is crucial to create less head loss to generate higher efficiency of the turbine for a GWVPP. The shaft power output, ($P_{\text{shaft_out}}$) is utilized with the torque generated and the impeller angular velocity. Based on momentum principles, the torque produced can be calculated by means of a force generated on the impeller-water interface by estimating the difference between the blade velocity and the initial velocity near the core. Combined vortex models of Rankine, Odgaard or Vatistas et al. can also estimate the torque so that the turbine efficiency is dependent on the operational impeller velocity, which can be determined by:

$$P = \frac{P_{\text{out}}}{P} = \frac{(v_1 - v_b) r \omega}{gH} \quad (8)$$

SCOPE FOR GWVPP SYSTEM

The main factors that are important for the scope installation and development of a GWVPP system are described in this section through optimized parameters that can be improved in terms of performance and efficiency of the system.

Site selection is crucial to starting a GWVPP project from a social, environmental, economic and technical aspects. The choice of suitable sites can be done by using remote sensing and geographical information systems (GIS) using different method of multi-criteria decision making analysis (Vidhya and Sarvani 2018). For that purpose, usage of a weir, head, mass flow, flow rate, and elevation difference are determined. Technically, when a

candidate site for GWVPP development is examined, estimation of river flow and water head must be predictable as two factors. There are different types of methods to estimate river flow, as known site discharge and streamflow, using a variety of factors including the type of flow system, expected range of flow rates, the configuration of a site, overall cost. The classification of common flow measurement methods in Table 3 is represented. According to the specifications of the methods and water condition (using a separated canal), we concluded that site discharge methods can be more appropriate to measure river flow for a GWVPP project.

Table 3. *Common Flow Measurement Methods* (Michaud and Wierenga 2005)

Site Discharge Methods			Stream Flow Methods	
No	Method Name	Equipment Needed	Method Name	Equipment Needed
1	Bucket&Stopwatch	A container to fill of known volume Timer (Stopwatch) Measuring Tape	Using Stream Gage Data	Flow monitoring sites (gage sites) Receiving water flow statistics & the term of 7Q10 Measuring Tape
2	Float Method	Markers (Flags, cones, etc.) Timer (Stopwatch) Float (a plastic bottle half filled with water)	Float Method	Markers (Flags, cones, etc.) Timer (Stopwatch) Float (a plastic bottle half filled with water)
3	Meter (For Wadeable streams and Non-Wadeable streams)	Flow Meter (Measure both velocity and depth) Top setting rod (if available) or measuring stick Waders or boots	Meter (For Wadeable Streams and Non-Wadeable Streams)	Flow Meter (Measure both velocity and depth) Top setting rod (if available) or measuring stick Measuring tape or ruler
4	Manning's Equation	Measuring tape or ruler		

Due to the complexity in GWVPP design, technical parameters, which are the most challenging aspects of the technology are identified and summarized in Table 4. These parameters and their combinations lead readers to investigate different combinations to investigate the efficiency and performance of an entire GWVPP system.

Since there have been studies focusing on turbines and their developments in the last decade, the parameters used in chapter related to the efficiency of a single turbine and the other parameters corresponding to these parameters are represented here separately. Taking these parameters into consideration, it is also emphasized that how various and newer correlations can be established among these parameters.

Table 4. *The Key Factors Influencing a GWPP System (Afgan, Carvalho, and Hovanov 2000; Bakiş and Demirbaş 2004; Balat 2007; Kaygusuz 2009; Kentel and Alp 2013; Klimpt et al. 2002; Lalitha 2013; Sarkar and Karagöz 1995; Scannapieco, Naddeo, and Belgiorno 2014).*

Schedule		Technical	Social	Environment	Economical	
	Key factors in General	Efficiency and Performance Related Factors including Geometry, Turbine and others				
Site Selection	Weir Usage	Feasibility	Inlet width, height, length, notch angle, width, & water velocity	Job creation,	Fish migration,	Efficiency
	Head (m)	Flexibility	An angle of inlet passage and Geometric factor (α)	Capital produced	CO ₂ emission	Affordable power
	Mass flow	Availability	Basin shape, diameter, height, and cone (inclination) angle	Public participation	Species extinction	Unit electricity cost
	Flow velocity	Accessibility	Outlet Shape (Flat, cylinder, and cone), diameter and length	Visual impact	Landslides and land use	Project cost, IRR, NPV
	Flow rate	Construction	Blade position, Runner Position and Submergence	Shared benefits	Hydrologic regime,	Unit price of energy
		Performance	Shape of propeller (flat, twisted, curved, and cross-flow)	Displacement	Water quality	Operation costs
		Productivity	Rotors diameters ratio and radius of curvature	Drought protection	Topographic condition	Levelized cost of electricity
		Demand Response	Shaft position arrangement for multi-stage propellers	Safety and social conflict	Fishery	Proven technology
		Development period	Blade number, size, and Length of chord	Water resource issues	Climate benefits	Impact on local economy
		Head	Booster runner w/main runner	Legal obstacle	Aquatic habitat	Investment per unit power
	Flow, Flow pattern	Blade height, Inlet and outlet blade angle	Innovative ability	Flow pattern	Capital & maintenance cost	

Installed capacity	Baffle Plates attaching main blades	Functional Impact	Habitat loss, land use	Resource availability
Capacity factor	Impact & taper angles and Turbine weight	Accessibility	Sedimentation,	Incentives,
Discharge	Diameter, Number, of intensifier nozzles	Impact on locals	Protected areas,	Annual benefit
Turbine Efficiencies	Blade shape & Configurations (Flat, twisted, curved and cross-flow)	Irrigation, fishing	Environmental flow	Payback period
System Efficiencies	Turbine materials (Al, Steel, Acrylonilite Butadiene Styrene (ABS))	Employment opportunities	Natural flow disruption	Regional development
Technical limitations	Related parameters of Turbine break force (F)	Public perception	River bank collapse	Capital & operating cost
Sensitivity Analysis	Cavitation on Turbines based on temperature, suction head and flow velocity	Public acceptance	Hydrological condition	Installation cost per kWh
	Hydraulic loss parameters	Irrigation, heritage sites	Hydrological risks,	Construction cost
	Velocity triangles of turbine	Human Health concerns	Deforestation	Cost per KWh
	Vortex height	Living standards	Dust and noise	Investment costs
	Rate of flow coefficient based on Fr, Re, We	Flood protection	Temperature	IRR compensation fees
	Load (kg), Force (N), Torque (N.m)	Land use,	Sedimentation	
	Rotational Speed (rpm) Angular velocity	Infrastructure	Erosion, soil fertility	

The International Association for Hydro-Environment Engineering and Research (IAHR) (Spain water and IWHR C. 2020) recognizes that social impacts are important in hydropower evaluation. Rehabilitation of local public, reluctant resettlement, and potential conflict, as well as enhancing cases of water-based diseases are main factors in discussion. The benefits of reported GWVPP development often include employment, public acceptance and perception, investment, fish migration, irrigation, etc.

The environmental parameters generally related to water quality, flooding, fish migration, bio-diversity loss, land use, and sedimentation. Increased water temperature, low dissolved oxygen, loss of soil fertility, and erosion are other mentioned parameters in the literature. In studies that focus solely on hydropower systems such as GWVPP, emissions prevention is less often cited as an environmental advantage. Fisheries impact, environmental visibility, and other type of emissions (as methane) are also rarely studied.

Economic parameters associated with GWVPP development have received less attention while technical, social, and environmental issues are relatively discussed in detail at the accessible literature.

DESIGN HIGHLIGHTS

General concepts for a GWVPP research are provided. Water vortex hydroelectric theory is described here as a general power generation down to power output, including the classification of vortices, water-turbine interaction, scale effects, surface tension and viscous effects. In addition, it is urgent to establish an appropriate institutional framework for operating a customer and environmental-friendly GWVPP units. Since a GWVPP system is placed in rural areas, project development and completion processes should be prepared, taking into account state-sourced investments and loans. It was emphasized that the development and completion processes of the project should be completed as legal institutional structures.

The highlights selected regarding the geometry and turbine are summarized as follows:

- Reasonable correlations among the technical, social, economic and environmental parameters should be established in a way that positively affect the efficiency and performance of the entire system or turbine. For example, the optimized conical basin structure can be more efficient than cylindrical basin alone or conical basin.
- The vortex height and the achievement of symmetrical vortices contribute significantly to a GWVPP performance. In addition, the correlation between blade submergence and vortex height, rotation speed, torque, brake power and mechanical efficiency

have been identified as important factors determining GWVPP performance and layout.

- The performance of GWVPP system can be increased by supporting multi-stage turbine configurations.
- Higher angle of orifice may increase power output.
- The number and the distance of blades, as well as baffle plates mounted on the main turbine blades are effective in capturing right amount of water and producing higher torque.
- Using alternative materials with fixed size and blades numbers can increase the system efficiency to make lightweight turbines.
- Although higher speed is better to generate power, the tank losses, friction losses of a tank or runner can cause extra losses with high speed in water turbine.

The highlights selected regarding numerical related studies are summarized as follows:

- For GWVPP projects, Reynold, Froude, and Weber numbers are important parameters according to momentum versus viscosity, momentum versus gravity, kinetic energy versus surface tension relations, respectively.
- Mathematical models describe water flow properties. The flow coefficient rate is relying on Froude's, Reynolds', and Weber's numbers, whereas it did not exhibit any dependency for $Fr \geq 2.5$, $Re > 3 \cdot 10^4$ and $We > 250$.
- The circulation fields and the tangential velocity can be found at various sub-surface depths using particle tracking techniques.
- Cavitation depends on flow rate, suction head, atmospheric pressure, temperature, gas content in the liquid, and turbine operating hours. Therefore, cavitation must be estimated using a fixed water speed.

The highlights selected regarding the social, environmental, and economic are summarized as follows:

- The cost analysis should be made by dividing into sub-categories such as transportation, equipment, construction. During the life of the plant, the O&M costs are determined and their costs should be re-covered.
- For a system with fish-friendly properties, the volumetric flow must be kept constant.
- Quantitative data should be produced for mechanisms that cause damage. Thus, turbine designers can design more advanced fish-friendly turbines improving performance criterion.

GENERAL APPROACH FOR COMPUTATIONAL FLUID DYNAMICS MODELING

Experience is really matters when developing Computational Fluid Dynamics (CFD) models. It is because in the real world there exist a lot of problems that come up and we need to know how to solve them efficiently and quickly. Let's get into some practical solutions and tips for how we actually can do modeling. Some of skills which is covered here are: (i) Modeling approach and basic modeling, (ii) Access convergence, (iii) Turbulence, (iii) Volume of Fluid, (iv) Time variation, and (v) Mesh deformation.

For a roadmap, we need to have a basic roadmap of how a CFD project is going to be to move forward and anticipating how that will affect the project.

It is a need to be planning and understanding how that will affect next steps, which are very essential to CFD. Characterizing a problem should be the first step to understand which type of a problem are we dealing with (Is it slow flow? Is it fast flow? Is it a simple or complicated problem? Are there lots of interacting equations? so on). The major tools, which is used for characterization are non-dimensional coefficients such as Reynold, Froude, and Courant numbers. Also, a skecth path is required to characterize how the flow patterns look like. All of these items provide an idea of where the areas of complicated flow and a mesh refinement are obtained. In that way, meshing strategy has informed estimating first guess for meshing. Then, additional refinement may be needed depending on the results, which is the iterative process. Therefore, it is better to begin with the possible simplest initial setup without any problems. Designers should be able to identify any problems quickly during the process. Once they have identified problems and created a working solution adding complexity, turbulence, and extra equations, they ensure to execute the project with a stable simulation before adding extra complexity. Therefore, the best way is to proceed step by step.

Let's begin with a geometry for a CFD simulation as a basic process. The geometry set up as whole simulation geometry to create the domain defined. Then, diagnostic runs can be proceeded running the results, which are looked for. Here, basic modeling strategies are mentioned:

Domain size: Ask questions, which are “how big your geometry to create fluid domain”, “boundaries are far enoguh away for a predictable flow”, “boundaries are predictable to be dictated”, and much farther than the flow patterns show”. If it is not ensured about the domain size, one thing, which is a simple test case picking some distances for the boundaries, positions, etc. can be made. Then the process flows using different boundaries or positions when running two comparisons and checking out whether they have any difference. It is recommended to check pressure changes on the body instead

of flow patterns. If a big change is obtained or there exists a doubt, then boundaries further out applied ones should be picked.

Physics: A software has quite a few different options, which set different values picked. In general, there exist four major categories of physical boundary conditions, which can be applied on all of physical solid objects. Skin friction where the fluid cannot actually pass through the wall typically. If the object is actually moving relative to the flow, a velocity at the wall, which is another effect to be considered. Velocity inlet conditions where specifying a vector velocity, pressure, which is allowed to be freely calculated at that condition, including pressure inlet/outlet conditions are other parameters for consideration. Inlet and outlet cases are pressed specifying the static pressure, not the stagnation pressure so that the velocity is allowed to freely vary in those cases. Later, all the gradients are set to zero obtaining symmetry conditions. Every CFD simulation including at least one boundary condition for velocity and one boundary condition for pressure have these two variables (velocity and pressure), which are coupled in the equations used. If a boundary condition for one of them (the other one is unconstrained) is specified, that leads problems for the solution. Specifying boundary conditions for both velocity and pressure in a simulation is required.

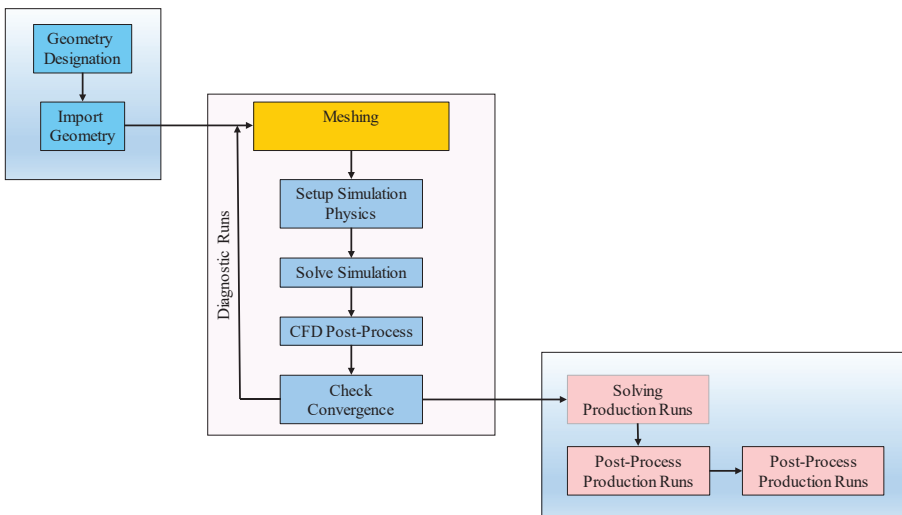


Figure 3. *CFD Modeling Approach*

An Example of CFD Application for GWVPP

Using Ansys Fluent 2019 R3 academic version as a CFD tool, this example is to design of a basin structure mounting an upstream rectangular canal, an orifice, which is able to form a gravitational vortex stream. Here, the formation of a water vortex flow formed by gravity is under focus as an example of a GWVPP. The governing equations are Navier-Stokes

equations. The finite volume method is employed to discretize the governing equations, while the SIMPLE method is adopted to solve the discretized equations. For an incompressible, isothermal Newtonian flow (density(ρ) and viscosity (μ) are constant), with a velocity field $\vec{V}=(V_r, V_\theta, V_z)$, incompressible continuity equation is shown as flows:

$$\frac{1}{r} \frac{\partial(rV_r)}{\partial r} + \frac{1}{r} \frac{\partial V_\theta}{\partial \theta} + \frac{\partial V_z}{\partial z} = 0 \quad (9)$$

and Navier-Stokes equations in the cylindrical coordinates are shown as flows:

$$\rho \left(\frac{\partial V_r}{\partial t} + V_r \frac{\partial V_r}{\partial r} + \frac{V_\theta}{r} \frac{\partial V_r}{\partial \theta} - \frac{V_\theta^2}{r} + V_z \frac{\partial V_r}{\partial z} \right) = - \frac{\partial P}{\partial r} + \rho g_r + \mu \left[\frac{1}{r} \frac{\partial}{\partial r} \left(r \frac{\partial V_r}{\partial r} \right) - \frac{V_r}{r^2} + \frac{1}{r^2} \frac{\partial^2 V_r}{\partial \theta^2} - \frac{2}{r^2} \frac{\partial V_\theta}{\partial \theta} + \frac{\partial^2 V_r}{\partial z^2} \right] \quad (10)$$

$$\rho \left(\frac{\partial V_\theta}{\partial t} + V_r \frac{\partial V_\theta}{\partial r} + \frac{V_\theta}{r} \frac{\partial V_\theta}{\partial \theta} + \frac{V_r V_\theta}{r} + V_z \frac{\partial V_\theta}{\partial z} \right) = - \frac{1}{r} \frac{\partial P}{\partial \theta} + \rho g_\theta + \mu \left[\frac{1}{r} \frac{\partial}{\partial r} \left(r \frac{\partial V_\theta}{\partial r} \right) - \frac{V_\theta}{r^2} + \frac{1}{r^2} \frac{\partial^2 V_\theta}{\partial \theta^2} + \frac{2}{r^2} \frac{\partial V_r}{\partial \theta} + \frac{\partial^2 V_\theta}{\partial z^2} \right] \quad (11)$$

$$\rho \left(\frac{\partial V_z}{\partial t} + V_r \frac{\partial V_z}{\partial r} + \frac{V_\theta}{r} \frac{\partial V_z}{\partial \theta} + V_z \frac{\partial V_z}{\partial z} \right) = - \frac{\partial P}{\partial z} + \rho g_z + \mu \left[\frac{1}{r} \frac{\partial}{\partial r} \left(r \frac{\partial V_z}{\partial r} \right) + \frac{1}{r^2} \frac{\partial^2 V_z}{\partial \theta^2} + \frac{\partial^2 V_z}{\partial z^2} \right] \quad (12)$$

The CFD is a technique, which is used computer programs and high performance computers. Thus, a large number of calculations per unit of time can be performed, thereby reducing time and design costs in analysis, and obtaining results based on the accuracy of the established assumptions, estimates and idealizations (Wilson et al. 2019).

Methodology and Simulation

Geometry of solid model was created including an upstream canal, a cylindrical basin structure, and an orifice using Ansys design model of Workbench R3 in Ansys Fluent R3 academic version (Ansys 2020). The length (l), width (w), and height (h) of the upstream canal are 0.5m, 8cm, and 8cm, respectively. None of any notch angle was applied between the upstream canal and the basin so that the upstream canal was tangentially mounted to upper side of the basin. The basin structure was generated with 1m long upper diameter and 31cm long height with an orifice including 20cm height and 10cm diameter at the center of bottom side. Solid model is created using Ansys Fluent workbench academic version in the module of

“the Design Modeler” (Ansys 2020). The material for a GWVPP system is chosen Aluminum (al) with its properties, which are shown in Table 5.

Table 5. *Mechanical Properties of Aluminium*

No	Property	Value	Unit
1	Density	2719	kg/m ³
2	Cp (Specific Heat)	871	j/kg-k
3	Thermal Conductivity	202.4	w/m-k

The solid model geometry depending on the dimensions mentioned above is designed and shown in Figure 4.

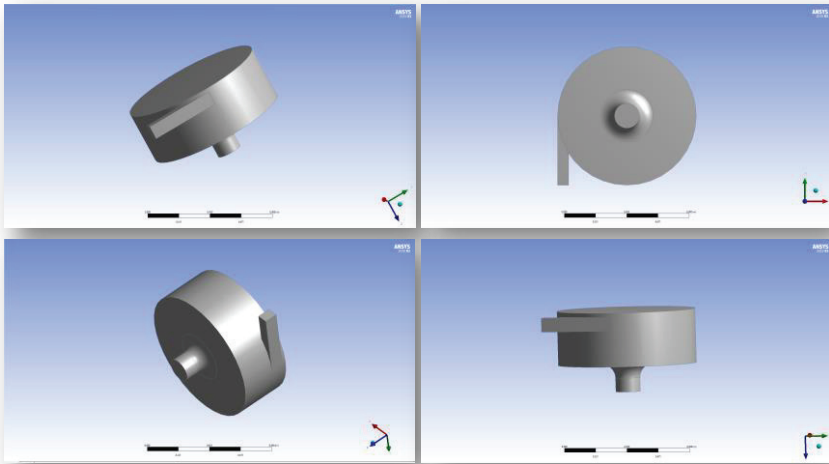


Figure 4. *Solid Model Geometry*

For meshing the geometry, it needs to be determined by some criteria to verify that the mesh is done correctly, these are the parameters that ANSYS Fluent recommends to obtain an adequate solution of the system. A mesh method within the reliable values were carried out via CFD Physics preference and Fluent solver preference including element size of 5e-002m, max size of 5e-002m resulting from 10949 nodes and 35537 elements.

ANSYS is used to define preprocessing simulation parameters so that the whole system with the initial parameters can be provided by the software when starting up. A faster convergence can be achieved by replacing these parameters with those that most closely match the reality. The governing equations for this GWVPP application are the Navier-Stokes equations so that the “coupled method” was approved solving the discretized equations. It is well known that the pressure-based solver is used to solve flow problems

in either a separated or coupled method. There exist some advantages over the non-coupled approach when using the coupled one. The coupled structure including pressure-velocity coupling acquires a healthy and efficient single-phase implementation for steady-state flows with better performance compared to the separated solution structures. Using the coupled method is relatively required when the mesh quality is weak. The coupled method creates a solution including the momentum and pressure-based continuity equations together.

The details of the meshing properties and meshing appearance are shown in Figure 5 and Figure 6, respectively.

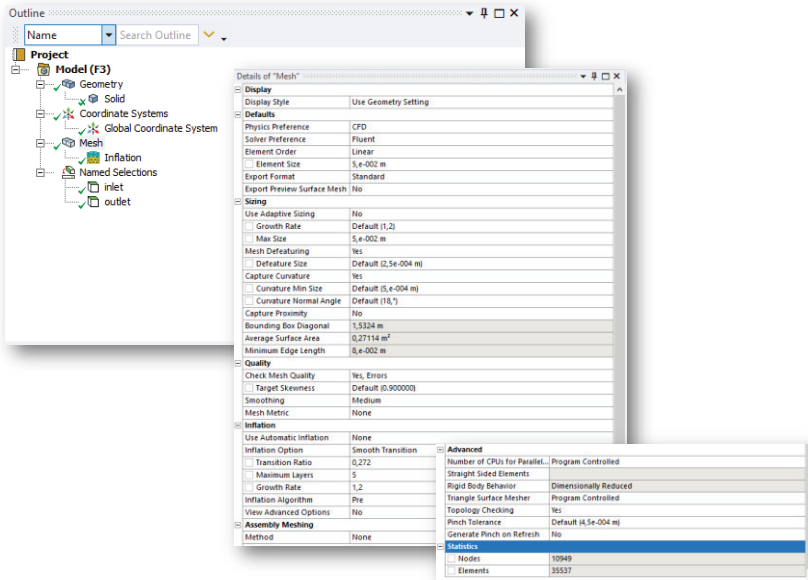


Figure 5. Meshing Properties

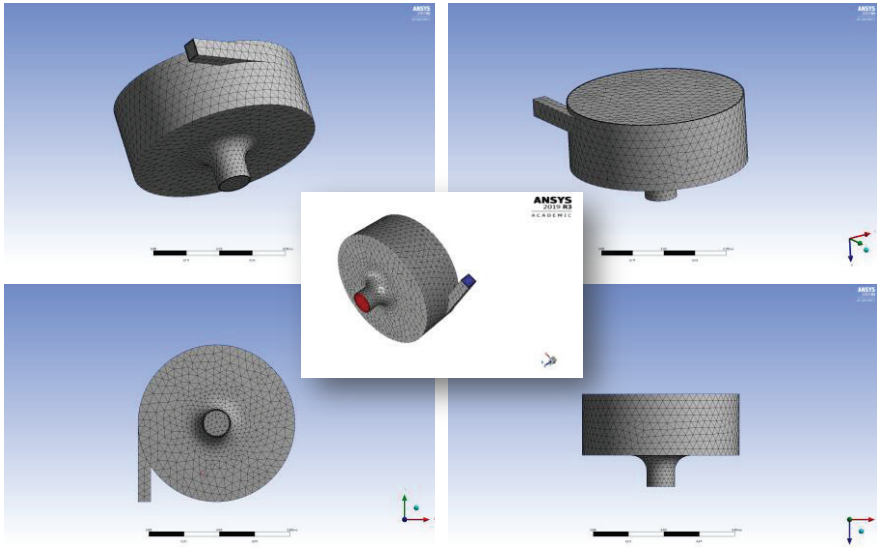


Figure 6. Mesh (with Inlet and Outlet Configurations)

Steady time option, the pressure-based solver, and absolute velocity formulation were activated for this application. Also, fluid time scale was set up automatic as a time step method with time scale factor was 1 where the length scale method was conservative with zero verbosity. Finally, the iteration number was entered 600. In this simulation, there exists an interaction between water and air so that two types of materials as water and air were created as requirements. The reference pressure was placed in the model domain, which is equal to atmospheric pressure.

Under the models, energy was turned on when the realizable viscous model was k-epsilon (2 eqn) with an option activated scalable wall functions. Inlet velocity magnitude was entered 0.4 m/s with the thermal temperature of 353 Kelvin. After initialization was done, calculation was run to observe the residuals for continuity, velocities (x, y, z), energy, k, and epsilon. The solution was converged at the end of the 497 iterations (Figure 7).

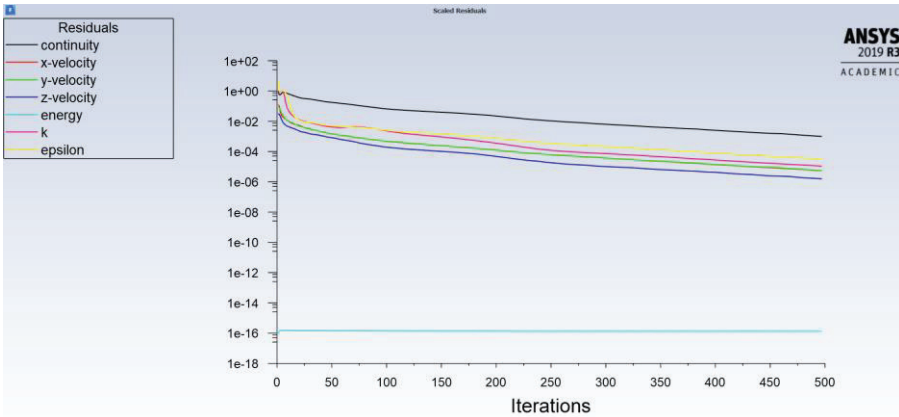


Figure 7. *Scaled Iterations*

CFD solvers use an iterative process to solve equations so that convergence should be judged and refine the initial guess. It means that CFD operator needs to be decide when the process is done. For that approach, the residuals plot is primary tool but it is not the only tool to build up a preponderance of evidence. In the process of judging convergence, the other things are to create monitors and checking flow patterns of the scaled residuals whether or not the scaled residuals are converged. Some reminders are required regarding residuals whether the scaled residuals are converged. Depending on these parameters, the answers of some questions for equation solutions should be sought according to the convergence results: Is the meshing done correctly? Do we have any wrong input parameters? Is there any small changes in residuals levels and fluctuations?

In this way, it is necessary to look for monitored values and trying to understand whether real-world physical values are reliable. In short, it is checked whether a stable convergence has been obtained. If troubles such as no good stable lines are appeared in the scaled residuals:

- If only one equation was a problem, the need is to find out the trouble spot in mesh such as poor mesh cell, quality, and resolution
- If bad residuals are constantly occurred, the need is to check momentum and fraction equations trying to change the order of interpolation such as first order in terms of second order. However, changing the order of interpolation is not recommended for the momentum equation.
- If the scaled residuals are oscillating but not converging, then the need is to reduce relaxation factor for momentum and fraction equations.

Later, the velocity, the pressure in a selected plane, and the pressure at the solid wall view are plotted using the results option in Ansys Fluent (Figure 8). Each process of the simulation for a GWVPP is shown in Figure 9.

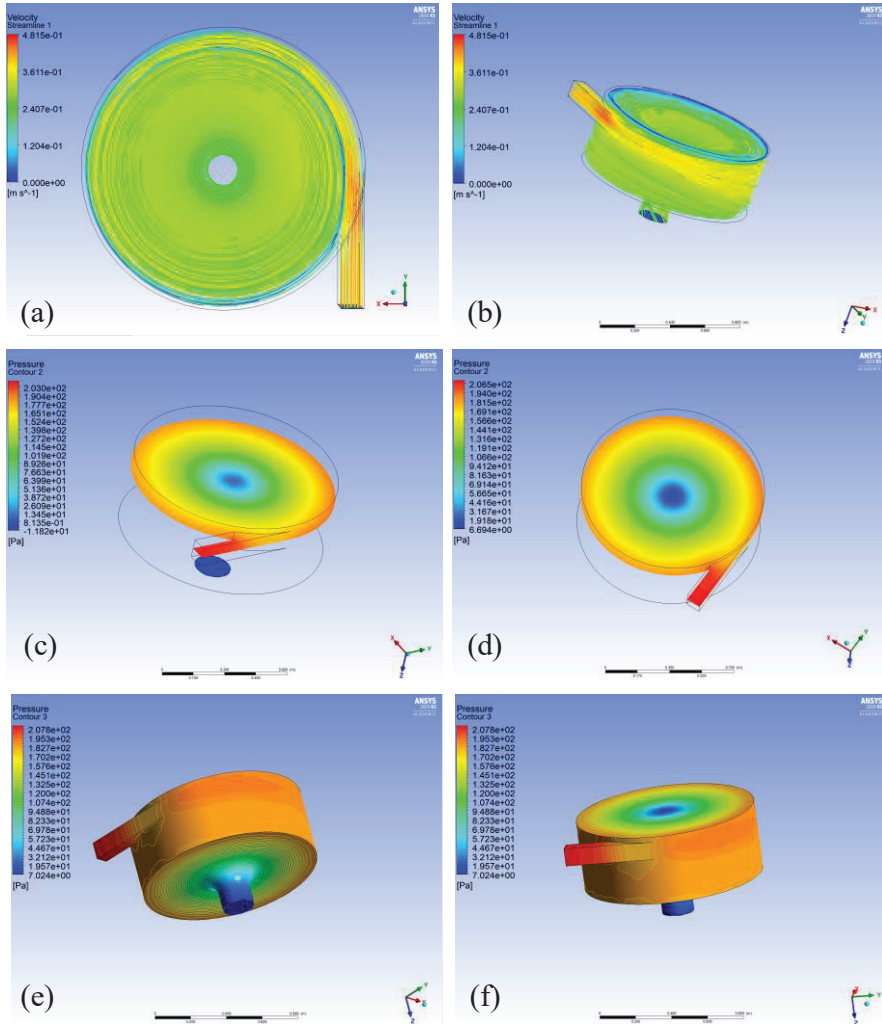


Figure 8. Simulated (a-b) Velocity View, (c-d) Pressure View, (e-f) Pressure at the Solid Wall View

Finally, Ansys Fluent methodology is shown step-by-step in Figure 9.

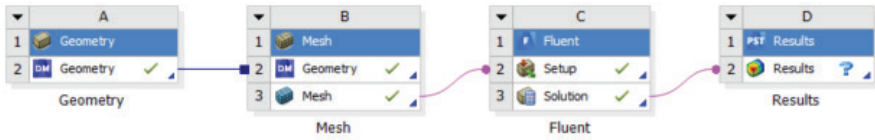


Figure 9. *Methodology for CFD*

CONCLUSION

GWVPP technology is an innovative and environmental-friendly hydroelectric technology under the river-type electricity generation class. The technology has wider range of benefits including social, environmental and economic aspects, which are provided in this study. This chapter for the gravitational water vortex power plant (GWVPP) is demonstrated providing the definition, fundamentals, scope and design highlights, and general approach of CFD modeling with an application by using Ansys Fluent R3 version.

REFERENCES

- Afgan, Naim H., Maria G. Carvalho, and Nikolai V. Hovanov. 2000. "Energy System Assessment with Sustainability Indicators." *Energy Policy* 28(9):603–12. doi: 10.1016/S0301-4215(00)00045-8.
- Agency, Japan International Cooperation. 2011. *Project for Operation and Maintenance of the Rural Electrification on Micro-Hydropower in Mondul Kiri*. Mondul Kiri, Kingdom of Cambodia.
- Ak, Mümtaz, Elçin Kentel, and Serhat Kucukali. 2017. "A Fuzzy Logic Tool to Evaluate Low-Head Hydropower Technologies at the Outlet of Wastewater Treatment Plants." *Renewable and Sustainable Energy Reviews* 68(October 2016):727–37. doi: 10.1016/j.rser.2016.10.010.
- Ansys. 2020. "Ansys Academic Research Fluent, Release 19.3."
- Anwar, Habib O., James A. Weller, and Michael B. Amphlett. 1978. "Similarity Of Free-Vortex At Horizontal Intake." *Journal of Hydraulic Research* 16(2):95–105. doi: 10.1080/00221687809499623.
- Anwar, Zaizuliana Rois. 2013. "Formation of a Weak Vortex." *Journal of Hydraulic Research* 4(1):1–6.
- Bakiş, Recep, and Ayhan Demirbaş. 2004. "Sustainable Development of Small Hydropower Plants (SHPs)." *Energy Sources* 26(12):1105–18. doi: 10.1080/00908310390265932.
- Balat, Havva. 2007. "A Renewable Perspective for Sustainable Energy Development in Turkey: The Case of Small Hydropower Plants." *Renewable and Sustainable Energy Reviews* 11(9):2152–65. doi: 10.1016/j.rser.2006.03.002.
- Chen, Yun liang, Chao WU, Mao YE, and Xiao ming JU. 2007. "Hydraulic Characteristics of Vertical Vortex at Hydraulic Intakes." *Journal of Hydrodynamics* 19(2):143–49. doi: 10.1016/S1001-6058(07)60040-7.
- Cooke, Lacy. 2018. "Fish-Friendly Whirlpool Turbine Makes Hydropower Green Again." *InHabitat*. Retrieved (<https://inhabitat.com/fish->

friendly-whirlpool-turbine-makes-hydropower-green-again/).

- Dhakal, R., Shrestha, S., Neupane, H., Adhikari, S. and Bajracharya, T. 2020. "Inlet and Outlet Geometrical Condition for Optimal Installation of Gravitational Water Vortex Power Plant with Conical Basin Structure." Pp. 163–74 in *In Recent Advances in Mechanical Infrastructure (ICRAM)*. Singapore.
- Domfeh, Martin Kyereh, Samuel Gyamfi, Mark Amo-Boateng, Robert Andoh, Eric Antwi Ofori, and Gavin Tabor. 2020. "Free Surface Vortices at Hydropower Intakes: – A State-of-the-Art Review." *Scientific African* 8:e00355. doi: 10.1016/j.sciaf.2020.e00355.
- European Commission. 2009. "General Framework of EU Water Law Legal Basis for Water Policy." *EU Water Legislation*. Retrieved (https://www.era-comm.eu/EU_water_law/part_2/index.html).
- GH Keulegan, LLDaggett. 1974. "Similitude in Free-Surface Vortex Formation." *Journal of Hydraulics Divisions* 1565–81.
- Grant, Gordon E. 1997. "Critical Flow Constrains Flow Hydraulics in Mobile-Bed Streams: A New Hypothesis." *Water Resources Research* 33(2):349–58. doi: 10.1029/96WR03134.
- Gulliver, Alan J. Rindels; John S. 1983. *AN EXPERIMENTAL STUDY OF CRITICAL SUBMERGENCE TO AVOID FREE-SURFACE VORTICES AT VERTICAL INTAKES*. Minneapolis, Minnesota.
- H. A. Einstein, Huon Li. 1951. "Steady Vortex Flow in a Real Fluid." Pp. 33–43 in *Proc. Heat Transfer and Fluid Mechanics Institute, Stanford University*. Stanford, CA.
- H. O. Anwar. 1965. "Flow in a Free Vortex." *Water Power* 4:153–61.
- Hamed Sarkardeh, Amir Reza Zarrati, Ebrahim Jabbari, Reza Roshan. 2011. "Prediction of Intake Vortex Risk by Nearest Neighbors Modeling by Quentin B.Travis and Larry W. Ways." *Journal of Hydraulic Engineering* 137(6):701–5. doi: 10.1061/(asce)hy.1943-7900.0000344.
- Hecker, G. E. 1987. *Fundamentals of Vortex Intake Flow, Swirling Flow*

Problems at Intakes.

- Hite, John E., and Walter C. Mih. 1994. "Velocity of Air-Core Vortices at Hydraulic Intakes." *Journal of Hydraulic Engineering* 120(3):284–97. doi: 10.1061/(asce)0733-9429(1994)120:3(284).
- Kaygusuz, K. 2009. "The Role of Hydropower for Sustainable Energy Development." *Energy Sources, Part B: Economics, Planning and Policy* 4(4):365–76. doi: 10.1080/15567240701756889.
- Kentel, Elçin, and Emre Alp. 2013. "Hydropower in Turkey: Economical, Social and Environmental Aspects and Legal Challenges." *Environmental Science and Policy* 31:34–43. doi: 10.1016/j.envsci.2013.02.008.
- Klimpt, Jean Étienne, Cristina Rivero, Hannu Puranen, and Frans Koch. 2002. "Recommendations for Sustainable Hydroelectric Development." *Energy Policy* 30(14):1305–12. doi: 10.1016/S0301-4215(02)00092-7.
- Knauss J. 1987. *Swirling Flow Problems at Intakes*. A.A. Balkema, Rotterdam, Netherland.
- Kosnik, Lea. 2010. "The Potential for Small Scale Hydropower Development in the US." *Energy Policy* 38(10):5512–19. doi: 10.1016/j.enpol.2010.04.049.
- Kumar, Pradeep. 2020. "Turbulent Hydro- A Whole New Level of A Hydropower Plant." *All Sustainable Solutions*. Retrieved (<https://allsustainableolutions.com/turbulent-hydro-a-whole-new-level-of-a-hydropower-plant/>).
- Lalitha, O. R. 2013. "Sustainable Development of Hydroelectric Power - An Overview." *Water and Energy International* 70(12):39–43. doi: 10.1080/0090831029008672.
- Lecler, Yveline. 2018. "Small and Micro-Scale Hydropower in Japan: Potential, Incentives and Regulation." Pp. 31–63 in *Proceedings of the XV East Asia Net Research Workshop (Studi e ricerche 12)*, Edizioni Ca' Foscari.

- Lugt, H. J. 1983. *Vortex Flow in Nature and Technology*. New York: Wiley-Interscience.
- Michaud, J. P., and M. Wierenga. 2005. *Estimating Discharge and Stream Flows. A Guide for Sand and Gravel Operators*.
- Mulligan, Sean. 2015. “Experimental and Numerical Analysis of Three-Dimensional Free-Surface Turbulent Vortex Flows with Strong Circulation.” Institute of Technology, Sligo.
- Mulligan, Sean, Leo Creedon, John Casserly, and Richard Sherlock. 2019. “An Improved Model for the Tangential Velocity Distribution in Strong Free-Surface Vortices: An Experimental and Theoretical Study.” *Journal of Hydraulic Research* 57(4):547–60. doi: 10.1080/00221686.2018.1499050.
- Odgaard, A. Jacob. 1986. “Free-Surface Air Core Vortex.” *Journal of Hydraulic Engineering* 112(2):610–20. doi: 10.1061/(ASCE)0733-9429(1986)112:7(610).
- OECD. 2020. “Renewable Energy (Indicator).” *Renewable Energy*. Retrieved October 26, 2020 (<https://data.oecd.org/energy/renewable-energy.htm>).
- P.B. Zielinski , J.R. Villemonte. 1968. “Effect of Viscosity on Vortex Orifice Flow.” *Journal of Hydraulics Division* 94(3):745–52.
- REN21. 2020. “Renewables 2019 Global Status Report.” *Global Overview*. Retrieved October 26, 2020 (https://www.ren21.net/gsr-2019/chapters/chapter_01/chapter_01/#sub_4).
- Rosenhead, L. .. 2011. “The Spread of Vorticity in the Wake Behind a Cylinder.” Pp. 590–612 in *Proceedings of the Royal Society of London . Series A*. Vol. 127. The Royal Society Stable.
- Rott, Nicholas. 1959. “On the Viscous Core of a Line Vortex.” *Zeitschrift Für Angewandte Mathematik Und Physik ZAMP* 10(1):73–81. doi: 10.1007/BF01637199.
- Sarkar, Amin U., and Serkan Karagöz. 1995. “Sustainable Development of

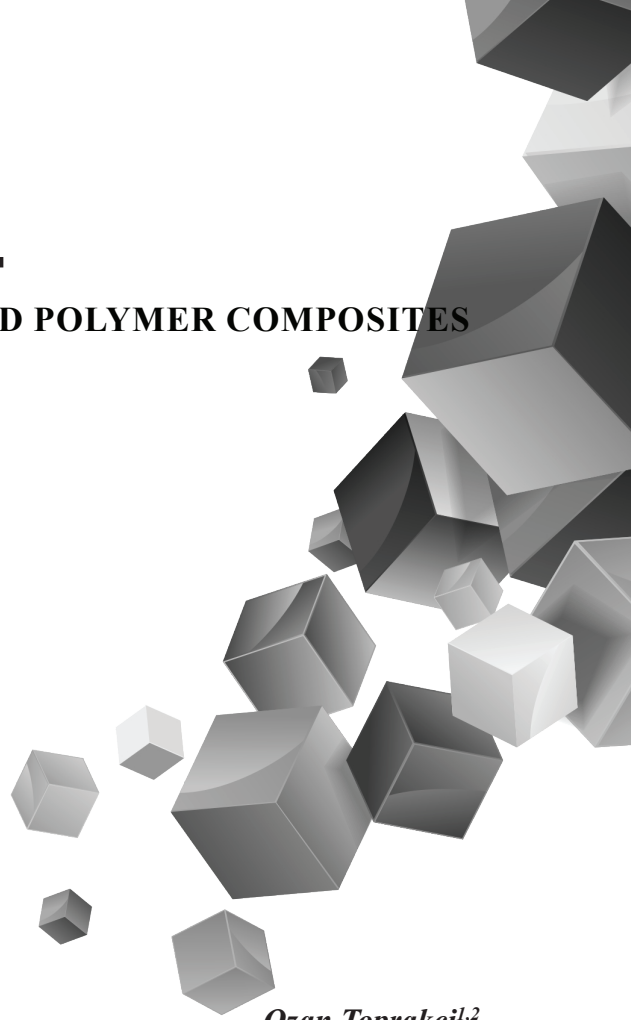
- Hydroelectric Power.” *Energy* 20(10):977–81. doi: 10.1016/0360-5442(95)00059-P.
- Scannapieco, D., V. Naddeo, and V. Belgiorno. 2014. “Sustainable Power Plants: A Support Tool for the Analysis of Alternatives.” *Land Use Policy* 36:478–84. doi: 10.1016/j.landusepol.2013.09.008.
- Spain water and IWHR C. 2020. “International Association for Hydro-Environment Engineering and Research.”
- Timilsina, Ashesh Babu, Sean Mulligan, and Tri Ratna Bajracharya. 2018. “Water Vortex Hydropower Technology: A State-of-the-Art Review of Developmental Trends.” *Clean Technologies and Environmental Policy* 20(8):1737–60. doi: 10.1007/s10098-018-1589-0.
- Vatistas, G. H., V. Kozel, and W. C. Mih. 1991. “A Simpler Model for Concentrated Vortices.” *Experiments in Fluids* 11(1):73–76. doi: 10.1007/BF00198434.
- Vidhya, S., and Lakshmi G. Reddi Sarvani. 2018. “Selection of Suitable Sites for Small Hydropower Plants Using Geo-Spatial Technology.” *International Journal of Pure and Applied Mathematics* 119(17):217–40.
- Wang, Yingkui, Chunbo Jiang, and Dongfang Liang. 2011. “Comparison between Empirical Formulae of Intake Vortices.” *Journal of Hydraulic Research* 49(1):113–16. doi: 10.1080/00221686.2010.534279.
- Williamson, S. J., B. H. Stark, and J. D. Booker. 2014. “Low Head Pico Hydro Turbine Selection Using a Multi-Criteria Analysis.” *Renewable Energy* 61:43–50. doi: 10.1016/j.renene.2012.06.020.
- Wilson, Sánchez Ocaña, Haro Valladares Jonathan, Sanaguano Jiménez Edison, and Salazar Jácome Elizabeth. 2019. “Investigation of the Behavior of the Fluid of a Micro Hydroelectric Gravitational Vortex, by Means of the Computational Dynamics of High Performance Fluids, for the Generation of Electric Power.” *International Journal of Mechanical Engineering and Robotics Research* 8(1):79–86. doi:

10.18178/ijmerr.8.1.79-86.

WJM Rankine. 1872. *A Manual of Applied Mechanics*. Sixth. London:
Charles Griffin and Company.

Chapter 7

VERMICULITE FILLED POLYMER COMPOSITES



Ozan Toprakci^{1,2}

Mukaddes Sevval Cetin^{1,2}

Hatice Aylin Karahan Toprakci¹

¹ Department of Polymer Materials Engineering, Yalova University, Yalova, Turkey

² Graduate School of Natural and Applied Sciences, Yalova University, Yalova, Turkey

1. Introduction

Vermiculite is a micaceous natural mineral which belongs to the group of phyllosilicate materials. Since vermiculite is formed underground, its structure mostly depends on the geological conditions. South Africa, China, and the United States are the leaders of the vermiculite production in the world. Vermiculite can be expanded to 20 or 30 times when compared with their original size and various exfoliation methods can be used including thermal, chemical and microwave. As shown in Fig. 1, after the exfoliation process, it expands and turns into a curved, accordion like (worm-like) shape. The exfoliation is caused by the evaporation of the water that are found between the layers of the vermiculite. The expanded vermiculite (EV) has distinctive properties such as porous structure, low thermal conductivity, and resistance to the high temperature. In addition to aforementioned properties, the vermiculite has a good ion exchange performance that is important in terms of removing undesired species from water (Aristov, Restuccia, Tokarev, Buerger, & Freni, 2000; Bar-Tal, Saha, Raviv, & Tuller, 2019; Bush, 2001; de la Calle, 1988; Feng et al., 2020; Malamis & Katsou, 2013; Motokawa et al., 2014; Schulze, 2005; Suvorov & Skurikhin, 2003; Marta Valášková, Martynkova, & application, 2012; Wang & Wang, 2019).

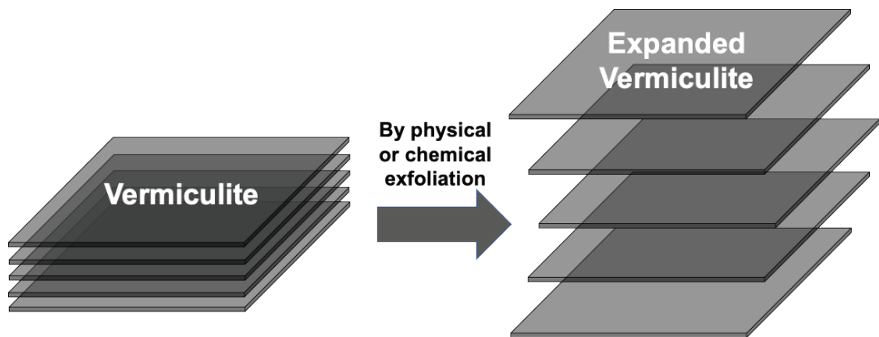


Figure 1. Schematical representation of expanded vermiculite production process

2. Structural and Physical Properties of Vermiculite

Vermiculite is a member of phyllosilicate material or sheet silicates. As shown in Fig. 2, vermiculite is a 2:1 type layered aluminosilicate mineral, consisting of octahedral layer between two tetrahedral layers.

The general formula for the vermiculite is $A_4(B_{2-3})O_{10}(OH)_2C \cdot nH_2O$ (A: Si, Al; B: Mg^{2+} , Fe^{2+} , Fe^{3+} , Al^{3+} ; C: Mg^{2+} , Ca^{2+} , Ba^{2+} , Na^+ , K^+). A, B and C represents octahedral sites, tetrahedral sites and exchangeable cations located in the interlayer space, respectively.

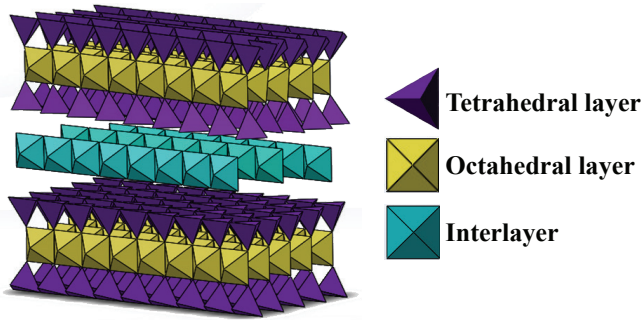


Figure 2. *Crystal structure of vermiculite*

Different varieties of vermiculites can be found in the nature including macroscopic vermiculite and vermiculite clays. The vermiculites are generally in brown color with bronze appearance. Actually, the color is based on the amount of the components. Depending on type and ratio of the components, color change from black to dark brown and even to green, yellow and yellowish-brown. The differences between the compositions of minerals affect not only the color but also some other properties. The common properties of vermiculite and expanded vermiculite can be seen from Table 1 also optical images of expanded vermiculite are given in Fig. 3.

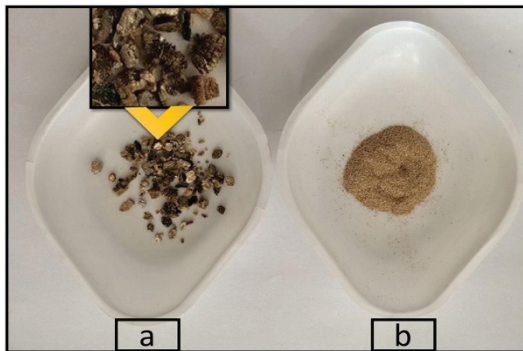


Figure 3. *Optical images of expanded vermiculite a) before and b) after grinding*

Table 1. *Some properties of vermiculite and expanded vermiculite*

Property	Vermiculite	Expanded Vermiculite
	Golden-yellow	
Color	Light to dark brown Silver-gold (Karatat, Benli, & Toprak, 2019; Suvorov & Skurikhin, 2003)	Silver to gold (de la Calle, 1988; Gencel et al., 2014)
Shape	Layered structure, particle (Bar-Tal et al., 2019; Liu, Feng, Mo, Su, & Fu, 2020)	Accordion shaped granule (de la Calle, 1988; Gencel et al., 2014)

Density (g cm ⁻³)	2.0-2.9 (Duman & Tunç, 2008; Suvorov & Skurikhin, 2003)	0.06-0.9 (Bar-Tal et al., 2019; de la Calle, 1988; Gellert, 2010)
Specific surface area (m ² g ⁻¹)	7.8 (Duman & Tunç, 2008)	4.5-9.8 (Duman & Tunç, 2008; Shoukry, Kotkata, Abo-El-Enein, Morsy, & Shebl, 2016)
Thermal conductivity (W (m K) ⁻¹)		0.0633-0.0738 (Low, 1984)
Melting point (°C)	1200-1320 (Chung, Jeong, & Kim, 2015; Karatas et al., 2019)	1240 – 1430 (Suvorov & Skurikhin, 2003)
Specific heat (kJ (kg K) ⁻¹)	0.84–1.08 (Chung et al., 2015)	0.8-1.08 (Karatas et al., 2019)
pH	6.0-9.0 (Chung et al., 2015; Karatas et al., 2019)	6.1-8.1 (Bar-Tal et al., 2019; Gencel et al., 2014; Papadopoulos, Bar-Tal, Silber, Saha, & Raviv, 2008)

Since vermiculite has unique properties, the material can be used in different applications from oil adsorption to water treatment and from sound insulation to thermal insulation. Since vermiculite is in particle or powder form, it needs to be mixed with some binding materials for giving a solid 3D shape. Vermiculite can be incorporated into the polymers not only to functionalize the polymer and but also to improve its properties. The resultant product can be classified as thermoplastic, thermoset, elastomer-based composites in various forms such as film, sheet, foam or gel.

3. Vermiculite Filled Polymer Composites

Composites are systems that are basically formed by combining at least two different materials to improve the desired properties of raw materials. Recent developments in technology and increasing requirements of modern life force producers to design more functional and high-performance composites. As known, a composite basically consists of a matrix and a filler material. Due to the distinct characteristics such as lightness, easily processable and low cost, polymers can be used as the matrix in the composites. Since polymeric composites offer many advantages, they are dominating the composite industry and they are used in many fields such as automotive industry, aerospace industry, medical industry, etc. Fibers, additives, and minerals can be used as filler materials. Minerals are widely preferred in polymer composites. Minerals are inorganic materials occurring naturally in earth. Therefore, using natural materials such as vermiculite, perlite, or bentonite as a filler in a polymer matrix provides ecological sustainability to petroleum-based materials such as polyolefins. In addition to that vermiculite improves the thermal and sound insulation

properties, oil and water absorbency, flame retardancy, and gas barrier behavior of the composites.

Vermiculite can be used in polymer composites in various forms including expanded, pristine-unexpanded, intercalated, organomodified and in various size from micro to nanometer.

As shown in Fig. 4, vermiculite can be organically modified or intercalated by various chemicals. As reported by Isci, anionic surfactants was more effective intercalants compared to cationic and nonionic surfactants in order to get intercalated vermiculite (Isci, 2017).

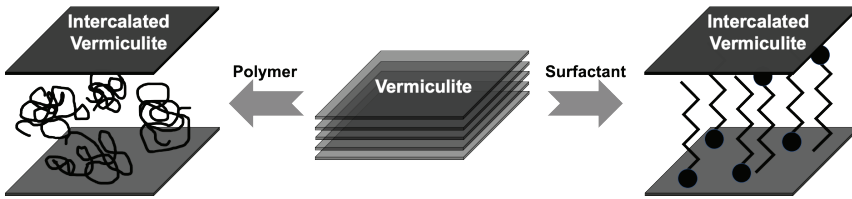


Figure 4. Schematic representation of intercalated vermiculite production routes

3.1. Vermiculite Filled Thermoplastic Composites

Thermoplastics are polymers that can be processed by melting. Vermiculite filled thermoplastic polymer composites can be produced by using a wide variety of polymers. In the literature, most common thermoplastics are polystyrene (PS) (Koksal, Mutluay, & Gencil, 2020), polyvinyl alcohol (PVA) (Kim et al., 2018), polyethylene (PE) (Hundáková et al., 2015; Tjong & Bao, 2005; Tjong & Meng, 2003b; Marta Valášková et al., 2013), low-density polyethylene (LDPE) (Marta Valášková et al., 2013), polypropylene (PP) (Chen et al., 2013; Elaine, Leila, & Elen, 2009; Gomes, Visconte, & Pacheco, 2008, 2009; Tjong & Meng, 2003a; Valášková et al., 2009), polyamide (PA) (Macheca, Focke, Kaci, Panampilly, & Androsch, 2018), thermoplastic starch (TPS) (Lu, Zhang, Liu, Li, & Xin, 2012), and their copolymers or blends (Tjong, Meng, & Xu, 2002).

Gomes et al. dispersed maleated-PP into vermiculite/PP blend by using a twin-screw extruder in order to investigate the effects of filler on mechanical properties. They found that mechanical properties improved by 3–5 wt% vermiculite addition, but that improvement was not as good as expected (Gomes et al., 2008). In order to overcome this issue, Gomes et al. also produced PP/vermiculite composite by using organically modified vermiculite (OMV) to improve thermal properties of PP. Although, crystallinity of the composite increased by incorporation of small amount of OMV, thermal stability of the composites improved significantly (Gomes et al., 2009).

Chen et al. produced PP/OMV composite to improve flame retardancy of composite. They found that limiting oxygen index (LOI) value increased from 30.7% to 32.9% with 1 wt% OMV addition into the composite (Chen et al., 2013).

In order to understand mixing behavior of OMV in the polymer matrix, Valášková et al. prepared three different maleated-PP/OMV nanocomposites by using three different procedures including low-temperature melt intercalation of OMV, mechanical exfoliation of OMV by jet-milling, and chemical exfoliation of OMV. They found that homogeneous distribution and better exfoliation of OMV in the composite was observed by using jet milled OMV and slower mixing speed (M. Valášková et al., 2009). Tjong and Bao investigated the effects of OMV addition on crystallization kinetics of PE composite. They found that exfoliated vermiculite layers acted as effective nucleation sites for the secondary nucleus of the nanocomposites during crystallization (Tjong & Bao, 2005). In order to understand thermomechanical properties of composites, Tjong and Meng prepared PE/OMV nanocomposite by direct melt compounding in a twin-screw extruder and injection molding. According to their results, 50% increment in storage modulus was achieved with 4 wt% OMV addition into PE (Tjong & Meng, 2003b).

In another study, Hundáková et al. conducted research about the antibacterial properties of PE/OMV composites. Vermiculite was modified by a simple cation exchanging process with hexadecyltrimethylammonium (HDTMA⁺) bromide at three concentrations and used as OMV nanofillers in PE matrix. The composites were prepared by melt compounding technique. As reported in the study, PE chains diffused into the gaps between layers of OMV caused by alkyl tails of HDTMA⁺ molecules. This was assumed to be caused by formation of a non-polar, water-free area in the structure. Also, the antibacterial activity tests were performed to approve the productivity of the OMV/PE composites. The test was carried out on Gram-positive (G⁺) (*Staphylococcus aureus*, *Enterococcus faecalis*) and Gram-negative (G⁻) (*Escherichia coli*) bacterial strains. The positively charged ammonium groups reacted with anionic groups on the cell surface of the bacterium. This reaction reported to affect the permeability of the cell membranes of bacteria and cause the loss of intracellular components and dead of microorganism. The dissimilarity between the cellular structures of two bacterial groups G⁺ and G⁻ was given as the reason of differences between the sensitivities of G⁺ and G⁻ bacteria against the prepared composite samples. The composites including the higher quantity of HDTMA⁺ were found more effective against bacterial colonies (Hundáková et al., 2015).

In another study, Valášková et al. fabricated and characterized vermiculite/LDPE composites, by using two different types of vermiculite

(ball-milled and jet-milled). Smaller particle size and narrow particle size distributions were obtained by jet-milling for vermiculite. Smaller crystallite size was found for compression molded jet-milled vermiculite/LDPE composites (Marta Valášková et al., 2013).

Lu et al. carried out a study about vermiculite reinforced thermoplastic starch via the solution-casting process. The vermiculite was used to increase the mechanical properties of thermoplastic starch. Urea was used as a plasticizer for the composites. The vermiculite/starch composites showed better mechanical properties than pure starch. The elongation at break values were decreased with incorporation of vermiculite particles to the composites that were assumed to be caused by increased rigidity (Lu et al., 2012).

Fernández et al. prepared PLLA/OMV nanocomposites by melt compounding. They found that OMV addition accelerated the thermo-mechanic oxidation of PLLA and molecular weight of PLLA decreased during melt compounding (Fernández, Fernández, & Aranburu, 2013).

Tjong et al. prepared PA6/PP/OMV ternary nanocomposite by melt compounding followed by injection molding. They reported that thermal properties of PA6 improved with PP/OMV addition (Tjong et al., 2002).

Macheca et al. prepared PA11/EV bio-nanocomposite by melt compounding. 10 wt% addition of EV improved mechanical properties and fire retardancy of composite (Macheca et al., 2018).

Xu et al. have reported the direct melt intercalation of polypropylene carbonate (PPC) into OMV by direct melt compounding. The mechanical properties of PPC/OMV nanocomposites i.e. the strain at break and the yield strength were reduced dramatically with a higher amount of OMV loading (Xu, Li, Xu, Li, & Meng, 2005).

In order to understand the barrier properties of vermiculite, Essabti et al. prepared chitosan/vermiculite coating onto corona treated PET film by bar coating technique. They have reported that helium and oxygen permeability of composite decreased with increased amount of vermiculite addition (Essabti et al., 2018).

Kim et al. coated PVA/OMV nanocomposite onto multilayered LDPE packaging film for understanding the oxygen barrier property against high moisture content. They found that oxygen barrier properties significantly affected by relative humidity (RH%). When RH% increased more than 50%, oxygen transmission rate increased exponentially (Kim et al., 2018).

3.2. Vermiculite Filled Thermoset Composites

Thermosets are polymers that are irreversibly cured from prepolymers or resins. Thermoset polymer composites are produced by using a wide variety of polymers. In the literature, most common thermosets are polyglycerol (PG) resin, phenolic resin, and urea formaldehyde (Fig. 5).

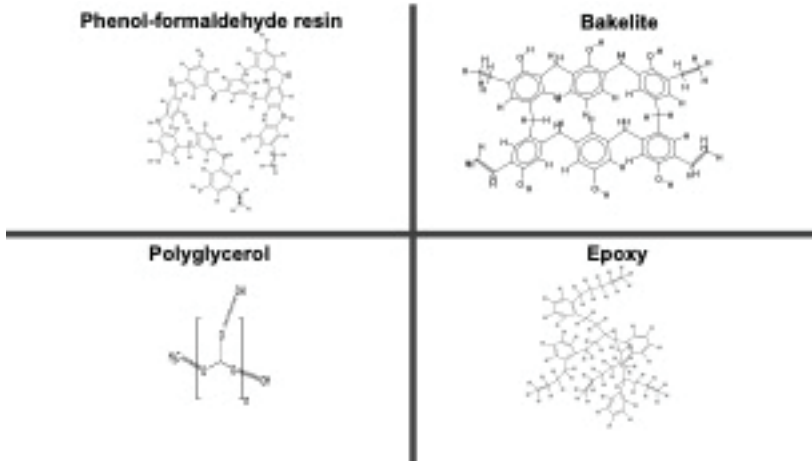


Figure 5. Chemical structures of various thermoset polymers

Medeiros et al. modified exfoliated vermiculite by polymerization and carbonization of glycerol to improve oil removal efficiency. Small amounts of carbon were formed around 300–400 °C. When the temperature was increased, porous carbon was formed by the decomposition of PG. They found that oil absorbency was increased from 0.8–1.2 $\text{g}_{\text{oil}}/\text{g}_{\text{EV}}$ to 4–5 $\text{g}_{\text{oil}}/\text{g}_{\text{EV}}$ with increasing carbonization temperature from 380 °C to 750 °C (de Araújo Medeiros, Sansiviero, Araújo, & Lago, 2009).

You et al. produced epoxy/OMV nanocomposite by *in situ* melt blending of bisphenol A epoxy resin in the presence of amino modified vermiculite. They found that the affinity between epoxy and OMV was good and OMV was easily intercalated by epoxy (You, Yang, Tsai, Wu, & Su, 2016). In another study, Mittal produced epoxy/OMV nanocomposites by solution casting for gas barrier applications. They found that incorporation of OMV into epoxy matrix improved oxygen barrier properties, also water barrier properties of composites could be improved significantly by grafting of large alkyl chains onto vermiculite layers (Mittal, 2008).

Křístková et al., prepared composite samples by thermal curing of Mg-vermiculite (Mg-V), phenolic resin, and fine pulverized Al_2O_3 mixture. They found that porosity and crack density decreased with the increment in phenolic resin ratio in the composite. Also, better encapsulation of vermiculite particles in the phenolic matrix was observed for lower

phenolic resin amounts. (Křístková, Weiss, & Filip, 2004).

Machado et al. studied about polymer coated EV–iron composites as floatable magnetic adsorbents for water spilled contaminants. In their study, they have used vermiculite-iron based materials coated by epoxy resin and PS and characterized magnetic, morphological, thermal and structural properties of composites. Since, hydrophobicity increases oil removal capacity of composite systems. PS and epoxy were chosen for their hydrophobic and good adhesion behavior, respectively. When the polymer ratio was increased, the gaps between exfoliated vermiculite layers were filled by the polymeric material. The oil absorption capacity of the polymer coated hydrophobized composites was found approximately $2.3 \text{ g}_{\text{oil}}/\text{g}_{\text{composite}}$ for the Fe_{0.1}/EV/0.1 epoxy (Machado et al., 2006).

3.3. Vermiculite Filled Elastomer Composites

Elastomers are flexible, elastic polymers. They can be stretched-deformed at various levels and they turn back to their original size easily. Their properties can be tuned by many factors including type of elastomer and cross-linking density. Vermiculite can also be compounded with elastomers. Zhang et al. produced natural rubber (NR)/OMV nanocomposites by combination of melt mixing and vulcanization. They found that OMV incorporation into NR improved the mechanical properties (Zhang, Liu, Han, Guo, & Wu, 2009). In addition to NR, PU is also used in many areas including foams, coatings, adhesives, etc. The properties of PU such as flexibility or rigidity significantly based on the type of polyols and amount of isocyanate used in the polymerization process. Qian et al. conducted research about the synthesis and properties of EV/PU nanocomposites. According to their findings, rheological behavior of EV/PU nanocomposites was pseudo-plastic (shear-thinning) compared to Newtonian-type vermiculite and polyol slurry/solution. Also, mechanical properties of EV/PU nanocomposites were better than pure PU and vermiculite/PU composites and gas permeability of the system. As reported, both dispersion and modification of the surface were found significant in terms of gas barrier properties. Also, Qian et al. synthesized PU/OMV nanocomposites through solvent-free *in situ* intercalative polymerization. According to their results, tensile modulus of the nanocomposite increased by 4 times and CO₂ permeation decreased 40% with 5.3 wt% loading of OMV into composite (Qian et al., 2012).

El-Nemr et al. studied effects of gamma irradiation on physico-chemical properties of SBR/maleic anhydride (MA)/vermiculite nanocomposites. They found that crosslinking activity increased with increasing amount of irradiation dose and also vermiculite and MA addition improved thermal stability (El-Nemr, Ali, El-Sayed, & Zahran, 2018). They also conducted

similar study for EPDM/MA/vermiculite nanocomposite by direct melt compounding. They found similar behavior for nanocomposites like their previous study (El-Nemr, Khaffaga, Saleh, & Zahran, 2018).

Szadkowski et al. prepared ethylene-propylene rubber (EP)/vermiculite composite by melt compounding. According to their results, vermiculite tear resistance and barrier performance of composite (Szadkowski, 2020).

In another study, Tjong et al. incorporated styrene-ethylene-butadiene-styrene (SEBS) into PP/vermiculite nanocomposite to improve impact strength. They found that impact resistance increased exponentially with the increased amount of SEBS in the composite (Tjong & Meng, 2003a).

3.3.1. Vermiculite Filled Foam Composites

Polymeric foams are also another form of the polymers with very low weight and density. The sound absorption, thermal insulation, gas barrier properties of vermiculite can be improved by creating foamy structures. Closed cell type rigid polyurethane (PU) foams are generally used as thermal insulation materials. The loss of blowing gases makes a problem that affects the thermal conductivity of the system. The fillers such as plate-like nanomaterials construct a gas barrier hence decrease gas transportation and increase the resistance to insulation aging. Typical vermiculite filled polymer composite foam production process was given in Fig. 6. According to this, modified or unmodified vermiculite firstly mix with polyol, this mixture is casted into a mold and finally is cured in this mold to get final product.

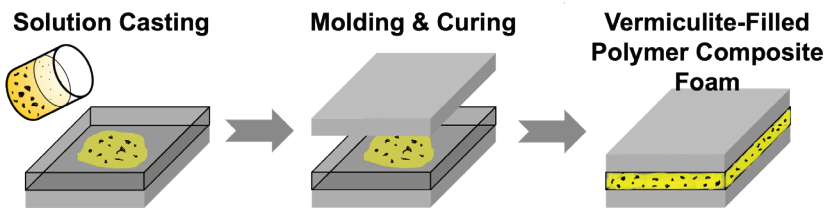


Figure 6. Schematic representation of vermiculite filled polymer composite foam production process

Li et al. incorporated vermiculite fillers into PU foam to improve sound absorbing, thermal insulating and resilience properties. They found that increased vermiculite content increased the resilience of the system. Sound absorption capacity of PU foam composites was better than pure PU foam. Also, smaller vermiculite fillers showed better sound absorption for all composites. When foam density increased, cell morphology became more compact, heat flow through cell wall became easier that led to a decrease in thermal insulation. When vermiculite is added in PU foam, regardless of the filler content, thermal conductivity value increased (Li,

Chuang, Huang, Lou, & Lin, 2015).

In another study, Patro et al., synthesized exfoliated and unmodified vermiculite/ rigid polyurethane nanocomposites. The effect of clay addition on polymerization and foaming reactions were investigated by the gel and rise times. The cell morphology and closed cell content of the nanocomposite were also examined. Both polyol and the polyol–vermiculite blend exhibited Newtonian behavior due to weaker interaction between vermiculite and polyol. When the vermiculite content in foam increased, cell size become smaller and the structure seemed more uniform due to the inducing effect of vermiculite on gas bubble nucleation. And it also led to a higher number of finer cells in the foam structure. According to their results, when vermiculite content in foam increased, the closed cell content also increased; a significant reduction of thermal conductivity was observed due to reduction in cell size; the brittleness of foam increased, and the bulk density of the foams increased slightly (Patro, Harikrishnan, Misra, & Khakhar, 2008).

Park et al., carried out a study about the dispersion of vermiculite into PU with in-situ intercalative polymerization. They found that the full exfoliation of vermiculite had been seen only in the presence of masterbatch mixing. The films prepared with the masterbatch method also showed a significant reduction in CO₂ gas permeation which was around ~40 % compared to pristine PU rigid films (Park et al., 2013).

3.3.2. Vermiculite Filled Polymeric Gel Composites

Gels are materials composed of a three-dimensional physically or chemically crosslinked polymer or colloidal network immersed in a fluid. They are usually soft and weak but can be made hard and tough. Polymer gels are crosslinked networks of polymers which behave like viscoelastic solids (Fig. 7). Aerogel is an ultralight material which shows excellent adsorption performance thanks to its high specific surface area and pore volume. Aerogels show very effective insulation properties since they are extremely porous which are in the nanometer range. The presence of these pores makes the aerogel so useful for insulation applications.

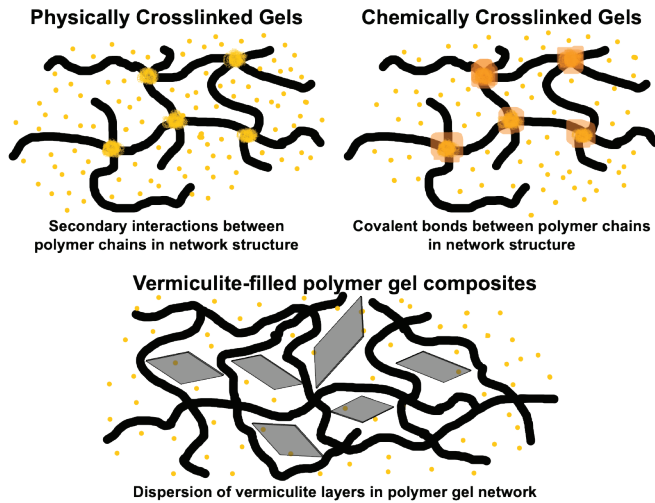


Figure 7. Schematic illustration of polymer gels

Zhou et al. modified expanded vermiculite by an in-situ gel method. Gelation time and the effect of propylene oxide (PO) on some properties were investigated. As given in the study, modified EV had better insulation properties. EV had higher thermal conductivity value when compared with modified EV since its nano-level porous structure restricted the heat transfer (Zhou, Gu, & Wang, 2013).

Jin et al. synthesized polymer gel/vermiculite fiber reinforced composite for oil removal application through *in situ* intercalation and exfoliation technique. As given in the results, vermiculite composite showed good oil absorbency (Jin, Liu, Pu, & Wen, 2014).

He et al. prepared OV/PMMA/1-butyl-3-methylimidazolium hexafluorophosphate composite gel polymer electrolytes (CGPEs) by solution casting method. Crystallinity of CGPE was decreased with the presence of OV. Ionic conductivity and electrochemical window of CGPE was improved with 8 wt% OV addition into composite (He, Chen, Wang, Xie, & Dong, 2013).

4. Conclusions

Vermiculite is a natural mineral with many superior properties. Although its general structure and properties are affected by the geological conditions during its formation and nature of the vermiculite, it can be modified by delamination/exfoliation, intercalation or chemical modifications. The unique and tunable structure makes it preferable material in many applications such as adsorption (oil, organic solvent,

gas, and metal ions), separation, waste water treatment, electrical, thermal sound, and insulation. In addition to these it can be used as a fire retardant, a barrier material for films, while it can be used in powder form, it is mixed with polymers to modify the properties of the polymers. It can be compounded with various types of polymers including thermoplastics, thermosets, elastomers and composites can be in various forms including films, sheet, foam or gel.

References

- Aristov, Y. I., Restuccia, G., Tokarev, M. M., Buerger, H. D., & Freni, A. (2000). Selective Water Sorbents for Multiple Applications. 11. CaCl_2 Confined to Expanded Vermiculite. *Reaction Kinetics and Catalysis Letters*, 71(2), 377-384.
- Bar-Tal, A., Saha, U. K., Raviv, M., & Tuller, M. (2019). Chapter 7 - Inorganic and Synthetic Organic Components of Soilless Culture and Potting Mixtures. In M. Raviv, J. H. Lieth, & A. Bar-Tal (Eds.), *Soilless Culture (Second Edition)* (pp. 259-301). Boston: Elsevier.
- Bush, A. L. (2001). Construction Materials: Lightweight Aggregates. In K. H. J. Buschow, R. W. Cahn, M. C. Flemings, B. Iilschner, E. J. Kramer, S. Mahajan, & P. Veyssi re (Eds.), *Encyclopedia of Materials: Science and Technology* (pp. 1550-1558). Oxford: Elsevier.
- Chen, S., Wang, B., Kang, J., Chen, J., Gai, J., Yang, L., & Cao, Y. (2013). Synergistic Effect of Organic Vermiculite on the Flame Retardancy and Thermal Stability of Intumescent Polypropylene Composites. *Journal of Macromolecular Science, Part B*, 52(9), 1212-1225.
- Chung, O., Jeong, S.-G., & Kim, S. (2015). Preparation of energy efficient paraffinic PCMs/expanded vermiculite and perlite composites for energy saving in buildings. *Solar Energy Materials and Solar Cells*, 137, 107-112.
- de Ara jo Medeiros, M., Sansiviero, M. T. C., Ara jo, M. H., & Lago, R. M. (2009). Modification of vermiculite by polymerization and carbonization of glycerol to produce highly efficient materials for oil removal. *Applied Clay Science*, 45(4), 213-219.
- de la Calle, C., & Suquet, H. (1988). Vermiculite. *Hydrous phyllosilicates* (pp. 455-496). Berlin, Boston: De Gruyter.
- Duman, O., & Tun , S. (2008). Electrokinetic Properties of Vermiculite and Expanded Vermiculite: Effects of pH, Clay Concentration and Mono- and Multivalent Electrolytes. *Separation Science and Technology*, 43(14), 3755-3776.
- El-Nemr, K. F., Ali, M. A. M., El-Sayed, S. N., & Zahran, M. K. (2018). Physical and chemical properties of gamma-irradiated styrene-butadiene rubber/vermiculite clay nanocomposites modified using maleic anhydride. *Polymer Bulletin*, 75(8), 3587-3606.
- El-Nemr, K. F., Khaffaga, M. M., Saleh, S. N., & Zahran, M. K. (2018). Physico-chemical and spectroscopic properties of gamma irradiated ethylene propylene diene monomer rubber/vermiculite clay/maleic anhydride nanocomposites. *Polymer Composites*, 39(7), 2469-2478.
- Elaine, G., Leila, V., & Elen, P. (2009). Thermal characterization of polypropylene/vermiculite composites. *Journal of Thermal Analysis and Calorimetry*, 97(2), 571-575.

- Essabti, F., Guinault, A., Roland, S., Régnier, G., Ettaqi, S., & Gervais, M. (2018). Preparation and characterization of poly(ethylene terephthalate) films coated by chitosan and vermiculite nanoclay. *Carbohydrate Polymers*, *201*, 392-401.
- Feng, J., Liu, M., Fu, L., Zhang, K., Xie, Z., Shi, D., & Ma, X. (2020). Enhancement and mechanism of vermiculite thermal expansion modified by sodium ions. *RSC advances*, *10*(13), 7635-7642.
- Fernández, M. J., Fernández, M. D., & Aranburu, I. (2013). Poly(l-lactic acid)/organically modified vermiculite nanocomposites prepared by melt compounding: Effect of clay modification on microstructure and thermal properties. *European Polymer Journal*, *49*(6), 1257-1267.
- Gellert, R. (2010). 8 - Inorganic mineral materials for insulation in buildings. In M. R. Hall (Ed.), *Materials for Energy Efficiency and Thermal Comfort in Buildings* (pp. 193-228): Woodhead Publishing.
- Gencil, O., del Coz Diaz, J. J., Sutcu, M., Koksall, F., Alvarez Rabanal, F. P., Martinez-Barrera, G., & Brostow, W. (2014). Properties of gypsum composites containing vermiculite and polypropylene fibers: Numerical and experimental results. *Energy and Buildings*, *70*, 135-144.
- Gomes, E. V. D., Visconte, L. L. Y., & Pacheco, E. B. A. V. (2008). Morphological, Thermal and Mechanical Properties of Polypropylene and Vermiculite Blends. *International Journal of Polymeric Materials and Polymeric Biomaterials*, *57*(10), 957-968.
- Gomes, E. V. D., Visconte, L. L. Y., & Pacheco, E. B. A. V. (2009). Thermal characterization of polypropylene/vermiculite composites. *Journal of Thermal Analysis and Calorimetry*, *97*(2), 571.
- He, P., Chen, B., Wang, Y., Xie, Z., & Dong, F. (2013). Preparation and characterization of a novel organophilic vermiculite/poly(methyl methacrylate)/1-butyl-3-methylimidazolium hexafluorophosphate composite gel polymer electrolyte. *Electrochimica Acta*, *111*, 108-113.
- Hundáková, M., Tokarský, J., Valášková, M., Slobodian, P., Pazdziora, E., & Kimmer, D. (2015). Structure and antibacterial properties of polyethylene/ organo-vermiculite composites. *Solid State Sciences*, *48*, 197-204.
- Isci, S. (2017). Intercalation of vermiculite in presence of surfactants. *Applied Clay Science*, *146*, 7-13.
- Jin, F., Liu, R., Pu, W., & Wen, C. (2014). Preparation and Properties of Polymer/ Vermiculite Hybrid Superabsorbent Reinforced by Fiber for Enhanced Oil Recovery. *Journal of Chemistry*, *2014*, 286091.
- Karatas, M., Benli, A., & Toprak, H. A. (2019). Effect of incorporation of raw vermiculite as partial sand replacement on the properties of self-compacting mortars at elevated temperature. *Construction and Building Materials*, *221*, 163-176.

- Kim, J. M., Lee, M. H., Ko, J. A., Kang, D. H., Bae, H., & Park, H. J. (2018). Influence of Food with High Moisture Content on Oxygen Barrier Property of Polyvinyl Alcohol (PVA)/Vermiculite Nanocomposite Coated Multilayer Packaging Film. *Journal of Food Science*, 83(2), 349-357.
- Koksal, F., Mutluay, E., & Gencel, O. (2020). Characteristics of isolation mortars produced with expanded vermiculite and waste expanded polystyrene. *Construction and Building Materials*, 236, 117789.
- Křístková, M., Weiss, Z., & Filip, P. (2004). Hydration properties of vermiculite in phenolic resin friction composites. *Applied Clay Science*, 25(3), 229-236.
- Li, T.-T., Chuang, Y.-C., Huang, C.-H., Lou, C.-W., & Lin, J.-H. (2015). Applying vermiculite and perlite fillers to sound-absorbing/thermal-insulating resilient PU foam composites. *Fibers and Polymers*, 16(3), 691-698.
- Liu, M., Feng, J., Mo, W., Su, X., & Fu, L. (2020). A novel quantitative analysis method of microwave energy absorption during vermiculite expansion process. *Thermochimica Acta*, 691, 178718.
- Low, N. M. P. (1984). The Thermal Insulating Properties of Vermiculite. *Journal of Thermal Insulation*, 8(2), 107-115.
- Lu, P., Zhang, M., Liu, Y., Li, J., & Xin, M. (2012). Characteristics of vermiculite-reinforced thermoplastic starch composite films. *Journal of Applied Polymer Science*, 126(S1), E116-E122.
- Machado, L. C. R., Lima, F. W. J., Paniago, R., Ardisson, J. D., Sapag, K., & Lago, R. M. (2006). Polymer coated vermiculite-iron composites: Novel floatable magnetic adsorbents for water spilled contaminants. *Applied Clay Science*, 31(3), 207-215.
- Macheca, A. D., Focke, W. W., Kaci, M., Panampilly, B., & Androsch, R. (2018). Flame retarding polyamide 11 with exfoliated vermiculite nanoflakes. *Polymer Engineering & Science*, 58(10), 1746-1755.
- Malamis, S., & Katsou, E. (2013). A review on zinc and nickel adsorption on natural and modified zeolite, bentonite and vermiculite: Examination of process parameters, kinetics and isotherms. *Journal of Hazardous Materials*, 252-253, 428-461.
- Mittal, V. (2008). Epoxy—Vermiculite Nanocomposites as Gas Permeation Barrier. *Journal of Composite Materials*, 42(26), 2829-2839.
- Motokawa, R., Endo, H., Yokoyama, S., Ogawa, H., Kobayashi, T., Suzuki, S., & Yaita, T. (2014). Mesoscopic Structures of Vermiculite and Weathered Biotite Clays in Suspension with and without Cesium Ions. *Langmuir*, 30(50), 15127-15134.
- Papadopoulos, A., Bar-Tal, A., Silber, A., Saha, U., & Raviv, M. (2008). Inorganic and synthetic organic components of soilless culture and potting mixes. *Soillless Culture*, 505-543.

- Park, Y. T., Qian, Y., Lindsay, C. I., Nijs, C., Camargo, R. E., Stein, A., & Macosko, C. W. (2013). Polyol-Assisted Vermiculite Dispersion in Polyurethane Nanocomposites. *ACS Applied Materials & Interfaces*, 5(8), 3054-3062.
- Patro, T. U., Harikrishnan, G., Misra, A., & Khakhar, D. V. (2008). Formation and characterization of polyurethane—vermiculite clay nanocomposite foams. *Polymer Engineering & Science*, 48(9), 1778-1784.
- Qian, Y., Liu, W., Park, Y. T., Lindsay, C. I., Camargo, R., Macosko, C. W., & Stein, A. (2012). Modification with tertiary amine catalysts improves vermiculite dispersion in polyurethane via in situ intercalative polymerization. *Polymer*, 53(22), 5060-5068.
- Schulze, D. G. (2005). Clay Minerals. In D. Hillel (Ed.), *Encyclopedia of Soils in the Environment* (pp. 246-254). Oxford: Elsevier.
- Shoukry, H., Kotkata, M. F., Abo-El-Enain, S. A., Morsy, M. S., & Shebl, S. S. (2016). Enhanced physical, mechanical and microstructural properties of lightweight vermiculite cement composites modified with nano metakaolin. *Construction and Building Materials*, 112, 276-283.
- Suvorov, S. A., & Skurikhin, V. V. (2003). Vermiculite — a Promising Material for High-Temperature Heat Insulators. *Refractories and Industrial Ceramics*, 44(3), 186-193.
- Szadkowski, B. M., Anna; Rybiński, Przemysław; Żukowski, Witold; Zaborski, Marian. (2020). Characterization of Ethylene–propylene Composites Filled with Perlite and Vermiculite Minerals: Mechanical, Barrier, and Flammability Properties. *Materials*, 13(3), 585.
- Tjong, S. C., & Bao, S. P. (2005). Crystallization regime characteristics of exfoliated polyethylene/vermiculite nanocomposites. *Journal of Polymer Science Part B: Polymer Physics*, 43(3), 253-263.
- Tjong, S. C., & Meng, Y. Z. (2003a). Impact-modified polypropylene/vermiculite nanocomposites. *Journal of Polymer Science Part B: Polymer Physics*, 41(19), 2332-2341.
- Tjong, S. C., & Meng, Y. Z. (2003b). Preparation and characterization of melt-compounded polyethylene/vermiculite nanocomposites. *Journal of Polymer Science Part B: Polymer Physics*, 41(13), 1476-1484.
- Tjong, S. C., Meng, Y. Z., & Xu, Y. (2002). Preparation and properties of polyamide 6/polypropylene–vermiculite nanocomposite/polyamide 6 alloys. *Journal of Applied Polymer Science*, 86(9), 2330-2337.
- Valášková, M. & Martynkova, G. S. (2012). Vermiculite: structural properties and examples of the use. *Clay Minerals in Nature* (pp.209-238). IntechOpen Ltd. London, UK.
- Valášková, M., Simha Martynková, G., Matějka, V., Barabaszová, K., Plevová, E., & Měřínská, D. (2009). Organovermiculite nanofillers in polypropylene. *Applied Clay Science*, 43(1), 108-112.

- Valášková, M., Tokarský, J., Barabaszová, K. Č., Matějka, V., Hundáková, M., Pazdziora, E., & Kimmer, D. (2013). New aspects on vermiculite filler in polyethylene. *Applied Clay Science*, 72, 110-116.
- Wang, W., & Wang, A. (2019). 9 - Vermiculite Nanomaterials: Structure, Properties, and Potential Applications. In A. Wang & W. Wang (Eds.), *Nanomaterials from Clay Minerals* (pp. 415-484): Elsevier.
- Xu, J., Li, R. K. Y., Xu, Y., Li, L., & Meng, Y. Z. (2005). Preparation of poly(propylene carbonate)/organo-vermiculite nanocomposites via direct melt intercalation. *European Polymer Journal*, 41(4), 881-888.
- You, C., Yang, C., Tsai, W., Wu, S., & Su, C. (2016, 12-13 Nov. 2016). *Preparation and characterization of epoxy/vermiculite nanocomposites*. Paper presented at the 2016 International Conference on Advanced Materials for Science and Engineering (ICAMSE).
- Zhang, Y., Liu, W., Han, W., Guo, W., & Wu, C. (2009). Preparation and properties of novel natural rubber/organo-vermiculite nanocomposites. *Polymer Composites*, 30(1), 38-42.
- Zhou, F., Gu, H.-Z., & Wang, C.-F. (2013). Preparation and microstructure of in-situ gel modified expanded vermiculite. *Ceramics International*, 39(4), 4075-4079.

Chapter 8

DESIGN AND IMPLEMENTATION OF A MOBILE CULTURAL HERITAGE KNOWLEDGE MANAGEMENT SYSTEM FOR THE INTERNET OF ARCHEOLOGICAL THINGS



Mehmet Erkan YÜKSEL¹

Hüseyin FIDAN²

¹ Assist. Prof. Dr., Burdur Mehmet Akif Ersoy University, Faculty of Engineering and Architecture, Department of Computer Engineering, Burdur-Turkey. Email: erkanyuksel@mehmetakif.edu.tr, Orcid ID: 0000-0001-8976-9964

² Assoc. Prof. Dr., Burdur Mehmet Akif Ersoy University, Faculty of Engineering and Architecture, Department of Industrial Engineering, Burdur-Turkey. Email: hfidan@mehmetakif.edu.tr, Orcid ID: 0000-0002-7482-8922

INTRODUCTION

Museums are cultural institutions exhibiting artifacts specific to social structures, thereby revealing the relations among cultures and ensuring that national values are recognized. International Council of Museums (ICOM) defined a museum as:

“A non-profit, permanent institution in the service of society and its development, open to the public, which acquires, conserves, researches, communicates and exhibits the tangible and intangible heritage of humanity and its environment for the purposes of education, study and enjoyment.” (ICOM, 2020).

According to ICOM's definition, museums are institutions that aim to display the material and immaterial heritages of historical value to the people. This purpose also contributes to the education of society and the establishment of relations between different cultural structures. In the literature, it is possible to find different researches that promote similar opinions. Museums, which constitute a communication bridge between people from different cultures and today's social life, are considered to play a unifying role in countries with cultural confusion and separation (Mercin, 2006). The primary mission undertaken by museums is to preserve cultural values and transfer them to society according to scientific patterns. In this context, museums are considered as institutions that carry out continuous education activities and develop cultural empathy (Siedel and Hudson, 1999; Tezcan and Ödekan, 2011). These interactions allow people to pay more attention to cultural heritages and thus museum and archaeological site visits increase. For this reason, the museum management should be fully aware of its place and functions in the social plan, not just protecting and presenting objects and collections (Kenderdine, 1998). The number of museum visitors between 2000 and 2019 in Turkey is shown in Figure 1 that shows people's interest in museums and archaeological sites is constantly increasing.

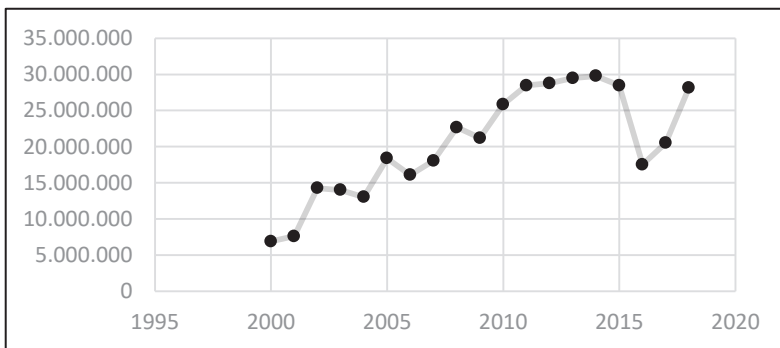


Figure 1: Number of visitors to museums and sites in Turkey (<https://kvmgm.ktb.gov.tr/TR-43336/muze-istatistikleri.html>)

The concept of digitalization, which has come into our lives with the developments of information and communication technologies, can be expressed as the transfer of process and objects to the electronic environment. The concept, which is technically defined as the digitization of data, is expressed as virtualization because data is transferred to the electronic environment (Fidan, 2013). The concepts such as e-government, e-school, e-book, e-commerce, e-invoice, and e-municipality have begun to be used as expressions emphasizing the transformation. Digital definitions of data have led to an increase in abilities related to transmission, access, and storage, a decrease in costs, and an increase in the efficiency of data analysis (Yılmaz, 2011). These technological developments have involved the rise of a research field called Knowledge Management (KM), which includes the processes of acquiring, storing, transmitting, and using data in digital format. The concept of KM, which has great importance in business processes, is also a crucial issue in museum management.

Digitalization, which becomes a part of our social life by developing technology, brings along cultural changes (Özbağ, 2013). In this context, the transferring of information, documents, and data of cultural heritage to electronic environments is seen as one of the important issues for archeological studies (Biedermann, 2017). Digitalization of cultural heritage data brings many advantages for data processing such as storing, transmitting, accessing, and analyzing with low cost (Özbağ, 2013). Due to these advantages, it cannot be expected that museums, which are institutions that undertake the mission of preserving cultural heritages and exhibiting them to the public, will not be affected by the virtualization. In the last two decades, it has been noticed that researches on digitalization on museum core tasks and the concept of KM in museums have gained importance in both literature and practice (Parry, 2010). KM, which is a concept generally encountered in industrial processes, has started to be used in cultural heritage studies (Hervy et al., 2013). Also, it is observed that studies on museum management systems carried out within the framework of KM are generally visitor-oriented such as virtual guides, e-tours, and web site presentations.

KM is defined as the process of producing, sharing, communicating, and managing knowledge using information and communication technologies (Onyancha and Ocholla, 2009). According to the definition, KM includes four general tasks such as conceptualize, reflect, act, and review. Conceptualization refers to the acquisition and concretization of data by different actors. Reflection is referring to improvements and shortcomings by highlighting the strengths and

weaknesses of the data. The act is taking the necessary measures according to the analysis results of the data and shaping the process according to the evaluations. The review is the evaluation of previous and reshaping processes (Wielinga, Sandberg, and Schreiber, 1997). This approach, which determines the framework of the KM process, also can be used in the museum management system. Kavakli and Bakogianni (2003) stated that the mission and processes of the museum should be defined in the conceptualization; the reflection should include the determination of the procedural deficiencies and relational deficiencies of public information about the object. The authors also emphasized that effective solutions to the problems should be determined in the action stage and evaluation of the changes should be made in the review task.

Technological systems used in museums have revealed some concepts in the literature such as virtual museum, digital museum, e-museum, smart museum, etc. The literature has two different views on these new concepts. Some authors argue that new approaches cannot replace the exhibition of real objects and physical museums (Niewerth, 2013; Biedermann, 2017). According to the other opinions, virtualized museums will increase the effectiveness of information organization (Parry, 2010), support their social and educational roles, and thus, cultural heritages will increase their value (Li and Liew, 2015). Due to the advantages of digital technologies, the positive contributions of these technologies to museum processes cannot be ignored. According to a study, the views of museum visitors about museum websites were determined. In the conclusion of the study, it was determined that visitor expectations regarding the use of digital resources on museum websites are quite high (Marty, 2008).

The studies conducted within the framework of information organization and presentation generally include practices and analyzes created for effective museum visits. Wang et al. (2007) created a Museum Guide System (MGS) based on handheld devices. MGS, which allows visitors to read or listen to information about the exhibitions, is an application that aims to provide independent guide service to each visitor. In another study called I-Muse, which was carried out to provide guide services to visitors, Fevgas et al. (2011) developed a mobile application that includes 3-D supported museum presentations. RFID (Radio Frequency Identification) tags were used to identify artifacts in the application, which included group service in group visits as well as personal use. Developing the I-Muse application by adding interactive education applications, Fevgas et al. (2014) thereby increased cultural interaction by contributing to cultural understanding. Lopez, Fernandez, and Burillo (2016) have developed an NFC (Near Field Communication) based mobile system to systematically record the data obtained about the

artifacts found in the excavation area. It has aimed to collect data entered by archaeologists working in different excavation sites in a common database. In the study, it is emphasized that aid of the NFC-based mobile system, access to data obtained in archaeological excavations is accelerated, efficiency is ensured in the next excavation decision and human-oriented errors in data entry are prevented. Khelifi (2018), who researched the level of technology usage in museums, emphasizes that archaeological excavations are behind in terms of technology usage, and insufficient use of technology in the museum-visitor-excavation triangle causes disconnection in the transfer of information to the next generations. One of the recent studies suggesting that the use of digital technologies in museum processes will increase personal and social interactions (Gran et al., 2019). It has been revealed in the study that technological systems can contribute to cultural wealth in society. In order to transfer information to future generations effectively, the cultural heritage data must be obtained, recorded, and presented using technological developments. In this way, the deficiencies in the creation of the information to be presented to the visitors only by the museum management will be prevented. In other words, recording the data of the artifacts found as a result of archaeological excavations into the system at the location where it is located will contribute to the museum management system and ensure the efficient realization of the data flow in the museum-visitor-excavation triangle. In this way, all artifacts data found in different excavations will be collected in a database and relational analysis will be possible.

This study, it is aimed to record the whole process from the discovery of artifacts to presentation in the museum, to eliminate the information gaps, and to increase the data access speed. In this context, three different interactive applications have been developed: museum manager, archaeologist, and visitor. The archaeological excavation is appointed by the museum manager by sharing the location and time interval of the archaeological excavation through the developed mobile application and assigning an archaeologist to the excavation. The archaeological excavation manager can assign RFID tags through the NFC service and record the artifacts found as a result of the excavation together with their location information. The decision to be exhibited in the museum is taken by the museum management by creating a QR code for the artifacts, and access to the artifacts information is provided through the mobile application developed for visitors. Thus, within the framework of KM, a relational management system based on museum management, excavation, archeologist, and visitor was established.

MATERIAL AND METHOD

Radio Frequency Identification

Radio Frequency Identification (RFID), which is used to obtain object information, is a technology consisting of two basic components: a tag carrying data and a reader receiving data from this tag. The RFID tag, whose structure is presented in Figure 2, consists of a silicon chip, antenna, and coating that allow answering queries by radiofrequency. The chip contains data about the object on which the tag is placed. The antenna transmits the object information to the reader using radiofrequency. The coating surrounds the chip and antenna so that the tag can be placed on an object (Wang et al., 2007).

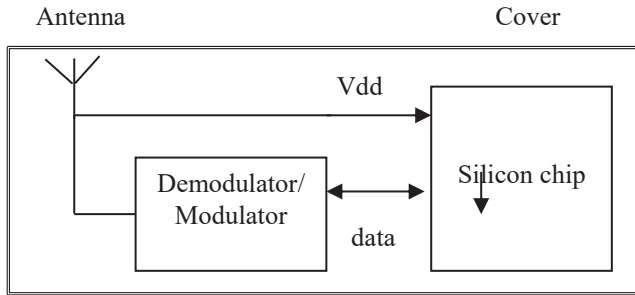


Figure 2: *Structure of RFID tag*

Although RFID technology has been available for a long time, its widespread usage has been adversely affected by problems related to cost and data standards (Pala and İnanç, 2007). With the use of RFID technology especially in automation systems, manual processes are minimized (Penttila, et al., 2006; Zhang, 2005). In this way, it provides significant contributions to companies by increasing employee and process efficiency (Higgins and Cairney, 2006). RFID technology, which has been used not only in industrial applications but also in service sectors such as health, education, and tourism, has been used for museum management and the presentation of archaeological artifacts. Especially, applications targeting museum visitors have become widespread in recent years.

RFID Reader

An RFID reader is a transmitter-receiver device working with radiofrequency. The RFID reader includes a microcontroller to analyze the tag information it reads, a communication module, and an I/O module for external device connections (Yüksel and Yüksel, 2011). The antenna is used to emit radio frequency signals and to catch the returning signals. In this sense, the antenna of the reader is used both to trigger RFID tags

and to capture incoming data from the RFID tag. It should be noted that antenna gain and polarization are among the most important factors determining the reading range. A basic RFID reader scheme is given in Figure 3.

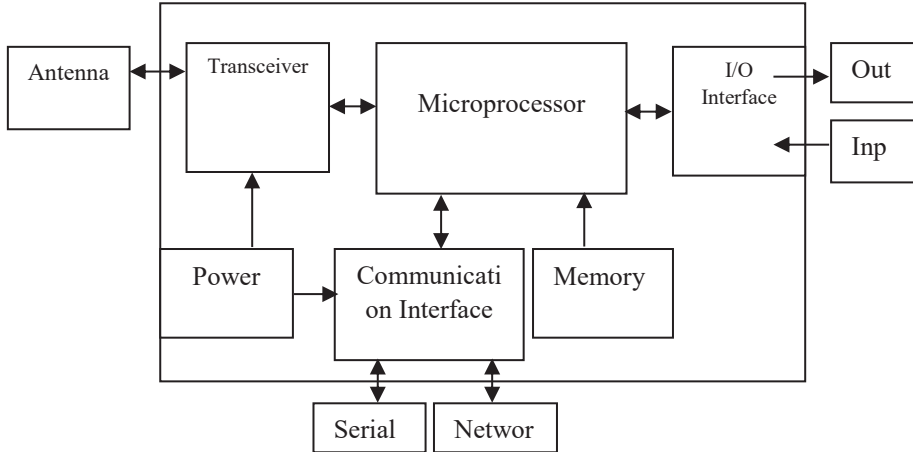


Figure 3: *Structure of RFID Reader (Yüksel and Yüksel, 2011)*

Near Field Communication

Near Field Communication (NFC) is a short-range wireless communication technology designed for interaction with mobile devices and computers. NFC, which allows users to perform contactless transactions and contactless payments, allows users to easily connect to electronic devices. In this context, NFC systems are one of the most ideal methods to establish a connection between other technologies with their bidirectional communication capability (Wang et al., 2007).

Quick Response Code

Quick Response (QR) code is a 2D barcode system developed by the Japanese company Denso Wave. While traditional barcode systems have the capacity to express 20 digits, QR code shown in Figure 4 can encode more than 7000 characters (Chang, 2014). It can be used for encoding data with long character strings such as text or hyperlink addresses, where barcode systems are insufficient due to its greater capacity.



Figure 4: QR codes in different dimensions

RESEARCH MODEL

The developed application has two interfaces, mobile, and web. Using a common database, the system has a functioning model that includes two flow charts for visitors and administrators. The use of archaeologists has been established within the management function and access restrictions have been imposed. In other words, archaeologists and administrator access are realized through the same application.

Museum Visitor System

The visitors who want to use the system are required to install the application on their devices and allow application access permission to the cameras of their phones to enable QR code identification. As seen in the visitor system flow chart given in Figure 5, firstly the QR code is controlled. If the QR code is defined in the system, information and pictures about the artifact will be displayed as far as the administrator allows visitor access. In addition, the system offers visitors the opportunity to hear written information about the artifact.

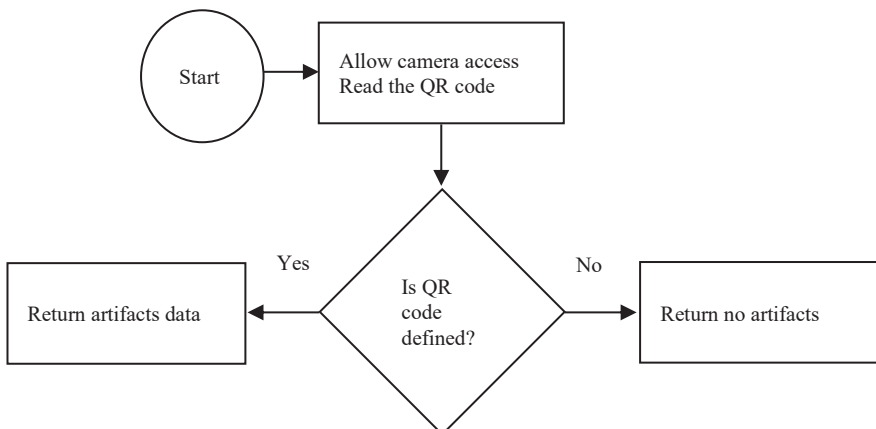


Figure 5: Diagram of museum visitor system

Archaeologist-Administrator System

The flow diagram of the archaeologist-administrator system is presented in Figure 6. Archaeologists added to the system by the administrator are given an RFID tag smart ID card. The archaeologist, who is identified with the RFID tag in the system, can enter the system with the defined RFID tag. If the mobile phone does not have NFC, login can be realized by the user name and password. Thus and view the information about the active excavations on the screen. In the artifacts section, it has the opportunity to examine the previously added works and add new works. The description, picture, and location data to be added to the system are presented to the administrator after identification with RFID. The admin who examines the artifacts uploaded to the system by the archaeologist decides whether the artifact is proper for showing in the museum or not.

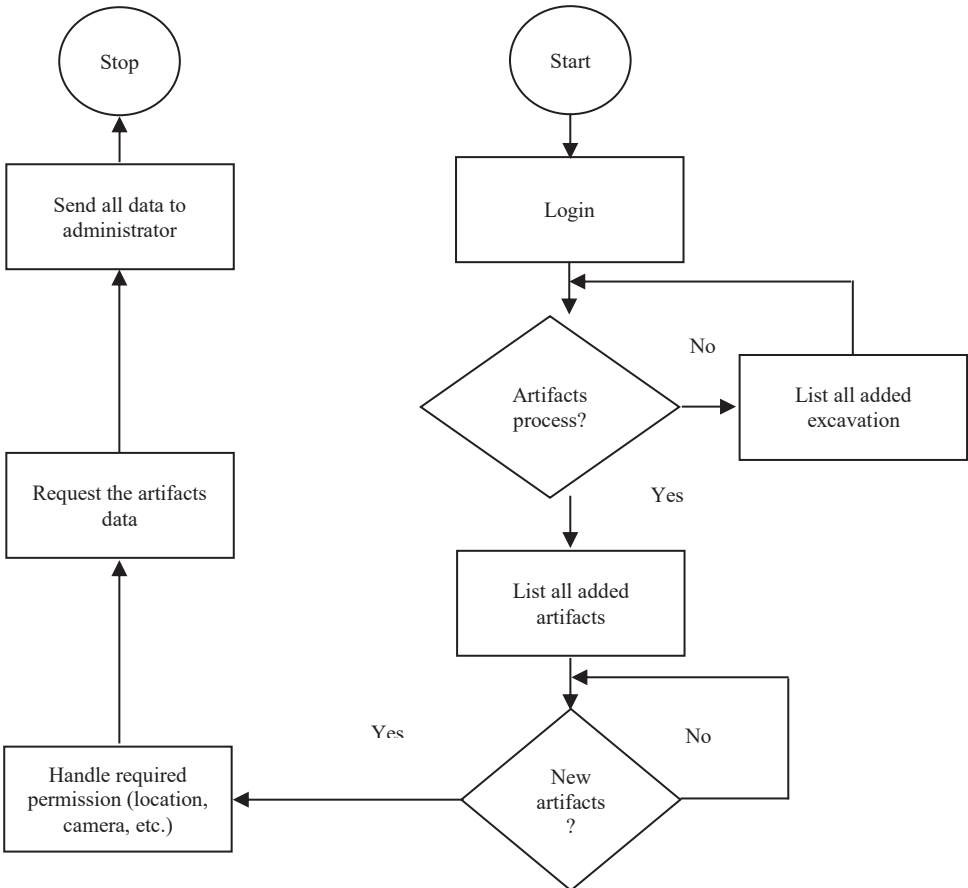


Figure 6: Diagram of Archaeologist-Administrator system

FINDINGS

In our study, a mobile and web-based relational system has been developed in order to maintain the processes in the museum management (administrator)-excavation-visitor triangle effectively. With the creation of the system integrated with each other, it has been ensured that the data to be produced in the field are collected in the same place.

Evaluation of Administrator System

Two applications have been developed for administrator operations, mobile and web-based management panel. Due to the similar nature of manager and archaeologist operations in the mobile application, a single application was prepared, and these two entry types were separated from each other with post-login restrictions. The web-based management module is used only by the administrator. A Web panel that has been designed for easy KM operations such as examining, editing, presenting to visitors as well as creating QR codes was performed.

In addition to being able to login to the system with a user name and password, the administrator will also be able to log in through an RFID defined mobile device with NFC support. Administrators are enabled to carry out transactions related to excavations, artifacts, archaeologists, and their personal information thanks to a menu added in the mobile application. By selecting the excavations option from the menus, the data related to the archaeological excavations defined by the administrator are displayed in Figure 7.

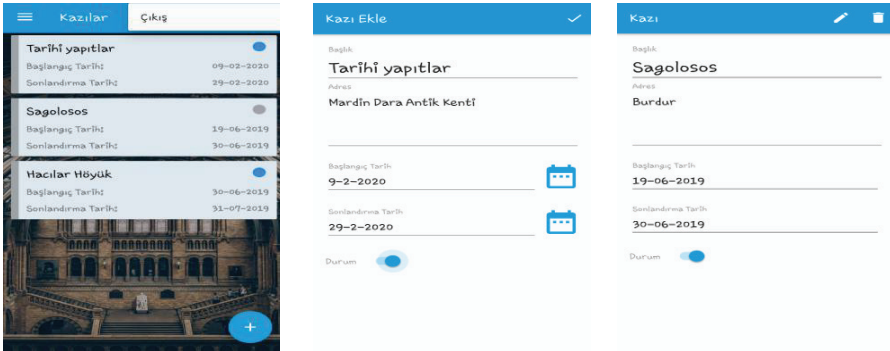


Figure 7: Screenshot of archeologic excavations option

Adding a new archeologist and editing an existing one are other operations that administrators can realize via using the system. As seen in Figure 8, archeologists can be saved to the system with their personal information. Archaeologists can log into the system with the e-mail and password information defined for them after they are registered in the system by the administrator.

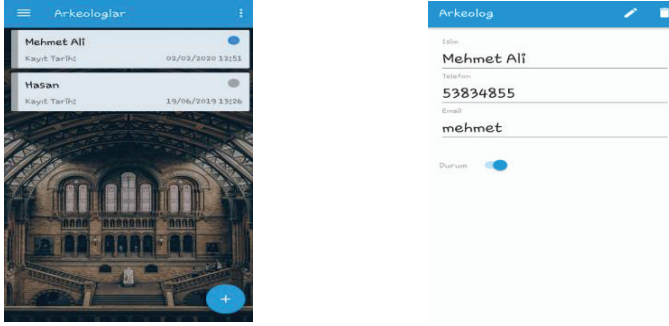










Figure 8: Adding archeologist

In the administrator system, in addition to the excavation and archaeologist management, it is also possible to organize and exhibit the artifacts recorded in the system by archaeologists. As can be seen in Figure 9, in addition to the inventory information about the artifacts, it is possible to register by location it was discovered. The administrator who performs the artifacts review can generate a unique QR code and activate it for the visitor exhibition. The QR code of artifacts was generated by using the RFID code that archeologist associated with the artifacts. Figure 10 shows the list of artifacts added to the system after generating a QR code.

Figure 9: Updating artifacts

Rfid Numarası	Bağlık	QR	Durum	Resim	İşlemler
1001	Kaşıklı Elması		Aktif		Düzenle Sil
1002	Sagalassos		Pasif		Düzenle Sil
1007	deniz atı brosu		Aktif		Düzenle Sil
1006	Denem		Aktif		Düzenle Sil

14 entries

Previous 1 Next

Figure 10: List of artifacts

Evaluation of Archaeologist System

Archaeologists log into the system with the username-password or smart ID card introduced by the administrator, by imposing some operation restrictions in the application prepared for managers. Archaeologists can only view active excavations. Archaeologists can carry out procedures related to the artifacts in order to send the artifacts they find in the excavation area to the administrator. As can be seen in Figure 11, the RFID number, the tags given to the archaeologists by the administrator who started the archaeological excavation, was read with the help of mobile devices with NFC service, and the id information was automatically written. Location is determined by the latitude and longitude data obtained by clicking the location icon.

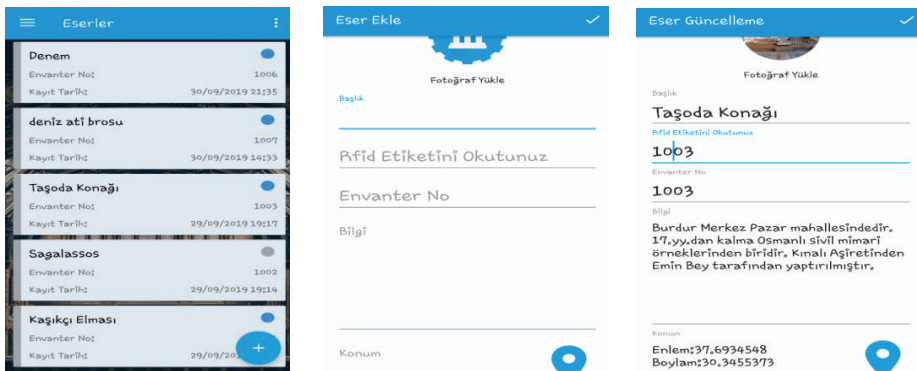


Figure 11: Artifacts operations of archeologists

Evaluation of Museum Visitor System

The administrator will be able to exhibit the artifacts worth to be exhibited in the museum by creating a special QR code. The application prepared for museum visitors presented in Figure 12 has been simplified

as much as possible. By pressing the icon in the application, the QR code that contains the information of the artifacts will be tried to be scanned. If the id information of the artifacts is matched with the RFID data embedded in the QR code, information about the relevant artifacts will be displayed on the screen. At the same time, an alternative to listening to the information of the artifacts has been added to the application.

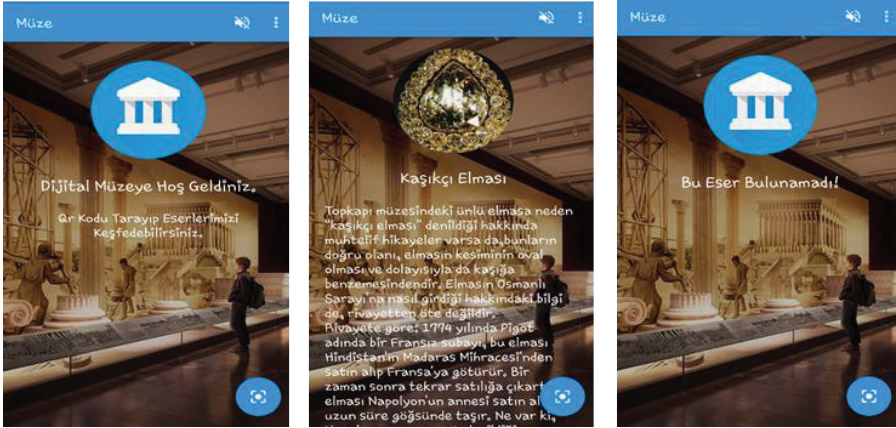


Figure 12: Screenshots of Visitor System

CONCLUSION

In this study, it has been ensured that the data are recorded in a database in all processes from archaeological excavations to the exhibition in museums. Failure to systematically recording large amounts of data leads to incomplete data errors in analysis and not being able to perform relational analyzes. In our study, data errors are minimized by recording the data about the work in an electronic environment. The data to be collected in the database will enable access to confidential information and perform relational analysis using data mining and machine learning techniques. In this way, archeological analysts will have a fast, impeccable, and comfortable analysis environment. Thus, they will reach healthier archeologic knowledge about the artifacts.

In traditional exhibitions, new information boards are prepared when artifacts' information needs to be arranged. Instead of this process, which has disadvantages in terms of cost and time, QR codes that contain information about the artifacts or archaeological sites to be exhibited in this study are used. The information of artifacts to be exhibited in a museum or archaeological sites can be reached with a text embedded in a QR code. If the artifact's information needs to be updated, the information can be corrected by the manager by updating the artifact's information without changing the QR code. At the same time, our

application will serve as a guide. With the information and pictures of artifacts in the QR code, visitors will be able to read the information about the artifacts and listen without a guide.

The developed system supports only Turkish language and can be developed by adding different languages. Saving the artifacts with the location information will pave the way for different analyzes such as relational analyzes, association rules, and prediction analyzes. In this sense, developing this study by instant mapping of the excavation areas will provide significant contributions to the literature.

REFERENCES

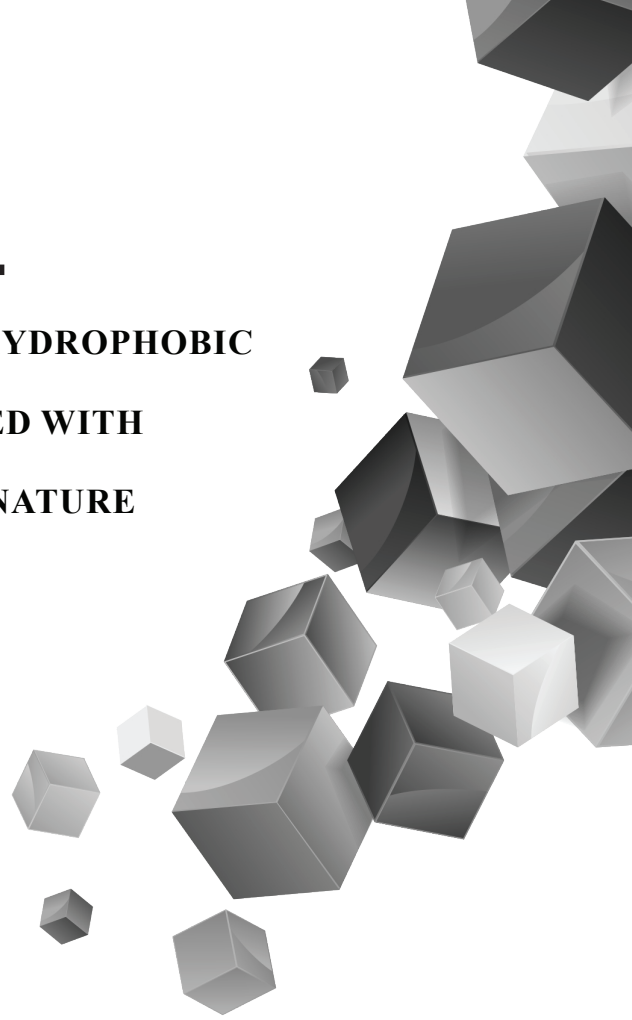
- Biedermann, B. (2017). Virtual museums as digital collection complexes. A museological perspective using the example of Hans-Gross-Kriminalmuseum. *Museum Management and Curatorship*, 32(3), 281-297, Doi: 10.1080/09647775.2017.1322916
- Chang, J. H. (2014). An Introduction to Using QR Codes in Scholarly Journals. *Sci Ed.*, 1(2), 113–117. <http://dx.doi.org/10.6087/kcse.2014.1.113>
- Fevgas, A., Tsompanopoulou, P., and Bozanis, P. (2011). iMuse Mobile Tour: A Personalized Multimedia Museum Guide Opens to Groups. In 2011 *IEEE Symposium on Computers and Communications (ISCC)*, 971-975.
- Fevgas, A., Fraggogiannis, N., Tsompanopoulou, P., and Bozanis, P. (2014). The iMuse Virtual Museum: Towards a Cultural Education Platform. In IISA 2014, *The 5th International Conference on Information, Intelligence, Systems and Applications*, 171-175.
- Fidan, H. (2013). İktisadi Açından Bilgi Kavramı ve Bilgi Kavramına Yaklaşımlar Üzerine Bir İnceleme. *Süleyman Demirel Üniversitesi Vizyoner Dergisi*, 4(9), 94-104.
- Gran, A. B., Vestberg, N. L., Booth, P., and Ogundipe, A. (2019). A Digital Museum's Contribution to Diversity – A User Study. *Museum Management and Curatorship*, 34(1), 58-78, DOI: 10.1080/09647775.2018.1497528
- Hervy, B., Laroche, F., Bernard, A., and Kerouanton, J. L. (2013). Co-working for Knowledge Management in Cultural Heritage: Towards a PLM for Museum. In *10th International Conference On Product Lifecycle Management*, Nantes, France. DOI: 10.1007/978-3-642-41501-2_32
- Higgins, N. L., and Cairney, T. (2006). RFID Opportunities and Risks. *Journal of Corporate Accounting & Finance*, 17(5), 51-57.
- ICOM (International Council of Museums), (2020). Museum Definition, <https://icom.museum/en/resources/standards-guidelines/museum-definition/>
- Kavakli, E., and Bakogianni, S. (2003). *Building Museum Information Systems: A Knowledge Management Approach*. In E. Lipitakis (Ed.), *Proceedings of the 6th Hellenic-European conference on computer mathematics and its applications*, 850–857. Athens: LEA Publishers.

- Kenderdine, S. (1998). Inside the Meta-Centre: A Wonder Cabinet. *Media International Australia Incorporating Culture and Policy*, 89(1), 63-74.
- Khelifi, A. L. (2018). The Archeology Field in the Mobile Era: A Roadmap to Catch-up. *International Journal of Interactive Mobile Technologies (iJIM)*, 12(1), 73-94.
- Li, R. Y. C., and Liew, A. W. C. (2015). An Interactive User Interface Prototype Design for Enhancing on-site Museum and Art Gallery Experience through Digital Technology. *Museum Management and Curatorship*, 30(3), 208-229, DOI: 10.1080/09647775.2015.1042509
- Lopez, A. M., Fernandez, G., and Burillo, F. (2016). Mobile Computing with Near Field Communication (NFC) Smart Objects Applied to Archaeological Research. In 2016 *12th International Conference on Intelligent Environments (IE)*, 88-94, IEEE.
- Marty, P. F. (2008). Museum Websites and Museum Visitors: Digital Museum Resources and Their Use. *Museum Management and Curatorship*, 23(1), 81-99.
- Mercin, L. (2006). Müzeler ve toplum. <http://www.https://www.ayk.gov.tr/wp-content/uploads/2015/01/Yrd.-Do%c3%a7.-Dr.-Levent-MERC%c4%b0N-M%c3%9cZELER-VE-TOPLUM.pdf>. (Accessed 18.06.2020).
- Niewerth, D. (2013). Heiße Töpfe. Digital Humanities und Museen am Siedepunkt (Museums and the Internet 2013 / Kunst- und Ausstellungshalle der Bundesrepublik Deutschland / 23. - 24.05.2013). Heiße Töpfe. Digital Humanities Und Museen Am Siedepunkt.
- Onyancha, O. B., and Ocholla, D. N. (2009). Conceptualising Knowledge Management in the Context of Library and Information Science Using the Core/Periphery Model. *South African Journal of Information Management*, 11(4). doi: 10.4102/sajim.v11i4.412
- Özbağ, D. (2010). Ulusal Dijital Kültür Mirasının Korunması ve Arşivlenmesine Yönelik Kavramsal bir Model Önerisi. Yayınlanmamış bilim uzmanlığı tezi, Hacettepe Üniversitesi, Ankara.
- Pala, Z., and İnanç, N. (2007). Smart Parking Applications Using RFID Technology. In *The First International RFID Eurasia 2007 Conference*, September 5-6, 2007, Istanbul, Turkey.

- Parry, R. (2010). *The Practice of Digital Heritage and the Heritage of Digital Practice*. In *Museums in a Digital Age*, edited by Ross Parry, 1–7. London: Routledge.
- Penttila, K., Keskilammi, M., Sydanheimo, L., and Kivikoski, M. (2006). Radio Frequency Technology for Automated Manufacturing and Logistics Control. *International Journal Of Advanced Manufacturing Technology*, 31(1-2), 116-124.
- Tezcan, M. K., and Ödekan, A. (2011). Müze eğitiminin tarihsel gelişimi. *İTÜ Dergisi*, 3(1), 47-58. http://itudergi.itu.edu.tr/index.php/itudergisi_b/article/view/1085/1074 (Accessed 22.07.2020)
- Wang, Y., Yang, C., Liu, S., Wang, R., and Meng, X. (2007). A RFID & Handheld Device-based Museum Guide System. In *2007 2nd International Conference on Pervasive Computing and Applications*, pp. 308-313, IEEE.
- Wielinga, B., Sandberg, J., and Schreiber, G. (1997). Methods and Techniques for Knowledge Management: What Has Knowledge Engineering to Offer? *Expert Systems With Applications*, 13(1), 73-84.
- Yılmaz, B. (2011). Dijital Kütüphane Becerileri Konusunda Türkiye’de Durum: AccessIT Projesi Çerçevesinde bir Değerlendirme. *Türk Kütüphaneciliği*, 25(1), 117-123.
- Yüksel, M. E., and Yüksel, A. S. (2011). RFID Technology in Business Systems and Supply Chain Management. *Journal of Economic and Social Studies*, 1(1), 53-71.
- Zhang, L. (2005). An Improved Approach to Security and Privacy of RFID Application System. *Wireless Communications Networking and Mobile Computing. International Conference*. (2): 1195- 1198.

Chapter 9

INNOVATIVE SUPERHYDROPHOBIC MATERIALS DESIGNED WITH INSPIRATION FROM NATURE



Ceyda BİLGİÇ¹
Şafak BİLGİÇ²

1 Assoc. Prof. Dr., Department of Chemical Engineering, Eskisehir Osmangazi University, Eskisehir, Turkey, Orcid No: 0000-0002-9572-3863

2 Assist.Prof.Dr. Department of Civil Engineering, Eskisehir Osmangazi University, Eskisehir, Turkey, Orcid No: 0000-0002-9336-7762

1. Introduction

Living nature has been the inspiration for the hydrophobic surface approach to achieve a self-cleaning surface. Some surfaces possessed by many plants and animals in nature exhibit high hydrophobic properties and keep themselves constantly clean by exhibiting cleaning properties. The wings of butterfly and leaves of many plants are examples of such surfaces. Lotus (*Nelumbo nucifera*) plant has the property of its excellent non-wettability, is recognized as a “King plant” among all natural water repellent plants. The hierarchical micro / nanostructure of a lotus leaf surface consists of a normal micro-relief cuticular about 1-5 μm in height. They compose of secreted low surface energy epicuticular wax crystalloids that evenly cover the surface (Nun et al., 2002:677; Cannavale et al., 2009:1233).

Biomimetics is a new science that studies models in nature and then aims to solve people’s problems by imitating or inspired by these designs. Biomimetics is a term that refers to the whole of the materials, tools, mechanisms and systems that humans make by imitating the systems found in nature. Tools made by modeling the designs in nature are especially needed for use in areas such as nano technology, robot technology and military equipment. Living nature is an inspiration for many improvement and serves us as a matchless resource for solving technical problems. Rice leaf and butterfly wings; combining with shark skin (anisotropic flow leading to low drag) and lotus plant (superhydrophobic and self-cleaning), a unique surface characteristic has been achieved called “rice and butterfly wing effect”. Systematic studies were conducted using rice leaves and butterfly wings, and a combination of actual and replica samples. Obtaining such surfaces, real samples were exposed to low adhesion nanostructured coating. Then, the artificial surface obtained and real samples were compared. Surface morphology characterization was made with scanning electron microscopy and optical profiler imaging using software analysis. The characteristics of surfaces associated with self-cleaning, low drag, antifouling properties have been tried to be understood and these studies conceptual models for development. For example, boots and swimsuits are made of shark skin and the windows producing from inspired by the lotus plant, which has features super water repellency and low surface energy (Bixler ve Bhushan, 2012:11271).

In 1997, Barthlott and Neinhuis first exposed the unique dual-scale micro / nanostructures of lotus leaves with the aid of a scanning electron microscope (SEM) and also examined the chemical material found on it (Barthlott and Neinhuis, 1997:1). Today, this material has been put on the market with two applications as self-cleaning paint and plaster for building facades. Since the mechanism needs water to clean itself, it can only be

used on external surfaces that are exposed to rain. A silicone resin-based, micro-scale external paint containing Lotus Effect is in use today.

The paint creates a wavy micro-structure on the surface it is coated, creating a lotus effect; It makes the surface superhydrophobic by creating a contact angle between the surface and the water droplet falling on it. Matt colored paint, which can be applied to masonry surfaces (concrete, masonry, etc.) with a brush, roller or airless spray, cannot be applied to wood and metal surfaces. There is also an acrylic resin-based exterior plaster with silicone additives, which has been released with the Lotus effect. This plaster functions by providing a lotus effect on the applied surface, just like the paint derivative. In addition, there are also hydrophobic surface coating applications to protect historical buildings against the effects of water and mold.

These are applied by spraying a solution of isobutyl trimethoxysilane in ethanol to provide waterproofing on masonry surfaces. As this application makes the surface hydrophobic, although it is not as strong as the Lotus Effect, it partially gives the surface the quality of self-cleaning with rain (Leydecker, 2008).

Liu et al. (2015) were examined the synthesis of Fluoroalkylsilanes (FAS) using a sol-gel method with a very simple one-step approach. The materials used them (Heptadecafluoro-1,1,2,2-tetrahydrodecyl) trimethoxysilane (17FTMS), ethanol and ammonia. They followed the following way to prepare of the coatings: firstly, 1 mL of deionized water and 0.5 mL of ammonia were added into 25 mL of ethanol and mixed gently for 5 minutes. Next, under continuous stirring to this solution was added slowly 100 μ L of 17FTMS. Also, the ammonia was used as a catalyst to initiate the sol-gel process. The cleaned glass substrates were placed under tap water and dipped, then allowed to dry overnight at room conditions. The results obtained from this study are; the coating showed a rough, wrinkled, hill-like surface morphology. The water droplets with a contact angle of 169° and a sliding angle of less than 5° formed a spherical shape on this surface. Therefore the prepared superhydrophobic coating exhibited excellent self-cleaning performance.

In addition, the superhydrophobic wetting condition was maintained under the effect of high speed water jet, but due to the poor mechanical strength of the coating it was easily scratched with a pencil. They control the scratch resistant property of the coating using pencil hardness test. The pencil was mounted at an angle 45° in contact with the coated surface and was moved horizontally over the surface. 9H (hardest), HB (average hard) and 9B (softest) pencil hardness was tested on having superhydrophobic coating; however, the coated surface is damaged and significant scratches were observed in all pencil tests (Liu et al., 2015:897).

Park et al. (2013), a sol-gel mixture containing 3,3,3-trifluoropropyltrimethoxysilane (FAS3) and tetramethoxysilane (TMOS) prepared successfully. It is coated on glass surfaces by spin coating method. They were coated on glass surfaces by a spin coating method. They obtained dynamically oleophobic repellent surfaces against liquids such as n-decane, n-dodecane and n-hexadecane. They have obtained dynamic repellent surfaces with low equilibrium contact angle values but less than 10° sliding angles. They made these surfaces without relying on conventional surface roughening and long-chain perfluoroalkylsilanes. Thus, they have created self-cleaning dynamic surfaces while maintaining surface transparency.

These findings further addition of TMOS and homogeneous / continuous formation of films as well as in improving the dynamic dewetting behavior against various alkene liquids offers clear evidence that play key roles. Unlike the traditional oleophobic / superoleophobic treatments reported thus far, their one-pot process is simple, effective and environmentally friendly. Because it does not require any long chain perfluoroalkylsilanes, thermal treatment or physical / chemical treatments to roughen the surfaces. Therefore, this technique is widely applicable to a variety of substrates and they expect to provide suitable oleophobic coatings and surface treatments (Park et al., 2013:100).

2. Superhydrophobic Surfaces

Superhydrophobicity formed by a combination of hierarchical surface structures and low surface energy materials. Self-cleaning ability (low contact angle hysteresis) with superhydrophobic surfaces can perform many functions. In order to provide these properties, natural hydrophobic materials must have a multi-scale or hierarchical surface. There is a need for a composite structure with a high rate of trapped air. This requirement fits with Cassie-Baxter's theory.

Over the past decade, superhydrophobic surfaces with water contact angle (CA) in excess of 150° have attracted great interest in potential applications as self-cleaning materials (Sas et al., 2012:824; Wang et al., 2007:27). Many studies have been done on lossless droplet manipulation (Wu et al., 2015:1) and anti-corrosion coatings (Arukalam et al., 2016:220; Barati et al., 2020:1763; Yin et al., 2010:816; Cui et al., 2011:398). The researchers determined that the wetting behavior of water droplets on superhydrophobic surfaces is managed by a combination of surface chemistry and topology. In particular, superhydrophobicity can be achieved on nano-structured surfaces exhibiting a low surface energy. Generally, these surface patterns were defined by Wenzel (1936) and Cassie (1994).

If the roughness of a solid surface, it must be taken into account as the actual contact area between the droplet and the rough surface differs from the flat surface area. In Wenzel model is assumed to be in contact with the whole rough surface of the water droplet. Therefore, the rough surface is completely wet. In this model, the water drop is attached to the superhydrophobic surface due to the large contact area with the surface. The Cassie-Baxter model droplets by contacting the top layer of the roughened surface causes the formation of air pockets in the liquid-solid interface. In this model, as a result of minimizing the liquid-surface contact area, superhydrophobic surface having a self-cleaning and water-repellent properties are obtained.

In 1997, Barthlott and Neinhuis first revealed that the lotus leaf has micro/nano-hierarchical structures consisting of randomly oriented papillae epidermal cells covered with hydrophobic epicuticular wax crystalloids (Barthlott and Neinhuis, 1997:1; Neinhuis and Barthlott, 1997:667; Bayer et al., 2011: 7939, Crawford et al., 2015). Later in their study, they also observed that the air could remain under the water droplets in accordance with the Cassie-Baxter equation. These findings revealed that highly water-repellent superhydrophobic surfaces like lotus leaves can be produced using micro / nano hierarchical structures coated with low surface energy materials.

Various methods have been developed inspired by lotus leaves; such as; wet chemical etching (Matin et al., 2016:322), electrochemical reaction (Gnedenkov et al., 2016:1241), lithography (Kavalenka et al., 2014:31079), electrodynamics (Sarkar et al., 2011:43), sol-gel methods (Shirtcliffe et al., 2010:124; Rao et al., 2011:5772; Kumar et al., 2015:205), layer-by-layer coating (Lee et al., 2006:2305) and etching to plasma methods to produce these surfaces (Lee et al., 2011:3907).

2.1. Natural Superhydrophobic Surfaces

It is possible to encounter many superhydrophobic surface samples in nature. The most well-known and most referenced of these are lotus leaves. The presence of randomly distributed structures with a diameter of 5-10 μm on the surface of the leaf is observed by high-resolution scanning electron microscopy (RTEM) images. These structures contain hairy infrastructures of 100-200 nm in length. Thanks to their complex hierarchical micro-nano structures and hydrophobic wax on their surfaces, they have 150-160° water contact angles and $\sim 2^\circ$ slip angles. These features ensure that the surfaces can clean themselves continuously and therefore receive daylight continuously. Other similar plant examples, Drosera (sundew), Eucalyptus, Euphobiaceae and Ginkgo biloba.

The contact angle of natural superhydrophobic surfaces varies between 150° and 160°. Water lily plants can be given as an example of these surfaces. The leaves of this plant, which grows in muddy and dirty environments, are constantly clean. Because the plant immediately shakes its leaves when the smallest dust gets on it and pushes the dust particles to certain points. Raindrops falling on the leaf are also directed towards these points and sweep the dust here, leaving a completely clean surface behind. The lotus leaf provides this with the roughness of a few millionths of a meter on it. This effect is the “Lotus Effect” as known. There are many self-cleaning surfaces in nature, such as water lily (lotus) leaves. Examples include the wings of birds, butterfly, and leaves of many plants (Özgür et al., 2007:52; Doğanç, 2007:19).

Lotus effect surfaces are hydrophobic and nanostructured surfaces that can be cleaned by the movement of water. These types of surfaces are generally expressed in words such as “easy to clean”, “dirt repellent”, “self cleaning” or “lotus effect”. Although each of these explanations is similar to the other actually, is different and used to describe the behavior of a surface. Easy-to-clean surfaces are hydrophobic and flat surfaces that have been well known for years. As is known, it is not difficult to remove dirt from such surfaces and “Lotus effect” and “self-cleaning effect” are used similarly. There is no need for any human impact to clean the contaminated surface.

After the unique surface properties of lotus leaves were discovered, it began to be applied quickly in many areas. These include laminates, protective films, traffic signs (not deteriorating even in foggy weather), window frames, tents and linoleum production, etc. can be counted. Studies on the application of the Lotus effect in the textile industry are still ongoing. Application of the Lotus effect on textiles, ease of cleaning and maintenance, no negative impact on the environment, time, material and energy savings, longer life of the products used, since it can replace some chemicals that are safer in terms of health and environment and provides advantages such as working with lower costs. Due to all these advantages, it is estimated that it will be widely used in many areas (Özdoğan et al., 2006:287).

Lotus leaves, hierarchical roughness (nano structures combined with micro-ridges) and water-repellent covering these structures by the presence of waxy super water repellent structure and exhibits self-cleaning properties. According to the investigations made in the past years, super water repellent plants have macroscopically flat surfaces. However, they usually show different sizes of roughness microscopically. Therefore, it has been understood that they show super water repellent properties thanks to the low surface energy water repellent waxy structures covering the micro

and nano structures on their surfaces. Like lotus leaves, rice leaves have nano-structures combined with micro protrusions that give the surface the ability to not getting wet. Rice leaves have papillary sizes ranging from 5 to 8 micrometers on the surface, which are aligned unidirectionally parallel to the surface in one direction (Guo et al., 2011:314).

Insects and birds may have superhydrophobic surfaces. For example, water striders' legs that don't get wet. In this way, they can walk on the surface of the water. Again, as in the lotus leaf example, with the micro - nanoscale and hydrophobic wax structure on the surface, they attain superhydrophobic properties. The superhydrophobic feature in the wings of the butterfly keeps the water away from the wings and prevents the wings from sticking together. (Wagner et al., 1996:213; Lee et al., 2004:7665). Namibia beetles use their superhydrophobic properties for a different purpose. The superhydrophobic regions on the way to their mouths allow the water droplets that accumulate on the leaves to go directly to their mouths. In this way, they managed to survive in the desert (Parker and Lawrence, 2001:33; Crawford and Ivanova, 2015).

In addition, superhydrophobic surface characteristics are encountered in many plant leaves, water strider, butterfly and cicadas. The force applied by each water striders' legs on a unit surface of water is 152 dyn (1 dyn = $1 \cdot 10^{-5}$ N), 15 times its own weight. The soles of the feet of this striders' are consisting of nanoscale slits, revealed by SEM images. This structure enables it to have hydrophobic legs. It is understood that there are nano sized slits at the ends of the legs. The roughness created by these slits prevents the legs of the water strider touching the water surface from getting wet.

Cicadas and butterflies are able to protect their wings from moving dust particles, moisture and water drops. This is the result of their micro/nano-rough wings. The wing of a cicada consists of 70 nm thick columns that are 90 nm apart from each other, and this gives its wings self-cleaning feature. Animals, on the other hand, have a microstructure between 10 nm and different micrometer scales. Examples of superhydrophobic animals include butterfly wings, duck feathers and bedbugs (Lee et al., 2004:7665). For these animals, this is the way they protect themselves in the area where they are. For example, after the duck comes out of the water, the wetness disappears and the wings of the butterfly approaching each other in the evening will not stick together due to the effect of the avalanche (Figure 1).

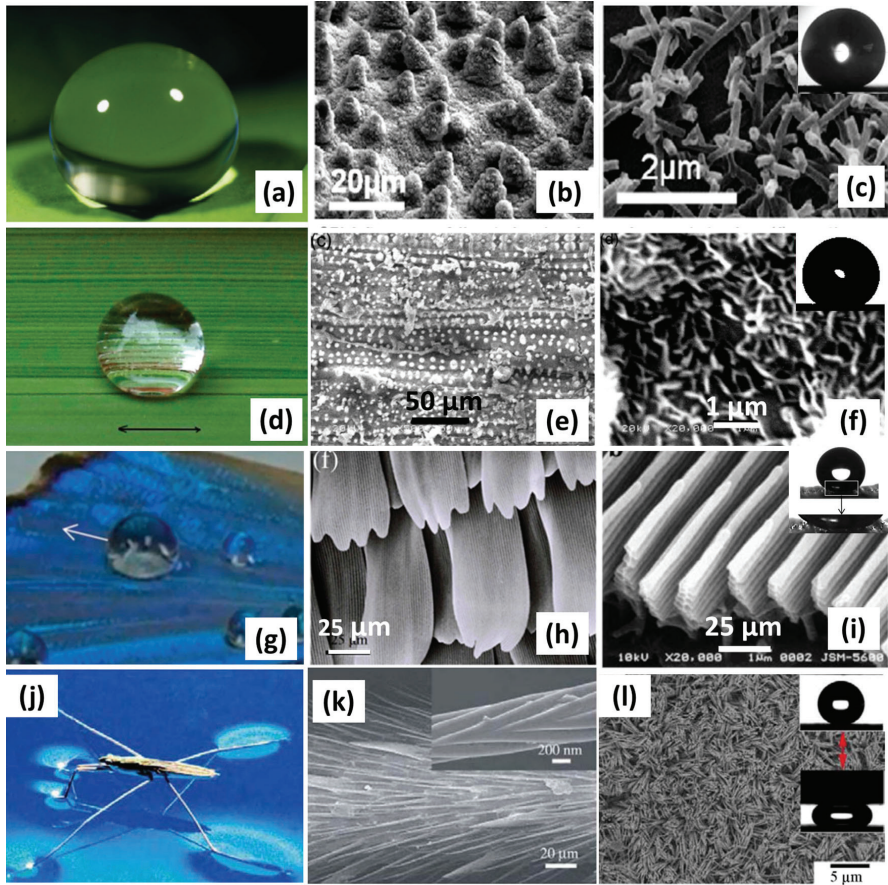


Figure 1. (a) Water droplet on the Lotus (*Nelumbo nucifera*) leaf and Lotus leaf surface (b) at low and (c) at high magnifications of SEM micrographs (Koch et al., 2009:137). (d) Water droplet anisotropic wetting of rice leaf and rice leaf surface (e) at low and (f) at high magnifications of SEM images (g) One-way wetting behavior of the butterfly wing and (h) at low and (i) at high magnifications of SEM micrographs (Bixler et al., 2014:114; Bixler et al., 2014:76; Bixler and Bhushan, 2012:11271; Kinoshita et al., 2002:1417; Yan et al., 2011:80). (j) Photograph of a water striders' legs capable of standing on the water surface. (k) The SEM micrograph of the leg with nano sized slits. (l) From SEM micrograph of water-strider' legs in the creation of ribbed nano-needle arrays biomimetic materials ($\text{Cu}(\text{OH})_2$) inspired. The inset at (l) shows squeezing and relaxing of water drops between two such surfaces. It shows the robust super hydrophobicity of biomimetic materials inspired by water-strider' legs (Liu et al., 2011:155; Gao and Jiang, 2004:36; Yao et al., 2010:656; Belhadjamor et al., 2018:85).

2.2. Artificial superhydrophobic surfaces

Samples of the natural superhydrophobic surfaces were used to create artificial superhydrophobic surfaces. Johnson and Dettre were sprayed wax on a flat glass surface to create waxy surfaces of different roughness. The surfaces of these samples were flattened by various heat applications. They observed that although the roughness scale was the only quantity, clusters ranging from 100μ to 10μ were formed. The static contact angle on these surfaces is 105° . Increase with increasing roughness, increase in the advancing contact angle causes the value of the decrease in the decreasing contact angle to change between 15° - 100° .

In cases where the roughness value is critical, the advancing angle becomes closer to 160° , while the receding angle approaches 150° . The contact angle hysteresis of the rough surface is smaller than the contact angle hysteresis on the flat surface. This study is an important experiment in terms of showing that surface hydrophobicity increases with surface roughness. Superhydrophobic solids have very little contact angle hysteresis. There are two reasons that cause these sticky drops to roll off the surface. The first of these is that the contact between solid-liquid is less, and the second is that this is achieved in small drops due to the presence of small hysteresis (Johnson and Dettre, 1964).

The Kao group has done many experiments on rough surfaces. To apply anode oxidation to give roughness to aluminium surfaces, followed by coating with fluorinated silanes was their first method. Fluorinated silanes bond covalently to the surface and form a hydrophobic monolayer on it. The second method is the surfaces created by making such substrates consisting of solidifying alkyl ketene dimer (AKD) solutions containing a small proportion of dialkyl ketone (DAK). The autonomy of Kao experiments is due to the measurement of different liquids and contact angles on the samples and the comparison of these data by observing the same liquids with different samples. With such comparisons, the relationship between contact angle and roughness factor has been tried to be understood (Shibuichi et al. , 1998:287).

The key feature observed in natural samples is that the hydrophobic property reaches the superhydrophobic level thanks to their surface textures. Based on this basic principle, various synthetic approaches to the development of superhydrophobic surfaces and coatings have been developed using hydrophobic surfaces, chemistry and geometric properties. The textile material (with rough surface due to being woven) was immersed in 4 wt% methylsilicon-toluene solution and then dried at 100°C . Thus, contact angles above 150° were obtained (Carre and Mittal, 2009).

A lot of research has been done on the preparation of superhydrophobic surfaces with self-cleaning properties based on the Lotus effect. A group in Kao worked on the preparation of superhydrophobic rough surfaces after preparing artificial hydrophobic surfaces in the mid-1990s. Most of the methods applied in the synthesis are processes that change the roughness of the hydrophobic surface.

Two main approaches are used to increase the contact angle, which is a measure of superhydrophobicity:

- Chemical method
- Geometric method

Chemical method:

To obtain surfaces has a lower surface energy achieved by playing with surface chemistry. It is known that surfaces containing $-\text{CF}_3$ groups have low free surface energy. Since fluorine has a small atomic radius and the greatest electronegativity of all atoms, therefore it forms a stable covalent bond with the C atom, forming a surface has low surface energy. The free surface energy increases as the element fluorine is replaced by other atoms such as carbon and hydrogen. Surface tension of functional groups; $-\text{CF}_3 < -\text{CF}_2\text{H} < -\text{CF}_2 < -\text{CH}_3 < -\text{CH}_2$. The lowest free energy for all surfaces is obtained with hexagonal tight pack $-\text{CF}_3$ groups. However, it has been determined that the contact angle of smooth hydrophobic surfaces containing fluorine obtained in this way does not exceed 120° . For this reason, micro/nano binary structures with the combining effect of low surface energy materials are generally recommended for superhydrophobic surfaces.

Geometric method:

The surface area and hydrophobicity of the contact surface are increased by increasing the roughness of the surface with the geometric method. When a small amount of liquid is placed on a hydrophobic surface, the shape of the drop formed depends on the equilibrium contact angle between the surface and the liquid and liquid volume. If the volume of the drop on the solid surface is microliters (μl) or less, gravity is less effective on the drop and the shape of the drop is spherical. In liquids, there is a dynamic balance between the liquid surface and the inside of the liquid. Therefore, the free surface energy is the same at all points, but for solid surfaces the free surface energy is not equal at all points. Equilibrium contact angle depends on surface conditions. The wetting behavior of smooth (flat, ideal) and rough solids was developed by Young and Wenzel and Cassie-Baxter equations, respectively. When a small amount of liquid is placed on a hydrophobic surface, the shape of the drop formed depends

on the equilibrium contact angle between the surface and the liquid and liquid volume.

Both high contact angle and low contact angle interference should having of superhydrophobic surfaces. The high contact angle indicates that the liquid is repelled by the solid. Low contact angle hysteresis indicates that the liquid has a low adhesion strength against the solid. Thus, the fluid can move easily with low energy loss.

3. Conclusions

In this study, the properties of superhydrophobic, natural and artificial superhydrophobic surfaces and studies using these properties have been investigated. Superhydrophobicity or super water repellency of the surface offers important solutions in many application areas such as self-cleaning, coating, corrosion resistance, biotechnology and low friction coatings. It is possible to adjust the surface topography by choosing the design parameters of the surface appropriately and thus to obtain the hydrophobicity afterwards. Hydrophobic surfaces with low surface free energy tend to attract gas bubbles although they repel the liquid droplet. Therefore, although a drop of liquid left on the superhydrophobic surface spreads over a very small area and stays close to the sphere, the gas bubble left on the surface immersed in the liquid spreads on the surface and stops with a small contact angle.

Wonderful things can be the result of continuously learning from nature. The mimicry of lotus leaves' micro/nanostructure is limited to the achieving of high water contact angles and low sliding angles on the surface. However, serious steps must be taken to achieve a durability similar to a lotus leaf. Various polymers were used due to their natural hydrophobicity and toughness in the synthesis of most of the superhydrophobic surfaces developed by mimicking of the lotus leaf-like micro nanostructure.

Acknowledgments

This study is a part of a project (2020-3139) supported by the Research Fund of Eskişehir Osmangazi University.

References

- Arukalam I.O., Oguzie E.E., Li Y. (2016) Fabrication of FDTS-modified PDMS-ZnO nanocomposite hydrophobic coating with anti-fouling capability for corrosion protection of Q235 steel, *Journal of Colloid Interface Science*, 484, 220-228.
- Barthlott, W., Neinhuis, C. (1997), Purity of the sacred lotus, or escape from contamination in biological surfaces, *Planta*, 202, 1-8.
- Barati Darband G., Aliofkhaezrai, M., Khorsand, S., Sokhanvar, S., Kaboli, A. (2020) Science and engineering of superhydrophobic surfaces: review of corrosion resistance, chemical and mechanical stability, *Arabian Journal of Chemistry*, 13(1), 1763-1802.
- Bayer, I. S., Fragouli, D., Martorana, P. J., Martiradonna, L., Cingolani, R., Athanassiou, A. (2011), Solvent resistant superhydrophobic films from self-emulsifying carnauba wax– alcohol emulsions, *Soft Matter*, 7, 7939-7943.
- Belhadjamor, M., El Mansori, M., Belghith, S., Mezlini, S. (2018) Anti-fingerprint properties of engineering surfaces: a review, *Surface Engineering*, 34(2), 85-120.
- Bixler G. D., Bhushan B., (2012) Bioinspired rice leaf and butterfly wing surface structures combining shark skin and lotus effects, *Soft Matter*, 44, 11271-11284.
- Bixler G.D., Theiss A., Bhushan B., Lee S.C. (2014) Anti-fouling properties of microstructured surfaces bio-inspired by rice leaves and butterfly wings, *Journal of Colloid and Interface Science*, 419, 114-133.
- Bixler G.D, Bhushan B. (2014) Rice- and butterfly-wing effect inspired self-cleaning and low drag micro/nanopatterned surfaces in water, oil, and air flow, *Nanoscale*. 2014, 6, 76-96.
- Cannavale, A., Francesco, F., Manca, M., Tortorici, G., Cingolani, R. ve Gigli, G. (2010) Multifunctional Bioinspired Sol-Gel Coatings for Architectural Glasses, *Building and Environment*, 45(5), 1233-1243.
- Carre A., Mittal K.L., editors. (2009) *Superhydrophobic Surfaces*, VSP: Leiden, The Netherlands, Leiden: VSP/Brill; CRC Press.
- Crawford R. J., Ivanova E. P. (eds), (2015) *Superhydrophobic surfaces*, 1st Edition, Elsevier Science, Oxford, UK: Elsevier, 165 pp.
- Cui, J.P., Zhou, F., Wang, Q.H., Wu, D., Li, D.H. (2011) Transflective blue phase liquid crystal display using an etched in-plane switching structure, *Journal of Display Technology*, 7(7), 398-401.
- Doğancı E., (2007), Cyclic olefin kopolimerden süperhidrofobik yüzey sentezi ve karakterizasyonu”, Yüksek lisans Tezi, *Gebze Yüksek Teknoloji Enstitüsü*, 19-43.

- Gnedenkov S.V., Sinebryukhov S.L., Egorkin V.S., Vyaliy I.E (2016) Wettability and electrochemical properties of the highly hydrophobic coatings on PEO-pretreated aluminum alloy, *Surface and Coatings Technology*, 307(C), 1241-1248.
- Gao X, Jiang L. (2004), Biophysics: water-repellent legs of water striders. *Nature.*, 432, 36-37.
- Guo, L., Liu, Y., Zhang, C., Chen, J., (2011) Preparation of PVDF-based polymer inclusion membrane using ionic liquid plasticizer and Cyphos IL 104 carrier for Cr(VI) transport, *Journal of Membrane Science*, 372, 314-321.
- Johnson R.E. and R. H. Dettre R.H., In: Gould RF, editor. (1964) Contact angle, Wettability and Adhesion, *Advances in Chemistry Series, American Chemical Society*, Washington DC, 43, 112-135 pp.
- Kavalenka M.N., Hopf A., Schneider M., Worgull M., Hölscher H. (2014) Wood-based microhaired superhydrophobic and underwater superoleophobic surfaces for oil/water separation. *RSC Advances*, 4, 31079-31083.
- Kinoshita S., Yoshioka S., Kawagoe K. (2002) Mechanisms of structural colour in the Morpho butterfly: cooperation of regularity and irregularity in an iridescent scale, *Proceedings of the Royal Society Biological Science*, 269,1417-1421.
- Koch K., Bhushan B, Barthlott W. (2009) Multifunctional surface structures of plants: an inspiration for biomimetics. *Progress in Materials Science*, 54(2), 137-178.
- Kumar D., Wua X, Fua Q., Hoa J., Pushkar D. Kanhereb., Lic L., Chena Z. (2015) Development of durable self-cleaning coatings using organic–inorganic hybrid sol–gel method, *Applied Surface Science*, 344, 205-212.
- Lee, H. J., Willis, C. R., Stone, C. A., (2011) Modeling and Preparation of A Super-Oleophobic Non-Woven Fabric, *Journal of Materials Science*, 46, 11, 3907-3913.
- Lee D., Rubner M. F., Cohen R. E. (2006) All-nanoparticle thin-film coatings, *Nanoletter* , 6, 2305-2312.
- Lee W., Jin M. K., Yoo W. C., Lee J. K. (2004), Nanostructuring of a polymeric substrate with well-defined nanometer-scale topography and tailored wettability, *Langmuir*, 20 (18), 7665-7669.
- Liu K, Jiang L. (2011) Bio-inspired design of multiscale structures for function integration. *Nano Today*, 6, 155-175.
- Liu S., Liu X., Lathe, S.S., Gao L., An S., Yoon S.S., Liu B., Xing R. (2015) Self-cleaning transparent superhydrophobic coatings through simple sol–gel processing of fluoroalkylsilane. *Applied Surface Science*, 351, 897-903.
- Leydecker, S., Marius, K., and Sascha, P. (2008). *Nano Materials in Architecture, Interior Architecture and Design,* Birkhäuser Basel; Elvin, G. (2006). “NanoBioBuilding: Nanotechnology, Biotechnology, and the Future

- of Building” in *Proceedings of 2nd International Symposium on Nanotechnology in Construction*, Bilbao, 192 p.
- Matin A., Merah N., Ibrahim A., 2016. Superhydrophobic and self-cleaning surfaces prepared from a commercial silane using a single-step drop-coating method. *Progress in Organic Coatings* 99:322-329.
- Neinhuis C., Barthlott W. (1997) Characterization and distribution of water-repellent, self-cleaning plant surfaces”. *Annals of Botany*, 79(6), 667-677.
- Nun, E., Oles, M., Scleich, B. (2002) Lotus Effect Surfaces, Macromolecular Symposia, 187, 677-682.
- Özgür, H., Gemici, Z., Bayındır M. (2007) Akıllı Nanoyüzeyler, *Bilim ve Teknik Dergisi*, 473, 52-56.
- Özdoğan, E., Demir, A., Seventekin, N. (2006) Lotus Etkili Yüzeyler, *Tekstil ve Konfeksiyon*, 16(1), 287-290.
- Park J., Urata C., Masheder B., Cheng D.F., Hozumi A. (2013) Long perfluoroalkyl chains are not required for dynamically oleophobic surfaces, *Green Chemistry*, 15, 100-104.
- Parker A. R., Lawrence C. R. (2001) Water capture by a desert beetle, *Nature*, 414 (6859), 33-34.
- Rao A.V., Latthe S.S., Mahadik S.A., Kappenstein C. (2011) Mechanically stable and corrosion resistant superhydrophobic sol-gel coatings on copper substrate, *Applied Surface Science*, 257, 5772-5776.
- Sarkar P., Bhui D.K., Bar H., Sahoo G.P., Samanta S., Pyne S., Misra A. (2011) DDA-based simulation of uv-vis extinction spectra of Ag nanorod synthesized through seed-mediated growth process. *Plasmonics*, 6, 43-51.
- Sas, I., Gorga, R.E., Joines, J.A., Thoney, K.A., (2012) Literature Review on Superhydrophobic Self-Cleaning Surfaces Produced by Electrospinning, *Journal of Polymer Science Part B-Polymer Physics*, 50, 12, 824-845.
- Shibuichi S., Yamamoto T., Onda T., Tsujii K. (1998) Super water- and oil-repellent surfaces resulting from fractal structure, *Journal of Colloid Interface Science*, 208, 287-294.
- Shirtcliffe, N.J., McHale, G., Atherton, S., Newton, M.I. (2010) An Introduction to Superhydrophobicity, *Advances in Colloid and Interface Science*, 161, 1, 124-138.
- Wagner T., Neinhuis C., Barthlott W., (1996) Wettability and Contaminability of Insect Wings as a Function of Their Surface Sculptures, *Acta Zoologica*, 77 (3), 213-225.
- Wang, C. X., Li, M., Jiang, G. W., Fang, K. J., Tian, A. L., (2007) Surface Modification with Silicon Sol on Cotton Fabrics for Water-Repellent Finishing, *Research Journal of Textile and Apparel*, 11, 3, 27-34.

- Wu, P., Li, J., Wei, K., Yue, W. (2015) Tunable and ultra-elongated photonic nanojet generated by a liquid-immersed core-shell dielectric microsphere, *Applied Physics Express*, 8(11), 112001.
- Yan Y.Y., Gao N., Barthlott W. (2011) Mimicking natural superhydrophobic surfaces and grasping the wetting process: a review on recent progress in preparing superhydrophobic surfaces. *Advances in Colloid and Interface Science*, 169(2), 80-105.
- Yao X., Chen Q.W., Xu L., Li, Q. K., Song, Y. L., Gao, X. F., Quere, D., Jiang, L. (2010) Bioinspired ribbed nanoneedles with robust superhydrophobicity. *Advanced Functional Materials*, 20 (4), 656-662.
- Yin, L., Wang, Q., Xue, J., Ding, J., Chen, Q. (2010) Stability of superhydrophobicity of lotus leaf under extreme humidity, *Chemistry Letters*, 39, 816-817.

Chapter 10

THE NOVEL MANUFACTURING TECHNIQUES OF THE AIRBORNE PARTS



Tamer SARAÇYAKUPOĞLU¹

¹ Istanbul Gelisim University, Aeronautical Engineering Faculty tsaracyakupoglu@gelisim.edu.tr

1. Introduction

Aviation is a well-regulated industry. The rules and regulations are well defined and the borders are bolt between the functions. The International Civil Aviation Organization (ICAO) is a top airworthiness organization that works as a conductor for the harmonization of air traffic. In accordance with the ICAO regulations, regional regulatory airworthiness bodies in Europe (European Aviation Safety Agency-EASA), the USA (Federal Aviation Administration-FAA) and Asia are responsible for the implementation of new technologies based on the manufacturer's dossier and ICAO Certification Specifications (CS).

The aviation industry can be considered as an indicator of a country's industrial level (Saraçyakupoğlu, 2021). It is a high value-added technology. Per the National Academies Press (NAP) report, the finished value of the land-vehicle per pound is only about 5 US Dollars, while the finished value of the commercial transport aircraft per pound is 300 US Dollars (NAP, 1993). In other words, the price of an airworthy part is 60 times higher than those in the automotive industry. It is noteworthy that, depending on its type, the modern commercial passenger aircraft consist of many million parts and complex components. For example, a Boeing 747-400 includes more than 6 million parts in the fuselage, landing gear, propulsion, avionics, aerodynamics, etc. parts and assemblies (Eugui & Bifani, 2014). It is worth emphasizing that the freighter conversions would have significantly fewer parts than the full passenger versions

Each part, assembly, and the component requires specific tests for being validated as an airworthy part. In the open literature, there are different names for the definition of "airworthy part" such as;

- Aviation-grade part,
- Airborne-part,
- Ready-to-take-off part,
- Ready-to-flight part,
- Flight-ready part,
- Flight-grade part (Saraçyakupoğlu, 2020).

For manufacturing an airworthy part, it is essential to follow the rules of airworthiness authorities that are dictated for design and manufacturing companies in the aviation industry. Airplanes can only operate with airworthy parts and waive off the airworthiness requirements of the parts is unacceptable by certification authorities (Saraçyakupoğlu, 2019). In the aviation industry, if a company concentrates on the design or manufacturing the airworthy parts/components should have Part 21 J/Design Organization

Approval (DOA) and Part 21 G/Product Organization Approval (POA) from the relevant airworthiness authorities.

On the other hand, the systems installed on an aircraft should provide, at least the given below items besides high performance;

- High flight reliability,
- Minimum maintenance requirement,
- Easy maintenance capability,
- Low maintenance-operating cost,
- Low engine fuel consumption,
- Being sustainable and eco-friendly (Ballı, 2020).

Each aircraft type-approved by a single airworthiness regulatory organization, based on the mutual recognition between the regulatory bodies. In other words "reciprocity is essential". For each and every individual aircraft a single certificate of airworthiness, recognized worldwide is granted by one Country Aviation Authority (CAA). The aircraft manufacturer companies are periodically and sometimes on-conditional audited by the authorities. This system provides the opportunity to operate worldwide without additional efforts (Gastineau, 2020). In accordance with ICAO Global Air Navigation Plan 2016-2030, the global air traffic has doubled size once every 15 years since 1977 (ICAO, 2016). Also, the International Air Transport Association (IATA) declares that almost 8 Billion people will fly in 2037, which means that there's an increasing demand from customers to fly more frequently on a global level (Bagamanova & Mota, 2020). It is also should be emphasized that the main forcer of the enlarging of the aviation industry is the increase in airfreight.

2. Challenges of the Manufacturing Technologies in the Aviation Industry

For figuring out the environment of a regular commercial passenger aircraft, the working conditions should be understood properly. It is not hard to explain that, these state-of-art machines (airplanes) working conditions are extremely difficult.

2.1. A Commercial Passenger Aircraft's Operation Conditions

A commercial passenger aircraft operates in a harmful condition. At the cruise altitude of a regular commercial flight, the outside temperature is about -55°C . This temperature is 3 times colder than regular kitchen deep freezers. In the Table 1, the altitude and temperature change is provided.

Table 1. *The Altitude and Temperature Values Change*

Altitude (Meters)	Temperature (°C)
0	15
1000	8,5
2000	2
3000	-4,5
4000	-11
5000	-17,5
6000	-24
7000	-30,5
8000	-37
9000	-43,5
10000	-50
11000	-55

At the same flight level, the outside pressure is about 200 mbar. This pressure is approximately 5 times smaller than the Mean Sea Level (MSL) pressure. In Table 2, the altitude and pressure change is provided.

Table 2. *The Altitude and Pressure Values Change*

Altitude (Meters)	Pressure (mbar)
0	1013,3
500	955
1000	900
1460	850
2000	795
3010	700
4000	616
5000	540
5570	500
7000	410
9160	300
10000	264
11790	200
16210	100

While an aircraft is floating through the clouds in these mean conditions the crew and the passengers breath approximately 8000 feet of cabin altitude air (ASEM, 2008).

2.2. The Temperature Inside The Gas Turbine Engine is Hotter Than “Lava”

Gas turbine engines (GTE) are used as the propulsion system in the most commercial passenger aircraft operating at present. A regular GTE is composed of more than 30, 000 components, operating above their melting point. The technology used in the GTE’s as complex as they have to

operate reliably in exceedingly harmful environments where temperature and pressure vary dramatically in different parts and components. In the new type of GTE's maximum temperature can be as high as $\sim 2.000\text{ }^{\circ}\text{C}$ as it is demonstrated in Figure 1.

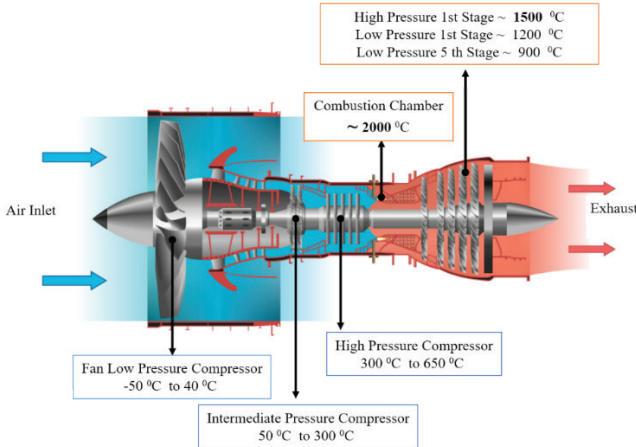


Figure 1. *The Sections and Temperatures Inside a GTE (Adapted from (Spittle, 2003))*

The GTE's are exposed to environments that vary from severe to mild conditions, therefore each one needs to have different characteristics to operate reliably (Ackert , 2009). For gases, it is known that pressure and temperature are in the right proportion while volume and pressure are in inverse proportion. The modules positioned near to the combustion chamber (High-Pressure Turbine and High-Pressure Compressor) are the ones that are exposed to the extremely harmful environment where pressure can go up to 40 Atm, while the temperature can go up to $\sim 2.000\text{ }^{\circ}\text{C}$. Figure 2 shows the temperature change through the engine gas flow path.

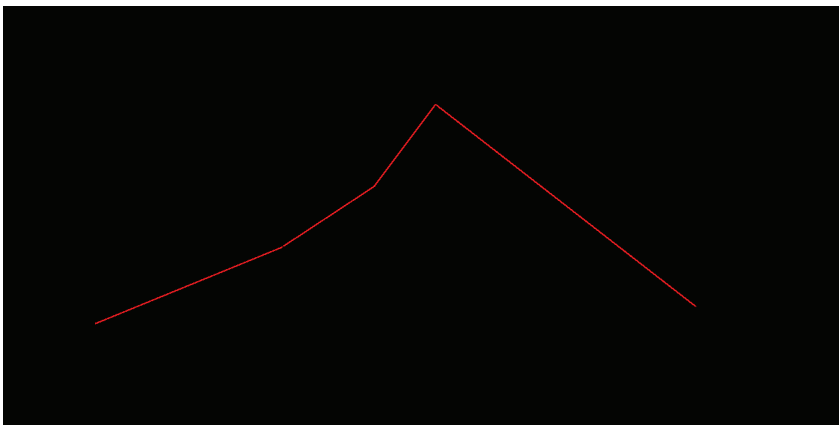


Figure 2. *Temperature Distribution in a GTE (Centrich, et al., 2014)*

It is worth underlining that, the temperature inside the GTE is hotter than lava that comes from the volcano. For example, the field temperature measurements at Erta’Ale Lava Lake, Ethiopia shows that inside the magma the maximum temperature is 1.187 °C (Burgi, Caillet, & Haefeli, 2002). In another study, that was done for Kilauea active volcano in Hawaii shows that the temperature of the lava was measured as 1230 °C (Carling, et al., 2015). Conclusively, in the hot sections of a GTE the ambient temperature is more than “lava”. Even in the mean conditions mentioned in 2.1. and 2.2. the GTE should run reliably.

A typical commercial passenger aircraft gas turbine engine takes approximately 1.2 tons/second of air during the take-off phase of the flight. This amount of air equals the air of a squash court with the dimensions demonstrated in Figure 3. The mechanism by which a jet engine sucks in the air is mainly a part of the compression stage (Gavrieli, 2004).

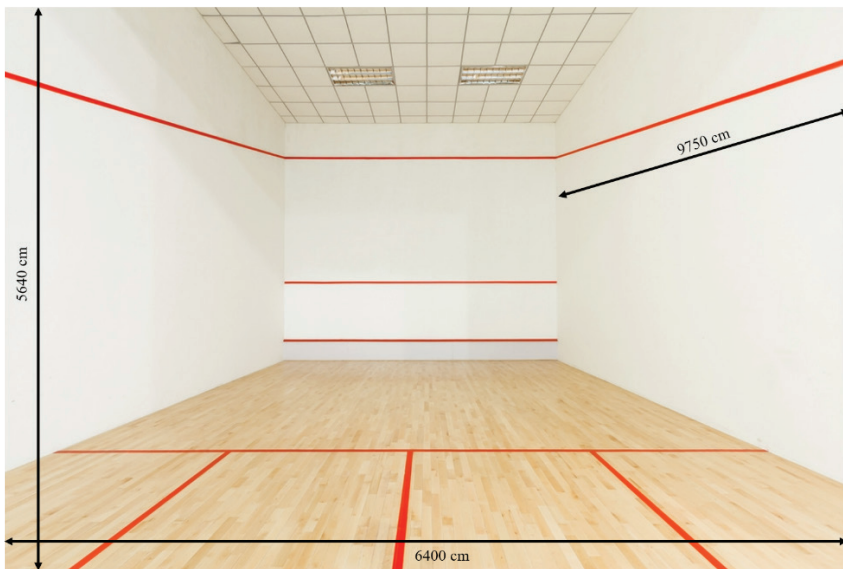


Figure 3. A Typical Gas Turbine Engine Takes Air of a Squash Court per Second (WSF, 2020)

2.3. The Challenges of Manufacturing Activities in the Aviation Industry

Undoubtedly, manufacturing a flight-ready gas turbine engine, in a multi-layered facility has many limitations. Mainly, extreme complexity for modern aircraft jet engines manufacturers is caused by many reasons such as;

- The complexity of products and technology regarding working conditions,

- Novel innovations and fast changes in products, technologies, equipment, toolsets, etc.,
- Large number and size of manufacturing plants,
- Many unpredictable events like demand and resource fluctuations,
- Real-time resource allocation, scheduling, and lean manufacturing line optimization for new orders,
- Interdependent schedules of many workshops such as mechanic, avionics and assembling workshops,
- Intensive use of sensors and robotic multi-functional units which make enterprises more flexible,
- Numerous constraints on products, operations, workers skills, equipment, materials, compatibility, etc.,
- Individual agreements with major clients, suppliers, workers, etc. (Shpilevoy, et al., 2013).

It is obvious that the emerging trend of production is keenly concentrated on increasing productivity. Plant-Layout studies and lean-manufacturing line arrangements are effective for better productivity as was mentioned before.

In the aviation industry, competition is fierce. While implementing the newest technologies into the industry companies are looking for opportunities to increase their capacities. For example, thanks to the implementation of the novel technologies, the Boeing company which is a main role player in the aircraft manufacturing sector has increased their manufacturing capacity from 52 to 57 per month in their Renton / Washington facility (Sutedja, Smith, Muilenburg, & Musser, 2018).

2.4. The Components and Manufacturing Structure For a Top Assembly (Aircraft)

Aircraft is the top assembly which is the end product of the manufacturing line. As it was mentioned earlier, there are almost 6 million parts in a Boeing 747-400 (Eugui & Bifani, 2014) and there are almost 30.000 parts in a GTE (Spittle, 2003). It is noteworthy that the aircraft is the top assembly as it is illustrated in Figure 4. Aircraft is composed of the manufactured parts with the compliance of Part 21 J-G requirements, consumables, standard parts, COTS' and loose-items.



Figure 4. An Aircrafts Components and Parts

Meanwhile, it should be underlined that an airworthy part should be tagged with the forms for authorization. In general, these forms are called as "Authorised Release Certificate" by both FAA and EASA. But in detail, EASA titles its form as "Form 1" and FAA titles its form as "Form 8130-3". The mentioned forms are provided in Figure 5.

1. Approving State/Authority FAA (United States)		3. Authorized Release Certificate EASA Form 1 (EUROPEAN APPROVAL / ETC)		2. Form Tracking Number	
4. Organization Name and Address		5. Work Order/Contract/Invoice		6. Remarks	
7. Description	8. Part No.	9. Qty.	10. Serial No.	11. Status/Work	
13a. Certify that the items identified above were manufactured in conformity to: <input type="checkbox"/> Approved design data and in accordance with applicable regulations. <input type="checkbox"/> Non-approved design data specified in block 12					
13b. Authorized Signature		13c. Approval/Authorization Number		14. Date (dd/mm/yyyy)	
13d. Name		13e. Date (dd/mm/yyyy)		14b. Name	
13f. Title		13g. Date (dd/mm/yyyy)		14c. Name	
13h. Signature		13i. Date (dd/mm/yyyy)		14d. Name	

a. FAA Form 8130-3

b. EASA Form 1

Figure 5. FAA and EASA Authorized Release Certificate Forms

Both Form 8130-3 and Form 1 can be released by a POA holder for stating that a product, a part, or a component was manufactured in accordance with the airworthiness' authorities' regulations (Bhopatkar, 2013).

From bottom to top, the parts and components are manufactured in a flow line. It is noteworthy that, aircraft manufacturers and airliner companies are propelling each other in a harmony (Saraçyakupoğlu,

2020). It is clear that a strong air cargo fleet contributes to the country's development. In that case, the Logistics Performance Index (LPI) is a robust indicator for giving clues about the countries industrial position. The studies show that there's a positive correlation between LPI and air cargo transportation (Düzgün, 2020).

2.5. The Novel Technologies Such as Additive Manufacturing Implementation in the Aviation Industry

The aviation industry is a pioneer in implementing novel technologies. The airworthiness bodies are leading the aviation industry for having eco-friendly aircraft and engines. Naturally, it requires exploring using the newest techniques and advanced materials (GE, 2013). As it was mentioned before the aviation industry is highly regulated. The manufactured parts and the components need to be authorized by airworthiness authorities prior to marketing.

Additive manufacturing is an emerging methodology used for meeting the requirements of airworthiness organizations. Basically, it is a process of manufacturing parts layer-by-layer which is contrary to that chip-away conventional techniques. The materials differ from one AM technique to the other one. In Figure 6, material types are provided.

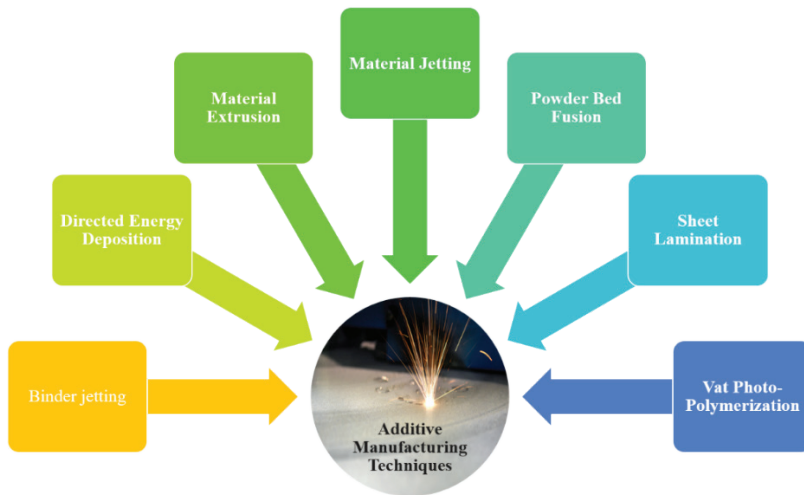


Figure 6. *Types of Additive Manufacturing Process (ASTM, 2013).*

For example, wax-like materials can be processed with material jetting and binder jetting. Metals such as nickel-based alloys and aluminum can be processed with directed energy deposition. Thermoplastic filaments can be processed with Material Extrusion. With powder bed fusion, polymers, maraging steel, stainless steel 316 L, 15-5PH, 17-4PH, nickel-

based superalloys, Inconel 718, Inconel 625, Hastelloy X, Titanium TA6V, chrome-cobalt, aluminum ALSi10Mg can be used as raw materials. Adhesive coated papers, metal tapes, and foils, the plastic sheet material can be processed with sheet lamination, and light-curable resin and photopolymers can be processed with Vat Photo-Polymerization.

During the standing jump, power output mean values of 5.23 HP for men and 3.15 HP for women were recorded (Davies, 2007). Considering, on a Boeing 777, a single-engine produces 52,000 HP the manufacturing ability of "human being" will be understood clearly. In that perspective, additive manufacturing technology provides many opportunities from aviation-grade production to generating human organs (Murr, 2016). It is noteworthy that both medical and aviation industry has precise manufacturing limitations. In other words, if a technology is implemented to either of them it is a reliable reference for implementation to others.

Because of the design freedom upon complex parts available with AM techniques of the airworthy parts which are used on the airplanes are perfect applications (Tomlin & Meyer, 2011). Additive manufacturing also provides opportunities to reduce operational man and machine hours and simplifying the manufacturing process (Despeisse & Ford, 2015). Since assessment of appropriate part candidates could be time-consuming, the part selection step is conducted in three phases as information, assessment, and decision (Poyraz & Kuşhan, 2019).

In Figure 7, an additively manufactured GTE hot section blade is provided. The material is selected as Ti6Al4V which is very common in the aviation industry. EOS M 290 Direct Metal Laser Sintering (DMLS) machine is used for manufacturing the blade.

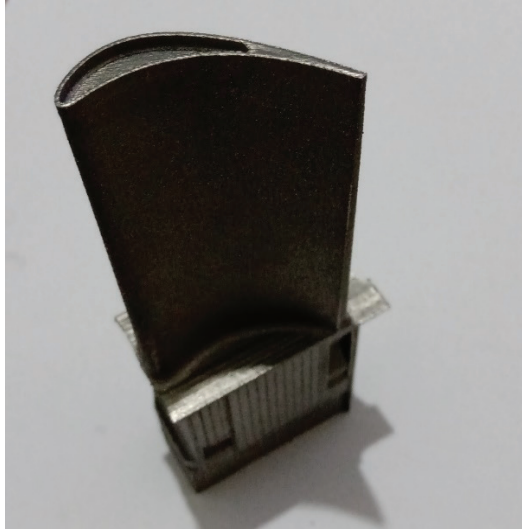


Figure 7. *Additively Manufactured GTE Hot Section Blade (Courtesy of Artuk Aviation)*

For manufacturing the upper mentioned blade a CAD model has been prepared with Catia V5 R21. As it is seen in Figure 8, this model is prepared only for training purposes. Albeit, the dimensions are very close to the genuine one, it still needs further numerical studies. This part can be considered as a sample for figuring out the behave of the process.

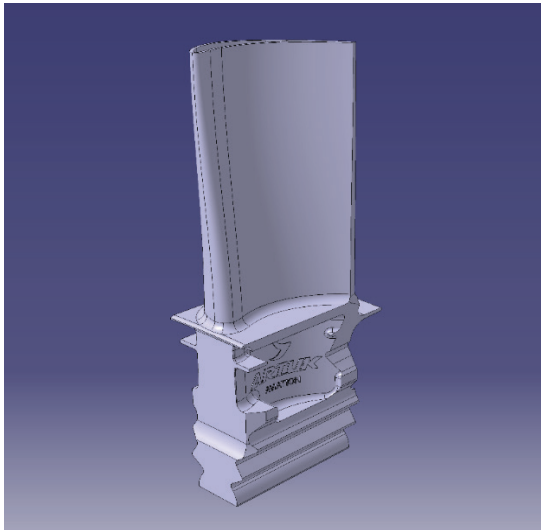


Figure 8. *CAD Model of the Hot Section Blade (Courtesy of Artuk Aviation)*

As demonstrated in Figure 9, for the GTE hot section blades, the cooling channels are the vital areas because of the extremely hot working

environment. As it was mentioned before both the combustion chamber and high-pressure combustion section have a temperature as high as lava from a volcano.

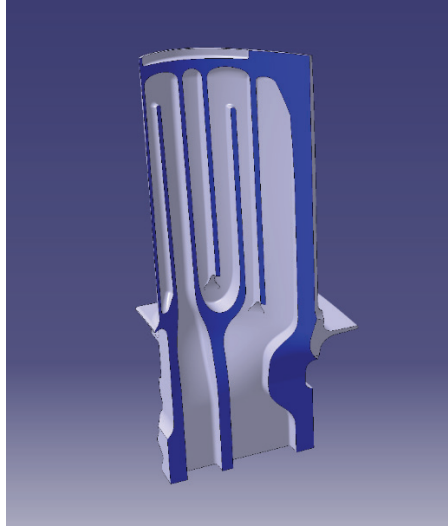


Figure 9. *Illustrated Cooling Channels Inside the Hot Section Blade (Courtesy of Artuk Aviation)*

Acknowledgment

The author's additive manufacturing studies are encouraged by Artuk Aviation Ltd. Company located in Afyonkarahisar/Turkey. The author is immensely grateful to Artuk Aviation Ltd. for supporting his engineering studies.

Conclusion

It is obvious that additive manufacturing has changed the face of the manufacturing industry. The ease of digitizing the technical data package and manipulation of the data is the main positivity of the process. The developments in additive manufacturing technology on behalf of the airworthy parts create a vast area of research criteria for producing the complex parts that are almost impossible with conventional manufacturing techniques. While reducing the labor and machine hours during the manufacturing phase it still needs process improvements because of its drawback of batch production of large-size components.

In the future, more additively manufactured airworthy parts will be encountered in the aviation industry.

References

- Ackert , S. (2009). Engine maintenance concepts for financiers: Elements of turbofan shop maintenance costs. *Proceedings of the Institution of Mechanical Engineers* (pp. 433-440). Part G: Journal of Aerospace Engineering.
- ASEM. (2008). *Cabin Cruising Altitudes for Regular Transport Aircraft*. Aerospace Medical Association. doi:10.3357/ASEM.2272.2008
- ASTM. (2013). *Standard Terminology for Additive Manufacturing Technologies*. American Society for Testing and Materials.
- Bagamanova, M., & Mota, M. M. (2020). Reducing airport environmental footprint using a disruption-aware stand assignment approach. *Transportation Research Part D*, 1-15. doi:10.1016/j.trd.2020.102634
- Ball, Ö. (2020). Failure analysis of inlet guide vane (IGV) actuator and bellcrank assembly used on J85 turbojet engines. *Engineering Failure Analysis*, 1-6. doi:10.1016/j.engfailanal.2020.104700
- Bhopatkar, N. S. (2013). Development of Production Organization Exposition (POE) to Include Requirements of AS/EN9100, EASA, FAA AND DGCA India. *3rd International Symposium on Aircraft Airworthiness, ISAA 2013*, (pp. 216-223). doi:10.1016/j.proeng.2014.09.076
- Burgi, Y. P., Caillet, M., & Haefeli, S. (2002). Field temperature measurements at Erta'Ale Lava Lake, Ethiopia. *Bulletin of Volcanology*, 472-485. doi:10.1007/s00445-002-0224-3
- Carling, G. T., Radebaugh , J., Saito, T., Lorenz, R. D., Dangerfield, A., Tingey , D. G., . . . Diniega, S. (2015). Temperatures, thermal structure, and behavior of eruptions at Kilauea and Erta Ale volcanoes using a consumer digital camcorder. *GeoResJ*, 47-57. doi:10.1016/j.grj.2015.01.001
- Centrich, T. X., Shehab, E., Sydor, P., Mackley, T., John, P., & Harrison, A. (2014). An Aerospace Requirements Setting Model to Improve System Design. *3rd International Conference on Through-life Engineering Services*, (pp. 287-292). doi:10.1016/j.procir.2014.07.127
- Davies, C. T. (2007). Human Power Output in Exercise of Short Duration in Relation to Body Size and Composition. *Ergonomics*, 245-256. doi:10.1080/00140137108931241
- Despeisse, M., & Ford, S. (2015). The Role of Additive Manufacturing in Improving Resource Efficiency and Sustainability. *IFIP WG 5.7 International Conference*, (pp. 129-137). doi:10.1007/978-3-319-22759-7
- Düzgün, M. (2020). Methodological Study on the Effect of Aviation on Service Export and LPI Mainly Based on the Cargo Data of All International and Turkish National Airlines'. *PARADOKS Economics, Sociology and Policy Journal*, (pp. 35-52).

- Eugui, V., & Bifani, P. (2014). Exploring Linkages between Aircraft Technologies, Climate Change Considerations and Patents. *CUTS International 2014*, (p. 8).
- Gastineau, T. (2020). What can vaccines learn from aviation. *Vaccine*, 2. doi:10.1016/j.vaccine.2020.06.027
- Gavrieli, K. (2004). *The Jet Engine: A Historical Introduction*. Retrieved 10 14, 2019, from <https://cs.stanford.edu/people/eroberts/courses/ww2/projects/jet-airplanes/how.html>
- GE. (2013). *Continuous Lower Energy, Emissions and Noise (CLEEN) Program, TAPS II Combustor Final Report*. Federal Aviation Administration.
- IATA. (2019, 07 19). *Forecast Predicts 8.2 billion Air Travelers in 2037*. Retrieved from IATA.org: www.iata.org/pressroom/pr/Pages/2018-10-24-02.aspx
- ICAO. (2016). *Global Air Navigation Plan 2016-2030*.
- Mélanie Despeisse, S. F. (2015). The Role of Additive Manufacturing in Value Chain Reconfigurations. *Advances in Production Management Systems, Innovative Production Management Towards Sustainable Growth*. Tokyo, Japan: IFIP WG 5.7 International Conference. doi:10.1007/978-3-319-22759-7
- Murr, L. E. (2016). Frontiers of 3D Printing/Additive Manufacturing: from Human Organs to Aircraft Fabrication. *Journal of Materials Science & Technology*, 988-995.
- NAP. (1993). *Materials Research Agenda for the Automobile and Aircraft Industries*. The National Academies Press.
- Poyraz, Ö., & Kuşhan, M. C. (2019). Design for Additive Manufacturing with Case Studies on Aircrafts and Propulsion Systems. *Scientific Research and Education in the Air Force – AFASES 2019*, (pp. 166-175). doi:10.19062/2247-3173.2019.21.23
- Saraçyakupoğlu, T. (2019). The Qualification of the Additively Manufactured Parts in the Aviation Industry. *American Journal of Aerospace Engineering*, 1-10. doi:10.11648/j.ajae.20190601.11
- Saraçyakupoğlu, T. (2020). The Adverse Effects of Implementation of the Novel Systems in the Aviation Industry in Pursuit of Maneuvering Characteristics Augmentation System (MCAS). *Journal of Critical Reviews*, 2530-2538. doi:10.31838/jcr.07.19.374
- Saraçyakupoğlu, T. (2020). The Manufacturing and Qualification Methodology of the Aviation-Grade Parts. *2nd Hezarfen International Congress of Science, Mathematics and Engineering*, (pp. 32-37).
- Saraçyakupoğlu, T. (2021). Failure analysis of J85-CAN-15 turbojet engine compressor disc. *Engineering Failure Analysis*, 1-8. doi:10.1016/j.engfailanal.2020.104975

- Shpilevoy, V., Shishov, A., Skobelev, P., Kolbova, E., Kazanskaia, D., Shepilov, Y., & Tsarev, A. (2013). Multi-agent system "Smart Factory" for real-time workshop management in aircraft jet engines production. *11th IFAC Workshop on Intelligent Manufacturing Systems The International Federation of Automatic Control*, (pp. 204-209). doi:10.1109/ETFA.2012.6489694
- Spittle, P. (2003). Gas turbine technology. *Physics Education*, 38, 504-511.
- Sutedja, M. B., Smith, G. D., Muilenburg, D. A., & Musser, P. (2018). *The Boeing Co. Q2 Earnings Call*. Boeing.
- Tomlin, M., & Meyer, J. (2011). Topology Optimization of an Additive Layer Manufactured (ALM) Aerospace Part. *7th Altair CAE Technology Conference*, (pp. 1-9).
- WSF. (2020). *Court Specifications*. Retrieved 12 06, 2020, from World Squash Federation: <http://worldsquashfederation.com/court-construction/>
- Zang, B. (2019). <https://www.businessinsider.com/boeing-737-max-profit-moodys-2019-3>. www.businessinsider.com. adresinden alındı

Chapter 11

TOPOLOGIES OF ISOLATED AND NON-ISOLATED DC-DC PWM CONVERTERS IN SOLAR PV APPLICATIONS



Naim Suleyman TING¹

Yakup SAHIN²

1 Associate Prof. Dr., Erzincan Binali Yildirim University, Department of Electrical Electronics Engineering, nsuleyman@erzincan.edu.tr

2 Assistant Prof. Dr., Bitlis Eren University, Department of Electrical Electronics Engineering, ysahin@beu.edu.tr

INTRODUCTION

With the technological development, that makes life easier and the increase in the world population, the energy need of people is increasing day by day. Most of the energy consumption in the world is met by fossil fuels. Nowadays, besides the increasing consumption of fossil fuels and the negative aspects it gives to the environment, interest in renewable energy sources is increasing for purposes such as ensuring energy efficiency and protecting environmental factors. Renewable energy can be defined as the ability to renew itself at an equal rate to the energy taken from the energy source or faster than the depletion rate of the resource. Solar energy as a renewable energy source and solar cells used in converting this energy into electrical energy and system components are among the most interesting subjects in research. While the supply inputs of most of the receivers used in daily life are alternating current (AC), photovoltaic (PV) panels generate direct current (DC). The fact that the energy demand amount and time of the users and the time and amount of the energy produced from the solar cell are generally not compatible reduces the reliability and operational efficiency of local systems fed by PV. The batteries used to ensure the continuity of energy increase the investment cost and reduce the efficiency of the system. It is only possible to eliminate these drawbacks and to benefit from the energy produced from solar cells only with grid-interactive systems (Koutroulis et al., 2001; Chiang et al., 1998).

It is clear that the use of fossil resources in energy production is no longer possible, and the damage caused by industrialization, fossil resources, and the fact that the use of renewable energy resources instead of these energy resources, which were previously ignored, is increasing day by day. For each type of power plant to be established to produce energy, while calculating the costs, it is necessary to consider the operation, production, disposal of waste, etc. details are taken into account. Considering these costs, it is seen that renewable resources are also economically advantageous (Walker et al., 2004; Li et al., 2011).

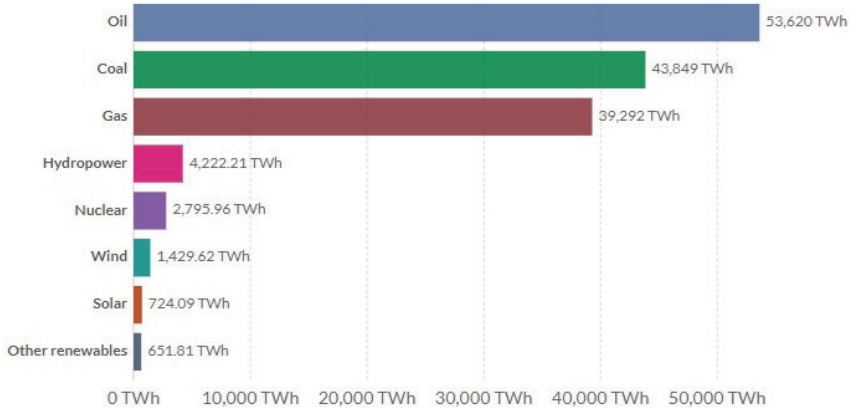


Figure 1. *Shares of energy resources in world electricity generation in 2019 (Ritchie, 2019).*

Renewable resources, which can be consumed where they are produced without connecting to the grid, can easily be used for energy generation, especially in regions where the access of transmission or distribution lines is difficult or where line construction is not economical due to small-scale energy needs. The shares of energy resources used in world electricity production in 2019 are isolated in Figure 1. As can be understood from here, electricity generation with solar energy corresponds to 0.5% of the total electricity generation (Ritchie, 2019).

SOLAR ENERGY AND PHOTOVOLTAIC PANELS

Solar energy is an electromagnetic radiation of 200 nm and 2500 nm wavelengths, which is called photon and propagates in energy beams, and it is the energy that comes out as a result of the transformation of hydrogen gas into helium through the fusion process that occurs in the Sun's core. This energy reaches the Earth as heat and light energy. As a result of this fusion reaction in the core of the sun, 4×10^{18} Joules of energy is sent to the Earth annually. However, up to 3×10^{14} Joules of this energy can be used by the world. Solar panels are materials that operate according to the photovoltaic principle, convert the sunlight coming on their surfaces directly into electrical energy as DC and consist of two semiconductor materials such as P and N types with electrically different properties. The first findings of the conversion of solar energy into electricity based on the photovoltaic principle emerged in 1839 as a result of the studies of Alexander Edmond Becquerel. In this study, Becquerel observed that the potential difference between the tips of the electrodes in a liquid electrolyte solution changes depending on the light falling on the electrodes. In the following years, studies of generating electricity from solar energy have become widespread due to their increasing efficiency (Kenar, 2019). In

order to determine the electrical properties and behavior of photovoltaic panels or arrays, they must first be modeled by simulation. For this, elements whose behavior and reactions are known or can be calculated are used. In the literature related to the modeling of photovoltaic panels, more than one electrical equivalent circuit model such as single diode structure and double diode structure can be used. Since it is simpler and 13 ideal models are accepted, a single diode model has been preferred in this thesis. Accordingly, the equivalent circuit model of a single diode solar cell is isolated in Figure 2 (Rasool et al., 2016).

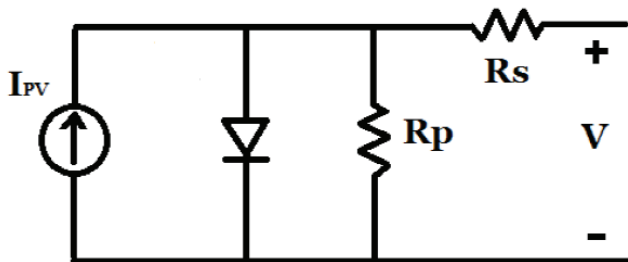


Figure 2. Solar cell equivalent circuit.

Abbreviations in electrical equivalent circuits;

I_{PV} : Electric current produced by solar

R_s : Serial resistance

R_p : Parallel resistance

The electric current generated in the solar cell is given as in equation (1);

$$I_{PV} = [I_{SC} + K (T - 298)] * \lambda \quad (1)$$

Here, λ indicates the radiation in kW/m^2 , I_{SC} indicates the short circuit current of the solar cell at 25° , K the short circuit current temperature constant of the solar cell, and T indicates the solar cell's operating temperature in Kelvin. The characteristic curves of photovoltaic panels produced by the manufacturers with different properties are obtained under constant test conditions of 25°C temperature and 1000 W/m^2 . Changes in temperature and radiation values cause changes in characteristic curves. In addition, in order to obtain current-voltage and power-voltage curves depending on different temperature and radiation values, it is necessary to know the open-circuit voltage and short-circuit current values of the measured photovoltaic panel.

The highest voltage value that can be obtained from the photovoltaic panel is the open circuit voltage value of the panel, while the highest current

value is the short circuit current value of the panel. However, in both cases, the power value that can be taken from the panel is zero. Because the panel current is zero in case of open circuit, and the panel voltage is zero in case of short circuit. Solar panels are the main element of the solar cell system that converts the sun's rays into electrical energy. Panels are connected in series to give higher voltage and in parallel to get higher current output. By-pass diode is used in serial connections of panels, and blocking diode is used in parallel connections. The function of the by-pass diode is to ensure that the current passes through the panels as short circuits that break down during operation. The function of the blocking diode is to block the damaged panels during operation and prevent them from absorbing the energy of other panels. Solar cells are connected in parallel or in series to increase the power output. This structure is called solar cell module. A typical silicon solar cell can generate as much as 0.5 volts of electricity. Solar cells are connected in series to give higher voltage and in parallel to give higher current. Usually 30-36 solar batteries can be connected together to give an output power of 15-17 volts. Panels are formed by connecting modules together. Each module is designed with a connection box that allows it to be connected in parallel or in series (Partain et al., 2010). The energy produced in solar cell systems is converted into chemical energy and stored in batteries in order to be used at night or on days when the weather is off. In addition, if the power produced in the batteries is insufficient, the difference can be met from the batteries. Although the stored energy is used at any time of the day and in all weather conditions, solar cells try to replace the spent energy only in a limited time in daylight (Doughty at al., 2010

). In addition, charge regulators are used in the solar energy system to prevent overcharging and discharging the battery. The control method of the charge regulator must meet the effect of the battery charge and the needs of the loads that the system must supply.

DC-DC PULSE WIDTH MODULATION (PWM) CONVERTERS

DC-DC converters are power electronics circuits that transfer the DC voltage at its input to the output as a different level DC voltage. They have a wide range of uses both in practical applications in the industrial field and in theoretical and experimental applications in the academic field. In this respect, DC-DC converters; It is widely used in renewable energy systems, switched power supplies, control and communication systems, battery charging circuits, electric vehicles and many more. DC-DC converters are circuits with a structure that can operate at high frequencies. The operation of these power electronics circuits at high frequencies causes them to be physically designed to be small and light. This provides an advantage in terms of cost. However, working at high frequencies also

causes harmonics and power losses as a result of fast switching. DC-DC converters are generally divided into linear power converters and switch mode power converters. Nowadays, with the developments in semiconductor technology, the fact that switch mode power converters can be designed smaller and more efficiently enables these converters to be widely used (Mohan et al., 2003).

Switched type DC-DC power converters are basically power electronic circuits formed by connecting two switching elements, one of which is controlled, and the coil in different ways. The semiconductor switching element that is operated in a controlled manner and functions in the circuit in full transmission or in full cut is called the active element, and the semiconductor element that changes position depending on the operating conditions of the circuit is called the passive element. SCR, BJT, MOSFET or IGBT are generally used as active semiconductor switching element for different frequency and power values. The working principle of switched DC-DC power converters is based on the coil in its structure to store and transfer energy according to the position of the semiconductor power switch. Depending on the structure of the circuit, it is realized by transferring the energy accumulated in the coil during the period when the semiconductor-switching element is in transmission to the output when the diode, which is the passive element, is active (Bodur, 2017).

DC-DC power converters are generally controlled by two different methods: Pulse Width Modulation (PWM) and Frequency Modulation (FM). In FM technique, the output value is controlled as a result of changing the transmission time of the semiconductor switching element by changing the pulse frequency, that is, the period. However, this technique is mostly used in forced state studies such as transient regime and low load. In addition, fluctuations and noises occur in the output voltage as a result of the use of this technique. Due to the fact that the frequency is constant, it allows the fluctuation and noise in the input and output to be filtered, so PWM technique is widely used in real studies. The PWM technique is a method in which the output value is controlled by adjusting the transmission time of the semiconductor switch by changing the pulse width and changing the period and the fixed frequency value (Bodur, 2017). The converters with inductance are commonly used in DC-DC converters. DC-DC converters with inductance are widely used in applications such as Switched Power Supply (SMPS), Power Factor Correction (PFC), computer, control and communication circuits. Inductance isolated converters can be applied at low powers up to a few kW, due to the limitations in the use of transformers. In applications requiring large power such as DC welding machine and inverter feeding, it is necessary to switch to DC-DC converters with inverter intermediate circuit. In these circuits, a high frequency AC voltage generated by an inverter is rectified and filtered. DC-DC converters are

known as high frequency and switched circuits. In switched circuits, a fully controlled power element is switched at high frequency. The power element is operated either at full transmission or at full cut, thus achieving high efficiencies between 70% and 90%. The use and design of capacitors, coils and transformers have an important place in these converters. The higher the frequency, the smaller the capacitor, coil and transformer sizes. The size and cost of the circuit decreases and the power density increases. In DC-DC converters, despite all the advantages listed above, due to fast switching and high frequency, Electro Magnetic Interference (EMI), current and voltage rise rates, maximum values of current and voltage and switching power losses increase. In these circuits, Soft Switching (SS) techniques that minimize or eliminate switching losses with snubber cells that limit the rise rates and maximum values of the current and voltage are becoming important (Bodur, 2017).

The most common type of DC-DC converters can be divided into two categories depending on how they transfer the power. The energy can go from the input through the magnetics to the load simultaneously or the energy can be stored in the magnetics to be released later to the load. Table 1 lists the most common DC-DC converters and their typical power limitation. When choosing a DC-DC converter, attention should be paid to the power values in the table below (Andersson, 2011).

Table 1. *Overview of DC/DC-converters and their typical power limitation*

Converters	Energy Flow	Energy Storage
<i>Non-Isolated</i>	Buck (<1 kW)	Boost (<150 W) Buck – Boost (<150 W)
	<i>Isolated</i>	Full-bridge (>1 kW)

NON-ISOLATED DC-DC PWM CONVERTERS IN SOLAR PV APPLICATIONS AND SIMULATION RESULTS

Non-isolated DC-DC converters are structurally obtained by differently connecting an active and a passive semiconductor switching power element and an inductance. The operating logic of inductive converters is based on the transfer of energy stored in the inductance. Semiconductor switching takes place by transferring the energy supplied by the source and stored in the inductance during the period when the power element is in transmission, to the load as a result of the semiconductor switching element being cut. The biggest disadvantage of these converters is the lack of isolation between output and input. These converters; while the types such as boost, buck, buck-boost are the most common ones.

1. BUCK CONVERTERS IN SOLAR PV APPLICATIONS

Buck converters are converters that produce an average output voltage lower than the input voltage. Figure 3 shows the solar panel application circuit in the PSIM model of the buck converter. PSIM is a power electronics simulation programme. A 22 Volt solar panel model is used in the figure. The operation of the converter basically, while the power switch is in transmission, the energy taken from the solar panel both feeds the output and provides energy storage in the inductance located on the current path. When the switch is cut off, the diode starts conducting and continues to feed the load with the energy accumulated in the inductance. Thus, energy continuity is ensured in the load. In buck converters, a controllable DC output voltage is obtained between zero and input voltage. The output voltage is expressed by the following equation, where D is the relative conduction time,

$$V_{Out} = V_{in} * D \quad (2)$$

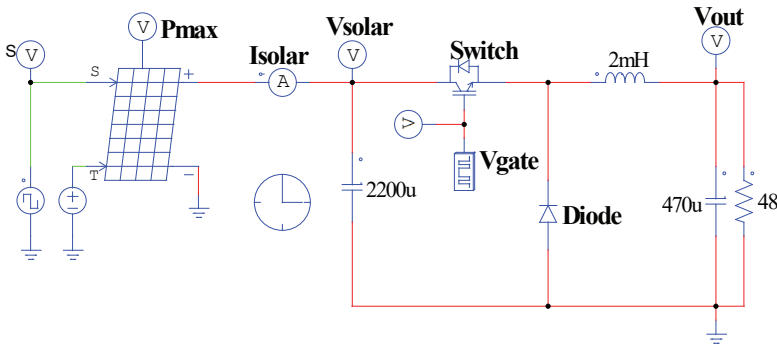


Figure 3. Buck converter PSIM model with solar panel application

In Figure 4, the solar panel voltage and the output voltage results are given. The input voltage obtained by solar panel is 22 V and this voltage duty cycle (D) was reduced to 11 volts at the output with the control made as 50%. Also, in Figure 5, the output, solar and inductance current results are given. In buck converter operating in continuous current mode, the average inductance current is equal to the average output current. This situation is clearly visible in Figure 5. Because in continuous current mode, the average capacitor current is zero. It is also seen in Figure 5 that the current drawn from the input voltage source is very fluctuating, but the fluctuation in the output current is very low. In these converters, the fluctuation in the output voltage is very small since the energy accumulated in the inductance in the interval where the power switch is in the cut is transferred to the load. Besides, in Figure 6, the current and voltage waveforms of the switch and diode of buck converter are given. As shown in figure, the semiconductor devices are exposed to the most input voltage obtained by solar panel.

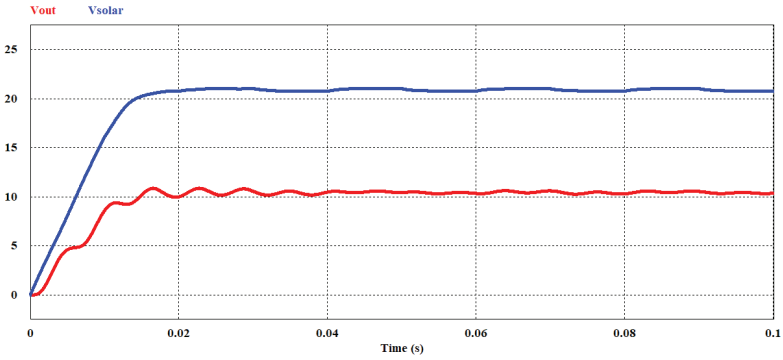


Figure 4. The solar and output voltage results of buck converter in solar pv application.

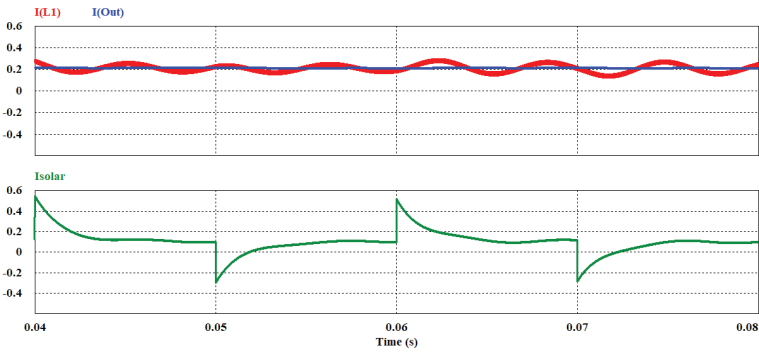


Figure 5. The currents of output, inductance and solar results of buck converter in solar pv application.

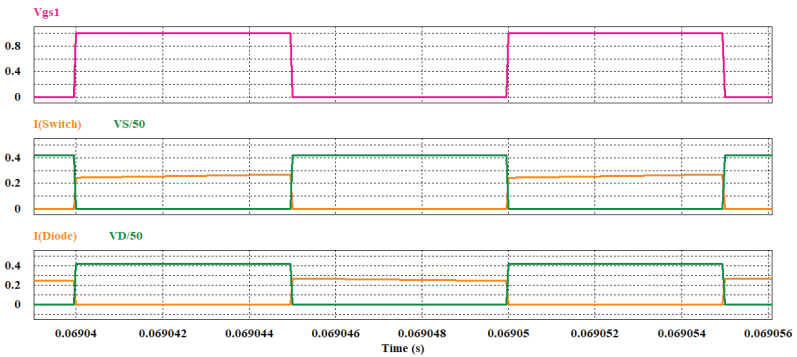


Figure 6. The currents and voltages results of switch and diode of buck converter in solar pv application.

2. BOOST CONVERTERS IN SOLAR PV APPLICATIONS

Boost converters are converters that produce a higher level of output voltage than the input voltage. Figure 7 shows the solar panel application

circuit in the PSIM model of the boost converter. A 20 Volt solar panel model is used in the figure. The operation of the converter is basically; the solar panel simply injects additional energy into the inductance while the power switch is on. Meanwhile, the diode is reverse polarized and only supplies the capacitor load. With the switch turned off, the diode turns on and both the input voltage supplies the output and the energy accumulated in the inductance is transferred to the output. In boost converters a controllable DC output voltage is obtained between input voltage and a specified maximum voltage. The output voltage is expressed by the following equation, where D is the relative conduction time,

$$\frac{V_{Out}}{V_{in}} = \frac{1}{1-D} \quad (3)$$

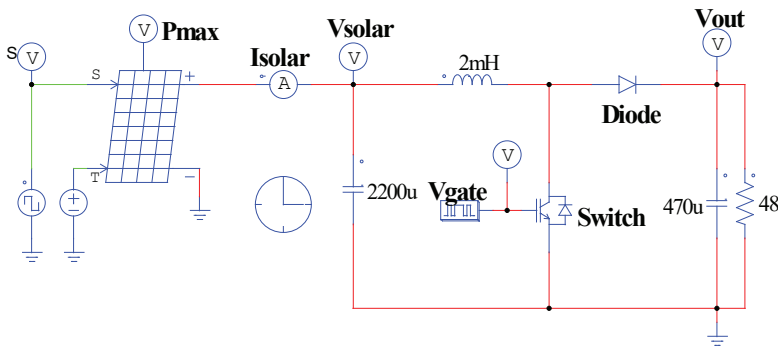


Figure 7. Boost converter PSIM model with solar panel application

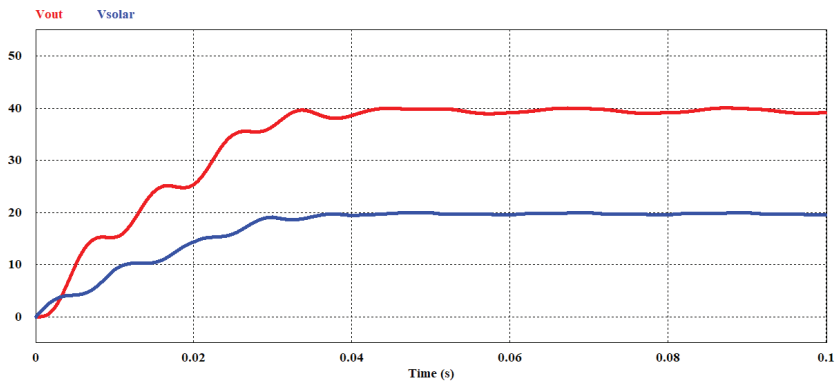


Figure 8. The solar and output voltage results of boost converter in solar pv application.

In Figure 8, the solar panel voltage and the output voltage results are given. The input voltage obtained by solar panel is 20 V and this voltage duty cycle (D) was increased to 40 volts at the output with the

control made as 50%. Also, in Figure 9, the output, solar and inductance current results are given. In this boost converter operating in continuous current mode, the ripple in the input current is very small as the inductance is connected in series with the input and the inductance current is equal to the input current. This situation is clearly visible in Figure 9. Since the output voltage is supplied solely by capacitor energy when the power switch is in transmission, fluctuations occur in the voltage. It is accepted that the parallel capacity in the output filter is too large to keep the output voltage constant. Besides, in Figure 10, the current and voltage waveforms of the switch and diode of boost converter are given. As shown in figure, the semiconductor devices are exposed to the output voltage. Also, these converters cannot be operated without load (Bodur, 2011).

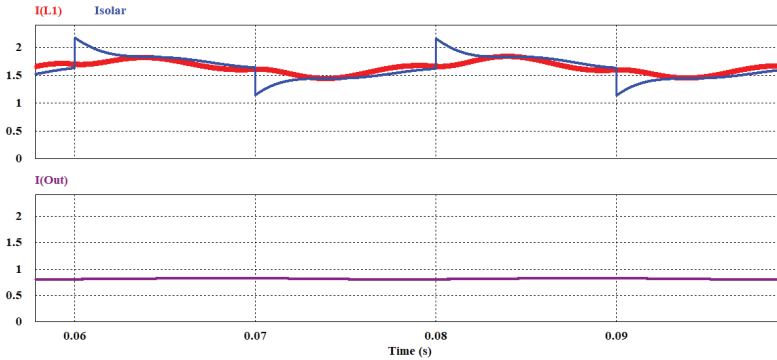


Figure 9. *The currents of inductance, solar and output results of boost converter in solar pv application.*

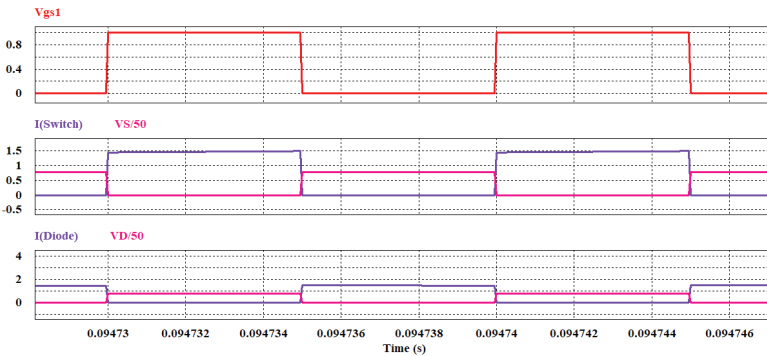


Figure 10. *The currents and voltages results of the switch and diode of boost converter in solar pv application.*

2. BUCK - BOOST CONVERTERS IN SOLAR PV APPLICATIONS

Buck - boost converters are converters that can both step down and step up the voltage. The different feature of this converter compared to

other converters is that the output voltage is opposite. That's why they are also known as reverse output converters. Figure 11 shows the solar panel application circuit in the PSIM model of the buck - boost converter. A 17 Volt solar panel model is used in the figure. The operation of the converter is basically, when the power switch is on, the input voltage source transfers additional energy to the inductance while the capacitor feeds the load. With the switch on, only the energy accumulated in the inductance is transferred to the output. In buck-boost converters, a controllable DC output voltage between zero and a specified maximum voltage is obtained. The output voltage is expressed by the following equation, where D is the relative conduction time,

$$\frac{V_{Out}}{V_{in}} = \frac{D}{1-D} \tag{4}$$

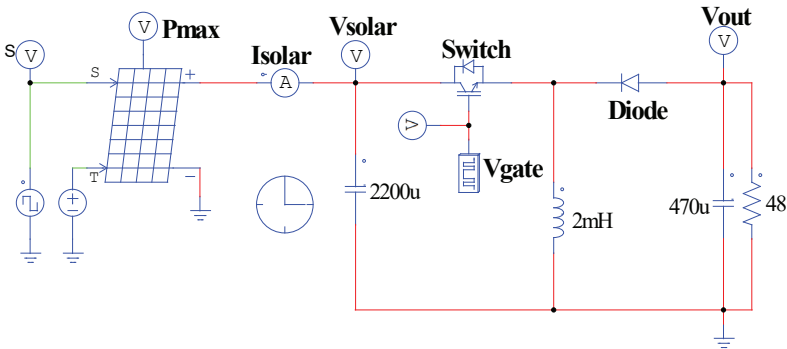


Figure 11. Buck - boost converter PSIM model with solar panel application

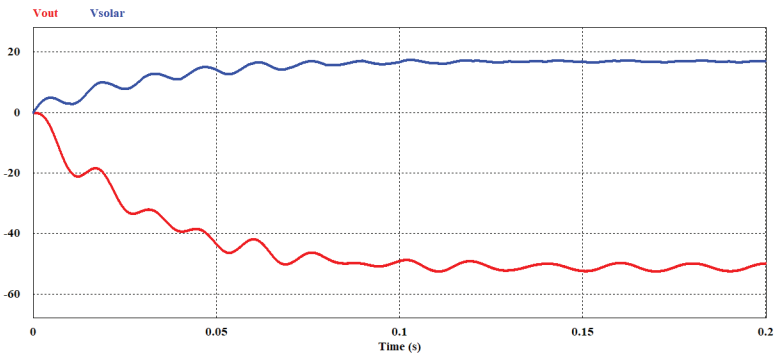


Figure 12. The solar and output voltage results of buck - boost converter in solar pv application.

In Figure 12, the solar panel voltage and the output voltage results are given. The input voltage obtained by solar panel is 17 V and and this voltage duty cycle (D) was increased to 51 volts at the output with the

control made as 75%. Also, in Figure 13, the output, solar and inductance current results are given. In the buck-boost converter operating in continuous current mode, inductance current is equal to the sum of input and output currents since inductance is not connected in series to input or output and fluctuations in input and output currents are large. This situation is clearly visible in Figure 13. Besides, in Figure 14, the current and voltage waveforms of the switch and diode of buck - boost converter are given. As shown in figure, the semiconductor devices are exposed the sum of input and output voltages. Also, these converters cannot be operated without load.

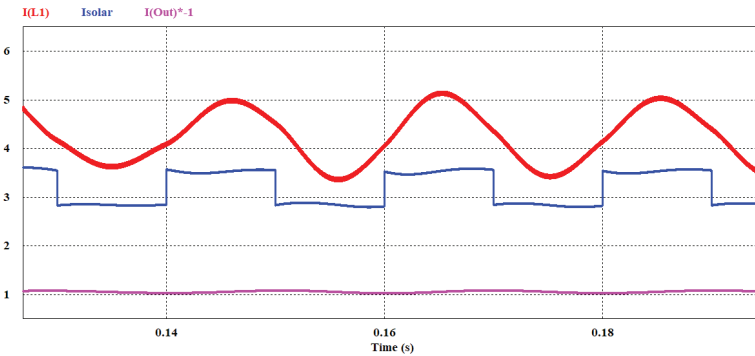


Figure 13. The currents of inductance, solar and output results of buck - boost converter in solar pv application.

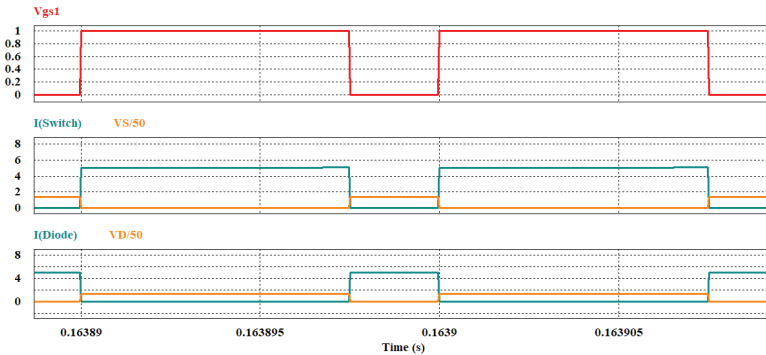


Figure 14. The currents and voltages results of the switch and diode of buck - boost converter in solar pv application.

ISOLATED DC-DC PWM CONVERTERS IN SOLAR PV APPLICATIONS AND SIMULATION RESULTS

Isolation is the process of electrically separating the input and output. Isolation can be done in two ways. Isolation can be made with either magnetic connectors or optical connectors. Either optic elements or transformers are used in the circuits to electrically isolate the input and

output, that is, to make insulation. Since electrical isolation is required in most of the DC-DC converter applications, isolated types of inductance converters have been developed. The isolated type of buck converter used is called forward converter. The isolated type of buck - boost converter used is called flyback converter. There is no applied isolated type of boost converter. The working principle of isolated converters is exactly the same as the non-isolated basic types. The properties of the inductance used here and the working conditions with CCM and DCM are also the same. Here, the use and properties of the transformer providing insulation become important. The magnetizing inductance is fully coupled and can be isolated either primary or secondary. The energy of this inductance can be transferred. The energy of non-coupled leakage inductances can cause high voltage pulses to occur and power elements to fail. The recovery, control or suppression of stray inductance energies is very important in these circuits (Bodur, 2017). In this section, flyback converter and full-bridge converter of isolated DC-DC converters are examined.

1. FLYBACK CONVERTERS IN SOLAR PV APPLICATIONS

The flyback converter is the easiest to design and the one with the least elements among the existing isolated converters. The advantages of this converter are that it can obtain high output voltage and give more than one output (Pressman at al., 2009). Figure 15 shows the solar panel application circuit in the PSIM model of the flyback converter. A 22 Volt solar panel model is used in the figure. The operation of the converter is basically, when the power switch is on, the input voltage is applied to the primary winding. Due to the reverse polarity of the secondary winding with respect to the primary winding, the diode is reverse polarized and no current flows from the secondary. Meanwhile, the capacitor feeds the load. When the switch enters the cut, the energy stored in the primary winding is transferred to the load through the secondary winding. The output voltage is expressed by the following equation, where D is the relative conduction time,

$$\frac{V_{Out}}{V_{in}} = \frac{D}{(1-D)*a} \quad (5)$$

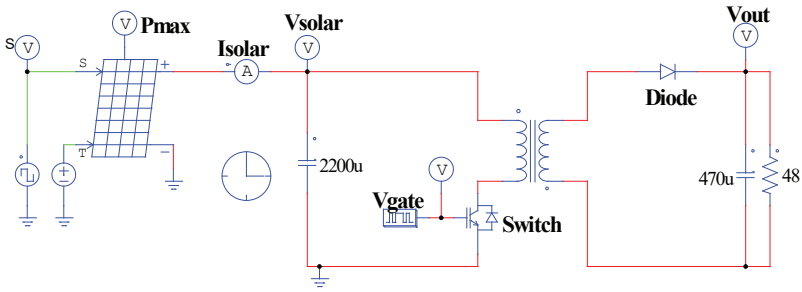


Figure 15. Flyback converter PSIM model with solar panel application

In Figure 16, the solar panel voltage and the output voltage results are given. The input voltage obtained by solar panel is 22 V and this voltage duty cycle (D) was reduced to 11 volts at the output with the control made as 50% and N_p/N_s is equal to 6. Also, in Figure 17, the output, solar and inductance current results are given. The flyback converter operating in continuous current mode basically has buck-boost converter features. However, due to the electrical isolation between the input and output, it is not possible for the output voltage to be reversed. This situation is clearly shown in Figure 17. Besides, in Figure 18, the current and voltage waveforms of the switch and diode of flyback converter are given. As shown in figure, the power switch is exposed to $(V_{in} + a \cdot V_{Out})$ voltage and the power diode to $(V_{in}/a + V_{Out})$ voltage.

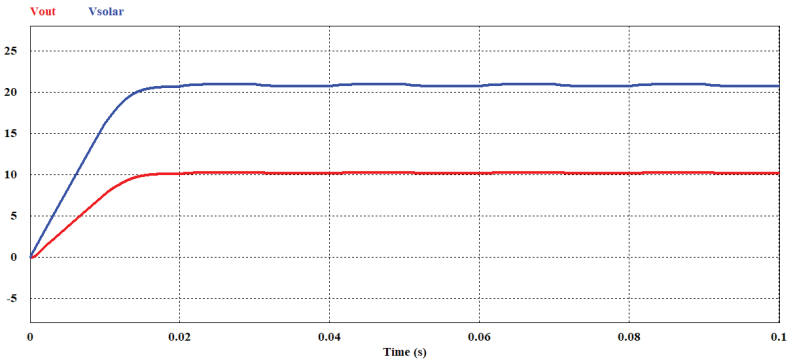


Figure 16. The solar and output voltage results of buck converter in solar pv application.

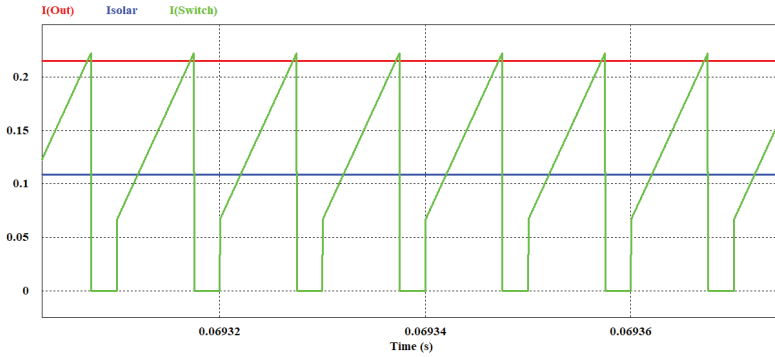


Figure 17. The currents of output, inductance and solar results of flyback converter in solar pv application.

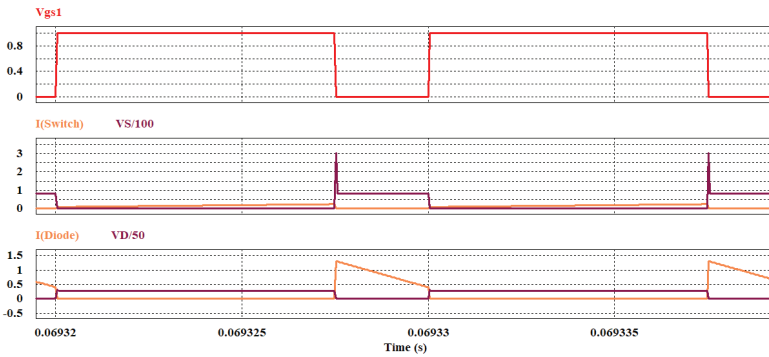


Figure 18. The currents and voltages results of switch and diode of buck converter in solar pv application.

2. FULL-BRIDGE CONVERTERS IN SOLAR PV APPLICATIONS

Full-bridge converters are one of the widely used isolated DC-DC converters. In this converter, an output voltage is obtained according to the transformer conversion ratio. Unlike the flyback converter, the primary and secondary windings of the transformer work simultaneously in this converter. Thus, the energy obtained from the primary can be transferred to the load through the secondary winding while the power switches are in transmission. Figure 19 shows the solar panel application circuit in the PSIM model of the boost converter. A 16 Volt solar panel model is used in the figure. The output voltage is expressed by the following equation, where D is the relative conduction time,

$$\frac{V_{out}}{V_{in}} = \frac{N_S}{N_P} \tag{6}$$

In Figure 20, the solar panel voltage and the output voltage results are given. The input voltage obtained by solar panel is 16 V and this voltage duty cycle (D) was increased to 48 volts at the output when N_p/N_s is equal to 3.

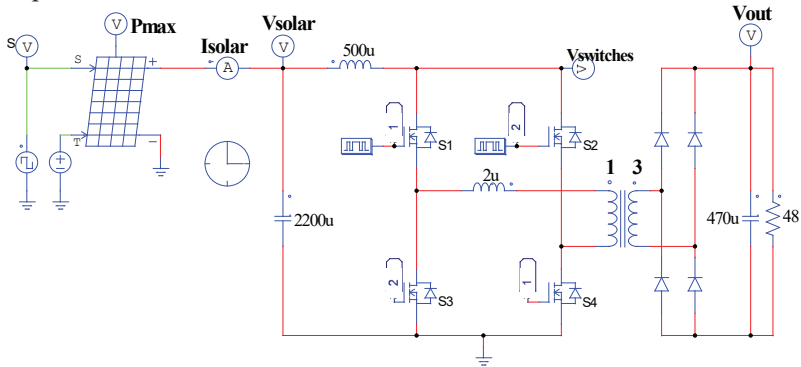


Figure 19. Full-bridge converter PSIM model with solar panel application

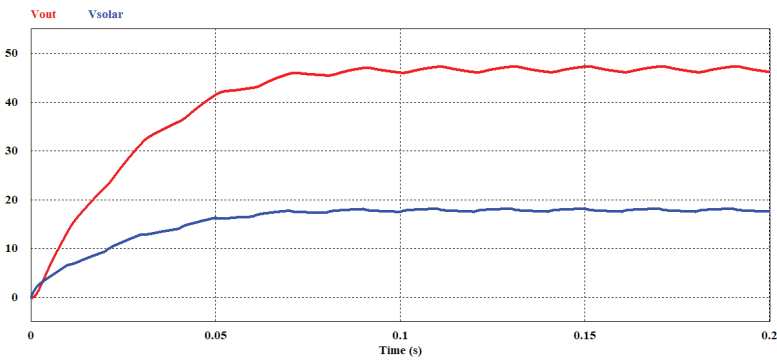


Figure 20. The solar and output voltage results of full-bridge converter in solar pv application.

CONCLUSION

In this chapter, the use of the most widely used isolated and non-isolated DC-DC converters in solar PV applications and the simulation results obtained are given and compared. In the chapter, isolated and non-isolated common converter topology is mentioned. In the selection of topology to be used in solar cells, parameters such as panel characteristics, load characteristics, ease of control, volume, reliability and system cost determine the system type. In addition, the fact that the necessary components are at low voltage and current increases the usefulness. Some properties of the converters analyzed in the section according to the data obtained from the simulation results are given in Table 2. Finally, when choosing a converter in applications where the voltage is required to be increased or decreased in solar panel applications, the appropriate converter can be selected by paying attention to the criteria in the table below.

Table 2. Comparison of Isolated and Non-Isolated DC-DC PWM Converters

DC-DC PWM Converter Used in Solar PV Applications					
Subject of Comparison	Non-Isolated Converters			Isolated Converters	
	Buck	Boost	Buck – Boost	Flyback	Full-bridge
Output Voltage V_{out}	$V_{in} * D$	$V_{in} * \frac{1}{1-D}$	$V_{in} * \frac{D}{1-D}$	$\frac{V_{in} * D}{a * 1-D}$	$V_{in} * \frac{N_S}{N_P}$
Input Current I_{in}	$I_{out} * D$	$I_{out} * \frac{1}{1-D}$	$I_{out} * \frac{D}{1-D}$	$\frac{I_{out} * D}{a * 1-D}$	$I_{out} * \frac{N_S}{N_P}$
Voltage Value to Which Power Switch are Exposed	V_{in}	V_{out}	$V_{in} + V_{out}$	$V_{in} + a * V_{out}$	$\frac{V_{out}}{a}$
Feature of Operation Without Load	Yes	No	No	No	No
Output Voltage Control Range	$0 \rightarrow V_{in}$	$V_{in} \rightarrow V_{out_max}$	$-(0 \rightarrow V_{out_max})$	$0 \rightarrow V_{out_max}$	$0 \rightarrow V_{out_max}$
Output voltage direction	Positive	Positive	Negative	Positive	Positive

REFERENCES

- Koutroulis, E., Kalaitzakis, K., Voulgaris, N. (2001). Development of a Microcontroller-Based, Photovoltaic Maximum Power Point Tracking Control System, *IEEE Transaction on Power Electronics*, 16(1): 46-54.
- Chiang, S. J., Chang, K. T., Yen, C. Y. (1998). Residential Photovoltaic Energy Storage System, *IEEE Transaction on Industrial Electronics*, 45(3): 385-394.
- Walker, G. R., Sernia, P. C. (2004). Cascaded DC-DC converter connection of photovoltaic modules. *IEEE Transaction on Power Electronics*, 19(4): 1130-1139.
- Li, W., He, X. (2011). Review of Nonisolated High-Step-Up DC/DC Converters in Photovoltaic Grid-Connected Applications, *IEEE Transaction on Industrial Electronics*, 58(4): 1239-1250.
- Ritchie, H. (2019). Energy, Published online at ourworldindata.org
- Kenar, M. (2019). Design of DC-DC and DC-AC Power Converters for Solar Power Systems and Control with Fuzzy-Pi, *Master Thesis*, Afyon Kocatepe University, Afyon, Turkey.
- Rasool, F., Driberg, M., Badruddin, N., Singh, B., & Singh, M. (2016). Modeling of PV panels performance based on datasheet values for solar micro energy harvesting. *In conference: Intelligent and Advanced Systems*, 1-5.
- Partain, L., Fraas, L. (2010), *Solar Cell and Their Applications*, 2nd Edition, Wiley, New York.
- Doughty, D., Butler, P., Akhil, A. Clark, N., Boyes, J. (2010). Batteries for Large-Scale Stationary Electrical Energy Storage, *Electrochemical Society Interface*, 19(3): 49-53.
- Mohan, U., Undeland, T. M., & William, P. (2003). *Robbins Power Electronics—Converters. Applications, and Design* 3rd Edition John Wiley & Sons Ltd.
- Bodur, H. (2017). *Güç Elektroniği Temel Analiz ve Sayısal Uygulamalar*, 4th Edition, Birsen Yayınevi, İstanbul.
- Andersson, C. (2011). Design of a 2.5kW DC/DC Fullbridge Converter, *Master of Science Thesis*, Department of Energy and Environment Division of Electric Power Engineering Chalmers University Of Technology, Göteborg, Sweden.
- Bodur, H. (2011). *Soft Switching Techniques in DC-DC Converters Lecture Notes*.
- Pressman, A., Billings, K., Morey, T. (2009). *Switching Power Supply Design*, 3rd Edition, The McGraw-Hill Companies.

Chapter 12

FLEXIBLE PIEZORESISTIVE STRAIN SENSORS BASED ON CARBONACEOUS FILLER/THERMOPLASTIC ELASTOMER COMPOSITES



Mukaddes Sevval CETIN^{1,2}

Ozan TOPRAKCI^{1,2}

Hatice Aylin KARAHAN TOPRAKCI¹

¹ Department of Polymer Materials Engineering, Yalova University, Yalova, Turkey

² Graduate School of Natural and Applied Sciences, Yalova University, Yalova, Turkey

1. Introduction

Sensors are systems that are used for the conversion of any type of stimuli into the meaningful electrical signal. Sensors can be fabricated by using various materials from metals to semiconductors and from ceramics to polymers. Recent requirements and trends in technology opened a new area as flexible electronics. Polymers are the common components of the flexible electronics because they are flexible, lightweight materials with easy processability. They have been used for various applications including switches, diodes, conductive adhesives, energy storage systems, actuators and sensors in various forms such as homopolymers, blends or composites. Since most of the polymers show relatively high resistivity, the easiest way to produce flexible electronics with electrical conductivity is to incorporate conductive fillers into polymer matrix. The polymer composites that show electrical conductivity with flexibility are referred to as “Flexible Conductive Polymer Composites” (FCPCs). Although FCPCs can be used for many applications including conducting adhesives, coating, electromagnetic interference shielding; they can be used as piezoresistive sensors because of their stretchable character and good resilience (Fraden, 2004; Hatice Aylin Karahan Toprakci, 2012; Hatice A. K. Toprakci & Ghosh, 2015; Hatice A. K. Toprakci et al., 2013; Turgut et al., 2018).

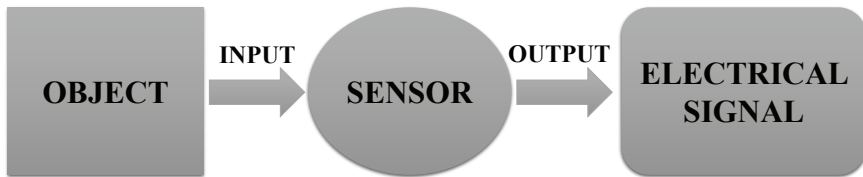


Figure 1. *Basic mechanism of sensors*

2. Piezoresistive Sensors

Sensors function based on their working mechanisms. The mechanism of sensing is not only important for the sensing systems requirements but also for the performance of the system. As known, there are various sensing mechanisms including capacitive, piezoelectric, chemical, optical, inductive and piezoresistive. Piezoresistive sensors are the common type of polymer-based sensors. Their mechanism is based on piezoresistance. Piezoresistance is basically change in resistance caused by dimensional deformation. The deformation can be induced by various factors such as applied mechanical force, temperature, humidity, chemical or gas exposure. Mechanical stress can be applied in various forms such as bending, strain or compression. The most important property for the piezoresistive sensors is the electrical conductivity. In the case of polymer based piezoresistive

sensors (PBPSs), polymers or polymer composites with semi-conductivity or conductivity is required.

3. Polymer Based Piezoresistive Strain Sensors

Sensors can be used to determine many variables including strain, pressure, force, concentration, temperature and gas exposure. Strain sensors are materials used to determine the applied strain under various conditions. Polymer based strain sensors are generally obtained from FCPCs. The requirements for a piezoresistive strain sensor can be given as: electrical conductivity, flexibility, stretchability, resilience, recoverability, durability and dimensional stability. For PBPSs, basically there are two basic responds obtained from the PBPSs as positive and negative piezoresistance. As given in Fig. 2, applied strain leads to separation of fillers, as a consequence of that, conducting networks start to break-down and resistance increases. The increase in resistance as a result of applied strain is called “Positive Piezoresistance”. Polymer type, filler type and concentration, composite fabrication method, test conditions are the most common factors those govern the piezoresistive response.

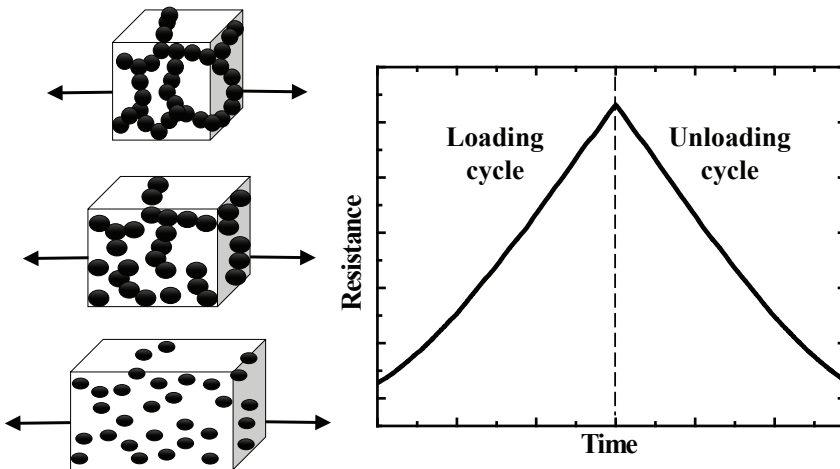


Figure 2. Positive piezoresistance

In some cases, as given in Fig. 3 (based on the filler geometry and filler concentration), under applied strain, fillers come closer, new conductive networks are formed and resistance drops. The decrease in resistance as a result of applied strain is called “Negative Piezoresistance”.

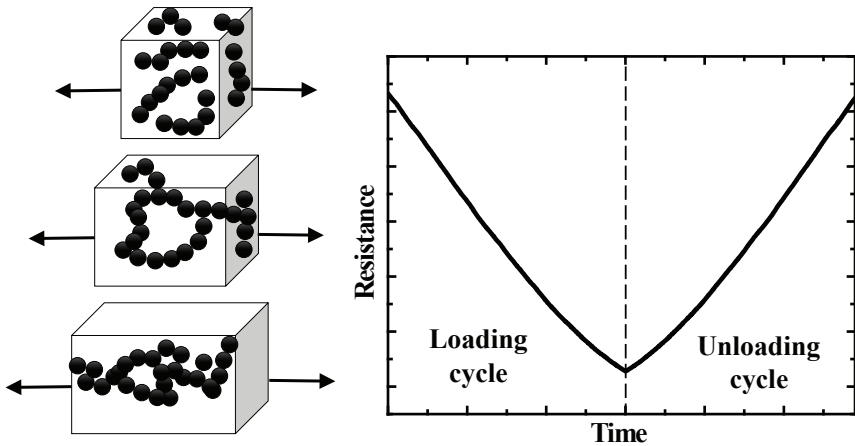


Figure 3. Negative piezoresistance

Another important concept for the polymer based piezoresistive strain sensors is the sensitivity. Sensitivity depends on the change in resistance under given strain level. This is expressed by “Gauge Factor” (GF). GF of a polymer based piezoresistive composite is defined as the fractional change in resistance ($\Delta R/R_0$) per unit strain, ε as given in Eq. 1. Higher GF value represents the higher sensitivity.

$$GF \text{ composites} = \left(\frac{\Delta R}{R_0}\right) / \varepsilon_{axial} \dots\dots\dots \text{Equation (1)}$$

4. Thermoplastic Elastomer Based Strain Sensors

Sensitivity is one of the most important performance factors for strain sensors. As mentioned above, higher GF represents higher sensitivity. When the polymer-based sensors are investigated, the most common problems faced with is hysteresis observed during electromechanical characterization. This is caused by the mechanical properties of the polymer composites. Although flexibility and stretchability are significance for PBPSs, recoverability in other words resilience is very critical in terms of obtaining repeatable and precise data. As known, under cyclic loading-unloading process samples deform and resilience shows the recoverability of the polymeric system. The polymers with low recoverability/resilience show higher hysteresis. On the other hand, polymers with good resilience show relatively low hysteresis. Elastomeric polymers are advantageous materials in the area of PBPSs. However, elastomers require vulcanization that results in harder materials. Another class of elastomers known as “Thermo Plastic Elastomers” (TPEs). TPEs are promising materials

for PBPSs because of their unique mechanical properties including flexibility, stretchability, bendability and high resilience. Since TPEs consist of thermoplastic and elastomer domains, they can be processed like thermoplastics and they do not require vulcanization. Thermoplastic domains function as physical crosslinks that increase the recoverability of the system.

In the literature the number of studies related with TPE based piezoresistive sensors are limited compared to elastomeric and thermoplastic based sensors. In these studies generally TPU (Bilotti et al., 2010; Duan et al., 2019; Zheng et al., 2017), poly(styrene-butadiene-styrene) (SBS) (Bautista-Quijano et al., 2018; Costa et al., 2013; Costa, Silva, et al., 2014; Costa, Silvia, et al., 2014; X. Wang et al., 2018), SEBS (Gonçalves et al., 2016; Mattmann et al., 2008; Pan et al., 2020; X. Yang et al., 2019), were used. The conductive fillers can be classified as carbon black (CB) (Clemens et al., 2013; Duan et al., 2019; Zhang et al., 2018), carbon nanofibers (CNFs) (Turgut et al., 2018), carbon nanotubes (CNTs) (Bilotti et al., 2010; Gonçalves et al., 2016), graphene (Costa et al., 2019; Xie et al., 2020), and mixture of various fillers (Pan et al., 2020; Xie et al., 2020). As can be seen from these studies carbonaceous fillers are dominant in this area. This is caused from many factors including high conductivity, inert structure and tunable filler geometry. Since all carbonaceous fillers have different size, geometry, aspect ratio and conductivity; sensitivity and performance of the sensors change.

As reported in the studies various factors (Avilés et al., 2018; Duan et al., 2020) were investigated such as filler type (Zheng et al., 2017), filler concentration (Duan et al., 2019; Y. Li & Shimizu, 2009; Liu, Li, et al., 2016; Mattmann et al., 2008; X. Wang et al., 2018), deformation ratio (Liu, Li, et al., 2016; X. Wang et al., 2018; Zheng et al., 2017), test speed (Liu, Li, et al., 2016; Turgut et al., 2018), cycle number (Turgut et al., 2018) and hysteresis (Liu, Li, et al., 2016; Turgut et al., 2018).

4.1 Carbon Black Filled Thermoplastic Elastomer Based Piezoresistive Strain Sensors

Carbon black is one of the most commonly used carbonaceous material for various applications from coloring to reinforcement and antistatic, conductive coating applications. CB can be fabricated by various methods and various types of CB, (with various physical, mechanical and electrical properties), can be found in the market. Generally, highly conducting CBs are preferred not only for low percolation value but also for easy processing for the conductive composites. Zheng et al. prepared piezoresistive sensors based on CB/TPU. Composite films were prepared, morphological, electrical and electromechanical properties were investigated. Solvent based process was combined with compression molding. CB particles were

found to be homogeneously dispersed in the TPU matrix and percolation concentration was determined around 1 wt%. Piezoresistive sensing tests were carried out under various strain ratios. 8 wt% CB filled TPU composite showed a GF of 10.8 under 20% strain. Samples were also tested in terms of their bending behavior and sensing performance was found good under bending load (Zheng et al., 2017).

In a study carried out by Duam et al., two types of CB were used with TPU matrix. CBs had different surface area values. Composites prepared by using CB with higher surface area showed lower percolation value. In order to determine the piezoresistive behavior, 10, 12, 15 wt% CB (CB with higher surface area) filled composites were prepared. All samples showed positive piezoresistance but at 10 wt% CB concentration, sensitivity was higher and resistance higher change was observed at relatively lower strain level (Duan et al., 2019).

Cochrane et al. fabricated SBS based sensors in two ways; melt mixing and solvent casting process. The effect of humidity and temperature on the sensing properties of the sensor were investigated. Percolation region was determined as 7.3 vol% CB for CB/SBS for both set of samples that were melt mixed and CB/SBS-solvent casted. According to the conductivity values, it was reported that the composites produced by solution casting showed higher conductivity since the particles dispersed more homogeneously in low viscous polymer solution. 27.6 vol% CB/SBS solvent mixed composite was chosen as a sensor. The sensor showed linear behavior above 15% strain. It was found that electrical response of the sensor was affected from environmental conditions such as humidity and temperature (Cochrane et al., 2007).

Clemens et al. fabricated strain sensor in the form of fiber. Three different SEBS, in terms of shore hardness, were used as matrix and 30-58 wt% CB was added. As given in the study, by applying the strain resistance values were reported to decrease. This was assumed to be caused by formation of new conductive networks in the polymeric matrix. It was reported that SEBS, with the highest hardness value, was chosen for further analysis. For this set of samples, above 45 wt% CB, the sensor had a stable electrical signal and low relaxation (Clemens et al., 2013). Poudel et al. fabricated CB/SEBS sensors via extrusion and supercritical fluid (SCF) assisted-extrusion. It was shown that CB particles dispersed more homogeneously in the composite produced by SCF-assisted extrusion. While, the conductive composite structure was observed around 5 wt% CB concentration by SCF, without using SCF method, conductive network formation was observed around 10 wt% CB concentration. The initial DC conductivity values of 10 wt % CB/SEBS composites were almost same with/without SCF process. The resistance change of 10 wt% CB/SEBS

fabricated with SCF had shown decreasing trend with under 5% strain, while without SCF had shown irregular change under the same strain because of agglomeration. Gauge factor was calculated under 2% strain for 5 and 10 wt% CB/SEBS, with SCF, and 10 wt% CB/SEBS, without SCF. It was reported that 5 wt% CB/SEBS, with SCF, had the highest sensitivity and its gauge factor increased with increasing strain value. The GF values under 2 wt% strain were reported as 5 wt% CB/SEBS-SCF, 10 wt% CB/SEBS-SCF, 10 wt% CB/SEBS 9, 1-2, 0.5-1 respectively (Poudel et al., 2019).

One of the most comprehensive studies in the area of strain sensors was carried out by Mattmann et al. They have fabricated 30, 40 and 50 wt% CB filled SEBS strain sensors for textile applications. As reported in the study, resistance increased for all samples under strain and the highest change in resistance was observed for 30 wt% CB filled sample. After characterization of sensor fibers, integration on the textile substrate was carried out by using a silicone film. 50 wt% CB filled sample was chosen for the textile sensor. 20, 40, 60, 80 % strain was applied on the textile sensor. In the case of pre-stretching to the desired value, any strain value in this range showed the same trend. They also investigated the effect of aging and washability on the sensing performance. Sensing properties were measured at certain intervals and it was shown that aging and washing did not affect the performance of the sensor (Mattmann et al., 2008).

Melnykowycz et al. fabricated CB/SEBS sensors in the form of fibers with various diameters and compared the sensing properties with three commercial monofilaments. Cycling tensile tests were performed to analyze sensing properties. Samples showed positive piezoresistance. When the filaments were compared sample with 0.3 mm diameter showed better sensing properties when compared with thicker monofilaments and commercial samples. The filament showed a nearly-linear behavior under loading 15-30% and GF was reported as 18 (Melnykowycz et al., 2014).

In another study, Melnykowycz et al. studied about the sensor that was covered on hand wrinkle and used to measure the hand movements and pulse to calculate the blood pressure of the human. A U-shape sensor, consisting of 50 wt% CB filled SEBS composite was produced. In order to analyze the electromechanical properties, cycling tensile test was conducted. The sensor showed a nearly linear positive piezoresistance behavior under high strain (up to 50%). GF of the composite was reported between 3.5 and 5 at 10 – 50 % strain. After determination of the electromechanical properties, sensor was tested for its motion capturing and pulse monitoring capacity. Sensor was found successful in terms of monitoring these properties (Melnykowycz et al., 2016).

4.2 Carbon Nanofiber Filled Thermoplastic Elastomer Based Piezoresistive Strain Sensors

Carbon nanofibers are fibrous nano structures obtained by carbonization of electrospun nanofibers or vapor grown deposition. The CNFs obtained by vapor grown deposition are referred as “Vapor Grown Carbon Nano Fibers” (VGCNFs). VGCNFs consist of graphene layers arranged in different forms depending on the processing conditions and catalysts. They are electrically conductive fillers with good mechanical properties. (Feng et al., 2014; Hatice Aylin Karahan Toprakci, 2012; Hatice A. K. Toprakci et al., 2013; Turgut et al., 2018). In the literature there are very limited studies in terms of CNF/TPE based strain sensors. In a study carried out by Turgut et al., VGCNFs were used for fabrication of SEBS based strain sensors. In the study, SEBS gels and neat SEBS were used as matrix materials. For the TPE gels, midblock-selective aliphatic oil was mixed with SEBS before the addition of VGCNFs. Various nanocomposites were prepared as a function of filler ratio from 1-7 wt%. Samples were evaluated in terms of their morphological, electrical, mechanical and electromechanical properties. For both polymers CNFs were found to be well dispersed in the matrix. Neat SEBS based composites showed lower percolation concentration and lower volume resistivity when compared with SEBS gels. Both composites showed negative piezoresistance but neat SEBS composite showed better performance such as low hysteresis and higher stability (Turgut et al., 2018).

4.3 Carbon Nanotube Filled Thermoplastic Elastomer Based Piezoresistive Strain Sensors

Carbon nanotubes are nano materials with a tube morphology. They are basically consisting of graphene layers. Because of that, they show high conductivity and good mechanical properties. Depending on the number of the graphene layers they are classified as single-walled carbon nanotubes (SWNTs) or multi-walled carbon nanotubes (MWNTs) (Ajayan et al., 1997; Iijima, 1991; Vairavapandian et al., 2008). Zheng et al. fabricated CNT/TPU composites that showed piezoresistive behavior. Composite films were prepared, morphological, electrical and electromechanical properties were investigated. CNTs were found to be homogeneously dispersed in the TPU matrix and percolation around 0.28 wt%. Piezoresistive sensing tests were carried out under various strain ratios. 4 wt% CNT filled TPU composite showed a GF of 6.8 under 20% strain. In cyclic test, samples started to sense around 135 % strain. Samples showed good cyclic performance with stability and durability. In addition to these, samples were used as bending sensors (Zheng et al., 2017).

Slobodian et al. fabricated non-woven TPU membrane via electrospinning. Filler material, MWCNT, was vacuum filtered on the membrane and then compression molded. Electromechanical characterization of MWCNT/TPU sensor was performed up to 4% strain and seven cycles were analyzed. The sample was deformed under 1.27 MPa tensile stress and when the stress was removed, relaxation time was found 1000s. Sensitivity of the sensor was analyzed between 0-400% strains. The sensor showed nearly linear positive piezoresistance behavior and resistance change increased with the increasing deformation. GF was about 100 under 100% strain, while 69 under 403% strain. It was also reported that the sensor could also be used in orthopedics to analyze knee movements (Slobodian et al., 2012).

Bilotti et al. fabricated 2 and 3 wt% MWCNT filled TPU strain sensors by extrusion method in the form of fiber. Percolation behavior of the composite fibers was analyzed depending on the extrusion die temperature (200, 220 and 240°C). The highest conductivity was obtained for 3 wt% MWCNT/TPU composite extruded at 240 °C. In order to characterize the electromechanical properties, the samples were deformed up to 50% strain. At lower temperatures, resistivity increased. Cyclic test was performed with the maximum strain of 10%. The highest sensitivity was obtained for the sensor fabricated at lower extrusion die temperature. According to electromechanical data, samples showed negative piezoresistance at the beginning and at higher levels behavior turned into positive piezoresistance. The highest sensitivity was observed for the sensor that was extruded at 200 °C (Bilotti et al., 2010).

Costa et al. fabricated 4, 6, 8 and 10 wt% MWCNT filled SBS composites via extrusion. Different butadiene/styrene content of SBS was used in the study and effect of block ratio on the morphological, thermal, mechanical and electromechanical properties were investigated. Percolation region was determined between 3-4 wt% MWCNT for SBS, with higher ratio of elastomeric content. For the other SBS with lower elastomeric block ratio, the percolation was determined higher than 4wt% filler loading. In order to analyze sensing performance under strain 1-5% with 1 mm/min test speed, 8 and 10 wt% MWCNT filled composites were chosen for both SBS. Composites showed positive piezoresistance. It was shown that 8 wt% MWCNT/SBS (near percolation threshold) had higher sensitivity for both polymers, compared to 10 wt% filler content. The highest GF was 16 for 8 wt% MWCNT filled composite, consisted of lower elastomeric ratio matrix, under 5% strain. 8 wt% MWCNT/SBS showed highest sensitivity under 20% strain with the test speed of 50 mm/min. When pre-stress applied on the 8 wt% MWCNT/SBS, lower elastomeric content, it was reported that the sensitivity of the sensor increased (Costa, Silvia, et al., 2014).

In another study, Costa et al. fabricated strain sensors by using four different SBS matrix with four different morphology (styrene/butadiene (S/B) content; 20/80, 30/70, 30/70, 40/60) with two different structures (linear/radial) of SBS. MWCNT, SWCNT, and their functionalized forms (non-covalent functionalized (NCF), and covalent functionalized (CF)) were used and filler ratio was between 0-8 wt%. Percolation behavior was investigated for SBS with the S/B ratio of 40/60 and linear structure. For pristine CNT, percolation region was around 1wt%, on the other hand percolation value was obtained 0.5 wt% MWCNT/SBS. GF was analyzed under 1 to 5% strain with a test speed of 1 mm/min. pristine 1 wt% MWCNT showed a highest sensitivity under 5% strain, about GF 8 (Costa, Silva, et al., 2014).

Costa et al. fabricated composites filled with 0-8 wt% MWCNT with four different block sizes and two different structures of SBS. Percolation region was determined around 1 wt% filler content for all types of SBS. Electromechanical behavior was analyzed under uniaxial stress for 4 wt% MWCNT/SBS with S/B ratio of 30/70 and radial structure. It was shown that the curves of resistance change and deformation were nearly overlapped for 10 loading-unloading cycles. GF was calculated for all SBS types under 5-20% level of strain. The highest sensitivity, (GF around 18), was obtained for SBS, lowest butadiene ratio with linear structure under 20% strain. Pre-stress effect on the GF was analyzed for SBS with S/B 40/60 morphology. This sample showed the highest GF and it was reported that applying pre-stress increased the sensitivity of the sensor. GF change depending on the test speed was also investigated for 4 wt% MWCNT/SBS, S/B of 40/60. Highest sensitivity (GF around 70) was obtained under 5% strain with 20 mm/min test speed. 4-point bending test with a deformation rate of 0.1 mm/min was also performed to analyze the electromechanical properties of 4 wt% MWCNT/SBS, for the polymer with S/B ratio of 30/70 and radial structure. It was shown that change in electrical resistance and deformation curves did not overlap. Highest sensitivity (GF ~100) under bending strain between 0.2-0.3% was obtained SBS, S/B ratio of 20/80 and radial structure. Higher GF (~122) was obtained with 5 mm/min test speed for the same SBS (Costa et al., 2013).

Gonçalves et al. fabricated 0, 0.5, 1, 2, 4, and 5 wt% filled MWCNT/SEBS sensor for biomedical applications. In contrast to general approach, they followed ecological approach and instead of toluene, cyclopentyl methyl ether (CPME) was used as a green solvent. Composite films were prepared by solvent casting method. Percolation region was determined between 1-2 wt% filler content. In order to analyze sensing properties of the sensor, 2, 4 and 5 wt% MWCNT/SEBS composites were chosen. Strain was increased up to 80% and test speed was adjusted to 1 mm/min. 10 cycles were analyzed under 2 and 40% strain for 5 wt% MWCNT. It was reported

that resistance decreased when the deformation rate was decreased. Electro-mechanical test was carried out for 500 cycles for 5 wt% MWCNT/SEBS strain sensor and it was shown that electrical resistance stabilized after 60 cycles. Gauge factor of 2, 4 and 5 wt% MWCNT/SEBS sensor varied between 1.3 and 2.7. GF of 5 wt% of filler content decreased from 2.5 to 2 with the increasing strain from 2 to 10%. In terms of GF, 2 and 4wt% MWCNT/SEBS sensors showed the same trend under increasing strain. Sensitivity of these sensor increased up to 5% strain and then, GF started to decrease after 5% strain. Sensitivity of 5 wt% filler loading sensor was analyzed at larger deformations (up to 80%). GF increased when strain was increased from 20% to 40% and then, sensitivity remained nearly same up to 80%. The GF value under 80% strain was lower compared with GF under 2% strain. The sensitivity of the sensor was also compared depending on the printing technique. Printed sensors were found suitable for applications from low to high strains (Gonçalves et al., 2016).

In another study about printed sensors was performed by Castro et al. In the study, Wheatstone bridge circuit with one or two embedded sensors were prepared. The conductive ink, 5 wt% MWCNT/SEBS, was deposited on the electrodes via screen printing, spray printing and drop casting method. Thickness of the screen printed-MWCNT/SEBS layer had lower than other techniques and it showed higher and broader resistance value. Resistivity of the screen-printed sensor depended on the width over length (W/L) channel ratio of Wheatstone bridge. For electromechanical analysis, screen-printed sensor with W/L 170 was chosen. It was reported that Wheatstone bridge circuit with two sensors performed better and stable response was obtained after about 60 cycles under 5% strain for 500 cycles (Castro et al., 2018).

Li and Shimizu designed a strain sensor by using multi wall carbon nanotubes (MWCNTs) and SEBS. The composites were obtained at various filler loadings from 1.25 to 15 wt%. Percolation concentration was reported between 1.25-2.5 wt% concentrations. Samples with 5 and 15 wt% MWCNT filled composites were evaluated. While the sample with 5 wt% MWCNT showed the resistance value around 10^6 ohm under 300 % strain; 15 wt% MWCNT showed the resistance value around 10^4 - 10^5 ohm. This is an indication of filler concentration effect on sensor sensitivity. In the case of higher conductivity, more saturated network was formed and even if same level of strain was applied, breakdown of the conducting network could not be achieved as in lower filler concentrations. Although effect of filler ratio was investigated, the dynamic cyclic tests were not given in the study (Y. Li & Shimizu, 2009).

4.4 Graphene Filled Thermoplastic Elastomer Based Piezoresistive Strain Sensors

Graphene is another nano filler used for the fabrication of piezoresistive strain sensors. Graphite is one of the oldest conductive fillers used in polymer science. It has a crystalline and layered structure. Each layer in graphite is referred as graphene. When evaluated from this aspect graphite can be defined as a planar, layered, crystal structure consists of graphene layers. It is electrically and thermally conductive filler (Chung, 2002; Tanzi et al., 2019). Each layer in graphite is called as graphene (Chung, 2002; Gómez-Navarro et al., 2010; Tanzi et al., 2019; G. Yang et al., 2018). Graphene has superior properties such as optical, mechanical, electrical and thermal. It became one of the most investigated fillers in the area of material science. Although there are many techniques for its fabrication, chemical vapor deposition (CVD) and graphene synthesis from graphite are the most common methods. While first method leads to fabrication of graphene, the structure obtained by the second method is referred as “Reduced Graphene Oxide” (rGO) that is obtained by a chemical route based on the reduction of graphene oxide (Gómez-Navarro et al., 2010; G. Yang et al., 2018).

Liu et al., fabricated graphene (GNP) filled TPU composites. Percolation value was reported to be between 0.1-015 wt%. Samples with 0.2, 0.4 and 0.6 wt% graphene were tested up to 5% strain. Although all three samples showed positive piezoresistance, sample with the lowest filler ratio (0.2 wt% graphene) showed the highest sensitivity. Because of that, same sample was further analyzed under 5, 10, 20 % strain. It was found that at higher level of strain, change in resistance increased. In the next step samples were analyzed at 30% strain at various test speeds such as 0.1, 0.3, 05 mm min⁻¹. At higher speeds sample could not find enough time to recover and higher level of hysteresis was observed (Liu, Li, et al., 2016).

In addition to films, 3D printed piezoresistive sensors were fabricated. In the study carried out by Xiang et al., in the first step 3D printable filaments were fabricated and sensors were printed. Percolation concentration was 1.67 wt% for GNP/TPU composites. For the electromechanical characterization, 2 wt% GNP/TPU sample was used. The composite showed positive piezoresistance under various levels of strain from 5-50 %. By increasing the strain level, GF value of the composite increased. At 30% strain GF was reported as 67.31 (Xiang et al., 2020).

Wang et al., fabricated GNP/SBS nanocomposite fibers by wet-spinning method and evaluated the sensing performance of the nanocomposites. Percolation concentration was determined as 2.7 wt%. 3, 5, and 7 wt% GNP/SBS composites were analyzed in terms of their piezoresistive

character. All 3 samples showed positive piezoresistance and 3 wt% GNP filled composite showed the highest sensitivity. This sensor was further tested under various strain levels (5, 10, 25, 50, 100 %) at various strain rates (50, 200, 500 % min⁻¹). GF increased by the increase in strain % and lower strain rates resulted in higher GF. For this sample strain range was determined more than 110 % and GF values were reported as 160 and 2546 for 50% and 100% strain respectively (X. Wang et al., 2018).

Costa et al., fabricated SEBS nanocomposites using various types of fillers such as graphene oxide (GO), reduced graphene oxide (rGO), and graphene nanoplatelets (G-NPLs). In the study percolation behavior of the samples were analyzed. rGO filled samples showed the lowest percolation value around 2 wt%. Electromechanical characterization of 4 wt% rGO filled samples was performed. That sample showed positive piezoresistivity and GF was reported between 10-90 depending on the strain level (1-10 %) (Costa et al., 2019).

4.5 Thermoplastic Elastomer Based Piezoresistive Strain Sensors with Mixture of Different Fillers or Modified Fillers

In addition to binary composite systems with one filler and one matrix, hybrid fillers and modified fillers were also reported in the literature. The main aim of these studies was to increase the sensing performance of the composite systems. In one of these studies, Zhang et al. used TPU as a matrix and carbon black and silver nanoparticles (AgNPs) were filler materials. Fabrication of CB/AgNPs/TPU composite was involved modification of CB, deposition of AgNPs, mixing CB/AgNPs with TPU solution and casting methods. CB/AgNPs mass fraction changed between 2- 50 wt%. Percolation concentration was reported as 20 wt% (0.06 S/m). It was reported that the sensitivity of the sensor increased with the addition of AgNPs and GF was reported as 21.12 at 100 % strain (Zhang et al., 2018).

Slobodian et al. investigated the piezoresistance of MWCNT/TPU strain sensor based on the functionalization method of the MWCNTs. Pristine, KMnO₄ oxidized and O₂ plasma treated carbon nanotubes were used in the study. Non-woven TPU filter membrane and MWCNT network were fabricated by electrospinning process and vacuum filtration, respectively and then, melt welded. Obtained structure involved three layers; electrically insulating layer (TPU), conductive interlayer (MWCNT/TPU) and second conductive layer (MWCNT). Electro-mechanical behavior was analyzed for pristine and KMnO₄ functionalized MWCNT/TPU sensors. Resistance change was 36% and 438% for MWCNT-N_(KMnO4)/TPU and MWCNT-N_(KMnO4)/TPU respectively. Sensitivity of the sensors was calculated between 0-12% strain. It was shown that MWCNT-N_(KMnO4)/TPU had the highest sensitivity and showed a linear increasing trend with increasing deformation. The other

sensors had low GF values and showed similar trend under all strain levels. Cycling test was performed for the KMnO_4 functionalized filler containing composite, and sensor showed a stable trend under strain between 2 and 7.9% (Slobodian et al., 2013).

Liu et al. fabricated hybrid graphene/CNT/TPU composites. In the first case in order to compare the hybrid composites, they have prepared CNT/TPU and graphene/TPU composites. These composites were prepared between 0.4-1.2 wt% filler loading. For the graphene/CNT/TPU composites, CNT ratio was determined as 0.5 wt% and the amount of graphene was varied between 0-0.12 wt%. Percolation values of graphene/TPU set was reported as 0.051 vol%. CNT/TPU set showed percolation concentration around 0.337 vol%, graphene/CNT/TPU composites 0.01 vol%. Although percolation concentration was lower for hybrid composites, CNT/TPU composites showed higher GF during electro-mechanical tests. Graphene/CNT/TPU composites 0.01 vol%. Graphene/CNT/TPU composites showed GF values 3.58, 12.89 and 35.78 under 5, 15, 30 % (Liu, Gao, et al., 2016).

In addition to composite films, 3D printing was also used for the preparation of piezoresistive strain sensors with graphene nanoplates and CNTs. In the first step, fillers were mixed and incorporated into polymeric matrix. Following that filaments were fabricated by using an extruder. Percolation concentration changed from 1.98 to 1.42 wt% and the conductivity of GNP/CNT/TPU composites were relatively higher. GF under 250% strain was reported as 136327.4. In addition to that, the monitoring performance of the 3D printed sensor was shown for limb motions, physiological activities, speech recognition (Xiang et al., 2020).

Another interesting study with hybrid fillers were carried out by Xie et al. In the study, CNT/rGO mixture was spray coated on the TPU film and this structure rolled-up. The final morphology was a spirally layered composite yarn. GF was reported as 2160.4. Since yarn sensor showed a wide range of applicable strain, it was used from pronunciation to knee bending monitoring (Xie et al., 2020).

Yang et al. developed strain sensors based on CNT/CB/SEBS composites. They have prepared CNT/SEBS, CB/SEBS and CNT/CB/SEBS composites. CNT:CB ratios were determined as 1:0, 1:1, 1:2, 1:3. CNT/SEBS and CB/SEBS composites showed percolation concentration 2.07 and 5.22 wt% respectively. Since CNTs had higher aspect ratio, conductive network formation was obtained at lower values. CNT:CB 1:3 showed the lowest percolation concentration around 1 wt%. In order to determine the piezoresistive behavior of the hybrid composites, CNT:CB 1:1 and 1:2 samples were chosen and total filler concentration was 6 wt%. Samples were tested under 5 and 10% strain. GF of the samples were

reported to be between 2-10, depending on the strain level, filler ratio and concentration (X. Yang et al., 2019).

In addition to two different fillers, a ternary hybrid SEBS based nanocomposite was prepared by using carbon nanotubes, graphene, and fullerene. Pan et al., developed CNT/SEBS, CNT/graphene/SEBS and CNT/graphene/fullerene-based sensors. In the first part, the maximum strain level and related GF were determined for all samples. Although GF for ternary hybrid was lowest (15) when compared others maximum strain level (200%) was higher than the others. After that, cyclic tests were carried out under 60 and 100% levels at 2, 4, 6 mm/s. Stable, positive piezoresistance was observed under given conditions. Although, by increasing the strain level GF increased, lower speed led to more stable piezoresistance. In addition to these, ternary hybrid sensor was used for monitoring human movements at various strain levels. As reported, it can be used for lower and higher strain sensing applications (Pan et al., 2020).

Simon et al. fabricated a piezoresistive strain sensor for civil engineering applications. After fabrication of CB/SEBS composite, it was mixed with cement and plasticizer. The samples classified as only CB-cement-water-containing and CB/SEBS-cement-water containing. Percolation was determined between 0.82-2.37 vol% for CB-cement composites. With the addition of SEBS, percolation was observed at lower values, 0.61-0.82 vol%. In order to investigate the sensing properties, eight samples were chosen with/without SEBS. The samples with SEBS showed a noise and non-linearity, compared with CB-cement containing samples and reported that it was related to the nonhomogenous filler dispersion in matrix. GF of samples with/without SEBS was around 1.3 (Simon et al., 2015).

4.6 Thermoplastic Elastomer Based Piezoresistive Strain Sensors those Fabricated by Using Different Polymers

In addition to single polymer matrix-based strain sensors, composites that consisted of more than one polymer were also reported in the literature. In one of these studies, bicomponent yarn was fabricated by integrating graphene/poly(vinyl alcohol) composites as the conductive sheath around TPU elastic core yarn. The yarns with the 0.8 and 1 wt% graphene showed positive piezoresistance with GF 28.48 and 86.86 respectively (X. Li et al., 2017). In another study, SBS was blended with 15 wt% CB filled TPU and filaments were extruded. Positive piezoresistance was observed and linear response was obtained up to 35% strain. Meaningful signal was obtained up to 50% and GF was reported as 26 (Bautista-Quijano et al., 2018).

In another study, Wang et al. fabricated CB/SBS conductive ink, and it was printed on PDMS surface. On this layer, silver or carbon paste was

coated in order to obtain brittle-stretchable strain sensor. The printed strain sensor had shown superior properties such as high GF>870, low hysteresis, high cyclic durability thanks to brittle-stretchable conductive network (Y.-F. Wang et al., 2020).

5. Conclusions

This review study provides detailed overview about the basic concepts of TPEs, conductive polymer composites, piezoresistive sensors and TPE based piezoresistive strain sensors. Strain sensors can be in various forms including films, nonwovens, fibers obtained by solution, melt processing or 3D printing. TPU, SBS and SEBS are the most common TPEs; CB, CNFs, CNTs, GNP and rGO are the significant conductive fillers used for the fabrication of piezoresistive sensors. TPE based strain sensors have potential in various areas including structural health monitoring to human motion monitoring. TPE based conductive composites are promising materials for piezoresistive strain sensors because of their high resilience, lightweight structure and high GF. Their structure can be tuned based on the polymer type, polymer morphology, filler type, filler content and testing conditions. In order to achieve the most sensitive and repeatable response, all these factors should be taken into consideration.

Acknowledgments

This study was funded by Yalova University, BAP (Scientific Research Project) Project Number: 2020/YL/0013, “Electromechanical Sensing Properties of Flexible Electronics From Functional Polymer Nanocomposites” and TUBITAK, Project number: 115E016 “Thermoplastic Elastomer Based Wearable Sensors”.

References

- Ajayan, P. M., Redlich, P., & Ru'hle, M. (1997). Structure of carbon nanotube-based nanocomposites. *Journal of Microscopy*, 185(2), 275-282. doi:<https://doi.org/10.1046/j.1365-2818.1997.1670730.x>
- Avilés, F., Oliva-Avilés, A. I., & Cen-Puc, M. (2018). Piezoresistivity, Strain, and Damage Self-Sensing of Polymer Composites Filled with Carbon Nanostructures. *Advanced Engineering Materials*, 20(7), 1701159. doi:<https://doi.org/10.1002/adem.201701159>
- Bautista-Quijano, J. R., Torres, R., & Kanoun, O. (2018, 7-8 Nov. 2018). *Flexible strain sensing filaments based on styrene-butadiene-styrene copolymer mixed with carbon particle filled thermoplastic polyurethane*. Paper presented at the 2018 Nanotechnology for Instrumentation and Measurement (NANOofIM).
- Bilotti, E., Zhang, R., Deng, H., Baxendale, M., & Peijs, T. (2010). Fabrication and property prediction of conductive and strain sensing TPU/CNT nanocomposite fibres. *Journal of Materials Chemistry*, 20(42), 9449-9455. doi:10.1039/C0JM01827A
- Castro, H. F., Correia, V., Pereira, N., Costab, P., Oliveiraa, J., & Lanceros-Méndez, S. (2018). Printed Wheatstone bridge with embedded polymer based piezoresistive sensors for strain sensing applications. *Additive Manufacturing*, 20, 119-125. doi:<https://doi.org/10.1016/j.addma.2018.01.004>
- Chung, D. D. L. (2002). Review Graphite. *Journal of Materials Science*, 37(8), 1475-1489. doi:10.1023/A:1014915307738
- Clemens, F. J., Koll, B., Graule, T., Watras, T., Binkowski, M., Mattmann, C., & Silveira, I. (2013). Development of Piezoresistive Fiber Sensors, Based on Carbon Black Filled Thermoplastic Elastomer Compounds, for Textile Application. *Advances in Science and Technology*, 80, 7-13. doi:10.4028/www.scientific.net/AST.80.7
- Cochrane, C., Koncar, V., Lewandowski, M., & Dufour, C. (2007). Design and Development of a Flexible Strain Sensor for Textile Structures Based on a Conductive Polymer Composite. *Sensors (Basel, Switzerland)*, 7(4), 473-492. Retrieved from <https://www.ncbi.nlm.nih.gov/pmc/articles/PMC3800360/>
- Costa, P., Ferreira, A., Sencadas, V., Viana, J. C., & Lanceros-Méndez, S. (2013). Electro-mechanical properties of triblock copolymer styrene-butadiene-styrene/carbon nanotube composites for large deformation sensor applications. *Sensors and Actuators A: Physical*, 201, 458-467. doi:<https://doi.org/10.1016/j.sna.2013.08.007>
- Costa, P., Gonçalves, S., Mora, H., Carabineiro, S. A. C., Viana, J. C., & Lanceros-Mendez, S. (2019). Highly Sensitive Piezoresistive Graphene-Based

- Stretchable Composites for Sensing Applications. *ACS Applied Materials & Interfaces*, 11(49), 46286-46295. doi:10.1021/acsami.9b19294
- Costa, P., Silva, J., Ansón-Casaos, A., Martínez, M. T., Abad, M. J., Viana, J., & Lanceros-Mendez, S. (2014). Effect of carbon nanotube type and functionalization on the electrical, thermal, mechanical and electromechanical properties of carbon nanotube/styrene-butadiene-styrene composites for large strain sensor applications. *Composites Part B: Engineering*, 61, 136-146. doi:https://doi.org/10.1016/j.compositesb.2014.01.048
- Costa, P., Silvia, C., Viana, J. C., & Lanceros Mendez, S. (2014). Extruded thermoplastic elastomers styrene-butadiene-styrene/carbon nanotubes composites for strain sensor applications. *Composites Part B: Engineering*, 57, 242-249. doi:https://doi.org/10.1016/j.compositesb.2013.10.006
- Duan, L., D'Hooge, D. R., & Cardon, L. (2020). Recent progress on flexible and stretchable piezoresistive strain sensors: From design to application. *Progress in Materials Science*, 114, 100617. doi:https://doi.org/10.1016/j.pmatsci.2019.100617
- Duan, L., Spoerk, M., Wieme, T., Cornillie, P., Xia, H., Zhang, J., . . . D'Hooge, D. R. (2019). Designing formulation variables of extrusion-based manufacturing of carbon black conductive polymer composites for piezoresistive sensing. *Composites Science and Technology*, 171, 78-85. doi:https://doi.org/10.1016/j.compscitech.2018.12.009
- Feng, L., Xie, N., & Zhong, J. J. M. (2014). Carbon nanofibers and their composites: a review of synthesizing, properties and applications. 7(5), 3919-3945.
- Fraden, J. (2004). *Handbook of modern sensors: physics, designs, and applications*: Springer Science & Business Media.
- Gómez-Navarro, C., Meyer, J. C., Sundaram, R. S., Chuvilin, A., Kurasch, S., Burghard, M., . . . Kaiser, U. (2010). Atomic Structure of Reduced Graphene Oxide. *Nano Letters*, 10(4), 1144-1148. doi:10.1021/nl9031617
- Gonçalves, B. F., Costa, P., Oliveira, J., Ribeiro, S., Correia, V., Botelho, G., & Lanceros-Mendez, S. (2016). Green solvent approach for printable large deformation thermoplastic elastomer based piezoresistive sensors and their suitability for biomedical applications. *Journal of Polymer Science Part B: Polymer Physics*, 54(20), 2092-2103. doi:https://doi.org/10.1002/polb.24118
- Iijima, S. (1991). Helical microtubules of graphitic carbon. *Nature*, 354(6348), 56-58. doi:10.1038/354056a0
- Li, X., Hua, T., & Xu, B. (2017). Electromechanical properties of a yarn strain sensor with graphene-sheath/polyurethane-core. *Carbon*, 118, 686-698. doi:https://doi.org/10.1016/j.carbon.2017.04.002

- Li, Y., & Shimizu, H. (2009). Toward a Stretchable, Elastic, and Electrically Conductive Nanocomposite: Morphology and Properties of Poly[styrene-*b*-(ethylene-co-butylene)-*b*-styrene]/Multiwalled Carbon Nanotube Composites Fabricated by High-Shear Processing. *Macromolecules*, *42*(7), 2587-2593. doi:10.1021/ma802662c
- Liu, H., Gao, J., Huang, W., Dai, K., Zheng, G., Liu, C., . . . Guo, Z. (2016). Electrically conductive strain sensing polyurethane nanocomposites with synergistic carbon nanotubes and graphene bifillers. *Nanoscale*, *8*(26), 12977-12989. doi:10.1039/C6NR02216B
- Liu, H., Li, Y., Dai, K., Zheng, G., Liu, C., Shen, C., . . . Guo, Z. (2016). Electrically conductive thermoplastic elastomer nanocomposites at ultralow graphene loading levels for strain sensor applications. *Journal of Materials Chemistry C*, *4*(1), 157-166. doi:10.1039/C5TC02751A
- Mattmann, C., Clemens, F., & Tröster, G. J. S. (2008). Sensor for measuring strain in textile. *8*(6), 3719-3732.
- Melnykowycz, M., Koll, B., Scharf, D., & Clemens, F. J. S. (2014). Comparison of piezoresistive monofilament polymer sensors. *14*(1), 1278-1294.
- Melnykowycz, M., Tschudin, M., & Clemens, F. (2016). Piezoresistive soft condensed matter sensor for body-mounted vital function applications. *Sensors*, *16*(3), 326.
- Pan, S., Pei, Z., Jing, Z., Song, J., Zhang, W., Zhang, Q., & Sang, S. (2020). A highly stretchable strain sensor based on CNT/graphene/fullerene-SEBS. *RSC advances*, *10*(19), 11225-11232. doi:10.1039/D0RA00327A
- Poudel, A., Karode, N., McGorry, P., Walsh, P., Lyons, J. G., Kennedy, J., . . . Coffey, A. (2019). Processing of nanocomposites using supercritical fluid assisted extrusion for stress/strain sensing applications. *Composites Part B: Engineering*, *165*, 397-405. doi:https://doi.org/10.1016/j.compositesb.2019.01.098
- Simon, L., Irvin, P., Hussam, S. S., Mohamed, E., Kejin, W., & Eric, C. (2015). *Conductive paint-filled cement paste sensor for accelerated percolation*. Paper presented at the Proc.SPIE.
- Slobodian, P., Riha, P., Olejnik, R., Cvelbar, U., & Saha, P. (2013). Enhancing effect of KMnO₄ oxidation of carbon nanotubes network embedded in elastic polyurethane on overall electro-mechanical properties of composite. *Composites Science and Technology*, *81*, 54-60. doi:https://doi.org/10.1016/j.compscitech.2013.03.023
- Slobodian, P., Riha, P., & Saha, P. (2012). A highly-deformable composite composed of an entangled network of electrically-conductive carbon-nanotubes embedded in elastic polyurethane. *Carbon*, *50*(10), 3446-3453. doi:https://doi.org/10.1016/j.carbon.2012.03.008

- Tanzi, M. C., Farè, S., & Candiani, G. (2019). Chapter 1 - Organization, Structure, and Properties of Materials. In M. C. Tanzi, S. Farè, & G. Candiani (Eds.), *Foundations of Biomaterials Engineering* (pp. 3-103): Academic Press.
- Toprakci, H. A. K. (2012). *Piezoresistive Properties of Polyvinyl Chloride Composites*: North Carolina State University.
- Toprakci, H. A. K., & Ghosh, T. K. (2015). Textile Sensors. In X. Tao (Ed.), *Handbook of Smart Textiles* (pp. 357-379). Singapore: Springer Singapore.
- Toprakci, H. A. K., Kalanadhabhatla, S. K., Spontak, R. J., & Ghosh, T. K. (2013). Polymer Nanocomposites Containing Carbon Nanofibers as Soft Printable Sensors Exhibiting Strain-Reversible Piezoresistivity. *Advanced Functional Materials*, 23(44), 5536-5542. doi:<https://doi.org/10.1002/adfm.201300034>
- Turgut, A., Tuhin, M. O., Toprakci, O., Pasquinelli, M. A., Spontak, R. J., & Toprakci, H. A. K. (2018). Thermoplastic Elastomer Systems Containing Carbon Nanofibers as Soft Piezoresistive Sensors. *ACS Omega*, 3(10), 12648-12657. doi:[10.1021/acsomega.8b01740](https://doi.org/10.1021/acsomega.8b01740)
- Vairavapandian, D., Vichchulada, P., & Lay, M. D. (2008). Preparation and modification of carbon nanotubes: Review of recent advances and applications in catalysis and sensing. *Analytica Chimica Acta*, 626(2), 119-129. doi:<https://doi.org/10.1016/j.aca.2008.07.052>
- Wang, X., Meng, S., Tebyetekerwa, M., Li, Y., Pionteck, J., Sun, B., . . . Zhu, M. (2018). Highly sensitive and stretchable piezoresistive strain sensor based on conductive poly(styrene-butadiene-styrene)/few layer graphene composite fiber. *Composites Part A: Applied Science and Manufacturing*, 105, 291-299. doi:<https://doi.org/10.1016/j.compositesa.2017.11.027>
- Wang, Y.-F., Sekine, T., Takeda, Y., Hong, J., Yoshida, A., Matsui, H., . . . Tokito, S. (2020). Printed Strain Sensor with High Sensitivity and Wide Working Range Using a Novel Brittle–Stretchable Conductive Network. *ACS Applied Materials & Interfaces*, 12(31), 35282-35290. doi:[10.1021/acsaami.0c09590](https://doi.org/10.1021/acsaami.0c09590)
- Xiang, D., Zhang, X., Han, Z., Zhang, Z., Zhou, Z., Harkin-Jones, E., . . . Li, Y. (2020). 3D printed high-performance flexible strain sensors based on carbon nanotube and graphene nanoplatelet filled polymer composites. *Journal of Materials Science*, 55(33), 15769-15786. doi:[10.1007/s10853-020-05137-w](https://doi.org/10.1007/s10853-020-05137-w)
- Xie, X., Huang, H., Zhu, J., Yu, J., Wang, Y., & Hu, Z. (2020). A spirally layered carbon nanotube-graphene/polyurethane composite yarn for highly sensitive and stretchable strain sensor. *Composites Part A: Applied Science and Manufacturing*, 135, 105932. doi:<https://doi.org/10.1016/j.compositesa.2020.105932>

- Yang, G., Li, L., Lee, W. B., & Ng, M. C. (2018). Structure of graphene and its disorders: a review. *Science and Technology of Advanced Materials*, 19(1), 613-648. doi:10.1080/14686996.2018.1494493
- Yang, X., Sun, L., Zhang, C., Huang, B., Chu, Y., & Zhan, B. (2019). Modulating the sensing behaviors of poly(styrene-ethylene-butylene-styrene)/carbon nanotubes with low-dimensional fillers for large deformation sensors. *Composites Part B: Engineering*, 160, 605-614. doi:https://doi.org/10.1016/j.compositesb.2018.12.119
- Zhang, W., Liu, Q., & Chen, P. (2018). Flexible Strain Sensor Based on Carbon Black/Silver Nanoparticles Composite for Human Motion Detection. *Materials (Basel, Switzerland)*, 11(10), 1836. doi:10.3390/ma11101836
- Zheng, Y., Li, Y., Dai, K., Liu, M., Zhou, K., Zheng, G., . . . Shen, C. (2017). Conductive thermoplastic polyurethane composites with tunable piezoresistivity by modulating the filler dimensionality for flexible strain sensors. *Composites Part A: Applied Science and Manufacturing*, 101, 41-49. doi:https://doi.org/10.1016/j.compositesa.2017.06.003

Chapter 13

MINI-REVIEW: SOME ARTICLES IN THE FIELD OF BIOTECHNOLOGY



Sevcan Aytaç KORKMAZ¹
Sümeyye GÜVENDİ GÜNDOĞDU²

¹ Fırat University Electronic Technology Department, Elazığ, Turkey

² Fırat University Biotechnology Department Elazığ, Turkey

Introduction

Fermentation of traditional foods, as a hurdle technology is an important advantage in terms of food quality. These include preservation and decontamination of toxins in which food has. The expectations of modern consumers must not meet only food safety but also the nutritional and flavour visions of the products. Training of communities as regards advantages of consuming fermented food is as important as health education. The fermentation technology must be developed to providing to increase safety and ease of application in rural area where has poor resource. Growth of development area of starter cultures and their methods will provide benefits that African people has got fermented foods and beverages during their daily activities and cultural ceremonies. Genetically modified foods are profitable on the environment as well as causes real noxious effects. But everybody uses genetically modified foods in some way with some reasons a live. It is more preferable because it is used to meet the world's largest population with healthy and nutritious food, so it dominates the harmful effects and is used all over the world in addition affects people more beneficial than their harms, so They try to create more genetically modified foods to increase the desired properties in food using a gene replacement mechanism. There are several laws that allow safe and healthy use of genetically modified foods and limit the harmful impact on the stage. In an term of rise awareness of the effect of human activities all around and human healthy, people of science take insipiration from organisms like bacteriocins and bacteriophages, the side of their antimicrobial activity shown take advantage in food and health areas. The search on these between antimicrobials will advantage definitely. Bacteriocins' activities (or bacteriocin producing), they are organizers of complicated bacterial populations, ought to know governing rules (about biological) of the interactions between phages and their hosts. Thus, bacterial resistance and microbial community factors must be analyzed with care. Nonetheless, the activity bacteriophages and phage lytic proteins in food biopreservation ought to profit bacteriocin inverstigate so that develop their effect in food setting and be inclusive of multi hurdle approaches. Nevertheless, just after this beginning era based on the exciting datas, another hurdles, like regulatory issues must be overcome previous to reach consumers. In high titrations with solid state fermentation milk coagulating enzyme from both *Mucor thermohyalospora* and *Rhizopus azygosporus* has been implemented. In our knowledge, milk from these fungi is the first report of clotting enzymes. The manufacturing of the non cell milk clotting enzyme was optimized with a single-factor approach using cost-effective agricultural industrial by products. Matching milk clotting enzymes (with minimal downward flow processing) with calf rennet and *Mucor* rennet has shown that these enzymes may develop in possible situations. Some extra

characterization of the enzyme, application on a bigger scale and work on the quality of reduced cheese can give an idea for commercial eligibility.

Traditional fermentation is one of food process methods that is used microorganisms like Lactic Acid Bacteria (LAB). The bacteria need substrate for their growth. The substrate is obtained from food. This is one of the ancient methods to preserve foods. It became part of the cultural and traditional norms among the local community with developing countries like Africa, over the years. The rural folk prefer to consume fermented foods rather than consume unfermented foods because they have more pleasant taste, colour and texture. Thanks to this popularity, fermented foods became one of the main dietary for the developing countries [1-3]. There are different types of food fermentation according to the major products of the fermentation process. They are alcoholic fermentation, lactic acid (non-alcoholic) fermentation, acetic acid fermentation, alkaline fermentation and amino acid/peptide sauce fermentations [4-6]. The pH of ferment must be lower than 5 as long as lactic acid is the main product of the fermentation process[7]. The main subject of the article is LAB fermentation. Some of the foods processed with fermentation technology are beverages, dairy products, cereals and meat products [8-9].

Genetically modified organisms (GMOs) are modified by changing the genetic materials which have not in natural habitat and genetically modified foods are developed for plants and animals by adding genes of desired properties to DNA that is an organism [10]. GMOs have some fields of application such as production of pharmaceutical drugs, experimental medicine, biological and medical research, and agricultural field. The area both provides supply of variety foods and improves the quality of foods thanks to genetic modification methods [11-13]. This area's advantages are combining the genes of desired properties with DNA of plant or DNA of animal, being resistance to diseases, increasing shelf life of foods. There are some disadvantages about production of genetically modified foods. These foods cause many chronic diseases related to high expression of used genes in which genetically modified organisms [14].

Lysine industry is the first and most successful biotechnology sector on the world, built on scientific researches and experienced rapid growth and changes in market organization. Patents and production confidentiality restricted the number of companies with three food manufacturers. Seven new companies have entered the lysine sector after 1990. When technological barriers grew, vertical integration backwards into starch manufacturing and firm-specific assets in the marketing of bulk animal feed materials gave advantages to experienced agricultural companies. Five companies continue to dominate global production, despite of vendors. Global price fixing has been documented in at least three parts of the lysine market, and current

levels of concentration become highly viable in future cartel formation [15]. The few social benefits of the discovered cartels is the huge amount of industry information released by their prosecution that would otherwise be fully registered. Five companies which made the 1992 - 1995 lysine cartel were charged, and in 1996 admitted the crime of price fixing in the U.S. federal court. The three top executives of the cartel's chief perpetrators were tried in 1998 and found guilty. These criminal acts and numerous civil litigation proceedings revealed most of the quantitative information that underpins this study [15]. The evolution of the lysine industry may be of broader significance to understand the change of cross-industry boundaries. The lysine industry has created an entirely new product market in the field of animal feed, lysine is a series of biotechnology products that in many cases replace manufacturers of many organic chemicals based on old chemical synthesis methods for production technologies. Paint and drug production 19. Thus, lysine and similar fermentation products have the potential for more dispersed geographical production models than the industry they are replacing. As a result, more diffuse ownership patterns are likely to appear in the biotechnology industry [15].

Bacteriocins and bacteriophages have a common biological result; both of them have strong and aim antimicrobial role. Bacteriocins cover a huge structurally and skilly varied group coping genes of antimicrobial peptides (AMPs) and proteins synthesised by bacteria. Bacteriocins, that in gram positive bacteria group mostly distrupction of cell envelope functions by the puncturing of the cell membrane or inhibition of the cell membrane syntheses [16-17], when colicins and colicin like bacteriocins synthesised by gram negative bacteria generally the aim intracellular area [18]. Bacteriophage is a virus which infects a bacterium. Bacteriophages transcribe within the cell and their own genetic material sent with lysis of the host bacterial during a lytic cycle. Because of the fact that bacteriophages have been known as an essential risk in food fermentation that starter bacteria acted. Bactericins and bacteriophages can be evaluated as encouraging biological means to decrease the effect of food production all around, to increase the activity gut flora for human healthy and to reduce the occurrence and distrubition of MDR (Multi Drug Resistant) bacteria, its source is connected with agro food circle unquestionably [19-20]. Furthermore their conventional function for food preservation to scope the shelf life of food and decrease the consume of chemical additives, bacteriocin investigate allow for an alteration in the direction of health-promoting activities. Besides bacteriophages gain acceleration as antimicrobial to decrease food borne outbreak likewise to cease the rise and dissemination of multi drug resistant zoonotic bacteria through the food chain. Nowadays, the most examples about for food biotechnology are procure in the review [17].

Proteases that are a group of enzymes act a important mission as physiological and pathological functions in cells. Proteolytic enzymes are used in leather industry, detergent industry, pharmaceutical and the most important food industry. Proteases' role to coagulate proteins, more particularly casein (milk proteins), is noteworthy. This situation is the main cause for these enzymes high demand in the food industry and other industry [21,22].

The global cheese industry is forecast reach \$124 billion as a cumulative annual growth rate of 7.3% from 2013 to 2019 [23]. Cheese is occurred after processing and coagulated milk. But the basic procedure has led the diversity in cheese production by source of milk, processing of milk, cheese ripening, taste, texture and the source and milk clotting enzyme used like rennet enzyme [24,25]. Milk clotting enzyme can be produced from four essential source. These are from animal as calf rennet, from plant like vegetable rennet, from genetically engineered chymosin, and from *Mucor* rennet as microbial sources [25,26].

Calf rennet do not only provide the coagulate casein but also cleave from κ -casein at the Phe¹⁰⁵-Met¹⁰⁶ position for obtaining para- κ casein and glycomacropeptide [27,28]. While maximum curd yield obtain with specific cleavage results, the recently available vegetable and microbial rennets are nonspecific. During cheese production non specific hydrolysis in low yields can turn into bitter peptides and off tastes during cheese ripening [26,29].

Worldwide, demand for cheese is predicted to reach 20 million metric tons by 2020 [24]. Shortage of calf veals, opposition to genetically engineered chymosin, resistance from animal rights groups, also choice of many varieties for cheese prepared from vegetable or microbial rennet, have driven the search for sustainable and viable sources for milk clotting enzymes from practically every class of living organism [26,28].

Microorganisms, specially fungi, have attracted attention recently, as potential source of a wide array of proteases, including milk clotting enzymes [30]. Fungi can improve in low costs and release a significant amount of enzymes, which can slow down the flow again. In addition, the ability to stay active in a wide variety of fungal protissis and temperature has made them particularly interesting [30,31]. A significant amount of work has been done recently to understand the biochemical engineering looks of solid state fermentation (SSF) and the nature of microorganisms that are most suitable for SSF [31,32]. For this reason, in our research to find milk clotting enzymes, which may be a suitable alternative to calf rennet, they scanned 15 fungi, which are GRAS (generally considered safe) fungi with solid state fermentation using agricultural industrial byproducts. Optimum temperature, pH and extraction conditions were ordinaried. The

conformity of enzyme preparations has been studied by comparing the yield of curd and whey and commercially usable animal feed and microbial rennet [32].

Encapsulation processes were developed about 30 years ago. This includes an overlay or a pure material or mixture overlay within another material. Coated or stuck material can usually be a liquid, but a solid or gas. This material is also known as core material, active, filler, internal phase or charge. Coating material can also be called capsule, wall material, membrane, carrier or shell. The purpose of encapsulation is to allow small molecules to enter and exit the membrane and protect its contents from potentially destructive media. Natural examples include bird's egg shells, plant seeds, bacterial spores, skin, and shells [33].

The first versions of the microcapsules were impermeable and often mechanically disintegrated to activate the internal components. Examples include the controlled release of flavors and flavors, perfumes, drugs, detoxicants, fertilizers and precursors in textile and printing [33-34]. Enzymes, plants, animal salads or microbial cells can be encapsulated to allow substrates to enter the membrane and products. This concept has been effective in the development of artificial kidneys, as its detoxifying enzymes can be placed in semipermeable membranes [36] and perform kidney function. Nylon membranes have been used by Desoize [35] to encapsulate enzymes such as casein and pepsin and provide crosslinking. Examples of enzyme encapsulation are pectin esterase and juice disclosure, invertase and sucrose inversion, rennet and milk coagulation [37].

Lactic acid bacteria, an important bacteria used in industry, were first immobilized in Berl saddles and *Lactobacillus lactis* in 1975 and alginate gel beads were encapsulated years later [38]. Seiss and Divies [34] suggested that immobilized lactic acid bacteria can be used to continuously produce yogurt. However, *L. lactis* susp cremoris alginate beads. leaked a large amount of cells. Other membranes, such as poly-L-lysine, nylon, and polyethylene, have recently been attempted to coat alginate beads [39]. But have not shown any improvement in lactic acid production compared to free cells [33, 39].

The encapsulation diameter contains about 5 to 300 micron capsules, including various substances [37]. Capsule sugars, gums, proteins, natural and modified polysaccharides, lipids and synthetic polymers can be made. The advantages of encapsulation include improved flow properties and easier handling because they are solid rather than liquid. The stability of the encapsulated material can be improved by protecting it from moisture or heat [33].

This technique has been used for many years in the pharmaceutical industry for time release, improved stability of formulations and flavor masking. Prescription drugs, over-the-counter drugs, vitamins and minerals have been encapsulated. Therefore, these applications will be useful in the food industry, among others [33].

As the technique was considered to be very expensive and highly specific, applications became increasingly slower. However, the number of encapsulated food products has increased significantly as production volumes have increased and more cost-effective preparation techniques and ingredients have been developed. Microcapsules can increase nutrition, as large storage of many products can add vitamins, minerals, and proteins that are sensitive to oxidation, resulting in loss of nutritional value [33].

Conclusion

Thirty years, the world's lysine sector will consist of two or three producers in East Asia, where marketplaces are protected by technological entry barriers. When Ajinomoto began to perform dextrose lysis using high-tech fermentation techniques in 1960, he also had fifty years of experience producing the world's first commercially important amino acid (monosodium glutamate). Kyowa Hakko, which started commercial production almost the same year, used a slightly different fermentation process in its design that uses the sac char as raw material. Both Japanese companies were heavily dependent on basic research on foodstuffs and pharmaceuticals, and received major R&D subsidies from the Japanese government targeted by the Ministry of International Trade and Industry. Biotechnology as a major recipient of positive subsidies. Both companies continue to hold the majority patents, but global shares have dropped about 35 percent overall [15]. The first leaders of the Lysine industry have been seized by the new generation companies with various competitive advantages in the modern market for Lysine. The most successful entrants are commodity-oriented agricultural sector companies with experience in starch production. The three most successful participants are eligible for this recognition: South Korea Sewon (entered in 1980), Archer-Daniels-Midland Co (1991) and Cargill Corporation (1998). These companies are now 90 percent of world lysine production of corn, soybeans and other feed ingredients. They have a history of selling to their consumers - animal feed manufacturers. Japanese pioneers aimed at selling food grade or pharmaceutical grade materials for most of their product lines, and thus had separate sales operations for their feed grade amino acids. Newcomers to the lysine industry also enjoyed economies in lysine production thanks to vertical integration with resources on the carbohydrate raw materials site. The final processing plants of the new Cargill and ADM lysine were built adjacent to the pipeline and maize wet milling plants that provide liquid

dextrose. These large corn refineries maize processing, milling and first stage fermentation equipment require large sunk investment costs. The first two plants built in Japan had to import relatively expensive dry dextrose or molasses from fairly remote sources. Most of the other facilities owned by Ajinomoto and Kyowa Hakko operate under the same cost disadvantages caused by the inability to return to raw material production [15]. In the second stage, costs of fermentation immersed discolor or sucrose into the lysine do not appear to exist. Evidence has emerged that fermenters built to make lysine can be used to produce other amino acids soon. Cheil plant of Indonesia is possible fermentors ethanol both lysine and MSG. ADM's Illinois plant (heavy demand in winter as a gasoline additive) makes it dedicated to making other uses in the summer [15]. Privacy and patent protection for lysine production is now a block that it was a decade or two years ago in the 1990s. While Japanese pioneers still hold the patent of the highest-yielding strains of lysine-producing microbes, other biotechnology companies are ready to license these technologies to newcomers. German companies with the necessary scientific skills are willing to establish joint ventures for the production of lysine. The leading lysine producers are growing lysine plants in similar East Asian economies, which are increasingly offering high levels of protection for China, Vietnam, Thailand and western intellectual property. These sites also offer very low production costs, due to cheap local sources of fermentable carbohydrates (sweet potato, molasses and tapioca starch, for example) and low plant construction costs [15]. The evolution of the lysine industry is illustrative of a broader trend: the invasion of the organic or "fine" chemical industry by the starch industry. The traditional organic chemicals industry produces relatively high-value chemicals using extraction or chemical synthesis. With more than \$ 100 billion in sales in the United States, this industry tends to have only two or three domestic suppliers for a small number of chemicals and overseas suppliers (USITC 1996). The average total cost of lysine produced by fermentation is only 15-25 percent of the cost of lysine produced by extracting it from vegetable matter. The last type of lysine sales continues because only some consumers prefer "natural" lysine for their drug use. Almost all feed grade lysine is now produced by modern biotechnology. Biotechnology companies have taken control of many food sweeteners and preservatives (citric acid, lactic acid, gums, sorbates, etc.) and various vitamins and pharmaceuticals (vitamin E, biotin, etc.), as well as 27 lysine and other amino acids. Old-tech chemical companies, which have a comparative advantage in synthetic chemistry, are increasingly challenged by low-cost manufacturers with expertise in fermentation Technologies [15]. A great number of improvements have been made in the field of captive food stuffs. Manufacturing techniques include spray drying, spray cooling or spray cooling, extrusion coating, fluid bearing coating, liposome trap, conassation, complexity, centrifugal

and rotational suspension separation. There are many requirements for the controlled and continuous release of foodstuffs. As developments in encaps continue, new markets will develop. Coacervation seems particularly promising because it can be reduced due to cost requirement. For low levels of food stuffs. Intercalarily, the flavors are more stable after processing with microwave, heat, oven drying and frying. In most encapsulation techniques, limitations occurred due to high production costs and the lack of food class available materials. Research is necessary to eliminate these limitations. Encapsulation is currently a difficult art for food scientists. The food scientist does not have the information available in databases that allow him to make informed choices about the most appropriate material and encapsulation process. For example, suitables of starch and malto dextrans can be extremely useful as encaps material sulation. The development of cyclo dextrans has led to new products with longer shelf life, less volatility and protection of heat-labile substances. Initial indications are many benefits for the food industry, including the protection of materials ranging from desired release or targeted delivery of liposomes. There is a lot of research to be done in the food industry regarding the use of liposomes. Unlike the pharmaceutical industry, which can excuse high costs, production costs for food applications will need to be reduced.

Reference

- [1] Aderiyi, B. I., and S. A. Laleye. "Relevance of fermented food products in southwest Nigeria." *Plant Foods for Human Nutrition* 58.3 (2003): 1-16.
- [2] Mosha TCE and Vicent MM. Nutritional value and acceptability of homemade maize/sorghum-based weaning mixtures supplemented with rojo bean flour, ground sardines and peanut paste. *International Journal of Food Sciences and Nutrition*. 2004;55(4):301 - 315.
- [3] Nout MJR and Sarkar PK. Lactic acid food fermentation in tropical climates. *Antonie van Leeuwenhoek*. 1999;76(1):395-401.
- [4] Anukam KC and Reid G. African Traditional Fermented Foods and Probiotics. *Journal of Medicinal Food*. 2009;12(6):177-1184.
- [5] Blandino, A., et al. "Cereal-based fermented foods and beverages." *Food research international* 36.6 (2003): 527-543.
- [6] Steinkraus KH. Classification of fermented foods: worldwide review of household fermentation techniques. *Food Control*. 1997;8(5/6):311-317.
- [7] Mokoena MP, Chelule PK and Gqaleni N. Reduction of Fumonisin B1 and Zearalenone by Lactic Acid Bacteria in Fermented Maize Meal. *Journal of Food Protection*. 2005;68:2095-2099.
- [8] Oyewole OB. Lactic fermented foods in Africa and their benefits. *Food Control*. 1997;8(5-6):289-297.
- [9] Chelule, P. K., M. P. Mokoena, and N. Gqaleni. "Advantages of traditional lactic acid bacteria fermentation of food in Africa." *Current research, technology and education topics in applied microbiology and microbial biotechnology* 2 (2010): 1160-1167.
- [10] Dizon, Francis, et al. "Genetically modified (GM) foods and ethical eating." *Journal of food science* 81.2 (2016): R287-R291.
- [11] Saeed, Muhammad, Misbah Miss Aslam, and Muhammad Asif Raheem. "Impact of Genetically Modified Food on Human Health." (2019).
- [12] Khoobchandani, Menka, and Arpita Saxena, eds. *Biotechnology Products in Everyday Life*. Springer, 2019.
- [13] Verma, Charu, et al. "A review on impacts of genetically modified food on human health." *The Open Nutraceuticals Journal* 4.1 (2011).
- [14] Mishra, Sanjay, et al. "Effects of nutraceuticals on genetic expressions." *The Open Nutraceuticals Journal* 2.1 (2009).
- [15] Connor, John M. "Evolution of the Global Lysine Industry, 1960-2000." Chapter 8 (2008): 237-66.

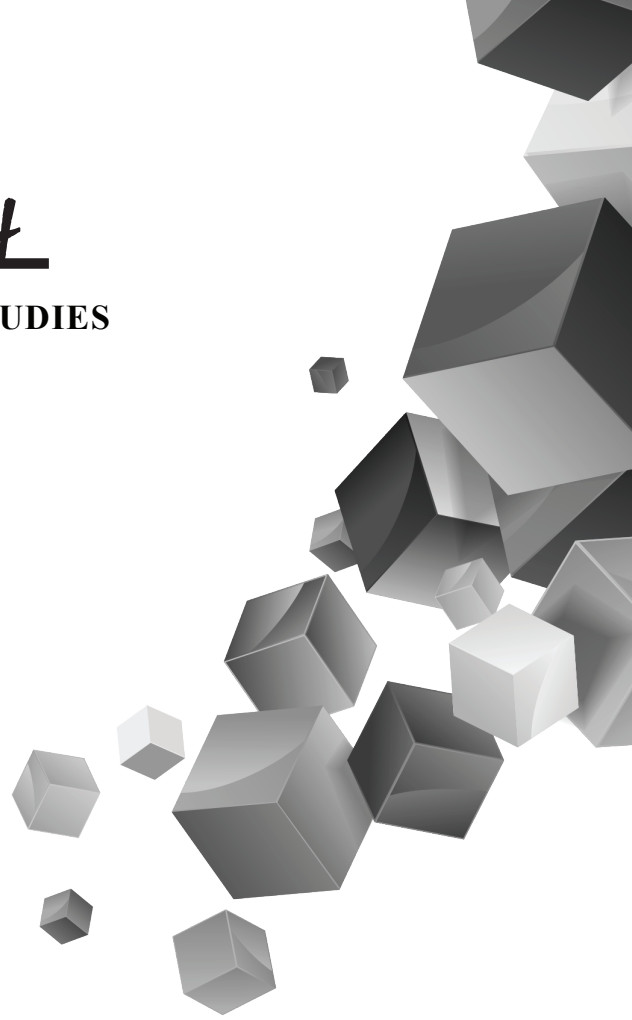
- [16] Alvarez-Sieiro, Patricia, et al. "Bacteriocins of lactic acid bacteria: extending the family." *Applied microbiology and biotechnology* 100.7 (2016): 2939-2951.
- [17] Martínez, Beatriz, Pilar García, and Ana Rodríguez. "Swapping the roles of bacteriocins and bacteriophages in food biotechnology." *Current opinion in biotechnology* 56 (2019): 1-6.
- [18] Cascales, Eric, et al. "Colicin biology." *Microbiology and molecular biology reviews* 71.1 (2007): 158-229.
- [19] García, Pilar, et al. "Food biopreservation: promising strategies using bacteriocins, bacteriophages and endolysins." *Trends in food science & technology* 21.8 (2010): 373-382.
- [20] Mills, Susan, R. Paul Ross, and Colin Hill. "Bacteriocins and bacteriophage; a narrow-minded approach to food and gut microbiology." *FEMS microbiology reviews* 41.Supp_1 (2017): S129-S153.
- [21] Lopez, O.C.; Bond, J.S. Proteases: Multifunctional Enzymes in Life and Disease. *J. Biol. Chem.* 2008, 283, 30433.
- [22] Theron, L.W.; Divol, B. Microbial Aspartic Proteases: Current and Potential Applications in Industry. *Appl. Microbiol. Biotechnol.* 2014, 98, 8853–8868.
- [23] Statista. Cheese market value world wide 2016–2022.
- [24] Mikkelsen, P. World Cheese Market 2000–2020. *Pm Food Dairy Consult* 2014.
- [25] Ullmann's Encyclopedia of Industrial Chemistry: Cheese, Processed Cheese, and Whey, 2012.
- [26] Jacob, M.; Jaros, D.; Rohm, H. Recent Advances in Milk Clotting Enzymes. *Int. J. Dairy Technol.* 2011, 64, 14–33.
- [27] Foltmann, B. A Review on Prorennin and Rennin. *C. R. Trav. Lab. Carlsberg.* 1966, 35, 143–231.
- [28] Shah, M.A.; Mir, S.A.; Paray, M.A. Plant Proteases as Milk-Clotting Enzymes in Cheesemaking: A Review. *Dairy Sci. & Technol.* 2014, 94, 5–16.
- [29] Visser, S. Proteolytic Enzymes and Their Relation to Cheese Ripening and Flavor: An Overview. *J. Dairy Sci.* 1993, 76, 329–350.
- [30] Hölker, U.; Hofer, M.; Lenz, J. Biotechnological Advantages of Laboratory-Scale Solid-State Fermentation with Fungi. *Appl Microbiol. Biotechnol.* 2004, 64, 175–186.
- [31] Singhania, R.R.; Patel, A.K.; Soccol, C.R.; Pandey, A. Recent Advances in Solid-State Fermentation. *Biochem. Eng. J.* 2009, 44, 13–18.

- [32] Chinmayee, Cirium V., et al. "Production of highly active fungal milk-clotting enzyme by solid-state fermentation." *Preparative Biochemistry & Biotechnology* 49.9 (2019): 858-867.
- [33] F. Gibbs, Selim Kermasha, Inteaz Alli, Catherine N. Mulligan, Bernard. "Encapsulation in the food industry: a review." *International journal of food sciences and nutrition* 50.3 (1999): 213-224.
- [34] Seiss W & Divies C (1975): *Microencapsulation*. *Angew. Chem. Int. Ed.* 14, 539±550.
- [35] Desoize B (1986): In vitro cytotoxic activity of cross-linked protein microcapsules. *J. Phar. Pharmacol.* 38, 8±13.
- [36] Chang TMS (1978): *Artificial Kidney, Artificial Liver and Artificial Cells*. New York: Plenum.
- [37] Lee BH (1996): *Fundamentals of Food Biotechnology*, New York: VCH Publishers.
- [38] Linko P (1985): Immobilized lactic acid bacteria. In *Enzymes and Immobilized Cells in Biotechnology*, ed. A Larson, pp. 25±36. Minto Park, CA: Benjamin Cummings.
- [39] Larisch B (1990): *Microencapsulation of Lactococcus lactis subsp. cremoris for application in the dairy industry*, MSc thesis, McGill University, Montreal, Canada.

Chapter 14

BIOTECHNOLOGY STUDIES

FOR MINI-REVIEW



Sevcn AYTAÇ KORKMAZ¹

Veysel ÇAKIR²

¹ Fırat University, Electronic Technology Department, Elazığ, Turkey

² Fırat University, Biotechnology Department, Elazığ, Turkey

Introduction

Growth in meat production and the risk of product contamination have caused in the food industry to keep rapidly, reasonable methods of analysis to protect health of consumers and safety of consumers. Moreover, the central principles that are food safety and food quality leads improvement and new ideas in the food area [1-2]. Dynamic practices have caused some hazards these are physical, chemical and biological hazards in terms of the product quality and consumer safety.

The growing risks, some pathogens(toxins), pesticides, drugs, heavy metals have been realised recently, owing to haphazard agriculture and animal husbandry areas having critical health effects from the point of causing diseases [3]. The more the quality and safety is challenged, the more strong equipments are needed to create a product of typical parameters. *Despite* traditional detection techniques are convenient, they spend a lot of time and to need serious protocol with an elaborate procedure and qualified personnel. *For instance*, traditional detection techniques and standard pathogen detection *techniques* such as culture counting and colony counting might take up a few days. Furthermore, physicochemical methods like liquid chromatography–tandem mass spectrometry (LCMS/MS), for contamination testing such as toxins, veterinary drug residues, heavy metals tend to be expensive, complicated to perform and to spend time [4]. But, chromatography and spectrometry can procure more safe and conclusive datas still a higher through put with less operator training are needed by screening tests [1].

A rapid method of screening these hazards in the bulk material handling industry to provide food safety and food quality could be the answer. In this conditions, in growing meat industry rapidly, for methods of quality control and safety of meat and meat products can become the biosensor an effective alternative. They have some advantages such as high degree of sensitivity and specificity of detection where minimum sample preparation is there, cost-effectiveness, miniaturization and portability for real time monitoring [5]. Furthermore, HACCP system can be used to verify that a given process is under control, since the sensitivity of high biosensor lets the detection of pathogenic microorganisms, pesticides and another contaminants in minutes or hours [1,6].

Biosensors can be described as an analytical instrument, which transforms a biological answer into an electrical signal and comes out of two main components: a bioreceptor or biorecognition element, which recognizes the target analyte and a transducer, which transforms the recognition event into a quantifiable electrical signal [7]. Therefore, biosensors can be classified on the main of type of biocomponent involved, mechanism or mode of signal transduction etc [8]. The recognition elements

can be systems containing enzymes, cell receptors, microorganisms, antigens, antibodies and nucleic acids. The transduction elements are usually electrochemical, optical or piezoelectric, and the electrical signals when based on a change in the measured current are amperometric; when change in the measured voltage between the electrodes are potentiometric and when a change in the functions to charge of transport, so then they are conductometric. The optical sensors are usually predicated on the absorbance principle, fluorescence, chemiluminescence, surface plasmon resonance etc. The sensors predicated on mass produce a mass dependent signal for the analyte that interact with the sensors and give information regarding analyte presence [1].

Even though the first progress in the biosensors was aimed to use in the medical diagnostic equipments, afterwards the principles of detection and quantification of biological molecules started to find its way in the food industry too. While biosensors can be uncomplicatedly applied for meat sample with the least processing methods such as mincing or homogenization, beginning enrichment activities may not be needed for pathogen or toxin detection, saving the analyses time. Even though little commercialization of the instrument has been done in the meat industry unlike the fields like medical diagnostics but with the increasing load of bulk handling it is going to be hard to continue the safety of products and the quality of products without a faster screening instruments like biosensor. This article envisages to discuss the possible area of the emerging instrument in the meat industry about ensure the quality and the safety of meat products [1].

Food biotechnology, together with use of plants and animals directly, is related the application of (live) food microorganisms, like yeasts, fungi, bacilli and lactic acid bacteria, in industrial areas. Basic purposes are increased production of ingredients and improved properties of starter cultures, such as reproducible growth characteristics, enhanced flavour formation and proteolytic activities or better autolytic properties. Investigation of the effect of food microorganisms on human health is also an essential area, for example, in prebiotics and probiotics research [9-10]. On the other part, attention are needed since the prevention of food-spoilage and pathogenic microbes. Food biotechnology' purpose are both directed towards improving food production and meet the requests by consumer for safe, natural, fresh, tasteful and convenient products [9,11].

The research programs that is for improvement of industrial activities of microorganisms used in fermentation progress were focussed in the beginning on microbial strain selection then classical mutagenesis, finally followed by more directed approaches using genetic engineering. These approaches' essential advantages are that they are time-consuming, side-

effects being in the selected or constructed strains are difficult to estimate and value, and the full range of engineering possibilities can not be exploited due to lack of knowledge of inter-related regulatory and metabolic processes going on in a cell. Moreover, the consumer population's part is worried seriously about the safety of the novel foods, and if undesirable spread of genetically modified microorganisms in environment can be controlled. Functional genomics can exactly provide solutions in the last two fields. Several criteria and options for safe biotechnology and for risk-assessment procedures for the environmental application of microorganisms have been discussed recently [9,12].

Within future decade, reaching various industrial aims will be possible for application of functional genomics programs on food microorganisms. For instance, to designate side-effects of genetic alterations on functionality in products, to occur wanted pleiotropic effects by specific regulatory mutations, to predict and develop stress responses, to develop novel antimicrobial systems, and to direct metabolic engineering efforts. Likewise, it will enable the identification of novel (enzyme) activities, the performance of high-throughput mutation analyses in strains of interest and the improvement of quick identification analyses for food spoilage or pathogenic microorganisms. The review provides an check of current improvements in high throughput technology and discusses their practicality about food biotechnology [9].

Riboflavin, also known as 7,8-dimethyl-10-[(2S,3S,4R)-2,3,4,5-tetrahydroxy pentyl]benzo[g]pteridine-2,4-dione, vitamin B2 is a water soluble vitamin naturally synthesized by plants and some microorganisms. It is an important micronutrient for animal and human diets, as it is not synthesized by higher animals. The product riboflavin that is used applications in small amounts as the colouring agent E101 or as a nutritional additive in animal feedstuffs besides as an additive in food [15-16]. In the beginning, riboflavin was fundamentally chemically synthesised for the production of very pure material. Biotechnological improvements have consequence in microbiological processes that can compete with the chemical synthesis and in our times commercial production of vitamin B2 is commonly done by fermentation.

In most instances, riboflavin's microbial synthesis involves genetically engineered selected strains of *Escherichia (E.) coli*, *Bacillus (B.) subtilis*, *Ashbya (A.) gossypii*, and *Candida (C.) famata* [16]. Genetically modified strains of *E. coli* and *B. Subtilis* are potentially the best known [17] within genetically modified micro-organisms (GMMs) as in these bacteria the riboflavin biosynthetic pathway has been studied in detail [18]. *B. subtilis* is an aerobic endospore forming bacterium prevalently found in nature and it has not a pathogenic or toxigenic potential. The large-scale fermentation

production of speciality chemicals of enzymes used in food production processes, and of several traditional ways of food preparation are used in direction of experiences about safe [15].

All the time, non-sporulating derivatives of the *B. subtilis* strain 168 were genetically modified (GM), it always carry natural mutations inducing riboflavin overproduction. Introduction of different plasmids harbouring both a recombinant *B. subtilis* riboflavin biosynthetic operon under the control of a strong promoter and antibiotic resistance genes as selection markers (like; cat, tet, ermAM), resulted in genetically modified *B. subtilis* strains with multiple copies of the rib operon (rib operon, also known as ribDEAHT operon, i.e. including the ribD, ribE, ribA, ribH, ribT genes). These strains can enhance riboflavin expression by 10 - 25 times the size [15,19-22].

In the last product, additives produced with GMM are show that neither the production strain nor its recombinant DNA can be detected according to EFSA guidance [22]. In September 2014, it was notified in RASFF (the European Rapid Alert System for Food and Feed) that a German official enforcement laboratory in Hesse detected viable GM *B. subtilis* spores in a consignment of vitamin B2 feed additive (80% feed grade) imported from China [15,23].

In April 2015, the Belgian official control laboratory published a report which about the genome sequence of a GM *subtilis* strain [24] This strain (isolate 2014-3557) was identified by a French competent authority in many vitamin B2 (riboflavin, 80% feed grade) imported to France from China. On basis of NGS (Next Generation Sequencing) result of a Belgian institution a TaqMan qPCR method (identified VitB2 - UGM) for specific detection of this EUunauthorized GM riboflavin overproducing *B. subtilis* was developed [24]. In addition to this, a junction between the riboflavin biosynthesis genes and the vector backbone are targeted by the TaqMan qPCR method. It remains unsolved if the aimed sequence is integrated into the bacterial genome or present on a plasmid. For the latter situation, the detection may fail if the plasmid is lost and the corresponding target sequence is therefore missing. Also, the comprehensive molecular characterization of the GM strains' genome and plasmids have not been reported by the authors [15].

In [15] review, microbiological and molecular analyses of the GM *B. subtilis* strain that is found in Germany in 2014 are presented. DNA is extracted from two independent isolates to characterize in detail the genome of these riboflavin-overproducing GM *B. subtilis* strains, and to reconstruct the putative plasmids present for performed whole genome sequencing (WGS). Later on, construct and event specific PCR based methods for its detection in food and feed were improved and applied [15].

DAS-44406-6 soybean was genetically engineered (GE) by use applications of three varied herbicides. Expression of the aryloxyalkanoate dioxygenase 12 (AAD-12) enzyme provides tolerance to 2,4-dichlorophenoxyacetic acid (2,4-D) by catalyzing its degradation, expression of the phosphinothricin acetyltransferase (PAT) enzyme inactivates glufosinate ammonium by acetylation of the l-isomer into *N*-acetyl-l-glufosinate ammonium, and expression of the double-mutated maize 5-enolpyruvyl shikimate-3-phosphate synthase (2mEPSPS) enzyme provides tolerance to glyphosate by replacing the function of the native soybean EPSPS enzyme (which is inactivated by glyphosate to control weeds/plants) [26]. These properties offer producers multiple additional choices for herb control in soybean [25-26]. The evidence's weight determines the food and feed safety of a genetically engineered crop [27-29]. This evidence has knowledge that is whole past of safety for the expressed proteins and/or the source organism about its identify. While assessing safety, certain properties of the expressed protein provide important evidence to consider. These traits include mode of action, amino acid sequence similarity to proteins with whole past of safe use and to those known to be allergenic or toxic, stability to standard food processing and cooking procedures and digestive stability. For some proteins, these properties are enough to robustly evaluate safety [30]. In addition, toxicity can be empirically evaluated in vivo via high-dose animal works with purified protein.

Unless a feedstuff in genetically engineered proteins remain spoilage whole-food animal-feeding works might provide benefit in term of the safety assessment for proteins that cannot be purified in an active form, and for which high margins of exposure can be obtained relative to actual exposure under standard use [31]. In practice, whole-food feeding works are usually used to investigate unwanted compositional changes within the genetically engineered crop that might not be detected in works that directly analyze the composition of the edible portion of the crop [31]. The large part of information shows that adverse unintended compositional changes in GE crops are a lower risk compared with traditionally bred crops, composition works are nearly globally wanted for all new GE events, and whole-food animal works are wanted by some regulatory authorities that assess GE crop safety [31,32]

In our review, the weight of evidence for the safety of DAS-44406-6 soybean based on: 1) the intended genetically engineered properties and 2) potential unintended adverse impact of the genetically engineered proteins (or the transgenesis process) on endogenous plant metabolic pathways. The approved GE crops that have been assessed universally for safety expresses proteins; the PAT and 2mEPSPS proteins. For the 2mEPSPS protein, these crops include GA21 maize, FG72 soybean, and Glytol cotton;

for the PAT protein, these crops include T25 maize, A5547-127 soybean, and 281-24-236 cotton [33-34]. Thus, the PAT and 2mEPSPS proteins are not among the novel food or feed risks [35-36]. For all of these datas, the present safety assessment focuses on the AAD-12 protein and any potential unexpected impacts in the DAS-44406-6 soybean event originating from transgenesis or the AAD-12 enzyme. It must not ignore that the AAD-12 protein is also expressed by event DAS-68416-4 soybean [25].

Conclusion

In last decade, biosensor technology has attracted attention, for it is a promising instrument to lower detection limit with quick analysis time at relatively low cost. In spite of the fact that conventional detection techniques are critical, they delay behind the analytical techniques despitedetection time. Biosensor usage in quick detection of contaminants can lead to release of products within hours or even minutes, rather than holding them since a few days. It can also be a well instrument for screening a big thorough put of samples and going for confirmation only for tiny number. The multiplexing a new and more advanced approach with the potential of detecting a num ber of pathogens, toxins, pesticides etc. have give to thanks to the raised use of array and multiple channel systems. Finally, the development of detection technique which is more reliable, rapid, accurate, simple, sensitive, selective and cost effective must be provided [1].

Food biotechnology will gain advantage from a functional genomics approach greatly; to constitute novel opportunities to ensure the safety of foods, to develop the quality of fermented products and to substantiate health claims related to the ingestion of specific microbes. Also, the better understanding of secretion processes, stress-responses and complex regulatory mechanisms will optimize industrial production of ingredients. Exciting new technologies for life sciences are being developed with incredible speed. Transcriptome and proteome research have some blanks which are being bridged by inventions recently, such as the synthesis of double-stranded oligonucleotide arrays for parallel investigations of DNA protein interactions [13]. While a study on the *S. cerevisiae* ribosome showed recently, advances in mass spectroscopy provide direct analysis of protein complexes, The procedure can identify more than 100 proteins in a single run, hence providing the simultaneous analysis of all components of huge macromolecular complexes [14]. Absolutely, these and other novel methods in genomics will profoundly change the nature of food biotechnology in the future millennium [9].

The value of the use of NGS approaches have been described; enforcement authorities and official control laboratories by assisting food/feed competent, the presence of GMMs in biotechnological products in their researches. The approach defined in the review showed to provide

a detailed molecular characterization of an unknown GMM and thus facilitated the risk assessment and together the improvement of specific PCR methods for its detection [15].

Nonetheless, the study showed that the bioinformatics analysis of the data produced by NGS is still a challenging task and would require the development of adapted bioinformatics instruments in order to be implemented for routine data analysis and management in the frame of GMO characterization and detection. The research of the GM *B. subtilis* strain showed at the same time, that indepth literature review is fundamental to interpret the series data and to fully understand and characterize the sample, specially if completely unknown [15].

In the [25] are current or past worker of Dow AgroSciences LLC, which develops and markets transgenic seed. Dow AgroSciences LLC and MS Technologies™ are co-developing DAS-44406-6 soybean. In the [25] demand the elimination of animal studies where datas are unlikely to meaningfully contribute to safety assessment [25].

Reference

- [1] Singh, P. K., Jairath, G., Ahlawat, S. S., Pathera, A., & Singh, P. (2016). Biosensor: an emerging safety tool for meat industry. *Journal of food science and technology*, 53(4), 1759-1765.
- [2] Ferreira S, De Souza MB, Trierweiler JO, Broxtermann O, Folly ROM, Hitzmann B (2003) Aspects concerning the use of biosensors for process control: experimental and simulation investigations. *Comput Chem Eng* 27:1165–1173
- [3] Kim SJ, Gobi KV, Iwasaka H, Tanaka H, Miura N (2007) Novel miniature SPR immunosensor equipped with all-in-one multimicrochannel sensor chip for detecting low-molecular-weight analytes. *Biosens Bioelectron* 23:701–707
- [4] McGrath TF, Elliott CT, Fodey TL (2012) Biosensors for the analysis of microbiological and chemical contaminants in food. *Anal Bioanal Chem* 403:75–92
- [5] Singh A, Poshtiban S, Evoy S (2013) Recent advances in bacteriophage based biosensors for food-borne pathogen detection. *Sensors* 13: 1763–1786
- [6] Luo J, Liu X, Tian Q, Yue W, Zeng J, Chen G, Cai X (2009) Disposable bioluminescence-based biosensor for detection of bacterial count in food. *Anal Biochem* 394(1):1–6
- [7] Velusamy V, Arshak K, Korostynska O, Oliwa K, Adley C (2010) An overview of foodborne pathogen detection: in the perspective of biosensors. *Biotechnol Adv* 28:232–254
- [8] Lavecchia T, Tibuzzi A, Giardi MT (2010) Biosensors for Functional Food Safety and Analysis. In *Bio-Farms for Nutraceuticals: Functional Food and Safety Control by Biosensors* edtd. Maria Teresa Giardi, Giuseppina Rea and Bruno Berra. chapter 20 Landes Bioscience and Springer Science + Business Media.
- [9] Kuipers, O. P. (1999). Genomics for food biotechnology: prospects of the use of high-throughput technologies for the improvement of food microorganisms. *Current opinion in biotechnology*, 10(5), 511-516.
- [10] Ricke SC, Pillai SD: Conventional and molecular methods for understanding probiotic bacteria functionality in gastrointestinal tracts. *Crit Rev Microbiol* 1999, 25:19-38.
- [11] Richardson DP: Functional foods — shades of grey: an industry perspective. *Nutr Rev* 1996, 54:174-185.
- [12] Doblhoff-Dier O, Bachmayer H, Bennett A, Brunius G, Bürki K, Cantley M, Collins C, Crooy P, Elmquist A, Frontali-Botti C et al.:

- Safe biotechnology 9: values in risk assessment for the environmental application of microorganisms. *Trends Biotechnol* 1999, 17:307-311.
- [13] Bulyk ML, Gentalen E, Lockhart DJ, Church GM: Quantifying DNA protein interactions by double-stranded DNA arrays. *Nat Biotechnol* 1999, 17:573-577.
- [14] Link AJ, Eng J, Schieltz DM, Carmack E, Mize GJ, Morris DR, Garvik BM, Yates JR: Direct analysis of protein complexes using mass spectroscopy. *Nat Biotechnol* 1999, 17:676-682.
- [15] Paracchini, V., Petrillo, M., Reiting, R., Angers-Loustau, A., Wahler, D., Stolz, A., ... & Pecoraro, S. (2017). Molecular characterization of an unauthorized genetically modified *Bacillus subtilis* production strain identified in a vitamin B2 feed additive. *Food chemistry*, 230, 681-689.
- [16] Abbas, C. A., & Sibirny, A. A. (2011). Genetic control of biosynthesis and transport of riboflavin and flavin nucleotides and construction of robust biotechnological producers. *Microbiology and Molecular Biology Reviews*, 75(2), 321–360.
- [17] Burgess, C. M., Smid, E. J., & van Sinderen, D. (2009). Bacterial vitamin B2, B11 and B12 overproduction: An overview. *International Journal of Food Microbiology*, 133 (1–2), 1–7.
- [18] Bacher, A., Eberhardt, S., Eisenreich, W., Fischer, M., Herz, S., Illarionov, B., ... Richter, G. (2001). Biosynthesis of riboflavin. *Vitamins and Hormones*, 61, 1–49.
- [19] Mander, L., & Liu, H. W. (2010). *Comprehensive Natural Products II: Chemistry and Biology: 10 Volume Set (Vol. 7 chapter 7.04.5.2 “Riboflavin Pathway Engineering”)*. Elsevier Science & Technology.
- [20] Perkins, B. J., Sloma, A., Hermann, T., Theriault, K., Zachgo, E., Erdenberger, T., ... Pero, J. (1999). Genetic engineering of *Bacillus subtilis* for the commercial production of riboflavin. *Journal of Industrial Microbiology and Biotechnology*, 22(1), 8–18.
- [21] Smolke, C. (2009). Riboflavin pathway engineering. In *The metabolic pathway engineering handbook: Fundamentals*. CRC Press.
- [22] EFSA (2011). Guidance on the risk assessment of genetically modified microorganisms and their products intended for food and feed use. *EFSA Journal*, 9(6), 2193.
- [23] RASFF (2014). Unauthorised genetically modified (*Bacillus subtilis*) bacteria in vitamin B2 from China, via Germany (Accessed 08.03.2017) https://webgate.ec.europa.eu/rasff-window/portal/?event=notificationDetail&NOTIF_REFERENCE=2014.1249.
- [24] Barbau-Piednoir, E., De Keersmaecker, S. C., Wuyts, V., Gau, C., Pirovano, W., Costessi, A., ... Roosens, N. H. (2015). Genome sequence of EU-unauthorized genetically modified *Bacillus subtilis* strain 2014–3557

overproducing riboflavin, isolated from a vitamin B2 80% feed additive. *Genome Announcements*, 3(2).

- [25] Herman, R. A., Ekmay, R. D., Schafer, B. W., Song, P., Fast, B. J., Papineni, S., ... & Juberg, D. R. (2018). Food and feed safety of DAS-44406-6 herbicide-tolerant soybean. *Regulatory Toxicology and Pharmacology*, 94, 70-74.
- [26] Lepping et al., 2013 M.D. Lepping, et al. Compositional equivalence of DAS-44406-6 (AAD-12 + 2mEPSPS + PAT) herbicide-tolerant soybean and nontransgenic soybean *J. Agric. Food Chem.*, 61 (2013), pp. 11180-11190
- [27] OECD, 1993 OECD Safety Evaluation of Foods Derived by Modern Biotechnology: Concepts and Principles (1993)
- [28] Hammond et al., 2013 B. Hammond, et al. Toxicological evaluation of proteins introduced into food crops *Crit. Rev. Toxicol.*, 43 (2013), pp. 25-42
- [29] Herman et al., 2015 R.A. Herman, et al. Percent amino-acid identity thresholds are not necessarily conservative for predicting allergenic cross-reactivity *Food Chem. Toxicol.*, 81 (2015), pp. 141-142
- [30] Delaney et al., 2008 B. Delaney, et al. Evaluation of protein safety in the context of agricultural biotechnology *Food Chem. Toxicol.*, 46 (2008), pp. S71-S97
- [31] Herman and Ekmay, 2014 R.A. Herman, R. Ekmay Do whole-food animal feeding studies have any value in the safety assessment of GM crops? *Regul. Toxicol. Pharmacol.*, 68 (2014), pp. 171-174
- [32] Herman and Price, 2013 R.A. Herman, W.D. Price Unintended compositional changes in genetically modified (GM) crops: 20 years of research *J. Agric. Food Chem.*, 61 (2013), pp. 11695-11701
- [33] CERA - ILSI Research Foundation, 2016b CERA - ILSI Research Foundation A Review of the Food and Feed Safety of the PAT Protein (2016)
- [34] CERA - ILSI Research Foundation, 2016a CERA - ILSI Research Foundation A Review of the Food and Feed Safety of the EPSPS Protein (2016) Herouet-Guicheney et al., 2009
- [35] C. Herouet-Guicheney, et al. Safety evaluation of the double mutant 5-enol pyruvylshikimate-3-phosphate synthase (2mEPSPS) from maize that confers tolerance to glyphosate herbicide in transgenic plants *Regul. Toxicol. Pharmacol.*, 54 (2009), pp. 143-153
- [36] Hérouet et al., 2005 C. Hérouet, et al. Safety evaluation of the phosphinothricin acetyltransferase proteins encoded by the pat and bar sequences that confer tolerance to glufosinate-ammonium herbicide in transgenic plants *Regul. Toxicol. Pharmacol.*, 41 (2005), pp. 134-149

Chapter 15

A HOUSE OF QUALITY APPLICATION BASED ON A DECISION SUPPORT SYSTEM FOR THE CREDIT CARD MONITORING UNIT OF A BANK



Yeliz BURUK SAHIN¹
Ezgi AKTAR DEMİRTAS²

1 Dr. Öğr. Üyesi, Eskisehir Osmangazi University, Department of Industrial Engineering, yelizburuk@ogu.edu.tr

2 Prof Dr., Eskisehir Osmangazi University, Department of Industrial Engineering, eaktar@ogu.edu.tr

1. Introduction

In an ever-increasing competitive environment, the establishment of customer relations based on loyalty providing high satisfaction levels is possible by properly perceiving clientele's expectations and delivering the proper service in a fast and effective way. Delivering services better than rival companies and adopting a customer service policy based on the voice of customers is of critical importance to establish a position in the market particularly for companies in the service sector. Finance and banking sectors have become new areas of process improvement methods. The greatest achievement in this respect will be a portfolio of the customers able to make use of fault-free and improved processes.

Quality Function Deployment (QFD) is an approach that enables the realisation of current or new products/services of an enterprise in the most effective way in line with the needs of clientele. For a self-sustainable existence of their companies, managers have to be able to meet the ever-changing needs of their clientele in a fast way while also maintaining high quality in products and services. QFD has been integrated into many services and manufacturing processes since its introduction. It essentially aims to create an optimised process in which the desires of clientele are transformed into measurable performance indicators. QFD is essentially a planning tool that aims at transforming the clientele's wishes into points of essential quality assurance to be used in the design and production phases with a focus on customers' needs and expectations (Akao, 2003). QFD can be considered as a technique that lays great importance on the voice of customers throughout the whole phases of production and service provision. It gives the companies a competitive advantage concerning corporate structure and customer satisfaction while, at the same time, allowing companies to design their products and services. It is an effective tool that transforms customers' wishes into production/service requirements (Sivasamy et al., 2016).

On the other hand, the decisions which are taken by the managers in the finance sector are of great importance for the success of a bank. A Decision Support System (DSS) is a computer-based system that is designed to support decision-makers in decision-making processes, also shortening the decision-making time (Turban et al., 2007). There exist different QFD definitions, but features such as providing support in all phases of decision-making, enabling users to design flexible and interactive systems, and offering support to individual and group decision-makers through mathematical methods are highlighted in all. QFD is a system that supports decision-makers in semi-structured decision-making phases but does not replace the decision-makers in evaluating the decisions taken (Turban and Aronson, 1998). Decisions that are right, timely and fast help companies

keep their business moving forward in a competitive environment. DSS allow decision-makers to have easy access to decision-making models and data to give them support in semi-structured and non-structured decision-making phases. Therefore, they are effective systems in overcoming the lack of information. Hence, decision-makers in managing positions can improve the quality of their decisions and increase the possibility of making the right decisions by way of analytical models. The aim of DSS is not to impose a decision on decision-makers, but it reveals solution alternatives. In this context, DSS enables users to process both the voice of customers that defines their wishes and technical requirements that reflect the voice of employees to the benefit of the company, and can thus guide companies in a fast and right way in development processes for new products (Sahin and Demirtas, 2019). Dogan (2014) summarises the purposes of a smart DSS-based QFD framework as determining the right actions to be taken to meet the satisfaction of customers using DSS and increasing the competitive advantage of the company through analysing rival companies.

In the current study, a DSS-based House of Quality (HOQ) was developed to improve credit card monitoring unit of a bank by analysing the credit card selection behaviours of university students. The calculations in the HOQ were performed based on the proposed proportional scale. The mathematical operations such as addition, extraction, multiplication, and division cannot be defined in traditional ordinal scales. However, such operations are often used in HOQ to calculate relative weights. Besides, the DSS method also allows even those decision-makers who have limited knowledge about proportional scales to comment results by performing fast and easy calculations utilising DSS. The study provides insights into the most important customer needs as well as the most important technical requirements. To our knowledge, no study is available in the literature that has discussed a DSS-based HOQ application in the finance and banking sector. The use of proportional scale in HOQ is also unique in this sector. The second section of the study contains a literature review on QFD and DSS-based QFD. The third and fourth parts present the proposed approach and the results of the application in the bank involved in the study. The concluding part contains the results obtained in the study and recommendations.

2. Literature Review

It has been observed that studies conducted in recent years on the QFD process have focused on different sectors, particularly on the fields of healthcare (Gündoğdu and Görener, 2017; Aktepe et al., 2018; Demirtaş and Köksal, 2018; Nursaçan and Çetinyokuş, 2020), construction (Kassela et al., 2017; Toptancı and Erginel, 2017; Moghimi et al., 2017), manufacturing (Vinodh and Kumar, 2011; Bhuvanesh and Parameshwaran, 2018; Sahin

and Demirtas, 2019) and so on. Besides these sectors, identifying the needs of customers and the studies of improvement processes are also gaining prominence day-by-day in the banking and finance sector (Shahin et al., 2016).

There have already been some applications in the banking and finance sector based on DSS. Carminati et al. (2015), for instance, developed DSS to analyse online banking fraud analysis in banking transactions. Fraud risks have been identified using data mining as well as statistical and mathematical techniques. Sariyer (2016) developed a DSS based on fuzzy Analytical Hierarchy Process (AHP) to compare the personnel of a bank in human resources. The proposed system is effective both to compare the employees and also to categorise them. Ignatius et al. (2018) proposed a decision support tool for a credit scoring model based on multi-criteria decision-making principles. While criteria weights are generated by fuzzy AHP, Fuzzy linguistic theory is applied to describe the uncertainties and vagueness arising from human subjectivity. Finally, TOPSIS is used to rank the alternatives by least risk exposure. Gaganis et al. (2020) developed a multi-criteria decision support tool for a credit analyst. They offer a visual of a bank's judgmental analysis, by providing a holistic multicriteria decision support tool in the hands of a credit analyst and enabling a rich inferential procedure to be conducted. Within this framework, a case study was presented, which evaluated the credit risk of 55 banks based in the European Union based on their financial fundamentals.

To the best of our knowledge, this study is the first in which the proportional scale was used in all stages of a DSS-based HOQ (customer importance weights, relationship matrices, improvement factor and selling point) in monitoring credit card unit of a bank.

3. Method

QFD is a systematic approach consisting of planning and communication processes, which ensure inter-disciplinary coordination within an organisation to design, produce, and market the products or services in line with customers' wishes. In other words, it is the whole of the processes that enable the establishment of a correlation between customers' demands and company functions as well as the adaptation of customers' demands into the product or service planning system.

HOQ, which is the most important tool within QFD, transfers customers' requirements into technical requirements. In a HOQ, customers' requirements (CR1 CRn) are indicated in rows, and technical requirements (TR1... TRn) are shown in columns. The related technical requirements are determined by a QFD team consisting of engineers, managers, specialists, and designers (Asadabadi, 2017). The distinctive

characteristic of this technique is to evaluate the customers' requirements in integration with current possibilities, rival companies, and solution proposals.

The use of proportional scale in HOQ and the application steps of this technique are represented below:

Defining and weighting the customers' requirements: The first phase in the HOQ is the proper definition of the target market. After the target market has been defined, the requirements regarding products/services should be expressed in the customers' own words. The needs of customers can be determined by way of different methods. The methods most frequently used to better define customers' needs are focus group interviews, questionnaires, face-to-face customer conversations, communications through telephone, fax, and e-mail for wishes, complaints, and proposals as well as feedbacks after events such as exhibitions, fairs, etc.

In a HOQ, relative significance levels are indicated next to the column of customers' requirements. In the traditional approach, a five, seven or nine-point Likert scale can be used regarding customers' requirements. The number "1" in the scale represents the lowest level of importance. Arithmetic means of the customer scores for each requirement is calculated, and the relative importance weight column is formed by normalising the mean values.

In this study, a proportional scale corresponding to the 5-point Likert was used while calculating the relative importance weights. As the arithmetical operations are undefined and invalid in the ordinal scale, a proportional scale was suggested by Demirtaş and Köksal (2018) based on the Analytic Hierarchy Process (AHP). This scale is shown in Table 1. Contrary to the ordinal scale, a fixed value is obtained all the time when the values in the proportional scale are proportioned to one another. Thus, any mathematical operation in the HOQ becomes valid.

Table 1 *Proportional versus Ordinal Scale*

Ordinal Scale	1	2	3	4	5
Proportional Scale	0.061	0.100	0.161	0.259	0.419

Forming the correlation matrices: In this phase, each customer requirement is translated into one or several technical requirements. At this point, several requirements can come into question from legal requirements such as security, legal regulations, quality levels, and product standards to other requirements such as machines and materials specific to the products produced, environment conditions, and company strategy. Then, the

correlation between customers' requirements and technical requirements is determined. Empty cells in the matrix indicate that no correlation exists between customer/technical requirement pairs. If any correlation exists, its degree is scored as 1 (weak), 3 (medium), and 9 (strong) in the traditional approach. Instead of numbers, relationships between customer and technical requirements can be recorded in the matrix as symbols showing the strength of the correlation (Table 2). Because the nature of the traditional 1-3-9 scale was compatible with the proportional scale, no conversion has been applied to traditional scale for technical requirements.

Table 2 *Proportional Scale for Technical Requirements*

Degree of Correlation	Strong (Θ)	Medium (O)	Weak (Δ)
Proportional Value	9	3	1

After determining the degree of correlation between customer/technical requirements, the relationship between technical requirements is investigated and the roof of HOQ is formed. Symbols are used to define the direction (positive or negative) of the correlation. While the sign (+) between two technical requirements indicates that improvement of one of the characteristics also has an improving effect on the other, the sign (-), on the other hand, indicates deterioration. It is important to take this fact into account in the improvement studies.

Forming the columns of benchmarking, improvement factor, and selling point: For effective planning, it is important to determine the importance of the requirements and the level of satisfaction with the product/service from the customers' perspective. In addition, it is important to determine the strengths and weaknesses of existing and competing products/services by benchmarking. It should also be determined what the selling point of the product/service will be if the customer requirements are met and how much improvement is required in the existing product compared to competing products/services. "Improvement factor" and "Selling point" columns are important for calculating the absolute and relative importance weights.

a) Improvement factor: According to the traditional approach, it can be defined as the ratio of the value targeted by firm in terms of a customer requirement to the actual performance of that company. Evaluations of the customer concerning rival companies are also taken into consideration in identifying the targets of the firm.

On the other hand, in the proposed proportional approach, four levels are identified based on the efforts to be made to reach the targeted scores:

‘getting much better’, ‘getting better’ ‘remaining at the same level’ and ‘getting worse’ when compared with the current status. For instance, while proceeding from 4 to 5 could mean ‘getting much better’ for a customer when considering the difficulties in business or the efforts to be made, it could mean ‘getting better’ in terms of another customer. Similarly, a ‘worse’ performance can be preferred to better focus on improvement efforts if an unjustifiable high performance comes into question in respect of the expectation of a customer. The scale in Table 3 was used to express AHP weighting of competitor level-up.

Table 3 *The proportional scale for the improvement factor*

Levels	Much better	Better	Same	Worse
Proportional Value	0.558	0.263	0.122	0.057

b) Selling point: It defines the influence of the planned improvement on the sales revenues. In the traditional approach, it is expressed in values of 1.0, 1.2, and 1.5, whereby 1.5 means ‘it can considerably increase the sales potential’, 1.2 means ‘it can increase the sales potential’ and 1.0 means ‘it would have no influence’. Table 4 presents a proportional scale developed for the “selling point”.

Table 4 *Proportional Scale for the selling point*

Levels	Major	Minor	No
Proportional Value	0.633	0.260	0.106

After “improvement factor” and “selling point” columns were created using the proportional scale, they were normalized and used in the stage of determining the absolute weights of customer requirements.

Formulas (1-3) were used to calculate the absolute weight of customer requirements (CAWs) and relative weight of customer requirements (CRWs).

i : indices for customer's requirements

CW_i : importance weight of customer requirement i

IF_i : Improvement factor for customer requirement i

SP_i : Selling point value for customer requirement i

CAW_i: Absolute weight of customer requirement *i*

CRW_i: Relative weight of customer requirement *i* (%)

SCAW: Sum of the absolute weight column of customer requirements

$$CAW_i = CW_i * IF_i * SP_i \quad \forall i \quad (1)$$

$$\sum_i CAW_i = SCAW \quad (2)$$

$$CRW_i = \frac{CAW_i}{SCAW} * 100 \quad \forall i \quad (3)$$

Technical evaluation

In this phase, the technical requirements that should be given high priority to meet customers' requirements are identified. The absolute and relative weights of each technical requirement are calculated using Formulas (4-6).

j: indices for technical requirement

TRAW_j: Absolute weight of technical requirement *j*

TRRW_j: Relative weight of technical requirement *j* (%)

STRAW: Sum of the absolute weight row for technical requirements

d_{ij}: the degree of the correlation between customer requirement *i* and technical requirement *j*

$$TRAW_j = \sum_i CAW_i * d_{ij} \quad \forall j \quad (4)$$

$$\sum_j TRAW_j = STRAW \quad (5)$$

$$TRRW_j = \frac{TRAW_j}{STRAW} * 100 \quad \forall j \quad (6)$$

After the absolute and relative weights of each column were calculated, the technical requirements having higher weights were determined. In the following phase, the company that conducts the research identifies whether the testing possibility for the measurement of technical requirements is available. The QFD team makes the arrangements necessary for the test and controls. The next phase after the comparative analyses performed by engineers on rival companies is the one in which the performance targets with respect to technical requirements are identified. Comparative analyses enable us both to detect the points needed to be improved and also to identify the strong and weak points compared to competitors.

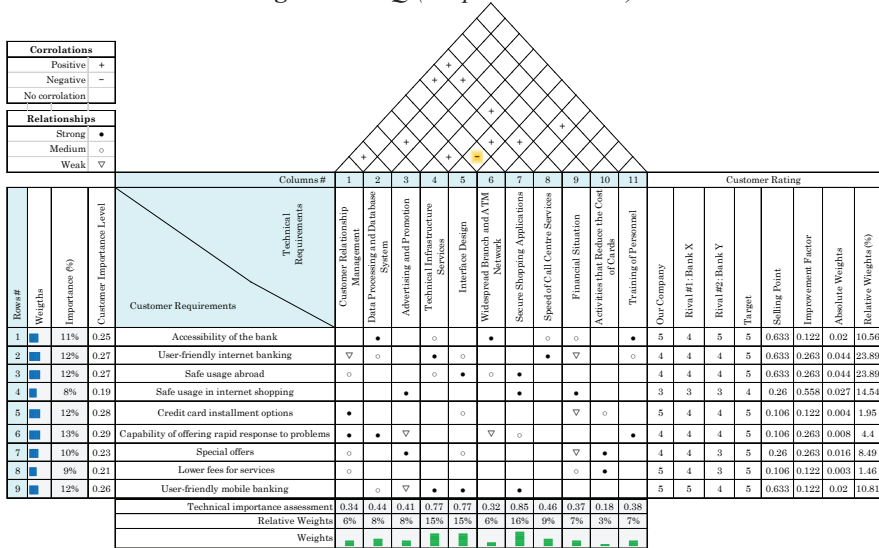
4. A case of application in the banking sector

In the banking sector application, the credit card selection procedure of university students has been analyzed. Then, a DSS has been developed to create HOQ and coded with Excel VBA. The interface developed in this way can be used in companies without the need of purchasing any new software. Even the decision-makers who have limited knowledge about this technique can easily use the Excel software.

The DSS developed in the present study was designed also to systematise the QFD process managed by specialist employees based on the results of customer questionnaires and interviews performed in different periods. In other words, it was designed to provide decision support even when customers' wishes and weights change. It is also possible to use the DSS developed in the study in other service processes with minor modifications. The DSS process aims to provide three main advantages: analysis of survey results through access to previous and current survey reports, assessment of the proportional method in the QFD dimension, and providing target-oriented recommendations on customer needs and technical requirements.

First of all, customer needs were determined with the information obtained from meeting with experts working in the bank and one-to-one interviews with customers of bank in order to listen to customers' voices. To identify the needs of customers, 20 customers were asked in individual interviews to evaluate their needs on a five-point scale. The "customer needs" listed in an Excel file using the macro "weight the customer needs" were transferred into the HOQ and presented in the column of customer significance degree in Figure 1.

Figure 1 HOQ (Proportional Scale)



Besides, the QFD team consisting of specialist, employees identified the technical requirements (Appendix-A) that could be connected with customers’ requirements. The list of technical requirements created by the same command was also transferred into the HOQ.

In the second phase, the significance scores were defined in the values of the proportional scale shown in Table 1, combined with geometric means, and transferred into the customer significance column in the HOQ.

The next step involves the identification of the correlation between customers’ and technical requirements. The term correlation refers to the influence of a technical requirement indicated in each column on meeting the customer requirement shown in each row. After the transfer of the weight values and other information regarding customer needs, the user is forwarded to the Excel page of HOQ. The input of data concerning the correlation between customers’ and technical requirements is easily done using “the dropdown list” displayed by clicking on the cells on the page.

Within the framework of the specialist team’s views and experiences, a strong correlation was detected between the accessibility of the bank and its data processing and database system, and widespread branch ATM network. The study also reveals a strong correlation between the accessibility of the bank and training of personnel. For example, it ensures fast execution of operations in the branch with the training given to the personnel and personnel who can solve potential problems quickly. The study results indicate a strong correlation between safe usage in internet shopping and advertisements, and promotions. Specialists underlined, in this respect, promotion of any security application is as much important

as the application itself. A weak correlation was detected between the capability of rapid response to problems and advertisements and promotions. Through advertisements, the customers are contacted not direct, but indirectly. It is suggested that while a strong correlation exists between user-friendly mobile banking and interface design, there exists a medium correlation between lower service fees and financial situation. The stronger the financial strength of a bank, the more likely its customers is to pay lower fees for the services they receive. Other correlations between technical requirements and customer requirements are shown in symbols in the HOQ.

The correlation on the roof matrix, on the other hand, is the part in which the effects of technical requirements on one another are discussed. This matrix aims to identify whether technical requirements affect each other negatively or positively (Kelesbayev, 2016). The study suggests that while a negative correlation exists between interface design indicating the user-friendly feature of mobile applications and widespread branch and ATM network, the results indicate the existence of a positive correlation between technical infrastructure services and interface design.

Thereafter, two rival banks with considerable market share were selected to observe the fields where rival companies had a better market position and accordingly take the necessary steps for the future. Apart from that, the customers were asked to evaluate the bank involved in the study and its rivals, as a result of which the QFD team defined the bank's target values for each customer request. Thus, the columns of improvement requirements and sales potential were created using the macro based on the projected and realised performance.

All the calculations in the HOQ (absolute and relative weights for customers' requirements, and absolute and relative weights for technical requirements) were performed in accordance with the proportional scale. In other words, the macro "Calculate According to the Proportional Scale" performed the calculations in all the cells in the HOQ based on the values that correspond to the ones of the proportional scale. The macro "Interpret" was used to evaluate the values calculated. The results of the analysis were presented to the customers utilising the inference mechanism available in the dimensions of "customer needs" and "technical requirements" in the DSS. Upon activation of the "Interpret" macro, customer wishes and technical requirements were ranged by relative weight values, and the technical requirements with the highest significance degree were displayed. Additionally, target values for technical requirements were extracted from the database created based on the views of the specialists in the QFD team and presented to decision-makers through the same macro. As it is, the system provides essential proposals to end-users.

The results obtained in the calculations performed in the DSS-based HOQ are discussed in the following paragraphs:

The customer wishes with the highest relative weight according to the proportional scale were ‘user-friendly internet banking’ and ‘secure usage abroad’ with 23.89%, followed by ‘secure usage in internet shopping’ with 14.54%, and ‘user-friendly mobile banking’ with 10.81%. The relative weight values of other customer wishes are presented in Figure 1. The technical requirement with the highest relative weight was ‘secure shopping applications’ with 16%, followed by ‘technical infrastructure services’ and ‘interface design’, both with a weight value of 15%, and ‘speed of call centre services’ with a weight value of 9%. To enhance these applications, ‘expanding the 3-D secure shopping domain’ was identified as the target value. ‘Providing individual services using artificial intelligence applications’ was identified as the target to enhance the technical infrastructure services. The target defined for interface design was ‘Providing a tailored interface based on the transactions frequently used by users’. The target identified to enhance the service quality in this respect was ‘being able to access to the call centre in less than two minutes’.

5. Results

In this study, QFD technique was used and improvement suggestions were presented for banks to meet the expectations of university students, who have an important place in the market share. The present study provides a HOQ based on the DSS developed through a proportional scale, which is relatively new used. This proposed method was implemented in the process of determining the technical requirements concerning the wishes and expectations of clientele for credit cards. The aim was to help the decision-making team managing the process to develop fast responses utilising DSS. The study has provided the target values regarding the wishes/expectations of the clientele, and the technical requirements that should come into focus. The DSS based HOQ aimed to enhance customer satisfaction through properly analysing the customers’ voice. In the proposed interface with Excel VBA support, ease of use and access for decision makers who are not experts in quality techniques are at the forefront. The mechanism that supports decision-makers in taking fast and proper decisions also enables users to take into account customer expectations in different periods using integrating survey data into the system. Thus, information regarding customers’ and technical requirements can also be easily transferred into the HOQ using the macros. In order to overcome the disadvantages of the traditional scale, absolute and relative weights are easily calculated for customers’ and technical requirements with the newly proposed proportional scale, so decision maker is supported in the

interpretation of the results. In addition, assistance is available on what the target values will be for key technical requirements.

When the importance weights of customer requirements are evaluated, convenient internet banking applications and safe usage in internet shopping abroad have come to the fore. It was followed by handy mobile banking. Nowadays mobile banking has gained importance thanks to the widespread usage of mobile phones. Providing special offers and discount to mobile banking users has become an important factor for banks to attract students in credit card selection decisions. The results regarding the relative weights of technical requirements show that secure shopping is the most important one, followed by technical infrastructure services, interface design, and speed of call centre services.

Customer satisfaction can be enhanced using customer-tailored service delivery when the services of a bank regarding technical infrastructure reach an adequate level. Interface design is another requirement that is important for students. Interface design is also important for students to enable them to complete the transactions in a shorter time both in mobile applications and internet banking.

Ultimately, call centre services are also very important concerning meeting the customers' expectations and solving their problems, because customers always prefer to have access to services in the most rapid way. Advertisements and promotion are important factors as well, but it has been observed that students lay less importance on these factors than other technical requirements. As a result of the rapid increase and change in the amount of data and customer requests, it is thought that the possible benefits of the predictability of customer expectations will spread the DSS-based QFD process. In future studies, it is possible to work on the DSS-based QFD process that can be integrated with mathematical modelling in order to optimize the target values.

Conflict of Interest

The authors have no conflicts of interest to declare.

Appendix-A. The list of technical requirements

Customer Relationship Management refers to the proper guidance of all the units in a bank to meet the expectations of customers and ensure the satisfaction.

Data Processing and Database System refer to the technical requirement that aims to provide and develop the necessary infrastructure for transactions and storing the database throughout the bank.

Advertising and Promotion refer to take part in the printed and

visual media to catch the attention of customers and awake curiosity in customers.

Technical Infrastructure Services refer to the strengthening and enhancing of a bank's security system using state-of-art technology.

Interface Design refers to the design and usefulness of mobile and online banking applications used today.

Widespread Branch and ATM Network refers to the number of branches and ATMs of a bank.

Secure Shopping Applications refer to the work of banks with companies in order to provide card security for the customers' credit card payments, especially in online shopping.

Speed of Call Centre Services refers to the waiting time in queue, fast processing time and fast services of call centre.

Financial Situation refers to the financing allocated to the bank by the holding or capital owner behind the bank.

Activities that Reduce the Cost of Cards refer to creating advantages to reduce the cost of the card reflected on the customer.

Training of Personnel refers to the requirements that involve the training given to the employees concerning essential banking services, human relations, and training programmes regarding customers.

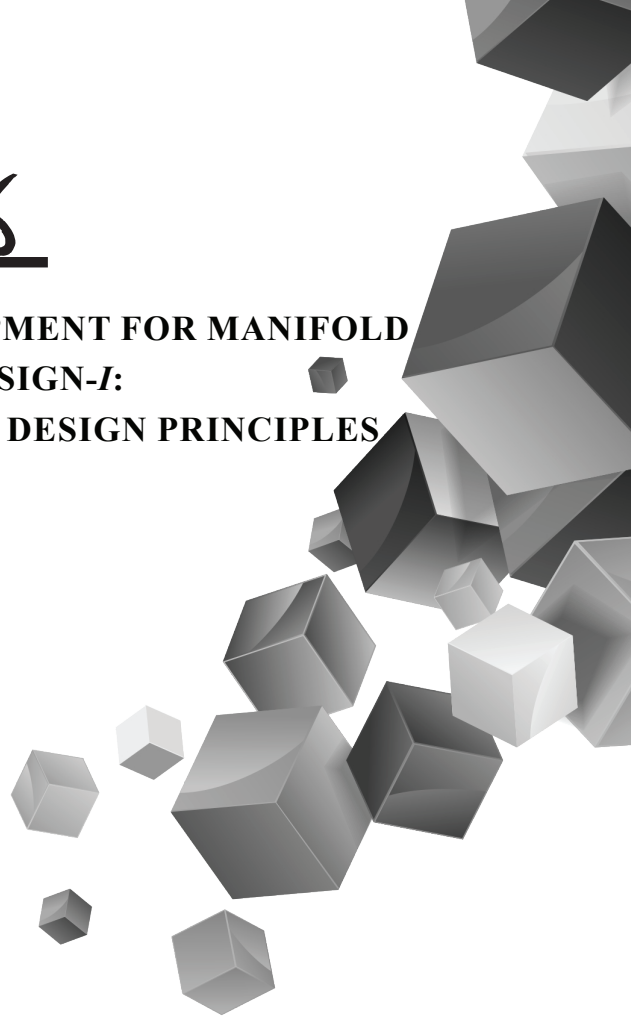
REFERENCES

- Akao, Y., & Mazur, G. H. (2003). The leading edge in QFD: Past, present, and future. *International Journal of Quality and Reliability Management*, 20 (1), 20-35.
- Aktepe, A., Ersöz, S., Hayyaoğlu, A. N., & Şakar, B. B. (2018). Kalite Fonksiyon Yayılımı Yaklaşımı İle Özel Bir Hastanede Hizmet Kalitesi İyileştirme Üzerine Bir Uygulama. *Uluslararası Mühendislik Araştırma ve Geliştirme Dergisi*, 10(2), 245-251.
- Asadabadi, M. R. (2017). A customer based supplier selection process that combines quality function deployment, the analytic network process and a Markov chain. *European Journal of Operational Research*, 263(3), 1049-1062.
- Bhuvanesh Kumar, M., & Parameshwaran, R. (2018). Fuzzy integrated QFD, FMEA framework for the selection of lean tools in a manufacturing organization. *Production Planning & Control*, 29(5), 403-417.
- Carminati, M., Caron, R., Maggi, F., Epifani, I., & Zanero, S. (2015). BankSealer: A decision support system for online banking fraud analysis and investigation. *Computers & security*, 53, 175-186.
- Demirtaş, E. A. & Köksal, G. (2018). Sağlık Hizmet Kalitesinin Servqual Temelli Kalite Evi İle Değerlendirilmesinde Yeni Bir Yaklaşım. *Verimlilik Dergisi*, 2, 29-52.
- Dogan, O. (2014). Yeni Ürün Geliştirmede Kalite Fonksiyon Göçerimi Kullanarak Zeki Karar Destek Sistemi Yaklaşımı. Yüksek Lisans Tezi, İstanbul Teknik Üniversitesi, Fen Bilimleri Enstitüsü.
- Gaganis, C., Papadimitri, P., & Tasiou, M. (2020). A multicriteria decision support tool for modelling bank credit ratings. *Annals of Operations Research*, 1-30.
- Gündoğdu, S., & Görener, A. (2017). Process Improvement Using Quality Function Deployment in the Healthcare Sector. *Alphanumeric Journal*, 5(1), 127-146.
- Ignatius, J., Hatami-Marbini, A., Rahman, A., Dhamotharan, L., & Khoshnevis, P. (2018). A fuzzy decision support system for credit scoring. *Neural Computing and Applications*, 29(10), 921-937.
- Kassela, K., M. Papalex, and D. Bamford. (2017). Applying Quality Function Deployment to Social Housing? *The TQM Journal*, 29 (3), 422-437
- Kelesbayev, D., Kalykulov, K., Yertayev, Y., Turlybekova, A., & Kamalov, A. (2016). A Case Study for using the Quality Function Deployment Method as a Quality Improvement Tool in the Universities. *International Review of Management and Marketing*, 569-576.

- Moghimi, V., M. B. M. Jusan, P. Izadpanahi, and J. Mahdinejad. (2017). Incorporating User Values into Housing Design through Indirect User Participation Using MEC-QFD Model. *Journal of Building Engineering*, 9, 76–83.
- Nursaçan, M. N. N., & Çetinyokuş, T. (2020). Hastane Hizmetlerinin İyileştirilmesinde Kalite Fonksiyonu Göçerimi (KFG) Yönteminin Kullanılması ve Nesnelerin İnterneti Model Önerisi. *Avrupa Bilim ve Teknoloji Dergisi*, (20), 181-195.
- Sahin, Y. B., Demirtas, E. A. (2019). Karar Destek Sistemi Tabanlı bir Kalite Evi için Oransal Bir Ölçek Önerisi. *Endüstri Mühendisliği*, 30(3), 173-186.
- Sarıyer, A. Z. (2016). A Fuzzy Ahp Weighted Decision Support System for Human Resources of a Bank, (Master's Thesis), Bahçeşehir University Istanbul.
- Shahin, A., E. Bagheri Iraj, and H. Vaez Shahrestani. (2016). Developing House of Quality by Integrating Top Roof and Side Roof Matrices and Service TRIZ with a Case Study in Banking Services. *The TQM Journal*, 28 (4), 597–612.
- Sivasamy, K., Arumugam, C., Devadasan, S. R., Muruges, R., & Thilak, V. M. M. (2016). Advanced models of quality function deployment: a literature review. *Quality & quantity*, 50(3), 1399-1414.
- Toptancı, Ş., & Erginel, N. (2017). Hata Türü Ve Etkileri Analizi Ve Kalite Fonksiyon Yayılımı İle Bir İnşaat Firması İçin Risk Değerlendirmesi. *Mühendislik Bilimleri ve Tasarım Dergisi*, 5, 189-199.
- Turban, E. & Aronson, J. E., (1998). Decision Support System and Intelligent System (5th Edition). New Orleans: Prentice Hall
- Turban, E., Aronson, J. E., Liang, T. P. & Sharda, R. (2007). Decision Support and Business Intelligence Systems. Noida: Pearson Education, Inc.
- Vinodh, S., & Kumar Chintha, S. (2011). Application of fuzzy QFD for enabling leanness in a manufacturing organisation. *International Journal of Production Research*, 49(6), 1627-1644.

Chapter 16

SOFTWARE DEVELOPMENT FOR MANIFOLD LINE HYDRAULIC DESIGN-I: METHODOLOGY AND DESIGN PRINCIPLES



Gürol YILDIRIM¹

¹ Professor of Civil Engineering, Aksaray University, Engineering Faculty, Civil Engineering Department, Head of Hydraulics Division, 68100, Aksaray, Turkey. E-mail: yildirim3@itu.edu.tr

This chapter was produced from the book author's Master's and Doctoral theses.

INTRODUCTION

Hydraulic design of multiple outlets sub-mains in a distribution network system, often referred to as manifolds, laterals or gated pipes, are extensively used in profession practice, has been a major problem tackled by many authors. This chapter presents a new mathematical model - stepwise computation algorithm- with software application regarding discrete-non-uniform outflow distribution approach for evaluating different forms of pressure head-discharge distributions along the sub-main line, and the required hydraulic flow characteristics along the energy-grade line, that takes into account to the velocity head change and variation of the Reynolds number, which affects the selection of the proper friction coefficient formula to be applied along the different reaches of the pipeline. Resulting, the improved user-friendly computer program in *Visual Basic 6.0* language named “*Multi-flowCAD*” was developed for hydraulic analyzing and designing of multiple outlets sub-main lines regarding certain hydraulics and uniformity criteria.

The present computer-aided computing technique can be efficiently used with the highest accuracy for different forms of pressure head profiles covering various design configurations regarding different flow regimes and uniform line slope situations with respect to alternative computing techniques, because only the basic equations of the hydraulics of steady-state pipe flow condition, were sensitively used in each pipe section between successive outlets. In profession practice, the present improved software simulation model is the most suitable, and can be efficiently used for hydraulic analyzing and designing of various types of multiple-outlets pipelines in sub-main distribution networks, for all performed simulations.

Multiple outlets pipelines in a sub-main unit, often referred to as manifolds, laterals or gated pipes, are extensively used in profession practice, such as in ocean out-falls with multiple diffusers, leakage assessment for branched networks, sediment transporting, sprinkling infiltration systems, sub-units of low-volume irrigation systems, gas pipe burners, thermal discharges, sewer line systems, submarine oil pipelines, e.g., general engineering applications in water distribution network systems (Yıldırım 2006, 2007a,b, 2008, 2009, 2010, 2015, 2016). In the available literature, a great deal of attention on this problem was successfully devoted by the earlier extensive investigations (Hathoot et al. 1993; Yıldırım and Ağralioğlu 2004a,b; Yıldırım 2006, 2007a,b, 2008, 2009, 2010a,b; Yıldırım and Singh 2010; Yıldırım and Singh 2013a,b; Yıldırım 2015, 2016). Hence, analysis of the hydraulic design of multi-outlets submain lines is very important concern for comprehensively

evaluating the proper hydraulic performance of these sub-main distribution network systems.

The objective of this chapter is to present an implementation of the improved user-friendly software simulation model in *Visual Basic 6.0* language named “*Multi-flowCAD*” based on the discrete-non-uniform outflow approach for multiple-outlets sub-mains, concerning different flow regimes and various uniform line slope situations, while determining the required pressure parameters along the energy-grade line (EGL) (Yıldırım 2001, 2007).

The present computer-aided computing technique takes into account to the velocity head change and variation of the Reynolds number, which affects the selection of the proper friction coefficient formula to be applied along the different reaches of the sub-main line. As a matter of fact, the present procedure has the highest accuracy for all performed simulations, because only the basic equations of the hydraulics of steady pipe flow were used in each pipe segment between successive outlets; hence it can be efficiently used for general purposes in engineering applications of multiple outlets pipe flow hydraulics.

PRINCIPLES ON MANIFOLD FLOW HYDRAULICS

Governing Equations

Hydraulically, flow in the sub-main line is considered to be a steady, spatially varied flow with decreasing outlet outflow along the downstream direction. The energy grade line (EGL) in a multiple outlets pipeline will not be a straight line but a curve of the exponential type, as shown in Figure 1.

This figure shows the sketch of the horizontal pipeline with multiple outlets, and the shapes of the hydraulic (HGL) and energy gradient (EGL) curves along its length. Generally, successive outlets are usually identical, and installed at an equal spacing on the sub-main line. The flow characteristics of the outlets are typically described by a function of the power form:

$$q_{(out)} = cH_{(out)}^x \quad (1)$$

in which $q_{(out)}$ is the outflow from an individual outlet; $H_{(out)}$ is the pressure head at the outlet under consideration; c is the outlet coefficient that accounts for areal and discharge effects and makes the units correct.

Let us consider the multi-outlets pipeline sketch with horizontal slope, as shown in Figure 1. If there are N outlets on the pipeline with a common spacing s , the number of spacing will be $(N - 1)$ and the length of the pipeline is the distance between the first and last outlet, $L = s(N - 1)$.

As indicated in this figure, $H_{(1)}$ is the initial inlet pressure head, $Q_{(1)}$ the initial discharge ($Q_{(1)} = N q_{(av)}$) upstream from the first outlet, and $q_{(1)}$ the outflow of the first outlet, which may be written as

$$q_{(1)} = c H_{(1)}^x \quad (2)$$

Assuming that the outflow varies continuously in space along the pipeline (the number of outlets is sufficiently large), the outflow per unit length (\bar{q}) can then be described by

$$\bar{q} = \left(\frac{c}{s}\right) H_{(n)}^x \quad (3)$$

If continuity is preserved along the pipeline, the conservation of mass is written in the general following form:

$$\frac{dQ}{dx} + \frac{dA}{dt} = -\bar{q} \quad (4)$$

where Q is the total discharge; x and t are space and time coordinates. For steady flow condition ($dA/dt = 0$), the continuity equation, Eq.(4), may be rewritten as follows

$$A \frac{dV}{dx} = -\bar{q} \quad (5)$$

where V is the average velocity of flow through the pipe.

Using the continuity equation, Eq.(5), the discharge, $Q_{(n+1)}$, at the pipe reach between successive outlets (n) and $(n+1)$, can be obtained from:

$$Q_{(i+1)} = Q_{(i)} - q_{(i)} \quad (6)$$

The discharge between the first and second outlets $Q_{(2)}$ can be evaluated from Eq. (6) in the special form :

$$Q_{(2)} = Q_{(1)} - q_{(1)} = (N \cdot q_{(av)}) - (c \cdot H_{(1)}^x) \quad (7)$$

The momentum effect resulting from decreasing the discharge in downstream direction, the conservation of momentum equation is given by the following form (Streeter and Wylie, 1979)

$$\sum F = \rho(Q_{(i+1)} \cdot V_{(i+1)} - Q_{(i)} \cdot V_{(i)}) \quad (8)$$

where $\sum F$ is the change of pressure force; ρ is the density of water; $V_{(i)}$ and $V_{(i+1)}$ are the flow velocity between successive emitters $(i-1) \sim (i)$ and $(i) \sim (i+1)$, respectively.

Using the conservation of momentum equation, Eq.(8), the change of pressure head, $\Delta H_{(i+1)}$, due to change of momentum between successive outlets (i) and $(i+1)$ resulting from decreasing the discharge from $Q_{(i)}$ to $Q_{(i+1)}$, may be written as follows

$$\Delta H_{(i+1)} = \frac{(Q_{(i+1)}^2 - Q_{(i)}^2)}{gA^2} \quad (9)$$

where g is the acceleration due to gravity.

The general form of the Darcy-Weisbach formula which proved to be the most accurate and reliable (von Bernuth and Wilson 1989, von Bernuth 1990) can be approximated by the following expression:

$$H_{f(i+1)} = f_{(i+1)} \frac{s}{D} \frac{Q_{(i+1)}^2}{2gA^2} \quad (10)$$

where $H_{f(i+1)}$ is the friction head loss between successive emitters (i) and $(i+1)$; $f_{(i+1)}$ is the Darcy-Weisbach friction coefficient for the pipe reach between successive emitters (i) and $(i+1)$; D is the internal diameter of the pipe.

Eq. (10) may be rewritten by simplifying

$$H_{f(i+1)} = \frac{8s}{\pi^2 g D^5} f_{(i+1)} Q_{(i+1)}^2 \quad (11)$$

With assuming the pipeline has a uniform slope S_0 , the difference in levels of points (i) and $(i+1)$ may be given by

$$(z_{(i)} - z_{(i+1)}) = \pm s S_0 \quad (12)$$

The positive sign is for pipeline sloping downward and the negative for upward slopes, $z_{(i)}$ and $z_{(i+1)}$ are elevations of successive outlets (i) and $(i+1)$ respectively, above an arbitrary datum.

Using conservation of the energy principle with Eq.(9) and Eq.(11), between successive outlets (i) and $(i+1)$, the following form can be obtained

$$H_{(i)} + \frac{V_{(i)}^2}{2g} + z_{(i)} = H_{(i+1)} + \frac{V_{(i+1)}^2}{2g} + z_{(i+1)} + H_{f(i+1)} + h_{(L)i} + \Delta H_{(i+1)} \quad (13)$$

where $H_{(i)}$ and $H_{(i+1)}$ are pressure head for the successive outlets (i) and $(i+1)$; $\frac{Q_{(i)}^2}{2gA^2}$ and $\frac{Q_{(i+1)}^2}{2gA^2}$ are velocity head under consideration; $h_{(L)i}$ is the local head losses due to pipe fittings or couplers.

Solving Eq.(13) for the pressure head at the individual outlet $(i+1)$, $H_{(i+1)}$ is related to $H_{(i)}$ by the following equation:

$$H_{(i+1)} = H_{(i)} + \left(\frac{Q_{(i)}^2}{2gA^2} \right) - \left(\frac{Q_{(i+1)}^2}{2gA^2} \right) + (z_{(i)} - z_{(i+1)}) - H_{f(i+1)} - h_{(L)i} - \Delta H_{(i+1)} \quad (14)$$

Combining conservation of mass and momentum principles Eq.(6) and Eq.(9) with Eq.(11) and Eq.(12), into conservation of energy principle, Eq.(14), and simplifying

$$H_{(i+1)} = H_{(i)} + \frac{3}{2gA^2} [Q_{(i)}^2 - (Q_{(i)} - q_{(i)})^2] - f_{(i+1)} \frac{8s}{\pi^2 gD^5} (Q_{(i)} - q_{(i)})^2 - h_{(L)i} \pm s S_0 \quad (15)$$

For convenience, Eq.(15) is put in the form

$$H_{(i+1)} = H_{(i)} + A^* [Q_{(i)}^2 - (Q_{(i)} - q_{(i)})^2] - B^* f_{(i+1)} (Q_{(i)} - q_{(i)})^2 - h_{(L)i} \pm s S_0 \quad (16)$$

$$A^* = \frac{3}{2gA^2}, \quad B^* = \frac{8s}{\pi^2 gD^5} \quad (17)$$

METHODOLOGY

As considered from the present hydraulic analysis, there are four basic equations in the multi-outlets pipe flow hydraulics. These equations are:

1. Outlet discharge-pressure head relationship as Eq. (1),
2. Continuity equation as Eq. (5),
3. Darcy-Weisbach friction formula as Eq. (10),
4. Conservation of energy equation coupled with the conservation of momentum equation as Eq. (13).

Hence, there are four unknown hydraulic variables ($Q_{(i+1)}$, $q_{(i+1)}$, $H_{(i+1)}$ and $H_{f(i+1)}$) at any location of lateral ($i+1$), with the previously known values ($Q_{(i)}$, $q_{(i)}$, and $H_{(i)}$), and the other design parameters ($z_{(i)}$, $z_{(i+1)}$, $f_{(i+1)}$, D , N , L , s , c , x , ε).

COEFFICIENT OF FRICTION (f)

Flow in a multi-outlets pipeline is generally turbulent ($3000 < R \leq 10^5$), sometimes fully turbulent flow ($10^5 < R < 10^7$) exists at the upstream end of the lateral and flow becomes laminar at the downstream reach where the velocity decreases to zero. Submain pipelines (manifolds or

laterals) are generally either plastic or aluminum pipes, therefore the analysis presents friction coefficients regarding both the materials.

Noting that, when couplers are used to connect two lengths of plain pipe, some additional energy loss takes place as the water passes through the coupler. The head loss in plastic couplers could be provided as equivalent length of the pipe. For aluminum pipes with couplers spaced 9 m, the energy loss can be determined by increasing the friction coefficient, f , by 11%; decreasing the spacing to 6 m increases the percentage to 17%, and increasing the spacing to 12 m decreases the percentage to 8%.

For Plastic Pipes

Plastic pipes are made of smooth materials. For laminar flow where Reynolds number R is less than 2000 ($R < 2000$), the friction coefficient is given by (Warrick and Yitayew 1988; Yitayew and Warrick 1988; Hathoot et al., 1993)

$$f = \frac{64}{R} = 64 \frac{\nu}{VD} \quad \left(R = \frac{VD}{\nu} \right) \quad (18)$$

in which R : the Reynolds number and ν : the kinematic viscosity of water.

For turbulent flow ($3000 < R \leq 10^5$), the Blasius equation can be used:

$$f = 0.316 R^{-0.25} \quad (19)$$

For fully-turbulent flow ($10^5 < R < 10^7$), we have:

$$f = 0.130 R^{-0.172} \quad (20)$$

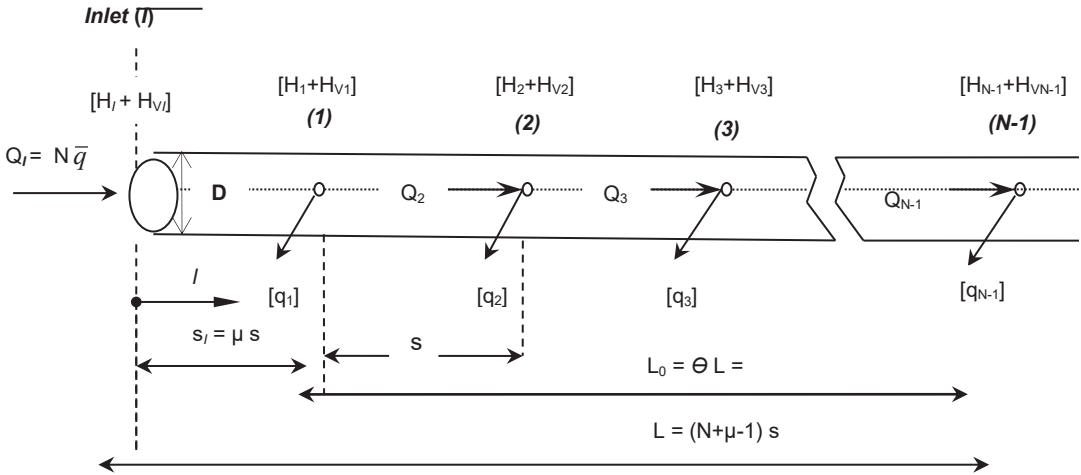
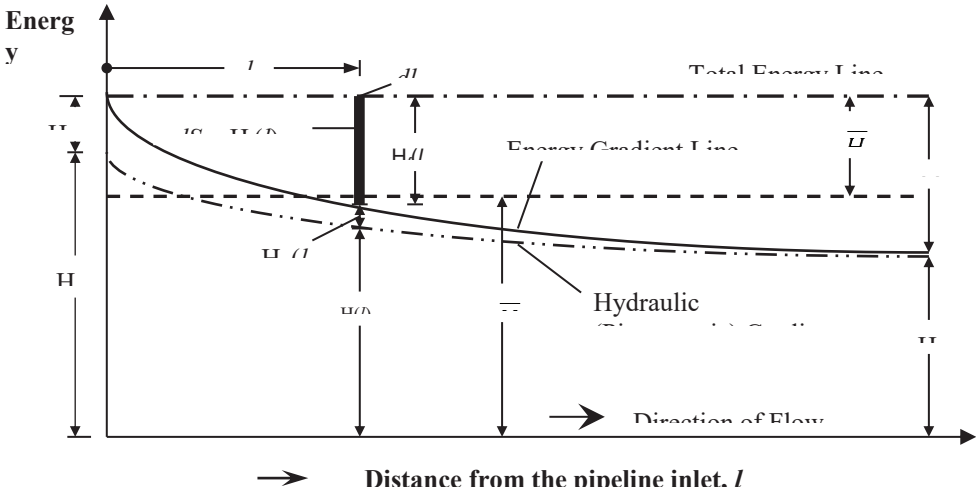


Figure 1. Shapes of hydraulic (piezometric) gradient line (HGL), and energy-gradient line

(EGL) along horizontal sub-main line with multiple outlets.

For Aluminum Pipes

In aluminum pipes, the absolute roughness ranges between 0.1 and 0.3 mm (“Design” 1981). For laminar flow regime, the coefficient of friction can be evaluated from Eq.(18). For turbulent flow, in general Churchill (1977) presented the following equation:

$$f = 8 \left[\left(\frac{8}{R} \right)^{12} + \frac{I}{(A' + B')^{3/2}} \right]^{1/12} \quad (21)$$

where A' and B' = empirical parameters for computing Darcy-Weisbach friction coefficient. A' and B' are computed from:

$$A' = \left(2.457 \ln \left[\frac{I}{(7/R)^{0.9}} + 0.27(\varepsilon/D) \right] \right)^{16} \quad (22)$$

$$B' = \left(\frac{37,530}{R} \right)^{16} \quad (23)$$

where ε = equivalent roughness height of the internal pipe surface. Eq. (21) covers a significant portion of the turbulent zone on the Moody's diagram. The present formulation yields errors less than $\pm 1\%$ in the range $10^{-6} \leq \varepsilon/D \leq 10^{-2}$ and $5 \times 10^3 \leq R \leq 10^8$.

Please note that, the recent comparative study (Yıldırım 2009, Özger and Yıldırım 2009) presented a comprehensive error analysis of the well-known explicit formulations (Swamee and Swamee 2006, Swamee and Rathie 2006) for the implicit Colebrook-White equation, with regarding commonly preferred performance evaluation criteria.

Water Application Uniformity

One of the main tasks of the multi-outlets pipeline hydraulic calculation is to provide a sensitive balance between the inlet pressure head, the water application uniformity, and the total frictional losses along the line. In designing, the variation of the outlet discharge within limited values, which are defined in the uniformity coefficients, namely the Christiansen's uniformity coefficient (U_C) and the lower-quarter distribution uniformity coefficient (DU_{LQ}), is very important concern, because it leads to a relatively short variation in the Reynolds number range, and therefore, in a short run along the Moody's diagram.

Essentially, successive individual outlets are convenient to consider expressions for emission uniformity, which is the relationship between the minimum and average outlet discharge within overall the

system. The uniformity coefficients (U_C and DU_{LQ}) are used here to express uniformity of emitter discharge throughout the system.

The uniformity coefficients are:

$$U_C = 1 - \frac{1}{Nq_{(av)}} \sum_{i=1}^{i=N} |q_{(i)} - q_{(av)}| \quad (24)$$

$$DU_{LQ} = \frac{4 \times \left[\sum_{i=\frac{3N}{4}}^{i=N} (q_{low})_{(i)} \right]}{N \times q_{(av)}} \quad (25)$$

where $q_{(av)}$: average outlet discharge along the pipeline; $q_{(i)}$: discharge of individual outlet (i) and $(q_{low})_i$: discharge of the lower-quarter outlet $i = 3N/4$.

CONCLUDING REMARKS

In this chapter, an improved computer-aided computation algorithm based discrete-non-uniform outflow approach was presented, and a user-friendly computer program in *Visual Basic 6.0* language named *Multi-flowCAD* was developed for multi-outlets sub-main lines in water distribution network system. In the present design methodology, the design of the sub-main line with uniform line slope and equally spaced individual outlets was examined within certain hydraulics and uniformity constraints.

In designing of the sub-main line by the present algorithm, for the given pipe length and inside diameter, firstly, the proper value of operating inlet pressure head was sensitively appointed within the design interval based on the initial and boundary conditions with the required hydraulic characteristics along the energy-grade line.

In profession practice, the present improved software simulation model is the most suitable because only the basic equations of the hydraulics of steady pipe flow were efficiently used in each pipe segment which was divided by successive individual outlets, and can be efficiently used for hydraulic analyzing and designing of various types of multiple-

outlets pipelines in sub-main distribution networks, for all performed simulations. Steps of the present algorithm, design criteria, computer visualization with engineering implementation, and program outputs are also presented in the companion chapter.

REFERENCES

- Churchill, S. W. (1977). Friction factor equation spans all fluid-flow regimes. *Chem. Eng.*, 84(24), 91-92.
- Hathoot, H. M., Al-Amoud, A. I., and Mohammad, F. S. (1993). Analysis and design of trickle irrigation laterals. *ASCE, J. Irrig. and Drain. Eng.*, 119(5), 756-767.
- Kang, Y. and Nishiyama, S. (1996a). Analysis and design of microirrigation laterals. *J. Irrig. and Drain. Eng., ASCE*, 122(2), 75-82.
- Kang, Y. and Nishiyama, S. (1996b). Design of microirrigation submain unit. *J. Irrig. and Drain. Eng., ASCE*, 122(2), 83-89.
- Özger, M. and Yıldırım, G. (2009). Determining Turbulent Flow Friction Coefficient Using Adaptive Neuro-Fuzzy Computing Technique. *Advances in Engineering Software*, 40(4): 281-287.
- Swamee, P.K. and Rathie, P.N. (2006). Exact equations for pipe-flow problems. *J. Hydraulic Research*, 1-4.
- Swamee, P.K. and Swamee, N. (2006). Full-range pipe flow equations. *J. Hydraulic Research*, vol.0 no: 0, 1-3.
- Vallesquino, P. and Luque-Escamilla, P.L. (2001). New algorithm for hydraulic calculation in irrigation laterals. *J. Irrig. and Drain. Eng., ASCE*, 127(4), 254-260.
- Vallesquino, P. Luque-Escamilla, P.L. (2002). Equivalent friction factor method for hydraulic calculation in irrigation laterals. *J. Irrig. and Drain. Eng., ASCE*, 128(5), 278-286.
- Valiantzas, J.D. (1998). Analytical approach for direct drip lateral hydraulic calculation. *J. Irrig. and Drain. Eng., ASCE*, 124(6), 300-305.
- Valiantzas, J.D. (2002). Continuous outflow variation along irrigation laterals: effect of the number of outlets. *J. Irrig. and Drain. Eng., ASCE*, 128(1), 34-42.
- Warrick, A.W. and Yitayew, M. (1988). Trickle lateral hydraulics.I: analytical solution. *J. Irrig. and Drain. Eng., ASCE*, 114(2), 281-288.

- Wu, and Gitlin, H.M. (1975). Energy gradient line for drip irrigation laterals. *J. Irrig. and Drain. Eng., ASCE*, 101(4), 323-326.
- Yıldırım, G. and Singh, V.P. (2013a). Operating Pressure for Uniformly Sloping Submain Lines with Different Types of Pressure Profiles-I: Improved Energy-Gradient Ratio (EGR) Approach. *6th International Perspective on Water Resources & the Environment” ASCE&EWRI, 7-9 January, Izmir, Turkey.*
- Yıldırım, G. and Singh, V.P. (2013b). Determination of Operating Pressure for Uniformly Sloping Submain Lines with Different Types of Pressure Profiles-II: Design Applications, Comparative Analysis and Verification. *6th International Perspective on Water Resources & the Environment” ASCE&EWRI, 7-9 January, Izmir, Turkey.*
- Yıldırım, G. (2015). An Assessment for Hydraulically-Efficient Design of Uniformly-Sloping Submain Lines. *Irrig. Drain. (ICID Journal)* 64(2),157-168.
- Yıldırım, G. and Singh, V.P.(2010). A *MathCAD* Procedure for Commercial Pipeline Hydraulic Design Considering Local Energy Losses. *Advances in Engineering Software*, 41(2), 489-496.
- Yıldırım, G. (2009). Computer-Based Analysis of Explicit Approximations to the Implicit Colebrook-White Equation in Turbulent Flow Friction Factor Calculation. *Advances in Engineering Software*, 40(11), 1183-1190.
- Yıldırım, G. and Özger, M. (2009). Neuro-Fuzzy Approach in Estimating Hazen-Williams Friction Coefficient for Small-Diameter Polyethylene Pipes. *Advances in Engineering Software*, 40(8): 593-599.
- Yıldırım, G. (2011). Closure to “Discussion of “Computer-Based Analysis of Explicit Approximations to the Implicit Colebrook-White Equation in Turbulent Flow Friction Factor Calculation by Dejan Brkic” *Advances in Engineering Software*, 40(11),1183-1190.
- Yıldırım, G. (2010). Total Energy Loss Assessment for Trickle Lateral Lines Equipped with Integrated In-Line and On-Line Emitters. *Irrigation Science*, 28(4), 341-352.
- Yıldırım, G. (2009). Simplified Procedure for Hydraulic Design of Small-Diameter Plastic Pipes. *Irrig. and Drain. (ICID Journal)*, 58(3):209-233.
- Yıldırım, G. (2008). Determining Operating Inlet Pressure Head Incorporating Uniformity Parameters for Multioutlet Plastic Pipelines. *J. Irrig. and Drain. Eng., ASCE*, 134(3), 341-348.

- Yıldırım, G. (2007a). An Assessment of Hydraulic Design of Trickle Laterals Considering Effect of Minor Losses. *Irrig. and Drain. (ICID Journal)* 56(4), 399-421.
- Yıldırım, G. (2007b). Analytical Relationships for Designing Multiple Outlets Pipelines. *J. Irrig. and Drain. Eng., ASCE*, 133(2), 140-154.
- Yıldırım, G. (2006). Hydraulic Analysis and Direct Design of Multiple Outlets Pipelines Laid on Flat and Sloping Lands. *J. Irrig. and Drain. Eng., ASCE*, 132(6), 537-552.
- Yıldırım, G., and Ağırlioğlu, N. (2004a). Comparative analysis of hydraulic calculation methods in design of microirrigation laterals. *J. Irrig. and Drain. Eng., ASCE*, 130(3), 201-217.
- Yıldırım, G., and Ağırlioğlu, N. (2004b). Linear solution for hydraulic analysis of tapered micro-irrigation laterals. *J. Irrig. and Drain. Eng., ASCE*, 130(1), 78-87.
- Yıldırım, G., and Ağırlioğlu, N., (2002). Variation of Total friction Head Losses and Uniformity Coefficients Based on Inlet Pressure Head in Trickle Irrigation Laterals, *Proc., International Conference On Water Resources Management in Arid Regions*, Kuwait Institute for Scientific Research, Kuwait.
- Yıldırım, G. and Ağırlioğlu, N. (2002). Variation of total friction head losses and uniformity coefficients based on inlet pressure head in trickle laterals. *Proc., International Conference on Water Resources Management in Arid Regions*, Kuwait Institute for Scientific Research, Kuwait.
- Yıldırım, G. and Ağırlioğlu, N. (2003). Discussion of 'Continuous outflow variation along irrigation laterals: effect of the number of outlets' by J. D. Valiantzas. *J. Irrig. and Drain. Eng., ASCE*, 129(5), 382-386.
- Yıldırım, G. and Ağırlioğlu, N. (2004a). Linear solution for hydraulic analysis of tapered microirrigation laterals, *J. Irrig. and Drain. Eng., ASCE*, 130(1), 78-87.
- Yıldırım, G. and Ağırlioğlu, N. (2004b). Comparative analysis of hydraulic calculation methods in design of microirrigation laterals. *J. Irrig. and Drain. Eng., ASCE*, 130(3), 201-217.

- Yıldırım, G. and Ağralıoğlu, N.(2004c). Variation of design parameters in microirrigation laterals. *ARI Interdisciplinary Journal of Physical and Engineering Sciences*, 54(1), 42-53.
- Yıldırım, G. and Ağralıoğlu, N. (2005a). Discussion of ‘Inlet pressure, energy cost, and economic design of tapered irrigation submains’ by J. D. Valiantzas.” *J. Irrig. and Drain. Eng., ASCE*, 131(2), 220-224.
- Yıldırım, G. and Ağralıoğlu, N. (2005b). Closure to ‘Linear solution for hydraulic analysis of tapered microirrigation laterals’ by G. Yıldırım and N. Ağralıoğlu.” *J. Irrig. and Drain. Eng., ASCE*, 131(5), 490-491.
- Yıldırım, G. (2007). Comparative analysis of hydraulic calculation methods in design oh micro-irrigation laterals and linear solution of hydraulic analysis of tapered laterals. *Doctoral thesis*, Istanbul Technical University (ITU) , Hydraulics Division, Istanbul, Turkey.
- Yıldırım, G. (2001). Computer-aided design of micro-irrigation laterals by using *LatCAD*, *Master’s thesis*, Istanbul Technical University (ITU), Hydraulics Division, Istanbul, Turkey.
- Yıldırım, G. (2016). Computer-Based Analysis of Hydraulic Design Variables for Uniformly Sloping Microirrigation System Laterals. *J. Irrig. and Drain. Eng., ASCE*, 141(7): 04014079.
- Yıldırım, G. (2015). An Assessment for Hydraulically Efficient Design of Uniformly Sloping Submain, Lines. *Irrigation and Drainage*, 64(2),157-168.
- Yıldırım, G. (2010). Total Energy Loss Assessment for Trickle Lateral Lines Equipped with Integrated In-Line and On- Line Emitters. *Irrigation Science*, 28(4), 341-352.
- Yıldırım, G. (2009). Computer-Based Analysis of Explicit Approximations to the Implicit Colebrook-White Equation in Turbulent Flow Friction Factor Calculation. *Advances in Engineering Software*, 40(11), 1183-1190.
- Yıldırım, G. and Özger, M. (2009). Neuro-Fuzzy Approach in Estimating Hazen-Williams Friction Coefficient for Small- Diameter Polyethylene Pipes. *Advances in Engineering Software*, 40(8): 593-599.
- Yıldırım, G. (2009). Simplified Procedure for Hydraulic Design of Small-Diameter Plastic Pipes. *Irrig. and Drain. (ICID Journal)*, 58(3):209-233.
- Yıldırım, G. (2008). Determining Operating Inlet Pressure Head Incorporating Uniformity Parameters for Multioutlet Plastic Pipelines. *J. Irrig. and Drain. Eng., ASCE*, 134(3), 341-348.

- Yıldırım, G. (2007). An Assessment of Hydraulic Design of Trickle Laterals Considering Effect of Minor Losses. *Irrig. and Drain. (ICID Journal)* 56(4), 399-421.
- Yıldırım, G. (2007). Analytical Relationships for Designing Multiple Outlets Pipelines. *J. Irrig. and Drain. Eng., ASCE*, 133(2), 140-154.
- Yıldırım, G. (2006). Hydraulic Analysis and Direct Design of Multiple Outlets Pipelines Laid on Flat and Sloping Lands. *J. Irrig. and Drain. Eng., ASCE*, 132(6), 537-552.
- Yıldırım, G. (2016). Discussion of “Statistical Analysis of Non-Pressure-Compensating and Pressure-Compensating Drip Emitters” by H. Perea, J. Enciso-Medina, V. P. Singh, D. P. Dutta, and B. J. Lesikar (DOI: 10.1061/(ASCE)IR.1943-4774.0000644). *J. Irrig. and Drain. Eng., ASCE*.
- Yitayew, M., and Warrick, A.W. (1988). Trickle lateral hydraulics.II: design and examples. *J. Irrig. and Drain. Eng., ASCE*, 114(2), 289-300.

Chapter 17

SOFTWARE DEVELOPMENT FOR MANIFOLD LINE HYDRAULIC DESIGN-II: STEPS OF ALGORITHM, IMPLEMENTATION AND COMPUTER VISUALIZATION



Gürol YILDIRIM¹

¹ Professor of Civil Engineering, Aksaray University, Engineering Faculty, Civil Engineering Department, Head of Hydraulics Division, 68100, Aksaray, Turkey. E-mail: yildirim3@itu.edu.tr

This chapter was produced from the book author's Master's and Doctoral theses.

INTRODUCTION

The increasing progress in computer technology has led to the development of the improved solutions of analytical and numerical methods of hydraulic design of multiple outlets sub-mains in a distribution network system. The present computer-aided computing technique was successfully implemented with the highest accuracy for different forms of pressure head profiles covering various design configurations regarding different flow regimes and uniform line slope situations with respect to alternative computing techniques, because only the basic equations of the hydraulics of steady-state pipe flow condition, were sensitively used in each pipe section between successive outlets.

In profession practice, the present improved software simulation model (*Multi-flowCAD*) is the most suitable, and can be efficiently used for hydraulic analyzing and designing of various types of multiple-outlets pipelines in sub-main distribution networks, for all performed simulations. Design criteria for the proposed program implementation with sample manifold line design, computer visualization, and program outputs are provided.

Large number of works were devoted on the development of analytical and numerical methods of the hydraulic analysis, as the differential method (*DM*) (Warrick and Yitayew 1988), Runge-Kutta numerical method (*RKM*) (Yitayew and Warrick 1988), the energy-gradient line method (*EGL*) (Wu 1975), and the revised method (*REGL*) (Yıldırım 2006, 2007a,b, 2008, 2009) the finite-element method (*FEM*) (Kang and Nishiyama 1996a, b), the forward-step method (*FSM*) (Hathoot et al. 1993, 1994), the successive-approximations method (*SAM*) (Vallesquino and Luque-Escamilla 2001, 2002), and others.

As a matter of fact, among these previous extensive researches, the computer-aided stepwise calculation procedure based discrete-non-uniform outflow distribution approach gives an exact solution applied to accurately establish the flow required hydraulic characteristics, and also determine pressure-discharge distributions along the energy-grade line. Essentially, two main concerns for the multi-outlets pipe flow hydraulics are first, to obtain a uniform flow distribution for all outlets, and second, to minimize the total head loss in the sub-main pipe system.

In water distribution networks, a sub-main line can be regarded as a typical hydraulic structure, whose design is limited by the operating inlet pressure head (H_{0l}), desired uniformity criterion for water application (i.e., uniformity coefficient), total friction drop at the end of line ($h_{f(L)}$), field topography, as well as outlet hydraulic characteristics.

Design of this sub-main distribution network system depends upon a good understanding of multi-outlets pipe flow hydraulics and outlet characteristics. In various types of the sub-main design problems, determination of the actual pressure head or outflow profile along the line is greatest important concern for the proper hydraulic design.

As a matter of fact, among the alternative design configurations, the operating inlet pressure head, H_{01} , is a key hydraulic component for the proper design and evaluation of pressure head or outflow distribution along the energy-grade line. This operating pressure head can be achieved in a stepwise manner, either starting from the required pressure head at the downstream closed end, H_d , working back to the inlet upstream direction, by computing the friction head loss in each pipe segment between successive outlets (*BSP*: backward-step procedure) (Kang and Nishiyama 1996); or starting from the inlet pressure head, H_{01} , computing forward in the downstream direction (*FSP*: forward-step procedure) (Hathoot et al. 1993).

In the present stepwise computation procedure in the forward form, the H_{01} will be determined by adding a reasonable head increment to the required average outlet pressure head, ensuring initial and boundary conditions to be based on the design algorithm earlier discussed (Yıldırım 2008). Adequate analysis of sub-mains with multiple outlets include the determination of the pipe length or the inside diameter, the required operating inlet pressure head and total friction head losses along the lateral assuming that the total flow rate at the inlet, characteristics of the outlets, and the acceptable level of uniformity are known previously.

CLASSIFICATION ON MANIFOLD DESIGN PROBLEMS

Design of a lateral pipe includes the determination of pipe geometric characteristics (pipe size and length), as well as operating inlet pressure head and total friction head losses along the line. Design engineers are often faced with three types of problems in most lateral hydraulic computations. In the first type of problem (energy grade-line determination) (Yıldırım and Singh 2013a,b, Yıldırım 2007a, 2008) for the given design values of uniform lateral slope (S_0) and average outlet pressure head (H_{av}), the required hydraulic variables concerning the pressure head profile [the operating inlet pressure head ($H_{01} = H_{in}$), downstream closed end pressure head (H_N), extreme pressure heads (H_{max} and H_{min}) with their locations along the line (i_{max} , i_{min} ; i : percentage of length, l is a length from the inlet in m, and L is the total length of the lateral line in m), and the total energy drop due to friction $H_{f(L)}$, can be determined ensuring the desired level of water application uniformity as well as the allowable pressure head variation along the line (Yıldırım 2007a).

With the help of the present computer-aided design technique,

knowledge of hydraulic properties for any type of pressure profile under consideration enables the design engineer to clearly evaluate the overall energy distributions with the required pressure parameters through the line sections between successive emitters, in a simple way. Variation of the emitter outflows along the line within certain limited values which defined as the uniformity coefficients for water application is also very important concern. In the second type of problem (water application uniformity evaluation) (Yıldırım 2007a,b, 2009), when H_{01} is given as an input parameter together with the required average emitter pressure head (H_{av}) and for a given design slope (S_0), proper values of the required water application uniformity coefficients can be directly approximated.

The design procedure which based on the uniformity coefficients depending on the acceptable level of outflow variation can be accepted or refused. In fact, the real value of these coefficients, should be just obtained with taking into account all the emitter outflows along the lateral line by implementing computer-aided stepwise procedure.

Designers are often faced with the problem of selecting the pipe size and length for a given desired uniformity level and given design slope range, in order to keep the design operating inlet pressure head and the allowed limit of total energy loss along the pipeline.

In the third type of design problem (direct sizing procedure) (Hathoot et al. 2000; Kang and Nishiyama 1996a,b; Valiantzas 2002, Yıldırım 2006a, 2009), the required parameters are the pipe inside diameter (D) or length (L) for a given design slope (S_0), the desired level of water application uniformity (U_c and D_{ULQ}), and the required average emitter outflow and pressure head (q_{av} , H_{av}), with the previously known design variables.

COMPUTATIONAL STEPS for PRESENT DESIGN ALGORITHM

As a notable reference, the algorithm was first programmed in *FORTRAN IV*, then a useful flowchart was presented by Hathoot et. al. (1993). Herein, the steps of the present algorithm was improved in the following section “*Implementation of the Design Criteria*” based on the initial and boundary conditions of the algorithm, and reprogrammed in *Visual Basic 6.0*, incorporating variable flow conditions through lateral segments, in a stepwise manner. Calculation steps of the proposed computer program (*Multi-flowCAD*) is also provided in Figure 1.

In practice the average emitter discharge q_{av} , the corresponding pressure head H_{av} , the flow exponent y , total number of emitters N , the spacing between emitters S , and the uniform line slope S_0 and the inside diameter of the lateral pipe D are assigned in advance, for a certain design. The following computational steps should be taken into consideration in the present algorithm:

1. The initial pressure head H_{\max} is first assumed by adding a reasonable head increment Δ_0 to the average head H_{av} (initial condition).

2. The outflow of each successive individual emitter q_i is evaluated in a stepwise manner, starting from the first emitter at the upstream lateral inlet; and in each step the corresponding lateral discharge Q_i is evaluated.

3. At each step, the Reynolds number valid for the pipe segment between successive emitters is calculated, then the proper friction coefficient formula is selectively used to evaluate the head loss due to friction, hence the new pressure head at the head of emitter, is determined by applying Eq. (16).

4. If Eq. (16) yields negative values of H at any emitter, this would indicate that the assumed H_{\max} should be increased by Δ_d (Boundary condition).

5. As negative values of H disappear, other conditions should be continued.

6. The velocity at any reach of the lateral pipe should be positive (boundary condition); otherwise, this would indicate that the sum of emitter outflows is greater than the total initial lateral discharge Q_{\max} , which means that H_{\max} should be decreased by Δ_d (Δ_d , being divided periodically by 10 on increasing or decreasing H_{\max}).

7. The discharge in the pipe segment from the last emitter toward the downstream lateral closed end should be zero, which forms an important boundary condition. Practically, this condition is satisfied if the relative velocity at that part becomes less than a sufficiently small quantity, ε .

8. As the proper value of H_{\max} is sensitively reached, outflow, pressure head for each emitter, the discharge and flow velocity at the corresponding reach of the lateral pipe can be determined. Finally, water application uniformity of the micro-irrigation system can be evaluated by computing the uniformity coefficients (U_C and DU_{LQ}) as given by Eq. (19) and Eq. (20), respectively.

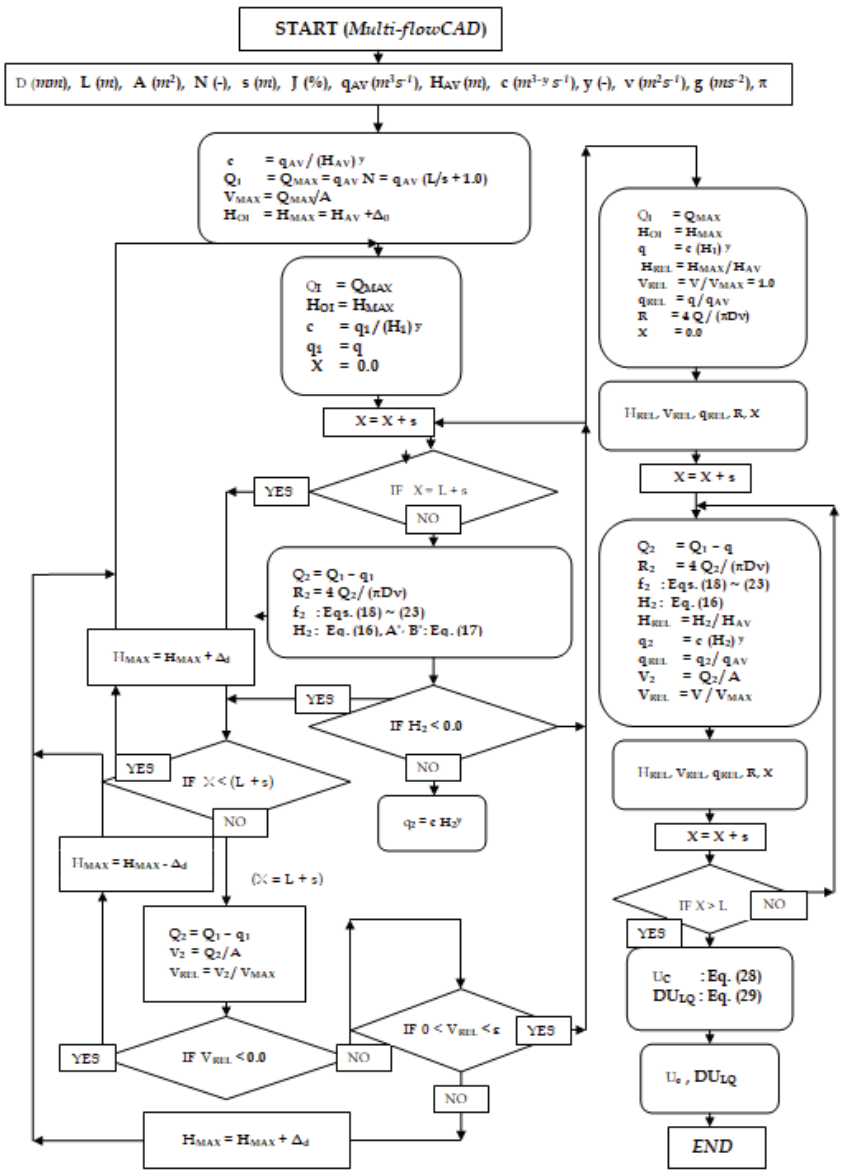


Figure 1. Flowchart (Steps of Algorithm) for the Present Computer Program (Multi-flowCAD)

IMPLEMENTATION of DESIGN CRITERIA

An important objective of the present analysis is the sensitively determination of the proper value of the operating inlet pressure head, H_{01} (H_{in}), which can be varied within limited constraints in the design algorithms (initial and boundary conditions). It clearly means, preliminary increase in average piezometric head (Δ_0) varies ranging from minimum inlet pressure head range [$\bar{H}_{min} = H_{01(min)}/H_a$] toward maximum inlet pressure head range [$\bar{H}_{max} = H_{01(max)}/H_a$]. Please note that, Fig. 3 presents visualization for sample input data generation for the proposed computer program (*Multi-flowCAD*), which sensitively performs the following calculations, in a stepwise manner:

a. Determine operating inlet pressure head ranges in which the operating inlet pressure head is located (\bar{H}_{min} and \bar{H}_{max} = minimum and maximum ranges for the operating inlet pressure head);

b. Obtain minimum operating inlet pressure head range [\bar{H}_{min}] based on the design algorithms (for H_{01} , if smaller values than \bar{H}_{min} are designed, this would indicate that a negative value of the pressure head at any outlet would be apparent);

c. Obtain maximum operating inlet pressure head range [\bar{H}_{max}], based on the design algorithms (for H_{01} , if larger values than \bar{H}_{max} are designed, this would indicate that the sum of outflows is greater than the initial pipe discharge, Q_p , which means that back-flow occurs from the downstream end toward the upstream direction of the pipeline);

d. As the proper interval of the reduced operating inlet pressure head [$\bar{H}_{min}(= H_{01(min)}/H_a) \leq (H_{01}/H_a) \leq \bar{H}_{max}(= H_{01(max)}/H_a)$] is obtained, the favorable value of H_{01} should be investigated. In line with this concept, the following considerations should be taken into account:

e. For H_{01} determination, if \bar{H}_{min} is selected for sub-main line design, the value of residual flow rate at the downstream end from the last outlet is larger than the acceptable small quantity (ε), approximately zero. Obviously, an important boundary condition for the downstream end does not keep to the right in the design algorithm. Meanwhile, the residual pipe discharge decreases from \bar{H}_{min} toward \bar{H}_{max} , increasingly; then, for \bar{H}_{max} it has a sufficiently small value, approximately zero.

f. For sub-main line design, the design parameters should be determined in order to minimize the total friction drop at the end of pipeline. In this respect, if \bar{H}_{min} is selected, the total friction drop would have major values; then, from \bar{H}_{min} toward \bar{H}_{max} , have minor values, increasingly. However, if \bar{H}_{max} is selected, the total friction drop is minimized.

g. In the design procedure, the water application uniformity is an

unknown parameter; other parameters should be varied to have the highest level of uniformity. Obviously, water application uniformity increases from \bar{H}_{min} toward \bar{H}_{max} , with the highest value at \bar{H}_{max} .

h. Resulting, the proper operating inlet pressure head is finally achieved at \bar{H}_{max} , and total friction drop ($h_{f(L)}$) and residual flow rate (Q_r) for the pipe segment from the last outlet toward to downstream closed end are minimized, whereas the water application uniformity (U_c) of the system is achieved to be maximized.

1. For all performed simulations it should be pointed out, for the *Multi-flowCAD*, the required design parameters ($H_{f(L)}$, Q_r , U_c and/or D_{ULQ}) vary versus the operating inlet pressure head range (H_{0l}/H_{av}) to achieve its acceptable proper value within the design criteria, while the available alternative procedures may have fixed values, for these unknown variables.

SAMPLE DESIGN APPLICATION

It is required to design the operating pressure head at the upstream end of the manifold (H_{0l}) and determine the required hydraulic characteristics along the energy-grade line (EGL) ($Q_{(i+1)}$, $q_{(i+1)}$, $H_{(i+1)}$ and $H_{f(i+1)}$), for the following given data: Total number of outlets along the manifold is 33 ($N = 33$) are equally spaced at 12.0 m ($s = 12.0$ m), the first outlet is located 12.0 m from the upstream end of manifold ($s_1 = s = 12.0$ m). Manifold pipe is of aluminum ($\epsilon = 0.1$ mm), and kinematic viscosity of water is at 20 °C ($\nu = 1.01 \cdot 10^{-6} \text{ m}^2\text{s}^{-1}$).

The average outlet discharge is 0.315 Ls^{-1} ($q_{av} = 0.315 \text{ Ls}^{-1}$), and the average outlet pressure head is 31.61 m ($H_{av} = 31.61$ m) with the outlet discharge exponent $x = 0.5$. The internal diameter of the horizontal ($S_0 = 0.0$) manifold is 4.0 in. ($D = 101.6$ mm). The localized head losses are neglected whereas the coupler head loss is considered. The distance between the first upstream and the last downstream outlets is $L_0 = (N-1) \cdot s = (33-1) \cdot 12 = 32 \cdot 12 = 384$ m, and the total length of the manifold is $L = L_0 + s_1 = 384 + 12 = 396$ m. In the computer program the friction factor was multiplied by 1.08 to account for head losses in couplers $s = 12.0$ m apart.

COMPUTER VISUALIZATION

Trials were made through the program to choose the proper value of operating inlet pressure head within certain hydraulics (initial and boundary conditions) and uniformity constraints. For demonstration purpose, the initial steps for inputs data generation (Figure 2), and outputs from the computer program were presented in Figures 3 and 4, respectively. As shown in Fig. 2, the operating inlet pressure head was sensitively

determined by trial-and error procedure within the limited interval based on the initial and boundary conditions in the design algorithm as $H_{01} = 33.8$ m with the higher level of overall system water application uniformity coefficient as $U_c = 98.8\%$. From Figure 3, the pressure head at the last outlet was 31.8 m ($H_{33} = 31.8$ m), that means head loss between the first upstream and last downstream outlets was about 6%. The execution time for the *Multi-flowCAD* implementation is only about 5 second for the complete hydraulic calculations.

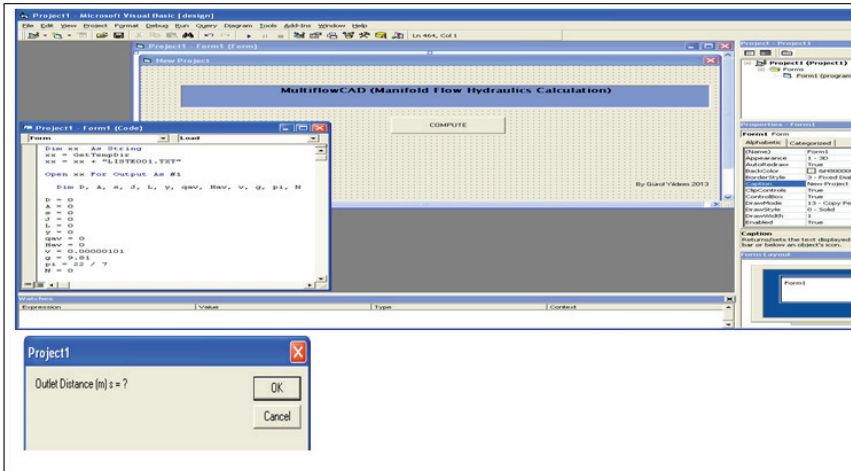


Figure 2. Computer Visualization: Program Code and Input Data Generation (Sample input parameter: Outlet Distance (m))

CONCLUDING REMARKS

In this chapter, an improved computer-aided computation algorithm based discrete-non-uniform outflow approach was presented, and a user-friendly computer program in *Visual Basic 6.0* language named *Multi-flowCAD* was developed for multi-outlets sub-main lines in water distribution network system. In the present design methodology, the design of the sub-main line with uniform line slope and equally spaced individual outlets was examined within certain hydraulics and uniformity constraints.

In designing of the sub-main line by the present algorithm, for the given pipe length and inside diameter, firstly, the proper value of operating inlet pressure head was sensitively appointed within the design interval based on the initial and boundary conditions with the required hydraulic characteristics along the energy-grade line. The level of water application uniformity of the system, and total head losses between the first upstream and last downstream outlets were finally determined. The examination

results of sample design application clearly indicate that, the proposed computer-aided design method has the highest accuracy and sensitivity rather than those of the traditional methods, in which their solution requires very long execution time and effort for the cumbersome iterative procedure.

In profession practice, the present improved software simulation model is the most suitable because only the basic equations of the hydraulics of steady pipe flow were efficiently used in each pipe segment which was divided by successive individual outlets, and can be efficiently used for hydraulic analyzing and designing of various types of multiple-outlets pipelines in sub-main distribution networks, for all performed simulations.

REFERENCES

- Churchill, S. W. (1977). Friction factor equation spans all fluid-flow regimes. *Chem. Eng.*, 84(24), 91-92.
- Hathoot, H. M., Al-Amoud, A. I., and Mohammad, F. S. (1993). Analysis and design of trickle irrigation laterals. *ASCE, J. Irrig. and Drain. Eng.*, 119(5), 756-767.
- Kang, Y. and Nishiyama, S. (1996a). Analysis and design of microirrigation laterals. *J. Irrig. and Drain. Eng., ASCE*, 122(2), 75-82.
- Kang, Y. and Nishiyama, S. (1996b). Design of microirrigation submain unit. *J. Irrig. and Drain. Eng., ASCE*, 122(2), 83-89.
- Özger, M. and Yıldırım, G. (2009). Determining Turbulent Flow Friction Coefficient Using Adaptive Neuro-Fuzzy Computing Technique. *Advances in Engineering Software*, 40(4): 281-287.
- Valiantzas, J.D. (1998). Analytical approach for direct drip lateral hydraulic calculation. *J. Irrig. and Drain. Eng., ASCE*, 124(6), 300-305.
- Valiantzas, J.D. (2002). Continuous outflow variation along irrigation laterals: effect of the number of outlets. *J. Irrig. and Drain. Eng., ASCE*, 128(1), 34-42.
- Vallesquino, P. and Luque-Escamilla, P.L. (2001). New algorithm for hydraulic calculation in irrigation laterals. *J. Irrig. and Drain. Eng., ASCE*, 127(4), 254-260.
- Vallesquino, P. Luque-Escamilla, P.L. (2002). Equivalent friction factor method for hydraulic calculation in irrigation laterals. *J. Irrig. and Drain. Eng., ASCE*, 128(5), 278-286.
- Warrick, A.W. and Yitayew, M. (1988). Trickle lateral hydraulics.I: analytical solution. *J. Irrig. and Drain. Eng., ASCE*, 114(2), 281-288.
- Wu, and Gitlin, H.M. (1975). Energy gradient line for drip irrigation laterals. *J. Irrig. and Drain. Eng., ASCE*, 101(4), 323-326.
- Yıldırım, G. and Singh, V.P. (2013a). Operating Pressure for Uniformly Sloping Submain Lines with Different Types of Pressure Profiles-I: Improved Energy-Gradient Ratio (EGR) Approach. *6th International Perspective on Water Resources & the Environment” ASCE&EWRI, 7-9 January, Izmir, Turkey.*
- Yıldırım, G. and Singh, V.P. (2013b). Determination of Operating Pressure for Uniformly Sloping Submain Lines with Different Types of Pressure Profiles-II: Design Applications, Comparative Analysis and Verification. *6th International Perspective on Water Resources & the Environment” ASCE&EWRI, 7-9 January, Izmir, Turkey.*

- Yıldırım, G. (2015). An Assessment for Hydraulically-Efficient Design of Uniformly-Sloping Submain Lines. *Irrig. Drain. (ICID Journal)* 64(2),157-168.
- Yıldırım, G. and Singh, V.P.(2010). A *MathCAD* Procedure for Commercial Pipeline Hydraulic Design Considering Local Energy Losses. *Advances in Engineering Software*, 41(2), 489-496.
- Yıldırım, G. (2009). Computer-Based Analysis of Explicit Approximations to the Implicit Colebrook-White Equation in Turbulent Flow Friction Factor Calculation. *Advances in Engineering Software*, 40(11), 1183-1190.
- Yıldırım, G. and Özger, M. (2009). Neuro-Fuzzy Approach in Estimating Hazen-Williams Friction Coefficient for Small-Diameter Polyethylene Pipes. *Advances in Engineering Software*, 40(8): 593-599.
- Yıldırım, G. (2011). Closure to Discussion of “Computer-Based Analysis of Explicit Approximations to the Implicit Colebrook-White Equation in Turbulent Flow Friction Factor Calculation by Dejan Brkic” *Advances in Engineering Software*, 40(11),1183-1190.
- Yıldırım, G. and Ağralıoğlu, N. (2002). Variation of total friction head losses and uniformity coefficients based on inlet pressure head in trickle laterals. Proc., *International Conference on Water Resources Management in Arid Regions*, Kuwait Institute for Scientific Research, Kuwait.
- Yıldırım, G. and Ağralıoğlu, N. (2003). Discussion of ‘Continuous outflow variation along irrigation laterals: effect of the number of outlets’ by J. D. Valiantzas.” *J. Irrig. and Drain. Eng., ASCE*, 129(5), 382-386.
- Yıldırım, G. and Ağralıoğlu, N. (2004a). Linear solution for hydraulic analysis of tapered microirrigation laterals, *J. Irrig. and Drain. Eng., ASCE*, 130(1), 78-87.
- Yıldırım, G. and Ağralıoğlu, N. (2004b). Comparative analysis of hydraulic calculation methods in design of microirrigation laterals. *J. Irrig. and Drain. Eng., ASCE*, 130(3), 201-217.
- Yıldırım, G. and Ağralıoğlu, N. (2004c). Variation of design parameters in microirrigation laterals. *ARI Interdisciplinary Journal of Physical and Engineering Sciences*, 54(1), 42-53.
- Yıldırım, G. and Ağralıoğlu, N. (2005a). Discussion of ‘Inlet pressure, energy cost, and economic design of tapered irrigation submains’ by J. D. Valiantzas, *J. Irrig. and Drain. Eng., ASCE*, 131(2), 220-224.
- Yıldırım, G. and Ağralıoğlu, N. (2005b). Closure to ‘Linear solution for hydraulic analysis of tapered microirrigation laterals’ by G. Yıldırım and N. Ağralıoğlu.” *J. Irrig. and Drain. Eng., ASCE*, 131(5), 490-491.
- Yıldırım, G. (2007). Comparative analysis of hydraulic calculation methods in design oh micro-irrigation laterals and linear solution of hydraulic analysis of tapered laterals, *Doctoral thesis*, Istanbul Technical University (ITU) , Hydraulics Division, Istanbul, Turkey.

- Yıldırım, G. (2001). Computer-aided design of micro-irrigation laterals by using *LatCAD*, *Master's thesis*, Istanbul Technical University (ITU), Hydraulics Division, Istanbul, Turkey.
- Yıldırım, G. (2016). Computer-Based Analysis of Hydraulic Design Variables for Uniformly Sloping Microirrigation System Laterals, *J. Irrig. and Drain. Eng.*, ASCE, 141(7): 04014079.
- Yıldırım, G. (2015). An Assessment for Hydraulically Efficient Design of Uniformly Sloping Submain, Lines, *Irrigation and Drainage*, 64(2),157-168.
- Yıldırım, G. (2010). Total Energy Loss Assessment for Trickle Lateral Lines Equipped with Integrated In-Line and On-Line Emitters. *Irrigation Science*, 28(4), 341-352.
- Yıldırım, G. and Singh, V.P. (2010). A *MathCAD* Procedure for Commercial Pipeline Hydraulic Design Considering Local Energy Losses, *Advances in Engineering Software*, 41(2), 489-496.
- Yıldırım, G. (2009). Computer-Based Analysis of Explicit Approximations to the Implicit Colebrook-White Equation in Turbulent Flow Friction Factor Calculation, *Advances in Engineering Software*, 40(11), 1183-1190.
- Yıldırım, G. and Özger, M. (2009). Neuro-Fuzzy Approach in Estimating Hazen-Williams Friction Coefficient for Small-Diameter Polyethylene Pipes, *Advances in Engineering Software*, 40(8): 593-599.
- Yıldırım, G. (2009). Simplified Procedure for Hydraulic Design of Small-Diameter Plastic Pipes, *Irrig. and Drain. (ICID Journal)*, 58(3):209-233.
- Yıldırım, G. (2008). Determining Operating Inlet Pressure Head Incorporating Uniformity Parameters for Multioutlet Plastic Pipelines, *J. Irrig. and Drain. Eng.*, ASCE, 134(3), 341-348.
- Yıldırım, G. (2007). An Assessment of Hydraulic Design of Trickle Laterals Considering Effect of Minor Losses, *Irrig. and Drain. (ICID Journal)* 56(4), 399-421.
- Yıldırım, G. (2007). Analytical Relationships for Designing Multiple Outlets Pipelines, *J. Irrig. and Drain. Eng.*, ASCE, 133(2), 140-154.
- Yıldırım, G. (2006). Hydraulic Analysis and Direct Design of Multiple Outlets Pipelines Laid on Flat and Sloping Lands, *J. Irrig. and Drain. Eng.*, ASCE, 132(6), 537-552.
- Yıldırım, G. (2016). Discussion of “Statistical Analysis of Non-Pressure-Compensating and Pressure-Compensating Drip Emitters” by H. Perea, J. Enciso-Medina, V. P. Singh, D. P. Dutta, and B. J. Lesikar (DOI: 10.1061/(ASCE)IR.1943-4774.0000644). *J. Irrig. and Drain. Eng.*, ASCE.
- Yitayew, M., and Warrick, A.W. (1988). Trickle lateral hydraulics.II: design and examples, *J. Irrig. and Drain. Eng.*, ASCE, 114(2), 289-300.

New Manifold Design Project.TXT - Not Defferi

Dosya Düzen Bgün Görünüm Yardım

New Project: Manifold design (Multi-FlowCAD) Manifold Flow Hydraulics Computations

INPUTS: D= ,051 (m) date Created: 28.01.2014
 A= ,00202683 (m²)
 S= 12 (m)
 J= 0 (m/m)
 L= 396 (m)
 j= 3 (-)
 Q_{AV}= ,000386 (m³/s)
 H_{AV}= 47,45 (m)
 v= 0,00000101 (m²/s)
 g= 9,81 (m/s²)
 P₁= 3,14285714285714 (-)
 N= 34 (-)

OUTPUTS:

Step Number	x(DON)	vrel(DON)	hrel(DON)	qrel(DON)	R(DON)
1	0	1,	2,018	1,421	326,962,315
2	12	,958219622	1,887	1,374	313,301,706
3	24	,917819232	1,756	1,325	300,092,301
4	36	,878842255	1,636	1,279	287,348,299
5	48	,841227968	1,524	1,235	275,049,844
6	60	,804957029	1,421	1,192	263,277,532
7	72	,769893242	1,327	1,152	251,712,377
8	84	,735974083	1,239	1,113	240,635,79
9	96	,703229225	1,159	1,077	229,929,154
10	108	,671563021	1,085	1,042	219,575,8
11	120	,640920927	1,018	1,009	209,556,99
12	132	,611250548	,956	,978	199,855,894
13	144	,582500085	,899	,948	190,455,576
14	156	,554618396	,847	,92	181,339,38
15	168	,527555963	,799	,894	172,490,929
16	180	,501262875	,756	,869	163,894,07
17	192	,475690813	,717	,847	155,532,969
18	204	,450792063	,681	,825	147,392,017
19	216	,426519734	,649	,806	139,455,88
20	228	,402827793	,62	,787	131,709,508
21	240	,379671117	,594	,771	124,138,148
22	252	,357005562	,571	,755	116,727,365
23	264	,334788044	,55	,742	109,465,074
24	276	,312976641	,532	,729	102,331,567
25	288	,2915307	,516	,718	95,319,553
26	300	,270409189	,502	,708	88,413,615
27	312	,249576254	,49	,7	81,602,03
28	324	,228997405	,479	,692	74,873,522
29	336	,208659657	,47	,686	68,217,305
30	348	,188472674	,463	,68	61,623,135
31	360	,16846392	,457	,676	55,081,35
32	372	,148598764	,452	,672	48,582,926
33	384	,128820722	,448	,669	42,119,522
34	396	,109136511	,	,667	,

Ş 1, Şm 1

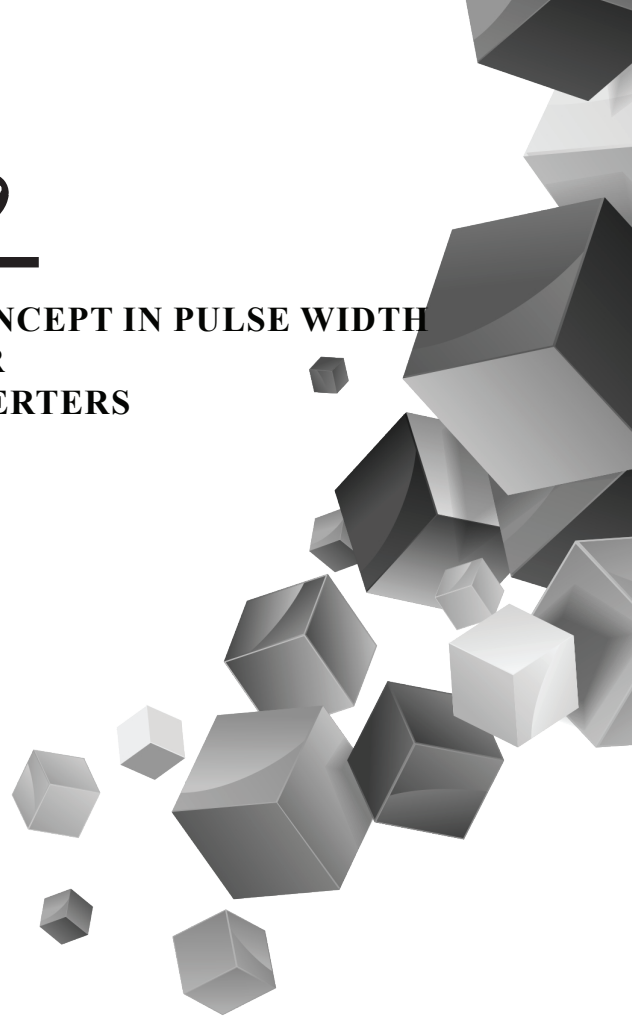
Figure 3. Inputs and Outputs from Computer Program (Multi-flowCAD) for Sample Design Application

New Manifold Design Project.TXT - Not Defteri			
Dosya Düzen Biçim Görünüm Yardım			
New Project: Manifold Design Multi-flowCAD) Manifold Flow Hydraulics Computations			
Outputs (Required Hydraulics Variables):			Date Created: 28.01.2014
Step Number	H(DON)	Q(DON)	qp(DON)
1,	95,75	,013124	,00054832568
2,	89,529	,01257567	,00053021471
3,	83,332	,01204546	,00051153385
4,	77,607	,01153393	,0004936499
5,	72,322	,01104028	,0004765449
6,	67,446	,01056373	,00046020195
7,	62,952	,01010353	,00044460515
8,	58,813	,00965892	,00042973957
9,	55,004	,00922918	,0004155912
10,	51,503	,00881359	,00040214684
11,	48,288	,00841145	,00038939406
12,	45,34	,00802205	,00037732108
13,	42,641	,00764473	,00036591666
14,	40,173	,00727881	,00035516999
15,	37,921	,00692364	,0003450705
16,	35,87	,00657857	,00033560774
17,	34,005	,00624297	,00032677119
18,	32,316	,0059162	,00031855004
19,	30,789	,00559764	,00031093303
20,	29,413	,00528671	,00030390822
21,	28,179	,0049828	,00029746275
22,	27,076	,00468534	,0002915827
23,	26,095	,00439376	,00028625286
24,	25,228	,00410751	,00028145652
25,	24,471	,00382605	,00027719871
26,	23,806	,00354885	,00027341145
27,	23,229	,00327544	,00027007681
28,	22,733	,00300536	,00026717508
29,	22,311	,00273819	,00026468462
30,	21,958	,0024735	,00026258189
31,	21,668	,00221092	,00026084142
32,	21,435	,00195008	,00025943578

Figure 4. Inputs and Outputs from Computer Program (Multi-flowCAD) for Sample Design Application

Chapter 18

SOFT SWITCHING CONCEPT IN PULSE WIDTH MODULATION POWER ELECTRONICS CONVERTERS



Yakup SAHIN

Naim Suleyman TING¹

¹ Assistant Prof., Bitlis Eren University, Department of Electrical Electronics Engineering, ysahin@beu.edu.tr ²Associate Prof., Erzincan Binali Yildirim University, Department of Electrical Electronics Engineering, nsuleyman@erzincan.edu.tr

Power electronics converters widely used in power plants, electrical vehicles, power factor correction applications and uninterruptible power supplies. These converters convert the energy into different forms as AC or DC by using semiconductor devices such as transistors and diodes. The conventional hard switching converters that illustrated in in Fig. 1, suffers from bulky and heavy filter components as filter inductance and filter capacitance. Because of unfavorable filter components, the power converters cannot be used in the mobile systems easily. For instance, on account of onboard charge systems are taken place on the electrical vehicles, the volume and weight of charger is quite important for the vehicle range. Consequently, the volume of power converters should be reduced for the preferable industrial applications.

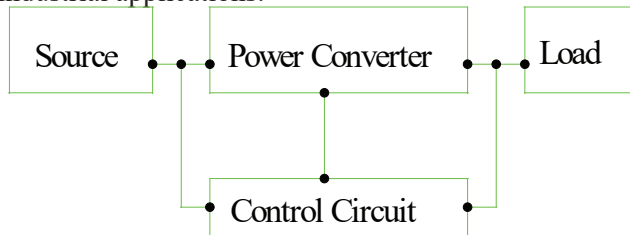


Figure 1. *Power conversion of simple power circuit.*

The power density of converters can be expressed as volume W/cm^3 or W/kg and the switching frequency of converter should be increased for increasing the power density. However, electromagnetic interference (EMI) and the switching power losses are increased when the switching frequency is increased. The switching power losses reduce the total efficiency of converter and lead high temperature. EMI creates noise and this noise disturbs both the control of converter and the devices near converter. To acquire higher power density, instead hard switching (HS) technique, the soft switching (SS) techniques should be applied.

The Scope of Soft Switching Technique

Soft switching aims to reduce EMI noises and switching power losses to obtain higher power density. The switching power losses occur while the power semiconductor is turned off and turned on. When the power transistor is turned on, the voltage of transistor starts to decrease and its current starts to increase during the rise time. The overlap of voltage and current of transistor leads turning on switching power losses. Similarly, the voltage of transistor starts to increase and its current starts to decrease during the fall time. Consequently, the turning of switching power losses occurs because of overlap the voltage and the current. The switching power losses are illustrated in Fig. 2 where include turning off and turning on switching

power losses. The switching power losses reduces total efficiency of the converter. Furthermore, fast switching leads RLC effects on the PCB ways and this concept causes EMI in the converter. To eliminate hard switching issues, soft switching techniques should be used instead hard switching.

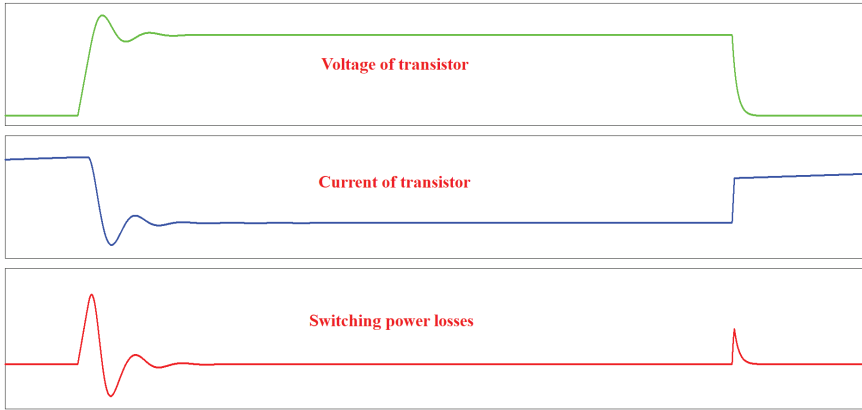


Figure 2. *The switching power losses of semiconductor transistor.*

1. Soft switching techniques

Soft switching techniques can be separated into two section as conventional techniques and advanced techniques.

1.1. Conventional soft switching techniques

The conventional soft switching techniques include two techniques as Zero Current Switching (ZCS) and Zero Voltage switching (ZVS). ZCS technique aims to reduce switching power losses at the turning on process while ZVS at the turning off process. In ZCS technique is illustrated in Fig. 3 (a), a series inductance is connected to semiconductor transistor and rising of transistor current is slowed down. Thence, the turning on switching power losses is reduced since the overlap of voltage and current of transistor is limited. A parallel capacitance is connected across the transistor to provide ZVS and ZVS application is presented in Fig. 3 (b). The rising of transistor voltage is slowed down by parallel capacitance when the transistor is turned off. Thus, the switching power losses at the turning off process is reduced by ZVS because of the overlap transistor voltage and current is limited.

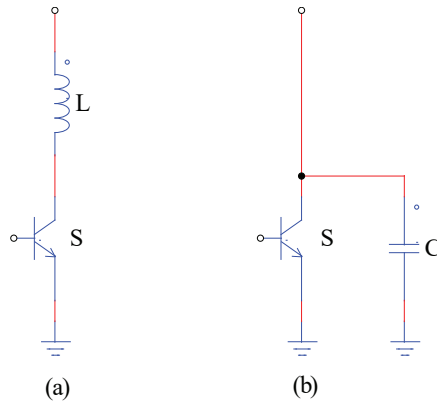


Figure 3. The Conventional SS techniques (a) Zero current switching (b) Zero voltage switching.

A simple ZCS-ZVS passive snubber PWM DC-DC buck converter (Bodur at al., 2003) is presented in Fig. 4 and the current and the voltage waveforms of transistor is illustrated in Fig. 5. It is clear from Fig. 5 where the transistor is turned on by ZCS since the current of transistor slowed down by series snubber inductance L_s . At the same time, the transistor is turned off by ZVS because the voltage of transistor is slowed down by parallel snubber capacitances C_{S1} and C_{S2} . ZVS reduces turning off switching power losses and ZCS reduces turning on switching power losses since the overlap voltage and current is limited.

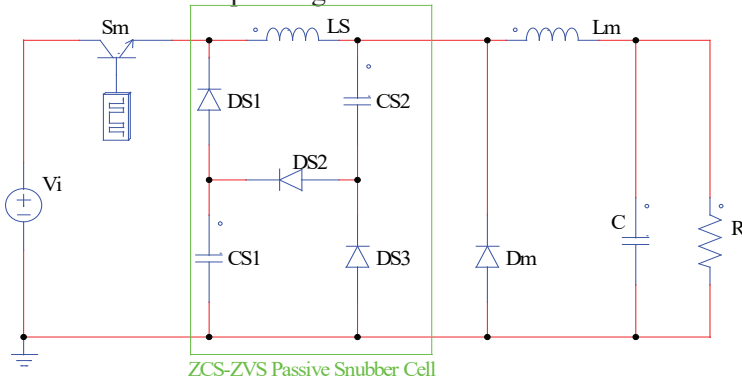


Figure 4. ZCS-ZVS passive snubber PWM DC-DC Buck converter.

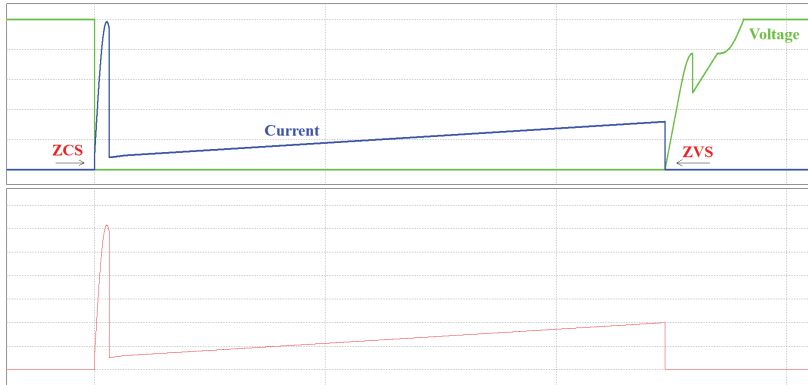


Figure 5. Voltage and current waveforms of transistor in ZCS-ZVS passive snubber PWM DC-DC buck converter.

Although the passive snubber cells has simple structure and cheap cost, the voltage or current stress occurs on the main or auxiliary semiconductor elements. Therewith, the cost of main semiconductor devices is increased slightly. Besides, the switching power losses of semiconductor devices cannot eliminate completely. To eliminate switching power losses completely and have better efficiency, instead conventional soft switching techniques, the advanced soft switching techniques should be used.

1.2. Advanced Soft Switching Techniques

The advanced soft switching techniques aims eliminate switching power losses completely and provide higher converter efficiency conventional soft switching or hard switching. The advanced soft switching techniques can be separated into two section as Zero Current Transition (ZCT) and Zero Voltage Transition (ZVT). Contrary passive snubber cells, advanced snubber cells include an active semiconductor device as MOSFET or IGBT.

1.2.1. Zero Voltage Transition (ZVT)

The first advanced soft switching technique introduced to literature is Zero Voltage Transition (ZVT) (Hua at al., 1994) presented in Fig. 6 and also, the current and voltage waveforms of main switch (S_m) is illustrated in Fig. 7. ZVT snubber cells aim to eliminate turning on switching power losses completely by an active semiconductor transistor.

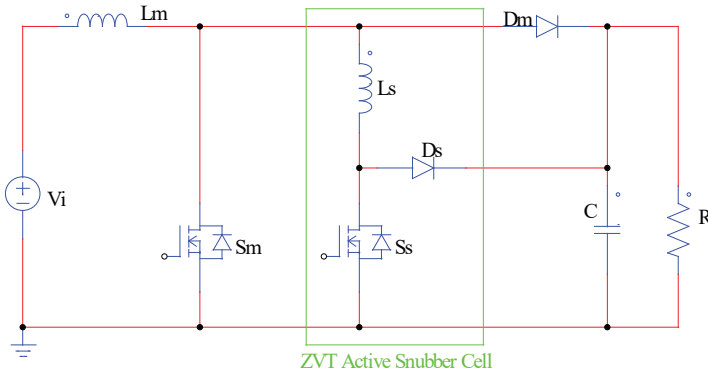


Figure 6. ZVT PWM DC-DC boost converter.

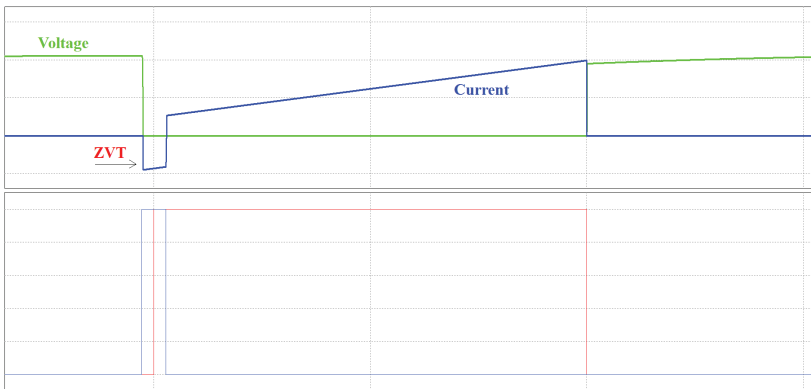


Figure 7. Voltage and current waveforms of main switch in ZVT PWM DC-DC boost converter.

In ZVT PWM DC-DC boost converter, before the control signal performed to the gate of main switch S_m , the voltage of main switch falls to zero by active snubber cell as can be seen in Fig. 7. Subsequently, the control signal of main switch performed while the internal diode of main switch is on-state. Because of the voltage and current are not overlapped at the turning on process, the turning on switching power losses are eliminated completely by aid of ZVT snubber cell.

The parasitic capacitance energies should be recovered in an advanced soft switching technique. A MOSFET has a parasitic capacitance between drain and source and the parasitic capacitance energies in the converter can be recovered by ZVT technique. ZVT technique can recover parasitic capacitance energies and eliminate switching power losses completely. So, ZVT snubber cell provide pretty good efficiency. Because of MOSFETs has large parasitic capacitance, ZVT technique applications is suitable for MOSFETs.

1.2.2. Zero Current Transition (ZCT)

Zero Current Transition (ZCT) PWM DC-DC boost converter (Hua at al., 1994) introduced to literature. ZCT snubber cell presented in Fig. 8 and the current and voltage waveforms of S_m are illustrated in Fig. 9.

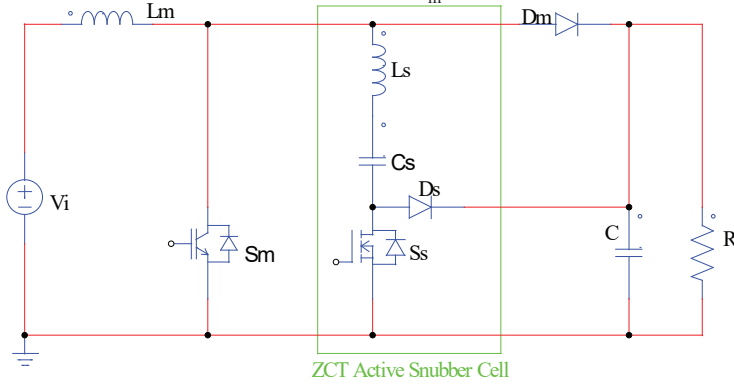


Figure 8. ZCT PWM DC-DC boost converter.

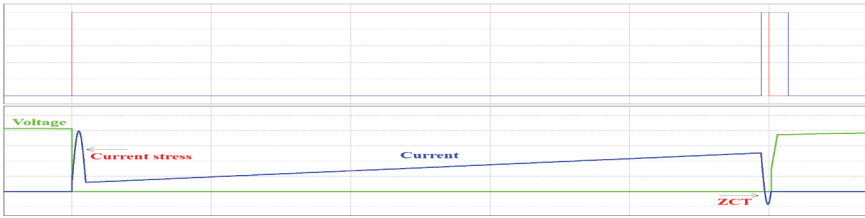


Figure 9. Voltage and current waveforms of main switch in ZCT PWM DC-DC boost converter.

ZCT technique aims to eliminate power losses completely at turning off process. In the PWM DC-DC boost converter, while the main switch is on-state, the gate signal of auxiliary switch is performed and a resonance starts between snubber inductance L_s and snubber capacitance C_s . the current of main switch falls to zero and then the internal diode of main switch is turned on since a negative current flows in S_m . The gate signal of S_m is removed when the current and voltage of S_m is zero. Thus, the turning off switching power losses of S_m is eliminated completely because the current and voltage of S_m are not overlapped.

Although ZCT technique eliminates turning off switching power losses completely, it cannot reduce turning on switching power losses. Also, current stress consists on S_m because of the resonance.

IGBTs has tail current when they are turned off. In this reason, ZCT technique suitable for IGBTs.

1.2.3. Zero Current-Zero Voltage Transition (ZCZVT)

Zero current-zero voltage transition (ZCZVT) combines both zero current transition (ZCT) and zero voltage transition (ZVT). Also, it can be seen as ZVZCT in the literature sometimes and it means same mean ZCZVT. ZCZVT aims not only to overcome the disadvantage of both ZCT and ZVT technique but also has advantages of these techniques. As mentioned above, ZVT technique eliminates the turning on switching losses perfectly but the turning off switching losses occur on the switch. Similarly, ZCT technique eliminates the turning off switching losses completely however switching losses occur on the switch at the turning on process. ZCZVT technique aims to eliminate both the turning off switching losses and the turning on switching losses simultaneously for semiconductor switch. A ZCZVT PWM DC-DC boost converter (Sahin and Ting, 2018) is presented in Fig. 10 and the waveforms of S_m in the converter is illustrated in Fig. 11.

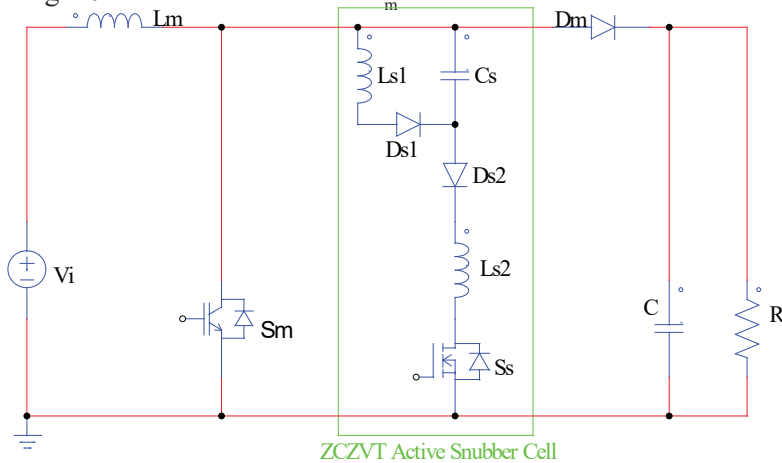


Figure 10. ZCZVT PWM DC-DC boost converter.

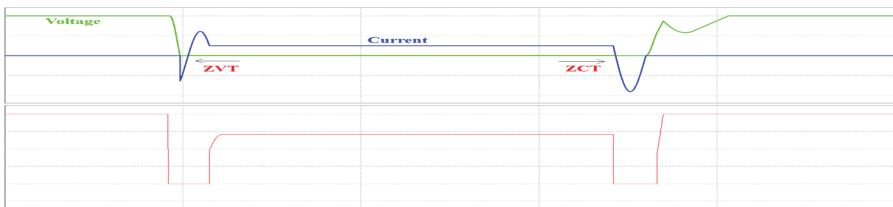


Figure 11. Voltage and current waveforms of main switch in ZCZVT PWM DC-DC boost converter.

In ZCZVT PWM DC-DC boost converter, as illustrated in Fig. 11, S_m is turned on by ZVT and the turning on switching power losses are eliminated completely at the turning on process. Similarly, S_m is turned off by ZCT and the turning off switching losses are eliminated completely at

the turning off process. The main switch has a fair current stress and does not has voltage stress.

The conventional (passive) and the modern (active) snubber cells are compared from many perspectives and the analyzes are presented in Table 1. As can be seen in the table, the modern snubber cells has more advantages compared with conventional snubber cells.

Table 1. Comparison of conventional and modern snubber cells.

	Passive Snubber	ZVT snubber	ZCT snubber	ZCZVT snubber
Need an auxiliary switch	No	Yes	Yes	Yes
Voltage stress on the S_m^*	No	No	No	No
Current stress on the S_m	High	No	High	No
Voltage stress on the S_s^{**}	No S_s	No	No	Low
Current stress on the S_s	No S_s	Low	High	High
Turning on Power losses on S_m	Reduced	Eliminated	High	Eliminated
Turning off Power losses on S_m	Reduced	High	Eliminated	Eliminated
Turning on Power losses on S_s	No S_s	No	No	No
Turning off Power losses on S_s	No S_s	High	No	No
Ease of control	Simple	Medium	Medium	Complex
Structure	Simple	Medium	Medium	Complex
Circulation losses	Medium	Ultra Low	Medium	Medium
Cost of snubber cell	Cheap	Medium	Medium	Expensive
Need for passive snubber cell	No	Yes	Yes	No
EMI on the converter	No	Low	Medium	No
Recovering of switching power losses	No	Low	No	Perfect
Saving PWM operation at high frequency	Bad	Good	Good	Medium
Operation at light loads	Bad	Medium	Good	Very good
Efficiency	Low	Medium	Medium	Perfect
Operation at high frequency	No	Yes	Yes	Yes
Operation at wide range load conditions	No	Yes	Yes	Yes
Recovering of parasitic capacitance energies	No	Yes	No	Yes
Reducing of reverse recovery power losses of the main diode	No	Yes	No	yes
Power density	Low	High	High	High
Dynamic response	Low	High	High	High

* S_m : Main switch, ** S_s : Auxiliary switch

2. Power Loss Calculation

In a power electronics converter, power losses can be separated in three sections which are fixed losses, conduction losses and switching losses. Fixed losses are control circuit losses that PWM control circuit is needed for turning on and turning off the power switch. Further, feedback circuit where occurs from resistance and operational amplifiers. Fixed losses cannot be affected and changed, therefore, they are static and independent from load current and frequency. Conduction losses are depending on-resistance and forward voltage drop of semiconductor switch and diode. Also, the copper resistance of inductance and internal resistance of capacitance create power losses and they are included to conduction losses. Finally, PCB copper losses are included to conduction losses as well. Conduction power losses are independent of switching frequency but output current. Switching power losses include power switch turning off and turning on losses and reverse recovery power losses of diode. Furthermore, the gate driver losses are included to switching power losses. Switching power losses depend on both switching frequency and output current.

2.1. Fixed Power Loss Calculation

There is no known method for calculating fixed power losses in power electronics converter. Fixed losses can be obtained when the switching power losses and the conduction losses are subtracted from total power losses.

2.2. Conduction Power Loss Calculation

The conduction power loss of MOSFET is depended on on-resistance of MOSFET. Also, the conduction power loss of IGBT is depended on Collector-Emitter Saturation Voltage of IGBT. Finally, the conduction power loss of diode is depended on Forward Voltage Drop of the diode.

Conduction power loss of a MOSFET can be calculated as follow.

$$P_{ConS} = I_o^2 R_{DSon} \frac{V_o}{V_{in}} \quad [W] \quad (1)$$

P_{ConS} : Conduction power loss of MOSFET

I_o : Output current

R_{DSon} : MOSFET on-state resistance

V_o : Output voltage

V_{in} : Input voltage

Conduction power loss of a diode approximately can be calculated as follow.

$$P_{ConD} \cong V_F I_{AV} \quad [W] \quad (2)$$

P_{ConD} : Conduction power loss of diode

V_F : Diode forward voltage

I_{AV} : Diode average current

2.3. Switching Power Loss Calculation

Switching power losses of MOSFET include turning off switching loss and turning on switching loss. Complete switching losses of MOSFET is calculated using following formulas.

$$P_{SWon} = \frac{1}{2} V_{in} I_o t_r f_{sw} \quad [W] \quad (3)$$

$$P_{SWoff} = \frac{1}{2} V_{in} I_o t_f f_{sw} \quad [W] \quad (4)$$

$$P_{SWtot} = P_{SWon} + P_{SWoff} \quad [W] \quad (5)$$

P_{SWon} : Turning on switching loss of MOSFET

P_{SWoff} : Turning off switching loss of MOSFET

P_{SWtot} : Total switching loss of MOSFET

t_r : Rise time

t_f : Fall time

f_{sw} : Switching frequency

Gate charge loss of MOSFET is calculated as follows.

$$P_{Gate} = Q_G V_G f_{sw} \quad [W] \quad (6)$$

P_{Gate} : Gate charge power loss of MOSFET

Q_G : Total gate charge

V_G : Gate-to-source voltage

3. Comparison of Hard Switching and Soft Switching PWM DC-DC Boost Converter

To show how switching power losses affect the total efficiency of the converter, hard switching PWM DC-DC Boost converter circuit presented in Fig. 12 is setup.

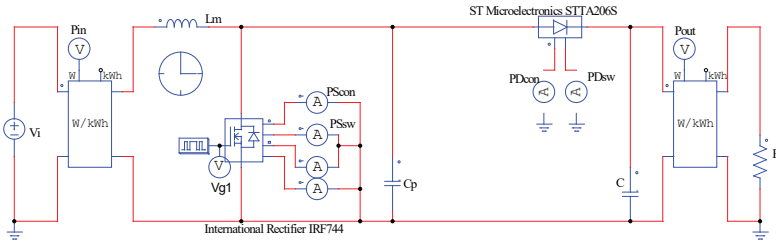


Figure 12. Hard switching PWM DC-DC boost converter.

Subsequently, ZCZVT soft switching snubber cell is connected to hard switching PWM DC-DC boost converter and then both converters are analyzed. ZCZVT PWM DC-DC boost converter is presented in Fig. 13.

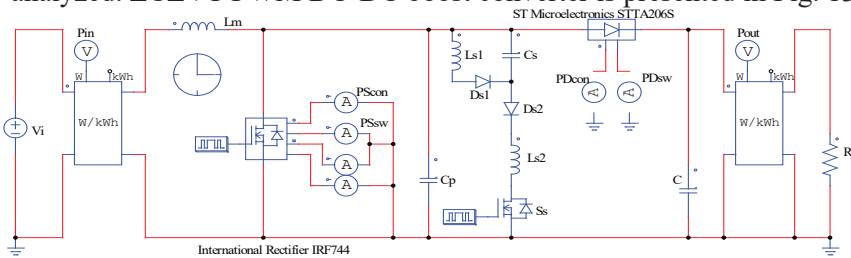


Figure 13. ZCZVT PWM DC-DC boost converter.

Both soft switching and hard converters are simulated in PSIM software and comparative analysis is presented in Table 2.

Table 2. Comparison of hard switching and soft switching PWM DC-DC boost converters.

ZCZVT PWM DC-DC Boost Converter Parameters								
Switch	Loss	Diode	Loss	Total Pcon and Psw	Other losses	Total losses	Efficiency	Output Power
Pcon	1.37 W	Pcon	1.8W	3.17 W	1.76 W	5 W	99%	500W
Psw	66 mW	Psw	4.9mW	70.9 mW				
Hard Switching ZCZVT PWM DC-DC Boost Converter Parameters								
Switch	Loss	Diode	Loss	Total Pcon and Psw	Other losses	Total losses	Efficiency	Output Power
Pcon	1.29 W	Pcon	2.21W	3.5 W	1.62 W	12 W	97.6%	500W
Psw	5.64W	Psw	1.24W	6.88 W				

Compared with hard switching PWM boost converter, it is clear from Table 2 that ZCZVT PWM boost converter has higher efficiency

at nominal output power. In an experimental application, hard switching PWM boost converter cannot be operated at this simulation condition since the operating frequency of converter is 100 kHz. At high switching frequency, the total losses of switch and diode rise and the temperature of semiconductors are raised. Consequently, the semiconductor devices are destroyed.

REFERENCES

- Bodur, H., Bakan, A. F., Baysal, M. (2003). A detailed analytical analysis of a passive resonant snubber cell perfectly constructed for a pulse width modulated d.c.–d.c. buck converter, *Electrical Engineering*, 85(1):45-52.
- Hua, G., Leu, C. S., Jiang, Y., Lee, F. C. Y. (1994). Novel Zero-Voltage-Transition PWM Converters, *IEEE Transactions on Power Electronics*, 9(2):213-219.
- Hua, G., Yang, E. X., Jiang, Y., Lee, F. C. Y. (1994). Novel Zero-Current-Transition PWM Converters, *IEEE Transactions on Power Electronics*, 9(6):601-606.
- Sahin, Y., Ting, N. S. (2018). A New Soft-Switched ZCZVT-PWM DC-DC Boost Converter, *Süleyman Demirel University Journal of Natural and Applied Sciences*, 22(2):435-442.

Chapter 19

CHANGE IN KEY MECHANICAL DESIGN QUANTITIES OF BI-2212 SUPERCONDUCTING SYSTEM WITH VARIOUS ANNEALING AMBIENT



*Asaf Tolga ULGEN¹
Gürcan YILDIRIM²*

1 Assoc.Prof, Sırnak University, Department of Electric-Electronic Engineering, Sırnak–Turkey, 73000

2 Assoc.Prof, Abant İzzet Baysal University, Department of Mechanical Engineering, Bolu–Turkey, 14280

1. INTRODUCTION

Materials science is known to be one of the most important branches of science and technology due to the usage in several application areas such as natural sciences, engineering astronomy, astrophysics, medicine, spintronics, refrigeration, particle accelerator, hydrogen society, pharmacology, veterinary, food, dentistry, power transmission, machine, mechatronics, buildings, electric and electronics, computer, textile, industry, radio and television technology, opto-electronics, heavy-industrial technology, electro-optic and innovative energy infrastructure a (whatever comes to our mind in daily life) [1–6]. Especially, nowadays we begin to frequently encounter the superconducting materials in a number of application fields. As well known that phenomenon of superconducting nature was initially discovered for mercury metal by Onnes in 1911 [7]. The phenomenon is shortly divided in two fundamental features: (I) exactly zero electrical resistivity at a certain lower temperature defined as the critical temperature for the transition and (I) expulsion of magnetic fluxoids at certain external magnetic field strengths [8]. During more than a century later, the scientists have endeavored to improve their fundamental identification properties; viz. the electrical, crystal structure, flux pinning, physical, opto-electronics, structural, morphological, superconducting, and especially mechanical performance and characterization due to the fact that the compounds can find much more application fields in technology, industry, motors, medicine and large-scale applications for the energy sectors [9–13]. It is to be mentioned here that of the characteristic features, the mechanical design performance is the most important aspect of every application area such as the metallurgical, technological, biological engineering and industrial fields for the materials [14–16]. Accordingly, it is not a surprising result from the explanations given above that the development in the mechanical performances has physically occupied several central positions for the application areas for the Bi-based solid compounds. The question appears here that how we can improve the fundamental mechanical design performance and mechanical characterization due to the fact that the Bi-containing superconducting ceramic compound parents with their inherit brittleness-fault feature and highly susceptible to cracking make some difficulties and faults for the technological, engineering and industrial application fields [17]. On this basis, the main aim should be to overcome the brittleness-fault feature. Once the omnipresent flaws related to the crack initiation sites, stress raisers and surface cracks in ceramic compounds can be eliminated in the crystal structure belonging to these kinds of materials, the key mechanical design features as regards the mechanical strength, stiffness, durability, ductility, hardness, toughness, fracture and especially flexural strengths can reach their maximum points due to the diversion or deceleration of

crack propagation, crack-producing flaws and dislocation movement. The considerable increment in the mechanical performance enables the mechanical engineers and scientists to pay much more attention to a new question about the application fields including the future heavy-industrial technology, electro-optic and innovative energy infrastructure application fields [18–24]. To sum up, the improvement in the mechanical performance of Bi-based superconducting parents is inevitably reality for the appearance of compounds in future application fields. In the current work, we search the effect of annealing ambient temperature (range from 830 °C to 850 °C) and time (24-48 h duration) on the mechanical performance features and mechanical identification of bulk Bi-2212 samples by making the micro hardness experimental tests at different indentation test loads (0.245 N-2.940 N). According to the results, the annealing ambient combination including the annealing temperature value of 840 °C and annealing time of 24 h is found to be the best annealing environment to improve the mechanical performance features and much more resist to the applied loads.

2. EXPERIMENTAL DETAILS FOR PURE AND BI-SITE GD PARTIAL SUBSTITUTED BI-2212 CERAMICS

The current work is the continuation of a systematic study of Bi-2212 superconducting ceramic compounds prepared at the different annealing conditions (830-850 °C annealing temperature and 24-48 h annealing time). In this work, we investigate the vital variations in the fundamental mechanical design performance and mechanical characterization via the microhardness test measurements conducted at the various applied loads of 0.245N-2.940N at the room-state temperature in air atmosphere. Shortly, we produce 9 different compounds within the chemical formula of $\text{Bi}_{2.1}\text{Sr}_{2.0}\text{Ca}_{1.1}\text{Cu}_{2.0}\text{O}_y$ with the assistant of standard solid-state reaction method. Firstly, all the chemical powders including the carbonates and oxides of CaCO_3 , CuO , SrCO_3 and Bi_2O_3 with higher purity value ($\geq 99.9\%$) are purchased from Alfa Aesar product distributor, and shortly after are accurately weighed within the grinding proportion of Bi: 2.1, Sr: 2.0, Ca:1.1, Cu:2.0 and O:y with the use of electronic balance in the medium of air. After, the chemicals of powder are grounded by a grinder machine for the duration of 9 h to possess homogenous mixture of powders. In order to obtain the desired particle sizes of chemicals, the homogenous mixture is pulverized in an agate mortar by a grinder for 30 minutes duration. The resultant powder is calcined at 800 °C for 36 h in a furnace at the heating-cooling rates of 5 °C/min under air atmosphere in the porcelain crucibles to remove the foreign particles, carbon related residuals (leading to the impurity phase) from the homogenous mixture. The calcined powder is removed from the furnace and reground in the agate mortar during the time of 30 min at the medium of air pressure. The last powder is pelletized into a rectangular bar with the volume size of $1.5 \times 0.5 \times 0.2 \text{ cm}^3$ in case of

300 MPa load during 5 min at room temperature in order to strengthen to bond the atoms with together. The bulk samples are separately sintered at the different annealing conditions, viz. annealing temperature between 830°C and 850 °C with the with the variation of every 10 °C and 24-48 h annealing time with the step of 24 h.

The differentiation of fundamental mechanical performances and mechanical characterization with the annealing temperature and annealing time of $\text{Bi}_{2.1}\text{Sr}_{2.0}\text{Ca}_{1.1}\text{Cu}_{2.0}\text{O}_y$ superconducting materials is searched with Vickers hardness tests based on SHIMADZU HVM-2 model digital microhardness tester under the indentation loads range of 0.245N-2.940N at the room-state temperature in air atmosphere. Every experimental measurement result is taken three times at the different places (due to the avoidance of hardening problems accumulated on the surface during the Vickers hardness measurements) for the duration of 10 seconds to increase the reliability (possessing the optimum microhardness parameters). A calibrated microscope is used to measure the diagonal tracks on the material surface. According to the diagonal lengths, we determine the variation of microhardness parameters with the annealing ambient (temperature and time) using the standard formulas present in the literature (will be discussed in the following sections in detail). Moreover, the microhardness values enable us to find other mechanical performance parameters, namely, fracture toughness (K_{IC}), ductility (D), Young's modulus (E), yield strength (Y) brittleness index (B), and elastic stiffness (C_{II}) coefficients. Lastly, we define the role of annealing ambient on the mechanical characteristic features founded on the typical indentation size (called as *ISE*) and reverse indentation size effect (named as *RISE*) feature pertaining to every superconducting ceramic sample under the applied test loads [25–27].

3. RESULTS AND DISCUSSION

Variation of Key Mechanical Design Parameters Founded on Micro Hardness Measurements

In the present work, we will discuss the differentiation of mechanical performances and corresponding experimental results of Bi-based superconducting samples produced with the annealing temperature (830°C-850 °C) and time (24-48h) via Vickers microhardness experimental measurements performed at the varied test loads between 0.245 N and 2.940 N. The recorded test findings are discussed in three main parts. (I) Definition of the best annealing ambient (temperature and time) for the pure Bi-2212 superconducting material exhibiting the highest mechanical performances and determination of a strong link between the structural deformation problems (crystal structure problems, porosity, voids, cracks,

disorders, strains, lattice strains, defects, distortions, crack-producing omnipresent flaws, grain alignment distributions and coupling problems between grain boundaries) founded on the production conditions and mechanical performances (mechanical durability, impact resistance, ductility, hardness, brittleness index, tensile and yield strength, stiffness, toughness, fracture, fatigue, modulus of elasticity and especially flexural strengths). On this basis, we discuss the role of annealing ambient on the active operable slip systems, crack initiation sites and stress raisers affecting directly the crack propagation and dislocation movement in the Bi-2212 crystal system. (II) Description of mechanical characteristic behaviors (*ISE* and *RISE*) of materials produced and determination of the change in the mechanical characteristic behavior with the different annealing ambient. (III) Expression of load-independent key mechanical design parameters such as K_{IC} , D , E , Y , B , and C_{II} parameters with the experimental micro hardness curves.

One can see the change in the micro hardness parameters over the test loads applied ($0.245\text{N} \leq F \leq 2.940\text{N}$) in Fig. 1 in detail for all the Bi-2212 superconducting ceramic materials prepared at the different annealing ambient conditions. It is obvious that the micro hardness parameters directly related to the mechanical performance are found to depend strongly on the annealing ambient (especially annealing temperature). It is well known that the general characteristic properties of bulk Bi-2212 compounds are seriously improved or degraded by the several factors as regards the ionic radius of dopant, magnetic dipole moment of dopant (especially under external magnetic field), formation of bonding between the atoms, different chemical valence and thus various electron configurations of outer Shell, easier integration with the surrounding atoms and particularly structural deformation problems (known as the crystal structure problems, porosity, voids, cracks, disorders, strains, lattice strains, defects, distortions, crack-producing omnipresent flaws, grain alignment distributions and coupling problems between the grain boundaries) in the bulk Bi-2212 crystal system. Among the factors mentioned above, the main reason for the change in the key mechanical design quantities and operable slip systems of our samples seems to be the structural deformation problems founded on the annealing ambient conditions. In this respect, the sample prepared at 840 °C annealing temperature and 24 hours annealing time exhibits the best mechanical performance features whereas the Bi-2212 superconducting ceramic material produced at the annealing ambient of the temperature of 850 °C and time of 48 h shows the lowest key mechanical design quantities. It is clear that the annealing ambient affects sensitively the durable tetragonal phase and the critical stress value of bulk Bi-2212 crystal system. It is stressed that the excess annealing ambient considerably induces permanently the crack initiation sites and stress raisers in the crystal system, hence the

flaws, voids, cracks and dislocations within the critical propagation speed propagate rapidly. Thus, the excess annealing temperature and period lead to make out of control for the dislocations and cracks. Namely, the Bi-2212 superconducting compound prepared by the excess annealing ambient is much easier broken in comparison with the materials produced with the optimum annealing temperature and period. Now, we will focus sensitively on the numerical values for the mechanical design quantities.

The Vickers hardness parameters (H_v) pertaining to the bulk Bi-2212 ceramic compounds are evaluated from a general formula of $H_v = 1854.4(\frac{F_{load}}{d^2})$ and all the computations are depicted graphically in Fig. 1. According to the relation, F_{load} displays the test load applied when d illustrates the mean diagonal length of tracks. The curves obtained allow us to picture the influence of annealing ambient on the micro hardness parameters for the Bi-2212 superconducting materials. On this context, we also give every numerical calculation related to the Vickers hardness in Table 1 in detail. It is apparent that the micro hardness parameters are sensitively dependent on the annealing ambient. That is to say, the H_v parameters are found to be about 3.0503 GPa, 3.4194 GPa and 2.9213 GPa at the constant indentation load of 0.245N the superconducting compound prepared at 830 °C annealing temperature for the different annealing period of 24 h, 36 h and 48 h while the H_v values of 3.5727 GPa, 3.2117 GPa and 2.7457 GPa ascribe to the bulk Bi-2212 samples produced at 840 °C temperature for varied annealing periods of 24 h, 36 h and 48 h. Besides, the compounds fabricated at the annealing temperature value of 830 °C for the different annealing time of 24 h, 36 h and 48 h exhibit the H_v values of 2.9027 GPa, 2.4977 GPa and 2.4021, respectively. One can easily realize the similar trends for the H_v parameters at any applied test loads. According to the results, similar to the maximum H_v value of 3.5727 GPa at 0.245N indentation test load, the same sample (produced at 840 °C annealing temperature for 24 h annealing time) presents the highest H_v values at any test loads applied. Conversely, the minimum H_v parameters are observed for the compound prepared at the excess annealing ambient as regards 850 °C annealing temperature for 48 h annealing time. On this basis, the smallest value (1.9424 GPa) is measured for the compound (850 °C for 48 h) at 2.940 N test load applied. The considerable change in the H_v parameters is directly related to the formation of new permeant structural deformations in the bulk Bi-2212 crystal system. Moreover, it is another probable result evaluated from the numerical values in Table 1 that the H_v values determined are found to decrease significantly with the augmentation in the test loads applied up to the highest level of 2.940 N. This means that the applied test load much harder tracks on the surface of specimen (840 °C for 24 h) as compared to those of other ones due to the rapid suppression in the local structural deformations in the crystal lattice. On the other hand, the applied

test load much easier damages the bulk Bi-2212 superconducting material prepared at the annealing combination of 850 °C temperature and 48 h period due to the enhancement of permanent structural deformations in the crystal system. Thus, it is not wrong to confirm that the excess annealing ambient directly harms on the mechanical performance and mechanical sensitivity founded on the Bi-2212 crystal structure.

The differentiations of Vickers micro hardness against the applied test load curves enable us to determine the fitting equations including the change between applied load and micro hardness values so that we can easily discuss the effect of annealing ambient on the mechanical performance of Bi-2212 superconducting materials. The fitting parameters (deduced from Fig. 1) are gathered numerically in Table 2 where one can see all the variation terms of x^4 in the range from 0.05853 (for the sample prepared at annealing temperature of 840 °C and annealing time of 24 h) to 0.23955 (for the Bi-2212 compound produced at excess annealing ambient of 840 °C annealing temperature and 24 h annealing time). It is shown that the optimum annealing ambient (840 °C for 24 h) makes the Bi-2212 superconducting material degrade the mechanical sensitivity (called as the load-dependence) whereas the mechanical sensitivity characteristic feature reaches to the maximum value for the Bi-2212 superconducting material produced at the annealing temperature of 850 °C for the duration of 48 h. This is attributed to the enhancement of mechanical sensitivity feature of Bi-2212 compound due to the rapid increment of structural problems in the crystal lattice. Hence, the movements belonging to the flaws, dislocations, and cracks in the material (850 °C for 48 h) highly increase at any small test load applied as compared to those in the others.

Moreover, with the re-check of the differentiations in the Vickers hardness parameters over the applied indentation test load curves, it is easy to realize that the Vickers hardness values tend to reduce significantly with increasing the test load applied until such a value of about 2 N (see Fig. 1). It is apparent that the H_v values reach to the saturation limit region due to the presence of permanent structural deformations in the Bi-2212 crystal system and after the critical test load value (≈ 2 N) any enhancement in the magnitude of indentation test load hardly any change meaningfully the micro hardness parameters. Figure 1 declares that of the bulk Bi-2212 superconducting materials the bulk sample prepared at 840 °C for 24 h reaches to its plateau region at further higher indentation test load value while the compounds produced at 850 °C for 48 h locates in the saturation limit region at rather lowest test loads because of the decreased critical stress, mechanical strength and durability founded on new induced crack initiation sites and stress raisers. In so doing, the micro hardness values of sample (850 °C for 48 h) rapidly degrade at relatively small test load applied. It is well known that an applying test load in the saturation region

is one of the most used methods to learn the load real (independent or true) micro hardness values for a material. Accordingly, the sample prepared at 840 °C (850 °C) annealing temperature for 24 h (48 h) duration has the maximum (minimum) real Vickers values

Role of Annealing Ambient on Mechanical Characterization of Bi-2212 Superconducting Ceramic Compound

A material can exhibit only two main mechanical characterizations under test load applied. The first of them is called as typical indentation size effect (*ISE*) behavior and is in association with the non-linear differentiation of real microhardness features (inverse relation to the applied load). The second one is the untypical reverse indentation size effect (*RISE*) behavior and is in relation to the direct relation to the test load applied [28–30]. The reversible (sometimes named as elastic) and irreversible (sometimes called as plastic) deformations form together under the applied test load in the bulk Bi-2212 ceramic material obeying the typical *ISE* behavior. On the other hand, the formation of only irreversible deformations is found in a material presenting the unusual *RISE* nature. According to the microhardness curves in Fig. 1, it is apparent that every Bi-2212 superconducting material shows the *ISE* feature (formation of reversible and irreversible deformations together in the crystal structure). Nevertheless, it is to be stressed here that all the samples prepared exhibit the different level of *ISE* characteristic feature. Namely, the sample produced at the annealing temperature of 840 °C for the annealing period of 24 h presents the highest *ISE* nature whereas the bulk Bi-2212 superconducting compound prepared at 850 °C for 48 h displays the lowest *ISE* feature against the moderate *ISE* characteristics for the other materials prepared at different annealing ambient. The change of *ISE* characteristics stems from the quality of crystallinity due to the variation of permeant structural deformations.

Differentiation of Mechanical Characteristics of Bulk Superconducting Material with Annealing Ambient

The microhardness curves in Fig. 1 allow us to determine the change in the key mechanical design performance quantities, viz. K_{IC} , D , E , Y , B , and C_{II} parameters with the annealing temperature and annealing time with the aid of following equations:

$$E = 8.9635H_V \quad (1)$$

$$Y \approx \frac{H_V}{3} \quad (2)$$

$$K_C = \sqrt{2E\alpha} \quad (\alpha, \text{ surface energy}) \quad (3)$$

$$B = \frac{H_v}{K_C} \quad (4)$$

$$C_I = H_v^{7/4} \quad (5)$$

$$D = \frac{1}{B} \quad (6)$$

We give numerically all the calculations performed in Table 1. It is seen in Table 1 that the preparation conditions founded on annealing ambient and test loads applied affect sensitivity the key mechanical design performance quantities mentioned above. Let us discuss numerically all the parameters in detail. However, it is to be mentioned here that we only discuss the maximum and minimum values for the parameters. In this regard, the first findings are Young's modulus values that are obtained to be in a range of 292.8310 GPa (for the bulk Bi-2212 superconducting material prepared at 840 °C annealing temperature for 24 h annealing time)-196.8876 GPa (for the sample produced at the annealing temperature of 850 °C for the annealing period of 24 h) at the external indentation test load of 0.245 N. Besides, in case of 2.490 N applied test load, the maximum and minimum values of 271.5861 GPa and 159.2070 GPa are attributed to the Bi-2212 ceramics produced at 840 °C for 24 h and 850 °C for 48 h, respectively. Other 7 samples fabricated at the different annealing ambient presents the moderate values. As for the yield strength parameters of Bi-2212 superconducting compounds, the similar trend is observed. The maximum value of 1.1909 GPa is experimentally recorded for the bulk compound produced at 840 °C for 24 h while the minimum value is obtained to be about 0.8007 GPa for the ceramic fabricated at 850 °C for 48 h at 0.245 N test load. Likewise, the smallest yield strength values for every material are obtained at the applied test load of 2.490 N. Among the samples, the compound prepared at 850 °C for 48 h displays the global minimum value of 0.6475 GPa. This means that the optimum annealing ambient (840 °C for 24 h) strengthens remarkably the mechanical durability, stiffness and mechanical strength of Bi-2212 ceramic materials. Conversely, the excess annealing temperature and time lead to induce new permanent and artificial structural deformation problems, casing the beginning points of plastic deformation (permanent deformation or irreversible deformation) at relatively smaller test load applied. Moreover, one can see the similar results for the other parameters computed. The experimental results demonstrate that the bulk

Bi-2212 superconducting sample prepared with the optimum annealing ambient (840 °C for 24 h) requires the highest energy value to break with the external test load applied due to the considerable enhancement in the strength, stability, stiffness and durability of the material.

4. CONCLUSION

We analyze thoroughly the differentiation of fundamental mechanical performance (founded on the key mechanical design quantities and operable slip systems) and mechanical characterization of bulk $\text{Bi}_{2.1}\text{Sr}_{2.0}\text{Ca}_{1.1}\text{Cu}_{2.0}\text{O}_y$ with the annealing temperatures intervals 830 °C - 850 °C and annealing period in a range of 24-48 h with Vickers hardness experimental measurements conducted at the various test loads changing between 0.245 N and 2.940 N. The measurement results are scientifically explained in three main sections. In the first section, we establish a strong link between the annealing ambient and fundamental mechanical performances for the bulk Bi-2212 material depending on the structural deformation problems. In the second part, we describe the variation of mechanical characteristic behaviors (*ISE* and *RISE*) of materials with the annealing ambient. And the last part is related to the role of annealing ambient on the key mechanical design parameters such as K_{IC} , D , E , Y , B , and C_{II} parameters with the experimental micro hardness curves. It is found that the annealing temperature and time affect seriously the mechanical performance features of Bi-2212 ceramic compounds due to the change in the active operable slip systems, crack initiation sites and stress raisers for the crack propagation and dislocation movement in the crystal system. In more detail, the sample prepared at 840 °C annealing temperature and 24 hours annealing time exhibits the best mechanical performance features whereas the Bi-2212 superconducting ceramic material produced at the annealing ambient of the temperature of 850 °C and time of 48 h shows the lowest key mechanical design quantities. Hence, in case of the excess annealing ambient, the propagation of flaws, voids, cracks and dislocations within the critical propagation speed accelerates rapidly and cannot be controlled. In conclusion, the Bi-2212 superconducting compound prepared by the excess annealing ambient is much easier broken as compared to the materials prepared with the optimum annealing temperature and period. In this respect, the optimum annealing ambient (840 °C for 24 h) degrades the mechanical sensitivity of Bi-2212 superconducting material. Conversely, the excess annealing ambient leads to considerably increase the mechanical sensitivity feature of Bi-2212 compound as a result of the significant increase in the number of cracks, voids and dislocations in the crystal lattice. As for the second important result inferred from the current work, every ceramic sample obeys the standard *ISE* feature (but in the different trend depending on the annealing temperature and duration), where both the formations (combination) of elastic and plastic deformations together

appear simultaneously in the crystal structure. In the paper, we find that the bulk Bi-2212 ceramic compound produced at the combination of 840 °C annealing temperature and 24 h annealing time presents the highest *ISE* nature whereas the bulk Bi-2212 superconducting compound prepared at 850 °C for 48 h displays the lowest *ISE* feature. The variation in the *ISE* behavior results from the quality of crystallinity due to the variation of permeant structural deformations in the crystal system. Finally, the differentiation in the key mechanical design performance quantities with the annealing ambient declares that the Bi-2212 superconducting material produced at the optimum annealing ambient obtains the highest mechanical durability, mechanical strength and stiffness features. Conversely, the excess annealing temperature and time cause to increase dramatically new permanent and artificial structural deformation problems. This is attributed to the beginning points of permanent plastic deformation at relatively smaller test load applied.

ACKNOWLEDGEMENTS

This work is supported by Şırnak University Research Fund Grant No:2019.FNAP.06.02.01.

REFERENCES

- [1] Choi, K. Y., Jo, I. S., Han, S. C., Han, Y. H., Sung, T. H., Jung, M. H., ... & Lee, S. I. (2011). High and uniform critical current density for large-size $\text{YBa}_2\text{Cu}_3\text{O}_{7-\delta}$ single crystals. *Current Applied Physics*, 11(4), 1020-1023.
- [2] Li, M., Zhang, Y., Li, Y., & Qi, Y. (2010). Granular superconductivity in polycrystalline $\text{Bi}_2\text{Sr}_2\text{CaCu}_2\text{O}_{8+\delta}$ by homovalent La substitution on Bi sites. *Journal of non-crystalline solids*, 356(50-51), 2831-2835.
- [3] Yaşar, E., Erdem, U., Tuna, M. A., Armağan, O., & Kırındı, T. (2018). The Effect of Ti Content on α' Martensite Phase Transformation, and Magnetic Properties by Mössbauer Spectroscopy in Fe-30% Ni-x% Ti (wt%) Alloys. *Acta Physica Polonica A*, 133(5), 1165-1169.
- [4] Turkoz, M. B., & Erdem, U. (2019). Physical and Chemical Characterization of Pure and Silver Doped Hydroxyapatite. *International Journal of Engineering Research and Development*. 11(2), 643-656.
- [5] K. Salama, V. Selymanickam, L. Gao, K. Sun, (1989). High-current Density in Bulk $\text{YBa}_2\text{Cu}_3\text{O}_x$ superconductor, *Appl. Phys. Lett.* 54, 2352-2354.
- [6] M.B. Turkoz, U. Erdem, (2020). Investigation of the Electrical and Structural Effects of Li Dopping on YBCO Ceramic Superconducting Materials Prepared with Nitrate Compounds. *International Journal of Engineering Research and Development*, 12, 210-216.
- [7] H.K. Onnes, Further experiments with Liquid Helium. D. (2011). On the change of Electrical Resistance of Pure Metals at very low Temperatures, etc. V. The Disappearance of the resistance of mercury, *Koninklijke Nederlandsche Akademie van Wetenschappen Proceedings*, 14, 113-115.
- [8] T. Turgay, G. Yildirim, (2018). Effect of Diffusion Annealing Temperature on Crack-initiating Omnipresent Flaws, Void/crack Propagation and Dislocation Movements Along Ni Surface-layered Bi-2223 Crystal Structure, *Sakarya University Journal of Science*, 22, 1211-1220.
- [9] W. Abdeen, S. Marahba, R. Awad, A.I. Abou Aly, I.H. Ibrahim, M. Matar, (2016). Electrical and mechanical properties of (Bi, Pb)-2223 substituted by holmium, *J. Advanced Ceramics* 5, 54-69.
- [10] G. Yildirim, E. Yucel, S. Bal, M. Dogruer, A. Varilci, M. Akdogan, C. Terzioglu, Y. Zalaoglu, (2012). Investigation of structural and superconducting properties of Cr added Bi-2212 superconducting ceramics, *J. Supercond. Nov. Magn.* 25, 231-237.
- [11] M. Runde, (1995). Application of high- T_c superconductors in aluminum electrolysis plants, *IEEE T. Appl. Supercond.* 5, 813-816.
- [12] W. Buckel, R. Kleiner, (2004). *Superconductivity: Fundamentals and applications*, 2nd ed., Wiley-VCH Verlag, Weinheim,.

- [13] B. Batlogg, Cuprate superconductors (1998). *Science beyond high T(c), Solid State Commun.* 107 639–647.
- [14] Y. Zalaoglu, E. Bekiroglu, M. Dogruer, G. Yildirim, O. Ozturk, C. Terzioglu, (2013). Comparative study on mechanical properties of undoped and Ce-doped Bi-2212 superconductors, *J. Mater. Sci: Mater. El.* 24, 2339–2345.
- [15] A.U. Metin, M. Doğan, U. Erdem, T. Babacan, H. Güngünes, (2020). Preparation of a novel functionalized magnetic nanobiocomposite as a carrier for protein adsorption. *Spectroscopy Letters*, 53, 289–305.
- [16] D.M. Newns, P.C. Pattnaik, C.C. Tsuei, (1991). Role of vanhove singularity in high-temperature superconductors - Mean field, *Phys. Rev. B* 43, 3075–3084.
- [17] Y. Zalaoglu, F. Karaboga, C. Terzioglu, G. Yildirim, (2017). Improvement of mechanical performances and characteristics of bulk Bi-2212 materials exposed to Au diffusion and stabilization of durable tetragonal phase by Au, *Ceram. Int.* 43, 6836–6844.
- [18] N.K. Saritekin, Y. Zalaoglu, M. Dogruer, G. Yildirim, C. Terzioglu, O. Gorur, (2014). *J. Alloy. Compd.* 610, 361–371.
- [19] S. Nagaya, N. Hirano, M. Naruse, T. Watanabe, T. Tamada, (2013). *IEEE T. Appl. Supercond.* 23, 5602804–5602807.
- [20] F.N. Werfel, U. Floegel-Delor, R. Rothfeld, T. Riedel, B. Goebel, D. Wippich, P. Schirrmeister, (2012). *Supercond. Sci. Technol.* 25, 014007.
- [21] A.T. Ulgen, T. Turgay, C. Terzioglu, G. Yildirim, M. Oz, (2018). Role of Bi/Tm substitution in Bi-2212 system on crystal structure quality, pair wave function and polaronic states, *J. Alloy. Compd.* 764, 755–766.
- [22] S.B. Guner, Y. Zalaoglu, T. Turgay, O. Ozyurt, A.T. Ulgen, M. Dogruer, G. Yildirim, (2019). *J. Alloy. Compd.* 772, 388–398.
- [23] T.A. Coombs, (2011). *IEEE T. Appl. Supercond.* 21, 3581–3586.
- [24] A.T. Ulgen, U. Erdem, Y. Zalaoglu, T. Turgay, G. Yildirim, (2020). Effect of vanadium addition on fundamental electrical quantities of Bi-2223 crystal structure and semi-empirical model on structural disorders-defects. *Journal of Materials Science: Materials in Electronics*, 31, 13765-13777.
- [25] Y. Zalaoglu, (2018). Determination of Solubility Characteristic of (Bi, Gd) Substitution in Bi-2223 Inorganic Compounds, *Sakarya University Journal of Science*, 22, 1221-1233.
- [26] A.A. Elmustafa, D.S. Stone, (2003), *J. Mech. Phys. Solid.* 5, 357
- [27] Y. Zalaoglu, T. Turgay, A.T. Ulgen, U. Erdem, M.B. Turkoz, G. Yildirim, (2020). A novel research on the subject of the load-independent microhardness performances of Sr/Ti partial displacement in Bi-2212 ceramics. *Journal of Materials Science: Materials in Electronics*, doi: <https://doi.org/10.1007/s10854-020-04724-6>

- [28] F. Poehl, S. Huth, W. Theisen, (2016). *Int. J. Solids Struct.* 84, 160–166.
- [29] M.M. Pasare, M.I. Petrescu, (2008). *Mater. Plast.* 45, 87–90.
- [30] R.K.A. Al-Rub, (2007). *Mech. Mater.* 39, 787–802.

Table 1. Key mechanical design properties including elastic modulus (E), yield strength (Y), brittleness index (B), fracture toughness (K_{Ic}), ductility (D) and elastic stiffness coefficient (C_{II}) parameters for all the bulk Bi-2212 superconducting compounds

Samples	F (N)	H_y (GPa)	E (GPa)	Y (GPa)	K_{Ic} (GPa $m^{1/2}$)	C_{II} (GPa) ^{7/4}	B (m ^{-1/2})	D (x10 ⁻³) (m ^{1/2})
830°C for 24 h	0,245	3,0500	250,0130	1,0170	1,1400	7,0400	2,6750	0,3738
	0,490	2,8630	234,6530	0,9540	1,1050	6,3010	2,5920	0,3858
	0,980	2,7640	226,5800	0,9210	1,0850	5,9270	2,5470	0,3926
	1,960	2,7340	224,0960	0,9110	1,0790	5,8130	2,5330	0,3948
	2,940	2,7210	223,0300	0,9070	1,0770	5,7650	2,5270	0,3957
830°C for 36 h	0,245	3,4190	280,2660	1,1400	1,1230	8,5980	3,0450	0,3284
	0,490	3,2680	267,8320	1,0890	1,0980	7,9420	2,9760	0,3360
	0,980	3,1860	261,1030	1,0620	1,0840	7,5960	2,9390	0,3403
	1,960	3,1430	257,6280	1,0480	1,0770	7,4200	2,9190	0,3426
	2,940	3,1320	256,7420	1,0440	1,0750	7,3750	2,9140	0,3432
830°C for 48 h	0,245	2,9210	239,4400	0,9740	1,2510	6,5280	2,3340	0,4284
	0,490	2,6990	221,2110	0,9000	1,2030	5,6830	2,2440	0,4456
	0,980	2,5820	211,6540	0,8610	1,1770	5,2600	2,1950	0,4556
	1,960	2,5280	207,1630	0,8430	1,1640	5,0670	2,1710	0,4606
	2,940	2,5250	206,9250	0,8420	1,1630	5,0560	2,1700	0,4608
840°C for 24 h	0,245	3,5730	292,8310	1,1910	1,1330	9,2840	3,1550	0,3170
	0,490	3,4650	284,0200	1,1550	1,1150	8,8010	3,1070	0,3219
	0,980	3,3880	277,6840	1,1290	1,1030	8,4600	3,0720	0,3255
	1,960	3,3370	273,4880	1,1120	1,0940	8,2380	3,0490	0,3280
	2,940	3,3140	271,5860	1,1050	1,0910	8,1380	3,0380	0,3292
840°C for 36 h	0,245	3,2120	263,2420	1,0710	1,1540	7,7050	2,7830	0,3593
	0,490	3,0450	249,5380	1,0150	1,1240	7,0170	2,7090	0,3691
	0,980	2,9500	241,8090	0,9830	1,1060	6,6410	2,6670	0,3750
	1,960	2,9060	237,4970	0,9660	1,0960	6,4350	2,6430	0,3784
	2,940	2,8980	238,1940	0,9690	1,0980	6,4680	2,6470	0,3778
840°C for 48 h	0,245	2,7460	225,0470	0,9150	1,4620	5,8570	1,8780	0,5325
	0,490	2,4510	200,9010	0,8170	1,3820	4,8020	1,7740	0,5637
	0,980	2,2840	187,1880	0,7610	1,3340	4,2430	1,7130	0,5838
	1,960	2,2000	180,3200	0,7330	1,3090	3,9740	1,6810	0,5949
	2,940	2,1960	179,9840	0,7320	1,3080	3,9610	1,6790	0,5956

850°C for 24 h	0,245	2,9030	237,9150	0,9680	1,3730	6,4550	2,1150	0,4728
	0,490	2,6410	216,4980	0,8800	1,3090	5,4730	2,0170	0,4958
	0,980	2,4950	204,4990	0,8320	1,2730	4,9530	1,9600	0,5102
	1,960	2,4280	198,9750	0,8090	1,2550	4,7210	1,9340	0,5171
	2,940	2,4270	198,9250	0,8090	1,2550	4,7190	1,9340	0,5171
850°C for 36 h	0,245	2,4980	204,7200	0,8330	1,2750	4,9620	1,9590	0,5105
	0,490	2,2440	183,9260	0,7480	1,2080	4,1140	1,8570	0,5385
	0,980	2,1070	172,7300	0,7020	1,1710	3,6860	1,8000	0,5556
	1,960	2,0510	168,0740	0,6840	1,1550	3,5140	1,7750	0,5634
	2,940	2,0480	167,8370	0,6830	1,1540	3,5050	1,7740	0,5637
850°C for 48 h	0,245	2,4020	196,8880	0,8010	1,2020	4,6350	1,9980	0,5005
	0,490	2,0900	171,2770	0,6970	1,1210	3,6320	1,8640	0,5365
	0,980	1,9620	160,7990	0,6540	1,0860	3,2520	1,8060	0,5537
	1,960	1,9430	159,2640	0,6480	1,0810	3,1980	1,7970	0,5565
	2,940	1,9420	159,2070	0,6470	1,0810	3,1960	1,7970	0,5565

Table 2. *Fitting parameters are computed to be the highest correlation value of $R^2=1$ for all the Bi-2212 ceramic compounds studied in this work

Materials	*Fitting relations for every Bi-2212 superconducting compounds
830°C for 24 h	$y = 0.12479x^4 - 0.83846x^3 + 1.94298x^2 - 1.86821x + 3.40327$
830°C for 36 h	$y = 0.10434x^4 - 0.69244x^3 + 1.58279x^2 - 1.51461x + 3.70528$
830°C for 48h	$y = 0.15571x^4 - 1.03139x^3 + 2.35299x^2 - 2.23819x + 3.34302$
840°C for 24 h	$y = 0.05853x^4 - 0.39619x^3 + 0.93884x^2 - 0.97526x + 3.7609$
840°C for 36 h	$y = 0.11015x^4 - 0.73505x^3 + 1.69587x^2 - 1.64436x + 3.52319$
840°C for 48 h	$y = 0.19571x^4 - 1.30077x^3 + 2.99113x^2 - 2.89755x + 3.29448$
850°C for 24 h	$y = 0.17372x^4 - 1.15627x^3 + 2.6626x^2 - 2.57603x + 3.39038$
850°C for 36 h	$y = 0.17176x^4 - 1.14395x^3 + 2.63061x^2 - 2.52623x + 2.97493$
850°C for 48 h	$y = 0,23955x^4 - 1,58924x^3 + 3,6025x^2 - 3,30829x + 3,01894$

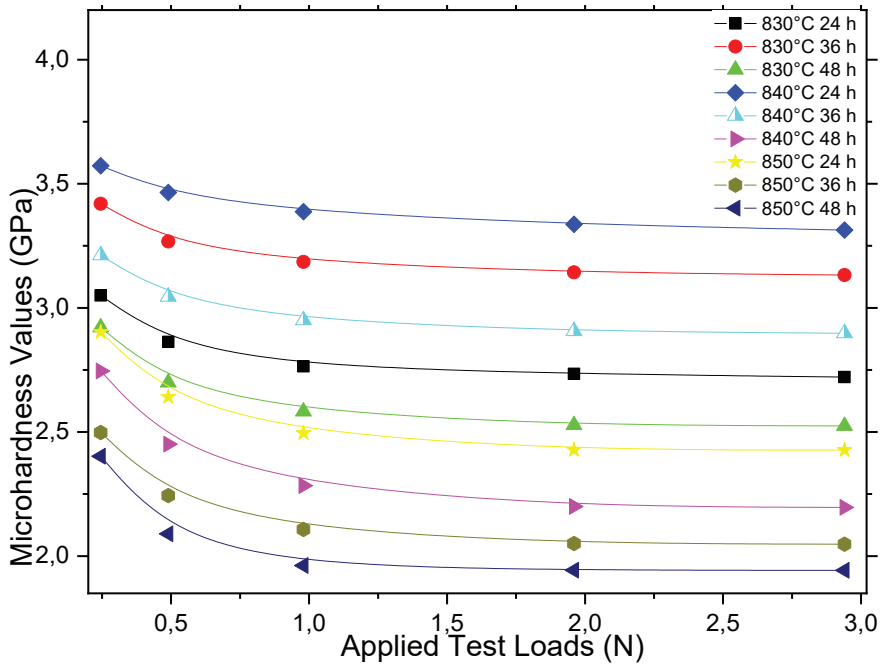


Figure 1. Differentiation of Vickers H_v hardness parameters against applied indentation test loads F .

Chapter 20

GEOGRAPHIC INFORMATION SYSTEM (GIS) AND MULTI CRITERIA DECISION ANALYSIS (MCDA) BASED APPLICATION FOR IDENTIFYING SUITABLE WIND TURBINE LOCATIONS IN KAHRAMANMARAS, TURKEY



Ozan ARTUN¹

¹ Dr. Cukurova University, Karaisali Vocational School, Department of Architecture and City Planning, Adana, Turkey (ORCID: 0000-0002-6122-2729)

INTRODUCTION

It is a well-known fact that energy is vital to sustain life on earth. Energy will continue to be the foundation of human and economic development and world peace. The energy demand of the world's countries is increasing exponentially. The world population is estimated to exceed 8 billion by 2020. On the other hand, traditionally called energy sources exist in limited quantities on earth. The rapid depletion of fossil fuel resources, the limited number of reserves and variable prices around the world required urgent research for alternative energy. This situation led to a significant increase in the interest in renewable energy sources (Nestmann and Maskey, 1998).

The development of Turkish industry has increased Turkey's energy demand. Our country's current energy resources are insufficient to meet this energy demand. Particularly, due to the scarcity of fossil fuels and the increase in costs in recent years, interest in alternative energy sources has increased day by day (Oner et al., 2009). In order to meet the increasing energy demand, the use of fossil fuels is mainly caused by environmental pollution. In recent years this situation has become a major issue on Turkey's agenda. In Turkey, as seen in the whole world, it is observed that there is a trend towards renewable energy sources. Considering the geographical location of Turkey, our country has a number of advantages for the most widespread use of renewable sources. In this regard, our country's renewable sources such as geothermal, solar and wind should not be used only to meet the growing energy demand. It is also essential to evaluate these resources for environmental reasons (Kaygusuz, 2002).

Knowing the environmental effects of fossil fuels has increased the need for clean and renewable energy sources. Wind energy is a renewable energy source with higher growth in recent years and can be considered as a hope for a clean and sustainable energy-based future (Ozgener, 2011; Erdogdu, 2009). When the advantages of wind energy are examined; It is seen that features such as cleanliness, abundance and low cost come to the fore. The harmful emissions released from diverse sources have been causing unfavorable effects on the atmosphere is a known fact. Renewable energy sources are defined as free, clean and inexhaustible. Also, when fuel is not burned, wind farms do not cause fuel or air pollution. This is one of the important indicators that wind energy is a clean fuel. High technology is not required to utilize wind energy, and there is no need for transportation. It can be said that the technology that converts wind energy into electrical and mechanical energy is a more economical technology than other energy conversion systems. In order to benefit from wind energy in the most profitable way, this energy must first be converted into mechanical energy and then into electrical energy. Installing wind energy conversion systems in regions with sufficient wind density is very important

in obtaining great economic benefits (İlkiliç, 2012). The researches show that projects related to wind energy are indeed one of the most suitable methods among sustainable energy development projects. Since large-scale wind farm projects are very costly, long-term wind feasibility is crucial to obtain effective and efficient results from wind power prior to power plant construction. In the planned studies, before feasibility, suitable areas should be determined and examined, especially according to the wind potential. With the help of economic, physical, environmental, social factors and a decision-making mechanism that should be taken into account for choosing the right location (Bennui et al., 2007).

Geographic Information System (GIS) is an important tool for determining the site locations in the renewable energy projects. In such complex applications, many systems such as high resolution remote sensing data and Geographic Information Systems (GIS) that support the decision-making process should be used. Site selection criteria can be developed to specify the appropriate locations for wind farms and even the positions of individual turbines for the highest use of resource potential. In order to choose between the main and sub criteria by examining the criteria to be selected in central location applications, the weighting of the criteria becomes easier with the functionality of the decision making mechanisms. Geographical information systems provide the opportunity to combine and analyze the obtained data. This makes these systems indispensable when solving complex problems and achieving the desired result (Yalçın and Yücel, 2020).

The location selection of wind turbines in GIS requires the analysis of many spatial factors. These factors can be specified as topography, land cover, slope, aspect, protection areas (protected area, etc.) and settlement centers. In wind energy studies, GIS, which has developed rapidly and its usage area has increased in recent years, is widely used. New generation wind energy atlases, which can be integrated with geographic information systems (GIS) is used to specify the most suitable areas for wind energy applications. These atlases have significant benefits in terms of both time and money. In Turkey, Wind Energy Potential Atlas (WEPA) was prepared in 2006, to prepare the information on the qualifications demanded of the wind energy sector and to provide services to the sector. With this atlas, that is prepared on a GIS basis, wind information can be provided in 3 dimensions for every 200x200 m areas of our country's land and sea areas (Malkoç, 2009; Nişancı et al., 2010). Despite everything, this atlas is still not enough. The reason for this is, problems such as sharing of spatial information among institutions, inadequate or outdated data, causes decision-makers make wrong decisions. In determining potential wind turbine areas, the local factors such as fault line, distance from residential areas, slope, etc. should also be included in the assessment (Nişancı et al.,

2010).

In this study, it is aimed to achieve the suitable Wind Turbine locations in Kahramanmaraş province, Turkey by using many variables. In the study area, Wind Energy Potential Atlas of the Turkey General Directorate of Renewable Energy (GDRE) may give investors an idea for the investments. But it was aimed to create a more comprehensive Land Suitability Index Map in GIS environment for the study area. In this context, different variables were used for choosing the suitable Wind Turbine locations. In this study, Analytical Hierarchy Process (AHP) combined with GIS is used for a preliminary site selection for wind turbines in Kahramanmaraş, Turkey (Saaty, 1980; Wind & Saaty, 1980). The suitable areas, alternative areas and unsuitable areas for Wind Turbines in the study area were determined in terms of Geographic Information System to guide investors and scientific researchers hereafter.

MATERIALS AND METHODS

Study Area

Kahramanmaraş province is selected for this study. This province is one of the provinces in Turkey's Mediterranean region (Figure 1). The city lies on a plain at the foot of the Ahir Mountain. The surface area of Kahramanmaraş province is 14.327 km². 59.7% of its territory is covered with mountains, 24% with plateaus and 16.3% with plains. Kahramanmaraş province is 568 m above from sea level. The northern parts of the province are quite mountainous. Landforms are generally composed of mountains that are extensions of the Southeast Taurus Mountains and depression plains between them. The high parts of the Kahramanmaraş mountains generally consist of bare rocks. The lower belts are covered with forest texture (Anonymous, 2020a).

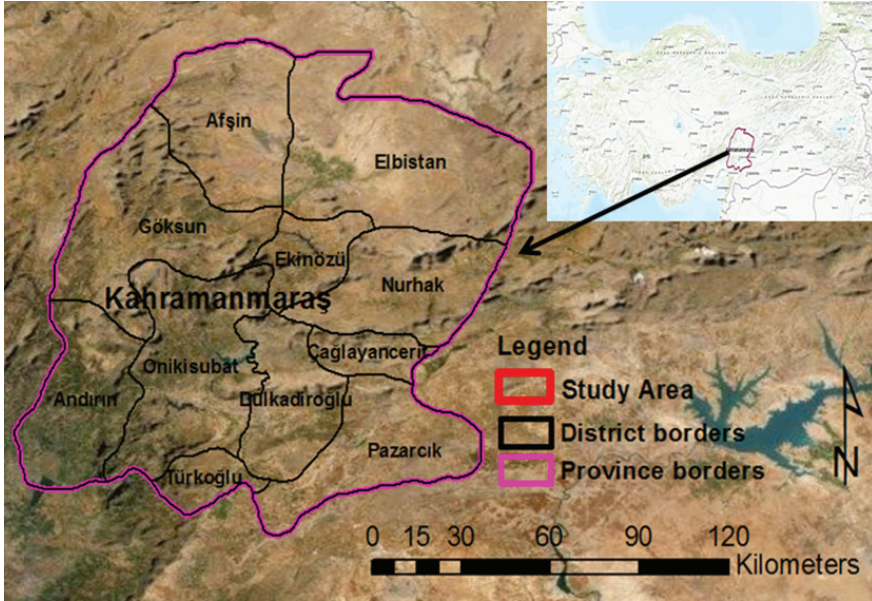


Figure 1 Map of Turkey and the Study Area

There are several important studies in the literature on wind turbine location selection using Geographical Information Systems (GIS). In this study, the mentioned studies were utilized to determine the criteria of wind turbine selection. In this study, firstly, the criteria that can define different constraints on wind turbine site selection are tried to be determined. The individual map layers, that are corresponding to each constraint were created then. The project area was divided into 30 m. - 30 m. grid cells in the study. Thus, each grid cell represented an alternative place for a wind turbine site. The chosen factors in the selection of wind turbine areas were determined according to the criteria used in related literature (Table 1.).

The altitude data of the study area were collected from ASTER Global Dem V.3 in GeoTIFF format. Slope criteria were derived from ASTER Global Dem V.3 (NASA, 2019). Distance, Roads and Transmission criteria were downloaded from OpenStreetMap (Anonymous, 2020b). Fault line criteria were obtained from the General Directorate of Mineral Research and Exploration (GDMRE)'s Turkey active fault map (Anonymous, 2020c). Capacity factor criteria were taken from Global Wind Atlas (Anonymous, 2020d). Annual precipitation criteria were downloaded from the Worldclim website (Anonymous, 2020e).

In the study, seven GIS layers stating physical criteria were identified. Then, these criteria subjected to a GIS analysis to select suitable sites for wind turbines. In order to calculate the land suitability index map of the area studied, the spatial analysis techniques mentioned below were

obtained using the ArcGIS:

- The attribute tables of each thematic layer were updated.
- Every selected criteria were converted to raster format.
- Slope criteria were derived from ASTER Global Dem V.3.
- All data were converted to 30 meter resolution.
- The Weighted Sum analysis combined with AHP is used to determine the appropriate sites for the wind turbine within the study area.

Table 1. MCDA modelling environmental data set. (Anonymous, 2020b), (Anonymous, 2020c), (NASA, 2019), (Anonymous, 2020d), (Anonymous, 2020e)

Criteria Name	Description	Source
Distance	Distance from Residential areas (m)	Derived from OpenStreetMap
Slope	Slope in degrees obtained from altitude (%)	Derived from ASTER/ASTGTM.003
Faults	Distance from Faults (m)	Derived from Active Fault Map of Turkey
Roads	Distance from Roads (m)	Derived from OpenStreetMap
Transmission	Distance from Transmission Lines (m)	Derived from OpenStreetMap
Capacity	Capacity Factor (%)	Derived from Global Wind Atlas
Precipitation	Annual precipitation (mm)	Derived from WorldClim

Analytic Hierarchy Process

In this study, the AHP technique, will be used for the determination of suitable places for Wind Turbines. The main reason for this is AHP is a frequently used multi-criteria decision-making technique in the literature. The selected criteria for the study area will be weighted according to this method. AHP technique is a structural technique. It is often used to analyze involved criteria in solving complex problems. In AHP model, the binary comparison matrix is provided based on the binary comparisons between the criteria. Subsequently, the weights of the criteria are determined.

Table 2. AHP evaluation scale (Saaty, 1980).

Numerical value of Pij	Definition
1	Equal importance of i and j
3	Moderate importance of i over j
5	Strong importance of i over j
7	Very strong importance of i over j
9	Extreme importance of i over j)
2,4,6,8	Intermediate values

Saaty developed the AHP mathematical method in 1977. The aim of this method is to analyze complex decisions involving various criteria (Table 2). Due to the literature, AHP method, is one of the most effective

methods used in spatial planning in recent years (Ayday et al., 2014; Uyan, 2017). In AHP method, taking into account the scale of importance, the criteria are weighted between 1 and 9, (Saaty, 1990). The weight of the criteria is actually important in obtaining the result in this method. Eventually the weights can be different, depending on the preferences of the decision makers’.

In this study, the seven criteria are identified for AHP analysis. The chosen criteria were evaluated in the AHP analysis software. Used software is prepared by Goepel (2018) and provided online. Therefore first of all, a binary comparison was made for AHP priorities. The selections were made in the range of 1-9 on the AHP scale and were calculated automatically, depending on the importance of the criteria, (Anonymous, 2020f).

Criteria

In this study the following factors were considered in the determination of the suitable areas for wind energy plants: Distance from Residential Areas, Slope, Distance from Faults, Distance from Roads, Distance from Transmission Lines, Capacity Factor and Annual precipitation.

Each criteria are explained below.

Distance from Residential Areas

The proximity of wind turbines to residential areas can be considered as an economic factor. Therefore, wind turbine placement should be done close to residential areas. In the study, for residential areas, with a <500 m. buffer zone is identified as 1, 500-1000 buffer zone is identified as 2, 1000-1500 m. buffer zone is identified as 3, 1500-2000 m. buffer zone is identified as 4, 2000-2500 m. buffer zone is identified as 5, 2500-3000 m. buffer zone is identified as 6, 3000-3500 m. buffer zone is identified as 7, 3500-4000 m. buffer zone is identified as 8 and > 4000 m. buffer zone is identified as 9 (Figure 2.).

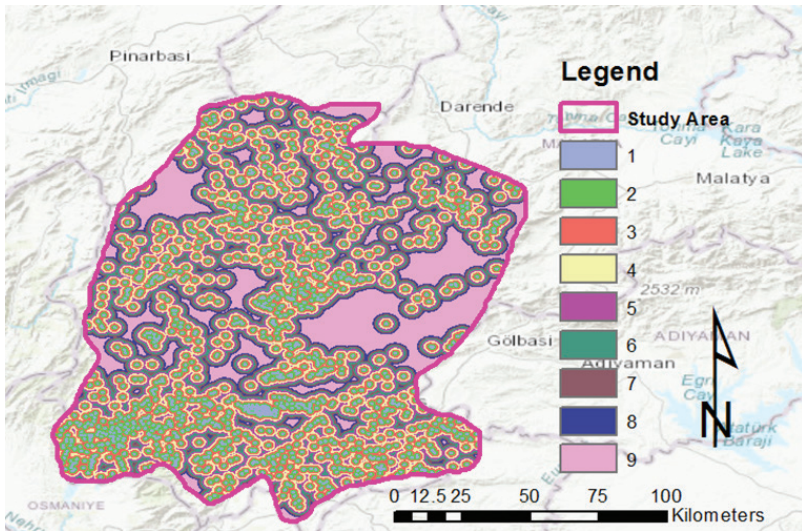


Figure 2. Suitability Index Map of the Distance from Residential Areas of the Study Area

Slope

It is seen that inclined and hilly regions prevent stable wind regime. It is the right decision to build wind turbines where the slope is low. The slope was divided into nine parts in the study. 0–1% buffer zone is identified as 9, 1–2% buffer zone is identified as 8, 2–4% buffer zone is identified as 7, 4–8% buffer zone is identified as 6, 8–12% buffer zone is identified as 5, 12–16% buffer zone is identified as 4, 16–20% buffer zone is identified as 3, 20–24% buffer zone is identified as 2 and >24% buffer zone is identified as 1. (Figure 3.).

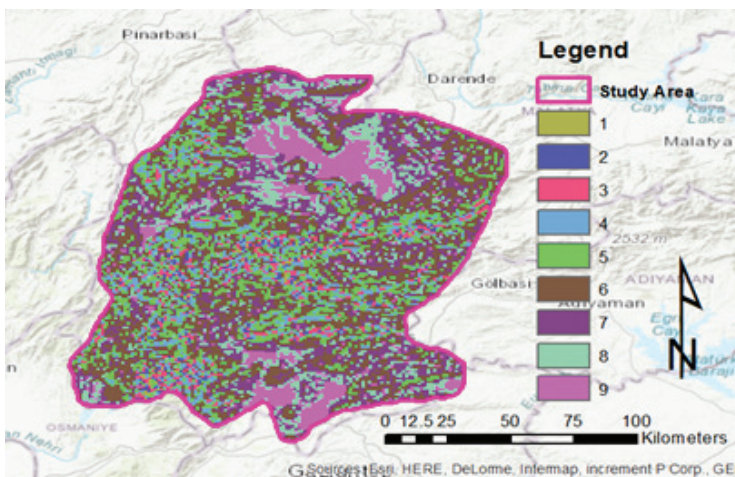


Figure 3. Suitability Index Map of Slope of the Study Area

Distance from Faults

Wind turbines should not be located in areas close to places with high earthquake risk. This situation was taken into account in the evaluation. In the study, for distance from faults, with a <1000 m. buffer zone is identified as 1, 1000-2000 m. buffer zone is identified as 2, 2000-3000 m. buffer zone is identified as 3, 3000-4000 m. buffer zone is identified as 4, 4000-5000 m. buffer zone is identified as 5, 5000-6000 m. buffer zone is identified as 6, 6000-7000 m. buffer zone is identified as 7, 7000-8000 m. buffer zone is identified as 8 and > 8000 m. buffer zone is identified as 9 (Figure 4.).

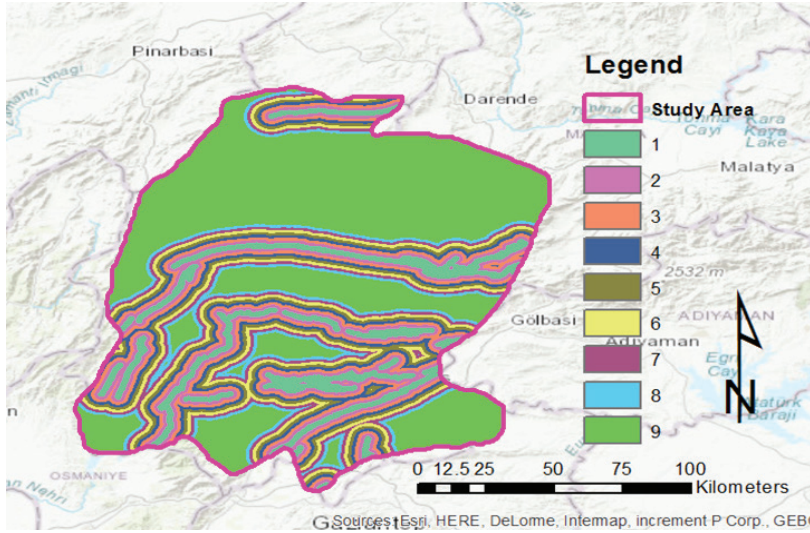


Figure 4. Suitability Index Map of Distance from Fault Lines of the Study Area

Distance from Roads

In wind turbine location selection roads are an economical and efficient criterion. Infrastructure works in areas close to main roads can reduce costs. (Uyan, 2017; Yalçın and Yüce, 2020). This situation has been taken into consideration in the evaluations.. In the study, for distance from roads, with a <250 m. buffer zone is identified as 9, 250-500 m. buffer zone is identified as 8, 500-1000 m. buffer zone is identified as 7, 1000-1500 m. buffer zone is identified as 6, 1500-2000 m. buffer zone is identified as 5, 2000-2500 m. buffer zone is identified as 4, 2500-3000 m. buffer zone is identified as 3, 3000-3500 m. buffer zone is identified as 2 and > 3500 m. buffer zone is identified as 1 (Figure 5.).

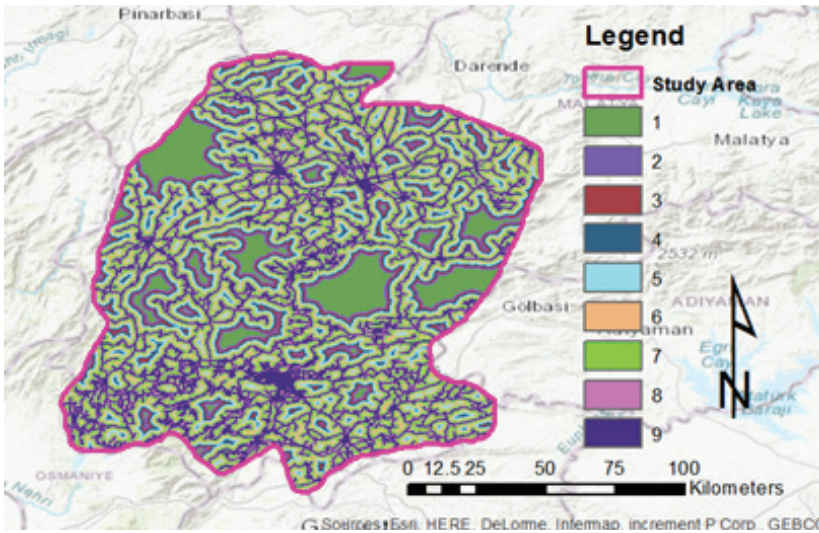


Figure 5. Suitability Index Map of Distance from Roads of the Study Area

Distance from Transmission Lines

The energy generated by the wind turbine should be easily transmitted to the transmission network. Therefore, it is more accurate to place wind turbines in areas close to transmission lines. In this study, for distance from the transmission lines, with a <1000 m. buffer zone is identified as 9, 1000-2000 m. buffer zone is identified as 8, 2000-3000 m. buffer zone is identified as 7, 3000-4000 m. buffer zone is identified as 6, 4000-5000 m. buffer zone is identified as 5, 5000-6000 m. buffer zone is identified as 4, 6000-7000 m. buffer zone is identified as 3, 7000-8000 m. buffer zone is identified as 2 and > 8000 m. buffer zone is identified as 1 (Figure 6.).

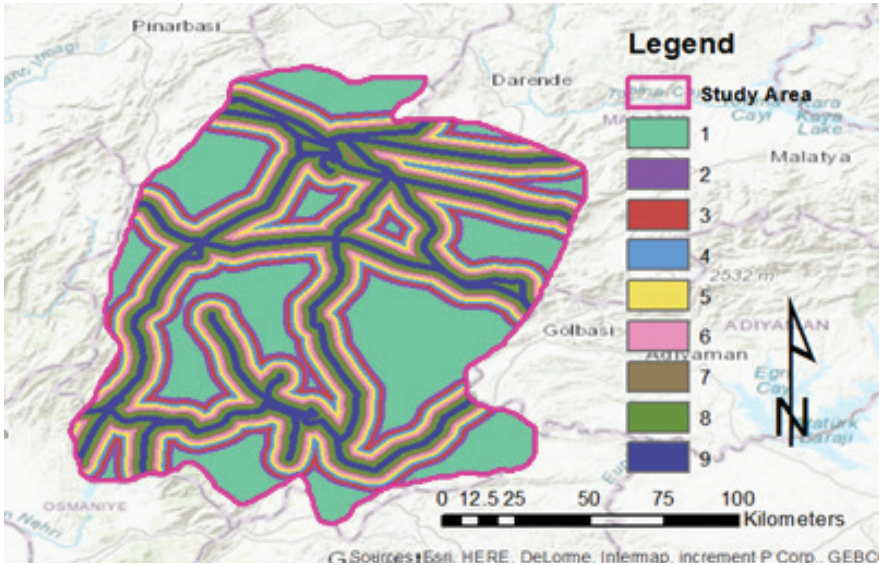


Figure 6. Suitability Index Map of Distance from Transmission Lines of the Study Area

Capacity Factor

The capacity factor is expressed as the ratio of the power produced by a power plant in a certain time period to the power it can produce at its maximum capacity. It is a known fact that more power and income is obtained in the wind turbine to be installed in places with higher capacity factor compared to places with low capacity factor. The capacity factor was divided into nine parts in the study. 1–6% buffer zone is identified as 1, 6–12% buffer zone is identified as 2, 12–18% buffer zone is identified as 3, 18–24% buffer zone is identified as 4, 24–30% buffer zone is identified as 5, 30–36% buffer zone is identified as 6, 36–42% buffer zone is identified as 7, 42–48% buffer zone is identified as 8 and >48% buffer zone is identified as 9. (Figure 7.).

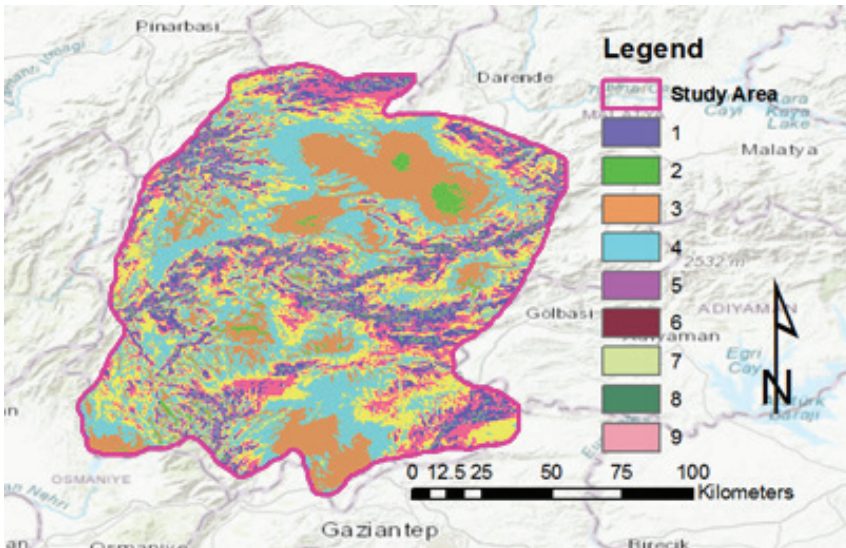


Figure 7. Suitability Index Map of Capacity Factor of the Study Area

Annual Precipitation

Precipitation is an important factor in wind turbine site selection. The areas with more rainfall will generate more runoff, and that will affect wind turbine sites. The annual precipitation was divided into nine parts in this study. In the study, for annual precipitation, with a <472 mm. buffer zone is identified as 9, 472-511 mm. buffer zone is identified as 8, 511-550 mm. buffer zone is identified as 7, 550-584 mm. buffer zone is identified as 6, 584-616 mm. buffer zone is identified as 5, 616-651 mm. buffer zone is identified as 4, 651-689 mm. buffer zone is identified as 3, 689-736 mm. buffer zone is identified as 2 and > 736 mm. buffer zone is identified as 1 (Figure 8.).

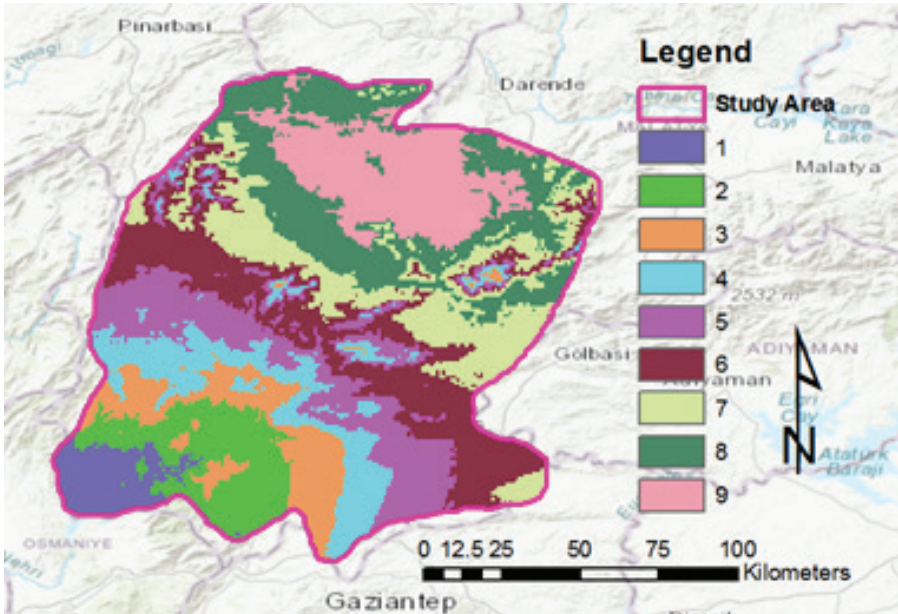


Figure 8. Suitability Index Map of Annual Precipitation of the Study Area

Factors belonging to the study area were interpreted in the GIS environment. Then, whole the obtained raster data were converted to 30 m. resolution. The Weighted Sum analysis in the Spatial Analyst Tool in the ArcGIS program was used in this study to create a Land Suitability Index Map for Wind Turbine siting. The criteria weights obtained in AHP method are used in the analysis (Figure 10).

RESULTS AND DISCUSSION

Multi-criteria decision making is using widely in spatial planning nowadays and AHP method is a significant method of multi-criteria decision making. When the literature on this subject is examined, it is seen that, AHP is one of the most effective methods used in spatial planning in recent years. In the AHP method, users are enabled to identify the weights of the criteria in the solution of a multi-criteria problem. In this method, a hierarchical model is used for every problem, consisting of objectives, criteria, sub-criteria and alternatives. (Saaty, 1990). For selecting suitable sites for the wind energy plants, in this study, it was targeted on the use of GIS together with MCE methods. The weights of the criteria, used in the site selection process were obtained separately by binary comparisons with the AHP. Determination of weights with AHP method gives very positive results. In this method, considering to the scale of importance, the criteria are weighted between 1 and 9. The weights of the criteria, creating the hierarchy are calculated, after the problem is set in a hierarchical structure (Öztürk & Batuk, 2010).

Scoring was made using the utilized preference scale suggested by Saaty (1980) in the study for evaluating the criteria included in a level compared with other criteria included in the next hierarchical level (Table 2). Subsequently, a pairwise comparison matrix is then created (Saaty, 1980, Saaty, 1990). The pairwise comparison matrix consists of $n(n - 1)/2$ comparisons, for n number of elements (Malczewski, 2010, Öztürk & Batuk, 2010).

In the study, seven criteria (distance from residential areas, slope, distance from faults, distance from roads, distance from transmission lines capacity factor and annual precipitation) obtained for AHP analysis are evaluated in the online software (Anonymous, 2020c), prepared by Goepel for making AHP analysis (Goepel, 2018).

Firstly, a double comparison was made for AHP priorities (Figure 8). Depending on the importance of the criteria, 1-9 selections were made in the AHP scale and then calculated automatically. As a result of the calculation, the Consistency Ratio was determined as 5.70% and the weights of the criteria were determined as a result of the double comparison (Table 3). It is considered that the judgments exhibit a sufficient degree of consistency and that the assessment can be continued, in the case where the consistency ratio calculated for the judgments is below 0.10, (Öztürk & Batuk, 2007; Akıncı et al., 2013).

A - wrt AHP priorities - or B?		Equal	How much more?
1	<input checked="" type="radio"/> Distance from residential areas <input type="radio"/> Distance from roads	<input checked="" type="radio"/> 1	<input type="radio"/> 2 <input type="radio"/> 3 <input type="radio"/> 4 <input type="radio"/> 5 <input type="radio"/> 6 <input type="radio"/> 7 <input type="radio"/> 8 <input type="radio"/> 9
2	<input type="radio"/> Distance from residential areas <input checked="" type="radio"/> Slope	<input type="radio"/> 1	<input checked="" type="radio"/> 2 <input type="radio"/> 3 <input type="radio"/> 4 <input type="radio"/> 5 <input type="radio"/> 6 <input type="radio"/> 7 <input type="radio"/> 8 <input type="radio"/> 9
3	<input type="radio"/> Distance from residential areas <input checked="" type="radio"/> Capacity Factor	<input type="radio"/> 1	<input type="radio"/> 2 <input type="radio"/> 3 <input type="radio"/> 4 <input checked="" type="radio"/> 5 <input type="radio"/> 6 <input type="radio"/> 7 <input type="radio"/> 8 <input type="radio"/> 9
4	<input checked="" type="radio"/> Distance from residential areas <input type="radio"/> Distance from transmission lines	<input type="radio"/> 1	<input checked="" type="radio"/> 2 <input type="radio"/> 3 <input type="radio"/> 4 <input type="radio"/> 5 <input type="radio"/> 6 <input type="radio"/> 7 <input type="radio"/> 8 <input type="radio"/> 9
5	<input type="radio"/> Distance from residential areas <input checked="" type="radio"/> Distance from faults	<input type="radio"/> 1	<input checked="" type="radio"/> 2 <input type="radio"/> 3 <input type="radio"/> 4 <input type="radio"/> 5 <input type="radio"/> 6 <input type="radio"/> 7 <input type="radio"/> 8 <input type="radio"/> 9
6	<input checked="" type="radio"/> Distance from residential areas <input type="radio"/> Rainfall	<input type="radio"/> 1	<input type="radio"/> 2 <input checked="" type="radio"/> 3 <input type="radio"/> 4 <input type="radio"/> 5 <input type="radio"/> 6 <input type="radio"/> 7 <input type="radio"/> 8 <input type="radio"/> 9
7	<input type="radio"/> Distance from roads <input checked="" type="radio"/> Slope	<input type="radio"/> 1	<input type="radio"/> 2 <input type="radio"/> 3 <input type="radio"/> 4 <input checked="" type="radio"/> 5 <input type="radio"/> 6 <input type="radio"/> 7 <input type="radio"/> 8 <input type="radio"/> 9
8	<input type="radio"/> Distance from roads <input checked="" type="radio"/> Capacity Factor	<input type="radio"/> 1	<input type="radio"/> 2 <input type="radio"/> 3 <input checked="" type="radio"/> 4 <input type="radio"/> 5 <input type="radio"/> 6 <input type="radio"/> 7 <input type="radio"/> 8 <input type="radio"/> 9
9	<input checked="" type="radio"/> Distance from roads <input type="radio"/> Distance from transmission lines	<input checked="" type="radio"/> 1	<input type="radio"/> 2 <input type="radio"/> 3 <input type="radio"/> 4 <input type="radio"/> 5 <input type="radio"/> 6 <input type="radio"/> 7 <input type="radio"/> 8 <input type="radio"/> 9
10	<input type="radio"/> Distance from roads <input checked="" type="radio"/> Distance from faults	<input type="radio"/> 1	<input type="radio"/> 2 <input checked="" type="radio"/> 3 <input type="radio"/> 4 <input type="radio"/> 5 <input type="radio"/> 6 <input type="radio"/> 7 <input type="radio"/> 8 <input type="radio"/> 9
11	<input checked="" type="radio"/> Distance from roads <input type="radio"/> Rainfall	<input type="radio"/> 1	<input type="radio"/> 2 <input type="radio"/> 3 <input checked="" type="radio"/> 4 <input type="radio"/> 5 <input type="radio"/> 6 <input type="radio"/> 7 <input type="radio"/> 8 <input type="radio"/> 9
12	<input type="radio"/> Slope <input checked="" type="radio"/> Capacity Factor	<input type="radio"/> 1	<input type="radio"/> 2 <input type="radio"/> 3 <input type="radio"/> 4 <input checked="" type="radio"/> 5 <input type="radio"/> 6 <input type="radio"/> 7 <input type="radio"/> 8 <input type="radio"/> 9
13	<input checked="" type="radio"/> Slope <input type="radio"/> Distance from transmission lines	<input type="radio"/> 1	<input checked="" type="radio"/> 2 <input type="radio"/> 3 <input type="radio"/> 4 <input type="radio"/> 5 <input type="radio"/> 6 <input type="radio"/> 7 <input type="radio"/> 8 <input type="radio"/> 9
14	<input type="radio"/> Slope <input checked="" type="radio"/> Distance from faults	<input checked="" type="radio"/> 1	<input type="radio"/> 2 <input type="radio"/> 3 <input type="radio"/> 4 <input type="radio"/> 5 <input type="radio"/> 6 <input type="radio"/> 7 <input type="radio"/> 8 <input type="radio"/> 9
15	<input checked="" type="radio"/> Slope <input type="radio"/> Rainfall	<input type="radio"/> 1	<input type="radio"/> 2 <input type="radio"/> 3 <input checked="" type="radio"/> 4 <input type="radio"/> 5 <input type="radio"/> 6 <input type="radio"/> 7 <input type="radio"/> 8 <input type="radio"/> 9
16	<input checked="" type="radio"/> Capacity Factor <input type="radio"/> Distance from transmission lines	<input type="radio"/> 1	<input type="radio"/> 2 <input type="radio"/> 3 <input checked="" type="radio"/> 4 <input type="radio"/> 5 <input type="radio"/> 6 <input type="radio"/> 7 <input type="radio"/> 8 <input type="radio"/> 9
17	<input checked="" type="radio"/> Capacity Factor <input type="radio"/> Distance from faults	<input type="radio"/> 1	<input type="radio"/> 2 <input checked="" type="radio"/> 3 <input type="radio"/> 4 <input type="radio"/> 5 <input type="radio"/> 6 <input type="radio"/> 7 <input type="radio"/> 8 <input type="radio"/> 9
18	<input checked="" type="radio"/> Capacity Factor <input type="radio"/> Rainfall	<input type="radio"/> 1	<input type="radio"/> 2 <input type="radio"/> 3 <input checked="" type="radio"/> 4 <input type="radio"/> 5 <input type="radio"/> 6 <input type="radio"/> 7 <input type="radio"/> 8 <input type="radio"/> 9
19	<input checked="" type="radio"/> Distance from transmission lines <input type="radio"/> Distance from faults	<input checked="" type="radio"/> 1	<input type="radio"/> 2 <input type="radio"/> 3 <input type="radio"/> 4 <input type="radio"/> 5 <input type="radio"/> 6 <input type="radio"/> 7 <input type="radio"/> 8 <input type="radio"/> 9
20	<input checked="" type="radio"/> Distance from transmission lines <input type="radio"/> Rainfall	<input type="radio"/> 1	<input type="radio"/> 2 <input checked="" type="radio"/> 3 <input type="radio"/> 4 <input type="radio"/> 5 <input type="radio"/> 6 <input type="radio"/> 7 <input type="radio"/> 8 <input type="radio"/> 9
21	<input checked="" type="radio"/> Distance from faults <input type="radio"/> Rainfall	<input type="radio"/> 1	<input checked="" type="radio"/> 2 <input type="radio"/> 3 <input type="radio"/> 4 <input type="radio"/> 5 <input type="radio"/> 6 <input type="radio"/> 7 <input type="radio"/> 8 <input type="radio"/> 9

CR = 5.7% OK

Calculate Download (.csv) dec. comma

AHP Scale: 1- Equal Importance, 3- Moderate importance, 5- Strong importance, 7- Very strong importance, 9- Extreme importance (2,4,6,8 values in-between).

Figure 9 The pairwise comparison module in the software (Anonymous, 2020f); AHP Evaluation Scale: 1- Equal importance, 3- Moderate importance, 5- Strong importance, 7- Very strong importance, 9- Extreme importance, 2,4,6,8- Intermediate values

Table 3. Resulting weights for the criteria based on pairwise comparison

Category	Priority	Rank
Capacity Factor	38.40%	1
Slope	14.90%	2
Distance from Faults	14.30%	3
Distance from Residential Areas	9.80%	4
Distance from Transmission Lines	9.10%	5

Distance from Roads	8.90%	6
Annual Precipitation	4.60%	7

In this study, selected criteria weights are calculated with AHP method. Resulting weights for the criteria based on pairwise comparison was calculated as 38.4% for Capacity Factor, 14.9% for Slope, 14.3% for Distance from Faults, 9.8 for Distance from Residential Areas, 9.1% for Distance from Transmission Lines, 8.9% for Distance from Roads and 4.6% for Annual Precipitation (Table 3). GIS is used for obtaining weights of the factors. Weighted Sum analysis, one of the analyzes of the Spatial Analyst Tool included in the ArcGIS program is used for creating the land suitability index maps for the Wind Turbine siting (Figure 9.). The validity of the created map was checked with the locations of the present wind turbines in the study area.

The criteria selected due to the general characteristics of the study area were integrated with ArcGIS software. The suitable areas for the WEP installation were determined by using the weight values obtained with AHP. The land suitability index map is created in the range of 1-9. The land suitability index map is divided into three categories subsequently: “unsuitable areas”, “alternative areas” and “suitable areas”. According to the obtained results, 26.05% of the working area are suitable for the establishment of a solar power plant. 42.15% of the study area are in an alternative suitability and 31.80% of the area is not suitable for building a wind energy plant.

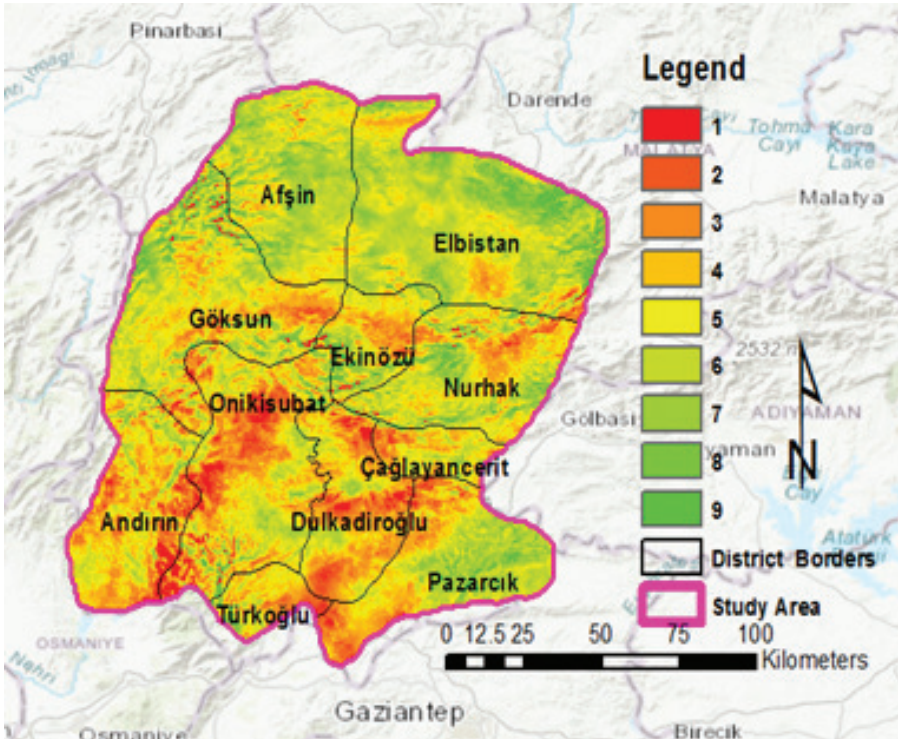


Figure 10. Land suitability index map of the study area

Conclusions

As a result of the study, the following results were obtained:

1. In Turkey, the majority of the energy needs are provided from imported fossil fuels. Our country has the opportunity to pursue a sustainable, secure and clean energy policy by making use of its renewable energy resources. In parallel to Turkey's development and economic growth, energy demand is in a continuous growth. Therefore, this study and similar studies support our country's policy of obtaining clean energy from renewable energy sources.

2. The amount of energy consumed per person in developed countries is higher than in Turkey. Recently, in the world and in Turkey, the concept of global warming and the negative impact it has come to the fore. This situation shows that an unsustainable economic development has a significant cost. In terms of energy production, fossil fueled power plants such as coal, fuel-oil and natural gas cause an increase in average temperatures due to the carbon dioxide and similar greenhouse gases they release into the atmosphere. Accordingly, the natural balance is also deteriorating. This study and similar studies can increase the interest of

people who want to invest in wind energy.

3. When Turkey's conditions examined, the investments in renewable energy are exposed to various risks and difficulties. For this reason, investments in wind energy can be very limited. This and similar studies can be used to reduce the risk of wind energy investors in the location selection process.

4. Wind energy is more advantageous than hydraulic and thermal power plants. Wind energy is a competitive form of energy and has many advantages. The result of this study specifies that the potential of wind energy in Kahramanmaraş and in the Eastern Mediterranean region of Turkey is sufficient to produce electricity.

5. Kahramanmaraş's power plant installed capacity is 4348 MW. There are 2 wind power plants in Kahramanmaraş, one in Caglayançerit and Andirin districts. Wind power plants in Kahramanmaraş produce approximately 85.10 MW of electricity annually. This constitutes 2% of the total electricity generation. In addition, 2 wind power plants are planned to be built. Despite this, it is seen that the share of wind power plants during electricity generation in Kahramanmaraş is low. It is thought that the study conducted may be effective in increasing this share.

6. In the land suitability index map, it was seen that a large part of Afsin and Elbistan districts consisted of suitable and alternative areas for the installation of a wind power plant. Also, southeast and southwest parts of Nurhak district, east and northeast parts of Pazarcik district, west and northwest parts of Goksun district, southeast parts of Onikisubat district, southwest parts of Ekinozu district have suitable or alternative areas for WEP siting. In the study area, Dulkadiroglu district is, the less suitable district for WEP siting.

7. In this article, a site selection study for WEP investment in the Kahramanmaraş province is conducted. A GIS based AHP method, based on seven different criteria is chosen for his purpose. In this study, the areas which are determined as suitable for WEP determined are very compatible with the current WEP locations. This showed that we used generally sufficient criteria in our study for evaluations. Therefore, the Land suitability index map of the study area can be used in preliminary evaluations for investors.

8. It is a well-known fact that determining suitable sites for wind turbine projects is a complex process that does not depend solely on physical criteria. It also includes other economic, physical, social, environmental and political criteria that can lead to different consequences. Based on this, further research is suggested to test their suitability for renewable energy purposes at selected wind turbine sites.

9. Today, our country provides attractive investment opportunities for domestic and foreign investors, especially in investments in wind and solar energy. By improving the investment environment and the provision of energy reform, in the coming years Turkey will become an increasingly more attractive market for the investors. In this context, this study is important for the investors, who will invest in the Kahramanmaraş province.

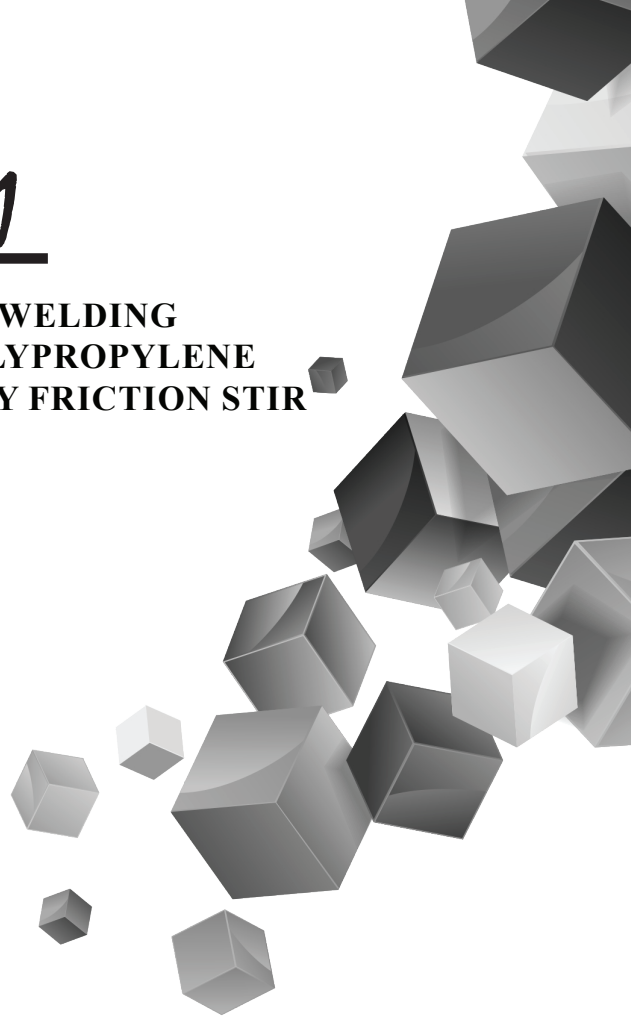
REFERENCES

1. Akinci H., Ozalp A. Y, Turgut B., (2013) Agricultural land use suitability analysis using GIS and AHP technique , *Computers and Electronics in Agriculture* 97; 71–82
2. Anonymous, (2020a). Kahramanmaraş province. Online Access Date:15.03.2020. web site: <https://tr.wikipedia.org/wiki/Kahramanmara%C5%9F>.
3. Anonymous, (2020b). OpenStreet Map <https://www.openstreetmap.org/#map=7/39.031/35>. Online Access Date:03.03.2020 web site:, 252
4. Anonymous, (2020c). <https://www.mta.gov.tr/v3.0/hizmetler/yenilenmis-diri-fay-haritalari>. Online Access Date:05.0.2020
5. Anonymous, (2020d). <https://globalwindatlas.info/downloads/gis-files> Online Access Date:05.0.2020
6. Anonymous, (2020e). <https://www.worldclim.org/>.Online Access Date:05.03.2020
7. Anonymous, (2020f). AHP Priority Calculator Access Date:15.01.2020 web site: https://bpmmsg.com/academic/ahp_calc.php.
8. Bennui A., Rattanamanee P., Puetpaiboon U., Phukpattaranont P., Chetpattananondh K., (2007). Site Selection For Large Wind Turbine Using GIS, *PSU-UNS International Conference on Engineering and Environment (ICEE-2007), Thailand.*)
9. Erdogdu E. (2009) On the wind energy in Turkey. *Renewable and Sustainable Energy Reviews* 13(6):1361–71.
10. İlkiliç, C. (2012). Wind energy and assessment of wind energy potential in Turkey. *Renewable and Sustainable Energy Reviews* Volume: 16, pp.: 1165– 1173.
11. Kaygusuz K. Renewable and sustainable energy use in Turkey: a review. *Renewable and Sustainable Energy Reviews* 2002;6:339–66
12. NASA/METI/AIST/Japan Spacesystems, and U.S./Japan ASTER Science Team (2019). ASTER Global Digital Elevation Model V003 [Data set]. NASA EOSDIS Land Processes DAAC. Accessed 2020-01-05 from <https://doi.org/10.5067/ASTER/ASTGTM.003>
13. Nestmann, F. and Maskey, R.K. (1998) Hydropower: A Regenerative Energy Source from the Sun. *Energi* , No. 2, 9-16.
14. Oner Y, Ozcira S, Bekiroglu N (2009) Prediction wind energy potential using by wind data analysis in Bababurnu-Turkey. In: *Proceedings of the IEEE 2nd International Conference on Clean Electrical Power, Italy*; 9–11 June 2009. p. 232–5.

15. Ozgener L. (2011) Investigation of wind energy potential of Muradiye in Manisa, Turkey. *Renewable and Sustainable Energy Reviews* 15(9):3232–6.
16. Ozturk, D., Batuk, F., 2007. Criterion Weights in Decision Making with Multiple Criteria. *Yıldız Technical University Sigma Engineering and Science Journal* 25 (1),86–98. (In Turkish)
17. Ozturk, D., Batuk, F., 2010 Using Analytical Hierarchy Method In Spatial Decision Problems. *Sigma Engineering Science Journal* Volume 28, Pages 124-137. (In Turkish)
18. Saaty, T. L., (1980). *The Analytic Hierarchy Process: Planning, Priority Setting, Resource Allocation*, ISBN 0- 07-054371-2, McGraw-Hill
19. Saaty T.L. (1990). How To Make A Decision: The Analytic Hierarchy Process. *European Journal of Operational Research*, 48(1), 9-26.
20. Uyan M., (2017) GIS-Supported mapping of solar power plant sites using AHP method . *Pamukkale Univ Muh Bilim Derg*, 23(4), 343-351, (In Turkish)
21. Wind, Y., Saaty, T. L., (1980). Marketing application of the analytic hierarchy process. *Management Science*, 26 (7): p. 641-658.
22. Yalçın, C , Yüce, M., (2020) Determination of Areas Suitable for Solar Power Plant (SPP) Investment in Burdur by GIS Method. *Geomatik* , 5 (1) , 36-46 . DOI: 10.29128/geomatik.561962 (In Turkish)

Chapter 21

DETERMINATION OF WELDING PARAMETERS OF POLYPROPYLENE SHEETS OF JOINED BY FRICTION STIR WELDING



İhsan KÜÇÜKRENDECI

1. Introduction

The use of friction stir welding method in the joining of metallic materials is increasing over time. Friction stir welding (FSW) offers superior mechanical properties in metal joining. This situation encourages researchers on the subject of metal joining. As a result of the studies, it was possible to combine Polymers with FSW. The joining of polymers with FSW is a new study issue. More courageous studies are needed in this area and much more investigations are needed on the subject.

A superior mechanical property and good a surface quality is aimed in joining polymer materials with FSW. A good tool design and suitable welding parameters are important for this. Vijendra and Sharma (2015) investigated the material flow and weld formation mechanism in joining of thermoplastics materials with FSW. In process, the welding tool was heated by induction. Banjare, Sahlot and Arora (2017) improved the tensile strength of friction stir welded polypropylene. In their studies was used heated tool and the welds was produced with more ductility than the conventional FSW. Sheikh-Ahmad, Alia, Devecib, Almaskaric and Jarrara (2019) studied on friction stir welding of HDPE carbon black composite. The effects of welding parameters were investigated on welding quality. The welding temperature was measured with special techniques. Azarsa and Mostafapour (2013) developed a new method of friction stir welding for producing of polymer metal surface or bulk composites in order to enhance the mechanical, electrical and thermal properties. The rotating pin with heating system was designed for a successful welding. Karagoz and Oksuz (2018) studied relationship between the microstructure and the mechanical properties and the joining performance by joining the thermoplastics with FSW. Lambiase, Paoletti, and Di Ilio (2015) investigated the influences of welding parameters on mechanical behaviour. The polycarbonate sheets were joined with friction stir spot welding (FSSW) and an artificial neural network (ANN) model was developed to relationship between experimental measurements and model. Kaddour, Miloud, El Bahri, and Abdellah (2019) studied on the weldability of high-density polyethylene (HDPE) using the friction stir welding technique. A parametric choice was made to optimize welding parameters. Eslami, Miranda, Mourão, Tavares, and Moreira (2018) et al. aimed to find the optimal welding set for polymer material joining by FSW. Taguchi method were used to select of welding parameters. Also welding temperature was recorded during process for study. Squeo, Bruno, Guglielmotti and Quadrini (2009) investigated FSW of polyethylene sheets with a single pass. Also, double passing was examined and introduced several technical problems in FSW process. Moochani, Omidvar, Ghaffarian and Goushegir (2019) introduced a new heat-assisted stationary shoulder FSW tool design. The constant tool temperature was provided during the FSW process. Effect of the process

parameters was investigated using Taguchi method and analysis of variance. Moreno-Moreno et al. (2018) investigated effects of rotational and welding speed on the mechanical properties and thermal behaviour in friction stir welded joints of high-density polyethylene. The non-rotational shoulder was used in the experiments. The mechanical properties were determined according to tensile and hardness values. Paoletti, Lambiase and Di Ilio (2016) studied the effect of the main FSSW process parameters on the developing forces (plunging force and torque), tool and weld temperature. Additionally, the mechanical behaviour and geometry of the joints was investigated. Polycarbonate (PC) materials was used for properties of high mechanical strength and toughness. Küçükrendeci (2019) investigated determine to suitable welding parameters in welding of polypropylene sheets with FSW method. The weld zone microstructure was examined and Shore hardness measurements were made. Charpy impact test was used to determine welding parameters.

Joining of polypropylene sheets with friction stir welding has recently gained value. In addition, the strength of the weld zone is also important. A strength joining of welding occur in suitable and controllable welding parameters. In this study is determinates welding parameters of polypropylene sheets joined by the friction stir welding (FSW). The values of tensile strength and elongation of welded joints were compared according to values of the main material. Same time, the microstructure properties of the welded section was examined.

2. Materials and Methods

2.1 Welding Method

Friction Stir Welding is a solid-state process, which means that the objects are joined without melting point. This opens up whole new areas in welding technology. The FSW is used as rapid and high in quality welds of alloys. The different materials can be joined with FSW and this method is very important a advantage. In FSW, a cylindrical shouldered tool with a profiled pin is rotated and plunged into the joint area. The parts have to be securely clamped to during FSW, because the joint faces from being forced apart. Frictional heat between tool and the materials causes to soften without reaching melting point, allowing the tool to traverse. The doughy material, transferred to rear edge of the tool pin through intimate contact with the tool shoulder and pin profile. During cooling, a solid phase created between the materials. For example, friction stir welding can be used to join aluminium sheets and plates. In FSW is not filler wire or shielding gas. Material thicknesses ranging from 0.5 to 65 mm can be welded from one side. The porosity or internal voids has not in welding zone.

In FSW method, the focus has traditionally been on non-ferrous alloys, but recent advances have challenged this assumption, enabling FSW to be applied to a broad range of materials. FSW has been proven successful on numerous of alloys and materials, including high-strength steels, stainless steel, titanium and polymer materials. A improvements on the existing methods and materials as well as new technological development, an improvement is expected.

The FSW process involves joint formation below the base material's melting temperature. With FSW, the heat input is purely mechanical and thereby replaced by force, friction, and rotation. Several studies have been conducted to identify the way heat is generated and transferred to the joint area.

The simple pin-shaped, non-profiled tool creates frictional heat and is very useful if enough downforce can be applied. Unfortunately, the oxide-layer breaking characteristics are not very good, and as material thickness is increased, welding heat at the lower part of the joint may be insufficient. With parameter adjustment and tool geometry optimisation, the oxide-layer could be broken more effectively. The need to generate more frictional heat and break the oxide-layer more effectively has been a driving force in tool development for light-metals. Especially as many of the intended applications are considered critical. The traces of the tool left in the seam is important.

The process of FSW is most suitable for components which are flat and long (plates and sheets) but can be adapted for pipes, hollow sections and positional welding. The welds are created by the combined action of frictional heating and mechanical deformation due to a rotating tool. The maximum temperature reached is of the order of 0.8 of the melting temperatures. The tool has a circular section except at the end where there is a threaded probe or more complicated flute; the junction between the cylindrical portion and the probe is known as the shoulder. The probe penetrates the workpiece whereas the shoulder rubs with the top surface. The heat is generated primarily by friction between a rotating--translating tool, the shoulder of which rubs against the workpiece. The welding parameters have to be adjusted so that the ratio of frictional to volumetric deformation--induced heating decreases as the workpiece becomes thicker (Figure 1).

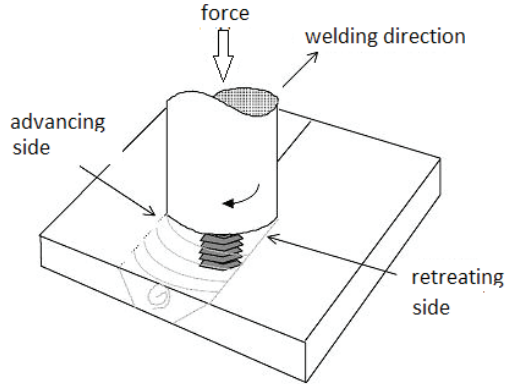


Figure 1: General FSW method

The microstructure of a friction stir welding depends in detail on the tool design, the rotation and translation speeds, the applied pressure and the characteristics of the material being joined. There are a number of zones. The heat-affected zone (HAZ) is as in conventional welds. The central nugget region containing the onion-ring flow-pattern is the most severely deformed region, although it frequently seems to dynamically recrystallise, so that the detailed microstructure may consist of equiaxed grains. The layered (onion-ring) structure is a consequence of the way in which a threaded tool deposits material from the front to the back of the weld. It seems that cylindrical sheets of material are extruded during each rotation of the tool, which on a weld cross-section give the characteristic onion-rings (Figure 2). The thermomechanically-affected zone lies between the HAZ and nugget; the grains of the original microstructure are retained in this region, but in a deformed state. The top surface of the weld has a different microstructure, a consequence of the shearing induced by the rotating tool-shoulder.

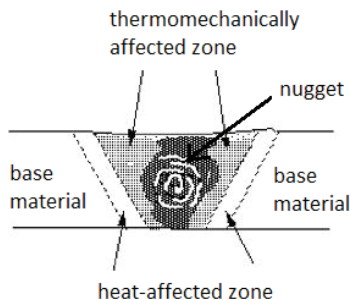


Figure 2: Characteristic microstructural zones

The process can be primarily used in industry to join aluminium alloys of all grades, whether cast, rolled or extruded. FSW has been shown to weld aluminium alloy butt joints with a thickness of between 0.3mm and

75mm in a single pass, depending on the alloy grade and capability of the FSW machine. Other materials that have been joined with FSW include magnesium, titanium, copper, nickel and steel alloys, while plastics and metal matrix composites (MMC). This process has also been shown to be able to join dissimilar combinations of these materials including aluminium to steel

2.2 Material and Tool Desing

In study, polypropylene (PP) sheets were used as main material. The sheets were acquired commercially and were thickness of 8 mm. PP has strong chemical resistance and it is low cost and it is used to very various applications. The physical and mechanical properties of PP was showed in Table 1.

Properties of PP material are permanent-heat stability, high chemical resistance, high corrosion resistance. Areas of use of PP materials are chemical installations, pharmaceuticals and bioindustry, livestock farming and agriculture, fish farming and food production. At the same time, PP material is used in the production of ventilation ducts and electrolysis coating pools. PP materials are particularly resistant to chemical abrasion.

Table 1: Physical and mechanical properties of polypropylene (Simona, 2020)

Yield Stress [MPa]	Elongation at yield [%]	Density [g/cm ³]	Shore hardness D	Melting temperature [°C]
32	8	0.9	70	160-165

The welding quality and tool wear are two important considerations in the selection of tool material, the properties of which may affect the weld quality by influencing heat generation and dissipation. The weld microstructure may also be affected as a result of interaction with eroded tool material. Tool wearing is a undesirable effect on the weld microstructure and same time this situation increases the processing cost of FSW. Owing to the severe heating of the tool during FSW, significant wear may result if the tool material has low yield strength at high temperatures. Stresses of tool are dependent on the strength of the workpiece at high temperatures.

Tool geometry affects the heat generation rate, traverse force, torque and the thermomechanical environment experienced by the tool. The flow of plasticised material in the workpiece is affected by the tool geometry as well as the linear and rotational motion of the tool. Important factors are shoulder diameter, shoulder surface angle, its shape and size of pin geometry and the nature of tool surfaces.

The dia meter of the tool shoulder is important because the shoulder generates most of the heat, and its grip on the plasticised materials largely establishes the material flow field. Both sliding and sticking generate heat whereas material flow is caused only from sticking. For a good FSW practice, the material should be adequately softened for flow, the tool should have adequate grip on the plasticised material and the total torque and traverse force should not be excessive. The shape of the tool shoulder surface is an important for tool design. The shape of the tool pin influences the flow of plasticised material and affects weld properties.

Compared with the tool shoulder, the tool pin suffers much more severe wear and deformation, and the tool failures almost always occur in the pin. This can be occurred several reasons. For example, the tool pin is completely immersed in the workpiece and, therefore, has been to face more resistance to it compared with the tool shoulder, only a small part of which is inside the workpiece.

Three different types of tools were used in the study. The pin shape of these tools has been designed and manufactured as conical. Each conical pin has different dimensions. Pins were produced in the form of grooves. The tools used to this experiment were made of 4140 steel tool and tool hardness was 44 HRC. Three different types of tools were used in experimental studies. The tool shape is designed and manufactured specifically for this work. Figure 3 showed the tool dimensions and shape. Table 2 showed the dimensions of the tools.

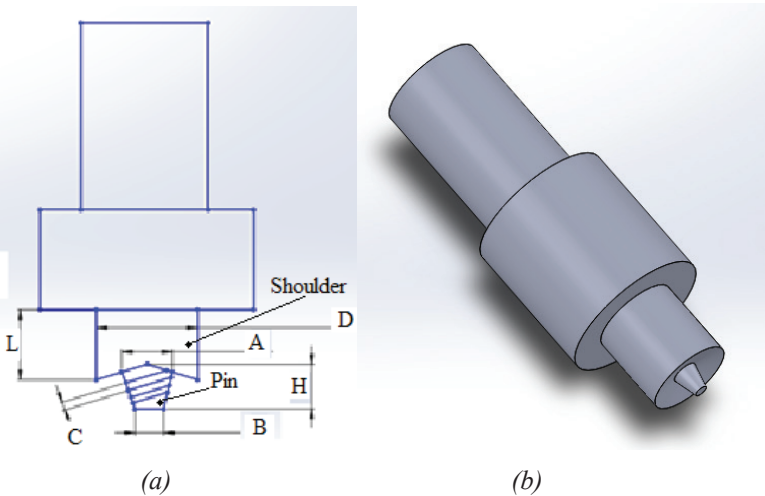


Figure 3: a-Tool dimensions, b-Tool shape

Table 2: The dimensions of tools

Tool Types	D(mm)	L(mm)	A (mm)	B(mm)	H(mm)	C(mm)
1	13	15	6	4.5	6	1.5
2	15	20	5	3	6	1.5
3	15	20	6	3.5	6	1.5

2.3 Experimental Procedure

The polypropylene sheets were joined in side to side with FSW. The universal milling machine were used in the welding process. This machine has mechanical setting and classical clamping fixtures. Figure 4 showed the welding process in study. A sample clamping fixtures was designed and manufactured to enable proper welding.

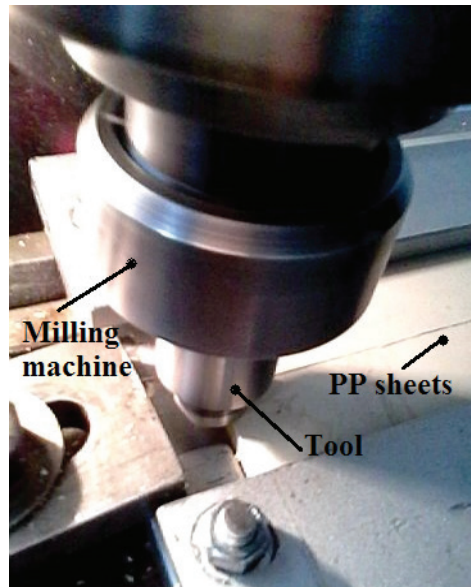


Figure 4: The welding process

In the experimentally analyses, classical experimental methods were used for the analyses of the mechanical testing. Tool type, rotation speed and welding speed were selected for each welding parameter. High mechanical behaviour is desirable from welded joints. In the analyses are taken into account tensile strength and elongation of welded joints. The welding parameters can be determined to test results.

Firstly, a series of welding parameters were selected. These are rotational speeds and welding speeds for three different tools. The tool rotational speed and machine table speed of the milling machine were

set. Selected parameters showed in Table 3. The PP sheets were securely attached to the workbench with the clamping fixture. The shoulder section of the tools is concave shape and this shape pushes dough material back into the welding zone without moving it out. The tool has a pin and the grooves are machined on the pin. The grooves regulate the downward flow of my material. PP sheets prepared with dimensions of 100x200x8 mm were combined with FSW according to selected parameters. The welded material was prepared in milling machine for tensile tests. The welding process was carried out at room temperature. Welded PP sheets are shown in Figure 5. In Figure 6, sample dimensions are seen for tensile tests.

Welding in the butt joint configuration is much more challenging than in the lap joint configuration, and a modification in the clamping setup was required to guarantee that the welding tool is always in-between the abutting plates, as well as avoiding lateral movements of the plates under the axial forces. Usually, the lateral movement of the plates occurs due to the tool's torque during the plunging stage, which pushes the plates aside from the tool, and consequently results in defect formation. In Figure 5 seen to adequate butt-welding configuration.

Standard test method for tensile properties of plastics (ASTM D638 standard) was used in the tensile testing. Tests was performed at room temperature with test speed of 10 mm/min. The average three sample were tested to determine tensile strength and elongation. The sample was moulded for the microstructure examination. Microstructure image of the welded section was taken from a Nikon MA 200 Eclipse Polarized Light Microscope (Figure 7)

ASTM D638 standard is test method covers the determination of the tensile properties of unreinforced and reinforced plastics in the form of standard dumbbell-shaped test specimens. This test is applied in conditions of pre-treatment, temperature, humidity, and testing machine speed. This test method is applicable for testing materials of any thickness up to 14 mm. Materials with a thickness greater than 14 mm (0.55 in.) shall be reduced by machining. In This test method can be determined Poisson's ratio at room temperature. Test data obtained by this test method have been found to be useful in engineering design. The specimen is added into tensile grips. The test is beginning by separating the tensile grips at a constant rate of speed. Speed depends on specimen shape and can range from 1.5 – 500 mm per minute. The target time from start of test to break should be from 30 seconds to 5 minutes. The test is ended after sample break (rupture). The values of tensile strength, elongation at yield, modulus of elasticity and poison's ratio can be obtained in results of tests.

Table 3: The selected parameters of FSW

Welding condition	Tool type	Tool rotational speed (rpm)	Welding speed (mm/min)
1	1	560	11.2
2	1	900	16
3	1	1400	22.4
4	2	560	16
5	2	900	22.4
6	2	1400	11.2
7	3	560	22.4
8	3	900	11.2
9	3	1400	16

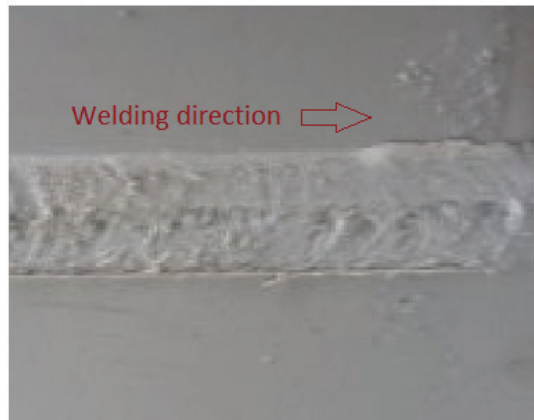


Figure 5: Welded PP sheets

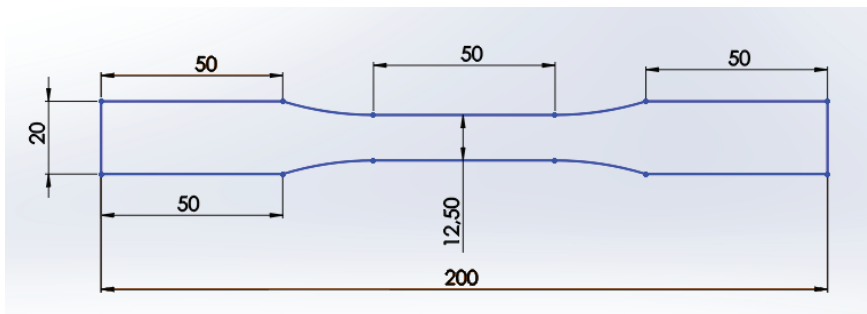


Figure 6: Sample dimensions

3. Results and discussion

PP sheets were successfully welded with FSW. Tensile tests of prepared samples were carried out and the results of the tensile tests are interpreted.

3.1 Microstructure of the Welded Section

Figure 7 shows the microstructure picture of the welded section for a sample. Welding parameters of microstructure of welded sample are tool type 3, tool rotational speed 560 rpm, welding speed 22.4 mm/min. The difference between the welded section and the base material is seen in Figure 7. Base or main material seem a regular structure and welded section seem difference in crystalline structure. Between two sections is a border line. The welding strength could be expressed with interface structure of between main material and the welded section. Main material has uniform structure. However, a grained structure is observed in welded section. The boundary line along has lack of contact. This situation could be occurred from warming and cooling. The tool quickly moves away from the molten zone in welding process. Fast warming and slow cooling is occurred in welded section and the grain structure differentiated. The contact lack of the boundary line can be reduced according to the welding parameters and process conditions. Thus, can be improved welding strength and values of welding strength is determined to experimental workings.

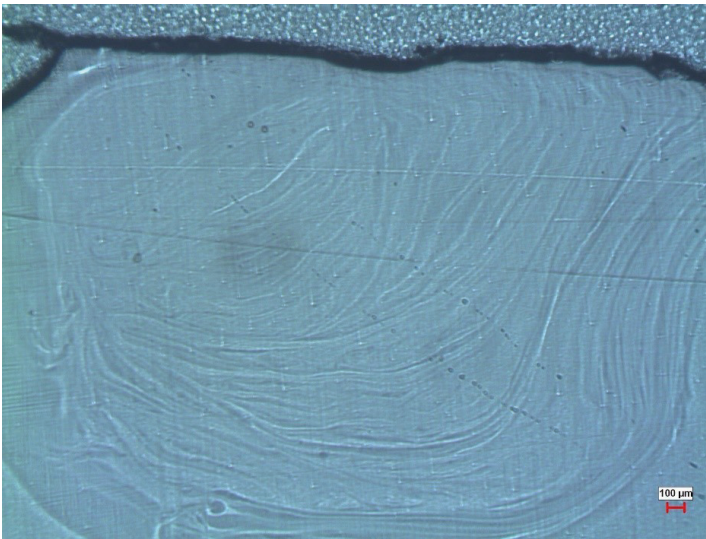


Figure 7: Microstructure of the welded section

3.2 Mechanical Properties of the Welded Joints

Tensile tests were performed by Zwick/Roll (device with autograph capability) and samples were extracted from each welded part in accordance with ASTM D638 standard. The specimens were obtained for evaluating properties of each welded sample. Three samples were tested under each welding condition.

In all processing conditions, the plunge depth was same and 6 mm. This value of plunge depth has been chosen according to the material thickness. In other words, designed tool is operated with about 6 mm of the tool on contact with the workpiece; any additional workpiece contact will produce significant amount of flash around the shoe. As the penetration depth of tool shoulder increases, more pressure applied to the material exists at the surface of the sheets. Since these surface materials are completely melted, increasing pressure will results in outpouring of them from weld nugget, consequently leads to thickness reduction. Therefore, tensile strength can be decrease due to stress concentration in this area. If the penetration depth is selected lower than 6 mm, the shoulder will ride on a cushion of material that will smear across the joint line, which in turn lead to low quality joints.

The average values of tensile strength and elongation of the welded samples are showed in Figure 8. The strength values of the joints changed according to the process parameters. Besides this, the elongation values change according to the process parameters. The tensile strength values of the welded section are in between 1.7 and 14.5 MPa. The elongation values were variated from 1 to 2.6%.

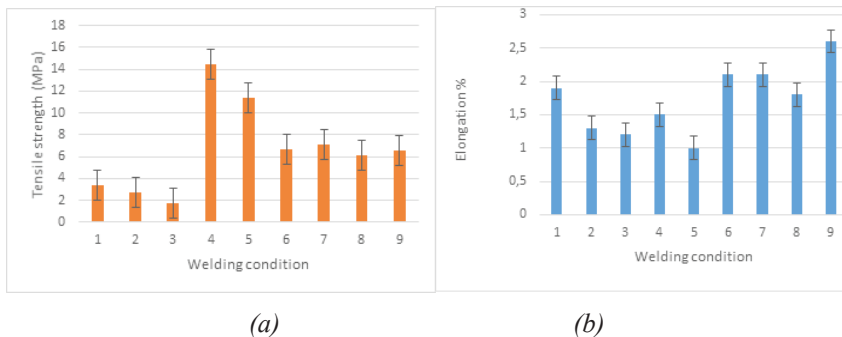


Figure 8: *a- Tensile strength values of the welded samples,*
b- Elongation values

4. Conclusions

The polypropylene sheets were joined by using friction stir welding. The tensile strength as 45% of base material strength (Figure 8a). The tensile strength values of the welded section are seen between 1.7 and 14.5 MPa. These values are seen between 5.3% to 45% of the main material strength. In Figure 8b, the elongation values are seen variated from 1 to 2.6% (12.5 to 32.5% of the main material elongation). Mechanical properties and microstructure of joined polypropylene sheets with friction stir welding process was affected from the process parameters.

Generally, higher tensile for welding zone can be obtained with optimal values of tool rotational and welding speed. The mechanical properties of welding zone can be determined through the various tests carried out.

The results obtained show the complex relationship between material and tool by several welding parameters such as the advance speed, the rotation speed and tool geometry. Besides, the behaviour of the welded joint FSW strongly depends on the geometry of the tool.

The determine of all welding parameters provides the strong and important results in FSW welding of PP. Also, it is very important also environmental conditions of FSW. In study, according to the results obtained of tensile strength, it is observed that the best result was obtained by welding condition 4. The same time, the best result of elongation % was obtained by welding condition 9. It is quite difficult to do experimental studies and it is very time consuming. Considering the wide usage area of PP, it is important to continue experimental studies on this subject.

References

- Vijendra, B. and Sharma, A. (2015). Induction heated tool assisted friction stir welding (i-FSW): A Novel Hybrid 2 Process for Joining of Thermoplastics. *Journal of Manufacturing Processes*, 20, 234-244. doi: 10.1016/j.jmapro.2015.07.005
- Banjare, P. N., Sahlot, P. and Arora, A. (2017). An assisted heating tool design for FSW of thermoplastics. *Journal of Materials Processing Technology*, 239, 83–91. doi:10.1016/j.jmatprotec.2016.07.035
- Sheikh-Ahmad, J.Y., Alia, D.S., Devecib, S., Almaskaric ,F. and ,Jarrara F. (2019). Friction stir welding of high-density polyethylene-Carbon black composite. *Journal of Materials Processing Technology*, 260, 402–413. doi:10.1016/j.jmatprotec.2018.09.033
- Azarsa, E. and Mostafapour, A. (2013). In the feasibility of producing polymer metal composites via novel variant of friction stir processing. *Journal of Manufacturing Processes*, 15 (4), 682-688. doi:10.1016/j.jmapro.2013.08.007
- Karagöz, İ. and Öksüz, M. (2018). Microstructures occurring in the joined thermoplastics sheets with friction stir welding. *Journal of the Faculty of Engineering and Architecture of Gazi University*, 33(2), 503-515. doi: 10.17341/gazimmfd.41635
- Lambiase, F., Paoletti, A. and Di Ilio, A. (2015). Mechanical behaviour of friction stir spot welds of polycarbonate sheets. *The International Journal of Advanced Manufacturing Technology*, 80, 301–314. doi:10.1007/s00170-015-7007-4
- Kaddour, H., Miloud, M. H., El Bahri, O. and Abdellah, L. (2019). Mechanical behaviour analysis of a Friction Stir Welding (FSW) for welded joint applied to polymer materials. *Frattura ed Integrità Strutturale*, 47, 459-467. doi:10.3221/IGF-ESIS.47.36
- Eslami, S., Miranda, J.F., Mourão, L., Tavares, P.J. and Moreira, P.M.G.P. (2018). Polyethylene friction stir welding parameter optimization and temperature characterization. *The International Journal of Advanced Manufacturing Technology*, 99, 127–136. doi:10.1007/s00170-018-2504-x
- Squeo, E.A., Bruno, G., Guglielmotti, A. and Quadrini, F. (2015). Friction stir welding of polyethylene sheets. *The Annals Of “Dunărea De Jos” University of Galați Fascicle V, Technologies in Machine Building*, ISSN 1221- 4566, 241-246.
- Moochani, A., Omidvar, H., Ghaffarian, S.R. and Goushegir, S.M. (2019). Friction stir welding of thermoplastics with a new heat-assisted tool design: mechanical properties and microstructure. *Welding in the World*, 63, 181–190. doi:10.1007/s40194-018-00677-x

- Moreno-Moreno, M., Romero, Y.M., Zambrano, H.R., Restrepo-Zapata, N.C., Afonso, C.R.M., and Unfried-Silgado, J. (2018). Mechanical and thermal properties of friction-stir welded joints of high-density polyethylene using a non-rotational shoulder tool. *The International Journal of Advanced Manufacturing Technology*, 97, 2489–2499. doi:10.1007/s00170-018-2102-y
- Paoletti, A., Lambiase, F. and Di Ilio, A. (2016). Analysis of forces and temperatures in friction spot stir welding of thermoplastic polymers. *The International Journal of Advanced Manufacturing Technology*, 83, 1395–1407. doi:10.1007/s00170-015-7669-y
- Küçükrendeci, İ. (2019). The investigation of suitable welding parameters in polypropylene sheets joined with friction stir welding. *Bulletin of The Polish Academy of Sciences Technical Sciences*, 67(1). doi:10.24425/bpas.2019.127342
- Simona (2020). www.simona.de

Chapter 22

FERROCHROMIUM SLAG

UTILIZATION IN HOT MIX ASPHALT



Altan YILMAZ¹

¹ Mehmet Akif Ersoy University, Department of Civil Engineering, Burdur/Turkey This study was produced from the author's master thesis.

1. INTRODUCTION

The main flexible pavement material in use today is asphalt concrete. This is a high-quality pavement surface composed of asphalt cement and aggregates, hot-mixed in an asphalt plant and then hot-laid. Asphalt concrete must provide a stable, safe and durable road surface. The properties of asphalt concrete depend on the quality of its components, binder, aggregates and filler, and the mix design proportions. Relative amounts of aggregate, binder and air void are very important [1].

In the meantime, as natural supplies of high quality granular materials used in highways have become less abundant, the highway engineer is faced with the challenge of finding alternative materials to meet the requirements for these materials. Some of these alternative materials are hydrated lime, Portland cement, marble dust [3], fly ash [4], coal dust [5], pumice dust [6], sewage sludge ash [7], steel slag [8] etc. Both environmental and economic factors also contribute to the growing need for the use of reclaimed materials in asphalt pavements. One of these reclaimed materials, ferrochromium slag, has not been used extensively in pavements even though it has got promising features.

A certain amount of filler is necessary in bituminous mixtures to obtain the required density and strength. The filler particles fill a portion of the space between sand and gravel particles, and thus contribute to increase density. The filler also influences the optimum binder content in bituminous mixtures by increasing the surface area of mineral particles. Several studies; Puzinauskas [2], Anderson et al. [9], Kandhal et al. [10], Shahrour and Saloukeh [11], Ishai et al. [12], Ishai and Craus [13], Tayebali et al. [14], Hussain Bahia [15] conclude that fillers largely influence the asphalt mixture performance. Different filler materials may have different mechanical properties in the asphalt mixture. Dukatz and Anderson [16] have investigated eight different filler materials to investigate the mechanical properties of asphalt and they found that different filler materials have different effects on stiffness and had almost no effect on Marshall stability and void ratio.

In this study, various percentages of asphalt cement, limestone filler and FeCr slag filler were used to prepare the Marshall specimens and then stability and flow tests and creep test were carried out on the specimens. After getting design parameters, utilization of slag filler in asphalt mixtures was investigated in comparison with limestone filler.

2. MATERIALS

2.1. Properties of Mineral Filler

Mineral filler is usually defined as a material which passes No.30 (0,600 mm) standard sieve. Moreover; at least 70 percent of this material passes No.200 (0,075 mm) standard sieve [18]. Mineral filler plays an important role in arranging the properties of the mixture; however, it covers a very little part of all aggregate. Filler is generally used at low rates such as 3% – 9%. This component change the aggregate gradation by filling air voids until a certain amount and this provides more touch points between aggregate particles and this contributing to obtain denser mixtures [19]. This situation is particularly important for surface layers, because increased composite and increased density gets good impermeability.

The function of mineral filler is more than filling voids. In addition, filler shows binder and slippery effects in the bituminous mixtures and helps to get mortar, this dual role differs mineral filler from other aggregates.

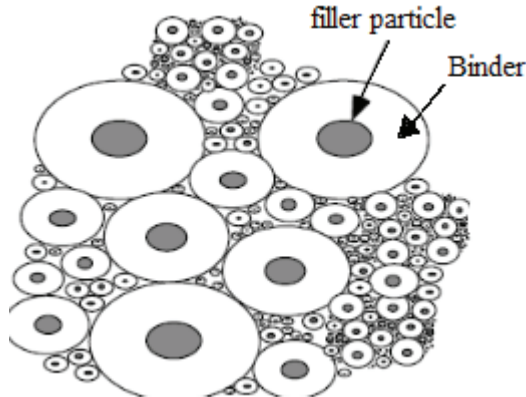


Figure 1. *Fillers' interaction with bitumen*

2.2. Properties of Slag Filler (FeCr slag)

Ferrochromium slag dust is used as artificial filler in this study. Slag was obtained from ETİ Electrometallurgy Establishment (ETİ E.E.) which is founded in Antalya-Turkey. Every day, approximately 70-80 tons of Ferrochromium slag (FeCr slag) are produced in ETİ E.E. and disposal of the waste slag constitutes a problem. Chemical analysis of FeCr Slag is shown in Table 1.

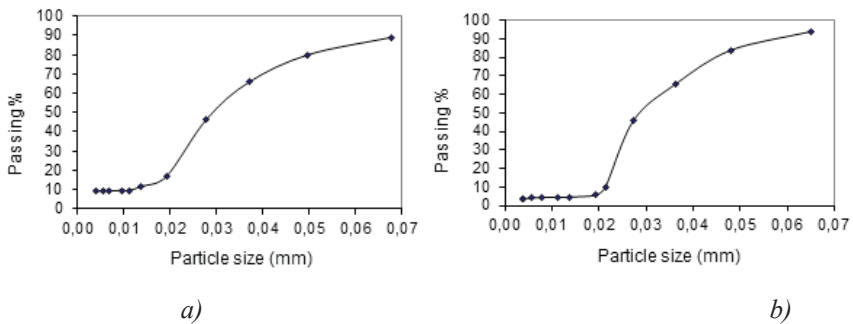
Table 1. Chemical properties of electric-arc furnace slag (Ferrochromium slag)

Element	Cr ₂ O ₃	SiO ₂	Fe ₂ O ₃	Al ₂ O ₃	CaO	MgO	S	C
Percentage	0.52	31.18	1.02	8.66	45.58	12.78	0.08	0.11

During the Ferrochromium and Silico-ferrochromium production process in the electric-arc furnaces, unreduced oxides and some SiO₂ form a liquid slag layer on the pots. Slag is poured into the slag molds and let to cool in open air. Air cooled FeCr slag is gradually transformed into powder form and it gains a crystal structure because of slow cooling process.

Only the minus No.200 sieve (0,075 mm) fraction of FeCr slag was evaluated in this study. The grading of slag filler and limestone filler were measured with a hydrometer analysis test. In this test, the filler is allowed to settle in solution and the rate of settling is related to particle size. Gradation curves for two fillers are shown on graphs given in Figure 2.a and 2.b).

Scanning electron microscopy (SEM) was used to observe the microstructure of slag filler particles (Figure 3). The SEM micrographs were obtained from Akdeniz University, Antalya/Turkey. The micrograph shows that the slag filler particles have rough and sharp surface with crystal structure. This phenomenon may cause the higher friction inside the samples.

**Figure 2.** Particle size distributions of filler (a- Slag filler, b- Mineral filler)

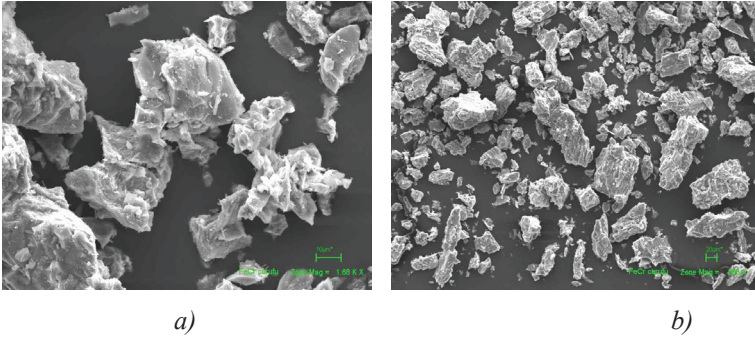


Figure 3. SEM images of FeCr slag (a- 1680x , b- 365x magnified)

2.3. Mineral Aggregate

Crushed aggregate of Antalya region was used in this study, aggregate gradation which is suggested from Turkish Highway Administration shown in Figure 4 [20]. Physical properties of aggregate and filler are shown in Table 2.

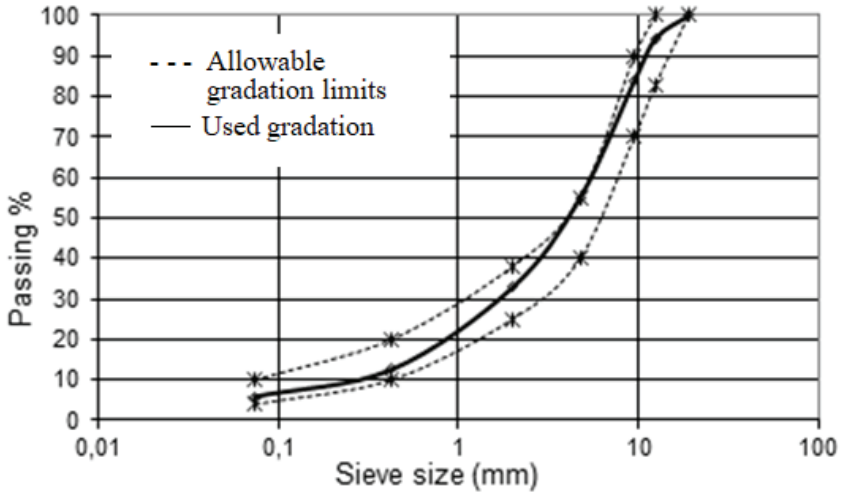


Figure 4. Aggregate gradations

Table 2. Physical properties of aggregate and filler

Properties	Value	Limits	Standard
Specific gravity of course aggregate	2,70 gr/cm ³	-	TS-EN 1097-6
Course aggregate, water absorption	0,37 %	Max 2,0	TS-EN 1097-6
Specific gravity of fine aggregate	2,65 gr/cm ³	-	TS-EN 1097-6

Los Angeles abrasion loss	20,2 %	Max 30%	TS EN 1097-2
Freeze thaw test with Na ₂ SO ₄	4,3 %	Max 12%	TS-EN 1367-2
Aggregate stripping resistance	72 %	Min 50%	ASTM D 1664
Limestone filler bulk specific gravity	2,69 gr/cm ³	-	ASTM D 854
FeCr slag filler bulk specific gravity	3,16 gr/cm ³	-	ASTM D 854

2.4. Asphalt Cement

50-70 penetration grade asphalt cement is selected. Determined properties of asphalt cement are shown in Table.3.

Table 3. Properties of asphalt cement [21]

Properties	Unit	Value	Related Standard
Penetration, 25°C, 100 g, 5 sec	1/10 mm	62	TS EN 1426
Ductility, 25 °C, 5 cm/min.	cm	100+	TS EN 13398
Softening point (ring and ball method)	°C	50,1	TS EN 1427
Flash point (Cleveland open pot)	°C	339	TS EN ISO 2592
Specific gravity	gr/cm ³	1,023	TS 1087

*TS: Turkish Standards

3. PERFORMANCE of ASPHALT MIXTURE

Diameter of 101.7 mm and a height of 63.5 mm Marshall specimens were prepared with various asphalt contents to determine the optimum bitumen content for each filler type. 7 different asphalt content at 0,5% increments (3,5% - 4,0% - 4,5% - 5% - 5,5% - 6% - 6,5%) and two filler materials (slag filler and limestone filler) were used for specimens.

The initial filler content was 7%. Marshall mixture design method, described in ASTM D.1559 was applied in the study. Stability and flow test were carried out on these specimens. The specimens were also tested for density and voids analysis. According to Marshall design method optimum bitumen contents were determined for each filler type. Average of the two optimum bitumen contents determined as optimum bitumen content (5,1%).

Marshall specimens were prepared with 75 standard compaction blow for each side, considering heavy traffic level. This is better simulates the required density for pavement construction. Mixing and compaction temperatures were controlled to produce viscosities of 170±20 cst and 280±30 cst, respectively [22]. Three specimens were manufactured for each combination.

In further tests, defined optimum bitumen content (5,1%) and various filler contents (2,5% - 5% - 7% - 10%) were used to prepare specimens. Aggregate gradations used for new specimens are shown in Table 5. When the filler content was increased from 0 to 10 percent, in order to accommodate the increased quantity of filler, an equal volume of fine aggregate (minus No.10) was removed and replaced by an equal volume of filler. Specimens were then tested for stability and flow, permanent deformation, air void content, density, voids filled with bitumen, voids in mineral aggregate. Test results are shown in Figure 5 to Figure 10.

Table 4. Hot mix asphalt design specifications (KGM*)

Specification	Binder Course		Friction Course	
	Min	Max	Min	Max
Std. Impact Number	75		75	
Stability, KN	7.5	-	9.0	-
Air voids in mixture, VTM %	4	6	3	5
Voids in Aggregate, VMA %	13	-	14	-
Flow, 1/100 in (mm)	8 (2)	16 (4)	8 (2)	16 (4)
Bitumen %	3.5	6.5	4	7
HMA Density*	2.30 – 2.50			

*Turkish Highway Administration Office

Minimum stability criteria suggested by Asphalt Institute for heavy traffic condition is 8006 N [23].

Table 5. Gradations for mixtures containing various filler percentages

Filler content (%)	0,0	2,5	5,0	7,0	10
Sieve Grade	Total Percentage Passing				
¾"	100	100	100	100	100
½"	91,5	91,5	91,5	91,5	91,5
3/8"	80	80	80	80	80
No.4	47,5	47,5	47,5	47,5	47,5
No.10	30	30,5	31	31,5	32
No.40	12	13	14	15	16
No.200	0	2,5	5	7	10

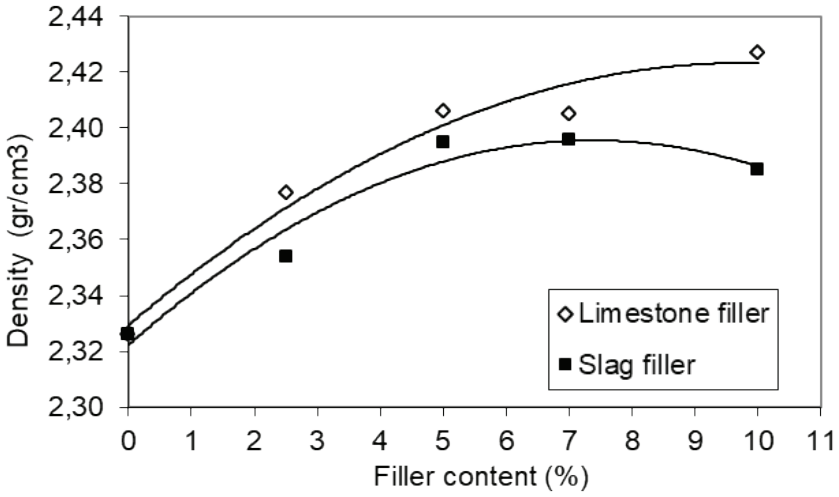


Figure 5. Filler content versus specimen density

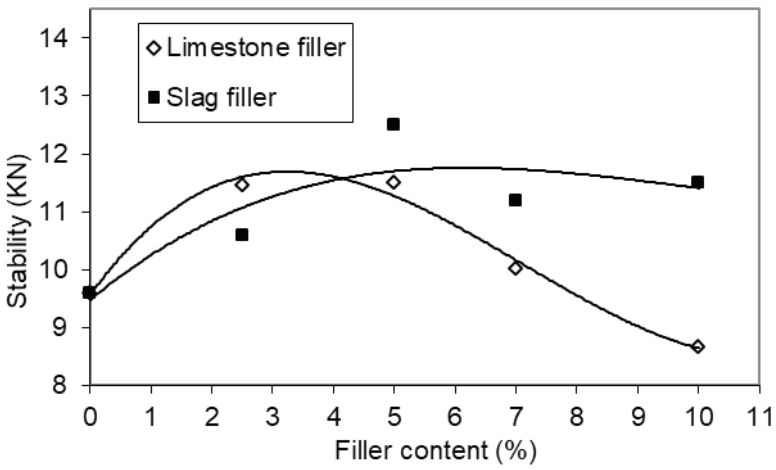


Figure 6. Filler content versus stability

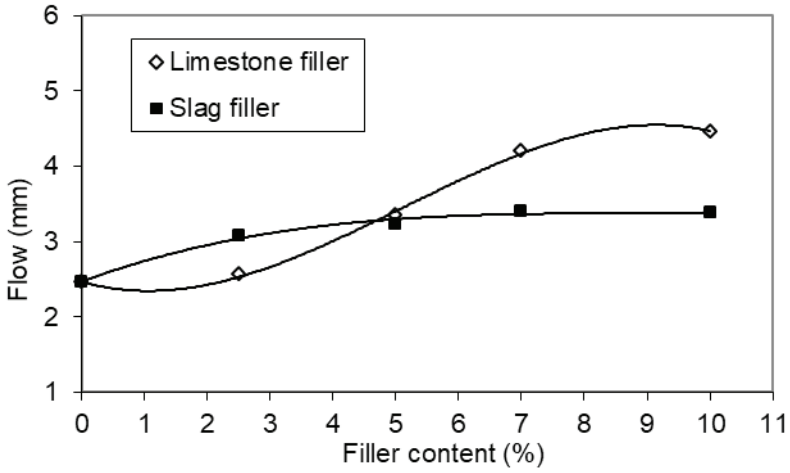


Figure 7. Filler content versus Marshall flow

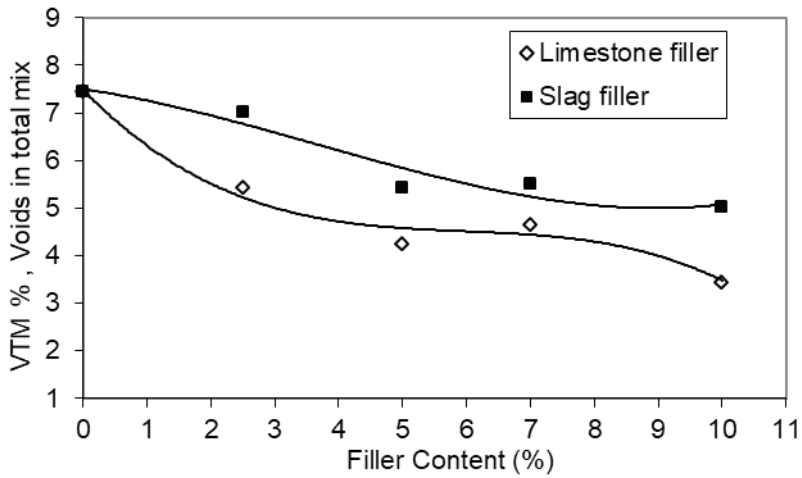


Figure 8. Filler content versus voids in total mixture

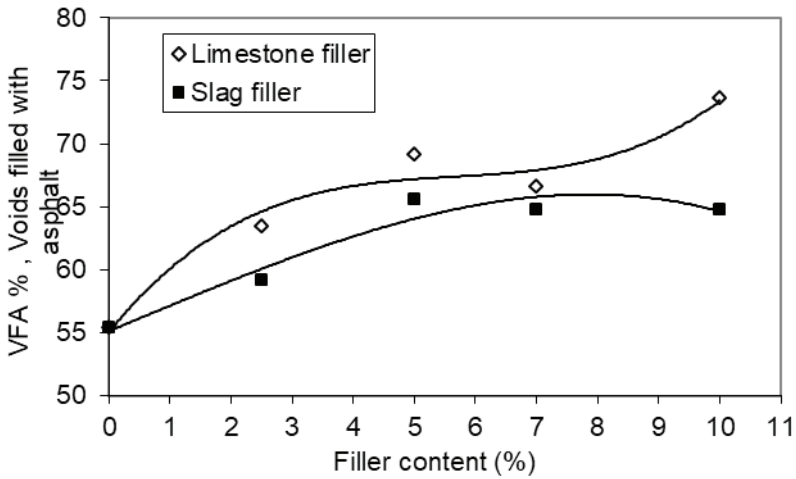


Figure 9. Filler content versus voids filled with asphalt
(Suggested VFA criteria by KGM, min: %65 – max: %75)

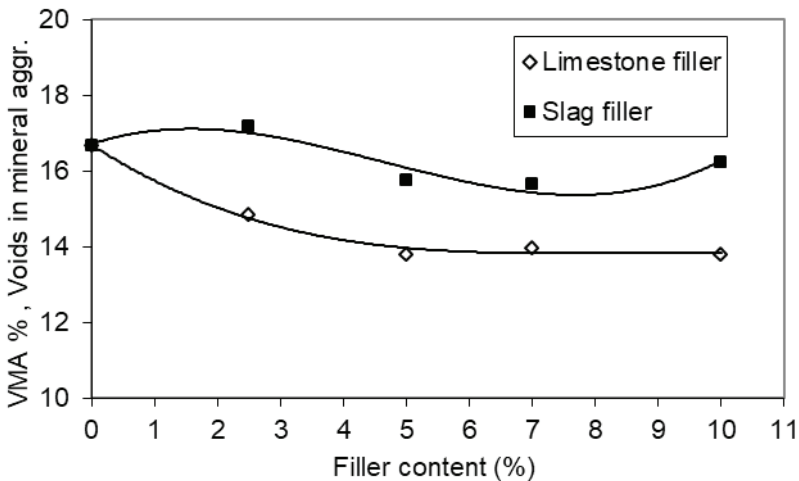


Figure 10. Filler content versus voids in mineral aggregate

Test results analyzed according to design parameters of hot mix asphalt and filler materials evaluated comparatively for use in asphalt pavements. With increasing of filler percentages, the densities of specimens were increased as expected (Figure 5). Densities of samples made with FeCr slag showed similarity to limestone filler.

Stability and flow results of the specimens produced with FeCr slag filler showed better performance than limestone filler. Especially at the higher filler percentages (7%, 10%), the significant improvement was

observed with FeCr slag filler. Specimens made with slag filler showed 15% improved stability in comparison with control specimens.

According to flow results, specimens with FeCr slag showed quite satisfactory values which doesn't go over criteria limits of 4 mm, also at 10% filler (the highest flow result was only 2,4 mm). On the other hand, flow result of the limestone filler were went up to max limit of flow at 7% and 10%percent. This situation can be explained by microstructure and surface properties of filler materials. The filler particles were observed by SEM as shown in Figure 3. The micrograph shows that the slag filler particles have rough and sharp surface with crystal structure. This phenomenon can be the possible reason of FeCr slag's lower flow and higher stability results. Mainly flow value of specimens could be assessing as a major indicator of inner friction. Hence, the increment of inner friction due to crystal structure and sharp surfaces of specimens are expected.

Specimens with slag filler showed higher VTM (voids in total mix) values compared to limestone filler (see Figure 8). However this is cannot asses as a preferred situation, until a certain amount of air void increment, it plays a preventive role to bleeding of asphalt pavements, particularly in hot climate regions bleeding is a key factor of proper pavement design.

McLeod [24] developed the volumetric criteria for the specimens compacted with a Marshall hammer with 75 blows on each side of the specimen. Since, McLeod recommended that the VMA, which is the volume of voids between the aggregate particles, should be restricted to a minimum value of 15%; also KGM recommends the minimum VMA value of 14%. Mainly, VMA value varies with air voids and aggregate size. Specimens with slag filler show higher VMA values than limestone filler specimens (see fig.10). Test results range between 15.6 – 17.2 for slag filler and 13.8 – 16.6 for limestone filler.

3.1. Dynamic Creep Test

The Dynamic creep test is a test that applies a repeated pulsed uniaxial stress on an asphalt specimen and measures the deformations in the same direction using Linear Variable Differential Transducers (LVDT's) [25]. The samples were prepared for dynamic creep test with different FeCr filler ratios and optimum bitumen content (5.1%). Three samples (101 mm diameter and 63.5 mm height) from each mix were tested and the average values of the accumulated (permanent) deformations were recorded [26].

After sample preparation, the samples have been kept overnight in room conditions then those have been put into the cabinet in which temperature is controlled and conditioned to the test temperature. The permanent deformation tests have been carried out at 40 °C. The samples are preconditioned to the testing temperature overnight. The samples were

mounted into the testing frame for dynamic creep test. 5000 cycles of 100 kPa axial stresses was applied on each sample. At the beginning, 100 cycles of 100 kPa axial stress was applied on each sample for conditioning. Five different types of samples which contain FeCr slag filler were prepared.

Fig.11 shows the relationship between the number of cycles and the axial accumulated permanent deformation for the tested groups.

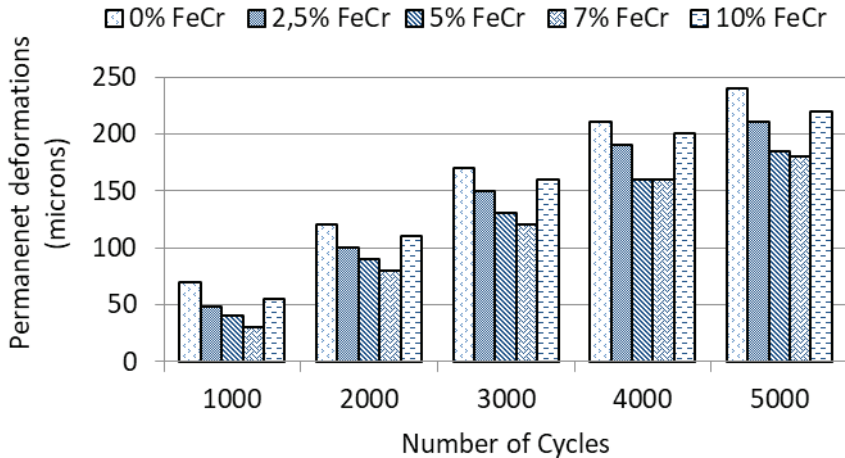


Figure 11. Relationship between axial accumulated permanent deformation and loading cycles

Control mixture (0% FeCr filler) has maximum permanent deformation about 240 microns at the end of test. For the mixes containing FeCr slag at different filler ratio, the plastic deformations decrease until 7% FeCr content, after that plastic deformation increase (Fig.11). Therefore it can be concluded that up to a certain value of the FeCr filler content in the sample plastic deformations decrease, after that it is increases. The reason behind is that certain amount of filler, fills the void inside the samples and increases the stability, but after a certain value, the filler material avoids the bounding between the grains and the asphalt.

4. CONCLUSIONS

This investigation was mainly undertaken to evaluate the FeCr slag performance of asphalt concrete mixes having different percentages of slag filler and find the optimum replacement percentage of the limestone filler by the slag. To fulfill this objective, laboratory evaluation of asphalt concrete mixes with different combinations of FeCr slag filler and limestone filler were conducted. Stability and flow properties, density and voids analysis of Marshall specimens were studied, including different types and various

percentages of fillers. Marshall mix design procedures and suggested criterions of Asphalt Institute and KGM were taken into account.

The test results showed that the use of FeCr slag as filler material in asphalt mixtures instead of limestone filler may be promising to obtain a material suitable for engineering purposes. It's recommended to use slag filler in current hot mix asphalt up to 7% where they are abundant. After 7% slag content, HMA density slightly decrease and plastic deformation of samples increases. Therefore it can be concluded that up to a certain value of the FeCr filler in the sample, fills the voids inside the sample and increases the stability, but after a certain value, the filler material avoids the bounding between the grains and the asphalt.

Consequently, electrometallurgy establishments generally don't expect an income from slag waste. They are looking for the utilization of slags which occupy large areas in factories. In fact, with the assistance of elements mentioned above, using FeCr slag as filler material in road pavements would provide economic and environmental benefits compared to conventional filler materials.

REFERENCES

1. Atkins, H. N. (1997). Highway Materials, Soils, and Concretes, 3rd ed., Pentice Hall Publication, 386p, USA.
2. Puzinauskas, V.P. (1983). Filler in Asphalt Mixture, Asphalt Institute, Research Record, 69/2, 30 p, Kentucky USA.
3. Karaşahin, M. and Terzi, S. (2007). Evaluation of marble waste dust in the mixture of asphaltic concrete. *Construction and Building Materials* 21, 616–620.
4. Güngör, M.M. (1996). An investigation on the use of Afşin-Elbistan fly ash in flexible pavements as filler material. MSc Thesis, Fırat University, Institute of Science, Elazığ, Turkey.
5. Tyson, S. (1993). Present and future use of coal ash in construction and related applications In: Utilization of industrial by products for construction materials Proceeding of ASCE National Conc. Expo., New York (USA) ASCE, p. 1–14.
6. Karaşahin, M., Tığdemir, M., Fincanoğlu, A., Saltan, M. (1997). Utilization of pumice as filler material in hot mix asphalt. In: 1. Isparta Pomza Sempozyumu, Isparta, Turkey.
7. Sayed, M.H, Madany, I.M, Buali, R.M. (1995). Use of sewage sludge ash in asphaltic paving mixtures in hot regions. *Constr Build Mater* 9(1):19–23.
8. Prithvi, S., Kandhall, Gary L. Hoffman (1997). Evaluation of steel slag fine aggregate in hot-mix asphalt mixtures, *Transportation Research Record: Journal of the Transportation Research Board* Volume 1583, pp 28-36.
9. Anderson, D.A., Bahia, H.U., Dongre, R. (1992). Rheological Properties of Mineral Filler-Asphalt Mastics and Its Importance to Pavement Performance, ASTM Special Technical Publication, 1147, pp. 131-153, San Diego, USA.
10. Kandhal, P.S., Lynn, C.Y., Parker, F. (1998). Characterization tests for mineral fillers related to performance of asphalt paving mixtures. *Transportation Research Record*, 1638, pp. 101-110.
11. Shahrour, M.A. and Saloukeh, B.G. (1992). Effect of Quality and Quantity of Locally Produced Filler (Passing Sieve No.200) on Asphaltic Mixtures in Dubai, ASTM Special Technical Publication, 1147, pp. 187-208, San Diego, USA.
12. Ishai, I, Craus, J. and Sides, A. A. (1980). Model for Relating Filler Properties to Optimal Behavior of Bituminous Mixtures, *Proceedings of The Association of Asphalt Paving Technologists*, 49, pp. 416-436.

13. Ishai, I., Craus, J. (1996). Effects of Some Aggregate and Filler Characteristics on Behavior and Durability of Asphalt Paving Mixtures, *Transportation Research Record*, 1530, pp. 75-85.
14. Tayebali, A.A. Malpass, G.A. and Khosla, N.P. (1998). Effect of Mineral Filler Type and Amount on Design and Performance of Asphalt Concrete Mixtures, *Transportation Research Record*, 1609, pp. 36-43.
15. Hussain U. Bahia. (2010). Test Methods and Specification Criteria for Mineral Filler Used in HMA. NCHRP Report 9-45 From University of Wisconsin-Madison, U.S. National Cooperative Highway Research Program.
16. Dukatz EL, Anderson DA. (1970). The effect of various fillers on the mechanical behavior of asphalt and asphaltic concrete. *Trans Res Rec* 38:46–58.
17. Mogawer WS, Stuart KD. (1996). Effect of mineral fillers on properties of stone matrix asphalt mixtures. *Trans Res Rec* 1530:86–94.
18. ASTM D242 (1992). Standard Specification for Mineral Filler for Bituminous Paving Mixtures, *Annual Book of ASTM Standards*, USA.
19. Umar, F., Açar, E. (1991). *Yol Üstyapısı*, Istanbul Technical University Publications, 260 p, Istanbul.
20. KGM (1994). Turkish Highway Administration Office, Scientific Specifications of Highways, KGM Publication, 170/2, 435 p, Ankara.
21. Yılmaz, A. (2002). Investigation of Electric-Arc Furnace Slag and Silica Fume of Antalya Ferrochrome Establishment, as Filler Material in Asphalt Concrete, M.Sci. Thesis, Akdeniz University, 76 p., Antalya.
22. ASTM D 1559-89 (1985). Standard Test Methods for Resistance to Plastic Flow of Bituminous Mixtures Using Marshall Apparatus, *Annual Book of ASTM Standards*, USA.
23. Asphalt Institute (1988). *Mix Design Methods for Asphalt Concrete and Other Hot Mix Types*, Manual Series No.2 (MS-2), Lexington.
24. McLeod N.W. (1957). Selecting the aggregate specific gravity for bituminous paving mixtures. *Proceedings of Highway Research Board* 36.
25. Ibrahim, A., Faisal, S., Jamil, N. (2009). Use of basalt in asphalt concrete mixes. *Construction and Building Materials* 23, pp. 498–506.
26. Ahmedzade, P., Tığdemir M., Kalyoncuoğlu, S.F. (2007). Laboratory investigation of the properties of asphalt concrete mixtures modified with TOP–SBS. *Construction and Building Materials* 21, pp. 626–633.

Chapter 23

A NOVEL RESEARCH ON DIFFERENT TYPES OF CELLULOSE USED IN COATING INDUSTRY



Bilge ÇELİK
Nil ACARALI¹

¹ Yıldız Technical University, Department of Chemical Engineering, Davutpasa Campus, 34210, Esenler-Istanbul, Turkey.

1. INTRODUCTION

Cellulose is a natural polymer that people have used from ancient times to the present day and are still widely effective [1]. More than 90% of cotton threads, 70% of flax, roughly 50% of wood, 30% of straw are cellulose. Although it is also used in the production of some plastics and fabrics, the biggest usage area of cellulose is the paper industry. Many products are obtained by chemical treatment of cellulose. These cellulose derivatives are used in the production of photographic films, various paints and varnishes, parchment, various textile products, cellophane and many plastics [2]. While some of these wastes, which are very rich in cellulose, are used as animal feed, the other part that is not stored and left in agricultural areas is used in the production process in factories. These wastes consist of leaves, stems and root parts of plants such as sisal, rami, linen, pine, etc., or different nuts shells such as nuts, peanuts, walnuts, etc. Studies show that it can be used in industry due to the high rate of cellulose in the waste mentioned [1].

2. COATING

Coating is defined as a substance that, when applied on a surface, provides color with a process that temporarily or permanently changes any crystal structure of the substances, and can be in liquid or powder form [3]. Dyes, which are usually applied in the form of an aqueous solution, are widely used in many areas of the industry such as textiles, food, medicines, cosmetics, paper [4]. Coatings that form a thin film layer on the material and have many properties can be applied to materials with different structures such as wood, ceramic, concrete [5]. Colors become visible when paints absorb light falling into the visible area between the electromagnetic spectrum (400-700 nm). Coatings, which generally have a conjugated double bond system and at least one chromophore, i.e., a group of molecules that determine the color property of the substance, exhibit electron resonance, which is the stabilizing force in organic compounds. Most coatings also contain color enhancers called "oxoromes". Carboxylic acids, sulfonic acid, amino and hydroxylic groups can be given as examples. Although oxoromes are not responsible for color, they are the electron donating group that shifts the absorption spectrum to a longer wavelength in the dye molecule with a conjugated-bond system. Examples of these groups that often affect the solubility of coating: $-\text{CH}_3$, $-\text{OH}$, $-\text{OCH}_3$, $-\text{NH}_2$, $-\text{NHCH}_3$ [6]. World paint production is around 35 million tons. It can be said that this growth is directly related to the rapid growth trend in the construction industry in the world. Considering the usage areas of the produced paints, the share of construction paints is 46%. Construction paints are followed by paints used in industrial products and automotive industry with 38% [7].

The coating industry is in an important position of chemical industry in Turkey. Most of the coatings in different structures produced for use in many fields such as construction, architecture, automotive and art are manufactured by large enterprises, and only a certain part of small enterprises is involved in this process. When the annual production volume of Turkey in the coating industry since 2014, growing an average of 800 tons/year, 55% water-based coatings, constitute the remaining 45% of the solvent-based coatings (Figure 1) [8].

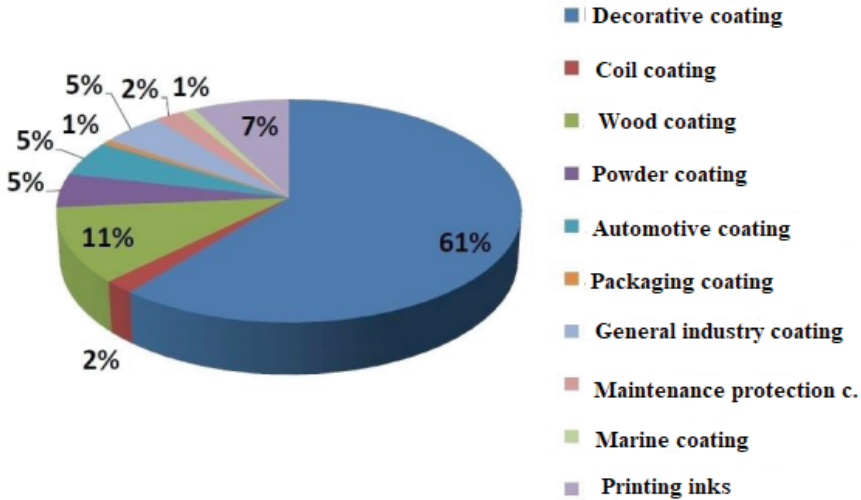


Figure 1. Percentage of sub-segments as amount in the Turkish Paint Industry, 2014 [8]

Except for the coating resins produced in the domestic market, three quarters of the Turkish paint industry is heavily dependent on imports, especially in terms of raw materials, pigments and solvents, but Eastern Europe, the Balkans, the Caucasus countries and Russia have a good potential for the national paint market [9].

Binder is an important component that participates in the paint in the production process and allows a thin layer to form on the surface on which it is applied. The main task of the binders that must be present in the structure of the coating is to hold and adhere to the surface on which the coating is applied. In addition, it also gives the coating characteristics such as flexibility, brightness, durability and corrosion resistance [10]. Pigments are substances that give color to coatings. Pigments show great changes in chemical structure, physical form and optical properties. The most important factor in the stability and quality of the coating is the dispersion degree of the pigment particles. A higher degree of pigment aggregation is observed in water-based coatings

compared to conventional solvent-based coatings. Pigments can be studied under two classes, organic and inorganic pigments in general [11]. Solvents are a paint component that allows paints to be applied in liquid state. The primary function of solvent is to distribute or decode the binder in paint so that it can make the paint formulation less viscous and ready for application. The properties of the solvent also affect the application properties of the paint such as consistency, drying time, flow. Solvents also help remove the rinse from the surface and wealer the surface, causing both the film to stick and its penetration to the surface. Solvents also help remove the rinse from the surface and wealer the surface, causing both the film to stick and its penetration to the surface. Toluene, quylene, methyl ethyl ketone are common solvents used in acetone solvent-based coatings [12]. Additives are chemicals that have very different properties and enter the paint in very small amounts. Additives are used to improve the properties of the paint and prevent unwanted and negative changes. Examples of additives used in the coating are: dryers, wetting agents, curing agents, anti-scaling, dispersing agents [13]. The various components used in the paint are classified on the basis of solvent in terms of waste control and reduction of the amount due to the environmental pollution and waste management that may occur after the production and use of the coating [14]. Water is used in certain proportions in the content of water-based coatings. It is generally used as interior and exterior coating. Satin coatings and plastic coatings are generally used in wall coatings. Pigments, additive chemicals and water are mixed during the production of water-based coatings. After the mixture is prepared, it is dissolved with water and mixed rapidly in order to distribute it homogeneously. Coloring is done by adding materials to color the coating. As the last step, substances such as dust and lime in the coating are removed by the filtering process [15]. Organic solvent dyes contain high third organic organic matter. In order to reduce this, coatings with high solids content are being developed. Solvent-based paint waste is often dangerous and flammable. However, it is also possible to evaluate solvent-based wastes in suitable areas such as waste recycling, reuse or management with its ease of solvent recycling and high thermal content [16]. Powder coatings do not contain solvents; It is a mixture based on resin, pigment, drying agents, catalysts, reinforcing fillers, flow control agents and small amounts of other additives. It is applied dry using electrostatic spray and fluidized bed techniques. Powder clings to the surface of the material by melting and applying heat to form a continuous film. It is environmentally advantageous since it does not contain any organic solvent. It also produces very little waste due to its high transfer efficiency. The biggest disadvantage is application difficulty [16]. Tests, which are an essential part of the functioning of a paint system, are carried out to verify that the coating meets the established quality standards and customer expectations. Multiple different mechanical or chemical tests can be applied

on the coatings. With these tests, controls are carried out in the coating and improvements are provided. These are corrosion test, adhesion test, viscosity test, covering test, impact resistance test [17].

3. CELLULOSE

Cellulose, the basic building agent of plants, is one of the most important natural substances that can be synthesized by living organisms. Cellulose is found in many creatures ranging from developed plants with green leaves to primitive organisms such as sea-grasses, flagellates and bacteria. The rate of cellulose in the structure of plants varies according to the structure of the plant. Cellulose is found in fewer quantities in plant fibers and seeds, while algae, attain and bacteria contain a smaller amount of cellulose than green plants. [18]. Cellulosic structure makes the cell walls of green plants mechanically strong. Cellulose is widely preferred in different sectors such as textile, cosmetics, paper etc. industries. [19]. Cellulose is a renewable, biocompatible, biodegradable polymer that is abundant in the world. Molecular structure of cellulose chains is shown in Figure 2. [20].

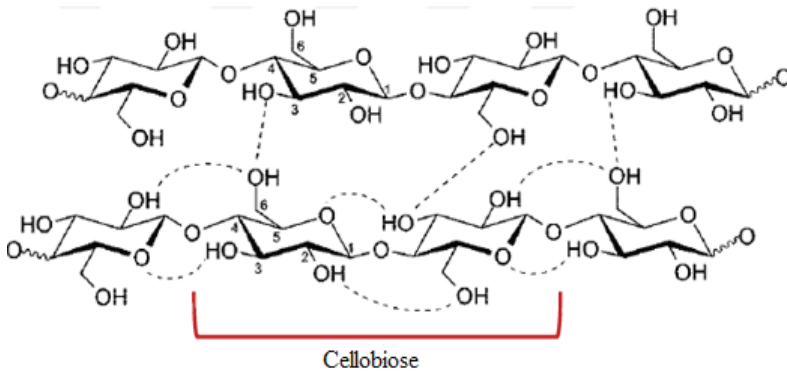


Figure 2. Chemical structure of cellulose [20]

As shown in Figure 2, cellulose is a linear polymer formed by the merger of glucose units connected by glycosidic ligaments. Cellobiose, a repeating cellulose unit, consists of two glucose molecules attached in opposite directions. Thus, repeating units can be connected to said positions continuously. A straight cellulose chain makes many hydrogen bonds both with itself and with other cellulose chains. The glucosidic and hydrogen bonds that make the molecules strong make them more resistant in terms of chemistry and mechanics. In addition, while glucosidic bonds bring hydrophobic properties to the structure, highly established hydrogen bonds add hydrophilic properties [20]. Cellulose derivatives dissolve in organic solvents or water and thanks to these properties, cellulose ethers and esters are used in many application areas [21]. Cellulose derivatives can be examined by dividing them into subtitles. Cellulose ethers are alkyl, intermediate

alkyl, hydroxy alkyl and carboxy alkyl ethers of cellulose. In esterification reactions, hydroxyl groups in the structure of cellulose can be partially etherified. Carboxymethylcellulose, one of the most used and important cellulose ethers, is a water-soluble substance that contains carboxyl groups in its structure, formed by etherification of cellulose with monochloroacetic acid. As a filler and binder in the coating industry, it has an important place in the production of paper, cosmetics, foil and building materials as well as the branches of industry mentioned above (Table 1) [22].

Table 1. Types of cellulose ethers and usage areas [23]

Cellulose Ethers	Functional Groups
Ethyl cellulose	$-\text{CH}_2\text{CH}_3$
Methyl cellulose	$-\text{CH}_3$
Hydroxyethyl cellulose	$-\text{CH}_2\text{CH}_2\text{OH}$
Carboxymethyl Cellulose	$-\text{CH}_2\text{COONa}$
Hydroxypropyl methyl cellulose	$-\text{CH}_2\text{CH}(\text{OH})\text{CH}_3$

Cellulose and its derivatives provide suspension stability, thickener, film forming, wetting processes in the paint industry [23]. Carboxymethyl cellulose is produced by carboxymethylation of cellulose. Carboxymethyl cellulose due to its properties such as thickener, adhesive, binder and stabilizer is used in different fields such as detergent, paint, wallpaper glue, paper and cardboard, textile, oil drilling muds, ceramics, foodstuffs, cosmetics and pharmaceutical industries [2]. It provides the formation of mono-, di- and tri-esters in three OH groups contained in each glucose molecule. OH groups, which are located in the molecular structure of cellulose and are connected by hydrogen bonds, partially or completely break during esterification. When cellulose attacks your chain in pieces, a change or deterioration occurs in the chain structure. It is technical possible to obtain cellulose esters from all inorganic and organic acids. [24]. Table 2 shows the widely used organic and inorganic cellulose esters.

Table 2. Types of cellulose esters [23]

Cellulose Esters	Functional Groups
Cellulose acetate	$-\text{C}(\text{O})\text{CH}_3$
Cellulose nitrate	$-\text{NO}_2$
Cellulose xanthate	$-\text{C}(\text{S})\text{SNa}$

Cellulose acetate propionate	$-C(O)CH_3$
Cellulose acetate butyrate	$-C(O)CH_3/-C(O)(CH_2)_2CH$

Cellulose nitrate, which is obtained as a result of nitration of cellulose with inorganic acids, is one of the important cellulose esters. Sulfuric acid or nitric acid is used in the nitration process in industry. Cellulose nitrate; depending on the nitrogen content in it, it is frequently involved in the production of explosives such as gunpowder, dynamite, adhesives, plastics and varnishes. Cellulose sulphate, another important component, is formed by the esterification reaction between cellulose and butyl sulphate added to concentrated sulfuric acid. It is used in industry to thin ink and varnishes [24]. Dissolved cellulose is regenerated cellulose, which has a different molecular structure and molecular weight than natural cellulose, and is obtained as a result of chemical dissolution and subsequent precipitation of cellulose. The dissolution process occurs as a result of breaking the network of hydrogen bonds in the molecular structure of cellulose by the solvent. Hydrophobic interactions between cellulose and solvent also play an important role in dissolution.

Dissolution of cellulose;

- solvent diffusion
- crystallization of cellulose
- inflatable including sample
- separation of cellulose chain
- diffusion of untied chains into solution

It is possible to sort in five steps [25]. Nanocellulose is a raw material that can be obtained from lignocellulosic raw material sources and gives positive effects to the industry with its physical, chemical and morphological properties. There are three different types of nanocellulose, fibrous nanocellulose (CNF), crystalline nanocellulose (CNC) and bacterial nanocellulose (BNC). CNF is a type that is formed by delamination as a result of a mechanical effect before and/or after chemical or enzymatic reactions, with a diameter of 3-60 nm and a length of up to several μm . Bacterial nanocellulose produced are nanocellulose types with a diameter of 20-100 nm. Among these types of nanocellulose, CNF product, which has high/aspect ratio and appropriate physical properties, is used extensively in material production [26]. There are three different general types of nanocellulose. These are crystalline nanocellulose, cellulose nanofibril and bacterial nanocellulose (Figure 3) [27].

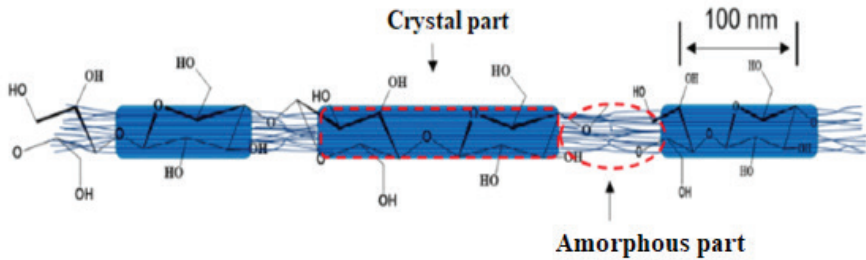


Figure 3. Theoretical configuration of crystalline and amorphous regions of cellulose nanofibril [27]

The wood that forms the basis of the trunks of large trees with green leaves; consists of cellulose, non-cellulosic polysaccharides (hemicelluloses and pectin) and lignin. Components are 97-99% naturally heterogeneous [28]. Figure 4 shows the cellulose found in the cell wall for the plants.

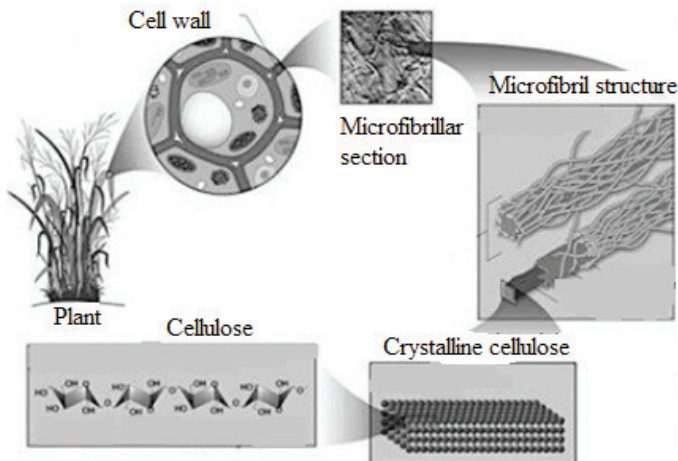


Figure 4. Cellulose structure in the cell wall for plants [1]

With the development of technology, it has been determined by studies that some bacterial species can also synthesize cellulose. Examples of cellulose-producing bacteria are *Alcaligenes*, *Sarcina*, *Escherichia*, *Acetobacter*, and *Komagataeibacter*. The presence of high amounts of oxygen and low amounts of nitrogen in the culture medium of bacteria represents the best conditions for cellulose synthesis. Fructose, glucose, sucrose, molasses and glycerol can be used as carbon sources in the environment. The temperature of the culture medium (25-30°C), the pH (generally 4-6) and the duration of the environment are the parameters that are effective in the production of bacterial cellulose. Bacterial cellulose has a larger surface area compared to cellulose obtained from plants and has the ability to break down. Bacterial cellulose, which is flexible, insoluble in water, has pores and can hold water well, is used in many areas such as food, membrane, paint, health in the industry [29]. There are various algae

species that synthesize cellulose microfibrils in the cell walls. Researchers succeeded the synthesizing cellulose in nano-size in *Gelidium elegans* algae as a result of their studies. It has been determined that there are some differences in the synthesized cellulose molecules due to the use of different algae species. *Micrasterias denticulata*, *Boergesenia* and *Valonia* are among the algae species commonly used in cellulose production [30]. Seaborne animal type overalls have a cover made of cellulose in their outer layer. Cellulose molecules containing microfibrillar structures are obtained from the *Styela Plicate* and *Ciona intetinalis* species of the tulum [30].

4. ADDITIVES THAT CAN BE USED IN COATINGS

In many health-promoting functional components, carrots are one of the significant vegetables' rich in carotenoids and dietary fiber. Carrots are a globally grown food and the most significant source of carotenoids in the majority of Western countries [31]. The region with the most carrot cultivation is the Central Anatolia region [32]. The excess amount of carrot pulp left in carrot juice is rich in fiber and is used for different purposes. In a study, it was aimed to investigate the dietary fiber content in pulp with using carrot pulp. First, carrot pulp was kept for 4 days in an environment with enzymes and hydrolyzed. As a result of the experiment using 100 grams of carrot pulp, 77.3 grams of dietary fiber was obtained [33]. Carrot pulp contains 17% of α -carotenes and 31-35% of β -carotenes in fresh carrots. The carrot pulp remaining after the removal of water from the structure of carrots has been determined to be a compound with bioactive features that can be discovered in the development of foodstuffs and dietary supplements. When the carrot pulp was dried and examined, it was seen that it had 4-5% protein, 8-9% carbohydrate, 5-6% mineral and 37-48% fiber content [31]. Peanut is a plant like lentils, beans and chickpeas. Peanuts are produced predominantly in Asia, Africa, America and Oceania with different rates. The peanut industry is one of the primary elements for agricultural waste. The biomass residue has a high usable energy content [34]. Peanut shells are a by-product that is released in abundance in peanut operating facilities. Peanut shells, which have a very fibrous structure and therefore rich in cellulose, contain many elements in their structure (Table 3) [35]. The body of the shell consists of a fibrous skeleton supporting the cellulosic layer as shown in Figure 5.



Figure 5. Fibrous skeleton of peanut shell [36]

Table 3. Structure of peanut shell [35]

Substance	Content (%)
Cellulose	45,3
Lignin	32,8
Hemicellulose	8,10
Protein	4,90
Ash	2,30

Volcanic lava stone is a stone obtained from slag with a highly porous structure, which is formed as a result of volcanic activities and the release of basic lava from cavities due to compression of volcanic rocks. There are volcanic slags in different regions of our country as well as in different parts of the world (in most countries of Europe such as Austria, France and Germany). For example, especially Samsun and Çorum located in the north of Anatolia, Malatya and Diyarbakır in Southeastern Anatolia, İzmir and its surroundings in the Aegean region are very rich with volcanic slag [37]. When the chemical analysis of the volcanic lava stone was made, it was determined that it contains oxide compounds and has a very rich structure in terms of silicon, iron, calcium and potassium. The most abundant compound in its structure is silicon dioxide, followed by aluminum dioxide and iron (III) oxide [38]. Perlite is a glassy volcanic rock belonging to the family of riolite surface rocks. When the temperature increasing to 900°C, it can expand up to 4-40 times its original volume. Perlite can be compact, thin, porous, brittle, sandy and in different appearances in a spectrum from white to black [39]. Perlite has a light, elastic and fireproof structure. As it provides a good level of heat and sound insulation, it is used for binding purposes in building materials in the construction industry, in increasing the

durability of cement, in plaster raw materials. Due to its porous structure, it is used in the agricultural sector to allow the plants to breathe in the soil and to enable the soil to absorb water better because it does not dissolve in any form. Perlite stone, which is very rich in silicon, also contains alkali elements such as aluminum, potassium, iron, calcium, magnesium [40].

REFERENCES

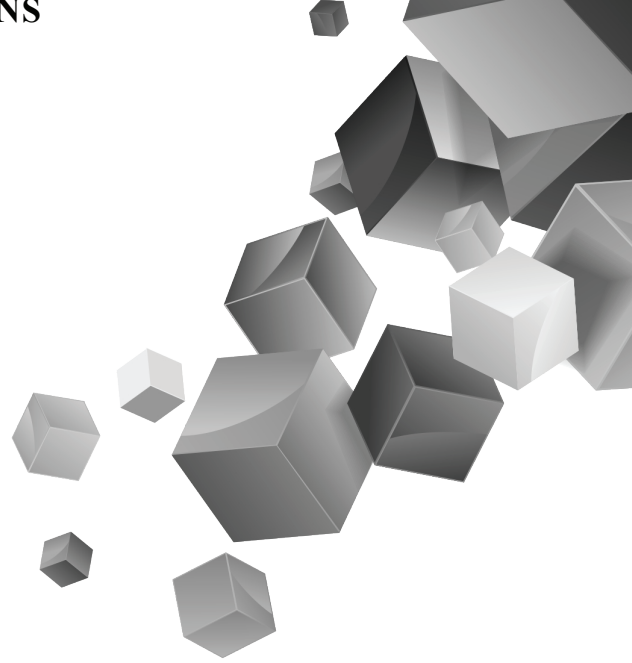
- [1] Bilek, S., Melikoğlu, A.Y., Cesur, S., (2019). Production of Cellulose Nanocrystals from Agricultural Wastes, Characteristics and Application Areas. *Academic Food Journal*, 17 (1), 140-148.
- [2] Ayten, A., (2011). Rheological Behavior of Carboxymethyl Cellulose Produced from Lemon Peel Cellulose and Its Use as a Hydrophy Polymer in Fruit Coating Films. Master Thesis. Firat University, Institute of Science, Elazig.
- [3] Abrahart, E.N. (1977). *Dyes and Their Intermediates*. (2nd edition). New York: Chemical Pub.
- [4] Tunç, M.S., Hanay, Ö. (2016). Use of Kaolin for Remazol Brilliant Green 6B Removal from Aqueous Solutions. *Adıyaman University, Journal of Engineering Sciences*, 4, 1-10.
- [5] Alicılar, A., Ökenek, F., Kayran, B., Tutak, M., (2015). Flame Retardancy, Smoke Suppression and Antibacterial Activities of Boron Doped Styrene Acrylic Paints. *Gazi University, Journal of Engineering and Architecture Faculty*, 30 (4), 701-709.
- [6] Malomo, D., Abimbade, S.A., Oluwaseun, A.K., Eghareba, O., (2017). Likely Mechanism of Dye Adhesion on Fabrics. *Proceedings of 62nd ISERD International Conference*, January Boston, USA.
- [7] Türkmen, M., Bayhan, M., Kılıcı, E., (2015). Investigation of Production Problems in the Construction Paint Industry in the Context of Value Chain and Five Competitive Power Model: Case Study. *Ege University. Faculty of Economics and Administrative Sciences. 15. Production Research Symposium*, 979-988.
- [8] Plums, H., (2019). Turkey and Paint Industry Contribution Assessment of the Economy and Tax Revenue in the world. Master Thesis. Pamukkale University, Institute of Social Sciences, Denizli.
- [9] Kocabaş, E., (2009). Treatment of Water-Based Paint Production Wastewater by Physico-Chemical Methods. Master Thesis. Istanbul Technical University, Institute of Science, Istanbul.
- [10] Ökenek, F., (2013). Investigation of Flame Retardant Properties of Alkali-Earth Alkali Borate Additives in Water Based and Styrene Acrylic Based Paints. Master Thesis. Gazi University, Institute of Science, Ankara.
- [11] Otani, J., (2015). Preparation of Novel Azo Pigments and Clarification of the Emitting State of a Unique Fluorescent Pigment. Doctoral Thesis. Ritsumeikan University, Institute of Science, Kyoto.
- [12] Tellus Institute, (1993). *Alternatives to Solvent-Based Paints*. Technical Report 4 University of Massachusetts Lowell, Massachusetts.

- [13] Çağlar, D., (2011). Synthesis of Flax Seed Based Alkyd Resins: Development of Paint Formulations. Marmara University, Institute of Science, Istanbul.
- [14] Uslu, B., (2019). Improving Flame Resistance of Water Based Interior Paints with Boric Acid Additive. Gazi University, Institute of Science, Ankara.
- [15] Gümrah, B.G., (2019). Compostability of Paint Sludges with Different Types of Additives. Uludağ University, Institute of Science, Bursa.
- [16] Aydın, S., (2013). Pretreatment of Paint Industry Wastewater by Coagulation, Istanbul University, Institute of Science, Istanbul.
- [17] Talbert, R., (2008). Paint Technology Handbook. Boca Raton: Taylor & Francis Group.
- [18] Fengel, D., Wegener, G., (1989). Cellulose. D. Fengel, (Eds.), Wood Chemistry, Ultrastructures, Reactions (1st ed.) (66-100). Berlin, New York: De Gruyter.
- [19] Gupta, P., Raghunath, S., Prasanna, D., Venkat, P., Shree, V., Chithananthan, C., Choudhary, S., Surender, K., Geetha, K., (2019). An Update on Overview of Cellulose, Its Structure and Applications. Intechopen, 1 (14).
- [20] Durmaz, E., (2017). Investigation of Phase Inversion Behavior of Cellulose-Ionic Liquid Solutions in Relationship with Membrane Formation. The Degree of Master of Science. Middle East Technical University, Institute of Science, Ankara.
- [21] Koç, A., Zıba, C.A., Akarsu, S., Orhan, B., Dolaz, M., (2016). Cellulose Production from Textile Wastes, Methyl Cellulose Synthesis, Characterization and Use in Cement Paste. Kahramanmaraş Sütçü İmam University, Journal of Engineering Sciences, 19 (3), 115-123.
- [22] Günel, B., (1999). Increasing the Solubility of Carboxymethylcellulose. Master Thesis. Istanbul Technical University, Institute of Science, Istanbul.
- [23] Zıba, Z.A., Akarsu, S., Çelikçi, N., Dolaz, M., (2017). Hydroxypropylmethyl Cellulose (HPMC) Synthesis and Characterization from Air Conditioning Powder, Kahramanmaraş Sütçü İmam University, Journal of Engineering Sciences, 20 (4), 23-29.
- [24] Kırıcı, H., Ateş, S., Akgül, M., (2001). Cellulose Derivatives and Their Uses. Kahramanmaraş Sütçü İmam University, Science and Engineering Journal, 4 (2), 119-130.
- [25] Tsianou, M., Ghasemi, M., Alexandridis, P., (2018). Fundamental Understanding of Cellulose Dissolution can Improve the Efficiency of Biomass Processing. Agricultural Research & Technology Journal, 16 (2), 1-5.
- [26] Poyraz, B., Arslan, R., Akıncı, A., Tozluoğlu, A., (2018). Chemical and Morphological Analysis of Modified Nanocellulose, Artvin Coruh University, Journal of Forestry Faculty, 19 (1), 39-47.

- [27] Tanis, S., (2019). Development of Golden Cellulose Nanofibril Material for the Determination of E. Coli. Master Thesis. Hacettepe University, Institute of Science, Ankara.
- [28] Hamad, A., Ateş, S., Durmaz, E., (2016). Evaluation of the Possibilities for Cellulose Derivatives in Food Products. Kastamonu University, Journal of the Faculty of Forestry, 16 (2), 383-400.
- [29] Güzel, M., Akpınar, Ö. (2018). Production and Properties of Bacterial Celluloses and Their Use in Food and Non-Food Applications. Academic Journal of Food, 16 (2), 241-251.
- [30] Yıldırım, N., (2018). Nanotechnology and the Environmental Polymer of the Future Nanocellulose. Forestry Research Journal, 5 (2), 185-195.
- [31] Sharma, K., Attri, S., Thakur, N., Karki, S., (2012). Chemical Composition, Functional Properties and Processing of Carrot. Journal of Food Science and Technology, 49 (1), 22-32.
- [32] Uğurluay, S., (2019). Orange Carrot Harvest, Labor Requirement and Harvest Cost in Kırıkhan. Turkish Journal of Agriculture and Natural Sciences, 6 (2), 235-242.
- [33] Ünlü, U.M., (2017). The Effect of Carrot Fiber and Sugar Beet Fiber on Tarhana Quality. Master Thesis. Aksaray University, Institute of Science, Aksaray.
- [34] Moreno, M., Agugliaro, F., Escobedo, Q., Moreno, A., (2018). Peanut Shell for Energy: Properties and Its Potential to Respect the Environment. Sustainability Journal, 10 (1), 1-15.
- [35] Bilir, M.H., (2009). Investigation of Adsorption of Saffron and Remazol Brilliant Blue R with Polyurethane Type Foam Produced from Peanut Shell. Master Thesis. Kilis 7 Aralık University, Institute of Science, Kilis.
- [36] Bieak, N., George, B., (2003). Utilization of Peanut Shell Fibers in Nonwoven Erosion Control Materials. International Nonwovens Journal, 3 (2), 60-65.
- [37] Coşkun, İ., (2009). Investigation of Some Durability Properties of Concretes with Fly Ash and Volcanic Slag. Master Thesis. Kahramanmaraş Sütçü İmam University, Institute of Science, Kahramanmaraş.
- [38] Aktepe, M., (2012). Development of Volcanic Slag Aggregate Screed Concrete and Investigation of Its Technical Properties. Master Thesis. Süleyman Demirel University, Institute of Science, Isparta.
- [39] Kaya, E.S., (2019). Usability of Raw Perlite and Expanded Perlite as Pozzolanic Materials. Master Thesis. Balıkesir University, Institute of Science, Balıkesir.
- [40] Arıkan, A.K., (2019). Investigation of the Use of Expanded Perlite in Wood Plastic Composite. Master Thesis. Kahramanmaraş Sütçü İmam University, Institute of Science, Kahramanmaraş.

Chapter 24

UP-TO-DATE APPROACHES TO WORKPLACE NUTRITION RELIGIONS



Abdulkadir BİNGÖLBALİ¹

Dilek ÖZTAŞ²

Ergün ERASLAN³

1 Abdulkadir BİNGÖLBALİ, Ankara Yıldırım Beyazıt University, Institute of Science, Occupational Health and Safety Program (PhD Student), a.kadirbingol@outlook.com, 05074641725, Orcid No: 0000-0003-2063-7706

2 Doç. Dr. Dilek ÖZTAŞ, Ankara Yıldırım Beyazıt University, Faculty of Medicine, Department of Internal Medical Sciences, doztas@ybu.edu.tr, 05070117140, Orcid No: 0000 0002 8687 7238

3 Prof. Dr. Ergün ERASLAN, Ankara Yıldırım Beyazıt University, Faculty of Engineering and Natural Sciences, Department of Industrial Engineering, eraslan@ybu.edu.tr, 05426477700, Orcid No: 0000-0002-5667-0391

1. Introduction

Work, which is at the equilibrium center of social, economic and cultural life in human life, is an indispensable element of life and most of the lives of the working population are passed on in the workplace. Healthy living standards, which can be achieved with an adequate and balanced eating habit in working environments, are important for employees and society to have a longer and higher quality life. Chronic disorders that do not have infectious properties such as hypertension, diabetes, obesity and cardiovascular worldwide are based on irregular and malnutrition habits that occur in workplaces (Çil, 2019). In a society with unhealthy eating habits, there are significant decreases in production and productivity throughout the country, with an increase in budget planning for education and health areas. This leads to a negative picture for the country's economy (Üner and Yılmaz, 2020). Using man power to increase production is an indicator of economic development (Bekar and Ersoy, 2011).

In order to live and operate, one has to feed on various foodstuffs and provide the calories needed for his body (Türkoğlu, 2011). Nutrition; it is not only feeding the snow and eating and drinking everything desired, but taking the necessary nutrients into the body so that the human being can grow, develop and live healthy. Healthy eating is only possible with an adequate and balanced diet (Yılmaz, 2003). Adequate and balanced nutrition is defined as “*adequately taking the energy, nutrients and nutritional components needed according to the age, gender, special condition and physical activity of the individual with nutrients and using them in his body.*” It is important to increase the productivity of workers by providing adequate and balanced nutrition opportunities (Bekar and Ersoy, 2011). Health and occupational safety of workers who play an important role in production and therefore in the country's economy; it is possible to get enough of the necessary nutrients in quantity and quality according to the work they do.

Inadequate and unbalanced nutrition reduces the body resistance of workers, causing them to get sick more often, negatively affecting their attention and attention, ingring out the rate of occupational accidents and occupational diseases. When the nutrients that will provide the energy and nutrients necessary for the efficient operation of the workers are not consumed, the physical power required for production decreases and the working capacity decreases. This reduces the continued work and individual initiative of workers (Tanır, et al., 2001). In a study, it was determined that the relationship between the number of days workers spent in the hospital due to their nutritional status and the number of days they spent in the hospital due to illness and the days they left the job unfinished due to various health problems or worked in the background was statistically

significant (Reime, et al., 2000). Adequate and balanced nutrition reduces national efficiency by 20%, while the 1% increase in energy consumption is reflected in efficiency by 2.27% (Wanjek, 2005).

Worker nutrition is the correct and effective application of the criteria and stages of nutrition on workers. Considering the impact of workers' nutritional status on their biological and psychological health, and therefore on working performance, it is important to regulate the nutritional status of workers and to enlighten workers and employers in this regard. Providing a healthy worker's diet in workplaces; it is possible to exhibit a multi-component intervention approach in an organizational, individual and environmental context. In order to implement and ensure the continuity of the measures to be implemented in this context, workers, employers, governments, trade unions and experts must exhibit a collective work and work in harmony with each other (Bor, 2020).

2. Nutrition Overview

Nutrition is one of the indispensable basic needs of living things in all periods of life. Adequate and balanced nutrition is perhaps the most important conditions in protecting and improving the health of society and the individuals who make it up, developing economically and socially, increasing the level of well-being. Attitudes and behaviors related to nutrition affect the performance of the individual in the educational and working life, and therefore its success, to a significant extent. Adequate and balanced nutrition is the taking of each of the nutrients in sufficient quantities and proper use in the body, taking into account the age, gender and physical activity statuses of each of the nutrients for the growth, renewal and functioning of the body (Bilici, 2008).

In the process of transitioning from agricultural society to industrial society with technological developments affecting our world, feeding people with meals prepared by others outside the home revealed the concept of collective nutrition systems and thus the collective nutrition system took its place in daily life. Hotels, restaurants, fast food restaurants and catering companies are organizations that provide mass nutrition services in our country. The bulk nutrition organizations that provide this service; it needs to please consumers by offering them meals that will ensure a timely, proper, adequate and balanced diet. In addition, it is possible for these organizations to gain consumer trust by producing reliable food, to establish and implement food safety and quality management systems (Sezgin and Özkaya, 2014).

The main goal of planning an effective worker nutrition is to protect the health of the worker and at the same time improve the work performance by meeting the energy and nutritional requirements in accordance with

the age, gender, nature, characteristics and physical activities of the work performed both in the working environment and at home (Bilici, 2006). Considering that a worker spends an average of a third of his life at work, he spends at least one meal during the day in a working environment. Food service can be provided by workplaces, as is possible for employees to bring it from home. The International Labour Organization (ILO) mandates that nutrition services be operated under the responsibility of doctors and dietitians in industrial organizations. In addition, the ILO states that within the scope of nutrition service services, employees in workplaces should be provided with adequate and balanced nutrition and food hygiene in terms of energy and nutrients, and trainings on nutrition and health (Çil, 2019).

2.1. Energy and Nutrient Requirements in Worker Nutrition

Adequate and balanced nutrition of employees is of great importance in terms of continuity of production in workplaces, decreased frequency of work accidents and effective work performance. Among the nutritional problems generally detected in workplaces are economic reasons, lack of educational status, lack of food in workplaces, wrong habits and compatibility with the person (Üner and Yılmaz, 2020).

It was determined that the rates of work accidents increased by experienced focus and attention deficiencies in workers who did not meet enough energy situation during the day. As a result of malnutrition, the body and brain's inability to obtain the necessary glucose, the lack of vitamin A, the inability to function adequately, excessive weight gain as a result of over-nutrition and nervous system disorders due to vitamin B deficiency, employees' conditions of having work accidents increase (Bor, 2020). It is reported that vitamin D deficiency in terms of workers will negatively affect work performance and safety due to its consequences such as weakness in muscles, decreased ability to balance and increased risk of falling. Workers working shifts and working underground are at risk for vitamin D because they make less use of the sun's rays (Murad, et al., 2011).

It has been reported that there is an inverse relationship between being productive and Body Mass Index (BMI). Work productivity tends to decline in high-weight individuals. In a study, it is thought that there is a relationship between occupational asthma and obesity and it is stated that occupational mortality, morbidity and obesity are common national problems. It has also been reported that obese workers tend to be more absent from work than workers in the normal weight range (Yılmaz, 2003).

There is an accurate ratio between the work activity of the worker and the energy required to be taken (Gallis and Panagopoulou, 2007). The energy needs of the workers working in various lines of work may also

vary according to the work they do. Therefore, it is not entirely possible to say anything definitive about the amount of energy a worker should receive daily (Atkoşar, 2018). However, as seen in Table 1, it is possible to make a general classation by refer to the physical mobility of the workers during the day (Müftüoğlu and Parlakyiğit, 2020).

Table 1. *Energy Requirement by Activity Types*

Activity	Male	Woman
Light Activities	2500 (Calories)	2100 (Calories)
Medium Activities	3000 (Calories)	2300 (Calories)
Medium Heavy Activities	3500 (Calories)	2600 (Calories)
Heavy Activities	4000 (Calories)	3000 (Calories)

Occupations that are in the *Light Activities* group; office workers, lawyers, doctors, accountants and teachers. The professions that belong to the *Medium Activities* group are industrial workers, sailors who work in a less dangerous group. The professions that belong to the *Medium Heavy Activities* group are agricultural workers, unskilled workers. Occupations that are in the *Heavy Activities* group; mine workers, forestry workers, iron and steel industry workers (Bor, 2020).

The amount of energy the employee needs to receive depends on the gender, the type of work he/she does and the temperature of the working environment. As the temperature of the working environment increases, the amount of energy required to the worker increases. In addition to the amount of energy to be taken, which types of nutrients the energy should be taken from are also very important in terms of healthy and balanced nutrition. In the daily energy intake of workers, macro (protein-fat-carbohydrate) and micro (vitamin-mineral) nutrients should be shared in a balanced way and this variety should be utilized in one meal (Abaoğlu, 1956). 55-60% of daily energy needs should be provided from carbohydrates, 25-30% from fats and 12-15% from protein-containing sources (Türk İş, 2014). In the nutrition programs of employees in environments where toxic substances and radiation are high, it is important for the health of employees to include foods rich in vitamins and minerals such as vegetables, fruits, milk and dairy products (Meng, et al., 2017). Menus should be adjusted so that the energy and nutrient needs to be taken during the day are in the form of three main meals and at least one of these main meals is met at work. In this arrangement, it should be arranged as 1/5 for morning meal, 2.5/5 for lunch and 1.5/5 for dinner. A business that only serves lunch must meet

half of its employee's requirement. Considering that the daily energy need of the worker, who usually works with his body standing for 8 hours, is considered as 3500 calories, half of this (1750 calories) will be covered by the food given at work. This amount of energy should be provided with 3 or 4 containers of food and bread using at least one type of nutrient from each food group (Büyükpamukçu, 2003).

2.2. Menu Planning Processes in Workers

In Gastronomie, the menu definition is “*details of the dishes that make up a lunch or dinner*” (Larousse, 2005). The nutritional needs and eating habits of the group of workers to be planned should be taken into account, and when planning the menus, attention should be paid to color, consistency, taste and shape harmony. Again, nutrient requirements, habits, individuals in need of special diets, budget, capacity, standard recipes, seasons and regional geographical factors are factors that will affect menu planning (Bor, 2020).

When planning an efficient menu in workers, factors such as the state of hunger and appetite that will affect their eating, the attraction and appearance, taste and taste of the food to be eaten should be taken into account (Baysal, 2009). Instead of meeting the intensive energy needs of workers working in heavy physical jobs with foods high in fat and sugar, it should be preferred for their health to meet the necessary energy needs by supplementing the intermediate meals (Tüber, 2015).

The nutrition of workers outside of work is also effective on their healthy and productive status. Workers who do not feed well outside of work can provide a part of their daily needs at work. Thus, the consequences of inadequate and unbalanced nutrition can be mitigating (Saltık, 1995).

There are some considerations when creating menus and nutrition plan according to the energy and nutritional requirements of employees at work. Workers in heavy and dangerous jobs should not take the increased energy burden in a single meal. Main and intermediate meal menus should be planned to meet half of the daily energy and nutrients requirements for these workers. Employees as drinks in intermediate meals; They can consume milk, buttermilk, lemonade, herbal teas, juices, various sandwiches as food, cakes, biscuits, pastries, pastries, fruits, walnuts, nuts and dried fruits. Attention should be paid to the consumption of liquids, especially those working within the scope of heavy and dangerous work. In addition to water, water should be included in order to contribute to liquid intakes, as well as juicy foods such as fresh juices, buttermilk, milk, open tea, herbal teas, lemonade and soups. Workers who work under the sun for a long time or are exposed to X-rays; The pre-ingredient of vitamin A is rich in carotene; should consume enough vegetables and fruits such as

carrots, curly, lettuce, aruga, tomatoes, apricots, oranges. In cases where the workplace does not provide food, the employee should bring the ration menus with the employee. The food-producing institution should prepare and offer menus that are hygienic, appetizing and high in subjective quality. In addition, nutrient diversity should be provided from each food group (Çil, 2019).

It is important to include the thoughts of workers in making meal plans in workplaces, to make necessary arrangements by identifying meals not consumed by the majority and the reasons why they are not consumed, to pay attention to hygiene and sanitation rules, to ensure worker and nutrition compliance (Bekar and Ersoy, 2011).

2.3. Measures That Can Be Taken Against Unhealthy Nutrition in Workplaces

In order to ensure healthy eating, employers take some measures for this and can implement various programs. In addition, for workers' health, the state, unions and managers can impose legal obligations and sanctions on these programs. Many administrations work to create a healthy eating program in their workplaces and develop a variety of plans and guides. In this context, some recommendations have been presented in line with many guides and evidence-level studies. Employees can be given group or individual interactive and/or computer-web based healthy eating trainings. Using posters and brochures, information about healthy eating can be made continuous. If it is an institution or organization that provides bulk nutrition services, the menus can be arranged according to the macro and micronutrition requirements of the employees. With food labeling, the energy, carbohydrate, fat and protein values of menus, dishes and foods can be indicated and healthy choices can be marked. A healthy food selection alternative can be put on the menus. Vegetables and fruits can be included more often in meals offered to the employee at work. In workplace cafeterias, canteens can be encouraged to offer healthy foods with reduced fat, high pulp content. Anthropometric measurements of employees (such as weight, height, body mass indecencies, waist and hip perimeter), body compositions and various biochemical parameters can be monitored at regular intervals. Individuals deemed risky can be directed to a health care organization (Çil, 2019).

3. Food Safety and Hygiene

World Health Organization (WHO) improves food safety; “*Compliance with the necessary rules and taking precautions during the production, processing, preservation, transportation and distribution stages of food in order to ensure healthy and flawless food production*” explains. By the Food and Agriculture Organization of the United Nations (FAO), the term

food safety is defined as “*always physical, social and economic access to adequate, reliable and nutritious food to meet nutritional requirements and food preferences so that all people can lead active and healthy lives*” (Er, 2015).

One of the most important conditions of healthy life is to ensure the consumption of reliable foods. Food safety can be defined in many ways. In general, food safety covers the package of measures taken to ensure that food is presented to the consumer in a healthy and reliable way, maintaining its chemical, physical, sensory and biological qualities from its production to recent consumption (Taşdan, et al., 2014). In other words, food safety is a condition in which all employees have continuous access to adequate, healthy, reliable and nutritious food physically and economically in order to meet the nutritional needs and food priorities necessary for an active and healthy life at all times (Ülgüray, et al., 2003).

Hygiene and sanitation should be applied effectively in order to ensure that the produced foods are presented safely and high quality in accordance with the consumption of people, so that there is no negativity in the stages leading up to the product’s table until the product comes to the consumer’s table. End consumers are highly vulnerable to any danger of contamination that may arise from manufacturing processes. Therefore, in food production, the quality of the food to be produced is an important requirement. Quality; The absence of errors and mistakes in products and services can also be defined as the high degree of product meets the needs, while maintaining consumer health at the highest level is one of the criteria of quality. For this, activities on hygiene and sanitation should be established and carried out (Kışla, 2013).

Food Hygiene; in order to produce the foods to be offered for human consumption, the purpose of use of food in food production facilities is taken into consideration, food hazards are controlled, the necessary rules are followed in the production stages and all precautions are taken. To put it another way; In order to produce healthy food, it covers the activities carried out in order to create and design appropriate production conditions at every stage from the farm to our table. Sanitation is a science. The way to protect, improve and regain human health includes the basic principles to be applied. When it comes to sanitation in the food industry, the environment and the product are brought into compliance with hygienic rules and production is carried out smoothly in terms of health. It ensures that the production of foodstity, which forms the basis of human nutrition, is physically, chemically and biologically reliable. In order to protect public health, the study includes all of the surfaces to be carried out, food residues as a result of previous production, microorganisms in the environment and the removal of contamination elements and debris from

the production environment, such as the remains of cleaning agents from previous processes (Parlak, 2020).

Physically, chemically or microbiologically grouped hazards along the food chain threaten food safety and can cause food to become a health disruptor. These hazards should be evaluated separately in the stages from the production of food to the consumption stage such as processing, transport, storage, purchase, storage, preparation, cooking (Giray and Soysal, 2007).

3.1. Physical Hazards

Glass shards that should not be present in food, plastic, bone, paper, stone, soil, wood, metal fragments, hair, nails, cigarette ash, flies, insects, radioactivity and dirt are physical hazards. These can be contaminated or fraudulently added to food from the environment during the stages of obtaining raw materials, production, storage, packing, transport or consumption (Erkmen, 2010).

Physical hazards do not normally cause foodborne diseases, but they can cause damage to the human body. Stones, for example, can break teeth, glass and hard plastic can make cuts in the mouth and throat, fish hairs, chicken bones can escape into the throat. These hazards and their resources are given below in Table 2 (Şahin, 2010).

Table 2. *Physical hazards and sources of danger*

Physical Hazard	Source of Danger
Piece of glass	Lamp, window glass, glass containers
Piece of metal	Equipment, personnel, raw materials
Hair, feather, hair impurities	Personnel, equipment
Impurities belonging to insects, rodents and birds	Building, equipment, inadequate pest control
Stone, wood, plastic, gasket	Packaging, equipment, building, process
Dust impurities	Air, building equipment

3.2. Chemical Hazards

Contamination with some chemicals that are transmitted to foodsting from various sources such as air, water and soil or specifically added for another purpose. The chemicals in question; toxic metals, pesticides used during the cultivation of food, detergent and disinfectant residues left on them due to the lack of good rinsing of the tools used in eating, are especially colored plastics used in food packaging. Additional additives are chemicals added to food in order to give color, smell, flavor, develop consistency

and increase its durability (West, et al., 1998). These chemicals, which are mixed into food from various sources or added for a specific purpose, may not be toxic when taken in trace amounts. But they can cause poisoning if they pass a certain level (Bulduk, 2010).

3.3. Microbiological Hazards

Microorganisms are invisible small creatures found in the composition of food and are also widely found in nature. Unless sterilized, each foodst agent has a certain level of microorganisms. Foodborne diseases caused by microbiological hazards are a growing health problem in both developed and developing countries (Türk-İncel, 2005). Since microbiological elements are living beings, they need certain nutrients (carbohydrates, proteins, fats), a certain degree of heat, neme, the amount of acid contained in food, and some need oxygen to multiply.

Microorganisms that are effective in the degradation of food; bacteria, yeasts, molds and viruses (Bulduk, 2010). Deterioration of a food; it is an indication that microorganisms may have developed and reached high numbers during the supply, transportation, processing and storage of raw materials. Meanwhile, if the food is also infected with a pathogenic microorganism and has multiplied and reached dangerous numbers, it can cause various infections and food poisonings in humans (Cömert and Özkaya, 2008).

Bacteria cause these infections and food poisonings through food the most. Bacteria are very small microorganisms and are found all around us. There are thousands of different types of bacteria. Bacteria multiply under certain conditions and spread through the easiest foods. Therefore, microorganisms play an important role in food spoils and foodborne poisoning (Erbil, 2000).

One of them is; *Salmonella spp.*, *Bacillus cereus*, *Bacillus subtilis*, *Bacillus licheniformis*, *Staphylococcus aureus*, *Clostridium boutulinium*, *Clostridium perfringens*, *Campylobacter jejuni*, *Shigella spp.*, *Vibrio cholerae*, *Escherichia coli*, *Listeria monocytogenes* *Yersinia enterocolytica* (Babür, 2007).

Another important microbiological hazard, yeasts, are single-celled organisms. Yeast cells multiply, develop and grow when they merge with warm temperature, air, humidity and sugar. Although they are of great importance in the production of foods such as bread, beer and wine, some species can cause negativity in the food industry. Some yeast species are known to be important contaminatants in fermentation and food industry. When yeast cells come into contact with food, when they start dividing carbohydrates and chemically change, foodstuffs deteriorate. As a result of the contamination of yeasts and unwanted porous structure, bitter taste and

bad smell, spoils can be seen in foods such as pickles, meat, jelly, syrup, juice, wine (Çetiner, 2010; Aratoğlu, 2015).

Viruses are the simplest and smallest microorganisms in terms of their properties. They are considered parasites, as they need the host to breed. Viruses can't reproduce in food, but they're transported through food. When taken into the body through the digestive system, they lead to infectious diseases. Among the foods that are intermediary in the transportation of viruses; there are seafood, drinking water, milk and dairy products, salads, bread and other bakery products and foods that are consumed raw or hand-processed after cooking (Bulduk, 2003).

3.4. Food Hygiene in Workplaces

All service stages from food supply to consumption in places where mass nutrition is used by the vast majority of society are of great importance for the protection and development of human health. The main goal in mass consumption enterprises is to achieve economic gain. They want to earn money in exchange for the goods and services they will offer, and increase market share and profitability. For this purpose, businesses aim to please them by meeting the wishes and needs of the customer group they target, to have a solid place in a competitive market, to have a reliable image and to offer reliable, hygienic products that consumers have a natural right (Sökmen, 2003). Accordingly, the most important task of a mass nutrition organization is to ensure adequate and balanced nutrition of consumers, as well as reliable food delivery that does not threaten health.

Two basic factors concerning the health of employees emerge in bulk nutrition systems. The first is balanced nutrition, which directly concerns the health of the worker and forms the ideal combination of all compositions such as vitamins, minerals, proteins and the necessary calories that the worker needs, and the other is hygiene and food safety, which covers all stages of producing, transporting and serving the food to consumption under hygienic conditions.

The bulk food sector should be evaluated according to these two elements in terms of both producers, buyer organizations and supervisory institutions and perceived as a strategic product and sector (Bozdağ, 2005).

Hygiene and food safety are extremely important in terms of protecting consumer health in bulk nutrition systems where the nutritional needs of a large number of people are met. Therefore, all the drivers such as people, nutrients, places, tools, etc. used in the whole process from the purchase of food to its service to the removal of garbage should be healthy. Unhealthy meals offered to consumers as a result of inadequate food purchase, production and service hygiene and minor carelessness endanger the health of hundreds or even thousands of people and cause economic losses. One

of the objectives of the institutions that provide mass nutrition services is to protect the health of the group that is fed (Ünsal, 2018).

It is very important for the personnel who are in charge of the preparation and service of food in public nutrition institutions and who have important responsibilities in terms of human health to be trained and knowledgeable about personal and culinary hygiene, both in terms of the quality of the nutrition service and the continuity of the place of service and the protection of the health of the consumer. Because a small omission can disrupt the health of hundreds and thousands of people, ingesting food poisoning and deaths (Çiğirim, et al., 1995). The efforts of the staff working in this sector to keep the food poisoning microorganisms and other contaminating agents from getting into the food is a legal obligation. Therefore, it is necessary to select the staff from healthy individuals who do not carry any infectious diseases and to carry out health checks at regular intervals. It is mandatory to provide hygienic cleaning of hands, bodies and clothes as well as healthy personnel, especially when dealing with food. All staff must know the relationship between their work and human health (Beyhan, 1999).

Protection in food hygiene, which is a very important concept; it is possible to know well the environmental factors that are effective in the development and toxins of the agents involved in food poisoning and to consciously implement protective measures (Alpakın, 2002). In this context, in order to ensure food hygiene, it is necessary to comply with the following hygiene rules during the purchasing, storage, preparation, cooking and service stages of food.

- Buying solid, clean, reliable food.
- Storing food that will not be consumed immediately with the appropriate method.
- Prepare the amount of food to be consumed, if possible, serve the meals immediately after cooking.
- To choose to cook meals in a short time and at high temperatures.
- To consider the interaction of microorganism temperature in the storage, preparation, cooking and service stages of food.
- To ensure that the internal temperature is at least 70 degrees in reheating.
- Do not keep cooked hot meals at room temperature for more than 4 hours.
- Dissolving frozen foods at refrigerator temperature.

- Washing raw vegetables and fruits abundantly with clean water so that pesticide residues can be minimized.
- To perform all food and beverage transactions with clean water.
- To make the food waiting for hot service at least 65 degrees (Demirci, 2005).

4. Conclusion and Suggestions

The health and safety of workers who play a role in production and in the economy of countries is only possible if they get enough of the necessary nutrients according to their work conditions. In industrially developed countries, it is a legal obligation to have nutrition services when the number of workers belonging to the workplaces passes certain levels. Workers are considered to be in the risk group in terms of nutrition and health. In various cases, not meeting these needs of workers with increased nutritional and energy needs can result in work accidents, decrease in production and increase in costs. The menus to be planned taking into account the characteristics of each business will contribute to the health and safety of both workers and increase productivity in the workplace. This area, which is closely related to production and therefore the country's economy, further research will contribute to the development of applications to be applied in various industrial organizations. Staff and their families should be given nutrition training to help them gain healthy eating habits. If adequate and balanced nutrition is not provided in the workplace, there will be many health problems and absenteeism problems, an increase in the likelihood of occupational accidents and a decrease in worker productivity. It is also recommended to establish cooperation between dietitians and workplace physicians on occupational health and nutrition, to plan and carry out related studies, and to provide in-service training to the worker in terms of health and nutrition.

The level of training of staff working in bulk nutrition services is generally low. They do not know what it is like to be contaminated with food and how it can be prevented. Some unconscious applications in the preparation of food can lead to food poisoning in bulk. Therefore, food processors should be given trainings including the basic principles of preparing healthy foods and personal hygiene issues. In particular, time and temperature control, personnel hygiene, sources of cross-contamination and factors affecting the reproduction of pathogens in food should be taught and these trainings should be carried out at regular intervals.

REFERENCES

- Abaoğlu, C., (1956). İşçi Sağlığı ve Beslenme [Occupational Health and Nutrition]. *Sosyal Siyaset Konferansları Dergisi* [Journal of Social Politics Conferences], (8).
- Alpakın, L., (2002). Gıda Maddelerinde Üretim Hijyeni ve Ambalaj [Production Hygiene and Packaging in Food Materials]. *Gıda Dergisi* [Food Journal], 9: 34-36.
- Aratoğlu, C., (2015). Mesleki ve Teknik Anadolu Lisesinde ve Meslek Yüksekokulunda Aşçılık Eğitimi Alan Öğrencilerin Gıda Güvenliği Konusundaki Bilgi ve Uygulama Düzeyleri [Knowledge and Application Levels on Food Safety of Students Studying Cooking at Vocational and Technical Anatolian High School and Vocational School], Yüksek Lisans Tezi [Master Thesis], Gazi Üniversitesi Eğitim Bilimleri Enstitüsü [Gazi University Institute of Educational Sciences], Ankara.
- Atkoşar, Z., (2018). Beslenmenin Temel İlkeleri [Basic Principles of Nutrition]. Eskişehir: Anadolu Üniversitesi [Anadolu University].
- Babür, T.E., (2007). Muğla'daki Birinci Sınıf Tatil Köylerinde Çalışan Mutfak Personelinin Aldıkları Hizmet İçi Eğitimi ve Mutfak Hijyen Durumunun Değerlendirilmesi [Evaluation of In-Service Training and Kitchen Hygiene Status received by The Kitchen Staff in The First Class Resorts in Muğla]. Yüksek Lisans Tezi [Master Thesis], Selçuk Üniversitesi Sosyal Bilimler Enstitüsü [Selçuk University Institute of Social Sciences], Konya.
- Baysal, A., Küçükaskan, N., (2009). Beslenme İlkeleri ve Menü Planlaması [Nutrition Principles and Menu Planning]. Bursa: Ekin Yayınları [Ekin Publications].
- Bekar, A., Ersoy, A.F., (2011). Sanayide Çalışan İşçilerin Enerji Harcamaları ve Beslenme Durumlarının Değerlendirilmesi [Evaluation of Energy Expenditures and Nutrition Status of Industrial Workers]. *Vocational Education* 6, p: 84-108.
- Beyhan, Y., (1999). Çalışma Hayatında Beslenme Hizmetlerinin Yönetimi [Management of Nutrition Services in Working Life.]. *Türkiye İşçi Sendikaları Konfederasyonu* [Confederation of Workers' Unions of Turkey], Türk-İş Yayın No: 189, 102s, Ankara.
- Bilici, S., (2006). Farklı İş Kollarında Çalışan Yer Altı Maden İşçilerinin Enerji Harcamaları ve Beslenme Durumlarının Saptanması [Detection of Energy Expenditures and Nutrition Status of Under-Ground Mine Workers Working in Different Lines of Business.]. Hacettepe Üniversitesi [Hacettepe University], Sağlık Bilimleri Enstitüsü [Health Sciences Institute], Beslenme ve Diyetetik Anabilim Dalı [Department of Nutrition and Dietetics], Doktora Tezi [PhD Thesis], Ankara, 35-57.

- Bilici S (2008). Toplu Beslenme Sistemleri Çalışanları İçin Hijyen El Kitabı [Hygiene Handbook for Collective Nutrition Systems Workers]. T.C. Sağlık Bakanlığı Temel Sağlık Hizmetleri Genel Müdürlüğü [T.R. Ministry of Health, General Directorate of Primary Health Services], Klasmat Matbaacılık [Klasmat Printing House], Sağlık Bakanlığı Yayın No [Ministry of Health Publication Number]: 726, 48s, Ankara.
- Bor, H., (2020). The Relationship between Nutrition and Worker Efficiency. *Turkish Journal of Family Medicine and Primary Care*. 305-311.
- Bozdağ, H., (2005). Yemek Sanayinin Gelişimi [Development of the Food Industry], *Gıray Karanlık*. İstanbul, 93-94.
- Bulduk, S., (2010). Gıda ve Personel Hijyeni [Food and Personnel Hygiene]. *Detay Yayıncılık* [Detay Publishing], 188s, Ankara.
- Bulduk, S., (2003). Gıda ve Personel Hijyeni [Food and Personnel Hygiene]. *Detay Yayıncılık* [Detay Publishing], 179s, Ankara.
- Büyükpamukçu, M., Oğuz, S., İlhan, M.N., (2003). Endüstride Beslenme [Nutrition in Industry]. *TTB Mesleki Sağlık ve Güvenlik Dergisi* [TTB Occupational Health and Safety Journal]. 4, 40-45.
- Ciğirim, N., Beyhan, Y., Çelikleş, N., (1995). Ankara'da Yüksek Öğrenim ve Kredi Yurtlar Kurumuna Bağlı Yurt Mutfaklarında Hijyen Durumunun Değerlendirilmesi [Evaluation of Hygiene Status in Dormitory Kitchens Affiliated to Higher Education and Credit Dormitories Institution in Ankara]. *Beslenme ve Diyet Dergisi* [Nutrition and Diet Journal]. 24(2): 273-278.
- Cömert, M., Özkaya, D., (2008). Otellerde Gıda Güvenliği [Food Safety in Hotels]. Türkiye 10. Gıda Kongresi Bildiriler Kitabı [Congress Proceedings of the 10th day in Turkey]. Türkiye 10. Gıda Kongresi [Turkey 10. Food Congress], Erzurum, 121-123.
- Çetiner, H., (2010). Yiyecek-İçecek İşletmelerinde Hijyen, Sanitasyon ve Personelin Hijyen Kurallarına İlişkin Davranışlarında Eğitim Faktörü [Education Factor in Hygiene, Sanitation and Behavior of Personnel Regarding Hygiene Rules in Food and Beverage Businesses]. Yüksek Lisans Tezi [Master Thesis], Gazi Üniversitesi [Gazi University], Eğitim Bilimleri Enstitüsü [Institute of Education Sciences], Ankara.
- Çil, A.M., (2019). İş Yerlerinde Beslenme ve Gıda Hijyeni [Nutrition and Food Hygiene in Workplaces]. Atatürk Üniversitesi Açıköğretim Fakültesi Yayını [Atatürk University Open Education Faculty Publication]. Erzurum.
- Demirci, M., (2005). Beslenme [Nutrition]. Onur Grafik [Onur Graphics], 297s, İstanbul.
- Er, S.S., (2015). Gıda Güvenliği Açısından Tarımsal Biyolojik Çeşitliliğin Önemi [Importance of Agricultural Biodiversity in Terms of Food Safety], T.C. Gıda Tarım ve Hayvancılık Bakanlığı [T.R. Ministry of Food, Agriculture and Livestock], Avrupa Birliği ve Dış İlişkiler Genel Müdürlüğü [General

- Directorate of European Union and Foreign Relations], AB Uzmanlık Tezi [AB Specialization Thesis], Ankara, 4-50.
- Erbil, S., (2000). İstanbul'da Toplu Beslenme Üretimi Yapan Yemek Fabrikalarının Sanitasyon ve Hijyen Koşullarının Değerlendirilmesi [Assessment of Sanitation and Hygiene Conditions of Food Factories Producing Mass Nutrition in Istanbul]. Yüksek Lisans Tezi [Master Thesis], İstanbul Üniversitesi Sağlık Bilimleri Enstitüsü [Istanbul University Institute of Health Sciences], İstanbul.
- Erkmen, O., (2010). Gıda Kaynaklı Tehlikeler ve Güvenli Gıda Üretimi [Foodborne Hazards and Safe Food Production]. *Çocuk Sağlığı ve Hastalıkları Dergisi* [Journal of Child Health and Diseases], 53(3): 220-235.
- Gallis, C., Panagopoulou, P., (2007). Nutrient Intakes of Greek Forest Workers and Researchers Do Not Meet All Reference Dietary Intakes. *Nutrition Research*; 27 (6), 321-326.
- Giray, H., Soysal, A., (2007). Türkiye'de Gıda Güvenliği ve Mevzuatı [Food Safety and Related Laws in Turkey]. *TSK Koruyucu Hekimlik Bülteni* [TSK Preventive Medicine Bulletin], 6(6): 485-490.
- Kışla, D., (2013). Gıda İşletmelerinde Hijyen [Hygiene in Food Business]. <http://www.gidateknolojisi.com.tr/haber/2013/01/gida-isletmelerinde-hijyen> Erişim: 05.12.2020
- Larousse gastronomique. (2005). Larousse Gastronomique: Dünyanın En Büyük Mutfak Ansiklopedisi [Larousse Gastronomique: The World's Largest Culinary Encyclopedia.]. (Çev. Ed. Haznedaroğlu, S.). İstanbul: Oğlak Yayınları [Oğlak Publications].
- Meng, L., Wolff, M. B., Mattick, K. A., DeJoy, D. M., Wilson, M. G., Smith, M. L., (2017). Strategies for worksite health interventions to employees with elevated risk of chronic diseases. *Safety and Health at Work*, 8(2), 117-129.
- Murad, M. H., Elamin, K. B., Abu Elnour, N. O., Elamin, M. B., Alkatib, A. A., Fatourechi, M. M., Almandoz, J.P, Mullan, R.J., Lane, M. A., Liu, H., Erwin, P. J., Hensrud, D. D., Montori, V. M., (2011). The effect of vitamin D on falls: a systematic review and meta-analysis. *The Journal of Clinical Endocrinology & Metabolism.*; 96 (10), 2997-3006.
- Müftüoğlu, S., Parlakyiğit, A., (2020). Vardiyalı Çalışan İşçilerin Fiziksel Aktivite, Duygudurumu ve Beslenme Alışkanlıkları Arasındaki İlişkinin Belirlenmesi [Determining the Relationship Between Physical Activity, Mood and Eating Habits of Workers Working in Shifts]. *Türkiye Klinikleri Journal of Health Sciences* 5, 10-21.
- Parlak, T., (2020). Gıda Ürünleri Üretiminde Hijyen Kavramına Farklı Bir Bakış [A Different Perspective on the Concept of Hygiene in Food Products Production]. *Ohs Academy.* (3), 73-101.

- Reime, B., Novak, P., Born, J., Hagel, E., Volker, W., (2000). "Eating Habits, Health Status, and Concern About Health: A Study Among 1641 Employees in The German Metal Industry". *Preventive Medicine*, Number:30, 295-301.
- Saltık, A., (1995). İşçi Beslenmesi [Worker Nutrition]. *Beslenme ve Diyet Dergisi* [Nutrition and Diet Journal], 24 (1), 123-149.
- Sezgin, A.C., Özkaya, F.D., (2014). Toplu Beslenme Sistemlerine Genel Bir Bakış [An Overview of Mass Nutrition Systems]. *Akademik Gıda* [Academia Food], 12, 124-128.
- Sökmen, A., (2003). Ağırılama Endüstrisinde Yiyecek ve İçecek Yönetimi [Food and Beverage Management in Hospitality Industry]. *Detay Yayıncılık* (1.baskı) [Detay Publishing (1st edition)], Ankara.
- Şahin, S., (2010). Gıda Güvenliği ve Gıda İşletmecileri İçin Business Support Programme (BSP) Uygulaması Semineri [Business Support Program (BSP) Application Seminar for Food Safety and Food Businesses]. Kilis 7 Aralık Üniversitesi Fen Bilimleri Enstitüsü [Kilis 7 Aralık University Institute of Science], Kilis.
- Tanır, F., Şaşmaz, T., Beyhan, Y., Bilici, S., (2001). "Doğankent Beldesinde Bir Tekstil Fabrikasında Çalışanların Beslenme Durumu [Nutritional Status of Employees in a Textile Factory in Doğankent Town]". *Türk Tabipleri Birliği Mesleki Sağlık ve Güvenlik Dergisi* [Turkish Medical Association Occupational Health and Safety Journal], 22-25.
- Taşdan, K., Albayrak, M., Gürer, B., Özer, O.O., Albayrak, K., Güldal, H.T., (2014). Geleneksel Gıdalarda Tüketicilerin Gıda Güvenliği Algısı: Ankara İli Örneği [Consumers' Perception of Food Safety in Traditional Foods: The Case of Ankara Province]. 2. Uluslararası Davraz Sempozyumu [2nd International Davraz Symposium], Süleyman Demirel Üniversitesi [Suleyman Demirel University], Isparta.
- Türk-İncel, E., (2005). Yetişkin Tüketicilerin Besin Güvenliği Konusunda Bilgi ve Davranışları [Knowledge and Behaviors of Adult Consumers on Food Safety.]. Yüksek Lisans Tezi [Master Thesis], Hacettepe Üniversitesi Sağlık Bilimleri Enstitüsü [Hacettepe University Institute of Health Sciences], Ankara.
- Türkoğlu, A., (2011). Dünya Nüfusu ve Beslenme Problemi [World Population and Nutrition Problem.]. İstanbul Üniversitesi İktisat Fakültesi Mecmuası [Istanbul University Faculty of Economics Magazine], 20.
- Türk İş. Türkiye İşçi Sendikaları Konfederasyonu [Confederation of Labor Unions of Turkey], İş Sağlığı ve Güvenliği Ders Notları [Occupational Health and Safety Lecture Notes]. Ankara: Grup Matbacılık [Grup Publications], (2014). Erişim: [http:// www.turkis.org.tr/dosya/IIeZkbGK8Lyp.pdf](http://www.turkis.org.tr/dosya/IIeZkbGK8Lyp.pdf)
- Tüber. Türkiye Beslenme Rehberi [Turkey Nutrition Guide], (2015). Ankara: T.C. Sağlık Bakanlığı [T.R. Ministry of Health].

- Ülgüray, D., Varlık. M., Kıymaz. T., (2003). Ulusal Gıda ve Beslenme Stratejisi Çalışma Grubu Raporu [National Food and Nutrition Strategy Working Group Report]. Devlet Planlama Teşkilatı [State Planning Organization], Yayın No: 2670.
- Üner, M.H., Yılmaz, İ., (2020). İşçi Beslenmesi, İş Kazaları ve Üretkenlik İlişkisinin İncelenmesi [Investigation of Worker Nutrition, Work Accidents and Productivity Relationship.]. *Haliç Üniversitesi Sağlık Bilimleri Dergisi* [Haliç University Journal of Health Sciences] 3, 169-179.
- Ünsal, C., (2018). Hazır yemek üretim ve toplu tüketim sektöründe çalışanların gıda hijyeni bilgi düzeylerinin ölçülmesi: Tekirdağ/Hayrabolu örneği [Measuring the food hygiene knowledge levels of those working in the catering sector: Tekirdağ / Hayrabolu example], Yüksek Lisans Tezi [Master Thesis], Tekirdağ Namık Kemal Üniversitesi Fen Bilimleri Enstitüsü [Tekirdağ Namık Kemal University Institute of Science and Technology], Tekirdağ.
- Wanjek, C., (2005). “Food at Work, Workplace Solutions For Malnutrition, Obesity and Chronic Diseases”. Geneva: *International Labour Organization*. First published.
- West, B., Wood, L., Harger, V.F., (1998). Food Service in Institutions. *New York Millan Publishing*, 73(6): 45-51.
- Yılmaz, C., (2003). Sağlıklı Beslenme ve Özellikleri [Healthy Nutrition and Its Features]. *Sosyoloji Dergisi* [Journal of Sociology]. 65-78.

Chapter 25

THE MODEL OF PREVENTING PSYCHOSOCIAL RISKS IN WORKPLACES WITH THE RISK ASSESSMENT METHOD A STUDY EXAMPLE FOR TURKEY MOBBING ISSUE



Adnan KARABULUT¹

Dilek ÖZTAŞ²

Ergün ERASLAN³

1 M.Sc. in OSHA, Chemical Engineer, Economist, Istanbul Technical University, Orcid No:0000-0002-0643-098X

2 Assoc. Dr. Dilek ÖZTAŞ, Ankara Yıldırım Beyazıt University, Faculty of Medicine, Orcid No:0000-0002-8687-7238

3 Prof. Dr. Ergun ERASLAN, Ankara Yıldırım Beyazıt University, Faculty of Engineering and Natural Sciences, Orcid No:

1. Introduction

In today's business life, the importance of psychosocial risk factors that reduce work efficiency and pose significant threats to health, safety and welfare is increasing. Psychosocial risks cause situations such as chronic stress, depression and burnout in business. Also increases significant costs for businesses and society. The subject of mobbing covers all businesses in the public and private sector.

Mobbing that is in the scope of the law since 1990 in developed countries, has been on the agenda of Turkey since 2010. "ALO-170" line was put into service in 2010. The Prevention Circular for Psychological Harassment in the Workplace was issued in 2011. A Board for Combating Psychological Harassment was established in 2012. Mobbing Information Guide was published in 2013.

ALO-170 service line received 55,046 calls between 2011-2017. It is seen that the most complaint subjects are ill-treatment, verbal abuse, discrimination and insult. As mobbing is difficult to prove, the solution based on formal procedures is not enough. In this study, it was aimed to build a preventive approach model by using risk assessment method to prevent mobbing, which is an important psychosocial risk.

2. The Importance of Preventive Approach Model in the Prevention of Mobbing

The concept of psychological harassment (psychological terror or mobbing) was first brought to the agenda by Psychologist Heinz Leymann in the early 1980s. Mobbing is an exclusionary behavior directed by one or more people to another. The cause of mobbing may be jealousy, racial and gender discrimination, hostility to religion and belief, and intolerance to different opinions. Mobbing is defined as a form of psychological terror that occurs as a systematic, hostile and immoral communication.

Today, one of the biggest psychosocial risks faced by workplaces (Organizations) is mobbing. The International Labor Organization (ILO) defines psychological harassment in the workplace as a repetitive, vengeful, brutal and humiliating action.

Workplaces are affected by the socio-political environments and contain psychosocial risks as well as financial risks. Because, mutual relations between institutions, businesses, society and stakeholders; shaped by socio-political values and it causes problems by increasing confusion, distrust and uneasiness over ethical and moral behaviors (Nivarthi et al., 2013). Therefore, workplaces is seen as a system that has to be kept under control in order to minimize risks (Kirsten, 2012). Although there are legal regulations and environments in the countries and policies are developed

in this subject, the main problem is the existence of a gap between policies and implementation (EU-OSHA, 2007).

The World Bank and World Health Organization bring psychological disorders to the agenda as one of the critical problems in societies. Mobbing is accepted as one of the most important causes of psychological disorders.

Some literature studies about mobbing in Turkey has made in recent years. Keser (2014) Kocabas, Aydin, Canbey private, Ilhan, Demirkaya, (2017), Sahan (2016), Sahan and Demiral, (2019). Şahan and Demiral study (2019) shows that employees and employers are aware of the psychosocial risk and this study indicates that a law on the prevention of psychosocial risks in Turkey is necessary supporting role in the definition of the attitude of the manager. On the other hand, organizational justice, openness and reward systems are important functional element in preventing psychosocial risks. Therefore, it is important to create a preventive approach model to prevent mobbing.

2.1 Psychosocial Risk Factors in Working Lives

Psychosocial health factors are work-related factors that disturb the peace of the employees (Goetz, 2015: 2). European OHS Agency defines “psychosocial risks as the risks that cause serious deterioration in physical and mental health over time. The economic and social conditions of the work and the design too effects psychosocial risks (EU-OSHA, 2007).

ILO ranks psychosocial risk factors in order of importance; 1. Unemployment 2. Lack of job security 3. Low wages 4. Shift work 5. Monotonous work. These factors all are a cause of mobbing

According to literature studies, for an action to be considered as mobbing, it must be a) Intentional b) Systematic repetition c) lasting for a long time (minimum 6 months).

In the fifth European working conditions survey (EWCS) grouped Psychosocial risks into six dimensions. These are job intensity and workload, emotional efforts, degree of autonomy at work, ethical conflicts, weak social relations and lack of job security (Eurofound, 2010).

Non-standard and flexible working hours in business life reveal many risks and dangers. In addition, situations such as unbalanced distribution, workload, indifference of managers, fear of losing their jobs, working hours, shift system, overtime, ergonomic conditions are important psychosocial risk factors (Richards, 2003).

Conditions that determine psychosocial situations may be categorized as follows according to the conditions and environment of the work.

- ↪ Organization culture; lack of communication, problems in solving problems, uncertainties in organizational goals
- ↪ Organizational role; role ambiguity, conflict, and inadequacy and overwork
- ↪ Career development; career development uncertainty, over-status attribution, uninsured employment, and inadequate social values for work
- ↪ Freedom to make decisions; insufficient participation in the decision-making process, lack of control on the issue
- ↪ Lack of interpersonal communication at work; interpersonal conflicts, violence and lack of social support
- ↪ Business and home conflict; conflict of expectations, insufficient support at home, career conflict.

The criteria to be considered when evaluating psychosocial risks are listed as follows (AISGA, 2007).

- ↪ Number of people exposed to dangers
- ↪ Frequency of exposure to the hazard
- ↪ Duration of exposure to the hazard
- ↪ Danger information / education level
- ↪ Frequency of control and recovery
- ↪ Work conditions

Psychosocial risks that may be encountered in workplaces are listed in another study as follows (Vatansever, 2014).

- ↪ Monotony at work
- ↪ Technological changes
- ↪ Dangerous factors at work, working environment and environmental conditions
- ↪ Excessive workload, evaluation and promotion mechanisms
- ↪ Fear of losing a job
- ↪ Ambiguities in roles
- ↪ Interpersonal relations
- ↪ A sense of responsibility
- ↪ No governance and competition

- Violation of the psychological contract
- An aging workforce
- Stress
- Intimidation

2.2 Psychosocial Risks Related to the Business Content

The characteristics of the production tools and environment in the workplaces and the physical environment in the social areas, the lack of suitable equipment, the lack of space, insufficient lighting, excessive noise, potentially damaging or stressful situations are psychosocial risks related to the workplace.

Under objective working conditions; by examining workload, repetitive or variable jobs, monotony, job satisfaction, etc., a positive relationship was found between job complexity and job satisfaction (Judge et al.2000).

Higher use of ability results in less emotional exhaustion and alienation which is a final of mobbing (Lee and Ashforth 1996).

Workload is the physical and mental effort a person takes to achieve his or her job. Although excessive workload causes adverse health effects, little workload too creates problems.

The pace and pace of work is an important workload factor and is accompanied by work stress. High pace of work can negatively affect work stress.

2.3 Psychosocial Risks Related to Business Environment

Excessive workload causes mental and musculoskeletal disorders. It has been observed that those working in non-autonomous jobs have lower motivation and job satisfaction (Pearson, 1992).

The level of participation in decisions is negatively related to the pressure and strain at work. Low participation causes a high degree of emotional exhaustion and alienation (Parker et al., 2002).

Poor communication, poor leadership, not defining goals and lack of consensus are risk factors related to organizational culture. Job insecurity, lack of promotion expectation, inability to be promoted, excessive promotion, low wage, unclear personal evaluation systems can be used as mobbing tools as (EU-OSHA, 2012, Leka, S., Griffi ths, 2004).

Physical and social abstraction, weak relationships of superiors, interpersonal conflicts, lack of support, psychological harassment and violence, bullying and rude behavior are psychosocial risks and can cause harm.

Among the sectors, the health sector is the area where mobbing is the most and men are exposed to more negative social behaviors than women.

According to a survey conducted in 2008 in the health sector in Turkey the ratio of exposed to psychological abuse changes from 23.2% to 46.5%. (Karatuna and Tınaz, 2010).

In Turkey, medical, bank and insurance employees, sales and technical staff are at high risk of bullying and mobbing. Frequency ranges between 25-29% (Gül, 2009).

Mobbing is deliberate and negative attitudes and behaviors in workplaces and behaviors of one or more people aiming to intimidate, pacify and dismiss other persons (ÇSGB, 2013).

Mobbing that people are exposed to in the workplace should include some factors (ÇSGB, 2013). It should be continuous and repeated frequently. It must be on purpose. It should aim to pacify. It should have a detrimental effect on personality, health or work life. Environmental factors and the personalities of the parties can be the cause of psychological terror. Role conflict, severe workload, tense and stressful atmosphere, low job satisfaction and leadership problem may be given as examples

Mobbing can start with a disagreement and can occur as a continuation of this behavior. The hierarchical organizational structure in workplaces can provide a basis for psychological reasons. This structure becomes a suitable environment for mobbers to hide themselves. Poor management, communication problems, poor leadership, fear of losing a job in a competitive environment, not being able to fulfill the expected jobs, a different structuring, and constant repetition of the same events create a mobbing environment (Yılmaz, Kaymaz, 2014).

One of the factors that create an environment for mobbing is workplace culture. Culture is a concept that has broad meanings, and it is a way of transferring thoughts, feelings and behaviors to future generations. Cultural transfer is a dynamic process. Security is a frequently used concept in all areas of daily life and is a part of culture. Maslow's need theory hierarchy includes the need for security. Following the basic needs, it is a natural behavior for the individual to want to secure himself. A culture must be created to ensure a safe environment in a business (Ültanır, 2003).

Psychosocial factors can also cause work accidents. Safety culture gains importance in preventing work accidents and ensuring safe working. The goals of safety culture can be summarized as follows (Uslu, 2014). To ensure safety in important matters, to ensure the safety commitment of employees through interest and participation, to establish behavioral norms by sharing opinions about risks, accidents and diseases (Uslu, 2014).

Flexible working hours, vacations, policies to ensure balance between work and home world are important for establishing a safety culture in organizations. In addition, communication, management organizations, information sharing are important to solve problems and increase efficiency (Hofstede, 2011).

It is stated that education is one of the important factors in the establishment of organizational culture. Employees' behaviors, knowledge, skills and abilities affect the development process. It is important to raise awareness with education in order to minimize psychosocial risk factors and provide a healthy work environment. The purpose of a good safety culture is to protect employees and prevent unsafe behaviors (Soft, 2008).

There are some reasons that affect the health of employees in workplaces and create psychosocially problems and the reasons of these factors have been examined under five categories separately (Çöğenli, 2019).

- Non-Institutional Workplaces
- Late Payment of Fees
- Long working hours
- Education level
- Management Issues

When the causes and consequences of the psychosocial dangers and risks that employees are exposed to are analyzed, it is seen that the responses of each employee to the problems, resistance and coping methods differ. While some of the employees overcome this process easily, it is observed that the duration of mobbing and the severity of damage increase especially with the decrease in the level of education.

Mobbing increases health expenses, absenteeism, accidents, mistakes, complaints, lawsuits, compensation expenses, results in decreased performance and efficiency.

In the process of psychological harassment, factors such as bad management and corporate culture are also effective in addition to individual factors. (Karatuna and Tınaz, 2010)

Employees experience discomfort when they cannot balance the increased burden of their work with their personal lives. According to the findings of the Fifth European Working Conditions Research (EWCS) conducted in 2010 18% of the employees state that they are not satisfied with the work-life balance.

3. Improved Measures Against Psychosocial Risk in Turkey

According to the Occupational Health and Safety Law enacted in 2012, employers are obliged to ensure the health and safety of their employees. These obligations are preventing risks, training and informing the employees, making the necessary organization, adapting health and safety measures according to changing conditions. The employer is responsible for the current situation and supervision (article 4). The employer is obliged to take precautions regard the design of work equipment and workplaces, the choice of working style and production methods. In case of irregular negativities the employer must take necessary technical and administrative measures (Article 5). According to the 18th article, the employer is obliged to educate the employees on occupational safety and obtain their opinions.

With the Alo-170 line, which was put into service in 2010, psychologists record the injustices of employees. These complaints are then forwarded to the government agencies in charge. This service received 55,046 applications between 2011 and 2017.

The Prime Ministry Circular on the prevention of mobbing in workplaces was published in 2011

The “Committee for Combating Psychological Harassment” was established within the Ministry of Labor and Social Security with the participation of NGOs and related parties in 2012. This is in Turkey’s Human Rights Council is established, the State Department and the staff are union representatives. The Board meets regularly twice a year. The Board is responsible for determining policies, training and informing activities, preparing guiding documents and raising awareness throughout the country.

Information guide on Mobbing in 2013 and Psychological Harassment in 2017 were published.

In a comprehensive study on psychological harassment in the health sector (Karatuna & Tinaz, 2010 p. 132), it was determined that there were factors such as bad management and corporate culture in addition to individual factors in the process of psychological harassment. Some solution suggestions were determined in the same research. 1-Getting information about psychological harassment from a third person, namely an expert (Expert / Judge). 2-The consultant person must be from within the institution, otherwise the victim suffers greater harm. (Karatuna ve Tinaz, 2010)

Research shows that a positive workplace safety culture reduces the impact and frequency of psychological harassment and violence in the workplace. Therefore, the purpose of prevention initiatives is to create a

culture that decreases psychological abuse and violence. Therefore, the first step in understanding this type of culture is to agenda psychosocial risks in company. It is important to develop workplace management that includes practices that promote a culture of mutual respect.

On the other hand, it is also important to consider whether the discomfort occurring in the employee due to psychological harassment in the workplace can be counted as an occupational disease within the scope of the Social Insurance and General Health Insurance Law No. 5510.

Occupational disease concept is not defined in the Labor Law numbered 4857. Occupational Disease is defined in Article 14 of the Social Insurance Law No. 5510. Occupational disease is defined as a temporary or permanent illness, physical or mental disability, which the insured suffers due to a recurring reason or the conditions of the work execution. However, diseases caused by psychological harassment are not included in the list of occupational diseases in the annex of Law No. 5510. Likewise, the psychosocial dimension is not regulated in the Occupational Safety Law No. 6331.

Occupational Diseases are divided into five groups as A, B, C, D and E according to the 18th article of the Regulation on Determination of Profession Earnings and Profession Gaining Rates. Diseases that fall under the scope of psychosocial health such as mobbing are not included in this classification. However, psychosocial diseases; It is listed under the title 2.4 in the ILO 2010 Occupational Diseases List. (2.4. Mental and Behavioral Disorders) The European Union directive no. 89/131, issued in 1989, includes legal regulations and risk analysis for the prevention of psychosocial risks.

Group A: Occupational diseases with chemical substances

Group B: Occupational skin diseases

Group C: Pneumoconiosis and other occupational respiratory system diseases

Group D: Profession infectious diseases

Group E: Occupational diseases due to physical factors

According to the decisions of the Supreme Court in the Turkish legal system, for a disease to be an occupational disease, there must be a causal link between the disease and the work done. Therefore, it is possible that mental illnesses caused by psychological abuse in the employee are occupational diseases.

4. Assessment of Psycho-social Risk Factors with the Risk Assessment Model

As it is known, Ombudsman means representative or deputy. The classical ombudsman handles and investigates complaints about public policies. The ombudsman has the authority to investigate and make recommendations for appropriate compensation or policy change (Met, 2016).

Today, companies have ombudsman units. Most of the S&P 500 companies have ombudsman units as well as ethics and social compliance units. These units conduct research and prepare reports to prevent bad and negative behavior within the organization (Singer, 2010).

Organizational ombudsman can be defined as a person or unit that has been appointed impartially within an organization and assists the organization members in resolving their conflicts and problem solving processes. (www.ombudsassociation.org, 2012) According to another definition, the organizational ombudsman is an independent and impartial institution within the company or an institution where employees can talk about their problems or complaints in private without keeping an official record. (Holmes, 2012)

The organizational ombudsman can be applied in state institutions, universities, companies, non-profit non-governmental organizations.

The organizational ombudsman function has changed due to developments in demographic, technological and globalization. (Singer, 2010) Although mobbing can be solved within the scope of the Ombudsman Model, the subject of this article is to analyze Mobbing with the risk assessment model.

According to the 3rd article of the Occupational Health and Safety Law, risk assessment is the determination of the dangers that exist in the workplace or that may come from outside. Risk assessment includes the studies required to be done in order to analyze and grade the risks arising from hazards and to decide on control measures. According to Article 4 of the Law, the employer has to have a Risk assessment done. When making a risk assessment, the employer takes the opinions of the employees according to the 18th article of the law and informs the employees according to the 6th article. If the risk assessment is not made in mining, metal, construction works and works with hazardous chemicals, the work is stopped according to Article 25 of the Law and administrative fines are imposed according to Article 26.

According to the Article 12 of the Risk Assessment Regulation, the risk assessment is renewed at the latest every two, four and six years

respectively in very dangerous, dangerous and less dangerous workplaces.

According to the 22nd article of the Occupational Safety Law, the employer has to establish an occupational safety board if he has 50 or more employees. One of the important duties of the board is to make a risk assessment. Psychosocial risks are an area of occupational health and safety that is less well known to other risk groups. Increasing workload, working hours and pace of work cause many negative effects on employees. These negative effects lead to some undesirable consequences such as low organizational commitment and absenteeism. The Occupational Safety Law requires risk assessment, even if there is one employee.

There are many qualitative and quantitative risk assessment methods. Preliminary Hazard Analysis, Primary Risk Analysis, Security Function Analysis, Risk Map, Occupational Safety Audit, Occupational Safety Analysis, Process / System Checklists, Process Review Technique, Relative Ranking-Dow and Mond Index Analysis, Risk Analysis, What If Happens? Analysis, Hazard and Operability Analysis, Error Types, Effects and Criticality Analysis, Error Tree Analysis, Event Tree Analysis, Cause - Result Analysis, Human Error Analysis, Human Error Identification, Human Reliability Assessment, Human Error Rate Estimation Technique, Hierarchical Task Analysis, Management View and Risk Tree Analysis, Energy Analysis, Safety Barrier Diagrams, Kinney Model, Zurich Hazard Analysis, Machine Risk Assessment, Hazard Early Warning Model, Deviation from Averages Technique, Weighted Average Deviation Technique and Risk Assessment Table are some of these methods. (Ceylan et al., 2011)

Although there are many qualitative and quantitative risk assessment methods, documents and guidelines on psychosocial risk assessment are quite limited (Vatansever, 2014).

5. Results and Recommendations

Psychosocial hazards and exposure risks have social consequences. Negative experiences and the number of workplace doctors affect both social and family life of individuals. It is important to educate employees about psychosocial hazards and risks.

At this stage, Security culture gains importance. Although all precautions are taken, it is not possible to completely prevent psychosocial risks, especially mobbing. Because there will always be factors that trigger mobbing such as competition, unemployment, greed and jealousy. Therefore, the early prevention system that will detect and reduce the risk of mobbing gains importance.

In our model, when we consider the Occupational Safety Board as an Organizational Ombudsman and the Chairman of the Board as the Chief Auditor; Especially prevention of mobbing caused by psychosocial risk factors will be easier and more effective.

Occupational Safety legislation is based on a self-management model rather than a rule maker. Therefore, the risk assessment model including ombudsman will be effective in developing and maintaining workplace culture (Gülnur, 2012)

Occupational Safety Law, Risk Assessment Regulation, Occupational Safety Boards Regulation, Penal Code and Labor Law provisions contain regulations that will enable the model to work more efficiently.

There are difficulties in determining psycho-social risk factors, especially mobbing. It is considered more appropriate to use risk assessment methods including linguistic elements in the detection of psychosocial risk factors.

Risk assessment methods such as Fuzzy Delphi Method (FDM) and Fuzzy Interpretive Structural Modeling (FISM) seem to be appropriate.

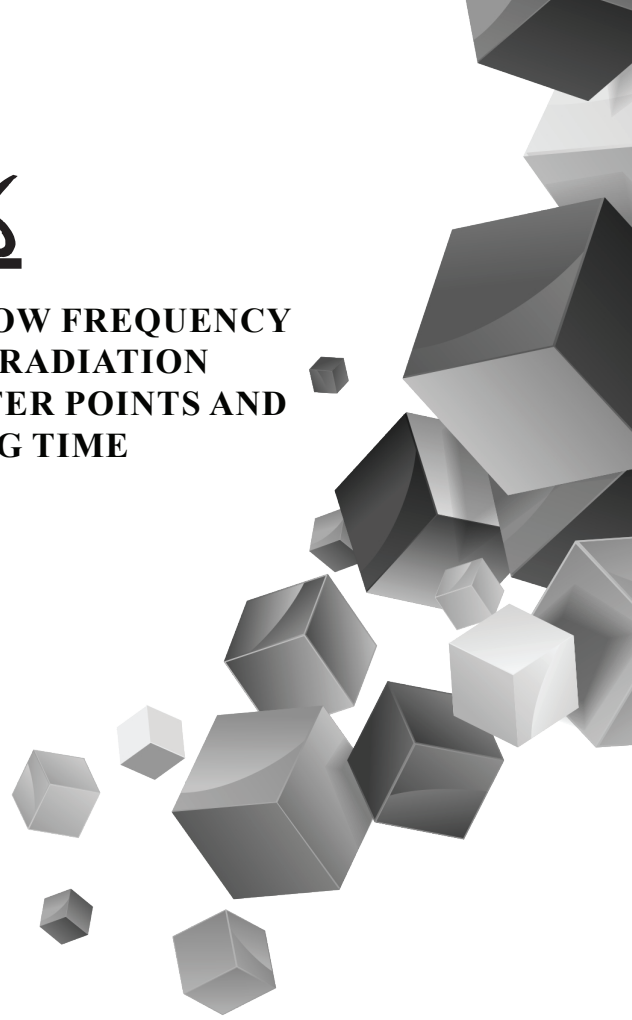
REFERENCES

- Nivarthi S., Quazi A. Saleh, A.(2013), Corporate Social Responsibility Ombudsman: A Proactive Perspective, Proceedings of 9th Asian Business Research Conference 20-21 December, , BIAM Foundation, Dhak
- Kirsten A Way, (2012) Psychosocial Hazards: Bullying, Aggression and Violence, Safety Institute of Australia Ltd, Tullamarine, Victoria, Australia
- EUROFOUND (2010) European Foundation for the Improvement of Living and Working Conditions, 5th European Working Conditions Survey
- Goetz K, Berger, S., Gavartina, A., Zarotil S., Szecsenyi J., (2015) How psychosocial factors affect well-being of practice assistants at work in general medical care? – a questionnaire survey, BMC Family Practice (2015) 16:166 2-7
- EU-OSHA (2007), European Agency for Safety and Health at Work, Expert forecast on emerging psychosocial risks related to occupational health and safety, Office for Official Publications of the European Communities
- Richards, J. (2003). Management Of Workplace Violence Victims. ILO/ICN/WHO/PSI Joint Programme on Workplace Violence in the Health Sector, 20-22
- AISGA. (2007). Psychosocial Risks in Occupational Health and Safety. ISG Bulletin. 74/TR, 1681.
- Vatansever, Ç. (2014). A New Dimension in Risk Assessment: Psychosocial Hazards and Risks. *Work and Society*, 117-138.
- Judge, T. A., Bono, J. E. and Locke, E. A. (2000), ‘Personality and job satisfaction: the mediating role of job characteristics’, *Journal of Applied Psychology*, 85, 237–249.
- Lee, R. T. and Ashforth, B. E. (1996), ‘A meta-analytic examination of the correlates of the three dimensions of job burnout’, *Journal of Applied Psychology*, 81, 123–133.
- Pearson, C. A. L. (1992), ‘Autonomous workgroups: an evaluation at an industrial site’, *Human Relations*, 45, 905–936
- Parker, S. K., Griffin, M. A., Sprigg, C. A. and Wall, T. D. (2002), ‘Effect of temporary contracts on perceived work characteristics and job strain: a longitudinal study’, *Personnel Psychology*, 55, 689–719.
- EU-OSHA, 2012, Leka et al., 2004, Leka, S., Griffiths, A. and Cox, T. (2004), *Work organisation and stress — Systematic problem approaches for employers, managers and trade union representatives*, World Health Organisation, Geneva
- Hülya Gül (2009) An Important Psychosocial Risk in Occupational Health: Mobbing

- ÇSGB. (2013). Psychological Abuse at Workplaces (Mobbing), Information Guide, 10.
- Ankara: Ministry of Labor and Social Security, General Directorate of Labor.
- Yılmaz, H., Kaymaz, A. (2014). A Risk Factor: Mobbing (Psychological Abuse in the Workplace). Public Internal Auditors Association (KIDDER), 75.
- Ültanır, G. (2003). The Relationship Between Education and Culture-The Anxiety of Which Dimensions of Culture in Education to Transfer to Young Generations. Gazi University, Gazi Education Faculty Journal, 23(3), 291-309.
- Uslu, V. (2014). The Relationship Between Occupational Safety Performance and Occupational Safety Culture in Enterprises: A Research in Eskişehir Metal Industry. Eskişehir Osmangazi University, 38- 39.
- Hofstede, G. (2011). Dimensionalizing cultures: the hofstede model in context. International Association for Cross – Cultural Psychology, 21-22.
- Soft, S. (2008). A Field Study on Investigation of Factors Affecting Employee Efficiency.
- Süleyman Demirel University Journal of Economics and Administrative Sciences, 13, 241-247. Çögenli Mehmed Zahid Journal of Business Studies Journal of Business Research-Turk 2019, 11(3), 1911-1926
- Karatuna, I., Tınaz P.(2010), Psychological Harassment in the Workplace: A cross-Sectional Healthcare Industry Research, Türk-İş, Ankara
- Met, Ö . (2016). A PROACTIVE TO PSYCHOSOCIAL RISKS IN WORKING LIFE APPROACH: ORGANIZATIONAL OMBUDSMANLIK MODEL
- Dumlupınar University Journal of Social Sciences, (49), 95-114. Received
- Singer, Andrew (2010) On The Evolving Corporate Ombudsman, ETHİKOS March/april, vol.23 No.5 s.10-13
- Merediith, Holmes, (2012) Creating A Better workplace, SWE Winter
- Hüseyin Ceylan, Volkan S. Başhelvacı International Journal of Engineering Research and Development, Vol.3, No.2, June 2011).
- Çiğdem Vatansever (2014) Calisma ve Toplum . 2014, Vol. 40 Issue 1, p117-138. 22p.).Erdoğan Gülnur, Legal Evaluation of Mobbing Behaviors in the Workplace, 2012

Chapter 26

MEASUREMENT OF LOW FREQUENCY ELECTROMAGNETIC RADIATION LEVELS AT MUŞ CENTER POINTS AND PREDICTION BY USING TIME SERIES MODELS*



*Zeydin PALA¹
İbrahim Halil ÜNLÜK²
Çağrı ŞAHİN³*

1 * This study was produced from the project numbered BAP-18-MMF-4901-01, whose results were accepted and supported by the Muş Alparslan University BAP unit.

Muş Alparslan University, Faculty of Architecture and Engineering, Department of Computer Engineering, Mus, Turkey, z.pala@alparslan.edu.tr

2 Department of Computer Programming, University of Mus Alparslan, Mus, Turkey, ih.unluk@alparslan.edu.tr

3 Muş Alparslan University Faculty of Architecture and Engineering, Department of Computer Engineering, Mus, Turkey, c.sahin@alparslan.edu.tr

1. Introduction

Electromagnetic radiation (EMR) is the type of energy around us that can take many forms, such as radio waves, microwaves, X-rays, and gamma rays. Sunlight is also a form of EMR energy. Visible light is only a small part of the EMR spectrum and includes a wide range of electromagnetic wavelengths.

Throughout the 20th century, the initially poor EMR engulfed us, man-made, an unforeseen byproduct of modern electricity. EMR flies and is invisible to humans at the speed of light. Typically it is structured based on frequency and wavelength. The frequency of EMR corresponds to the Hertz (Hz) number of cycles per second. The physical size of the wave refers to the wavelength and the wavelength is inversely proportional to the frequency. The longest wavelength is extremely low frequency (ELF), and high frequencies (HF) have a shorter wavelength, such as radio frequencies (RF) or microwaves.

Alternating current (AC) fields, direct current (DC) fields, magnetic fields, electrical fields, RF waves/microwaves, ionizing and non-ionizing radiation are composed of electromagnetic radiation. AC refers to an alternating current that continuously changes polarity, generating a repulsive force effect, from positive to negative. DC refers to a continuous field or constant power, which is a direct current. Ionizing radiation is made up of particles that have enough energy individually or may release sufficient energy to expel an electron from an atom or molecule.

The concern of people being exposed to electromagnetic radiation and its negative effects has been going on for over thirty five years. We are faced with insidious enemies that are invisible but have negative effects on living things. We live with electromagnetic fields of different frequencies in almost every point we breathe, especially in environments where all electrical devices are in operation. Therefore, depending on the work done, it is exposed to the effects of these areas. When radiation is defined broadly, it is seen that electromagnetic waves cover the entire spectrum. Over the past century, the research community has gained a great deal of information on radiation physics and the effects of radiation on humans, animals and plants (Habbash, 2008). Since then there has been continuous discussion of the impact of electromagnetic radiation on humans, animals and the environment.

Animal experiments, studies on cells, clinical studies, computer simulations, and epidemiological studies so far provide valuable information about the effects of electric and magnetic fields on human health (Çal, 2016). Especially in children, the rate of exposure to extremely low frequency electromagnetic fields is higher, and the research conducted

on children with leukemia in 27 member countries in the European Union clearly shows this (Grellier et al., 2014). The heating effects produced by Radio Frequency (RF) radiation scanning are a source of biological damage. The authors suggested that children who are exposed to magnetic fields of greater strength have a higher chance of developing leukemia than children who are not exposed (Redlarski et al., 2015). In another study, it is stated that electromagnetic waves can increase the level of estrogen in women, and testosterone hormone in men (İspirli et al., 2015: 1).

The number of users using communication systems increases day by day with the advancement of technology, and the electromagnetic radiation generated by the expansion of the systems' capabilities increases accordingly. Unfortunately, the important cell phones and base stations to which they are connected are the largest source of this contamination (Pala et al., 2015).

Many studies have been conducted in city centers (Güler et al., 2010; Özgümüş et al., 2010; Karadağ et al., 2014; Polat, 2013; Uygunol, 2009; Cansız, 2010; Sorgucu et al., 2011; Şahin et al., 2013) university campuses (Düzgün, 2009; Kunter, 2015; Mousa, 2009; Olubosede, 2012; Nassiri et al., 2012; Güneşer et al., 2007; Ema, 2020; Sarıkahya, 2014; Etem et al., 2016; Çeçen et al., 2016) and metropolises (Usikalu et al., 2012) to measure and evaluate the intensity of electric and magnetic fields, and important results have been presented. Narda brand SRM 3000 model measuring device was used in high-frequency electric field measurements made in close proximity of 33042 base stations in various parts of our country in 2010 and values close to the limit values determined by the Information Technologies Authority (BTK) were obtained (Cansız et al., 2014).

Some studies have been carried out to investigate the effects of radiation emitted by base stations according to the type of installation (Seyfi, 2015). On the other hand, the health effects of very low frequency radiation (such as 3-3000 Hz) have been studied and studies have shown that in those living near to high voltage lines, the health risk is higher (Tükkan and Pala, 2009; Kulkarni and Gandhare, 2012). Significant research, both domestically and abroad, have also been carried out, showing that electromagnetic fields released from base stations and wireless devices have a significant impact on the environment and living things (Sivani and Sudarsanam, 2012; Mollaoğlu and Özgüner, 2006; Bold et al., 2003; Verkasalo, 1996). In a doctoral dissertation study conducted by Ankara University, the effects of electromagnetic radiation on hospital staff in a hospital were investigated and significant results were obtained (İlhan 2008). All of these studies point out that electromagnetic radiation should be measured periodically, otherwise we will face unavoidable consequences.

The aim of this project is to determine low frequency based radiation sources by measuring electromagnetic pollution values with scientific methods in certain points of Muş province and to contribute to the literature in this field.

In this project, low frequency electromagnetic radiation values, in other words electric field measurements of 11 different points under the control of VEDAŞ firm located in the central points of Muş were made periodically. Periodic measurements were made over 12 months and four times a month and were evaluated by taking the monthly average of the measurements. A 12-month time series was created for the measurements of the 11th point in Yeşilce District and future predictions were made with the help of time series functions of the R programming and modeling environment. This study, which is the first in this field, was supported by the Scientific Research Projects Unit (BAP) of the Rectorate of Muş Alparslan University with the project coded BAP-18-MMF-4901-01.

Within the framework of the project, it is aimed to achieve the following results by comparing the low frequency electromagnetic radiation measurements obtained in different parts of Muş province with different regions:

1. Investigation of low frequency EMR effects emitted by energy cabins located in the most fundamental points of Muş province.
2. Investigation of low frequency EMR effects released due to high voltage lines passing through certain parts of the city.
3. Modeling the exposure with the support of artificial intelligence algorithms (Stuart, 2010) and estimating with the help of time series at points where energy cabinets are located in the city

2. Exposure Standards

The International Commission for Non-ionizing Radiation Protection (ICNIRP) and the Institute of Electrical and Electronics Engineers/American National Standards Institute (IEEE/ANSI) have set limit values as a precaution (ICNIRP, 1998; ICNIRP, 2009).

According to the national public exposure limits defined cities in Turkey 50 Hz electric fields in the network frequency limit value of 5000 V/m and magnetic field of public exposure and the intensity of 80 A/m respectively. Table I shows all limit values in low frequencies. These limit values were taken into consideration while making measurements.

Table I: Public exposure limit values in the 1 Hz-300 GHz frequency band determined by ICNIRP (ICNIRP, 2009; webarchive, 2020)

Frequency range	Electric field strength (V / m)	Magnetic field strength (A / m)
1 Hz' e kadar	-	3.2 x 104
1-8 Hz	10000	3.2 x 104/f
8-25 Hz	10000	4000/f
25 Hz - 3 kHz	250/f	5
3-150 kHz	87	5
0.15-1 MHz	87	0.73/f
1-10 MHz	87/f0.5	0.73/f
10-400 MHz	28	0.073
400-2000 MHz	1.375/f0.5	0.0037/f0.5
2-300 GHz	61	0.16

According to the limit values given in Table I, measurements are made with devices that have the properties specified in the calibrated regulation and express the limit values for a single device. The safety distance to be taken into account when making measurements; It is calculated by the formula given in equation (1), determined by the International Radiation Protection Board (IRPA), considering the antenna's broadcast direction and from the antenna (REGA, 2015).

$$d = \frac{\sqrt{30 \cdot P \cdot 10^{\frac{G}{10}}}}{E} \quad (\text{meter}) \quad (1)$$

In this formula;

d: Safety distance (meters),

P: Device output power (Watt),

G: Antenna gain (dBi),

E: It refers to the limit value of the electric field (Volt / meter).

3. Material and Method

3.1 Data Collection Studies

The SMP2 measuring device of the Wavecontrol company shown in Figure 1 was used in field measurements. This device fully meets the standards set by our country and many world countries. This device also complies with the measurement instrument standards determined by BTK and its calibration was performed in accordance with all standards by the manufacturer in the previous project period.



Figure 1: Wavecontrol SMP2 EMR device used in measurements

Depending on the probe used the SMP2 system will calculate values such as electric field, magnetic field, and electromagnetic power density in the range of 0 Hz-18 GHz. At frequencies up to 400 kHz, it can perform spectrum analysis. It can record the positions where the measurements are made automatically thanks to the integrated GPS system. It stores in its memory a large number of measurements and allows the measurement values to be passed to the computing world.

The same company's WP400 probe, shown in Figure 2, is the probe used in the measurements. This probe can be used to calculate values in the range of 1 Hz - 400 kHz, such as electric field, magnetic field, electromagnetic power density.



Figure 2: Wavecontrol WP400 low frequency probe

With the help of the above-mentioned measuring device and probe;

1- The electric field values emitted by the devices inside the panels and right next to the electrical panels at 10 different points in certain points of Muş province were measured as V / m. Measurements continued for 12 months. In a month, four measurements were taken for each point, and the average value for that point was obtained by taking the average of the measurements in a month. The Google Earth view of the points in the city where the measurements were made are given in Figure 3, the addresses of the measurement points in the city and the latitude / longitude information in Table II, and the field study image of one of the measurements is given in Figure 4.

2- Daily/weekly periodic measurements of the high voltage power line passing through Yeşilce district were made. Measurements continued for 12 months. By taking the average of the measurements taken four times a month, monthly data and the monthly values obtained during the 12-month period were combined to create a 12-month time series.

3.2 Measurements made at measurement Points

The EMR measurements of the transformer cabinets of the VEDAŞ Company, which provides electricity service to the city center and the city of Muş, were made not at a single point, but by visiting every point of the transformer cabin. Each measurement was carried out in a 6-minute time frame. Thus, it was evaluated whether the EMR values released from the cabins would have negative effects on human health by taking the average of the values obtained. The measurements were made at a height of 1 meter from the ground. Four times a month measurements were made for each transformer cabinet in the city center. The monthly EMR value was calculated by taking the average of the monthly values obtained for each point.



Figure 3: Google Earth view of the measurement points in the city center

Table II: Address, latitude / longitude information of the points in the city where measurements were made

Cabin number	Point Latitude and Longitude Information	
1	38,744772	41,497662
2	38,742731	41,496799
3	38,735669	41,492544
4	38,738203	41,488018
5	38,734914	41,484653

6	38,732666	41,488872
7	38,733964	41,489593
8	38,73643	41,496906
9	38,740606	41,501118
10	38,74343	41,513453



Figure 4: A view from the field study where the measurements were made (Yeşilce neighborhood under the high voltage power line)

The 12-month measurement averages of 10 points in the city, which are measured periodically, are graphically given in Figure 5. The highest EMR value measured during the project period was measured at M_5 and in December 2018 as $EM_5 = 20.14$ [V/m]. The most obvious reason for

the high EMR value obtained here compared to other points is that the partially collapsed cabin energy line is a little closer to the surface. The second highest value was measured at M8 point in March 2019 as $EM_8 = 9.00$ [V/m]. At this point, a higher value was obtained compared to other cabinets due to the measurement under the energy pole. The measured EMR value at other cabin points in the city remained at the level of $E_{other} \leq 2.00$ [V/m]. It has been determined that the average values measured at the transformer points, low frequency electromagnetic radiation (EMR) intensity is lower than national and international limits.

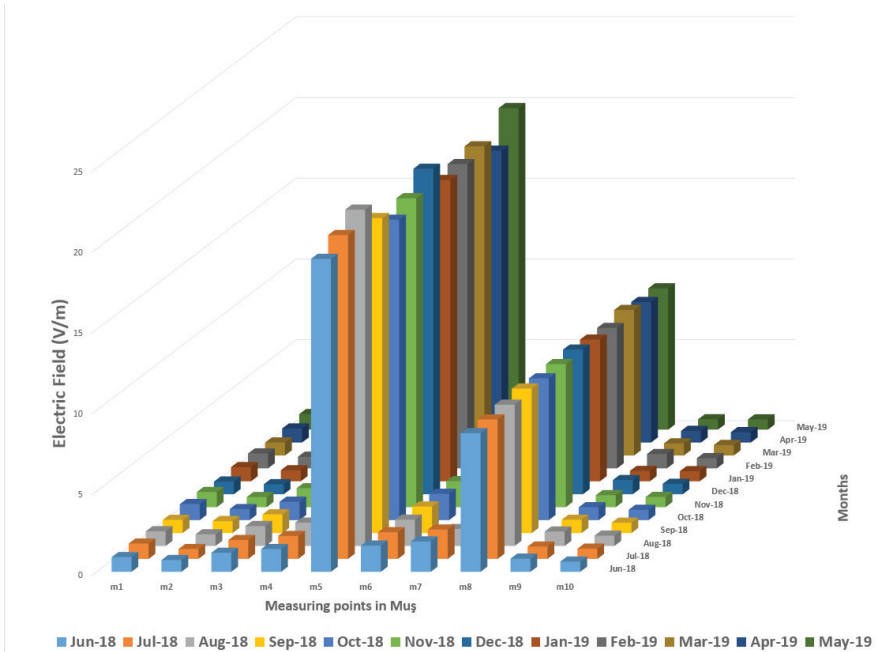


Figure 5: Monthly average EMR values measured in VEDAŞ cabinets

In the Yeşilce district, EMR values measured under the 30 kW power line and 2.5 m above the ground were in the band of 4010 V/m and 4700 V/m. The highest average value measured for 12 months at the high voltage point was 4809 V/m in March 2019 and the lowest average value was measured as 4010 V/m in May 2019. In this case, since the radiation at the high voltage point is below 5000 V/m, it does not pose a risk yet, but repeating the measurements from time to time is of great importance in terms of health.

4. Modeling Electromagnetic Radiation Values with Time Series

Artificial intelligence, or machine intelligence, is a field of study that aims to give cognitive powers to program computers to learn and solve problems. The purpose of artificial intelligence is to induce computers to think in a way similar to human intelligence. Artificial intelligence cannot completely mimic human intelligence, so computers can only be programmed to do certain aspects of the human brain.

Machine learning is a branch of artificial intelligence that helps computers program themselves based on input data. Machine learning offers data-based problem-solving capability compared to artificial intelligence. Artificial neural networks (ANN) are an example of machine learning algorithms.

Time series prediction is an important area of machine learning. This is important because there are too many estimation problems involving the time component (Ciaburro, 2017).

While creating the linear regression model, it is accepted that the errors are independent from each other. However, the situation is different in time series and it is accepted that the errors affect each other. To put it more clearly, the error terms are related to the previous one depending on the time. Time series are sequential measurements of the same variable over time (Brockwell and davis, 2016). The measurements that make up the time series can consist of different time periods. For example, these zones can range from small time units to large time units. Besides time zones such as seconds, minutes, hours; There are also daily, weekly, monthly and annual time frames. If we have a variable named y , which is expressed as a time series and consists of the annual air temperature values of a region, we can express the values measured in the time interval t as y_t . An automatic regression model emerges when each y_t value in the time series is subjected to regression in the same time series depending on previous values such as y_{t-1} . He can express such a model mathematically as follows:

$$y_t = \beta_0 + \beta_1 y_{t-1} + \epsilon_t \quad (2)$$

Where;

y_t independent variable,

y_{t-1} dependent variable expressing the previous year,

β_0 intersection value,

β_1 slope,

ϵ_t indicates the error term.

In such a model; a response variable belonging to the previous time frame becomes the input (predictor) variable for the next step this time. Errors have our usual assumptions about errors in the simple linear regression model.

4.1 Analysis of EMR Time Series in R Environment

The 12-month time series obtained at the end of the 12-month measurement within the scope of the project is given in Figure 6.

There was a partial decrease for the month after June 2018, when the measurements started on the time series, a slight increase in the next month, a decrease between August and September and an increase from October 2018. Although the ongoing increase decreased partially in February 2019, it peaked in March 2019. A decrease was observed in the April-May interval during which the measurements were carried out. In general, it has been observed that the EMR value released to the environment is higher because more electricity is consumed in winter than in summer.

ETS, TBATS and HoltWinters prediction models in forecast hybrid and forecast libraries are used to model time series in R environment. The ggplot2 library was also used for drawing graphics. However, the fact that the time series is very short and consists of only 12 data has emerged as a constraint, and algorithms that require more data for efficient operation could not be used.

The first 9 months of the EMR time series obtained at the end of the measurement were reserved for training processes, and the remaining 3 months for testing.

Various statistical measures, including Mean Absolute Percent Error (MAPE), root mean square error (RMSE), and mean absolute error (MAE), were calculated to examine the performance of the models using time series numerical values (Namin and Namin, 2018). MAPE represents the percentage of mean absolute error. The error is obtained by subtracting the predicted value from the actual or observed value. Equations for MAPE and RMSE and MAE metrics are given in Equations 3, 4 and 5, respectively.

$$MAPE = \frac{1}{T} \sum_{t=1}^T \left| \frac{\epsilon_t}{y_t} \right| \times 100 \quad (3)$$

$$RMSE = \sqrt{\frac{1}{T} \sum_{t=1}^T (\epsilon_{t+h})^2} \quad (4)$$

$$MAE = \frac{1}{T} \sum_{t=1}^T |e_{t+h}| \tag{5}$$

The t , T , e_t , y_t and h given in the equations show time, number of observations, prediction error, actual value and future forecast horizon, respectively.

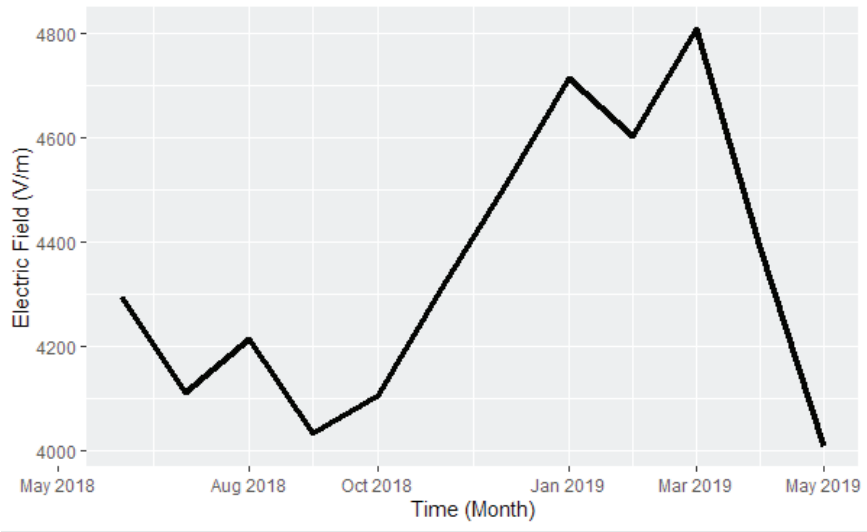


Figure 6: 12-month EMR time series

First Prediction Approach:

RMSE, MAE and MAPE metric values of EMR time series for ETS and TBATS models are given in Table III.

Table 3: Metric values of ETS and TBATS models

Model Name	RMSE	MAE	MAPE
ETS	382.21	337.00	7.96
TBATS	291.61	258.72	6.12

In this case, it is possible to say that the TBATS model makes less error in the prediction process with a value of 1.84% compared to the MAPE value. Figure 7 shows the estimation graphics. Clear lines in the forecast charts show the estimate, Dark colors show an 80% estimate, and light areas show a 95% estimate.

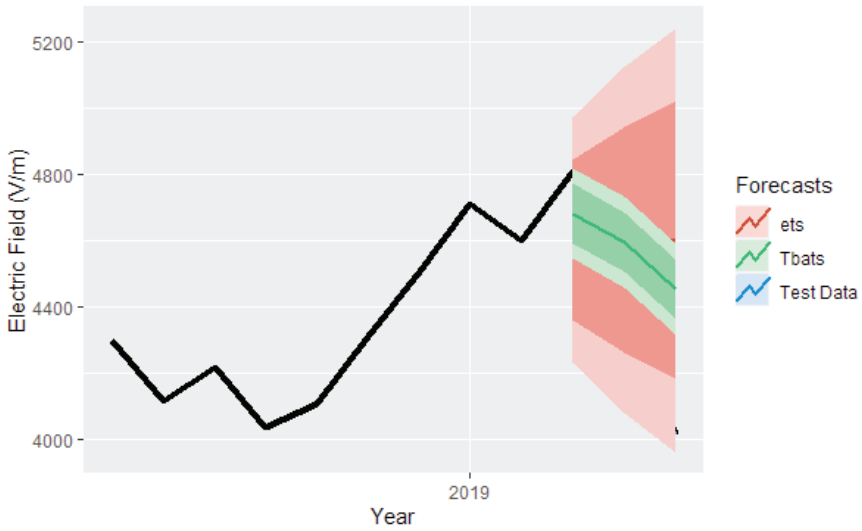


Figure 7: ETS and TBATS quarterly forecast charts

Second Prediction Approach:

In the second approach, the prediction process was made by using more than one model with the HybridModel library of the R programming environment. In the prediction process of the hybrid model in which ETS and TBATS models are used together, the RMSE, MAE and MAPE metrics have values of 102.71, 90.08 and 2.06, respectively. This shows that the result is more successful if the algorithms are used jointly rather than one by one. Figure 8 was produced for the results of the quarterly estimates and Figure 9 for the 12-month forecast results.

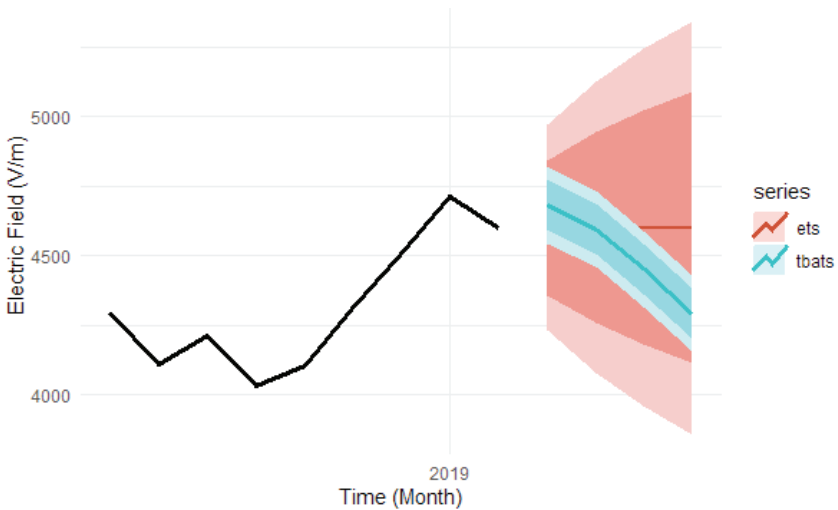


Figure 8: Collaborative prediction graph with Hybrid Model

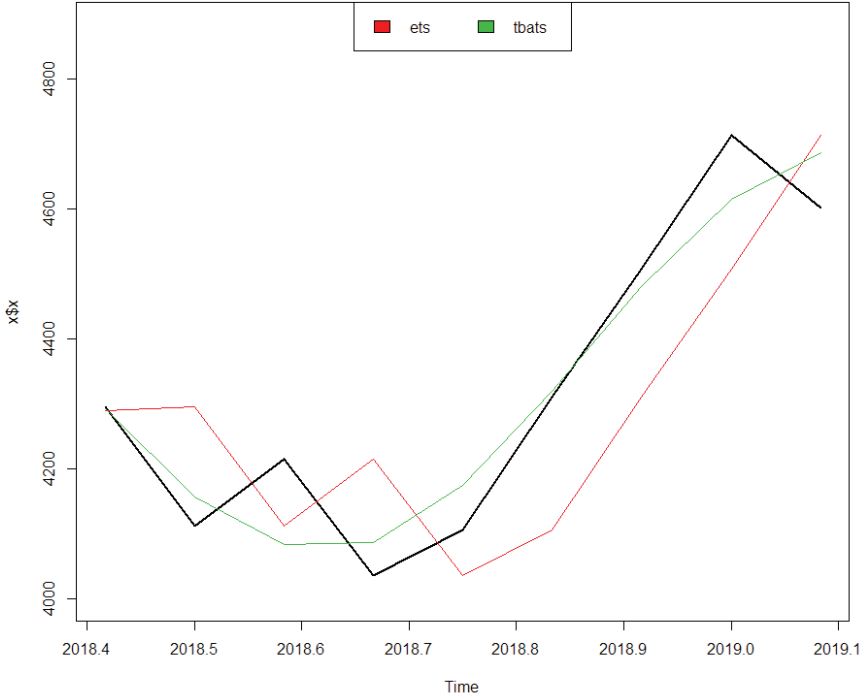


Figure 9: 12-month forecast graph with HybridModel

Third Predictive Approach:

It is possible to use HoltWinters, a simple exponential smoothing prediction model, to make predictions using simple exponential smoothing in the R environment. To use the HoltWinters () property for simple exponential smoothing, it is necessary to set the beta = FALSE and gamma = FALSE parameters in the HoltWinters () function. The 12-month forecast graph of the EMR time series using the HoltWinters model is given in Figure 10. It can be said that the logarithmic estimation is better than the normal estimate according to the SSE metric.



Figure 10: Modeling plot with HoltWinters (left: Normal forecast, right: logarithmic forecast)

5. Conclusion

1. In this study, the electromagnetic radiation values emitted by the low frequency VEDAŞ energy cabinets were obtained from the measurements made with the Wavecontrol SMP2 EMR device at 10 different points in the city center of Muş. The effects of the obtained values on human health and the environment were evaluated.

2. In addition, a 12-month time series was created based on the periodic measurement results of the 30 kW high voltage power line passing through the Yeşilce district. Future predictions of EMR values were made with the help of R programming libraries and prediction models using the created time series.

3. The following conclusions have been reached for the electromagnetic radiation values measured in the city:

4. When the average of all the measurements made around the energy cabinets in the city, the value reached is 3.68 V/m. The partial demolition of the electrical cabinet located at the top of the Tuba Mosque in the city caused a higher EMR value. At this point, the largest and smallest values measured are $E_{\max} = 20.81$ [V/m] and $E_{\min} = 18.06$ [V/m], respectively. The measured values in the city, the exposure limits defined for Turkey remains far below. Therefore, EMR values emitted by cabins in the city do not yet pose a danger to living things and the environment.

5. In the measurements made in Yeşilce neighborhood where the high voltage power line passes, the average highest value was measured as 4809 V/m in March 19 and the lowest value as 4010 V/m in May 19. The measured average values are well below international standards.

These values are based on nationally defined limit at 50 Hz for electrical equipment in Turkey 5000 V/m electric field does not exceed the limit, but was found to be 80% and 96%, respectively.

6. In general, it has been determined that electromagnetic pollution increases more in winter months when electrical devices are used intensively.

7. In the study, a value above the national and international limit values was not measured at any point in the city center of Muş. It is of great importance to regularly measure electromagnetic fields, especially at risk points. In this project, low frequency electromagnetic radiation values were studied. It was found that these values changed over time. It is probable that it will be useful to examine changes in electromagnetic pollution with regular measurements in order to identify possible risk factors in advance.

8. It has been observed that the TBATS prediction model is more successful in the estimation process using time series, which are accepted as a sub-branch of Machine Learning. It is a constraint that the time series consists of only 12 values per month, and many deep learning and other statistical algorithms in the R environment could not be used due to the lack of data in the prediction process. However, the estimation process was successfully performed with 6% error with three different approaches used in the study.

Acknowledge

This study was funded by the Scientific Research Projects Unit of Muş Alparslan University, with project code BAP-18-MMF-4901-01.

6. References

- Bold A, Toros H, Şen O. (2003). The Effect of Magnetic Field on Human Health, II. Atmospheric Sciences Symposium, 19-21 March, ITU, Istanbul. ISBN.975-561-236-X, 62-68.
- Brockwell, P. J, Davis, R.A. (2016). Introduction to Time Series and Forecasting, 3rd ed. Switzerland, Springer.
- Cansız M, Çelik AR, Kurt MB. (2014). Measurements of Electric and Magnetic Field Intensities at 50 Hz Mains Frequency and Comparison of Measurement Results to ICNIRP's Reference Levels for General Public Exposure, Pamukkale Univ J Eng Sci, 20(8), 294-299.
- Cansiz, M. (2010). Electromagnetic Field Map of Diyarbakır City Center and Evaluation of the Situation, Dicle University Institute of Science, Master's Thesis.
- Çal, S. (2016). Determination of Electromagnetic Field Exposure of Workers in Health Sector and Development of Solution Proposals (Master's thesis). Ministry of Labor and Social Security, General Directorate of Occupational Health and Safety, Ankara.
- Çeçen M., Pala Z, Etem T. (2016). Detection of Electromagnetic Fields Effect Rating On Health by Aid of Fuzzy Logic, International Conference on Natural Science and Engineering(ICNASE'16), March 19-20, 2016, Kilis, pp. 372-377.
- Ciaburro G, Venkateswaran B. (2017). Neural Networks with R, BIRMINGHAM, MUMBAI.
- Düzgün, S. (2009). Harmful effects of electromagnetic fields on human health, Çukurova University FBE, Adana.
- Etem T, Pala Z, Çeçen M. (2016). Investigation of Electromagnetic Pollution Changes Over Time in a University Campus, International Conference on Natural Science and Engineering(ICNASE'16), March 19-20, 2016, Kilis, pp. 482-488.
- Grellier, J., Ravazzani, P., Cardis, E. (2014). Potential health impacts of residential exposures to extremely low frequency magnetic fields in Europe, Environment International 62, 55–63.
- Güler, İ., Çetin, T. (2010). Ozdemir A. R., Extreme, N., Turkey Electromagnetic Field Exposure Report, Information and Communication Technologies Authority, 1-50.
- Güneşer, C., Şahin, Ö., Öztura, H. (2007). Determining the health risk of 154 kV, 50 Hz., power transmission line, EHE'07 - 2nd International Conference on Electromagnetic Fields Wroclaw, Poland, September 10-12, 4-6.

Habbash RWY. (2008). *Bioeffects and Therapeutic Applications of Electromagnetic Energy*, Taylor & Francis Group, LLC, ISBN: 978-1-4200-6284-7.

<http://ema-olcum.btk.gov.tr/>, Last accessed December 13, 2020.

<http://www.resmigazete.gov.tr/eskiler/2015/10/20151009-2.htm>, Last accessed December 13, 2020.

https://webarchive.nationalarchives.gov.uk/20140714123226/http://www.hpa.org.uk/webc/HPAwebFile/HPAweb_C/1194947383619, Last accessed December 13, 2020.

ICNIRP. (1998). Guidelines for limiting exposure to time-varying electric, magnetic and electromagnetic fields (up to 300 GHz), *Health Phys.* 74, 494-522.

İlhan MN. (2008). *Making an Electromagnetic Field Map in a Medical Faculty Hospital and Determination of Health Effects on Health Workers*, Ankara University Institute of Health Sciences, PhD Thesis, 1-79.

ICNIRP. (2009). International Commission on Non-Ionizing Radiation Protection, Exposure to high frequency electromagnetic fields, biological effects and health consequences (100 kHz-300 GHz), ICNIRP.

Karadağ, T., Özdemir, A. R. & Abbasov, T. (2014). Measuring and Mapping Long-Term and Continuous Electromagnetic Pollution Levels in a Selected Pilot Area, *Gazi University Journal of Science*, 2 (3), 239-246.

Kulkarni G, Gandhare WZ. (2012). Proximity Effects of High Voltage Transmission Lines on Humans, *ACEEE Int. J. on Electrical and Power Engineering*, Vol. 03, No. 01, pp. 28-32.

Kunter, F. (2015). Students Exposure to Radio Frequency Electromagnetic Fields in Marmara University, *Marmara Journal of Science*, 1:48-56.

Mollaoğlu H, Özgüner F. (2006). Biological effects of magnetic field on organism, *S.D.Ü. Faculty of Medicine. Journal.* 13 (1), 38-41.

Mousa, A. (2009). Exposure to Electromagnetic Radiation at the Campus of An-Najah University, *Proceedings of the 2009 IEEE 9th Malaysia International Conference on Communications 15 -17 December 2009 Kuala Lumpur Malaysia*, 154-158.

Namin S.S., Namin A.S. (2018). *Forecasting economic and financial time series: Arima vs. LSTM*, Texas Tech University, TX, USA.

Nassiri,P., Monazzam,M.R., Yunesian,M., Sowlat,M.H, Safari,M.H., Bellah, S.M., Lotfi, S. (2012). Investigation of Extremely Low Frequency Magnetic Field (ELF-MF) Flux Densities in the Vicinity of Schools in Tehran, *World Applied Sciences Journal* 20 (6): 848-853.

Olubosede, O. (2012). *Measurement of Magnetic Field Radiation from Selected High-Tension wires inside Adekunle Ajasin University Campus, Akungba*

- Akoko Nigeria, International Journal of Engineering Research and Dev., 3(3), 01-06.
- Özgümüş, B. (2010). Investigation of Electromagnetic Pollution in 100kHz-3GHz Frequency Band of Zonguldak City Center , Zonguldak Karaelmas University Institute of Science, Master's Thesis.
- Pala Z, Etem T, Çeçen M. (2015). Measuring Electromagnetic Radiation Values and Determining Risk Areas in Muş Alparslan University Campus, ESCROW-2015 Symposium for Healthy Tomorrows, 13-15 November 2015, Mersin.
- Polat, A. Ö. (2013). Karamanoğlu Mehmetbey University Electromagnetic Pollution Map of Yunus Emre Campus Mersin University Institute of Science, Master's Thesis.
- Redlarski G, Lewczuk B, gak A, Koncicki A, Krawczuk M, Piechocki J, Jakubiuk K, Tojza P. (2015). The Influence of Electromagnetic Pollution on Living Organisms: Historical Trends and Forecasting Changes, Hindawi Publishing Corporation BioMed Research International Volume 2015, Article ID 234098, pp. 1-18.
- Şahin, M.E, As, N., Karan, Y. (2013). Selective Radiation Measurement for Safety Evaluation on Base Stations, Gazi University Journal of Science, 26(1):73-83.
- Sarıkahya, N.M. (2014). Measuring electromagnetic field in a workplace, and evaluating the results in terms of occupational health and safety, T.C Ministry of Labor and Social Security, General Directorate of Occupational Health and Safety, Ankara.
- Seyfi L. (2015). Assessment of Electromagnetic Radiation with Respect to Base Station Types, International Journal of Information and Electronics Engineering, Vol. 5, No. 3. pp. 176-179.
- Sivani S, Sudarsanam D. (2012). Impacts of radio-frequency electromagnetic field (RF-EMF) from cell phone towers and wireless devices on biosystem and ecosystem – a review, Biology and Medicine, vol 4. No:4, pp. 202-216.
- Sorgucu, U., Kabalcı, Y., Develi, İ. (2011). Development in Turkey GSM Base Station System and the Role of the Electromagnetic Pollution, 6th International Advanced Technologies Symposium, 16-18 May 2011, Elazığ, Turkey, 29-32.
- Stuart J. Russell and Norvig P. (2010). Artificial Intelligence A Modern Approach, Pearson
- Tükkân A, Pala K. (2009). Very Low Frequency Electromagnetic Radiation and Health Effects, Uludağ University Faculty of Engineering and Architecture Journal, Volume 14, Number 2, 11-22.

- Usikalu M.R, Akinyemi M.L. (2012). Analysis of Radiation Dose around Some Base Stations in Ota and Lagos Environ, International Journal of Basic & Applied Sciences, Vol. 12, No. 05.
- Uygunol, O. (2009). Determination of Electromagnetic Field Pollution in GSM Base Stations with the Help of Geographical Information System and the Case of Konya, Selçuklu University Institute of Science, Master's Thesis.
- Verkasalo, P.K, Pukkala, E,Kaprio, J, Heikkilä, K.V, Koskenvuo, M. (1996). Magnetic fields of high voltage power lines and risk of cancer in Finnish adults: Nationwide cohort study, British Medical Journal, Vo. 313, Issue 7064, pp.1047-1051

Chapter 27

THE STATE AND IMPORTANCE OF FPGAs IN COMPUTATIONAL ELECTROMAGNETICS



*Ali Recai Celik*¹

¹ Dr., Dicle University, Engineering Faculty, Department of Electrical and Electronics Engineering, Diyarbakir, Turkey

1. INTRODUCTION

Several electromagnetic (EM) applications like designing and modelling of the antennas, waveguides, communication systems, fiber optic technologies, radar and satellite systems are not analytically computable due to irregular shapes of the devices. Therefore, some numerical techniques are needed to make these calculations.

There are many computational electromagnetics methods used to solve the problems. The most common of these methods are Finite Element Method (FEM), Finite Difference Time Domain (FDTD) and Method of Moment (MoM). While the first two of these methods are used as differential equation solvers, the other is used as integral equation solver. Implementations of the numerical methods are complex and time consuming since millions of equations must be solved simultaneously when making computations. Hence, accelerating the solver part of these methods is very important and necessary. Field Programmable Gate Arrays (FPGA) can overcome this problem thanks to their many features, especially their parallel processing capabilities.

In this study, FEM, FDTD, MoM and FPGA are introduced and some prominent works related with the FPGA implementations in computational methods are mentioned.

1.1. Electromagnetic Computation Methods

EM computations have an important place in the design of various electrical engineering applications. These computations are made by using some numerical techniques. One of these approximations is FEM which is widely used in modelling the EM problems having complex geometries. It has attracted great attention from researchers with the advancement in technological developments [1]. However, it has many linear equations in large sparse systems. Hence, the great part of the solution run-time is consumed when solving these equations.

Another powerful computational technique is FDTD. This technique provides a direct time-domain solution of Maxwell's Equations whose differential form is given in Fig. 1. The reason this method has become a powerful method for solving a wide variety of electromagnetic areas is that it can solve Maxwell's equations with almost any type of medium [2]. Just like in FEM method, the 3D simulation in FDTD method involves millions of computational cell volumes. It is computationally intensive and simulations must run for a long time on multiprocessor supercomputers. A flowchart for the complete process of the FDTD method is given in Fig. 2 as an example [3].

$\nabla \times \vec{E} = -\frac{\partial \vec{D}}{\partial t} - \sigma_m \vec{H} - \vec{M}$	(1)	\vec{E} : electric field
$\nabla \times \vec{H} = \frac{\partial \vec{D}}{\partial t} + \sigma_e \vec{E} + \vec{J}$	(2)	\vec{D} : electric flux density
$\nabla \cdot \vec{D} = \rho_e$	(3)	\vec{H} : magnetic field
$\nabla \cdot \vec{B} = \rho_m$	(4)	\vec{B} : magnetic flux density
$\vec{B} = \mu \vec{H}$	(5)	\vec{J} : electric current density
$\vec{D} = \epsilon \vec{E}$	(6)	\vec{M} : equivalent magnetic current density
		σ_e : electric conductivity
		σ_m : equivalent magnetic loss

Figure 1. Differential form of the Maxwell's Equations and definitions of the symbols

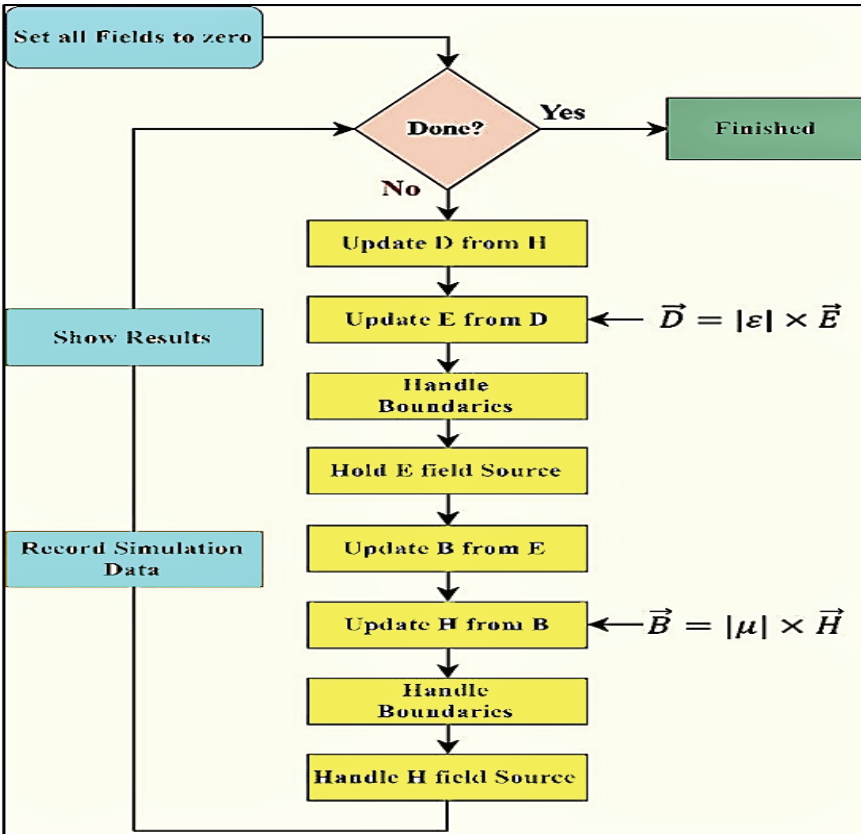


Figure 2. The process of FDTD method [3]

MoM is another basic method used to model the EM problems, which was first proposed by Harrington [4] and is still used in many applications. MoM is a numerical method based on integral equations in the frequency domain. The main formulation of the method is the integral equations obtained using Green's functions. In this method, the examined structure

should be divided into segments. It then needs to be written and resolved as a matrix system. The size of the matrix system depends on the number of segments. As the number of segments increases, the numerical difficulties arise when taking inverse of the impedance matrix. Thus, the calculation volume and its duration increase exponentially in this method.

In summary, implementations of the FEM, FDTD, MoM and other numerical methods are complex and time consuming since millions of equations must be solved simultaneously when making computations. Thus, the solver part of these methods must be very fast.

Software-based solvers are fed into microprocessors and computed serially. Every software instruction must be decoded before starting to execution. The microprocessor must read and decode each instruction sequentially and then execute it. This situation creates an extra overhead for each operation [5]. They don't scale well when the number of equations increase and they are often too slow to be practical for many real-time applications [6].

The usage of Application Specific Integrated Circuit (ASIC) may be another option. However, it has a long development period, costly, and also inflexible. What's more, once the ASIC chip is fabricated, it cannot be modified. If any part of the logic needs to be changed, the chip must be redesigned and refabricated.

FPGAs may be a suitable alternative which can overcome the mentioned problems thanks to their low costs, reconfiguration capabilities, parallel processing features, and speeds enough to work in complex systems. In the next section, the introduction, features and advantages of the FPGA will be mentioned.

1.2. What is FPGA?

FPGA is a general-purpose logic device containing a large number of chips, successfully performs the arithmetic operations and multiplexers can be embedded in. FPGAs are programmable in the field to create logical functions what designers need. They can be defined as integrated circuits whose hardware structures can be changed after production according to the desired function. In other words, FPGAs are the circuits whose transistors are produced independently and freely. Transistors are connected to each other according to the user specified function. Then, the desired application is performed [7]. They can also be reprogrammed run-time, namely reprogramming FPGA partly is possible in case that the system is running on the other part of the chip. These characteristics offer higher elasticity for the FPGAs and appropriateness for several practices. From the outside view, FPGA is a single chip, while the inside structure consists of the adjustable logic blocks, input-output (IO) units around these

blocks and programmable connections that connect all these units. The FPGA structure is illustrated in Fig. 3 [8,9].

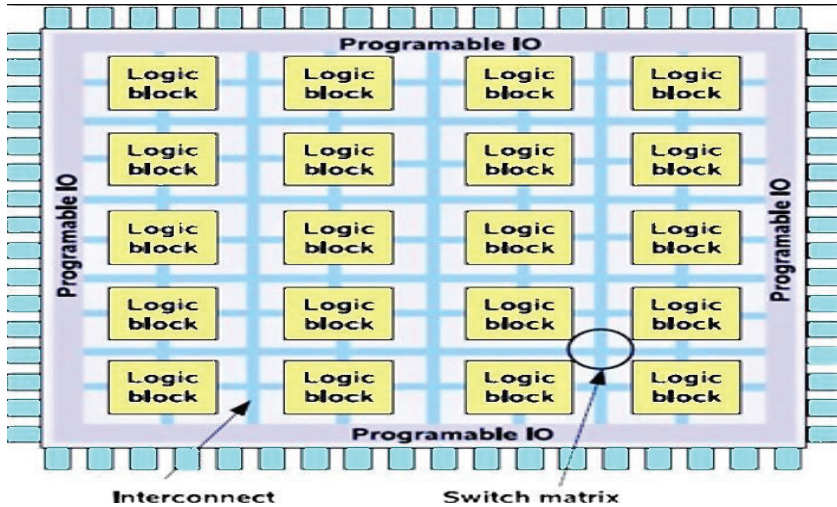


Figure 3. The inside structure of an FPGA

In summary, FPGAs provide the benefits of both ASICs and software-based solvers. Similar to the ASICs, FPGAs could potentially manage a myriad of logic gates, which are optimally designed for a specific function and in a single integrated circuit. Even though FPGA-based designs do not challenge the performance of ASICs, there are few applications that deserve the high cost of very expensive ASICs. Also like software, FPGAs are reprogrammable by designers at any time. Hence, there are flexible and convenient. Although the FPGA-based developments are costly compared to the software, they can show extremely high performance surpassing any programmable solutions [10]. Therefore, the usage of the FPGAs accelerates the solving of numerical methods and has an important role in EM computations. In the next section, some prominent works related with the FPGA implementations in numerical methods will be mentioned.

2. RELATED WORKS

2.1. FPGA Implementations of the FEM

Accelerating the FEM using FPGA for EM computations is one of the most significant works. There are many studies prepared for this purpose. For example, in the study of [11], the researchers introduced a hardware solver going through the most time-inefficient phase in FEM. The device and software of choice were Altera Cyclone II FPGA and Quartus II 9.0 in the study. Pipelining process was fulfilled and the clock speed was recorded nearly at 114.61 MHz. The hardware solver was used to solve the EM boundary value problems. Based on the measurements, the speed was raised by 4 times more than the software performance on a standard computer.

A deeply pipelined FPGA design for efficient sparse matrix-vector multiplication (SpMV), which is a kernel for several iterative numerical techniques to discover sparse linear systems, was developed in [12]. The authors of the paper developed their own pipelinable striping scheme in order to improve the total usability of their own hardware design.

In another study of Zhuo and Prasanna, LU factorization method implemented a direct solver. For the calculations on a Xilinx Virtex- II Pro XC2VP100, a circular linear array of processing elements in double precision became useful. The minimum latency period could be yielded using any design of LU decomposition in that study. The proposed design provided around 4 GFLOPS which was greater compared to the retainable operation of a LU decomposition algorithm exclusively optimized for a 2.2 GHz AMD Opteron processor [13].

Greisen et al. examined many solvent methods and presented a discussion on hardware trade-offs, with demonstration of FPGA architectures of Cholesky direct solver and BiCGSTAB iterative solver. In the study, it was concluded that 32K x 32K matrices were solved at less than 50 fps through the FPGA applications having higher performance than software applications by one or multiple orders of magnitude [14].

In another study related with the FPGA implementation of the FEM, Johnson et al. designed sparse direct LU decomposition and implemented a prototype on FPGA. They monitored the performance with reference to a platform based on universal processor. The results showed that the sparse LU decomposition hardware design application by using FPGA was capable of an order of magnitude speedup relative in comparison with the Pentium 4 based system. These results highlight the usage of FPGAs for high performance sparse direct LU decomposition [15].

2.2. FPGA Implementations of the FDTD

A number of works purposed to speed up the FDTD method for the EM computations. The first use of the FPGA device on this method was proposed in [16]. One-dimensional FDTD cell was implemented on FPGA and the activities were successfully simulated in that work. A pipelined bit-serial arithmetic architecture helped to transfer the algorithm to FPGA-based hardware. The results of the paper showed that the proposed hardware design made the one-dimensional algorithm quicker than the software design.

Kosmas et al. introduced and tested a pseudo-2D FDTD hardware architecture [17]. The study demonstrated that the results of software and hardware implementations. According to the obtained results, the qualified algorithms and the capable resources facilitated the hardware implementation to raise the computational speed up to the peak. The

hardware speed was corresponding to that of 24 times the fastest software implementation running on 3.0 GHz PC.

Durbano and Ortiz accelerated the FDTD using a customized accelerator board compatible with the specified configurations (DDR SDRAM \leq 16 GB, DDR SRAM=36 MB) as well as Xilinx Virtex-II 8000 FPGA and an external PCI controller. Although the accelerator cards used in that study required multiple-PC solutions, such weakness did not obstruct a 23-fold acceleration and an almost 6-fold hike at its zenith of problem size [18].

An FPGA-based architecture using OpenCL was shown in [19]. This architecture was proposed to apply the iteration level parallelism in order to decrease the external memory access. In that study, the processing speed reached up to relatively 4 or more times higher level to the GPU implementation and 13 times higher level to the CPU.

In the study [20], a method using the FPGA which employs a 32-bit operation machine was investigated to short the required time for the FDTD process. For this aim, an analysis about the processing time for an FPGA implementation was made. The authors of the paper focused on decreasing the number of data taken from the DDR memory. It was shown that the used techniques reduced the computation time by 22 times compared to the time required by a computer using commercial software.

2.3. FPGA Implementations of the MoM Studies

There are several studies presenting the FPGA-based accelerator for MoM solutions. Using an FPGA-based hardware implementation, the study of [21] offered parallelization of the iterative matrix solution for multiple RHS vectors in a low-rank compression-based fast solver scheme. This technique enhanced the capacity of multiple conductors to extract the electrostatic parasitic capacitance in a Ball Grid Array (BGA) package. In another study, the same researchers proposed similar hardware design toward a double-leveled parallelization scheme. The authors used a 2.4 GHz Intel Core i5 processor and observed that speedup was linearly scalable with FPGA resources and the software implementation had 10x higher velocity than equivalent one. Virtex-6 XC6VLX240T FPGA on Xilinx's ML605 board was used in that study. The authors also emphasized that the proposed method could be applied to other forms of EM extractions.

Another study investigated the CPU/FPGA application of the matrix assembly phase of the (MoM), based on the frequency-domain integral equation-based formulation including piecewise linear function and the image methods to appraise the radiation pattern of the antenna system [22]. The code executed on the device ran only one single work-item OpenCL kernel in order to take advantage of the proposed architecture. It was

reported that the speedup ratios were computed as relatively approximately $2.08\times$ with reference to the single-core CPU approach and as nearly $1.11\times$ to two-core CPU implementation.

3. CONCLUSIONS

There are several numerical methods used to solve computational EM problems. In this study, FEM, FDTD and MoM, which are the most known and preferred methods, have been briefly introduced. It has been mentioned that implementations of these methods are complex and time consuming since millions of equations must be solved simultaneously in calculation process. It has been emphasized that speed up the solvent part of the methods is very important and necessary. The merits and drawbacks of the software-based, ASIC-based and FPGA-based solver systems have been discussed. The properties and structures of the FPGAs have been shown in detail. Several works related with the FPGA implementations have been reviewed. The results of these works indicate that FPGA hardware implementation can achieve significant acceleration for solving numerical method algorithms. Finally, it can be concluded that the usage of FPGAs has an important role in computational electromagnetics.

REFERENCES

- [1] Strang, G. & Fix, G. (1973). *An Analysis of the Finite Element Method*: Englewood Cliffs. *Prentice Hall*, New Jersey, USA.
- [2] Kosmas, P., Wang, Y. & Rappaport, C. (2002). “Three-Dimensional FDTD Model for GPR Detection of Objects Buried in Realistic Dispersive Soil,” *SPIE Aerosense Conference*, Orlando, pp.330–338.
- [3] Memon, N., Naich, M.R., Pathan, A.Z., Mirjat, B.A. & Faiz, M. (2019). “Computational Investigations on CZTS Thin-Film Layers Adopting Grating Structures,” *SSRG International Journal of Electronics and Communication Engineering*, 6(8), pp. 38–43.
- [4] Harrington, R.F. (1968). “Field Computation by Moment Methods,” *Wiley IEEE Press*. ISBN: 978-0-780-31014-8
- [5] Compton, K. & Hauck, S. (2002). “Reconfigurable Computing: A Survey of Systems and Software,” *ACM Computing Surveys*, 34(2), pp.171–210.
- [6] Tarek Ibn Ziad, M., et al. (2015). “Finite Element Emulation-Based Solver For Electromagnetic Computations,” *IEEE International Symposium on Circuits and Systems (ISCAS)*, Lisbon, pp. 1434–1437.
- [7] Celik, A.R. & Alkan, A. (2015). “Implementation of Basic Image Processing Applications by FPGA Hardware,” *International Journal of Scientific and Technological Research*, 1(1), pp. 133–143.
- [8] Villasenor, J. & Mangione-Smith, W.H. (1997). “Configurable computing,” *Sci. Amer.*, 276(6), pp. 66–71.
- [9] Shawahna, A., Sait, S.M. & El-Maleh, A. (2019) “FPGA-Based Accelerators of Deep Learning Networks for Learning and Classification: A Review,” *IEEE Access*, vol.7, pp. 7823–7859.
- [10] Hauck, S. (1998). “The Roles of FPGAs in Reprogrammable Systems,” *Proceedings of the IEEE*, 86(4), pp.615–639.
- [11] Zhang, J., Zhang, M., He, H. & Song, Q. (2015). “Accelerating the finite element method using FPGA for electromagnetic field computation,” *2015 IEEE International Conference on Cyber Technology in Automation, Control, and Intelligent Systems (CYBER)*, Shenyang, pp. 1763–1768.
- [12] El-Kurdi, Y., Giannacopoulos, D. & Gross, W. J. (2007). “Hardware Acceleration for Finite-Element Electromagnetics: Efficient Sparse Matrix Floating-Point Computations With FPGAs,” *IEEE Transactions on Magnetics*, 43(4), PP.1525–1528.
- [13] Zhuo, L. & Prasanna, V.K. (2006). “High-Performance and Parameterized Matrix Factorization on FPGAs,” *International Conference on Field Programmable Logic and Applications*, Madrid.

- [14] Greisen, P., Runo, M., Guillet, P., Heinzle, S., Smolic, A., Kaeslin, H. & Gross, M. (2013). "Evaluation and FPGA Implementation of Sparse Linear Solvers for Video Processing Applications," *IEEE Transactions on Circuits and Systems for Video Technology*, 23(8), pp. 1402–1407.
- [15] Johnson, J., Chagnon, T., Vachranukunkiet, P., Nagvajara, P. & Nwankpa, C. (2008). "Sparse LU Decomposition Using FPGA," *Int. Workshop State-of-the-Art Scientific Parallel Comput. (PARA)*.
- [16] Schneider, R.N., Turner, L.E. & Okoniewski, M.M. (2002). "Application of FPGA Technology to Accelerate the Finite-Difference Time-Domain (FDTD) Method," *ACM/SIGDA Tenth International Symposium On Field-Programmable Gate Arrays (FPGA) Association for Computing Machinery*, New York, USA, pp. 97–105.
- [17] Kosmas, P., Wang, Y. & Rappaport, C. (2002). "Three-Dimensional FDTD Model for GPR Detection of Objects Buried in Realistic Dispersive Soil," *SPIE Aerosense Conference*, Orlando, pp.330–338.
- [18] Durbano J.P. & Ortiz, F.E. (2004). "FPGA-based Acceleration of the 3D Finite-difference Time-domain Method," *12th Annual IEEE Symposium on Field-Programmable Custom Computing Machines*, pp.156–163.
- [19] Waidyasooriya, H.M., Endo, T., Hariyama, M. & Ohtera, Y. (2017). "OpenCL-Based FPGA Accelerator for 3D FDTD with Periodic and Absorbing Boundary Conditions," *International Journal of Reconfigurable Computing*, vol. 2017.
- [20] Suzuki, H., Takagi, Y., Yamaguchi, R. & Uebayashi, S. (2005). "FPGA Implementation of FDTD Algorithm," *Asia-Pacific Microwave Conference Proceedings*, Suzhou, pp. 1–4.
- [21] Devi, A., Gandhi, M., Varghese, K. & Gope, D. (2016). "Accelerating Method Of Moments Based Package-Board 3D Parasitic Extraction Using FPGA," *Microw. Opt. Technol. Lett.*, vol. 58, pp. 776–783.
- [22] Topa, T. (2020). "Porting Wire-Grid MoM Framework to Reconfigurable Computing Technology," *IEEE Antennas and Wireless Propagation Letters*, 19(9), pp. 1630–1633.

Chapter 28

ON PERFORMANCE OF FLOWER POLLINATION ALGORITHM IN TRAINING ADAPTIVE-NETWORK-BASED FUZZY INFERENCE SYSTEM (ANFIS)



Ceren BAŞTEMUR KAYA¹

¹ Ceren BAŞTEMUR KAYA: ceren@nevsehir.edu.tr, ceren680@gmail.com, Department of Computer Technologies, Nevsehir Vocational College, Nevsehir Haci Bektas Veli University, 50300, Nevsehir, Turkey

1. INTRODUCTION

ANFIS is combined of fuzzy logic and artificial neural networks. Due to the advantages of both methods, it emerges as a powerful artificial intelligence technique. When the literature is examined, it is seen that it is used in the solution of many real world problems. Student modeling, medical system, economic system, traffic control, image processing and feature extraction, forecasting and prediction, manufacturing and system modeling, electrical and electronics system are some of the areas where it is used (Mitiku & Manshahia, 2018).

One of the important issues about ANFIS is the training process. There are two groups of parameters used in ANFIS training. These are premise and consequent parameters. In fact, training of ANFIS means determining the ideal value of these parameters. There are 3 different approaches in ANFIS training. These are derivative-based, heuristic algorithm and hybrid algorithms. The disadvantages of derivative based algorithms have recently enabled the use of heuristic algorithms in ANFIS training. On the other hand, hybrid algorithms have also been developed using the advantages of derivative-based and heuristic algorithms. Genetic algorithm (GA), particle swarm optimization (PSO), artificial bee colony (ABC) algorithm, differential evolution (DE), harmony search (HS), cuckoo search (CS), firefly algorithm (FA), simulated annealing (SA), mine blast algorithm (MBA) and artificial immune system (AIS) are some of the heuristic algorithms used in ANFIS training (Karaboga & Kaya, 2019).

There are many heuristic algorithms that have been proposed recently in the literature. While some heuristic algorithms are used very intensively in ANFIS training, some of them are used less. In fact, this may have several reasons. Some of these reasons are 1) it is successful in solving the real world problem 2) it has been accepted in the scientific world 3) it has been used for a long time 4) it is open to development. Scopus database are examined for the use cases of heuristic algorithms in models based on ANFIS. The filtering process is applied on title/keywords/abstract. ANFIS and the relevant heuristic algorithm are selected as the keyword in the filtering. The determined statistical information is presented in Table 1. As seen in Table 1, GA and PSO are used most frequently in ANFIS-based studies. DE, SA, ABC, FA and CS algorithms are also used extensively in this field. Methods such as HS and FPA have limited number of studies on ANFIS.

Examining some studies in the literature gives an idea about the areas which they are used and the importance of the subject. Calp (2019)

proposed a hybrid approach called (ANFIS-GA) based on ANFIS and GA for estimation of regional rainfall amount. Pereira, Patil, Mahadeshwar, Mishra, and D'Souza (2016) used ANFIS and GA to eliminate the Electrooculogram (EOG) artifact from the Electromyogram (EMG) and training of ANFIS was realized by utilizing GA. Noushabadi, Dashti, Raji, Zarei, and Mohammadi (2020) applied an approach based on PSO and ANFIS for estimation of cetane numbers of biodiesel and diesel oils. Zangeneh, Mansouri, Teshnehlab, and Sedigh (2011) trained ANFIS by using DE/current-to-best/1+1/bin & DE/rand/1/bin for predicting of Mackey-glass time series and identification of a nonlinear dynamic system. Haznedar and Kalinli (2018) realized training of ANFIS via SA for identification dynamic systems. (Karaboga & Kaya, 2020) optimized the parameters of ANFIS by using ABC algorithm to predict the number of foreign visitors coming to Turkey from the USA, Germany, Bulgaria, France, Georgia, the Netherlands, England, Iran and Russia. Kamarian, Yas, Pourasghar, and Daghigh (2014) combined FA and ANFIS for optimization of functionally graded beams. Mustapha, Salisu, Ibrahim, and Almustapha (2020) used a CS algorithm in ANFIS training and forecasted short-term load. Wang, Gao, Tanskanen, and Guo (2012) applied an approach called HS-ANFIS by adapting HS and ANFIS for epileptic EEG signal classification. Apart from these, there are different studies in the literature (Karaboga & Kaya, 2019).

Table 1. Statistical information about the number of publications based on ANFIS and heuristic algorithms

Algori thm	Number of publication
GA	875
PSO	559
DE	99
SA	55
ABC	45
FA	44
CS	20
HS	9
FPA	4

FPA is one of the heuristic optimization algorithms used extensively recently. Computer science, bioinformatics, operation research, imaging science, food industry, meteorology, medicine (ophthalmology), education, and engineering are among the areas where FPA is used

(Abdel-Basset & Shawky, 2019). When filtering the Scopus database according to the study title, it is seen that there are 400+ studies with FPA. This shows that FPA is utilized extensively in solving real world problems. Currently, there are a limited number of ANFIS and FPA-based studies. However, the success of FPA and its increasing popularity show that it can be used more in ANFIS training in the future. Therefore, the performance of FPA in ANFIS training is evaluated within the scope of this study. In other words, FPA is used in the process of determining ANFIS's premise and consequent parameters. An ANFIS and FPA based model has been created to solve XOR, 3 bit parity and 4 bit parity problems in applications.

2. METHODS

2.1. Flower Pollination Algorithm

FPA is an optimization algorithm inspired by the pollination process of plants in nature (Yang, 2012). In the pollination process, pollinators and types of pollination are important. Pollinators are divided into two groups as biotic and abiotic. Wind can be given as an example for abiotic pollinator. Insects are an examples of biotic pollinator. Pollination is divided into two groups depending on whether the pollination process takes place from the same or different plants: self-pollination and cross-pollination. These processes are illustrated in Figure 1 (Abdel-Basset & Shawky, 2019). There are four basic rules in FPA. These are:

- Biotic and cross-pollination are elements of global pollination. Levy distribution is effective in the flight of pollinators.
- Unlike the global pollination process, abiotic and self-pollination occurs in local pollination.
- Flower constancy is a reproduction probability associated with the similarity of the two flowers.
- Global or local pollination status is determined by a switch probability (p).

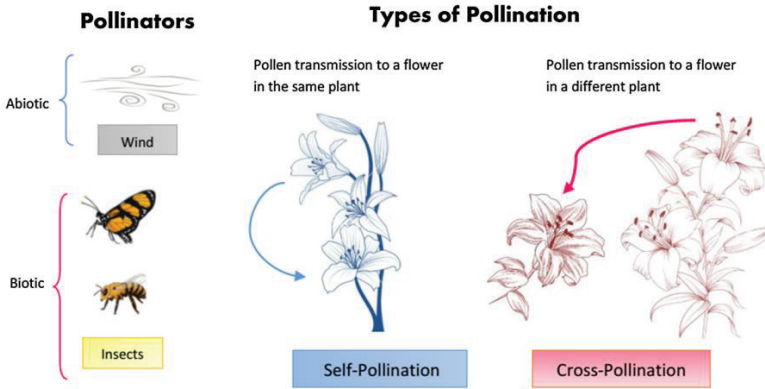


Figure 1. The pollinators and pollination types (Abdel-Basset & Shawky, 2019)

Flower Pollination Algorithm (or simply Flower Algorithm)

```

Objective min or max  $f(\mathbf{x})$ ,  $\mathbf{x} = (x_1, x_2, \dots, x_d)$ 
Initialize a population of  $n$  flowers/pollen gametes with random solutions
Find the best solution  $\mathbf{g}_*$  in the initial population
Define a switch probability  $p \in [0, 1]$ 
while ( $t < \text{MaxGeneration}$ )
    for  $i = 1 : n$  (all  $n$  flowers in the population)
        if  $\text{rand} < p$ ,
            Draw a ( $d$ -dimensional) step vector  $L$  which obeys a Lévy distribution
            Global pollination via  $\mathbf{x}_i^{t+1} = \mathbf{x}_i^t + L(\mathbf{g}_* - \mathbf{x}_i^t)$ 
        else
            Draw  $\epsilon$  from a uniform distribution in  $[0, 1]$ 
            Randomly choose  $j$  and  $k$  among all the solutions
            Do local pollination via  $\mathbf{x}_i^{t+1} = \mathbf{x}_i^t + \epsilon(\mathbf{x}_j^t - \mathbf{x}_k^t)$ 
        end if
        Evaluate new solutions
        If new solutions are better, update them in the population
    end for
    Find the current best solution  $\mathbf{g}_*$ 
end while
    
```

Figure 2. Pseudo code of Flower Pollination Algorithm (FPA)

Pseudo code of FPA is given in Figure 2. As can be seen, global pollination or local pollination occurs according to the value of p . The effect of biotic pollinators is observed in global pollination and the new solution is created using (1) and (2).

$$x_i^{t+1} = x_i^t + \theta L(x_i^t - g_b) \tag{1}$$

$$L \sim \frac{\lambda \Gamma(\lambda) \sin(\pi\lambda/2)}{\pi} \frac{1}{s^{1+\lambda}}, \quad (s \gg s_0 > 0) \tag{2}$$

Here x_i^t is the pollen i , g_b is also the current best solution. θ is a scaling factor to control the step size. L is a value found from the Levy distribution. $\Gamma(\lambda)$ is the standard gamma function. Value of λ is 1.5.

$$x_i^{t+1} = x_i^t + \sigma(x_j^t - x_k^t) \tag{3}$$

(3) is used to obtain a new solution in local pollination. x_j^t and x_k^t are pollens belong to different flowers of the same plant species in their neighborhood. σ is a local random walk and a random value that conforms to a uniform distribution in $[0,1]$.

2.2. Adaptive-Network-Based Fuzzy Inference System (ANFIS)

ANFIS, one of the neuro-fuzzy approaches using the characteristics of fuzzy logic and artificial neural networks, was developed by Jang (1993). ANFIS consists of two parts basically. These are: premise and consequence parts. These parts connect to each other with IF-THEN rules. Unlike artificial neural networks, it is an important advantage that ANFIS structure can be expressed with IF-THEN rules.

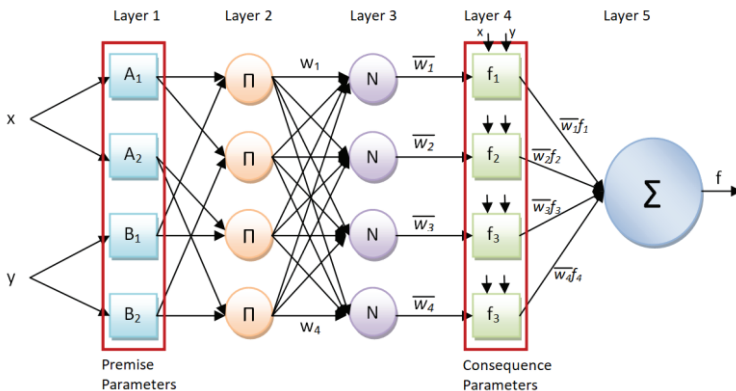


Figure 3. The ANFIS structure that has two inputs and one output

An ANFIS structure that has 2 inputs and 1 output is given in Figure 3. As can be seen, a basic ANFIS structure consists of 5 layers. Calculations are performed on each layer and the relationship between input and output is determined. In other words, an output is obtained against the input/inputs.

Layer 1 is called as fuzzification layer. In this layer, fuzzy clusters are obtained from input values through MFs. Parameters in MFs are called as primese parameters. It is one of the parameter groups that should be optimized in ANFIS training. There are many types of MFs that can be used in Layer 1. Generalized bell, gaussian, triangular, sigmoid and trapezoidal are some of them. The number of parameters each MF can be different. Generalized bell MF (Gbellmf) includes 3 parameters such as $\{a, b, c\}$. The membership value of each MF is calculated using (4) and (5). All MFs used here have been accepted as Gbellmf.

$$\mu_{A_i} = gbellmf(x; a, b, c) = \frac{1}{1 + \left| \frac{x-c}{a} \right|^{2b}} \quad (4)$$

$$O_i^1 = \mu_{A_i}(x) \quad (5)$$

Layer 2 is called as rule layer. Firing strengths (w_i) are found by utilizing the membership values obtained in Layer 1. Firing strengths are calculated by multiplying the membership values as stated (6).

$$O_i^2 = w_i = \mu_{A_i}(x)\mu_{B_i}(y) \quad (6)$$

Layer 3 is called as normalization layer. Normalized firing strengths (\bar{w}_i) are calculated via (7) by using the firing strengths found in Layer 2.

$$O_i^3 = \bar{w}_i = \frac{w_i}{w_1 + w_2 + w_3 + w_4} \quad (7)$$

Layer 4 is called as defuzzification layer. Weighted values of rules are calculated as in (8) using normalized firing strengths and first order polynomial. The parameters $\{p_i, q_i, r_i\}$ in the first order polynomial are called as consequence parameters. These parameters are the other parameter group used in ANFIS training.

$$O_i^4 = \bar{w}_i f_i = \bar{w}_i (p_i x + q_i y + r_i) \quad (8)$$

Layer 5 is called as summation layer. The actual output of ANFIS is obtained by summing the output of each rule found in Layer 4. It is calculated as in (9).

$$O_i^5 = \sum_i \bar{w}_i f_i \quad (9)$$

3. RESULTS

This study evaluates the performance of FPA in training ANFIS. For this, three test functions are used. These are XOR, 3 bit parity and 4 bit parity test problems. XOR test problem as shown in Figure 4 includes two inputs and one output. So ANFIS structure that has two inputs and one output is utilized for solving this problem. 3 bit parity problem and 4 bit parity problem have three and four inputs respectively. Both problems are also one output. Input and output values used in both problems are given in Figure 5 and Figure 6. ANFIS structure with 3 input is used for 3 bit parity problem, while ANFIS structure with 4 inputs is utilized for 4 bit parity problem. Four different membership functions such as generalized bell (Gbellmf), triangular (Trimf), gaussian (Gaussmf), trapezoidal (Trapmf) membership functions (MFs) are used in the applications. The results are obtained by using two, three and four MFs for each input in XOR problem and 3 bit parity problem. Two and three MFs are utilized for each input in the 4 bit parity problem. Therefore, the total number of parameters to be optimized in ANFIS training has changed according to the applications. The values of the control parameters of the FPA such as probability switch, population size and total number of iterations are given in Table 2. RMSE (root mean square error) calculated using (10) is utilized as the error value in the applications. Here, y_j is a real output and \bar{y}_j is a predicted output. Each application was run 30 times for statistical analysis. In this way, the best error value (Best), worst error value (Worst), average error value (Mean) and standard deviation (Std) are obtained.

$$RMSE = \sqrt{\frac{1}{n} \sum_{j=1}^n (y_j - \bar{y}_j)^2} \quad (10)$$

Input 1	Input 2	Output
0	0	0
0	1	1
1	0	1
1	1	0

Figure 4. XOR test problem (Example-1)

Input 1	Input 2	Input 3	Output
0	0	0	0
0	0	1	1
0	1	0	1
0	1	1	0
1	0	0	1
1	0	1	0
1	1	0	0
1	1	1	1

Figure 5. 3 bit parity test problem (Example-2)

Input 1	Input 2	Input 3	Input 4	Output
0	0	0	0	1
0	0	0	1	0
0	0	1	0	0
0	0	1	1	1
0	1	0	0	0
0	1	0	1	1
0	1	1	0	1
0	1	1	1	0
1	0	0	0	0
1	0	0	1	1
1	0	1	0	1
1	0	1	1	0
1	1	0	0	1
1	1	0	1	0
1	1	1	0	0
1	1	1	1	1

Figure 6. 4 bit parity test problem (Example-3)

Table 2. The used control parameters (p: switch probability, n: population size, iter: total number of iterations)

Example	Control Parameters
Example-1	p=0.8 n=10 iter=2500
Example-2	p=0.8 n=10 iter=10000
Example-3	p=0.8 n=10 iter=10000

ANFIS training results obtained by using FPA for Example-1 are presented in Table 3. The results are found for Gbellmf, Trimf, Gaussmf and Trapmf MFs. When 2,3 and 4 Gbellmf in each input are used, the best average error value is obtained as $4.0511e-05$ with 2 Gbellmf. The best error value, the worst error value and the best standard deviation are obtained by using 2 Gbellmf. When it is evaluated in terms of Trimf, the better results are found than 3 and 4 MFs with 2 MFs. Unlike Gbellmf and Trimf, the more successful results are obtained with higher number of MF in Gaussmf. The best average error value is found $5.15591e-05$ with Gaussmf. In Trapmf, the increase in the number of MF increases the error. The best average error value is found with 2 Trapmf. When Example-1 is evaluated in general, except Gaussmf, the best results are obtained with less MF numbers. For Example-1, the best average error value is found with 2 Gbellmf. At the same time, it is effective in results obtained by using 4 Gaussmf.

Table 3. The results obtained by utilizing FPA for Example-1

Type of MF	Number of MFs for Each Input	Number of Parameter	Results			
			Best	Mean	Worst	Std.
Gbellmf	2	24	0	$4.0511e-05$	$2.57903e-04$	$6.39761e-05$
	3	45	$2.91939e-07$	$1.06659e-03$	$2.57467e-02$	$4.626e-03$
	4	72	$1.17834e-06$	$1.56816e-03$	$2.07352e-02$	$4.42275e-03$
Trimf	2	24	$6.07455e-08$	$5.19485e-05$	$3.35858e-04$	$7.7602e-05$
	3	45	$2.08812e-07$	$2.69783e-04$	$1.86398e-03$	$4.07723e-04$
	4	72	$1.60196e-06$	$2.82801e-04$	$1.27423e-03$	$3.57084e-04$
Gaussmf	2	20	0	$7.03098e-04$	$1.64232e-02$	$2.94671e-03$
	3	39	$3.42379e-07$	$6.07555e-04$	$1.43326e-02$	$2.55841e-03$

	4	64	2.27488e-07	5.15591e-05	4.56088e-04	9.13763e-05
Trapmf	2	28	1.73422e-06	1.93957e-04	1.21691e-03	3.26088e-04
	3	51	2.17569e-06	2.17138e-04	1.99707e-03	3.84405e-04
	4	80	7.47123e-07	3.29448e-04	1.93675e-03	4.33965e-04

The results obtained for Example-2 are presented in Table 4. When 2 Gbellmf is used for each input, it is more effective than 3 and 4 Gbellmf. The error value is found as 1.64568e-02 with 2 Gbellmf. Unlike Gbellmf, more effective results are obtained when using 4 MFs for each input with Trimf. The average error value is 2.22386e-03 for 4 Trimf. The average error values found when is used 2, 3 and 4 Gaussmf are 4.34396e-03, 1.01483e-02 and 1.652e-02, respectively. The number of MF in Trapmf has a limited effect on the result. When all MFs are evaluated together, the best average error value for Example-2 is found with 4 Trimf. Also, the best error value is reached using 2 Trapmf. At the same time, the worst error value is obtained with 3 Trapmf. The most effective standard deviation is belonging to 4 Trimf. The most effective performance is found with low number of MF for Gbellmf and Gaussmf. Increasing the number of MF in Trimf increases the performance.

Table 4. The results obtained by utilizing FPA for Example-2

Type of MF	Number of MFs for Each Input	Number of Parameter	Results			
			Best	Mean	Worst	Std.
Gbellmf	2	50	1.67391e-05	1.64568e-02	2.39847e-01	4.42678e-02
	3	135	1.17628e-03	2.27185e-02	1.90368e-01	3.81667e-02
	4	292	2.90464e-03	6.38748e-02	2.13227e-01	4.730813e-02
Trimf	2	50	3.83011e-09	2.16892e-02	1.20011e-01	3.45091e-02
	3	135	1.33649e-09	7.96353e-03	1.13045e-01	2.36458e-02
	4	292	1.9087e-09	2.22386e-03	3.24197e-02	6.68812e-03
Gaussmf	2	44	1.78896e-05	4.34396e-03	3.96248e-02	7.69855e-03
	3	126	6.33963e-05	1.01483e-02	7.86094e-02	1.44589e-02
	4	280	4.20917e-04	1.652e-02	4.64782e-02	1.22833e-02
Trapmf	2	56	1.36982e-10	9.4119e-03	1.00433e-01	2.15737e-02
	3	144	3.98394e-10	9.00292e-03	8.32425e-02	2.02745e-02
	4	304	2.4897e-10	1.04044e-02	1.03111e-01	2.42223e-02

Table 5. The results obtained by utilizing FPA for Example-3

Type of MF	Number of MFs for Each Input	Number of Parameter	Results			
			Best	Mean	Worst	Std.
Gbellmf	2	104	5.04368e-02	2.34204e-01	5e-01	1.39178e-01
	3	441	7.86031e-02	2.21105e-01	3.75421e-01	7.19242e-02
Trimf	2	104	5.16702e-02	3.861853-01	5.04608e-01	1.60117e-01
	3	441	8.82838e-03	1.25246e-01	4.99951e-01	1.0151e-01
Gaussmf	2	96	3.88866e-02	2.49388e-01	5.00003e-01	1.4576e-01
	3	429	3.59583e-02	1.71342e-01	4.35065e-01	8.96384e-02
Trapmf	2	112	1.09403e-01	3.91771e-01	5.00002e-01	1.24867e-01
	3	453	7.55384e-02	2.25857e-01	5e-01	1.11764e-01

The results found for Example-3 are given in Table 5. Since this example has 4 inputs, the number of parameters to be optimized is more than the other examples. In fact, this situation indicates that the problem is more difficult. The results confirm this information. The results obtained using 2 Gbellmf are more successful than 3 Gbellmf. Using 3 MFs for each input in Trimf has increased the performance. Contrary to Example-2, in Gaussmf, 3 MFs are more effective than 2 MFs. In Trapmf, using 3 MFs instead of 2 MFs makes the result more successful. When all MFs are evaluated together, the best average result is found as 1.25246e-01 with 3 Trimf. At the same time, the best error value is also obtained with the same ANFIS structure. The most effective standard deviation is in structure with 3 Gbellmf. The worst error value is found as 5.04608e-01 with 2 Trimf. The best average results obtained for Example-1, Example-2 and Example-3 appear more clearly in Table 6. While Gbellmf is more successful in Example-1, Trimf is more effective in the other 2 examples.

Table 6. The best results obtained for all examples

Example	Type of MF	Number of MFs for Each Input	Number of Parameter	Train	
				Mean	Std
1	Gbellmf	2	24	4.0511e-05	6.39761e-05
2	Trimf	4	292	2.22386e-03	6.68812e-03
3	Trimf	3	441	1.25246e-01	1.0151e-01

In addition to results, convergence is also an important argument in the training process. The effect of MFs on the convergence speed is given for Example-1 in Figure 7. Especially when using 2 Gbellmf, a faster

convergence is observed compared to 3 and 4 Gbellmf. Although 3 Gbellmf is more effective than 4 Gbellmf up to about 2000 iterations, they exhibit similar convergence after about 2000 iterations. Better convergence is achieved with 3 and 4 Trimf up to about 1000 iterations. When 2 Trimf are used, it is observed that the convergence speed is better in the following iterations. When the effect of Gaussmf on convergence is examined, 2 Gaussmf converge better in low iterations. However, 4 Gaussmf converge better in high iterations. 2 and 3 Trapmf have a similar convergence characteristic.

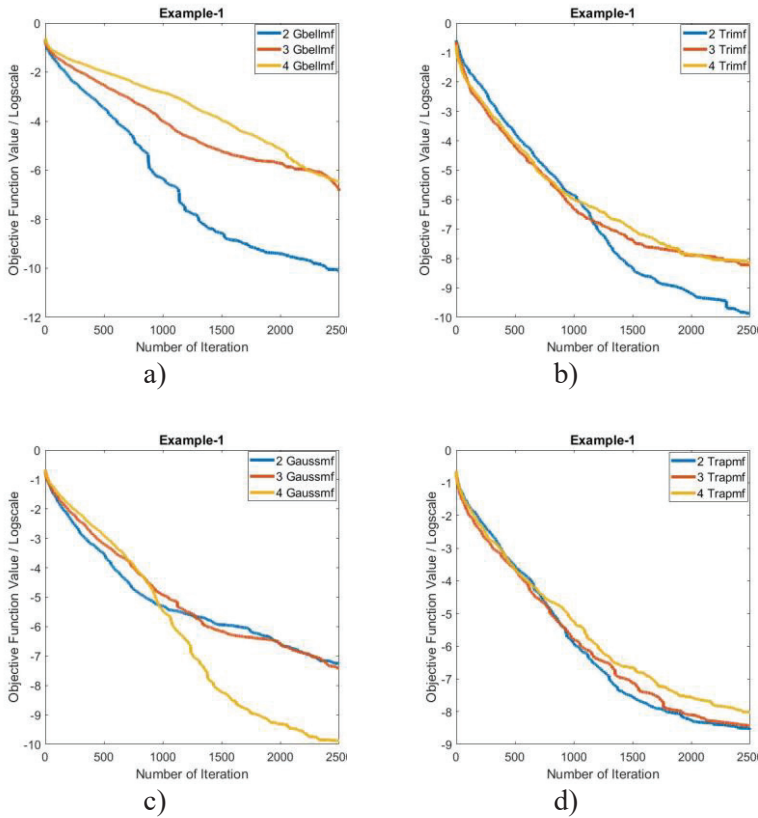


Figure 7. Comparison of convergence for membership functions on Example 1

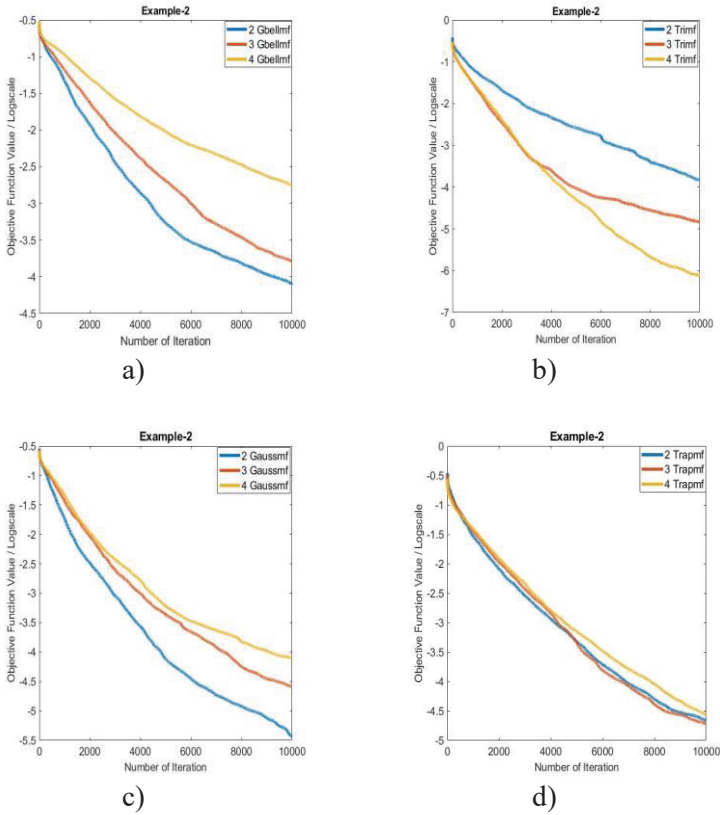


Figure 8. Comparison of convergence for membership functions on Example 2.

The effect of MFs on the convergence speed is given for Example-2 in Figure 8. It seems clear that increasing the number of MFs in Gbellmf and Gaussmf decreases the convergence speed. In Trimf, the most unsuccessful convergence speed is reached with 2 MFs. 3 Trimf and 4 Trimf show similar convergence up to about 4000 iterations. After about 4000 iterations, the convergence speed of 4 Trimf is more effective. For trapmf, the number of MF is not very effective at convergence speed.

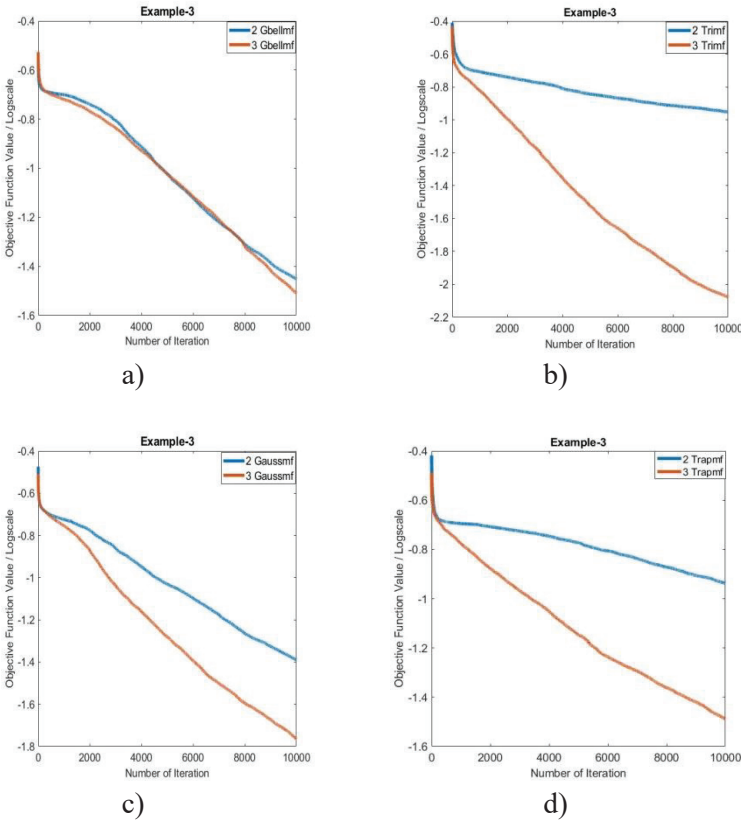


Figure 9. Comparison of convergence for membership functions on Example 3.

For Example-3, the effect of MFs on convergence is illustrated in Figure 9. Here, 2 and 3 MFs are used for each input. When 3 MFs are used for each input in Trimf, Gaussmf and Trapmf, a faster convergence is obtained compared to 2 MFs. On the other hand, the number of MF in Gbellmf does not significantly affect the convergence. When the examples are evaluated together, it is seen that the type and number of MF have different effects on convergence.

Table 7. Comparison of results obtained with PSO, HS and FPA

Example	Type of MF	Number of MFs for Each Input	PSO	HS	FPA (Proposed)
1	Gbellmf	2	5.02891e-03	7.04318e-03	4.0511e-05
2	Trimf	4	3.92009e-02	8.26843e-02	2.22386e-03
3	Trimf	3	1.30039e-01	1.64574e-01	1.25246e-01

The performance of FPA in ANFIS training is successful, as can be seen from the tables and figures, and low error values are achieved in all examples. To better analyze the performance of FPA, it is compared with PSO and HS based ANFIS training. These heuristic algorithms are chosen because they are popular and successful. Comparison of results obtained with PSO, HS and FPA are given in Table 7. The population size and number of iterations in PSO and HS are the same with FPA. In Example-1, the best result is obtained with FPA. The most successful method after FPA is PSO. The worst error value is reached as 7.04318×10^{-3} by using HS in Example-1. The error values obtained in FPA, PSO and HS in Example-2 are 2.22386×10^{-3} , 3.92009×10^{-2} and 8.26843×10^{-2} , respectively. In Example-3, the best result is again found with FPA. But the result of PSO is very close to FPA. The error value is found as 1.64574×10^{-1} with HS. When the solution qualities of three examples are evaluated together, the success order of the algorithms is FPS, PSO and HS. In addition to the solution quality, the convergence graphs of the algorithms are compared in Figure 10, Figure 11 and Figure 12. In Example-1 and Example-2, the convergence of FPA is better than PSO and HS. In Example-3, while PSO converges better until about 8000 iterations, FPA is more effective after 8000 iterations. Considering three examples, the best convergence belongs to the FPA. The least successful convergence graph belongs to HS.

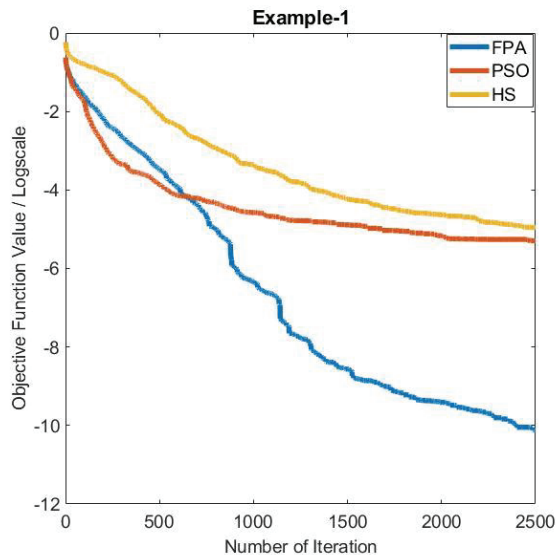


Figure 10. Comparison of the convergences of PSO, HS and FPA for Example 1.

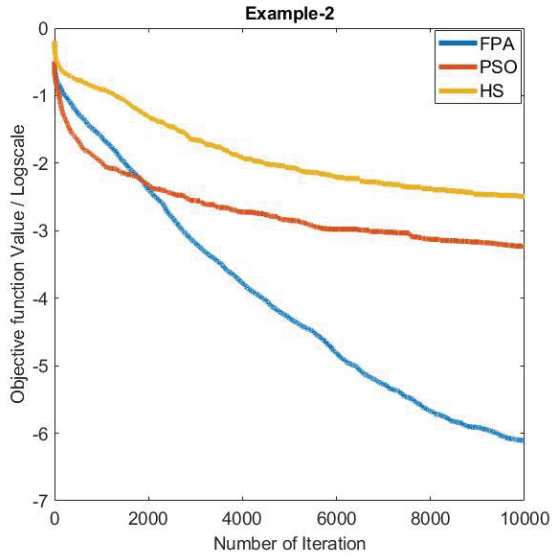


Figure 11. Comparison of the convergences of PSO, HS and FPA for Example 2.

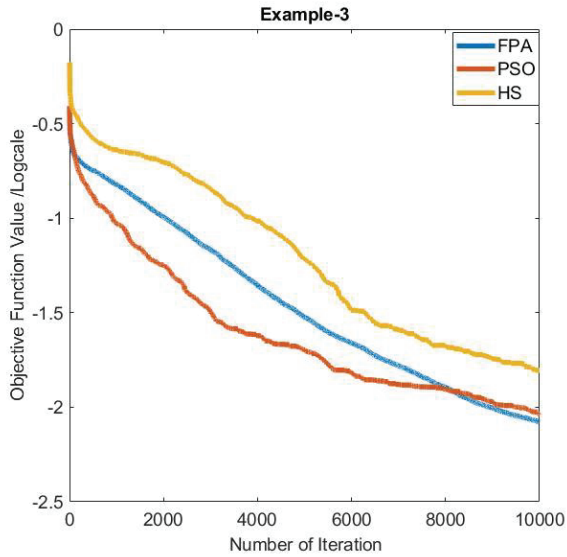


Figure 12. Comparison of the convergences of PSO, HS and FPA for Example 3.

4. CONCLUSION

In this study, the performance of FPA in ANFIS training is evaluated. As examples, XOR, 3 bit parity and 4 bit parity problems are examined. Performance of FPA-based ANFIS training has been evaluated in detail in terms of MF type and number. Four MFs such as Gbellmf, Trimf, Gaussmf and Trapmf are utilized in the applications. It has been observed that Gbellmf and Trimf are particularly effective in solving related problems. The effect of the number of MF on the result varies according to the related problem.

The performance of FPA in ANFIS training is compared with PSO and HS. It has been evaluated in terms of solution quality and speed of convergence. It has been determined that FPA is more effective than the other two algorithms in terms of both solution quality and convergence. High success rates and good error values are obtained for all examples with FPA. These results show that FPA can be effective in ANFIS training in terms of fast convergence and quality solution.

REFERENCES

- Abdel-Basset, M., & Shawky, L. A. (2019). Flower pollination algorithm: a comprehensive review. *Artificial Intelligence Review*, 52(4), 2533-2557.
- Calp, M. H. (2019). A Hybrid ANFIS-GA Approach for Estimation of Regional Rainfall Amount. *Gazi University Journal of Science*, 32(1).
- Haznedar, B., & Kalinli, A. (2018). Training ANFIS structure using simulated annealing algorithm for dynamic systems identification. *Neurocomputing*, 302, 66-74.
- Jang, J.-S. (1993). ANFIS: adaptive-network-based fuzzy inference system. *IEEE transactions on systems, man, and cybernetics*, 23(3), 665-685.
- Kamarian, S., Yas, M. H., Pourasghar, A., & Daghigh, M. (2014). Application of firefly algorithm and ANFIS for optimisation of functionally graded beams. *Journal of Experimental & Theoretical Artificial Intelligence*, 26(2), 197-209.
- Karaboga, D., & Kaya, E. (2019). Adaptive network based fuzzy inference system (ANFIS) training approaches: a comprehensive survey. *Artificial Intelligence Review*, 52(4), 2263-2293.
- Karaboga, D., & Kaya, E. (2020). Estimation of number of foreign visitors with ANFIS by using ABC algorithm. *Soft Computing*, 24(10), 7579-7591.
- Mitiku, T., & Manshahia, M. S. (2018). Neuro fuzzy inference approach: a survey. *Int JS Res Sci. Engg. Tech.*, 4(7), 505-519.
- Mustapha, M., Salisu, S., Ibrahim, A. A., & Almustapha, M. D. (2020). *Pattern-based Short-Term Load Forecasting using Optimized ANFIS with Cuckoo Search Algorithm*. Paper presented at the 2020 International Congress on Human-Computer Interaction, Optimization and Robotic Applications (HORA).
- Noushabadi, A. S., Dashti, A., Raji, M., Zarei, A., & Mohammadi, A. H. (2020). Estimation of cetane numbers of biodiesel and diesel oils using regression and PSO-ANFIS models. *Renewable Energy*.
- Pereira, L. F., Patil, S. A., Mahadeshwar, C. D., Mishra, I., & D'Souza, L. (2016). *Artifact removal from EEG using ANFIS-GA*. Paper presented at the 2016 Online International Conference on Green Engineering and Technologies (IC-GET).

Wang, J., Gao, X. Z., Tanskanen, J. M., & Guo, P. (2012). *Epileptic EEG signal classification with ANFIS based on harmony search method*. Paper presented at the 2012 Eighth International Conference on Computational Intelligence and Security.

Yang, X.-S. (2012). *Flower pollination algorithm for global optimization*. Paper presented at the International conference on unconventional computing and natural computation.

Zangeneh, A. Z., Mansouri, M., Teshnehlab, M., & Sedigh, A. K. (2011). *Training ANFIS system with DE algorithm*. Paper presented at the The Fourth International Workshop on Advanced Computational Intelligence.